Application of Fractional Calculus to Rainfall-Streamflow Modelling

Martin Borthwick

Let us know how access to this document benefits you

Recommended Citation

PEARL

PHD

Application of Fractional Calculus to Rainfall-Streamflow Modelling

Borthwick, Martin

Award date:
2010

Awarding institution:
University of Plymouth

[Link to publication in PEARL](#)

Application of Fractional Calculus to Rainfall-Streamflow Modelling

by

MARTIN FRANCIS BORTHWICK

A thesis submitted to the University of Plymouth
in partial fulfilment for the degree of

DOCTOR OF PHILOSOPHY

School of Marine Science and Engineering
Faculty of Science and Technology

January 2010

Application of Fractional Calculus to Rainfall-Streamflow Modelling

Martin Francis Borthwick

Abstract

There is evidence that hydrologic systems exhibit memory processes that may be represented by fractional order systems. A new theory is developed in this work that generalises the classical unit hydrograph technique for the rainfall-runoff transformation. The theory is based upon a fractional order linear deterministic systems approach subject to an initial condition and is taken to apply to the entire rainfall-streamflow transformation (i.e. including baseflow). The general equation for a cascade of time-lagged linear reservoirs of fractional order subject to a constant initialisation function is derived, and is shown to be a form of fractional relaxation model. Dooge's (1959) general theory of the instantaneous unit hydrograph is shown to fit within the new theoretical framework. Similarly the relationship to the general storage equation of Chow and Kulandaiswamy (1971) is demonstrated. It is shown that the correct initialisation of cascade models requires a substantial number of initial conditions which may limit the viability of applying them in practice. Consequently, the differential formulation of the classical Nash cascade has been corrected and reinterpreted.

The unbounded nature of the solution to the convolution integral form of the single fractional relaxation model is overcome by application of the Laplace transform of the pulse rainfall hyetograph following Wang and Wu (1983). The model parameters are fitted using the genetic algorithm.

The fractional order cascade equations are tested for classical rainfall-runoff modelling using a set of 22 events for the River Nenagh. The cascade of 2 unequal fractional-order reservoirs is shown to converge to that of the integer order case, whilst the cascade of equal reservoirs shows some differences.

For the modelling of the total rainfall-streamflow process the single fractional order reservoir model with a constant initialisation function is tested on a selection of events for a range of UK catchment scales ($22km^2$ to $510km^2$). A rainfall loss model is incorporated to account for infiltration and evapotranspiration. The results show that the new approach is viable for modelling the rainfall-streamflow transformation at the lumped catchment scale, although the parameter values are not constant for a given catchment. Further work is recommended on determining the nature of the initialisation function using field studies to improve the identification of the model parameters on an event-by-event basis.

Contents

List of Figures

List of Tables

Nomenclature

a	lower limit, constant
b	upper limit, constant
B	power-law exponent
c	constant
C	constant
d	uninitialized derivative
D	differ-integral operator
D^{α}	Riemann-Liouville fractional derivative
$^{c}D^{\alpha}$	Caputo fractional derivative
$E_{\alpha}(x)$	1-parameter Mittag-Leffler function
$E_{\alpha,\beta}(x)$	2-parameter Mittag-Leffler function
$E_{\alpha,\beta}^{\gamma}(x)$	3-parameter Mittag-Leffler function
f	arbitrary function, frequency
$g(t)$	unit step response function
$G(s)$	Laplace transform of $g(t)$
$h(t)$	impulse response function (instantaneous unit hydrograph)
$H(s)$	Laplace transform of $h(t)$
$i(t)$	effective (net) rainfall intensity
$i_{obs}(t)$	observed (total) rainfall intensity
$I(s)$	Laplace transform of $i(t)$
IUH	instantaneous unit hydrograph
j	integer index
k	integer index, storage delay time
K	storage delay time (relaxation time)
L	Laplace transform
L^{-1}	inverse Laplace transform
m	integer
n	integer, number of reservoirs
N	integer, number of hourly streamflow values
NSE	Nash-Sutcliffe efficiency
P	power-law exponent
$q(t)$	streamflow

$Q(s)$	Laplace transform of $q(t)$
q_0	initial streamflow
$\bar{q}_{obs}$	average observed streamflow
$q_{obs,t}$	observed streamflow at time t
q_t	streamflow at a particular time, t
$q_t(\theta)$	streamflow predicted by the model at time t
r	integer index
$r(t)$	stormflow (runoff)
$RMSE$	root mean square error
RMSslope	root mean square error of slope
s	complex variable of the Laplace transform
$S(f)$	power spectral density
t	time
T	lag time
$U(t)$	unit step function
V	storage volume
w	weighting
x	independent variable
$y(t)$	arbitrary function of t
α	fractional order
β	fractional order
$\delta(t)$	Dirac delta impulse
Δt	timestep
λ	constant
τ	time
ψ	initialisation function

Acknowledgements

AUTHOR'S DECLARATION

At no time during the registration for the degree of Doctor of Philosophy has the author been registered for any other University award without prior agreement of the Graduate Committee.

A programme of advanced study was undertaken, relevant scientific seminars and conferences were attended at which work was presented. The author is a lecturer in engineering hydrology and has taught computational hydrological modelling as part of the MSc Flood Risk course in the University. The author has been involved in a number of research projects in recent years in the University including modelling the effects of agricultural land-use changes on river flows; and the application of interactive visualisation for rainfall-runoff model calibration.

Publications:

Chadwick, A., Morfett, J. and Borthwick, M. (2004) *Hydraulics in Civil and Environmental Engineering*. London: Spon Press. 644 pp.

Williams, A. G., Borthwick, M. F., Mtika, E., Ternan, J. L. and Sullivan, A. (2004) *The influence of changes in farming patterns on the runoff characteristics of the River Camel, Cornwall, UK*. Webb, B., Arnell, N.W., Onof, C., MacIntyre, N., Gurney, R. and Kirby, C. (Eds) BHS International Conference on "Hydrology: Science & Practice for the 21st Century". London, UK. 12-16 Jul. pp 526-533. (Paper presented by author).

Borthwick, M. F., Packham, I. S. and Rafiq, M. Y. (2008) Interactive visualization for evolutionary optimization of conceptual rainfall-streamflow models. *Journal of Computing in Civil Engineering*, 22(1): 40-49.
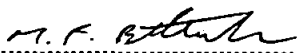
Rigden, T. and Borthwick, M. (2008) *Evolutionary computing approach to instantaneous unit hydrograph identification*. Rafiq, Y., de Wilde, P. and Borthwick, M. (Eds) Intelligent Computing in Engineering (ICE08) - 15th International Workshop of EG-ICE. Plymouth, UK. 2-4 Jul. pp 157-166.

Presentations and Conferences Attended:

BHS International Conference on "Hydrology: Science & Practice for the 21st Century". London, UK. 12-16 July 2004.

Intelligent Computing in Engineering (ICE08) - 15th International Workshop of EG-ICE. Plymouth, UK. 2-4 July 2008. (Co-Editor).

Word count of main body of thesis:

Signed _M. F. Borthwick_

Date _24/8/2010_

Chapter 1 Introduction

1.1 Context

The review of the literature presented herein indicates that a fractional calculus approach has not been used to model the rainfall-streamflow process at the storm event timescale. However, there is evidence from applications in the related areas of longer period time-series analysis, pollution-transport hydrology and systems analysis that the approach has potential for use in modelling the rainfall-streamflow transformation.

1.2 Aim and Objectives

The aim of the programme of study was to apply the fractional calculus to deterministic rainfall-streamflow modelling at the storm event timescale. The objectives of the work were:

- to develop a theory for the conceptual modelling of the rainfall-streamflow transformation using a fractional order systems approach;

- to fit the parameters to the derived models using observed rainfall-streamflow event data for a range of catchment scales;

- to assess the validity of the model forms and investigate the sources of uncertainty; and

- to identify potential areas for future development.

1.3 Contribution to knowledge

A programme of research was undertaken which involved the novel application of the fractional calculus technique to deterministic rainfall-streamflow modelling at the storm event timescale. A new theoretical framework was developed, tested and evaluated.

1.4 Thesis Structure

Chapter 2 presents a review of the research literature on the computational approaches to deterministic rainfall-streamflow modelling and identifies the limitations of existing methods and some of the key challenges for future research. This provides a context for the programme of work. The key features of the fractional calculus and the recent applications to science and engineering that are relevant to the problem of rainfall-streamflow modelling are reviewed in Chapter 3. The theory of fractional order hydrologic systems is developed in Chapter 4 and the new model equations are derived. The computational model testing methodology together with details of the catchments studied is presented in Chapter 5. Chapter 6 contains the model test results for a range of catchment scales and events. The validity of the theoretical models is discussed in the light of the test results in Chapter 7, and the conclusions and recommendations are summarised in Chapter 8.

Chapter 2 Review of Deterministic Computational Rainfall-Streamflow Modelling

2.1 Computational Rainfall-Streamflow Modelling

Computational modelling of the transformation of rainfall to streamflow is important for a number of civil engineering applications, for example flood and drought forecasting, flood defence design, and predicting the effects of climate and land use change on the hydrological response of catchments. The mathematical modelling of this transformation is not precise, however, because of the complex behaviour of the hydrologic processes, the heterogeneity of the flow pathways, and uncertainties in the measured data used. This is evident in the numerous models that have been developed (Beven 2000; Singh and Woolhiser 2002). The selection of the model by the user depends on the application, the physical and temporal scales of the catchment processes to be represented and the availability of data (in particular whether the catchment is gauged). These factors influence the "perceptual model" of the user (Beven 2000). The approximate formulation of the user's perceptual model as a mathematical model may be carried out in a number of different ways, and may be classified (Wheater 2002) as metric, conceptual, hybrid-metric-conceptual or physics-based. The model may also be categorised in terms of whether it represents the variation in physical processes across the area of the catchment explicitly (a distributed model) or uses spatially averaged processes (a lumped model). Furthermore it is possible to distinguish between stochastic and deterministic models where stochastic indicates that some of the model variables can take random values according to pre-defined probability distributions.

2.2 Metric Models for Runoff

2.2.1 Linear models

Metric (black box) models use a systems-based approach to transform inputs to outputs through fitting parameter values to a predefined mathematical transfer function using observations. They do not describe processes. The most commonly used in rainfall-

6

runoff modelling is the unit hydrograph (UH) technique developed from the work of Sherman (1932). It assumes that the system is a causal, linear, time-invariant process that represents the conservation of the volume of rainfall that becomes outflow (Dooge 1973). Causality refers to systems where the output only depends on inputs up to the present time, which is true for streamflow. The linearity assumption permits the use of the principles of superposition and proportionality in the solution of the system equations. In addition, the time-invariance assumption implies that the catchment characteristics are unchanged over the duration of the streamflow event so that the coefficients in the system equations are constants. These latter two assumptions are approximations for streamflow systems (Minshall 1960).

Typically, in the development of the perceptual UH model for effluent streams, the total streamflow hydrograph associated with a given rain storm event is assumed to be made up of *stormflow* (sometimes referred to as *runoff*) from the event rainfall plus *baseflow* draining from water stored in the catchment following infiltration from previous rainfall events. In order to satisfy volume conservation over storm event timescales, the *effective* rainfall that is net of "losses" due to infiltration, evapotranspiration, and surface ponding, needs to be derived from the observed rainfall. Similarly the stormflow needs to be derived from the observed streamflow hydrograph. Consequently, the assumed closed system of effective event rainfall transformed into stormflow may be approximated by the unit hydrograph analysis. This can be expressed mathematically as the stormflow (runoff), $r(t)$, at a time t due to an impulsive, effective rainfall input, $i(\tau)$, at an earlier time τ which is obtained through the convolution integral for a linear system on a continuous time scale (equation (2.1)):

$$r(t) = \int_0^t i(\tau)h(t-\tau)d\tau \qquad (2.1)$$

7

where $h(t)$ is the impulse response function or instantaneous unit hydrograph (IUH). The IUH is a theoretical construct that represents the runoff response to a given volume of effective rainfall falling instantaneously rather than in a finite duration.

The effect of the rainfall losses and the baseflow on the relationship of the observed (total) rainfall to the observed (total) streamflow is sufficiently non-linear to warrant modelling separately to the process of short term stream response (i.e. effective rainfall to stormflow) to a rainfall event. Consequently, over storm event timescales, the actual catchment system is open (non-conservative). In order to use the UH technique it is necessary, therefore, to apply a loss model to estimate the effective rainfall hyetograph, calculate the stormflow using the UH, and separately predict the baseflow so that the total streamflow can be obtained.

However, the identification of a definitive loss model remains an open problem, and a number of approaches have been proposed. Horton (1933) assumed that the generation of runoff takes place when the rainfall intensity exceeds the rate of infiltration into the soil. Field measurement of infiltration capacity at the plot scale typically shows a power law decay curve with time, tending towards a constant rate as the soil becomes saturated. Horton (1940) showed that this rainfall loss rate by infiltration can be modelled as an exponential decay curve. However, in practice, there is often substantial variation in infiltration rate across the catchment area making it difficult to identify uniquely and antecedent conditions influence the starting infiltration rate (Beven 2000). A simplification, at catchment scale, is to assume a constant loss rate such that the volume of effective rainfall equates to the runoff volume. This is the basis of the W-index and ϕ-index methods, where the former allows for the interception of water by vegetation and the retention of water in surface ponding (Cook 1946). However, these

indices are event specific, and, therefore, somewhat arbitrary for a given catchment. Correlation of rainfall-streamflow records with meteorological and catchment characteristics including antecedent moisture conditions has been used to develop catchment-specific predictor charts and equations for losses, including the antecedent precipitation index, *API* (Kohler and Linsley 1951), and the related catchment wetness index, *CWI* (Natural Environment Research Council 1975a). The *CWI* concept has been further utilised in the formulation of non-linear filters that separate losses from rainfall (Whitehead *et al.* 1979; Jakeman *et al.* 1990). In this approach the *CWI* represents catchment soil moisture content and is estimated by applying a first-order discrete time filter (i.e. low pass filter) to antecedent observed rainfall (similar to the calculation of the *API*). The rainfall can be adjusted to take account of evapotranspiration changes through empirical multipliers that depend on temperature. Young and Beven (1991; 1994) simplified the rainfall filter by replacing *CWI* by streamflow on the basis that streamflow results from a low pass filtered rainfall series. In this way the effective rainfall can be calculated as a function of the product of observed rainfall and time-lagged streamflow. The alternative approach of a water balance at the lumped catchment scale to calculate losses based on the conservation of volume allowing for evapotranspiration and soil moisture deficit has been successfully applied for daily data rather than at the hourly timescale (Natural Environment Research Council 1975a; Evans and Jakeman 1998). The UK Flood Studies Team (Natural Environment Research Council 1975a) developed a percentage runoff (*PR*) to represent conceptually the contributing area effect of a proportion of the whole catchment to stormflow. As with the *W*-index and ϕ-index methods, the *PR* is estimated such that the volume of effective rainfall equates to the volume of runoff. However, Webster and Ashfaq (2003) found that the predictor equations obtained from regression analysis of observed event runoff estimates with catchment characteristics were not robust. Consequently the

revitalised FSR/FEH rainfall-runoff method (Kjeldsen *et al.* 2005) in the UK uses a moisture balance approach but with the Probability Distributed Model (PDM) of Moore and Clarke (Moore and Clarke 1981; Moore 1985) to represent the assumed distribution of soil moisture storage capacity over the area of a catchment.

The separation of baseflow from the observed streamflow so that the stormflow can be identified and matched to effective rainfall (e.g. for estimation of *PR* or the ϕ-index) is also subject to considerable uncertainty (Tallaksen 1995). Horton (1933) defined the "master depletion curve" (master recession curve) as that part of the observed streamflow recession hydrograph that results from baseflow after the stormflow has ceased and noted that it can be modelled by Maillet's (1905) exponential decay equation which assumes that baseflow is proportional to the remaining storage volume for no recharge. This is equivalent to a linear reservoir model with no inflow. However, Clark *et al* (2009) have found that single linear reservoir modelling of baseflow recession becomes less accurate with increasing catchment size. The parameters of the exponential decay equation form of the master recession curve can be found by curve fitting to the recession limb of observed hydrographs. The point at which the master curve departs from the observed hydrograph denotes the end of stormflow and continuation of baseflow. Simpler methods for determining this end point include evaluating the change in curvature of the recession hydrograph or the use of filters Tallaksen (1995). However tracer experiments by Sklash and Farvolden (1979) have shown the significant contribution of groundwater stored in the catchment (prior to a storm event) to the whole streamflow hydrograph, emphasising that stormflow and baseflow are not independent processes and, consequently, the premise of baseflow separation is no longer appropriate.

A key aspect of the linear systems approach is to identify the unit hydrograph (i.e. the deconvolution problem). For gauged catchments (i.e. with records of observed rainfall and stormflow) it is possible to express equation (2.1) in discrete form as equation (2.2):

$$r_k = \sum_{j=1}^{k} i_j h_{k-j+1} \quad \text{for } k = 1, 2, 3 \ldots \tag{2.2}$$

where the rainfall, outflow and unit hydrograph are sampled at the same time interval. The resulting set of simultaneous linear equations is over-determined for the unknown ordinates of the unit hydrograph. The methods of solution that have been attempted (including substitution, iterative, least squares, linear and quadratic programming, and transformation techniques) with varying degrees of success are discussed in full by Dooge and O'Kane (2003). In general the unit hydrographs identified from the observed data tend to be sensitive to errors in the measurements, often magnifying the effects. Furthermore, some methods can produce conceptually unrealistic hydrographs with negative or oscillatory ordinates. Smoothing techniques have been developed (Boorman and Reed 1981) together with the use of catchment average hydrographs to account for the variation in hydrographs identified from different storms. However, the latter variation can be substantial for small catchments (Minshall 1960; Pilgrim 1976; Wang *et al.* 1981) and has been observed in larger areas also (Robinson *et al.* 1995; Goodrich *et al.* 1997). This observed behaviour is counter to the proportionality and superposition properties of the linearity assumption as well as the time-invariance underlying equation (2.1).

An alternative approach has been to prescribe the shape for a synthetic IUH and fit its parameters using observed data, for example the kinked triangle used in the Revitalised Flood Hydrograph (ReFH) model in the UK (Kjeldsen *et al.* 2005) and the triangle used in the Natural Resources Conservation Service (formerly the Soil Conservation Service,

SCS) in the USA (Natural Resources Conservation Service 2007). A particular merit of this approach is that it can lend itself to more parsimonious models (i.e. with fewer parameters than the unit hydrograph deconvolution). These parameters can be related to physical characteristics from gauged catchments by using regression techniques with a view to developing predictor equations for ungauged catchments. For example see the Flood Estimation Handbook (FEH) catchment descriptors (Institute of Hydrology 1999) and their use in the ReFH model in the UK (Kjeldsen *et al.* 2005). The development of conceptual model approaches that approximate the synthetic IUH are reviewed in section 2.3. In spite of the imperfections of the unit hydrograph technique such models require relatively little data and are often used in real-time flow forecasting but are restricted to the calibration range used in fitting the UH and for individual storm events (Young 2002).

2.2.2 Non-Linear models

Non-linear models of rainfall-runoff have been found to provide closer approximations to observed streamflow than linear models and can be used to relate the gross measured rainfall to the total streamflow, $q(t)$, without the need for separating out the net rainfall and runoff used in UH methods. Amorocho (1973) gives an overview of the initial development of non-linear black box models in terms of Volterra series which take the general form:

$$q(t) = \sum_{n=1}^{N} \int_0^t \cdots \int_0^t i_n(\tau_1,\ldots,\tau_n) \prod_{i=1}^{n} h(t - \tau_i) d\tau_i \qquad (2.3)$$

the first term of which is the linear convolution relationship of equation (2.1).

The difficulty with this approach is that the identification of the kernels of these models is generally ill-posed because of the size of the function space being searched, and the goodness of fit of the model to the data can be misleading (Napiorkowski and

12

Strupczewski 1984). A possible way forward would be to reduce the function set to that which generates a unique stable solution when there is uncertainty in the observed data (Napiorkowski and Strupczewski 1984). In a similar way to linear metric models, the general non-linear approach has no direct physical interpretation. However, Napiorkowski and Strupczewski (1979) have developed a conceptual model of a cascade of non linear reservoirs which can be approximated by the first two terms of the Volterra series.

2.3   Conceptual Models

Conceptual models use a simplified representation of actual processes at large scale but usually do not have physically based measurable parameters.

2.3.1   Cascades of Reservoirs

Typically the conceptual representation has taken the form of a virtual reservoir storage component through which an inflow is routed. The conservation of mass for a single reservoir can be expressed using the continuity equation assuming negligible acceleration (Chadwick *et al.* 2004):

$$i(t) - q(t) = \frac{dV}{dt} \qquad (2.4)$$

where $i(t)$ is the inflow rate at time t,

$q(t)$ is the outflow rate, and

V is the storage volume in the reservoir.

In order to solve for the outflow, a relationship between the outflow and the storage is required. This is often assumed to take the following form (Dooge and O'Kane 2003):

$$V = Kq^c \qquad (2.5)$$

where K and c are parameters specific to the reservoir's behaviour.

13

The simplest type of conceptual reservoir is the linear case proposed by Zoch (1934) where:

$$V = Kq \qquad (2.6)$$

and K is defined as the storage delay time of the reservoir ($K > 0$).

Nash (1957; 1960) applied the conceptual reservoir approach to represent the rainfall-runoff process for a catchment by routing a delta impulse function through a series (cascade) of n identical linear reservoirs (i.e. with identical K values) and applying the convolution integral (equation (2.1)). The resulting equation for the ordinates, $h(t)$, of the IUH is:

$$h(t) = \frac{1}{K(n-1)!}\left(\frac{t}{K}\right)^{n-1} e^{-t/K} \qquad (2.7)$$

For integer values of n, $\Gamma(n) = (n-1)!$ (Spanier and Oldham 1987) so equation (2.7) has the form of the 2-parameter gamma distribution (with n the equivalent shape parameter and nK the equivalent scale parameter):

$$h(t) = \frac{1}{K\Gamma(n)}\left(\frac{t}{K}\right)^{n-1} e^{-t/K} \qquad (2.8)$$

For application to a particular catchment the parameters n and K need to be fitted using observed rainfall-runoff data. In order to use the model for ungauged catchments Nash (1960) obtained 2 predictor equations based on multiple linear regression of catchment characteristics for a range of gauged catchments in the UK. Whilst the fit for the first equation was good (correlation coefficient of 0.9) that of the second was less reliable (coefficient of 0.5).

Numerous variants on the use of linear stores for representing the flow routing have been developed; for a comprehensive review see Singh (1988). Of particular note is the inclusion of linear channels that represent a time delay which a single linear reservoir does not model. Dooge (1959) introduced the linear channel and derived a general theory for the unit hydrograph that was based on a cascade of linear channels and reservoirs in series. Chow and Kulandaiswamy (1971) showed that the cascade models can be derived from a general ordinary linear differential equation relating storage and flow continuity. Valdes *et al* (1979) extended the reservoir cascade concept to the modelling of natural surface drainage channel networks – the geomorphological instantaneous unit hydrograph and Wang *et al* (1981) generalised the IUH to allow for time variation in the rainfall history (the instantaneous response function).

Dooge (1973) warns that strictly any proposed form of equation for the IUH can only be described as a "synthetic" unit hydrograph model if its parameters can be demonstrated to be related to physical characteristics of a catchment. This is particularly important when the model is to be applied to the prediction of streamflows for ungauged catchments. Kachroo and Liang (1992) and Dooge and O'Kane (2003) present reviews of a number of forms of synthetic IUH. Jeng and Coon (2003) have identified improvements that could be made to Nash's original IUH model in terms of the validity of the assumed initial condition of zero inflow and the use of spatially distributed rainfall inputs by means of sub-catchment IUH's. Furthermore Singh (1964; 1988) has derived other UH forms using classical methods which could also be investigated from a fractional calculus viewpoint, and could be extended to the case of a cascade of equal non linear reservoirs (Diskin *et al.* 1984; Ding 2005; Dooge 2005).

2.4 Physics-Based Models

Physics-based models have developed from the blueprint of Freeze and Harlan (1969), for example the "SHE" model (Abbott *et al.* 1986a; Abbott *et al.* 1986b). They are based on the coupled partial differential equations representing the conservation of mass and momentum for free surface overland flow and the sub-surface saturated and unsaturated flow processes solved numerically on a grid. Through the use of physics-based theoretical and semi-empirical equations derived from laboratory scale tests it is possible to make use of measurable parameters, which makes this approach attractive for scenario testing, for example land use change predictions (Williams *et al.* 2004). However, the "upscaling" to represent the flow processes at the much larger catchment grid scale assumes without proof that the grid point parameters are an averaged (lumped) representation of the sub-grid heterogeneity of the catchment (e.g. topography, soil, vegetation, etc); and that the process scales are the same (Beven 1989; Bloschl and Sivapalan 1995). The number of parameters required to solve the different process equations at each grid point is substantial and the values are likely to vary over the time of the rainfall events being simulated. This leads to problems in the calibration of the model given the limited quantity and resolution of observed data for a given catchment (Beven 2006a). Yawson *et al* (2005) have demonstrated the utility of systems-based models over higher complexity models particularly where data is scarce. Furthermore, there are issues concerning the use of different time steps for the stable solution of the coupled overland and subsurface flow equations; the non-linearity introduced by the modelling of soil moisture characteristics; and the difficulty in representing preferential flow pathways (Loague and VanderKwaak 2004).

In an attempt to overcome the issues of these point scale equations for distributed physics-based models is the formulation of the conservation law integral equations for

control volumes at the megascale of representative elementary watersheds (REWs) (Reggiani *et al.* 1998; 1999; Reggiani and Rientjes 2005). The subdivision of a catchment into REWs (i.e. subcatchments) is based primarily on topography. For each REW the conservation balance equations for each phase of flow in each internal zone (overland, channel, unsaturated, saturated, etc) are derived. This results in an unknown flux term for each equation which represents the area-integrated rate of exchange of the mass, momentum or energy between each phase, zone and REW. In order to solve these equations it is necessary to propose closure relations that express the unknown fluxes over the control surface of the REW in terms of either physically measureable quantities or a conceptual function of the internal states (which requires parameter fitting by approximate methods). As yet there is no method for measuring the boundary fluxes at REW scale nor an agreed functional relationship (Beven 2006b).

2.5 Data-Driven and Hybrid-Metric-Conceptual Models

A generalisation of the metric approach is to apply data-driven models such as artificial neural networks and genetic programming where both the model structure and parameters are unspecified in advance and a heuristic computational search technique is used to fit a model to the observed data.

2.5.1 Data-Based Mechanistic Modelling

Young and Beven (1994) advocate a top-down approach particularly where the lack of data does not support model complexity – the data-based mechanistic model. The important feature of this approach over a pure systems identification technique is that the user proposes a model structure in response to the outcome of initial tests using catchment data. In this way the model form becomes catchment-specific (Sivapalan *et al.* 2003). This does not restrict the user to a specific model form, although some

knowledge of viable mathematical forms is necessary. Young (2003) has successfully developed a technique for identifying linear models for catchments on the basis of 2 transfer functions: one to represent fast response (runoff); the other to represent slow response (baseflow) and incorporates a power law rainfall loss model. Lees (2000) has demonstrated how the technique can be used with nonlinear models.

2.5.2 Artificial Neural Networks

Artificial neural networks (ANNs) are based on conceptualisations of the learning behaviour of the human brain. They comprise several simple computational units ("neurons") that have weighted connections with other neurons to form a network. Observed rainfall data is passed to a set of input units, which, depending on the weightings, pass a signal to connected units, and so on through the network until an output is produced. This is compared with observed streamflow data and the weights of the connections are iteratively adjusted until the error between the network output and the observation is minimised (i.e. the network is "trained"). Hall and Minns (1993; Minns and Hall 1996) were the first to apply ANNs to rainfall-runoff modelling. In this form ANNs are non-linear black box models although some work has been done to attempt to derive physically-interpretable process relationships from the network (Sudheer 2005). Jain and Srinivasulu (2004; 2006) have developed "grey-box models" by coupling an ANN with a deterministic and a conceptual model. Napiorkowski and Piotrowski (2005) compared an ANN with a non-linear model based on the Volterra series and found similar performance. In general, ANNs have been observed to forecast well provided the input data is consistent with the training set used (Schütze et al. 2005; Shrestha et al. 2005), but are subject to the risk of over-fitting during the training (calibration) with a consequential loss of predictive performance when used with new input data (Gaume and Gosset 2003).

2.5.3 Genetic Programming

Symbolic regression using Genetic Programming (GP) (Koza 1992) is an automated search of a user defined set of mathematical functions and sets of arguments (i.e. constants and the rainfall data for a catchment). It is guided by an evolutionary computation technique in which an initial population of randomly selected models (combinations of functions and arguments) is tested for model fitness (by comparing predictions with observed streamflow) and a new population of models is evolved by applying reproduction, crossover and mutation operations on selected members of the parent population. The selection is made using a probabilistic rule weighted according to fitness. The process is repeated with a view to evolving fitter populations. Whigham and Crapper (1997) were one of the first to apply GP to rainfall-streamflow modelling. Davidson *et al* (2003) used a GP constrained by user-defined rules to allow polynomial expressions to be generated in order to control the growth of the model code (bloat) and to improve parameter fitting in each model of the population. Dorado *et al* (2002) constrained the GP function and argument sets to search for unit hydrographs for rainfall-runoff modelling in urban catchments. Babovic and Keijzer (2002) showed that, particularly for flow forecasting, the identification of GP-based models is improved through the use of domain knowledge (i.e. coupling with conceptual model output). Similarly, Jayawardena *et al* (2006) found that the GP approach was not as accurate as a conceptual model for smaller catchments. Minns (2000) has compared the performance of an ANN and GP and found that the ANN performed better but gave no insight to the processes unlike the GP, although some GP runs produced equations with no recognizable interpretation in terms of physical processes.

2.6 Rainfall-Streamflow Model Identification

2.6.1 Parameter Calibration

An essential aspect of computational rainfall-streamflow modelling is calibration of the parameters for the model to fit a set of field observed data. However, the multi-dimensional nature of many models (particularly conceptual types), parameter interaction and sensitivity often results in non-smooth, multimodal response surfaces leading to problems in the attempt to identify the model uniquely (Gupta *et al.* 2003b). In many instances this behaviour is due to over-parameterisation (Kirchner 2006).

Duan *et al* (1992) identified the existence of a number of regions of attraction in the parameter space for a typical conceptual model where the calibration algorithm can converge to a solution. These regions were found to contain numerous minor local optima. The response surfaces tended to be discontinuous and non-convex with areas of parameter interaction. These types of spaces make the search for an optimum set of parameter values by traditional gradient-based methods difficult or impossible. Consequently, emphasis has been placed on the use of evolutionary search techniques, such as genetic algorithms (GA). GA search operates in a similar manner to Darwinian natural selection (Holland 1975; Goldberg 1989). In the algorithm an initial population of randomly selected sets of parameter values is tested for fitness (by comparing model predictions using each set of parameters with observed streamflow) and a new population of parameter sets is evolved by applying reproduction, crossover and mutation operations on selected members of the parent population. The selection is made using a probabilistic rule weighted according to fitness. The process is repeated with a view to evolving fitter populations. Goldberg and Kuo (1987) were the first to apply the GA to a flow problem in civil engineering, by optimization of a pipeline. Wang (1991) first used a genetic algorithm-based automatic calibration of multi-

parameter conceptual rainfall-runoff models. This application has been further tested by a number of researchers (Liong *et al.* 1995; Franchini 1996; Wang 1997; Yang and Douglas 1998; Ndiritu and Daniell 1999).

Similarly, Dong (2008) achieved improved fitting of the Nash cascade IUH model using the GA for an observed flood hydrograph on the Qing river in China. Furthermore, Rigden and Borthwick (2008) studied a Genetic Algorithm (GA) used to identify the parameters of 7 conceptual IUH model forms. The GA outperformed the traditional method of moments (Dooge and O'Kane 2003) for IUH model fitting, and was shown to be better suited to parameter identification for observed hourly rainfall-runoff data from 4 different sized UK catchments.

2.6.2 Uncertainty Measures

Although techniques have been developed for automatic calibration of models (Duan *et al.* 2003), there is evidence to suggest that there are different sets of parameter values with similarly acceptable fitness, which Beven (1993) defines as "equifinality" (Beven 2006a). Furthermore, the equifinality concept can be extended to multiple behavioural models (acceptable predictions) rather than just different parameter sets for the same model structure. In this way the problem is one of mapping the landscape space to a model space containing several behavioural models (Beven 2002) and uncertainty is manifest in the model structure, parameters and data. For example, Uhlenbrook *et al* (1999) showed that even conceptually unrealistic sets of parameter values could produce good predictions.

In order to attempt to investigate the equifinality problem a number of methods of quantifying the uncertainty have been proposed. Kuczera (1983) used a Bayesian

approach to estimate the posterior probability distribution of the model parameters, expressing the uncertainty using a statistical likelihood function based upon an assumed behaviour of the measurement errors. This technique was later developed into the "Metropolis algorithm" using a random walk (Kuczera and Parent 1998). Beven and Binley (1992) introduced the Generalised Likelihood Uncertainty Estimation (GLUE) technique where the user pre-selects a likelihood objective function (to allow for the combined effect of structural, parameter and input errors) for evaluating models the parameter values for which are sampled with a Monte Carlo simulation. Non-viable models can be automatically rejected and the likelihood values of the remaining models can be rescaled before ranking to generate the cumulative distribution of output which can be interpreted in terms of the uncertainty (Beven and Freer 2001; Montanari 2005). In the light of criticism of the potentially arbitrary choice of likelihood in the GLUE method Gupta *et al* (1998) have noted that it may not be possible to propose a statistically correct likelihood function. Additionally, the statistical properties of the model prediction errors can depend on the catchment or the flow processes and may be both spatially and temporally correlated (Engeland and Gottschalk 2002). Furthermore a Bayesian Total Error Analysis (BATEA) framework (Kavetski *et al.* 2002) has been developed to attempt to account for all sources of error as well as the error model structure.

2.6.3 Objective Functions

The fitness of a given set of parameter values for a model is defined by one or more objective functions which provide a numerical measure of the level of agreements between model predictions and observed streamflow. A number of reviews have been undertaken of the use of common single objective functions in rainfall-streamflow model calibration (Diskin and Simon 1977; Cooper *et al.* 1997; Legates and McCabe

1999). In many cases the simple least squares (or root mean square error, RMSE) or the Nash-Sutcliffe efficiency, NSE (a normalized version of the RMSE) has been used, but these tend to emphasize the fitting of peak flows.

Jakeman and Hornberger (1993) have indicated that the use of single measures of fitness for calibration of models with just rainfall and streamflow data enables up to 5 or 6 parameters to be identified. Consequently to avoid the proliferation of behavioural models, multi-objective calibration to reflect the application requirements rather than single measures of fitness has been employed which extracts more information from the observed data and thereby constrains the calibration. Yapo *et al* (1998) developed a multi-objective complex evolution technique (MOCOM-UA) derived from the shuffled complex evolution (SCE-UA) method (Duan *et al.* 1992) which uses Pareto ranking and has been tested using 2 objective functions on the Sacramento soil moisture accounting model with observed data; and extended to 3 objectives (Gupta *et al.* 1998). Madsen (2000) used 4 objectives to represent the runoff volume, hydrograph shape, peak flows and low flows and then computed an overall fitness measure using the Euclidean distance incorporating user-defined transformation constants for each component objective function. This was then optimized using the SCE-UA. Gupta *et al* (2003a) followed Boyle *et al* (2000) and partitioned the streamflow hydrograph into driven and non-driven components and used the root mean square error for each component as the objectives in the MOCOM-UA technique, but found that the endpoints of the Pareto optimal parameter sets identified were not well defined. Consequently, Vrugt *et al* (2003) developed the multi-objective shuffled complex evolution Metropolis (MOSCEM-UA) algorithm based on the SCE-UA but using the Metropolis Hastings sampling strategy in place of the downhill simplex to avoid convergence on a single optimum. This permits the estimation of the most likely parameter set based on Pareto

dominance and the underlying posterior probability distribution to attempt to quantify uncertainty. However, the use of multi-objective calibration involves large numbers of model runs with the associated computational overhead. With the exception of selecting at least one objective function which takes account of the error in the measurement data (for example Sorooshian and Dracup (1980) have introduced the heteroscedastic maximum likelihood estimator (HMLE) to account for non-constant variance error in the observed streamflow data) there does not appear to be a consensus on which group of objective functions should be used in multi-criteria calibration.

An alternative approach has been to measure the correspondence between predicted and observed hydrograph peaks (using the RMSE) coupled with that of the hydrograph slopes, using a simple weighted average. This permits a comparison of both the shape and timing of the hydrographs with a relatively small computational overhead, overcoming the limitations of the single RMSE measure. This approach has been successfully applied to conceptual models (de Vos and Rientjes 2007; Borthwick *et al.* 2008).

Alongside the development of automatic calibration tools has been work on incorporating the expertise of the hydrological modeller through user interaction. Visualization helps the modeller to observe the complexity of the parameter and objective function spaces and assists in the process of selecting a set of parameter values for the particular watershed application. Wagener *et al* (2001) have developed a toolkit for identifying both the model structure and calibration of the parameters which uses Monte Carlo sampling of the parameter space over the time scale of the rainfall-streamflow process being modelled using low order (parsimonious) conceptual or metric models and provides the user with a selection of visualization techniques for the

parameter and objective function spaces. Borthwick *et al* (2008) have demonstrated the use of clustering and visualization, together with interactivity to exploit the expertise of the user for the calibration of a conceptual rainfall-streamflow model using the interactive visualization system developed by Packham *et al* (2005).

2.7 Summary

The multitude of computational modelling forms highlights the difficulty in representing the rainfall-streamflow transformation for natural catchments in a consistent manner. For a model to be useable it needs to be based on some agreed observed (or assumed) behaviour that can be represented in the form of parsimonious equations that can be applied to recorded rainfall data, such as the unit hydrograph approach. One of the simple IUH models is the 2-parameter gamma function developed by Nash (1957) given in equation (2.7). In the derivation Nash suggests that the resulting equation can be used for a fractional number of reservoirs (equation (2.8)) in spite of using integer order integrals in the proof. Interestingly, using non-integer values of n enables flexibility in fitting the parameter values (and hence fitting the UH model to the catchment data). This has been selected to be a suitable starting point for applying a fractional calculus approach to conceptual rainfall-runoff modelling.

Chapter 3 Review of Fractional Calculus Relevant to Hydrology

3.1 Typical Applications of the Fractional Calculus

Fractional calculus is concerned with derivatives and integrals of arbitrary order (i.e. including non-integer order). Although it was first conceived in correspondence between L'Hôpital and Liebniz in 1695 and has been developed in the mathematics literature since, its broader application to science and engineering problems, including hydrological modelling, has really only been undertaken in the last 40 years (see Oldham and Spanier (1974) for a review of the range of early applications). In recent years there have been advances in the solution techniques for fractional differential and integral equations suited to the mathematical modelling of the behaviour of systems and materials that exhibit memory, many of which occur in science and engineering (Podlubny 1999). Debnath (2003b; 2003a) reviews a number of recent applications in science and engineering, including fractional order dynamical systems control, fractional order impedance in electrical circuits, viscoelasticity, electrostatics, electrochemistry, the behaviour of neurons, and fluid mechanics. Oustaloup *et al* (1999) have developed the CRONE controller which uses fractional order integrators and differentiators as more efficient alternatives to Proportional-Integral-Derivative (PID) controllers for the control of fractional order dynamical systems. In a related aspect of the development of the CRONE controller, Oustaloup and Sabatier (1995) proposed an electrical analogue model that is equivalent to a fractional order dynamical system for the damping effect of water flowing into a porous flood embankment.

3.2 Applications of Fractional Calculus Relevant to Rainfall-Streamflow Modelling

3.2.1 Stochastic Analysis of Hydrologic Time Series Exhibiting $1/f^\beta$ Noise

The existence of long-range statistical dependency (persistence or long memory) in hydrologic time series was first identified by Hurst (1951) in assessing the design

28

capacity of reservoirs using annual flow records for the River Nile, and has since been observed in a wide variety of other geophysical time series (Koutsoyiannis 2002; Mandelbrot 2002). It is commonly referred to as the Hurst phenomenon. The examination of very long records of geophysical data such as rainfall, river flow, wind power, and temperature, when averaged over relatively long durations (e.g. annually) for several locations shows periods of persistent positive or negative departures from the mean. For stationary time series this behaviour appears to indicate a very long memory process (longer than the timescale of easily identifiable causative physical processes that would give rise to short-memory effects). Such a series can be classified as a type of $1/f^\beta$ noise whose power spectral density, $S(f)$, follows a power law relationship proportional to $1/f^\beta$ where f is frequency. For a series of statistically independent variables $B = 0$ and is defined as a white noise process, where white noise is the derivative of classical Brownian motion (Bras and Rodriguez-Iturbe 1985). Series exhibiting long-memory are characterised by the range $0 < B < 1$. Mandelbrot and Van Ness (1968) were the first to apply a fractional Brownian motion process to simulate the long term memory effect in hydrological time series. This was obtained from the moving average of a past white noise and is represented by the fractional derivative of classical Brownian motion (i.e. the fractional derivative arises because of the convolution operation of the noise with a power law function (Lovejoy and Schertzer 2006)). Hosking (1981) extended the application by fractional differencing of discrete-time white noise to generate the fractional autoregressive integrated moving-average process (FARIMA) which has the flexibility to represent both long term and short term memory effects. It should be noted that the use of these fractional Brownian motion (and the associated fractional Gaussian noise) models theoretically assumes an infinite memory process, which can only be approximated computationally. In view of the lack of a physically-based theory (Klemes 1974) to explain the long-memory behaviour then

29

these models can be classed as conceptual. Indeed other model forms have been proposed, for example the use of lag-one autoregressive random processes that are subject to random fluctuations of the mean over multiple time scales to simulate irregular climate changes (Koutsoyiannis 2002).

A further feature of hydrologic time series exhibiting $1/f^{\beta}$ noise is that the same power law relationship is often observed over a wide range of time scales i.e. the exponent B is scale invariant indicating that the series is isotropically scaling (or fractal). Studies of the precipitation input to streamflow generation, however, have shown that rain fields display intermittent bursts and are better represented by multifractals - a generalisation of fractals requiring a spectrum of an infinite number of dimensions to represent the anisotropic scaling behaviour (Schertzer and Lovejoy 1987). Similarly multiscaling has also been observed for river channel networks and topography, as reviewed by Rodriguez-Iturbe and Rinaldo (1997). Such multifractals may be represented by multiplicative cascade processes involving a reduced number of parameters. In a similar manner to the generation of fractional Brownian motion, the multifractal process can be simulated by means of fractional integration, this time of a cascade process (the fractionally integrated flux, FIF). A review of the development and application of this technique for multifractal modelling in geophysical data has been made by Lovejoy and Schertzer (2006). Tessier et al. (1996) and Pandey et al. (1998) extended this approach to the time series modelling of daily streamflow. They showed that the low frequency (greater than 1 week) region of the series could be simulated by a fractional integration of the FIF with parameters derived from the observed daily rainfall series. The fractional integration arises from a causal power law convolution process (i.e. a linear transfer function for the time series transformation of rainfall to streamflow). Furthermore detrended fluctuation analysis of hourly rainfall and streamflow series

indicated that short-term fluctuations in streamflow were smoother than the corresponding rainfall because of damping by the land surface and soil storage (Matsoukas *et al.* 2000). This damping behaviour is increasingly evident at the storm event timescale. Field measurements of the travel times of conservative tracers that occur naturally in rain (e.g. chlorides) show a long-memory effect indicating that "old" (pre-storm event) water released from prior storage in the catchment dominates the streamflow response to a rain storm (Kirchner *et al.* 2000), i.e. paradoxically water appears to be stored over a long time period but is discharged in a relatively short period (Kirchner 2003).

3.2.2 Cavallini's Proposed Fractional Instantaneous Unit Hydrograph

Cavallini (2002), following successful applications of fractional calculus to convolution equations in solid earth geophysics, has suggested as an ansatz (i.e. without proof) that a possible form of synthetic instantaneous unit hydrograph (IUH), $h(t)$, could be obtained from a fractional differential equation. Using the classical IUH for a cascade of 2 unequal linear reservoirs from Singh (1988) where

$$h(t) = \frac{k_1 k_2}{k_2 - k_1}\left(e^{k_2 t} - e^{k_1 t}\right)$$

(3.1)

Cavallini suggests (without derivation) that a "fractional IUH" should have a similar form, namely

$$h(t) = \frac{k_1 k_2}{k_2 - k_1}\left[\exp_{v, k_2}(t) - \exp_{v, k_1}(t)\right]$$

(3.2)

where k_1 and k_2 are the storage delay times of the 2 reservoirs, respectively; t is time, and $\exp_{v, k}(t)$ is the Miller-Ross function (Miller and Ross 1993) defined as

$$\exp_{v, k}(t) = t^{v-1} E_{v, v}\left(k t^v\right)$$

(3.3)

and $E_{\alpha, \beta}(x)$ is the 2-parameter Mittag-Leffler function (refer to section 4.2.5 for the definition).

However, Cavallini (2006) remarks that that expressing the IUH as the difference of two solutions of first-order fractional differential equations may not always produce a positive definite result, and has not developed the IUH further.

3.2.3 Anomalous Diffusion Modelling in Subsurface Hydrology

Anomalous diffusion (fractional Brownian motion) is observed for certain natural diffusion processes that do not appear to obey the classical Fick's law where the rate of spatial spreading of the diffusing particles is not proportional to $t^{\frac{1}{2}}$ where t is time (i.e. the spread is asymmetric). The mathematical modelling of anomalous diffusion using fractional differential equations together with comparisons with observed pollution transport processes has been undertaken by several researchers for pollution transport in groundwater flow (Baumann *et al.* 2000; Caputo 2000; Benson *et al.* 2001; Baeumer *et al.* 2005; Chang *et al.* 2005; Zhang *et al.* 2005). The fractional advection diffusion equation (FADE) has been applied to urban storm water pollution modelling (Deng *et al.* 2005) and for pollution modelling in rivers (Kim and Kavvas 2006). Furthermore the FADE has been used to model solute transport in soils by Pachepsky et al (2000) who have gone on to propose a fractional form of Richards equation for the modelling of unsaturated flow in soil (Pachepsky *et al.* 2003). A FADE approach has been taken by Scher et al (2002) to model the travel times for tracer movement from rainfall on a catchment hill slope into a river, as a development of the work of Kirchner et al (2001) who applied a simple conceptual model of classical advection-diffusion to produce an approximate gamma-type distribution of travel times to match those observed in the Plynlimon experimental catchment data set.

3.3 Summary

The fractional calculus has not been applied to rainfall-streamflow modelling at the storm event timescale. There is evidence that long memory processes exist in hydrologic systems and, given that the fractional order systems approach has been applied to the related field of hydrogeological pollution transport modelling, then there is the potential for a fractional order theory to be developed for rainfall-streamflow modelling, including the problem of identification of the resulting system equations.

Chapter 4 A Fractional Order Hydrologic Systems Theory

4.1 Methodology

A new theory that generalises that for the classical unit hydrograph technique for the rainfall-runoff transformation is developed in the following. The theory is based upon a fractional order linear deterministic systems approach and is taken to apply to the rainfall-streamflow transformation (i.e. including baseflow).

A comprehensive treatment of the fractional calculus can be found in the standard reference works, for example Miller and Ross (1993), Samko *et al* (1993), Carpinteri and Mainardi (1997), Podlubny (1999), and Kilbas *et al* (2006). The fundamental principles and key results necessary for the derivation of the theoretical equations in this thesis are presented in section 4.2. It should be noted that there are several forms of fractional integrals and derivatives detailed in the foregoing references; however, those adopted in this work have been selected on the basis of physically based initial conditions and applications made in other branches of engineering science.

The solution of ordinary linear differential equations (of arbitrary order) using Laplace transforms is adopted following common practice (Podlubny 1999). Full details of the theory of Laplace transforms may be found in Doetsch (1974).

Dooge and O'Kane (2003) and Singh (1988) provide introductions to the application of classical integer-order linear systems theory to rainfall-runoff modelling. The essential results for the general unit hydrograph and general storage equations are presented in section 4.3. This sets the context for the development of the fractional order hydrologic theory which is proposed in section 4.4.

4.2   Essential Concepts from the Fractional Calculus

4.2.1   The Riemann-Liouville Fractional Integral

Fractional calculus is concerned with derivatives and integrals of arbitrary order (i.e. including non-integer order). In this way it generalises the integer (n) order n-fold integrals and n-fold derivatives. For example equation (4.1) is the familiar formula (Samko $et\ al.$ 1993) for the n-fold integral (usually attributed to Cauchy) of a function, f, of a variable t.

$$\int_a^t dt \int_a^t dt \dots \int_a^t f(t)dt = \frac{1}{(n-1)!} \int_a^t (t-\tau)^{n-1} f(\tau)d\tau \tag{4.1}$$

τ is the dummy variable of integration. Since the gamma function $\Gamma(n)=(n-1)!$ (Spanier and Oldham 1987) then this equation can be generalised for non-integer values of n to define ${}_aD_t^{-\alpha}$ the fractional integral of order α where $\alpha > 0$. This can be expressed as a left-sided integral for $t > a$:

$$_aD_t^{-\alpha}f(t) := \frac{1}{\Gamma(\alpha)} \int_a^t \frac{f(\tau)}{(t-\tau)^{1-\alpha}} d\tau \tag{4.2}$$

and as a right-sided integral for $t < b$:

$$_tD_b^{-\alpha}f(t) := \frac{1}{\Gamma(\alpha)} \int_t^b \frac{f(\tau)}{(\tau-t)^{1-\alpha}} d\tau \tag{4.3}$$

Equations (4.2) and (4.3) are the Riemann-Liouville fractional integrals. Where t is time only the left-sided derivative is of relevance to this work since this represents a causal system, typical of hydrologic processes. It should be noted that the symbol I or J is sometimes used for fractional integrals as distinct from D for derivative. The operator D-notation is used in this work, following Podlubny (1999), to indicate a "differintegral" where ${}_aD_t^{-\alpha}$ denotes the fractional integral of order α for $t > a$, and ${}_aD_t^{\alpha}$ denotes the fractional derivative of order α for $t > a$.

4.2.2 The Riemann-Liouville Fractional Derivative

The Riemann-Liouville fractional derivative can be obtained by finding the inverse of the fractional integral. Denoting the derivative of any integer order as

$D^n f(t) = \dfrac{d}{dt^n} f(t) = f^{(n)}(t)$ then the left inverse of the integral holds according to the following composition rule

$$_aD_t^n {}_aD_t^{-n} f(t) = f(t) \tag{4.4}$$

However, using equation (4.2) with $\alpha = n$ the right inverse does not hold (Gorenflo and Mainardi 2000) since

$$_aD_t^{-n} {}_aD_t^n f(t) = {}_aD_t^{-n} f^{(n)}(t) = \frac{1}{(n-1)!} \int_a^t \frac{f^{(n)}(\tau)}{(t-\tau)^{1-n}} d\tau$$

$$_aD_t^{-n} {}_aD_t^n f(t) = f(t) - \sum_{k=0}^{n-1} f^{(k)}(a+) \frac{(t-a)^k}{k!} \tag{4.5}$$

Consequently, the Riemann-Liouville fractional derivative of order α is defined as the left inverse of the α-order fractional integral by incorporating a positive integer m such that $m-1 < \alpha \le m$ as follows:

$$_aD_t^\alpha f(t) := {}_aD_t^m {}_aD_t^{-(m-\alpha)} f(t) \tag{4.6}$$

and hence

$$_aD_t^\alpha f(t) := \frac{d^m}{dt^m} \left[\frac{1}{\Gamma(m-\alpha)} \int_a^t \frac{f(\tau)}{(t-\tau)^{\alpha-m+1}} d\tau \right] \tag{4.7}$$

The integral of the product of the 2 functions in equation (4.7) where one function is shifted by $t - \tau$ and the lower limit, $a = 0$, is a Laplace convolution integral (Doetsch 1974). For example, for $m = 1$, it can be written

$$_0D_t^\alpha f(t) := \frac{d}{dt} \left[f(t) * \frac{t^{-\alpha}}{\Gamma(1-\alpha)} \right] \tag{4.8}$$

38

where $t > 0$ (i.e. causal). The presence of the convolution integral highlights the non-local property of the fractional derivative operator which, unlike an integer order derivative, depends on the "history" of the function between the lower limit, a, and t. Hilfer (2008) shows that for causal physical systems non-locality in time represents the non-equilibrium (or non-conservative) phenomena of hysteresis, which is observable, but non-locality in space is difficult to prove as it implies action at a distance.

4.2.3 The Caputo Fractional Derivative

Using the Riemann-Liouville fractional derivative enables fractional differential equations to be defined, for example the simple α-order initial value problem of equation (4.9) where y is a function of t, with $m - 1 < \alpha \leq m$ and m a positive integer.

$$_0D_t^\alpha y(t) = f[t, y(t)] \tag{4.9}$$

The unilateral (one-sided) Laplace transform is commonly used in the solution of such fractional order initial value problems, and which is defined (Doetsch 1974) for $t \geq 0$ as the image function, $Y(s)$ in terms of a complex variable, s, of the original function, $y(t)$, by

$$L\{y(t)\} = Y(s) = \int_0^\infty y(t) e^{-st} dt \tag{4.10}$$

For convergence $|y(t)| \leq Me^\alpha$ for $Re(s) > c$ (for M and c constants). Unless otherwise stated the term Laplace transform in this work will be taken to mean the unilateral form.

The Laplace transform for the Riemann-Liouville derivative in equation (4.9) takes the following form (Podlubny 1999).

$$L\{_0D_t^\alpha y(t)\} = s^\alpha Y(s) - \sum_{k=0}^{m-1} s^k {}_0D_t^{\alpha-k-1} y(0^+) \tag{4.11}$$

From the right hand side of equation (4.11), for a unique solution of the differential equation, m initial conditions are required of the form:

$$\left.\frac{d^{\alpha-k-1}y(t)}{dt^{\alpha-k-1}}\right|_{t=0^+} = b_k, \quad k=0, 1, ..., m-1 \tag{4.12}$$

However, it is difficult to identify physically meaningful fractional order derivatives necessary for the initial conditions of (4.12). Consequently, Caputo (1967) derived the following fractional derivative.

$$_0^C D_t^\alpha y(t) :=\, _0D_t^\alpha \left[y(t) - \sum_{k=0}^{m-1} \frac{t^k}{k!} y^{(k)}(0^+) \right] = f[t, y(t)] \tag{4.13}$$

where $^C D^\alpha$ denotes the Caputo fractional derivative of order α to distinguish it from D^α the Riemann-Liouville derivative. It should be noted that the symbol D_*^α is sometimes used for the Caputo fractional derivative; however the $^C D^\alpha$ form is used in this work to facilitate the inclusion of the terminals (limits). Taking the Laplace transform of the Caputo derivative (Podlubny 1999) produces:

$$L\{_0^C D_t^\alpha y(t)\} = s^\alpha Y(s) - \sum_{k=0}^{m-1} s^{\alpha-k-1} y^{(k)}(0^+) \tag{4.14}$$

which shows that the Caputo derivative requires m initial conditions in terms of the usual integer order derivatives which are more meaningful in physical problems. From equation (4.13), the Caputo derivative can be expressed as follows.

$$_a^C D_t^\alpha f(t) :=\, _aD_t^{-(m-\alpha)} {}_aD_t^m f(t) \tag{4.15}$$

The Caputo has a further property that is shared with the integer order derivative, in that the derivative of a constant, C is zero, i.e.

$$_a^C D_t^\alpha C = 0 \tag{4.16}$$

This is unlike the Riemann-Liouville derivative, where it can be shown (Podlubny 1999) that for a finite value of the lower limit, a:

$$_aD_t^\alpha C = \frac{Ct^{-\alpha}}{\Gamma(1-\alpha)} \tag{4.17}$$

Further properties of the Caputo derivative may be found, for example, in Li and Deng (2007).

4.2.4   Sequential Fractional Derivatives

Since integer (n) order differentiation comprises a sequence of first order differentiations then a sequential fractional derivative can be defined (Miller and Ross 1993) as:

$$D^\sigma f(t) = \underbrace{D^\alpha D^\alpha \dots D^\alpha}_{n} f(t) \tag{4.18}$$

where $\sigma = n\alpha$. Alternatively the overall order of the derivative σ can be composed of sequences of unequal order derivatives of the form:

$$D^\sigma f(t) = D^{\alpha_1} D^{\alpha_2} \dots D^{\alpha_n} f(t) \tag{4.19}$$

where $\sigma = \alpha_1 + \alpha_2 + \dots + \alpha_n$. The operator D^σ can represent the Riemann-Liouville, Caputo or other definition of fractional derivative.

4.2.5   Ordinary Linear Fractional Differential Equations

In many applications of fractional differential equations to physical problems the unilateral Laplace transform technique has used been to obtain solutions to initial value problems. As a consequence the Laplace transforms have been found and tabulated for a number of the forms of ordinary linear fractional differential equations that arise in practice (Kilbas *et al.* 2006). In order to investigate the influence of the order of the derivative on the behaviour of such differential equations the simple case of the following homogeneous ordinary linear fractional differential equation expressed in terms of the Caputo derivative is considered (Gorenflo and Mainardi 1996).

$$_0^C D_t^\alpha y(t) + \lambda y(t) = 0 \tag{4.20}$$

with $\lambda > 0$ and initial conditions $y^{(k)}(0) = b_k$, $k = 0, 1, ..., m\text{-}1$ for $m - 1 < \alpha \leq m$ where m is a positive integer.

Taking Laplace transforms and using the result from equation (4.14) gives

$$s^\alpha Y(s) - \sum_{k=0}^{m-1} s^{\alpha-k-1} y^{(k)}(0^+) + \lambda Y(s) = 0$$

so

$$Y(s) = \frac{\sum_{k=0}^{m-1} s^{\alpha-k-1} y^{(k)}(0^+)}{s^\alpha + \lambda} \qquad (4.21)$$

The inverse Laplace transform of equation (4.21) requires the standard result (Podlubny 1999):

$$L\left[t^{\beta-1} E_{\alpha,\beta}\left(-\lambda t^\alpha\right)\right] = \frac{s^{\alpha-\beta}}{s^\alpha + \lambda} \qquad (4.22)$$

where $E_{\alpha,\beta}(x)$ is the 2-parameter Mittag-Leffler function defined as (Wiman 1905; Argawal 1953):

$$E_{\alpha,\beta}(x) = \sum_{r=0}^{\infty} \frac{x^r}{\Gamma(\alpha r + \beta)}, \quad \alpha > 0, \ \beta > 0 \qquad (4.23)$$

It should be noted that this reduces to the original 1-parameter Mittag-Leffler function (Mittag-Leffler 1903) when $\beta = 1$, giving

$$E_\alpha(x) = \sum_{r=0}^{\infty} \frac{x^r}{\Gamma(\alpha r + 1)} \qquad (4.24)$$

which further simplifies to the classical exponential function when $\alpha = 1$.

Taking the inverse Laplace transform of equation (4.21) gives the solution to equation (4.20) as

$$y(t) = \sum_{k=0}^{m-1} b_k t^k E_{\alpha,k+1}(-\lambda t^\alpha) \qquad (4.25)$$

Taking $\lambda = 1$ and $b_k = 1$ the solutions for different orders of derivative are plotted in Figure 4.1 and Figure 4.2.

For $0 < \alpha < 1$ (Figure 4.1) the solution $y(t) = b_0 E_\alpha(-\lambda t^\alpha)$ decays more rapidly than the classical exponential solution (for $\alpha = 1$) as $t \to 0^+$ but more slowly as $t \to \infty$. This power-law asymptotic behaviour of the fractional system exhibits long term memory loss (i.e. the system is dominated by more recent states as t increases). This is termed a fractional relaxation equation.
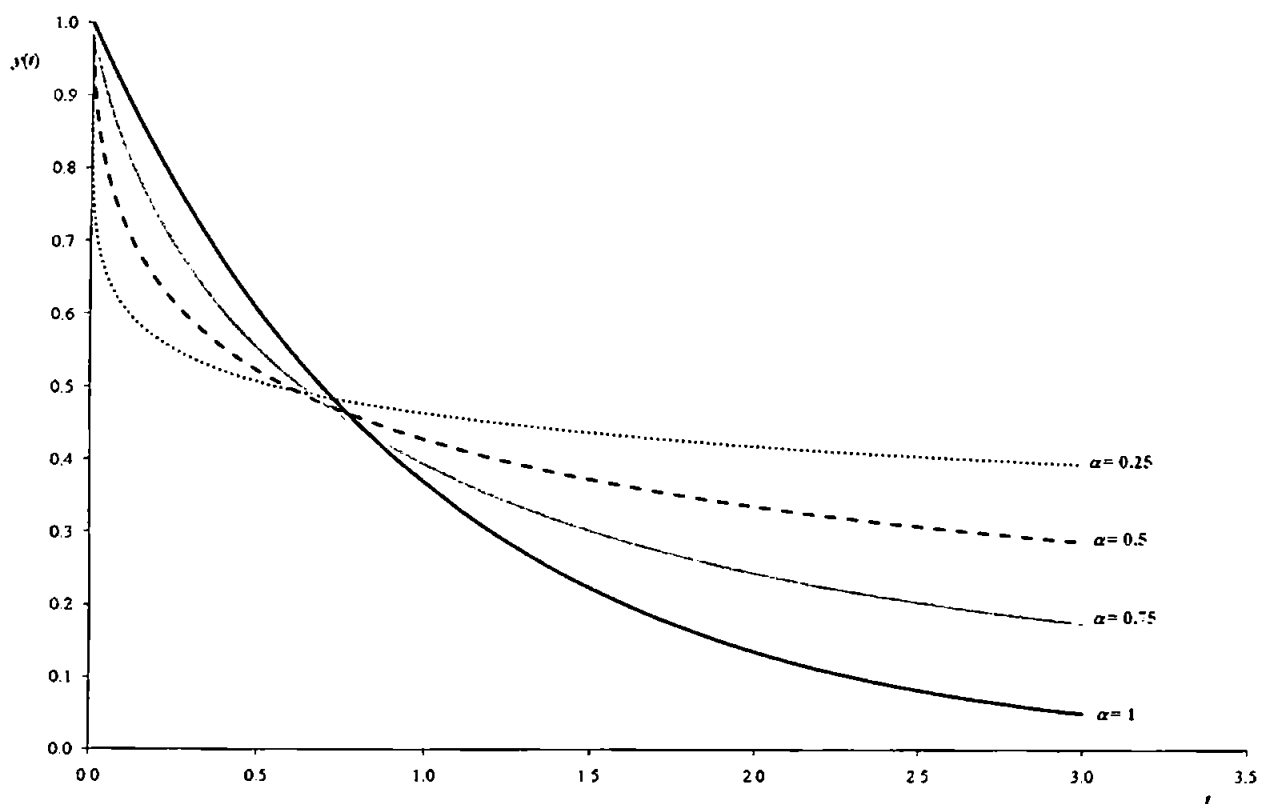
Figure 4.1 Solutions to the homogeneous fractional relaxation equation
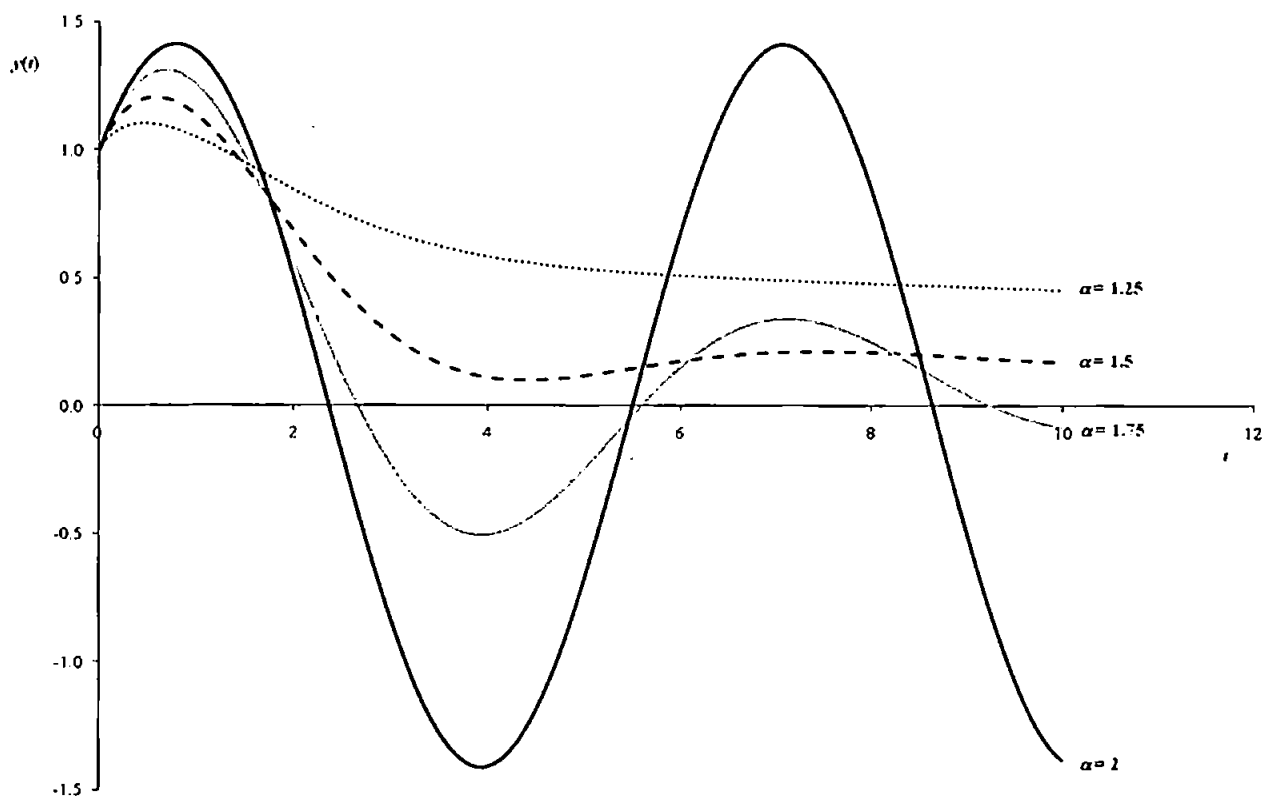
Figure 4.2 Solutions to the homogeneous fractional oscillation equation

44

For $1 < \alpha < 2$ (Figure 4.2) the solution takes the form $y(t) = b_0 E_\alpha(-\lambda t^\alpha) + b_1 t E_{\alpha,2}(-\lambda t^\alpha)$ which oscillates whilst decaying (unlike the periodic solution for the classical $\alpha = 2$ case), and this is termed a fractional oscillation equation.

4.2.6 The Generalised 3-Parameter Mittag-Leffler Function

In the solution of ordinary linear fractional differential equations use can be made of the generalised 3-parameter Mittag-Leffler function introduced by Prabhakar (1971) which takes the form for an argument, x:

$$E_{\alpha,\beta}^\gamma(x) = \sum_{r=0}^{\infty} \frac{\Gamma(r+\gamma)x^r}{\Gamma(\gamma)\Gamma(\alpha r + \beta)r!} \quad \text{for } \alpha,\beta,\gamma > 0 \tag{4.26}$$

When $\gamma = 1$ this reduces to equation (4.23), the 2-parameter Mittag-Leffler function.

Furthermore, Kilbas *et al* (2004) provide a Laplace transform of the 3-parameter Mittag-Leffler function for use with functions of a variable t in the following form

$$L\{t^{\beta-1} E_{\alpha,\beta}^\gamma(\lambda t^\alpha)\} = \frac{s^{\alpha\gamma-\beta}}{(s^\alpha - \lambda)^\gamma} \tag{4.27}$$

where λ is a constant.

4.2.7 Initial Conditions

A significant feature of the fractional calculus is the dependence on the definition of the integral for the selection of the initial conditions. For example comparing the Laplace transforms in equations (4.11) and (4.14) show the different initial conditions required for fractional differential equations expressed in terms of the Riemann-Liouville and Caputo derivatives, respectively. In addition, these definitions of the derivative show the effect of different sequencing of the differintegral operators. As section 4.2.4 shows there are many combinations of differintegrals that can be used to compose a definition

45

of a fractional derivative, each of which will have associated initial conditions. Furthermore Lorenzo and Hartley (1998) have investigated the initial conditions required for fractional differential equations using the Riemann-Liouville derivative and show that a time-varying initialisation function is required in place of initial conditions as single point values. Similarly, solutions to differential equations expressed in terms of the Caputo derivative with the associated initial conditions based on integer-order derivatives have been shown to be a restricted class of functions because of the assumption of constant initialisation (Ortigueira 2003; Orjuela *et al.* 2006; Achar *et al.* 2007).

For example Orjuela *et al* (2006) consider the solution of the non-homogeneous form of the ordinary linear fractional differential equation (4.20) expressed in terms of the Caputo derivative subject to a unit step input function, $U(t)$, as follows.

$$\begin{smallmatrix}C\\0\end{smallmatrix}D_t^\alpha y(t) + \lambda y(t) = U(t)$$

(4.28)

Taking Laplace transforms, using equation (4.14), for the case of $0 < \alpha \leq 1$ gives

$$s^\alpha Y(s) - s^{\alpha-1} y(0^+) + \lambda Y(s) = \frac{1}{s}$$

so

$$Y(s) = \frac{s^{-1}}{s^\alpha + \lambda} + \frac{s^{\alpha-1} y(0^+)}{s^\alpha + \lambda}$$

The inverse transform for each term is obtained from equation (4.22) resulting in the following solution.

$$y(t) = t^\alpha E_{\alpha,\alpha+1}(-\lambda t^\alpha) + y(0^+) E_\alpha(-\lambda t^\alpha)$$

(4.29)

The two terms in equation (4.29) represent the forced response plus the free response of the system, respectively. The forced response is the solution of the non-homogeneous part of equation (4.28) for zero initial conditions; and the free response is the solution of

46

the homogeneous part of equation (4.28) with the initial conditions included. In this way, only the free response of the system is affected by the definition of the fractional derivative used and the associated initial conditions.

For illustrative purposes, taking $\lambda = 1$ and subject to an initial condition $y(0^+) = 0.5$ then

$$y(t) = t^\alpha E_{\alpha,\alpha+1}\left(-t^\alpha\right) + 0.5 E_\alpha\left(-t^\alpha\right) \qquad (4.30)$$

In order to illustrate the influence of the history of the free response function (i.e. time-varying initialisation function) over the use of a point initial condition value (i.e. constant initialisation function) Orjuela *et al* use a reference response (2006). The reference response is the forced response solution for the case of a unit step input applied to an initially relaxed system at an earlier time, $t = -0.51$, such that the reference response when $t = 0$ is $y = 0.5$, i.e. equal to the initial condition $y(0^+) = 0.5$ for equation (4.30). If the initialisation is correct then the complete response predicted by equation (4.30) should correspond to the reference function for $t > 0$. Orjuela *et al* (2006) found that this only held for the integer order case when $\alpha = 1$. However, Figure 4.3 shows the discrepancy between the solutions for the fractional order case, e.g. when $\alpha = 0.5$.
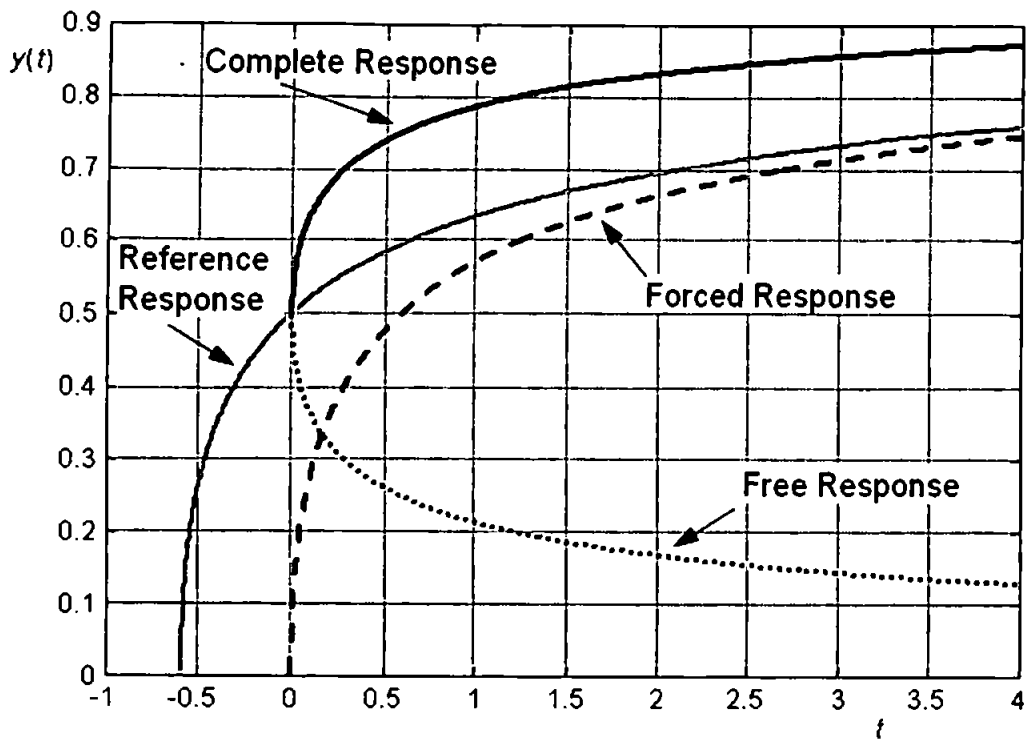
Figure 4.3 Solution of the inhomogeneous fractional relaxation equation

(after Orjuela *et al* (2006))

Similar results are found if the Riemann-Liouville derivative is used. Consequently, for the fractional order system constant initial conditions may not necessarily represent the true past history of the system response.

4.2.8 Initialisation Function

Lorenzo and Hartley (2008) provide a technique for the definition of the initialisation function for fractional differential equations expressed in terms of the Riemann-Liouville derivative. Figure 4.4 shows an arbitrary function $f(t)$ that originates at a time $t = -a$ which is subject to a differintegration operation at a later time of interest, $t = c$ (often taken as $t = 0$ for modelling the response of time varying systems).
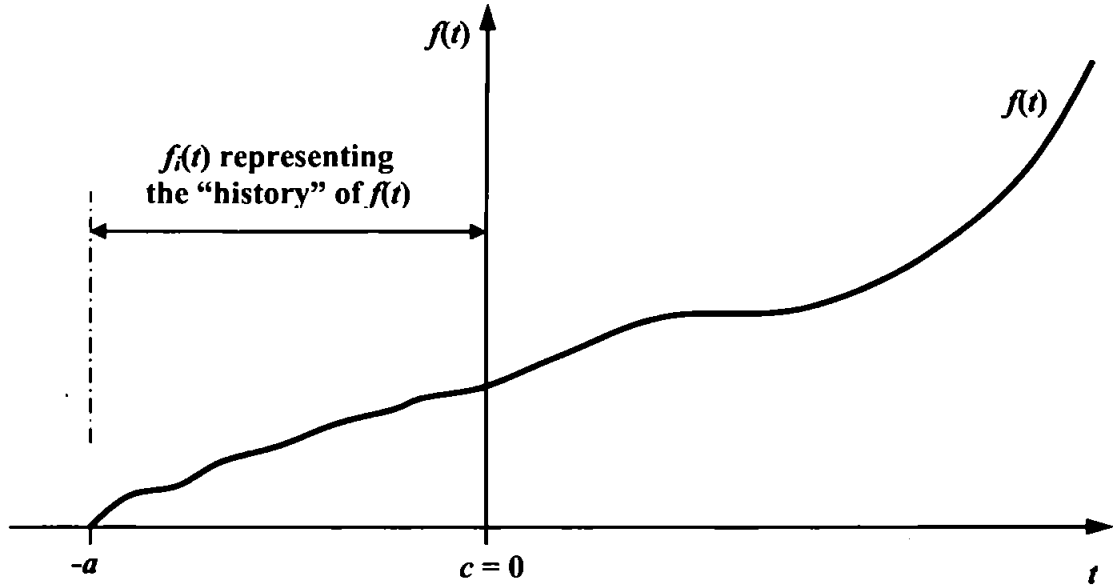
Figure 4.4 Conceptualisation of the initialisation function

The initialisation required of the function $f(t)$ can be defined by considering two uninitialized q-order fractional integrals of $f(t)$ starting at $t = -a$ and $t = c$, respectively, as follows.

$$_{-a}d_t^{-q}f(t) = \frac{1}{\Gamma(q)} \int_{-a}^{t}(t-\tau)^{q-1}f(\tau)d\tau \qquad t \geq -a \qquad (4.31)$$

$$_{c}d_t^{-q}f(t) = \frac{1}{\Gamma(q)} \int_{c}^{t}(t-\tau)^{q-1}f(\tau)d\tau \qquad t \geq c \qquad (4.32)$$

The d^q denotes an uninitialized integral. From Figure 4.1 $f(t) = 0$ for $t < -a$ so equation (4.31) does not require initialisation. However, the integral in equation (4.32) will only correspond with the integral in equation (4.31) for $t \geq c$ if an initialisation function, ψ, is added to it, i.e.

$$_{c}d_t^{-q}f(t) + \psi = {}_{-a}d_t^{-q}f(t) \qquad t > c$$

so

$$\psi = {}_{-a}d_t^{-q}f(t) - {}_{c}d_t^{-q}f(t) = \frac{1}{\Gamma(q)} \int_{-a}^{c}(t-\tau)^{q-1}f(\tau)d\tau \qquad t > c \qquad (4.33)$$

49

It follows that, in general, ψ is a function of time. This approach to initialisation by applying the function defined prior to $t = c$ is referred to as "terminal charging" by Lorenzo and Hartley (2008) as compared with applying an arbitrary initialisation function at $t = 0$ ("side charging"). The initialised form of the fractional integral can be stated now as

$$_cD_t^{-q}f(t){=}_cd_t^{-q}f(t)+\psi \qquad t > c \tag{4.34}$$

Substituting equation (4.34) into the definition of the Riemann-Liouville derivative in equation (4.6) expresses the initialised derivative as

$$_cD_t^{\alpha}f(t){=}_cD_t^{m}\,_cd_t^{-(m-\alpha)}f(t){+}_cD_t^{m}\psi \qquad t > c \tag{4.35}$$

for $m-1 < \alpha \leq m$. Using equation (4.32) the initialised derivative becomes

$$_cD_t^{\alpha}f(t) = \frac{d^m}{dt^m}\left[\frac{1}{\Gamma(m-\alpha)}\int_c^t(t-\tau)^{m-\alpha-1}f(\tau)d\tau\right]+\frac{d^m}{dt^m}\psi \qquad t \geq c \tag{4.36}$$

where ψ is given by equation (4.33).

Lorenzo and Hartley (2008) have derived Laplace transforms for the initialised fractional derivative for $c = 0$ and, consequently, $-a \leq t \leq 0$ so that physical systems represented as fractional order initial value problems can be formulated with time-varying initialisation. Referring to Figure 4.4 the function $f_i(t)$ on the interval from $t = -a$ to c, upon which the initialisation of the function $f(t)$ being differintegrated from $t = c$ onwards depends, does not have to be identical to $f(t)$. Evidently the form of the initialisation function must depend on the physical nature of the problem, i.e. the history of the system behaviour. However, as Malti *et al* (2006) point out, the identification of the initialisation function from data is an open problem for many systems. Furthermore, Lorenzo and Hartley's approach often involves finding the inverse Laplace transform of terms involving functions of the complementary incomplete gamma function which are not always available in closed form in standard tables (Hartley and Lorenzo 2008).

However, the concept of initialisation function does not preclude the use of the Caputo fractional derivative which incorporates constant initial conditions, but emphasises the restricted class of problems that it describes (recall section 4.2.7). Achar *et al* (2007) show that the inferred initialisation history (for $-\infty < t \leq 0$) for an α-order Caputo derivative is a polynomial of the form

$$f_i(t) = \sum_{n=0}^{m-1} \frac{f^{(n)}(0^+)}{\Gamma(n+1)} t^n \qquad (4.37)$$

where $m-1 < \alpha < m$. For example for $0 < \alpha \leq 1$ this reduces to $f_i(t) = f(0^+)$ which is consistent with the definition of the Caputo derivative in equation (4.13).

It should be noted that an alternative approach has been proposed by Ortigueira and Coito (2008) by treating the problem as a delay differential equation system and using the bilateral Laplace transform.

4.3 Classical Integer-Order Linear Hydrologic Systems

4.3.1 Integral Equation Approach - Instantaneous Unit Hydrographs

A lumped system can be conceptualised as shown in Figure 4.5 where a single input, $i(t)$ produces a single output, $q(t)$ as functions of time, t, only (i.e. spatially averaged).
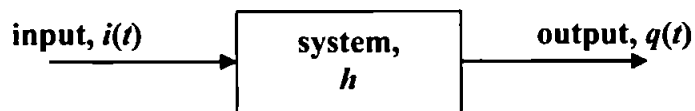

input, $i(t)$ → system, h → output, $q(t)$

Figure 4.5 Lumped system

In classical integer-order rainfall-runoff modelling, such as the unit hydrograph (Dooge 1973; Singh 1988) $i(t)$ is a continuous time history of effective rainfall that produces a continuous time-varying outflow, $q(t)$. The system is represented by a system function, h, such that

$$q(t) = hi(t) \tag{4.38}$$

In the classical integer-order unit hydrograph system the outflow is stormflow (runoff). In practice, rainfall measurements are usually made as total collected in a time interval (typically per hour). Consequently, the continuous input, $i(t)$, is approximated by n discrete rainfall pulses of duration Δt as shown in Figure 4.6.
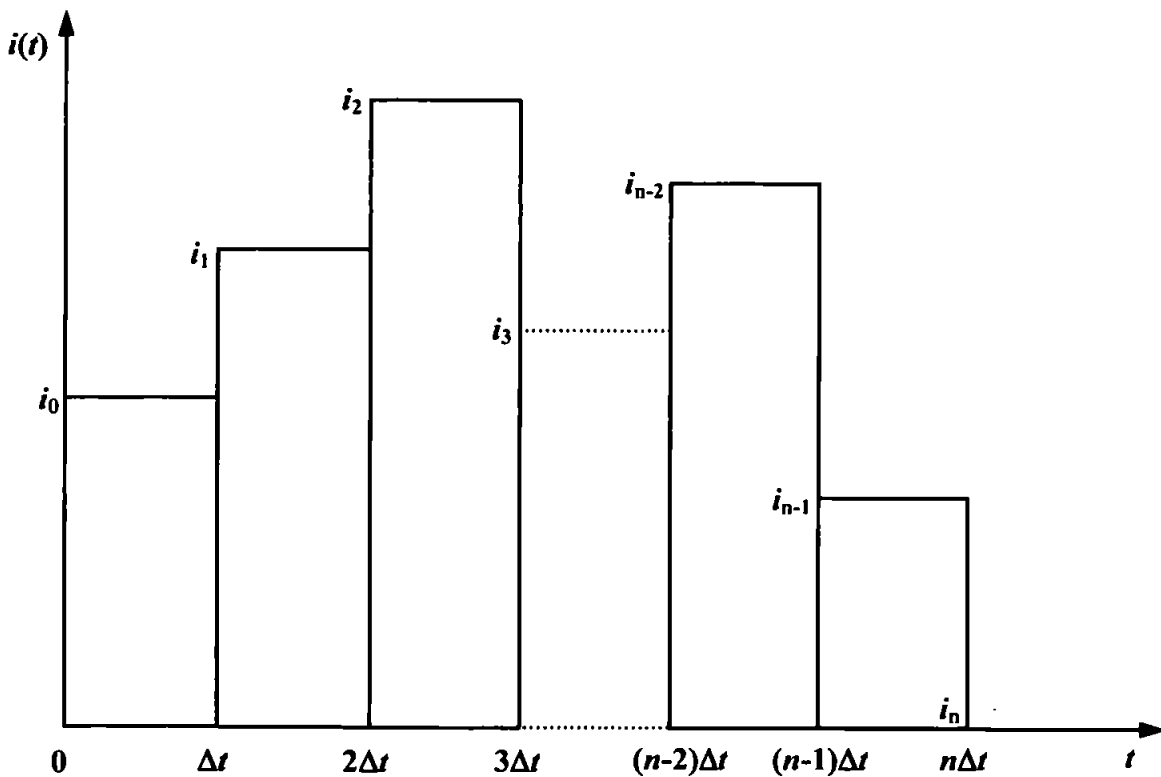
Figure 4.6 Pulse representation of rainfall data (hyetograph)

Wang and Wu (1983) represent this pulse hyetograph as a series of unit step functions, $U(t)$, whereby

$$i(t) = \sum_{j=0}^{n} w_j U(t - j\Delta t) \qquad (4.39)$$

and

$$w_j = i_j - i_{j-1} \quad \text{for } j = 1, 2, ..., n$$

Following Singh (1988), as $\Delta t \to 0$ the unit pulse, $U(t - j\Delta t)$ can be replaced by the Dirac delta impulse, $\delta(t)$; and, as $n \to \infty$ so that $n\Delta t = T$, then $j\Delta t$ can take all the values on the interval $[0, T]$. Hence the continuous rainfall function can be represented as

$$i(t) = \int_0^T i(\tau)\delta(t - \tau)d\tau \qquad (4.40)$$

which can be extended over the whole time line $-\infty < t < \infty$. Combining equations (4.38) and (4.40) gives

$$q(t) = h \int_{-\infty}^{\infty} i(\tau)\delta(t - \tau)d\tau \qquad (4.41)$$

Assuming an initially relaxed, linear system then the principles of superposition and proportionality apply so that

$$q(t) = \int_{-\infty}^{\infty} i(\tau)h\delta(t - \tau)d\tau \qquad (4.42)$$

For a $\delta(t)$ input to such a system the output is defined as the impulse response, $h(t, \tau)$, so that $h(t, \tau) = h\delta(t - \tau)$, and

$$q(t) = \int_{-\infty}^{\infty} i(\tau)h(t,\tau)d\tau \qquad (4.43)$$

Assuming the system is time-invariant, then $h(t, \tau) = h\delta(t - \tau) = h(t - \tau)$. Also assuming a causal system, $h(t, \tau) = 0$ for $\tau > t$ and $\tau < 0$, so that

$$q(t) = \int_0^t i(\tau)h(t - \tau)d\tau \qquad (4.44)$$

Equation (4.44) is a Laplace convolution integral which represents the response of an initially relaxed, lumped, linear, causal, time-invariant system. These conditions are the

fundamental assumptions underpinning the unit hydrograph approach to rainfall-runoff modelling (Dooge 1973).

The impulse response function, $h(t)$, is also referred to as the Green's function or transfer function. In hydrological modelling it is called the instantaneous unit hydrograph (IUH). It can be found from equation (4.44) by taking the Laplace transform of the convolution integral (Doetsch 1974):

$$Q(s) = I(s)H(s) \tag{4.45}$$

$h(t)$ is obtained from the inverse Laplace transform of equation (4.45) by considering the case of a Dirac delta impulse as input, since $L\{\delta(t)\} = 1$. Equation (4.44) can then be used to obtain the output, $q(t)$, for any input, $i(t)$.

4.3.2 Linear Differential Equation Approach

A lumped, linear, time-invariant system can be represented by an nth order ordinary linear differential equation with constant coefficients, a_j, as

$$[a_n D^n + a_{n-1} D^{n-1} + \cdots + a_0 D^0] q(t) = i(t) \quad t \geq 0 \tag{4.46}$$

with initial conditions $y^{(j)}(0^+) = b_j, j = 0, 1, ..., n-1$, and the solution takes the following form (Doetsch 1974; Miller and Ross 1993):

$$q(t) = q_{forced}(t) + q_{free}(t) \tag{4.47}$$

The forced response, $q_{forced}(t)$, is the solution of the non-homogeneous part of equation (4.46) for zero initial conditions

$$q_{forced}(t) = \int_0^t i(\tau) h(t - \tau) d\tau \tag{4.48}$$

This represents the convolution of the input function, $i(t)$ with the impulse response function, $h(t)$.

54

The free response, $q_{free}(t)$, is the solution of the homogeneous part of equation (4.46) with the initial conditions included

$$q_{free}(t) = \sum_{j=1}^{n} c_j h^{(j)}(t)$$ (4.49)

c_k are arbitrary constants, and $h(t)$ is the impulse response function.

Consequently, equation (4.44) is equivalent to equation (4.48), the solution of an initially relaxed non-homogeneous n^{th} order ordinary linear differential equation with constant coefficients ($q_{forced}(t)$). This result is consistent with Nash's (1957; 1960) work on the conceptual representation of the impulse response function as a cascade of equal linear reservoirs.

4.3.3 Reservoir Cascade Models

Recalling equation (2.4), the continuity equation for a lumped catchment system modelled by a single conceptual reservoir is given by

$$i(t) - q(t) = \frac{dV}{dt}$$ (4.50)

where V is the storage volume in the reservoir system. Zoch's (1934) linear reservoir (equation (2.6)) assumes that

$$V = Kq$$ (4.51)

where K is the storage delay (i.e. relaxation) time of the reservoir ($K > 0$). Differentiating gives

$$\frac{dV}{dt} = K \frac{dq}{dt}$$ (4.52)

Substituting equation (4.52) into equation (4.50) and rearranging gives

$$\frac{dq}{dt} + \frac{1}{K} q(t) = \frac{1}{K} i(t)$$ (4.53)

Nash (1957) assumed that the system that generates outflow from a rainfall input has zero initial conditions (i.e. starts from rest), so equation (4.53) is an initially relaxed homogeneous first order ordinary linear differential equation with constant coefficients (i.e. it is a first order relaxation system model). The solution is given by equation (4.48): the convolution of the impulse response function, $h(t)$, and the input function, $i(t)$. As before, the impulse response function is obtained as the output of equation (4.53) for the case of a delta input, $\delta(t)$, by taking Laplace transforms, so

$$sH(s) + \frac{1}{K}H(s) = \frac{1}{K}$$

$$H(s) = \frac{1}{K\left(s + \frac{1}{K}\right)}$$

or

$$H(s) = \frac{1}{1 + Ks} \tag{4.54}$$

hence

$$h(t) = L^{-1}\left\{\frac{1}{K} \cdot \frac{1}{\left(s + \frac{1}{K}\right)}\right\}$$

$$h(t) = \frac{1}{K}e^{-t/K} \tag{4.55}$$

Substituting into the convolution equation (4.48) gives the outflow of a single reservoir for an arbitrary input as

$$q(t) = \frac{1}{K}\int_0^t i(\tau)e^{-(t-\tau)}d\tau \tag{4.56}$$

This approach can be extended to a cascade of initially relaxed, unequal (different K value) linear reservoirs in series by determining the impulse response function where the output from the first reservoir given by equation (4.55) to the delta input becomes

the input to the second reservoir. From equation (4.54) the impulse response function for the second reservoir is

$$H_2(s) = \frac{1}{(1 + K_2 s)} \cdot \frac{1}{(1 + K_1 s)}$$

Continuing for n reservoirs gives

$$H_n(s) = \frac{1}{\prod_{j=1}^{n}(1 + K_j s)}$$ (4.57)

Taking the inverse Laplace transform (Dooge 1959) gives the impulse response function as

$$h(t) = \sum_{j=1}^{n} \frac{K_j^{n-2} e^{-t/K_j}}{\prod_{r=1}^{n-1}(K_r - K_j)} \qquad r \neq j, \quad K_r \neq K_j$$ (4.58)

However, Chow and Kulandaiswamy (1971) found that 3 unequal reservoirs were usually adequate for rainfall-runoff modelling applications. Cascades with higher numbers of unequal reservoirs lead to less parsimonious models, requiring many more parameters to be fitted. For n equal-K reservoirs equation (4.57) becomes

$$H_n(s) = \frac{1}{(1 + Ks)^n}$$ (4.59)

The inverse Laplace transform yields equation (2.7), the impulse response function for the Nash cascade:

$$h(t) = \frac{1}{K(n-1)!}\left(\frac{t}{K}\right)^{n-1} e^{-t/K}$$ (4.60)

To obtain the outflow of the Nash cascade for an arbitrary input, the impulse response function is substituted into the convolution equation (4.48). This is equivalent to substituting equation (4.59) into equation (4.45) in the Laplace frequency domain as

$$Q(s) = I(s)\frac{1}{(1 + Ks)^n}$$ (4.61)

Following Singh (1988) and recalling that the Laplace transform s variable appears because of the derivative, $\dfrac{d}{dt}$, in equation (4.53), then, using the operator D notation, equation (4.61) can be expressed as

$$q(t) = i(t)\frac{1}{(1 + KD)^n}$$

or

$$(1 + KD)^n q(t) = i(t) \tag{4.62}$$

Expanding as a binomial series for integer n (Spanier and Oldham 1987) gives

$$\left[\sum_{j=0}^{n} \binom{n}{j}(KD)^j \right] q(t) = i(t) \tag{4.63}$$

Letting $a_j = \dbinom{n}{j} K^j$ then

$$\left[\sum_{j=0}^{n} a_j D^j \right] q(t) = i(t) \tag{4.64}$$

which is the same as equation (4.46) for zero initial conditions

$$\left[a_n D^n + a_{n-1} D^{n-1} + \cdots + a_0 D^0 \right] q(t) = i(t) \quad t \geq 0 \tag{4.65}$$

i.e. the Nash cascade is modelled by an initially relaxed, n^{th} order ordinary linear differential equation with constant coefficients, a_j. This can also be derived from Chow and Kulandaiswamy's (1971) general storage equation for $b_r = 0$:

$$\sum_{j=0}^{n} a_j D^j q(t) = \sum_{r=0}^{m} b_r D^r i(t) \tag{4.66}$$

where j, r, m and n are integers, and a_j and b_r are constant coefficients.

4.3.4 Lag and Route Models

Dooge (1959) introduced the linear channel routing concept in the derivation of a general theory for the unit hydrograph to model lag effects in catchment response to rainfall. The linear channel represents a pure translation where the output is the input lagged by a time T:

$$q(t) = i(t - T)$$ (4.67)

Dooge's theory assumes that the instantaneous unit hydrograph (impulse response function) for the rainfall-runoff transformation can be obtained by routing a delta impulse through a series of initially-relaxed linear channels and equal-K linear reservoirs. In this way it combines the linear channel with the Nash cascade (i.e. lag and route). For the case of a single lag and route model the input to equation (4.53) is that from equation (4.67) giving

$$\frac{dq}{dt} + \frac{1}{K}q(t) = \frac{1}{K}i(t - T)$$ (4.68)

The impulse response function for the lag and route model is obtained for the case of a delta input, $\delta(t)$, to the linear channel element which, by equation (4.67) produces a $\delta(t - T)$ input to equation (4.68). Taking Laplace transforms gives

$$sH(s) + \frac{1}{K}H(s) = \frac{1}{K}e^{-Ts}$$

$$H(s) = \frac{e^{-Ts}}{(1 + Ks)}$$ (4.69)

Using the 2nd shift theorem for the Laplace transform (delay rule) (Doetsch 1974)

$$h(t) = U(t - T)\frac{e^{-(t-T)/K}}{K}$$ (4.70)

where $U(t)$ is the unit step function.

The extension to a cascade of n initially relaxed, equal (K, T) lag and route elements is made in a similar manner to that in section 4.3.3, by determining the impulse response function where the output from the first element given by equation (4.70) to the delta input becomes the input to the second element. This is repeated for the remaining elements. Combining equations (4.59) and (4.69) gives

$$H(s) = \frac{e^{-nTs}}{(1 + Ks)^n} \tag{4.71}$$

Using the 2nd shift theorem for the Laplace transform

$$h(t) = U(t - nT) \frac{(t - nT)^{n-1}}{K^n (n-1)!} e^{-(t-nT)/K} \tag{4.72}$$

This forms the basis for Dooge's general equation for the instantaneous unit hydrograph (Dooge 1959). As before, the solution for the lag and route models for an arbitrary input, $i(t)$, is found by convolution of $i(t)$ with the impulse response function, $h(t)$ (equation (4.48)).

4.4 Fractional Hydrologic Model

4.4.1 Assumptions

A general theory for the systems-based modelling of the transformation of observed (total) rainfall to observed streamflow (i.e. stormflow and baseflow together) is presented based on the following assumptions:

1. The output of the system, $q(t)$, is total streamflow to be modelled at the storm-streamflow event scale (typically hourly intervals) so that floods can be predicted.

2. The behaviour of the catchment system is spatially averaged (lumped) so that it is represented by an ordinary differential equations.

3. The system is linear so that the principles of superposition and proportionality can be used in the solution of the differential equations.

4. The catchment characteristics are constant over the total duration of the streamflow event (i.e. time-invariant) so that the coefficients of the differential equations are constants.

5. The system is casual so that Laplace convolution integrals can be utilised.

6. The effective (net) rainfall input, $i(t)$, to the system must be derived from the total observed rainfall, $i_{obs}(t)$, by a loss model to account for infiltration and evapotranspiration.

7. The differential equation is of arbitrary (α) order to represent the time-history of water storage/flow states in the surface/subsurface catchment system. This is expressed by a fractional order derivative form of the linear reservoir.

8. The streamflow system is not initially relaxed but is subject to an initial condition (i.e. a constant initialisation function using the Caputo fractional derivative) to represent the mixing effect of "old" (stored) water and "new" water observed in streamflow chemistry.

9. $0 < \alpha \leq 1$ to represent the heavily damped behaviour of the system over the duration of the flow event (i.e. non-oscillatory).

Assumptions 1 - 5 are consistent with those for Dooge's (1959) general unit hydrograph theory for rainfall-runoff systems. Assumption 6 is necessary in unit hydrograph models because only total rainfall is measured in practice, but water is "lost" through infiltration and evapotranspiration that does not contribute to the ensuing streamflow event. The further assumptions (7 – 9) generalise the theory to predict the total streamflow (i.e. stormflow and baseflow together) as a fractional relaxation model for which the classical unit hydrograph is a special case. The non-local property of the fractional order derivative is assumed to represent the memory loss in the catchment system where pre-storm event water released from storage in the catchment dominates

61

the streamflow response to a rain storm. Consequently, the system is not initially at rest (unlike the classical UH approaches for stormflow modelling) but is responding to previous event rainfall draining through the catchment. This gives rise to the need for an initial condition assumption.

4.4.2 Single Fractional Order Linear Reservoir

The simplest model element proposed is the fractional order linear reservoir. Recalling equation (4.52) for the integer-order linear reservoir

$$\frac{dV}{dt} = K \frac{dq}{dt}$$

From assumption 7 it is proposed that the rate of change of volume, V, with time, t, can be expressed by an α-order fractional time derivative of the outflow rate, q, so that

$$\frac{dV}{dt} = K^\alpha \, {}_0^C D_t^\alpha q(t) \tag{4.73}$$

K is the storage delay (i.e. relaxation) time of the reservoir ($K > 0$), and is raised to the power α, to preserve dimensionality. At this stage the Caputo fractional derivative has been used because it incorporates a physically observable initial condition (equation (4.13)). Substituting into equation (4.50), the continuity equation for a lumped catchment, and rearranging gives a fractional relaxation equation:

$$ {}_0^C D_t^\alpha q(t) + \frac{1}{K^\alpha} q(t) = \frac{1}{K^\alpha} i(t) \tag{4.74}$$

Taking Laplace transforms, using equation (4.14), for the case of $0 < \alpha \leq 1$ (assumption 9) gives

$$s^\alpha Q(s) - s^{\alpha-1} Q(0^+) + \frac{1}{K^\alpha} Q(s) = \frac{1}{K^\alpha} I(s) \tag{4.75}$$

$$Q(s) = \frac{I(s)}{K^\alpha \left(s^\alpha + \frac{1}{K^\alpha}\right)} + \frac{s^{\alpha-1} Q(0^+)}{\left(s^\alpha + \frac{1}{K^\alpha}\right)} \tag{4.76}$$

Recalling equation (4.47), the two terms in equation (4.76) represent the forced response plus the free response of the system, respectively. The forced response is the solution of the non-homogeneous part of equation (4.74) for zero initial conditions and takes the form of the convolution of the input function, $i(t)$ with the impulse response function, $h(t)$. As before, the impulse response function is obtained as the output of equation (4.74) for a delta impulse input, $\delta(t)$, and zero initial conditions. Substituting $L\{\delta(t)\} = 1$, then the first term of equation (4.76) becomes

$$H(s) = \frac{1}{K^\alpha \left(s^\alpha + \frac{1}{K^\alpha}\right)} \tag{4.77}$$

Using equation (4.22), the inverse Laplace transform yields the impulse response function which involves the 2-parameter Mittag-Leffler function, $E_{\alpha,\beta}(x)$ (refer to equation (4.23)):

$$h(t) = \frac{1}{K^\alpha} t^{\alpha-1} E_{\alpha,\alpha}\left[-\left(\tfrac{t}{K}\right)^\alpha\right] \tag{4.78}$$

$h(t)$ reduces to the Nash's single integer-order reservoir (equation (4.55)) when $\alpha = 1$. Hence the forced response for equation (4.74) is

$$q_{forced}(t) = \frac{1}{K^\alpha} \int_0^t (t-\tau)^{\alpha-1} E_{\alpha,\alpha}\left[-\left(\tfrac{t-\tau}{K}\right)^\alpha\right] i(\tau)d\tau \tag{4.79}$$

The free response is the solution of the homogeneous part of equation (4.74) with the initial conditions included, given by the inverse Laplace transform of the second term of equation (4.76) (again using equation (4.22)):

$$q_{free}(t) = q_0 E_\alpha\left[-\left(\tfrac{t}{K}\right)^\alpha\right] \tag{4.80}$$

where q_0 is the initial streamflow and $E_\alpha(x)$ is the 1-parameter Mittag-Leffler function (refer to equation (4.24)). Since the free response is the relaxation solution for zero input, it can be used as a general model for baseflow recession. When $\alpha = 1$, it reduces

to Maillet's (1905) exponential decay equation traditionally used for baseflow recession modelling (Tallaksen 1995).

The total solution to equation (4.74) is

$$q(t) = \frac{1}{K^\alpha} \int_0^t (t-\tau)^{\alpha-1} E_{a,a}\left[-\left(\tfrac{t-\tau}{K}\right)^\alpha\right] i(\tau) d\tau + q_0 E_a\left[-\left(\tfrac{t}{K}\right)^\alpha\right]$$ (4.81)

When $\alpha = 1$ and for zero initial conditions, this reduces to Nash's single linear reservoir equation (4.56).

4.4.3 Single Fractional Order Lag and Route Model

Using the outflow of a linear channel (equation (4.67)) as input to the fractional order linear reservoir gives the single fractional order lag and route model:

$$_0^C D_t^\alpha q(t) + \frac{1}{K^\alpha} q(t) = \frac{1}{K^\alpha} i(t-T)$$ (4.82)

where T is the lag time.

The impulse response function, $h(t)$, is obtained for the case of a delta input, $\delta(t)$, to the initially-relaxed linear channel element which produces a $\delta(t-T)$ input to equation (4.82). Taking Laplace transforms, using equation (4.14), for the case of $0 < \alpha \leq 1$ gives

$$s^\alpha H(s) + \frac{1}{K^\alpha} H(s) = \frac{1}{K^\alpha} e^{-Ts}$$

$$H(s) = \frac{e^{-Ts}}{K^\alpha \left(s^\alpha + \tfrac{1}{K^\alpha}\right)}$$ (4.83)

Using the 2nd shift theorem for a Laplace transform (Doetsch 1974)

$$h(t) = \frac{U(t-T)(t-T)^{\alpha-1} E_{\alpha,\alpha}\left[-\left(\frac{(t-T)}{K}\right)^{\alpha}\right]}{K^{\alpha}} \tag{4.84}$$

which reduces to Dooge's single integer-order lag and route model (equation (4.70)) when $\alpha = 1$.

Hence the forced response for equation (4.82) is given by the convolution of the input function, $i(t)$ with the impulse response function, $h(t)$. The free response is unchanged from that for the single fractional order reservoir (equation (4.80)), so the total solution for the single α-order lag and route model is

$$q(t) = \frac{1}{K^{\alpha}} \int_0^t U(t-T-\tau)(t-T-\tau)^{\alpha-1} E_{\alpha,\alpha}\left[-\left(\frac{(t-T-\tau)}{K}\right)^{\alpha}\right] i(\tau) d\tau + q_0 E_{\alpha}\left[-\left(\frac{t}{K}\right)^{\alpha}\right] \tag{4.85}$$

4.4.4 Cascade of Unequal Fractional Order Linear Reservoirs

The model of the cascade of fractional order linear reservoirs is derived in a similar manner to that for the integer-order cascade (section 4.3.3). In the first instance an initially relaxed cascade of unequal-K reservoirs in series by determining the impulse response function where the output from the first reservoir given by equation (4.78) to the delta impulse input becomes the input to the second reservoir. From equation (4.77) the impulse response function for the second reservoir is

$$H_2(s) = \frac{1}{K_2^{\alpha}\left(s^{\alpha} + \frac{1}{K_2^{\alpha}}\right)} \cdot \frac{1}{K_1^{\alpha}\left(s^{\alpha} + \frac{1}{K_1^{\alpha}}\right)} \tag{4.86}$$

assuming the reservoirs have the same order, α.

Continuing for n reservoirs gives

$$H_n(s) = \frac{1}{\prod_{j=1}^{n}\left(1 + K_j^{\alpha} s^{\alpha}\right)} \tag{4.87}$$

For $\alpha = 1$, this reduces to equation (4.57). Again, the issue of model parsimony limits the practical calibration of models with several unequal reservoirs. The case for $n = 2$ is

developed as an example (where $K_1 \neq K_2$ and $K_1 > 0$, $K_2 > 0$). Equation (4.86) can be rewritten as

$$H(s) = \frac{1}{(1 + K_1^\alpha s^\alpha)(1 + K_2^\alpha s^\alpha)} = \frac{A}{(1 + K_1^\alpha s^\alpha)} + \frac{B}{(1 + K_2^\alpha s^\alpha)}$$

Cross multiplying

$$1 = A(1 + K_2^\alpha s^\alpha) + B(1 + K_1^\alpha s^\alpha)$$

$$1 = A + AK_2^\alpha s^\alpha + B + BK_1^\alpha s^\alpha$$

$$1 = (A + B) + (AK_2^\alpha + BK_1^\alpha)s^\alpha$$

Equating coefficients of like terms in s

$$1 = A + B$$

and

$$0 = AK_2^\alpha + BK_1^\alpha$$

Substituting $A = 1 - B$ gives

$$B = \frac{-K_2^\alpha}{K_1^\alpha - K_2^\alpha}$$

and

$$A = \frac{K_1^\alpha}{K_1^\alpha - K_2^\alpha}$$

So

$$H(s) = \frac{1}{K_1^\alpha - K_2^\alpha}\left(\frac{K_1^\alpha}{1 + K_1^\alpha s^\alpha} - \frac{K_2^\alpha}{1 + K_2^\alpha s^\alpha} \right) \tag{4.88}$$

Taking the inverse Laplace transform (using equation (4.22)):

$$h(t) = \frac{t^{\alpha-1}}{K_1^\alpha - K_2^\alpha}\left\{ E_{\alpha,\alpha}\left[-(t/_{K_1})^\alpha \right] - E_{\alpha,\alpha}\left[-(t/_{K_2})^\alpha \right] \right\} \tag{4.89}$$

The foregoing provides a proof for Cavallini's (2002) proposed ansatz for a fractional instantaneous unit hydrograph model (equation (3.2) with $k_1 = -1/_{K_2}$, $k_2 = -1/_{K_1}$ and

$v = \alpha$). It should be noted that Cavallini's proposed equation is missing the powers on the k values required for dimensional consistency. When $\alpha = 1$, equation (4.89) reduces to the classical integer order IUH for a cascade of 2 unequal linear reservoirs (equation (3.1) and using Cavallini's k notation).

As before, the forced response for an arbitrary rainfall input is given by the convolution of the input function, $i(t)$ with the impulse response function, $h(t)$.

For the case where the cascade is not initially at rest the total solution also requires a free response (in accordance with equation (4.47)), and, hence an initial condition for each reservoir. In the absence of further information, it is assumed that the first reservoir of the cascade has an initial condition equal to the initial observed (total) streamflow, q_0, and the remaining reservoirs are all initially relaxed (although, strictly, this assumption is not proven for surface/subsurface catchment flow processes). Consequently, the free response is unchanged from that for the single fractional order reservoir (equation (4.80)).

4.4.5 Cascade of Equal Fractional Order Linear Reservoirs

The impulse response function for the fractional-order equivalent of the Nash cascade of initially relaxed equal-K reservoirs is derived from equation (4.87) as

$$H_n(s) = \frac{1}{\left(1 + K^\alpha s^\alpha\right)^n} \tag{4.90}$$

which can be rewritten as

$$H_n(s) = \frac{1}{K^{n\alpha}\left(s^\alpha + \frac{1}{K^\alpha}\right)^n} \tag{4.91}$$

Using equation (4.27) the inverse Laplace transform is

$$h(t) = \frac{t^{na-1}}{K^{na}} E^n_{\alpha,na}\left[-\left(\frac{t}{K}\right)^\alpha\right]$$ (4.92)

where $E^\gamma_{\alpha,\beta}(x)$ is the 3-parameter Mittag-Leffler function (refer to equation (4.26)).

Again, when $\alpha = 1$, this reduces to the Nash cascade (equation (4.60)).

The forced response for an arbitrary rainfall input is given by the convolution of the input function, $i(t)$ with the impulse response function, $h(t)$. For the case where the cascade is not initially at rest the same argument as for the unequal cascade in section 4.4.4 is used to obtain the free response (from equation (4.80)) and, hence the total solution.

4.4.6 Cascade of Time-Lagged Equal Fractional Reservoirs

The impulse response function for the fractional-order equivalent of the cascade of n initially relaxed, equal (K, T) lag and route elements to that used in the formulation of Dooge's (1959) general instantaneous unit hydrograph is derived in a similar manner to that in section 4.3.4. The output from the first element given by equation (4.84) to the delta input becomes the input to the second element. This is repeated for the remaining elements. Combining equations (4.83) and (4.91) gives

$$H_n(s) = \frac{e^{-nTs}}{K^{na}\left(s^\alpha + \frac{1}{K^\alpha}\right)^n}$$ (4.93)

Using the 2$^{\text{nd}}$ shift theorem for the Laplace transform

$$h(t) = \frac{U(t-nT)(t-nT)^{na-1} E^n_{\alpha,na}\left[-\left(\frac{(t-nT)}{K}\right)^\alpha\right]}{K^{na}}$$ (4.94)

Again, when $\alpha = 1$, this reduces to the equivalent form of Dooge's general instantaneous unit hydrograph (equation (4.72)). The solution for the lag and route cascade for an arbitrary input, $i(t)$, is found by convolution of $i(t)$ with the impulse

response function, $h(t)$. For the case where the cascade is not initially at rest the same tentative argument as for the fractional Nash cascade in section 4.4.5 is used to obtain the free response (from equation (4.80)) and, hence the total solution, i.e.

$$q(t) = \frac{1}{K^{na}} \int_0^t U(t - nT - \tau)(t - nT - \tau)^{na-1} E_{a,na}^n \left[-\left(\tfrac{(t-nT-\tau)}{K} \right)^a \right] i(\tau) d\tau + q_0 E_a \left[-\left(\tfrac{t}{K} \right)^a \right] \quad (4.95)$$

Equation (4.95) encompasses fractional order reservoir storage-outflow behaviour and takes account of initial conditions so that the rainfall-streamflow transformation can be modelled by unit hydrograph principles. Effectively, this further generalises Dooge's (1959) theory beyond the rainfall-runoff transformation.

4.4.7 A Fractional Order General Storage Equation – Initial Form

The relationship between the fractional order cascade models and a general storage equation akin to Chow and Kulandaiswamy's (1971) equation can be undertaken in a similar manner to that used in section 4.3.3. In order to investigate the form of such a fractional order general storage equation, and because of the implications for the interpretation of the Nash model, the case for a cascade of fractional order equal-K linear reservoirs is considered.

From section 4.3.2 the form of the differential equation depends on the forced response, $q_{forced}(t)$, namely the solution of the non-homogeneous equation for zero initial conditions expressed as the convolution of the input function, $i(t)$ with the impulse response function, $h(t)$ (equation (4.48)):

$$q_{forced}(t) = \int_0^t i(\tau)h(t - \tau)d\tau$$

The Laplace transform of this convolution integral is equation (4.45):

$$Q(s) = I(s)H(s)$$

Substituting for $H(s)$ from equation (4.90) for the fractional order cascade of equal-K reservoirs:

$$Q(s) = I(s)\frac{1}{(1 + K^\alpha s^\alpha)^n} \qquad (4.96)$$

As before, recalling that the Laplace transform s^α variable represents the fractional derivative (taken in the Caputo sense), ${}_0^C D_t^\alpha$, then

$$q(t) = i(t)\frac{1}{(1 + K^\alpha {}_0^C D_t^\alpha)^n}$$

or

$$(1 + K^\alpha {}_0^C D_t^\alpha)^n q(t) = i(t) \qquad (4.97)$$

Expanding as a binomial series for integer n (Spanier and Oldham 1987) gives

$$\left[\sum_{j=0}^{n} \binom{n}{j} (K^\alpha {}_0^C D_t^\alpha)^j \right] q(t) = i(t) \qquad (4.98)$$

Letting $a_j = \binom{n}{j} K^{j\alpha}$ then

$$\left[\sum_{j=0}^{n} a_j {}_0^C D_t^{j\alpha} \right] q(t) = i(t) \qquad (4.99)$$

which can be written as the following initially-relaxed ordinary $n\alpha$ order linear differential equation with constant coefficients, a_j.

$$\left[a_n {}_0^C D_t^{n\alpha} + a_{(n-1)} {}_0^C D_t^{(n-1)\alpha} + \cdots + a_0 \right] q(t) = i(t) \qquad t \geq 0 \qquad (4.100)$$

When $\alpha = 1$ this reduces to Nash's (1960) differential equation for the integer-order cascade (equation (4.65)) and to Chow and Kulandaiswamy's (1971) general storage equation (equation (4.66) for $b_r = 0$).

Replacing $(n - 1)!$ by the gamma function $\Gamma(n)$ in the impulse response function for the cascade of equal-K reservoirs, Nash (1957; 1960) allowed n to take on non-integer values, taken to mean a "fractional" number of reservoirs. This practice has continued since (Dooge and O'Kane 2003). However, when n is non-integer, say replaced by βn where $0 < \beta \le 1$, then equation (4.97) becomes

$$\left(1 + K^\alpha {}^C_0 D_t^\alpha\right)^{\beta n} q(t) = i(t) \qquad . \qquad (4.101)$$

For a positive integer, m, a binomial function $(1 + x)^m$ is equivalent to a finite m-term classical Taylor series expansion of the function about $x = 0$, where the Taylor series is comprised of integer-order differential terms, but for non-integer m the series is infinite (Spanier and Oldham 1987). Consequently, in the case of a non-integer value for βn the binomial expansion has an infinite number of terms and equation (4.99) becomes:

$$\left[\sum_{j=0}^{\infty} a_j {}^C_0 D_t^{j\alpha}\right] q(t) = i(t) \qquad (4.102)$$

which has an infinite number of fractional $j\alpha$-order differential terms. Furthermore, this implies that the free response part of the total solution requires an infinite number of initial conditions. Similarly, for the Nash cascade, where $\alpha = 1$, then the equation reduces to an infinite number of integer j-order differential terms. A further mathematical argument against this fractional n interpretation is that $\dfrac{1}{\left(1 + K^\alpha s^\alpha\right)^n}$ is not rational for non-integer values of n and cannot be expressed as partial fractions. Therefore the notion of a "fractional number" of reservoirs needs revising from a mathematical viewpoint.

4.4.8   A Fractional Order General Storage Equation – Final Form

In order to correctly interpret the Nash cascade model for non-integer βn value, it is proposed that a finite series expansion of the binomial function is necessary. Such an expansion is proved in the following.

Wheatcraft and Meerschaert (2008) have applied the generalised Taylor's formula of Odibat and Shawagfeh (2007) to give a finite representation of non-linear flux in a fractional conservation of mass equation for flow in porous media instead of the infinite series produced by the classical Taylor series. Consequently, the generalised Taylor's formula can be used to derive the finite series expansion of the binomial function of fractional order. Odibat and Shawagfeh's generalised Taylor's formula for a function $f(x)$ expanded about $x = a \geq 0$ is:

$$f(x) = \sum_{j=0}^{n} \frac{(x-a)^{j\beta}}{\Gamma(j\beta+1)} {}_0^C D_t^{j\beta} f(a) + R_n \qquad (4.103)$$

where $0 < \beta \leq 1$, n is a positive integer, and ${}_0^C D_t^{j\beta} f(x)$ is the sequential Caputo fractional derivative defined for $j = 0, 1, ..., n$ as ${}_0^C D_t^{j\beta} f(t) = \underbrace{{}_0^C D_t^{\beta} {}_0^C D_t^{\beta} ... {}_0^C D_t^{\beta}}_{j\text{-times}} f(t)$. R_n is the remainder term.

In the case of a binomial function $f(x) = (1+x)^{n\beta}$, the expansion about $x = 0^+$ is developed as follows.

For the first term ($j = 0^+$):

$$f(0^+) = 1$$

For the second term ($j = 1$):

$${}_0^C D_t^{\beta} f(x) = \frac{\Gamma(n\beta+1)}{\Gamma(n\beta-\beta+1)}(1+x)^{n\beta-\beta}$$

so

72

$$\,_0^C D_t^\beta f(0^+) = \frac{\Gamma(n\beta+1)}{\Gamma(n\beta-\beta+1)} \cdot 1$$

For the third term ($j = 2$):

$$\,_0^C D_t^\beta \,_0^C D_t^\beta f(x) = \,_0^C D_t^\beta \left[\frac{\Gamma(n\beta+1)}{\Gamma(n\beta-\beta+1)} (1+x)^{n\beta-\beta} \right]$$

$$= \frac{\Gamma(n\beta+1)}{\Gamma(n\beta-\beta+1)} \cdot \frac{\Gamma(n\beta-\beta+1)}{\Gamma(n\beta-\beta+1-\beta)} (1+x)^{n\beta-2\beta}$$

$$= \frac{\Gamma(n\beta+1)}{\Gamma(n\beta-2\beta+1)} (1+x)^{n\beta-2\beta}$$

so

$$\,_0^C D_t^\beta \,_0^C D_t^\beta f(0^+) = \frac{\Gamma(n\beta+1)}{\Gamma(n\beta-2\beta+1)} \cdot 1$$

For the fourth term ($j = 3$):

$$\,_0^C D_t^\beta \,_0^C D_t^\beta \,_0^C D_t^\beta f(x) = \,_0^C D_t^\beta \left[\frac{\Gamma(n\beta+1)}{\Gamma(n\beta-2\beta+1)} (1+x)^{n\beta-2\beta} \right]$$

$$= \frac{\Gamma(n\beta+1)}{\Gamma(n\beta-2\beta+1)} \cdot \frac{\Gamma(n\beta-2\beta+1)}{\Gamma(n\beta-2\beta+1-\beta)} (1+x)^{n\beta-3\beta}$$

$$= \frac{\Gamma(n\beta+1)}{\Gamma(n\beta-3\beta+1)} (1+x)^{n\beta-3\beta}$$

so

$$\,_0^C D_t^\beta \,_0^C D_t^\beta \,_0^C D_t^\beta f(0^+) = \frac{\Gamma(n\beta+1)}{\Gamma(n\beta-3\beta+1)} \cdot 1$$

For the (n+1)[th] term, $j = n$, so $\,_0^C D_t^{n\beta} f(x)$ is a constant. Consequently higher order sequential Caputo fractional derivatives are zero, so the series terminates for $j > n$. Therefore, the expansion of the fractional order binomial function is

$$(1+x)^{n\beta} = \sum_{j=0}^{n} \frac{\Gamma(n\beta+1)}{\Gamma[(n-j)\beta+1]\Gamma(j\beta+1)} x^{j\beta} \qquad (4.104)$$

It should be noted that when $\beta = 1$, equation (4.104) reduces to the classical binomial expansion for integer n.

Equation (4.104) is used to expand the binomial in equation (4.101) for the fractional order cascade

$$\left(1 + K^\alpha {}_0^C D_t^\alpha\right)^{n\beta} = \sum_{j=0}^{n} \frac{\Gamma(n\beta+1)}{\Gamma[(n-j)\beta+1]\Gamma(j\beta+1)} \left(K^\alpha {}_0^C D_t^\alpha\right)^{j\beta}$$

Letting $a_j = \dfrac{\Gamma(n\beta+1)}{\Gamma[(n-j)\beta+1]\Gamma(j\beta+1)} K^{j\beta\alpha}$ then

$$\left[\sum_{j=0}^{n} a_j {}_0^C D_t^{j\beta\alpha}\right] q(t) = i(t) \tag{4.105}$$

which can be written as the following initially-relaxed ordinary $\beta n\alpha$-order linear differential equation with constant coefficients, a_j.

$$\left[a_n {}_0^C D_t^{n\beta\alpha} + a_{(n-1)} {}_0^C D_t^{(n-1)\beta\alpha} + \cdots + a_0\right] q(t) = i(t) \quad t \geq 0 \tag{4.106}$$

where ${}_0^C D_t^{j\beta\alpha} q(t)$ is the sequential Caputo fractional derivative defined as

$$\underbrace{{}_0^C D_t^{j\beta\alpha} q(t) = {}_0^C D_t^\beta {}_0^C D_t^\beta \cdots {}_0^C D_t^\beta {}_0^C D_t^\alpha q(t)}_{j\text{-times}} \tag{4.107}$$

Equation (4.106) is a more generalised form of Chow and Kulandaiswamy's (1971) general storage equation (compare with equation (4.66) for $b_r = 0$). This is an ordinary fractional differential equation, with a finite number of terms representing a finite number, n, of virtual reservoirs of sequential order $\alpha\beta$, where $0 < \alpha \leq 1$ and $0 < \beta \leq 1$. When $\alpha = 1$ equation (4.106) reduces to an ordinary fractional differential equation form of Nash's (1960) model for a cascade of βn equal integer-order reservoirs. This corrects the interpretation for a "fractional number of reservoirs". When $\alpha = 1$ and

74

$\beta = 1$, Nash's equation (4.65) is recovered for integer n. Furthermore, the free response part of the total solution to equation (4.106) requires a finite number of initial conditions.

It follows that the new generalised cascade model is still achieved by using a single composite fractional order α in place of $\alpha\beta$ in equation (4.106). In this way conceptualisation of the model using an integer number of reservoirs (i.e. with $\beta = 1$) is adequate.

In order to investigate the form of the free response solution for the generalised fractional cascade model it is necessary to derive the Laplace transform of the Caputo sequential derivative, ${}_{0}^{C}D_{t}^{n\beta}f(t) = \underbrace{{}_{0}^{C}D_{t}^{\beta}\,{}_{0}^{C}D_{t}^{\beta}\ldots{}_{0}^{C}D_{t}^{\beta}}_{j\text{-times}}f(t)$. Since $0 < \beta \le 1$ then, from equation (4.14), for a single Caputo derivative

$$L\{{}_{0}^{C}D_{t}^{\beta}q(t)\} = s^{\beta}Q(s) - s^{\beta-1}q(0^{+}) \tag{4.108}$$

Let $q_{1}(t) = {}_{0}^{C}D_{t}^{\beta}q(t)$ with an initial condition $q_{1}(0^{+}) = {}_{0}^{C}D_{t}^{\beta}q(0^{+})$ then for the sequential derivative let $q_{2}(t) = {}_{0}^{C}D_{t}^{\beta}q_{1}(t)$ with an initial condition $q_{2}(0^{+}) = {}_{0}^{C}D_{t}^{\beta}q_{1}(0^{+})$

Continuing in this manner, then $q_{n}(t) = {}_{0}^{C}D_{t}^{\beta}q_{n-1}(t)$ with an initial condition $q_{n}(0^{+}) = {}_{0}^{C}D_{t}^{\beta}q_{n-1}(0^{+})$

Using equation (4.108) the corresponding Laplace transforms are:

$$L\{{}_{0}^{C}D_{t}^{\beta}q_{1}(t)\} = s^{\beta}Q_{1}(s) - s^{\beta-1}q_{1}(0^{+})$$

$$L\{{}_{0}^{C}D_{t}^{\beta}q_{2}(t)\} = s^{\beta}Q_{2}(s) - s^{\beta-1}q_{2}(0^{+})$$

$\vdots$

$$L\{{}_0^C D_t^\beta q_{n-1}(t)\} = s^\beta Q_{n-1}(s) - s^{\beta-1} q_{n-1}(0^+)$$

Substituting the sequential derivatives into these transforms gives:

$$L\{{}_0^C D_t^\beta q_1(t)\} = L\{{}_0^C D_t^\beta {}_0^C D_t^\beta q(t)\} = s^\beta \left(s^\beta Q(s) - s^{\beta-1} q(0^+)\right) - s^{\beta-1} q_1(0^+)$$

$$= s^{2\beta} Q(s) - s^{2\beta-1} q(0^+) - s^{\beta-1} q_1(0^+)$$

$$L\{{}_0^C D_t^\beta q_2(t)\} = L\{{}_0^C D_t^\beta {}_0^C D_t^\beta q_1(t)\} = s^\beta \left(s^{2\beta} Q(s) - s^{2\beta-1} q(0^+) - s^{\beta-1} q_1(0^+)\right) - s^{\beta-1} q_2(0^+)$$

$$= s^{3\beta} Q(s) - s^{3\beta-1} q(0^+) - s^{2\beta-1} q_1(0^+) - s^{\beta-1} q_2(0^+)$$

Continuing gives the general form for any integer number, n, of sequential derivatives of equal order β as

$$L\{{}_0^C D_t^{n\beta} q(t)\} = s^{n\beta} Q(s) - \sum_{j=0}^{n-1} s^{(n-1)j\beta-1} q^{(j\beta)}(0^+) \qquad (4.109)$$

It is worth noting that equation (4.109) is the equivalent to that for the Riemann-Liouville sequential derivative (Ortigueira 2003).

The consequence of equation (4.109) is that the free response part of the total solution to equation (4.106) requires a substantial number of initial conditions expressed as functions of the Caputo derivatives evaluated at $t = 0^+$. This raises the issue of the complexity of the generalised cascade model with multiple reservoirs for practical application where the system is not initially at rest (unlike the rainfall-runoff transformation system assumption). Furthermore, if Lorenzo and Hartley's (2008) approach is taken to overcome the restriction of using constant initialisation with the Caputo derivative and time varying initialisation functions are introduced then each derivative term requires an associated initialisation function. This would add

substantially to the model complexity. The implications for the development of parsimonious fractional order cascade models are significant. Consequently, it is proposed that a single fractional order time-lagged linear reservoir subject to a single initial condition will be adequate for modelling the rainfall-streamflow transformation. This proposal will be tested using observed flood event data (re. section 5.4).

4.4.9 Initialisation Function Considerations

In the derivation of the fractional order models considered the Caputo fractional derivative has been used which, in accordance with equation (4.37), infers that the $0 < \alpha \leq 1$ system is subject to a constant initialisation function in the sense of Lorenzo and Hartley (2008) to represent the mixing effect of "old" (stored) water and "new" water observed in streamflow chemistry. This initialisation function is taken as the initial streamflow at the start of the event. Given that the initialisation function representing the surface-subsurface storage-flux history is not easily defined (for example see Kirchner (2003)) then the identification of the true function is likely to require further field studies of the interaction between the "old" and "new" water in the generation of total streamflow. For the purposes of this work the constant initialisation has been used (recall assumption 8 in section 4.4.1).

A recommendation for potential future development is to assume that the baseflow recession characterises the surface-subsurface storage-flux history of a river and that it can be represented by the new theoretical general equation (4.80). It should be noted that the derivation of the required Lorenzo and Hartley (2008) initialisation function, ψ, involves determining Laplace transforms of terms which are not always available in closed form (Hartley and Lorenzo 2008).

4.5 Summary

Assuming that the time-history of water storage/flow states in the surface/subsurface catchment system can be represented by a fractional-order derivative form of an initially un-relaxed, lumped cascade of time-lagged, linear reservoirs a new theoretical model for the transformation of effective rainfall to total streamflow has been derived. The classical unit hydrograph for rainfall-runoff modelling appears as a special case (for initially relaxed, integer-order systems). The properties of cascades with equal and unequal storage characteristics and varying numbers of reservoirs have been investigated and, in particular, the implications of the initial conditions required. Consequently, the classical Nash cascade of n reservoirs has been reinterpreted for fractional n and Cavallini's (2002) proposed ansatz for one form of a fractional instantaneous unit hydrograph model has been proved (in a corrected form). Furthermore, two new mathematical results for the fractional calculus have been derived, namely a finite series expansion of the binomial function for a fractional power and the Laplace transform of the Caputo sequential derivative.

Chapter 5 Rainfall-Streamflow Model Testing

5.1   Methodology

The fractional order theory was tested using a selection of observed rainfall-streamflow events for a range of catchment scales provided from the UK Flood Event Archive (courtesy of the Centre for Ecology and Hydrology). The application of the fractional order theory to the special case of effective rainfall to stormflow (runoff) modelling was tested on the pre-processed data set published by Bree (1978). The mathematical limitations of the numerical evaluation of the fractional order impulse response function are identified and a novel series solution developed from the work of Wang and Wu (1983) is presented in section 5.2.

The calibration of the model equations was undertaken using the genetic algorithm (GA) technique to utilise its superior parameter-fitting capability over the classical method of moments reported by Dong (2008), and Rigden and Borthwick (2008). The GA control parameters and fitness functions used are presented in section 5.3.

In the light of the theoretical study of the influence of initial conditions on the development of parsimonious fractional order cascade models (re. section 4.4.8), particularly where sequential fractional order reservoirs are used, a single fractional-order, time-lagged, linear reservoir subject to a single initial condition was used to test the viability of the new theory for modelling the rainfall-streamflow transformation. For the simpler case of the effective (net) rainfall to stormflow (runoff) transformation uninitialized cascade models were tested against the classical Nash cascade. The details of the test catchments and flood events are given in section 5.4.

5.2 Numerical Methods

5.2.1 Limitations of the Convolution Formulation

Koutsoyiannis and Xanthopoulos (1989) exemplify the method commonly used for the identification of the parameters of a synthetic instantaneous unit hydrograph (i.e. the impulse response function) model, namely that parameter optimisation is done by minimisation of a fitness (objective) function. They present the following four steps:

1. calculation of the instantaneous unit hydrograph (IUH) ordinates using a chosen set of parameter values in the theoretical model equation,

2. scaling the IUH to calculate the synthetic unit hydrograph corresponding to the rainfall duration,

3. calculation of the predicted runoff hydrograph by convolution of the synthetic unit hydrograph with the effective rainfall hyetograph, and

4. calculation of the fitness function (i.e. the measure of the error between the observed and predicted hydrographs).

Step 3 is the classical unit hydrograph convolution integral (equation (4.44)) evaluated from the initial time, $t = 0^+$, to the time of interest t. This approach is almost universally used in unit hydrograph modelling (Dooge and O'Kane 2003). However, this presents a problem for the numerical evaluation of the fractional order impulse response function models of single (unique K value) reservoirs developed in section 4.4 at time zero, because of the $t^{\alpha-1}$ multiplier with $0 < \alpha \leq 1$. Recalling equation (4.77) for the Laplace transform of the impulse response function for a single fractional order reservoir:

$$H(s) = \frac{1}{K^\alpha \left(s^\alpha + \frac{1}{K^\alpha} \right)} \tag{5.1}$$

and applying the initial value theorem of the Laplace transform (Doetsch 1974) of a function $f(t)$

$$f(0^+) = \lim_{t \to 0^+} f(t) = \lim_{s \to \infty} s F(s) \tag{5.2}$$

gives

$$h(0^+) = \lim_{s \to \infty} \frac{s}{K^\alpha \left(s^\alpha + \frac{1}{K^\alpha} \right)} = \infty \tag{5.3}$$

This demonstrates the unbounded behaviour of the impulse response function at $t = 0$, which is a common feature of fractional relaxation equation modelling (Podlubny 1999). It also explains Cavallini's (2006) remarks that expressing the IUH as the difference of two solutions of first-order fractional differential equations may not always produce a positive definite result.

5.2.2 Unit Step Response Formulation

In order to overcome the initial value problem of the impulse response function it is necessary to note that if the expression in equation (5.3) is multiplied by $1/s$ it tends to zero as $s \to \infty$. From the integral theorem of the Laplace transform (Doetsch 1974)

$$L \left\{ \int_0^t f(\tau) d\tau \right\} = \frac{1}{s} F(s) \tag{5.4}$$

then this requires recasting the original model so as to obtain the integral form of the impulse response function (i.e. the step response function). Fortunately, this is possible given fact that the rainfall input function, $i(t)$, can be approximated by m discrete rainfall pulses of duration Δt as this is typically how it is measured in practice (re. section 4.3.1). Recalling equation (4.39), Wang and Wu (1983) represented this pulse hyetograph as a series of unit step functions, $U(t)$, whereby

$$i(t) = \sum_{j=0}^{m} w_j U(t - j\Delta t)$$

with

$$w_j = i_j - i_{j-1} \quad \text{for } j = 1, 2, ..., n$$

and expressed the Laplace transform as

$$I(s) = \sum_{j=0}^{m} \frac{w_j e^{-j\Delta t s}}{s} \tag{5.5}$$

Wang and Wu went on to incorporate this result in the Laplace transforms of the integer-order differential equations for the cascades of linear reservoirs and lag and route models (c.f. section 4.3.3 and 4.3.4) and produce solutions in terms of the step response functions that did not require the convolution integral for evaluation. This technique is developed here in order to utilise the common $1/s$ factor of equation (5.5).

Recalling equation (4.76), the Laplace transform of the differential equation of the fractional order reservoir model

$$Q(s) = \frac{I(s)}{K^{\alpha}\left(s^{\alpha} + \frac{1}{K^{\alpha}}\right)} + \frac{s^{\alpha-1}Q(0^+)}{\left(s^{\alpha} + \frac{1}{K^{\alpha}}\right)} \tag{5.6}$$

Only the first term (the forced response) need be considered since the free response (second term) is independent of $I(s)$. Replacing $I(s)$ with equation (5.5) then the forced response is

$$Q_{forced}(s) = \frac{\displaystyle\sum_{j=0}^{m} w_j e^{-j\Delta t s}}{sK^{\alpha}\left(s^{\alpha} + \frac{1}{K^{\alpha}}\right)} \tag{5.7}$$

Comparing with equation (5.1) this can be written

$$Q_{forced}(s) = \frac{H(s)}{s} \sum_{j=0}^{m} w_j e^{-j\Delta t s}$$

or

83

$$Q_{forced}(s) = G(s) \sum_{j=0}^{m} w_j e^{-j\Delta t s} \tag{5.8}$$

where

$$G(s) = \frac{1}{sK^\alpha \left(s^\alpha + \frac{1}{K^\alpha}\right)} \tag{5.9}$$

It should be noted that equation (5.8) can be used generally for other forms of $G(s)$ representing other models.

Using equation (4.22) the inverse Laplace transform of $G(s)$ is the unit step response function, $g(t)$

$$g(t) = \frac{1}{K^\alpha} t^\alpha E_{\alpha,\alpha+1}\left[-\left(\frac{t}{K}\right)^\alpha\right] \tag{5.10}$$

Now applying the initial value theorem to equation (5.9)

$$G(0^+) = \lim_{s \to \infty} sG(s) = \frac{1}{K^\alpha \left(s^\alpha + \frac{1}{K^\alpha}\right)} = 0 \tag{5.11}$$

which is now bounded.

Using the 2nd shift theorem then the inverse Laplace transform of equation (5.8) for the forced response of the single fractional order linear reservoir can now be found as

$$q_{forced}(t) = \frac{1}{K^\alpha} \sum_{j=0}^{m} w_j U(t - j\Delta t)(t - j\Delta t)^\alpha E_{\alpha,\alpha+1}\left[-\left(\frac{t - j\Delta t}{K}\right)^\alpha\right] \tag{5.12}$$

As noted above, the free response is unchanged from the original derivation (equation (4.80)), and can be added to the forced response to give the total solution.

5.2.3 General Unit Step Response Model

Consequently, from equation (4.93) the step response function for the cascade of n initially relaxed, equal (K, T) fractional-order lag and route elements can be obtained

$$G_n(s) = \frac{e^{-nTs}}{sK^{na}\left(s^{\alpha} + \frac{1}{K^{\alpha}}\right)^n}$$

(5.13)

Using equation (4.22) and the 2nd shift theorem the inverse Laplace transform gives

$$g(t) = \frac{U(t-nT)(t-nT)^{n\alpha} E_{\alpha,n\alpha+1}^n\left[-\left(\frac{(t-nT)}{K}\right)^{\alpha}\right]}{K^{n\alpha}}$$

(5.14)

Again using the 2nd shift theorem then the inverse Laplace transform of the general equation (5.8) is obtained as

$$q_{forced}(t) = \frac{1}{K^{n\alpha}} \sum_{j=0}^{m} w_j U(t-nT-j\Delta t)(t-nT-j\Delta t)^{n\alpha} E_{\alpha,n\alpha+1}^n\left[-\left(\frac{(t-nT-j\Delta t)}{K}\right)^{\alpha}\right]$$

(5.15)

As before, the free response can be added to the forced response to give the total solution.

Equation (5.15) is the most general form of the models. The other models can be obtained as particular cases as follows:

- $n = 1$ gives the single reservoir models

- $\alpha = 1$ gives the classical integer order reservoir models

- $T = 0$ gives the unlagged models

It should be noted that the case for the single integer-order lag and route model ($n = 1$, $\alpha = 1$) derived from equation (5.15) corrects that presented in Wang and Wu (1983).

The numerical solution of equation (5.15) was undertaken using a bespoke computer program written for this study. The 3-parameter Mittag-Leffler function (equation (4.26)) could only be approximated in a computer by truncating the infinite series for terms with vanishingly small values. For calibration of the models with the observed events the streamflow units (in m^3/s) were converted into mm/hour (over the area of the

85

catchment concerned) to be consistent with the rainfall units. For presentation and comparison purposes, the predicted streamflow units were converted back into m^3/s.

5.2.4 Rainfall Loss Model

If it is assumed that there is a "loss" of water from the measured rainfall due to infiltration and evapotranspiration, which does not contribute to the measured streamflow event, then a rainfall loss model has to be applied. However, it should be noted that infiltrated water has a contributory effect on subsequent streamflow events because of baseflow recharge to the stream. In order to test the influence of the loss model on the performance of the fractional order streamflow models studied, observed storm events were run for the case of the observed (total) rainfall, $i_{obs}(t)$ (i.e. without a loss model), and of effective (net) rainfall, $i(t)$ (i.e. having applied a loss model).

As reviewed in section 2.2.1, there are a number of approaches that have been proposed for loss modelling, including:

- an exponential decay function to simulate infiltration (Horton 1940);

- a constant loss rate, ϕ-index, such that the effective rainfall volume equals the runoff volume (Cook 1946);

- a proportional loss rate, percentage runoff (*PR*), to represent contributing areas to stormflow such that the effective rainfall volume equals the runoff volume (Natural Environment Research Council 1975a);

- a low pass filter applied to rainfall based on a catchment wetness index (*CWI*) to represent soil moisture content (Whitehead *et al.* 1979; Jakeman *et al.* 1990);

- a non-linear filter based on streamflow to replace the *CWI* (Young and Beven 1991; 1994); and

- a Probability Distributed Model (PDM) of catchment moisture storage (Moore and Clarke 1981; Moore 1985).

The fitting of an infiltration-type model is dependent on the initial infiltration rate and by variation across the catchment area (Beven 2000). However, no infiltration capacity data was available for the Flood Event Archive catchments. The PDM model used in the revitalised FSR/FEH rainfall-runoff (ReFH) method (Kjeldsen *et al.* 2005) needs an initial soil moisture content which, for the ReFH model, is estimated from a daily soil moisture accounting model applied to a year's record of daily catchment average rainfall and evaporation. Again this antecedent time series data was unavailable for the Flood Event Archive events. Young and Beven's (1991; 1994) simplified rainfall filter requires less data and fewer parameters than the *CWI* approach to simulate soil moisture storage change, so that the effective rainfall can be calculated as a function of the product of observed rainfall and time-lagged streamflow. Consequently the ϕ-index, *PR*, and non-linear filter based on Young and Beven (1994) were selected for loss model testing.

The effective rainfall, $i(t)$, for the ϕ-index model is given by

$$i(t) = i_{obs}(t) - \phi \qquad (5.16)$$

where ϕ is the constant loss rate.

The effective rainfall, $i(t)$, for the *PR* model is given by

$$i(t) = PR \cdot i_{obs}(t) \qquad (5.17)$$

where *PR* is the percentage runoff.

It should be noted that separation of the observed streamflow hydrographs into stormflow and baseflow (as undertaken in traditional UH analysis) is not required since the objective is to apply the fractional order systems models to predict the streamflow directly. Given that the actual catchment system is open (non-conservative) then the concept of matching the effective rainfall and stormflow volumes so as to specify the ϕ-index or PR is not applicable, unlike the integer order system. This, however, raises the question of the validity of these loss models in the context of the fractional order system approach.

The effective rainfall for the non-linear filter was assumed to be a product of the observed rainfall, $i_{obs}(t)$, and a power function of the calculated (total) streamflow $q(t)$ and the previous model timestep, Δt, after Young and Beven (1994) whereby

$$ i(t) = C i_{obs}(t) q^P(t - \Delta t) \tag{5.18} $$

and C and P are the parameters, such that $0 \le C \le 1$ and $0 \le P \le 1$.

The parameters of the loss models were fitted using observed total rainfall and streamflow event data as explained in section 5.3. Each model was tested on a set of storm events for a sample catchment in order to select a single loss model for use with a broader range of catchments (re. section 5.4.2).

5.3   Calibration

5.3.1   Genetic Algorithm

The principles of the genetic algorithm (GA) and its suitability for the calibration of rainfall-streamflow models have been summarised in section 2.6.1. In the GA an initial population of randomly selected sets of parameter values is allowed to "evolve" by applying reproduction, crossover and mutation operations on selected "individuals" of

the parent population (Goldberg 1989). Each individual is a single set of parameter values representing a unique model solution. The set of model parameters is encoded as a string of numerical values. Each model parameter can take values within a user-defined range so that the search space is constrained (e.g. to avoid unrealistic values being generated). The GA is repeated for a number of generations or until an adequately fit individual is found. The fitness of each individual is a numerical measure comparing model prediction with observations. The reproduction operator ensures that the best individuals of each population are retained. The key user-defined components of the GA are:

- the number of individuals in the population;

- the number of generations performed by the GA;

- the method of selecting individuals for reproduction, crossover and mutation;

- the probability of undertaking crossover between selected individuals;

- the probability of undertaking mutation on a selected individual; and

- the fitness function.

The population size and number of generations influence the extent of the search space during the GA run and are problem-specific. The selection techniques are based upon a probabilistic rule where the chance of a particular individual being selected is dependent on its fitness (e.g. proportional to the fitness as in a weighted "roulette wheel" simulation). A pseudorandom number generator is used in the implementation of the GA to pick values between 0 and 1. In practice, tournament selection is often used where a group of individuals is sampled at random from the population and the best in the group is selected based on fitness (Goldberg 1989). This avoids the potential with the roulette wheel approach for repeated selection of the same individuals which can

lead to convergence to a local optimum. The probabilities of crossover and mutation determine whether selected individuals are crossed or mutated. The crossover involves randomly selecting portions of the strings representing 2 parent individuals and crossing them between the 2 parents. Typically 2 points of crossover performs better than a single point (Goldberg 1989). Mutation involves randomly selecting a portion of the string representing an individual and replacing the model parameter values with new values drawn uniformly from the range for each parameter. The crossover and mutation operators simulate the evolution of fitter individuals whilst attempting to avoid convergence to a local optimum. Determining suitable values for these GA control parameters (population size, number of generations, tournament size, crossover probability and mutation probability) is problem specific and requires initial trials on sample data for the problem.

5.3.2   Fitness Function

In order to measure the error between the observed and model predicted streamflow necessary for the GA calibration a fitness function was evaluated based on two objective functions. The first objective was the commonly-used root mean square error, *RMSE* given by

$$RMSE = \sqrt{\frac{1}{N}\sum_{t=1}^{N}\left(q_{obs,t} - q_t(\theta)\right)^2} \qquad (5.19)$$

where $q_{obs,t}$ is the observed streamflow at time t, $q_t(\theta)$ is the streamflow predicted by the model at time t, θ is the set of model parameters, and N is the number of streamflow values used in the calibration.

To account for the limitations of the *RMSE* (re. section 2.6.3), a second objective function was proposed that would fit the observed hydrograph shape across the range of

flows. A novel approach was to compare the slopes (de Vos and Rientjes 2007; Borthwick *et al.* 2008) of the observed and predicted hydrographs, expressed as the root mean square error of slope, *RMSslope*, given by

$$RMSslope = \sqrt{\frac{1}{N}\sum_{t=1}^{N}\left(slope_{obs,t} - slope_t(\theta)\right)^2}$$

(5.20)

where

$$slope_t = \frac{q_{t+1} - q_{t-1}}{2\Delta t}$$

(5.21)

for $1 < t < N$ using a central difference approximation; and at the end points of the time series the slopes were estimated using forward and backward differences as follows:

$$slope_1 = \frac{q_2 - q_1}{\Delta t}$$

(5.22)

$$slope_N = \frac{q_N - q_{N-1}}{\Delta t}$$

(5.23)

where Δt is the timestep (hourly) and q_t is the streamflow at a particular time, t.

In a previous study Borthwick *et al.* (2008) have tested the effect of the fitness function based on *RMSE* and *RMSslope* using the conceptual daily rainfall-streamflow model, SIXPAR (Gupta 1982) which is a reduced parameter version of the Sacramento soil moisture accounting model, SAC-SMA (Burnash *et al.* 1973). For comparison with Duan et al's (1992) study the same 200 day synthetic daily series of precipitation and streamflow for a known set of parameter values was used. When used singly in a GA search, the *RMSE* and *RMSslope* objective functions identified different optima but failed to find the global solution. However, when combined as a weighted sum, the region of the global solution was detected.

To combine the influence of the two objective functions, therefore, a weighted average fitness measure was used given by:

$$Fitness = w_1 RMSE + w_2 RMS_{slope} \qquad (5.24)$$

where w_1 and w_2 are weightings such that $w_1 + w_2 = 1$.

In order to establish appropriate values of the GA control parameters and the fitness function weightings w_1 and w_2 initial calibration tests, where the key parameters were varied in turn, were undertaken to fit an initialised, single, fractional-order, time-lagged, linear reservoir with a non-linear rainfall filter to a sample observed catchment event.

5.3.3 Model Parameter Space

The problems of parameter interaction and sensitivity in the calibration of rainfall-streamflow models have been reviewed in section 2.6. The parameter space is defined by the values of parameters giving rise to model solutions of acceptable fitness. The space was investigated for a sample catchment by using a set of parameters calibrated for an observed event to run the fractional-order linear reservoir model and predict the streamflow for other observed events (i.e. validation). In this way the performance of calibration sets based on different events can be compared with each other for a given catchment. This is important for the assessment of how well the proposed model fits the catchment.

In addition, visualization of the parameter and fitness function spaces is valuable for identification of the robustness of the calibration process. In a previous study Borthwick *et al.* (2008) have tested the use of clustering and visualization for the calibration of the conceptual daily rainfall-streamflow model, SIXPAR (Gupta 1982) using the interactive calibration-support system developed by Packham *et al* (2005). The system uses the GA and clustering techniques to visualize the optimization of

multidimensional models and to evaluate robust regions of the parameter spaces. The system includes the following features:

- Rapid sampling of the feasible parameter and objective spaces by using short GA runs. The low number of generations avoids convergence onto a single optimum region, and the use of moderately high crossover and mutation rates, particularly if duplicate solutions are generated, maintains diversity.

- High dimensional visualization of the parameter and objective function spaces, including 2-D and 3-D views, and parallel coordinates to aid in identification of parameter interaction and model sensitivity to particular parameters.

- A kernel density estimation algorithm (Silverman 1986) to identify clusters of solutions in either the parameter or objective function space, and display using colour intensity in proportion to fitness. A univariate kernel density estimate of each variable is made and the minima from each estimate are computed. The bounds of each cluster are thus identified in each variable. The first cluster displayed to the user is that containing the highest fitness from the GA.

- Interactive features so that the user can quickly zoom into subspaces and select regions for additional GA searches to generate further solutions or for the identification of clusters – either automatically or manually. All the solutions (i.e. high and low fitness) generated by the GA search are retained by the system. In this way the user has control over both how and where the investigation of the search space takes place, including regions outside of clusters of good solutions found by the GA.

The parameter space for the initialised, single, fractional-order, time-lagged, linear reservoir model with a non-linear rainfall filter was visualised for a sample observed

93

flow event using the interactive calibration-support system developed by Packham *et al* (2005). Furthermore, the visualisation was undertaken for events exhibiting anomalous calibration behaviour.

5.3.4 Nash-Sutcliffe Efficiency

For presentation purposes and as a means of comparing the model performance against other published research the commonly used Nash-Sutcliffe efficiency, NSE (Nash and Sutcliffe 1970), was also evaluated using

$$NSE = 1 - \left(\frac{\sum_{t=1}^{N} (q_{obs,t} - q_t(\theta))^2}{\sum_{t=1}^{N} (q_{obs,t} - \bar{q}_{obs})^2} \right) \tag{5.25}$$

where $\bar{q}_{obs}$ is the average observed streamflow.

5.4 Test Catchments

5.4.1 Rainfall-Runoff Model Testing

In order to assess the applicability of fractional order cascades to the traditional effective (net) rainfall to runoff (stormflow) modelling problem an initially relaxed (i.e. zero initial condition) cascade of fractional reservoirs was tested for the following 3 conditions:

1. the cascade of n equal-K fractional linear reservoirs subject to a time lag, T;

2. the cascade of 2 unequal-K fractional linear reservoirs (Cavallini's ansatz); and

3. the cascade of n equal-K 1st order linear reservoirs (the classical Nash cascade).

A sample dataset of 22 rainfall-streamflow events recorded for the River Nenagh catchment, Ireland has been processed into effective rainfall and runoff by Bree (1978), and Mohan and Vijayalakshmi (2008) have successfully applied the GA to the

calibration of the classical Nash cascade for this dataset. This effective rainfall-runoff dataset was used to test the application of the initially-relaxed cascade of fractional order reservoirs. Bree's (1978) processing of the observed total rainfall and streamflow data is summarised below.

The Nenagh catchment has an area of 295km^2. Bree (1978) used the 3 hourly rainfall depth recorded by the single autographic rain gauge on the catchment for the mean areal rainfall. The 3 hourly streamflow discharges were obtained from the velocity-area gauging station at Clarianna. The 22 isolated flood flows comprised 19 winter and 3 autumn events. The percentage runoff loss model of the UK Flood Studies Report (Natural Environment Research Council 1975a) was used to derive the effective rainfall from the observed values for each event, so that the volume of effective rainfall equalled the volume of runoff. The runoff was obtained from the observed streamflow hydrograph by subtracting an assumed constant baseflow. For a given flow event, the baseflow value was taken as equal to the final observed streamflow from the recession hydrograph of the previous event (i.e. the streamflow at the start of the rising hydrograph for the current flood event).

For the model simulations the start time ($t = 0$) for each event was taken as that for the beginning of the effective rainfall hyetograph.

5.4.2   Rainfall-Streamflow Model Testing

For the testing of the initialised, single, fractional-order, time-lagged, linear reservoir for modelling the observed (total) rainfall-streamflow transformation a selection of flood events from 11 representative UK catchments was used. Catchments were chosen that covered a range of sizes (from 22km^2 to 510km^2). In addition, the events used were

those drawn from the Flood Event Archive (provided with the permission of the Centre for Ecology and Hydrology, UK) that were deemed reliable for use in previous published work (Institute of Hydrology 1999; Kjeldsen *et al.* 2005). A summary of each catchment is given in Table 5.1.

Gauge No.	River and Catchment	Area (km^2)	AAR (mm)	% Area Urbanised
46005	East Dart at Bellever	22.22	2096	0.00
30004	Lymn at Partney Mill	60.11	685	1.00
74001	Duddon at Duddon Hall	86.02	2265	0.00
25005	Leven at Leven Bridge	194.54	726	1.00
54004	Sowe at Stoneleigh	263.23	667	13.00
37001	Roding at Redbridge	301.12	607	4.00
66011	Conwy at Cwm Llanerch	339.62	2041	0.10
28026	Anker at Polesworth	370.50	653	6.00
7001	Findhorn at Shenachie	415.87	1217	0.02
57005	Taff at Pontypridd	451.88	1832	4.00
72006	Lune at Kirkby Lonsdale	509.98	1652	0.10

Table 5.1 Summary catchment properties

AAR is Average annual rainfall.

Full details of each catchment and river gauging station is available from HiFlows (Environment Agency 2009).

The UK Flood Event Archive comprises catchment average rainfall profiles (CARPs) and associated hourly streamflow data for isolated flood events used in the production of the Flood Studies Report (Natural Environment Research Council 1975a) and Flood Estimation Handbook (Institute of Hydrology 1999). The CARPs were derived from observed hourly point rainfall from autographic gauges on each catchment. The CARPs for events up to the end of 1975 were calculated using a weighted average of the

individual gauge observations based on the reciprocal of the distance from the centroid of the catchment (Natural Environment Research Council 1975b). For events from 1976, the CARPs were calculated using an area-weighted average based on a development of the Thiessen polygon approach (Diskin 1970) where a rectangular mesh was used to subdivide the catchment. The mesh space closest to a given gauge was used to estimate the proportion of the total catchment area associated with the gauge (Jones 1983; Institute of Hydrology 1999). In both techniques used in creating the CARPs for the Flood Event Archive where more than one autographic gauge was available the averaging involved adjusting the time origin of the observed point hyetographs so that the centroids were matched. This required selecting events where the timing of the centroids was close to avoid averaging very different profiles. This implies that each storm event included in the archive was reasonably stationary over the duration of the event.

The streamflow hydrographs in the Flood Event Archive were derived from the observed hourly stages from river gauges using the associated rating curve for the gauge. The flood events were selected on the basis of having a significant peak flow and so that the streamflow hydrographs were separated by a reasonably well defined recession (before and after the event).

For the model simulations the start time ($t = 0$) for each event was taken as that for the beginning of the rainfall hyetograph (CARP). The initial condition, q_0, required for the evaluation of the free response term, equation (4.80), of the fractional order reservoir model was taken as the observed streamflow at $t = 0$. This initial condition is the constant initialisation function implicit in the Caputo fractional derivative which is

assumed to represent the mixing effect of "old" (stored) water and "new" water observed in streamflow chemistry (re. section 4.4.1).

The influence of the selection of the rainfall loss model on the performance of the fractional order reservoir system was investigated by applying the ϕ-index, *PR* and non-linear filter approaches in turn on the observed rain storm events for the East Dart catchment at Bellever (river gauge no. 46005) and assessing the fit of the predicted and observed streamflow.

Chapter 6 Results

6.1 Rainfall-Runoff Model Results for River Nenagh

The summary results for the GA fitting of the parameters of an initially relaxed (i.e. zero initial condition) cascade of n equal-K fractional linear reservoirs subject to a time lag, T to Bree's (1978) pre-processed effective rainfall-runoff dataset for the River Nenagh (re. section 5.4.1) are shown in Table 6.1. K and T are presented in hours.

Event	K	n	α	T	nK^{α}	Fitness	NSE
1	7.898	1.123	0.990	0.569	8.688	0.027	0.953
2	4.309	1.466	0.999	0.836	6.308	0.015	0.988
3	3.387	1.289	0.820	0.969	3.505	0.035	0.923
4	4.083	1.572	0.908	0.917	5.639	0.081	0.839
5	3.071	1.106	0.701	1.603	2.429	0.030	0.876
6	4.219	1.205	0.818	1.668	3.912	0.031	0.953
7	7.538	1.108	0.993	1.817	8.235	0.028	0.943
8	5.155	1.327	0.991	0.317	6.740	0.015	0.990
9	3.986	1.041	0.878	1.379	3.505	0.014	0.991
10	1.954	2.232	0.846	0.305	3.934	0.014	0.988
11	2.215	1.357	0.700	1.078	2.368	0.031	0.937
12	2.631	1.531	0.918	0.537	3.721	0.067	0.970
13	2.900	1.578	0.842	1.013	3.868	0.034	0.976
14	2.715	1.594	0.834	0.950	3.667	0.020	0.988
15	3.468	1.746	0.827	0.815	4.883	0.024	0.943
16	4.130	1.409	0.910	0.915	5.122	0.018	0.956
17	2.044	1.532	0.701	0.744	2.529	0.034	0.921
18	1.372	1.711	0.837	1.556	2.230	0.069	0.924
19	2.879	1.434	0.833	1.762	3.460	0.033	0.979
20	1.616	3.321	0.950	0.445	5.239	0.049	0.973
21	4.755	1.075	0.964	1.617	4.833	0.049	0.991
22	5.611	1.051	0.968	0.738	5.581	0.019	0.990

Table 6.1 R. Nenagh results for cascade of time-lagged equal fractional reservoirs

The following Figures 6.1 and 6.2 show the predicted and observed runoff hydrographs together with the effective event rainfall hyetograph for the best and worst cases for the River Nenagh associated with Table 6.1. A full set of results plots is available in Appendix A.
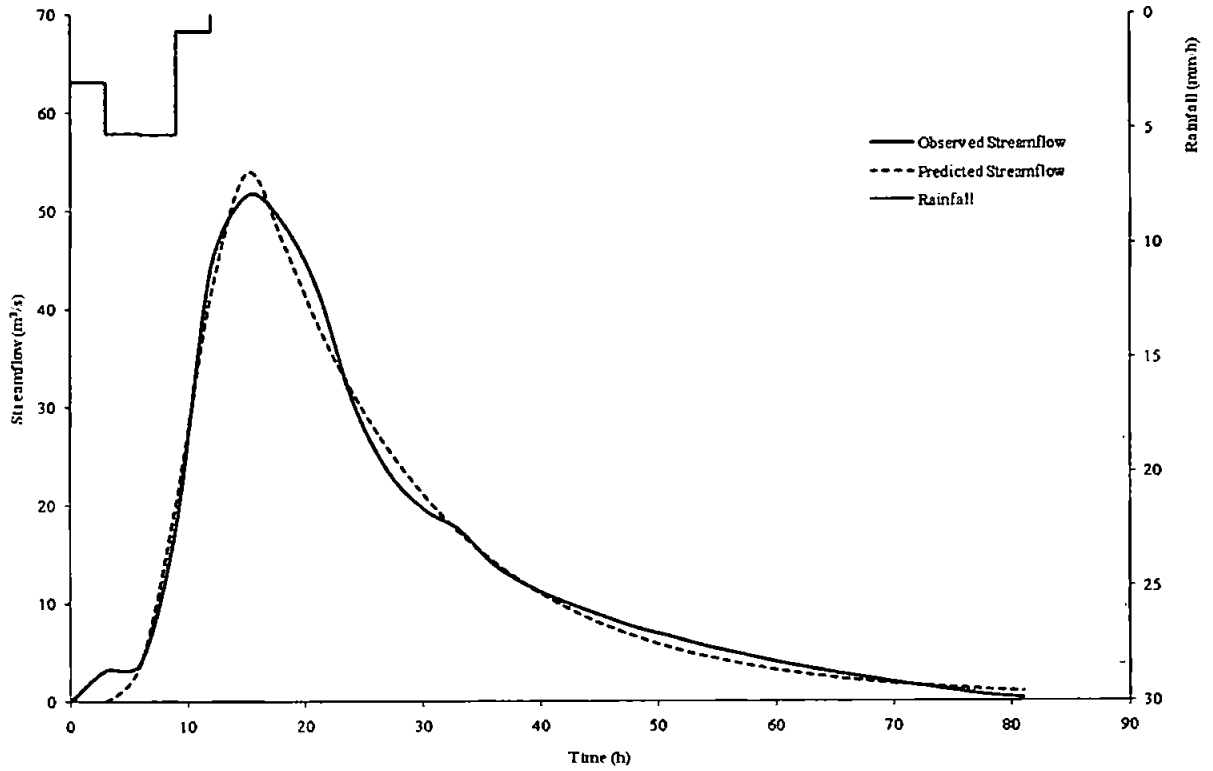
Figure 6.1 Predicted and observed results for event 21
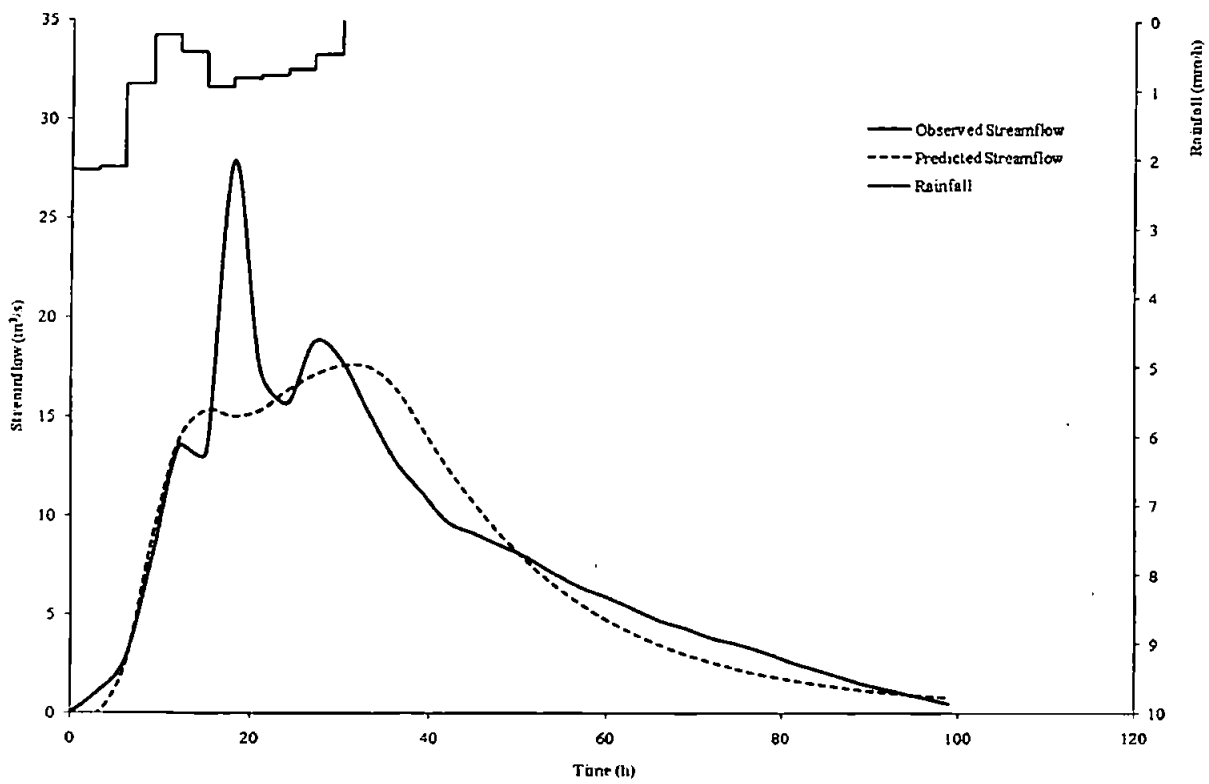
Figure 6.2 Predicted and observed results for event 04

The summary results for the GA fitting of the initially relaxed cascade of two unequal-K fractional linear reservoirs to the effective rainfall-runoff events on the River Nenagh are shown in Table 6.2.

Event	K_1	K_2	α	$K_1^\alpha + K_2^\alpha$	Fitness	NSE
1	1.012	8.278	0.997	9.238	0.028	0.950
2	4.044	3.107	1.000	7.151	0.021	0.973
3	4.467	1.201	0.939	5.265	0.038	0.904
4	2.586	5.109	0.972	7.399	0.082	0.833
5	1.486	4.063	0.891	4.910	0.048	0.755
6	3.722	2.929	1.000	6.651	0.073	0.792
7	5.911	3.532	0.997	9.398	0.036	0.907
8	2.126	4.747	0.944	6.389	0.015	0.990
9	1.305	3.589	0.999	4.889	0.029	0.953
10	4.268	1.573	0.999	5.834	0.020	0.974
11	4.166	1.002	0.957	4.920	0.055	0.859
12	1.595	3.315	0.986	4.844	0.079	0.955
13	3.808	2.262	1.000	6.070	0.063	0.915
14	2.084	3.884	0.992	5.914	0.044	0.943
15	5.589	2.249	0.989	7.713	0.032	0.932
16	4.981	2.122	0.995	7.055	0.022	0.931
17	2.618	1.563	0.875	3.799	0.051	0.852
18	2.832	2.974	1.000	5.806	0.147	0.735
19	3.261	3.698	0.998	6.942	0.091	0.856
20	4.078	4.169	0.999	8.235	0.153	0.746
21	2.917	3.208	1.000	6.125	0.124	0.937
22	1.483	4.498	0.927	5.471	0.024	0.984

Table 6.2 R. Nenagh results for cascade of 2 unequal fractional reservoirs

The following Figures 6.3 and 6.4 show the predicted and observed runoff hydrographs together with the effective event rainfall hyetograph for the best and worst cases for the River Nenagh associated with Table 6.2. A full set of results plots is available in Appendix B.
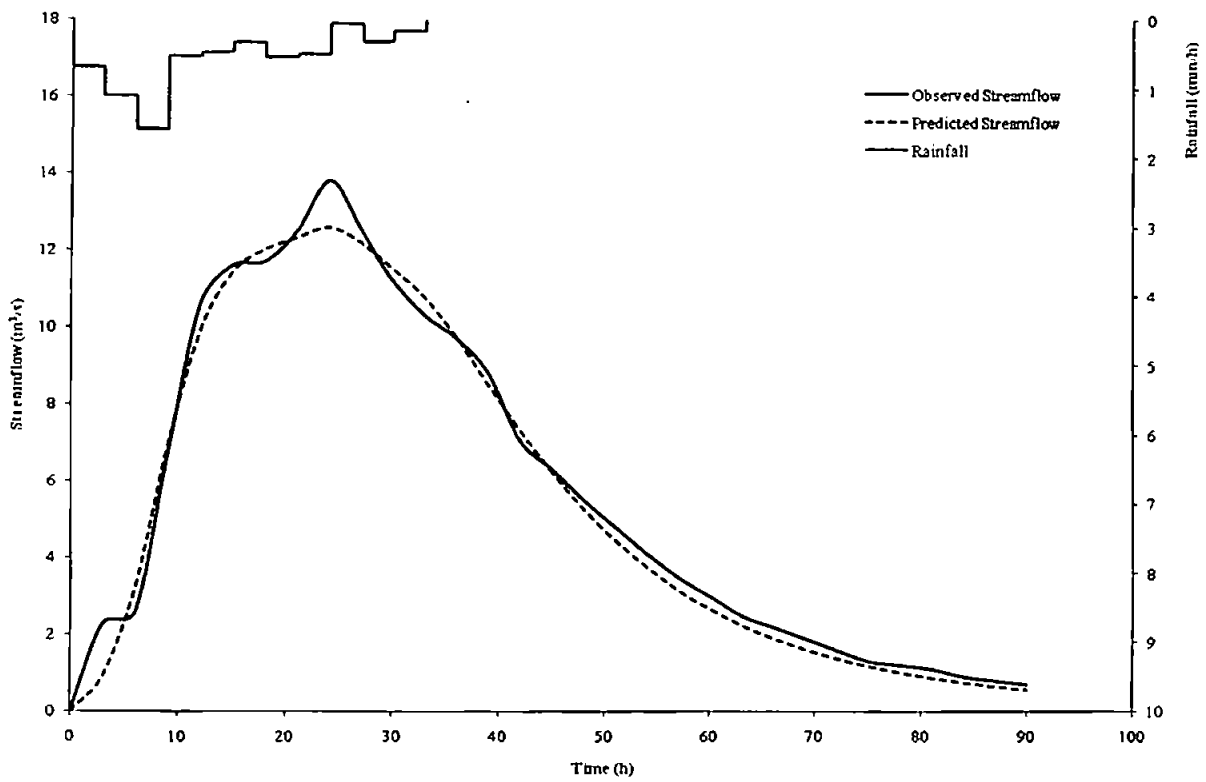
Figure 6.3 Predicted and observed results for event 08
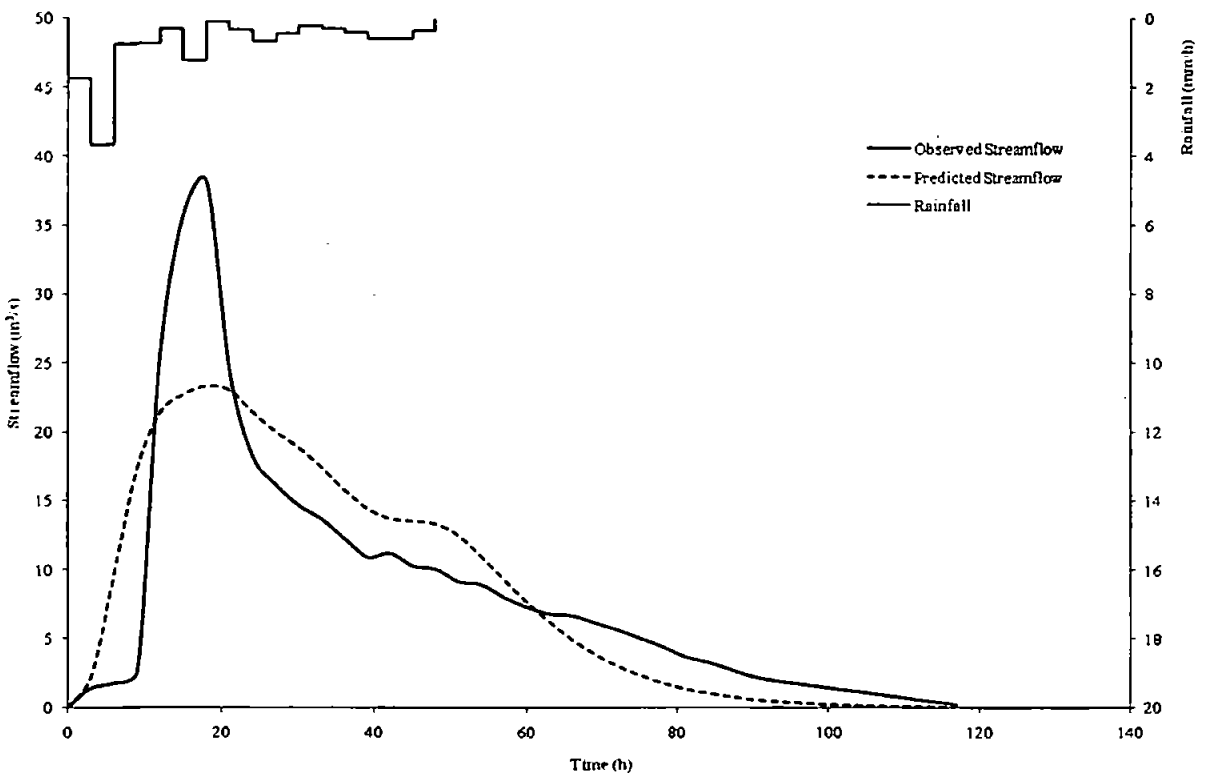
Figure 6.4 Predicted and observed results for event 18

104

For comparison with Table 6.1 and Table 6.2, the summary results for the GA fitting of the classical Nash cascade of n initially relaxed, equal-K 1st order linear reservoirs to the effective rainfall-runoff events on the River Nenagh are shown in Table 6.3. The nK values can be compared with the nK^{α} values in Table 6.1 and the $K_1^{\alpha} + K_2^{\alpha}$ values in Table 6.2.

Event	K	n	nK	Fitness	NSE
1	6.087	1.445	8.797	0.034	0.931
2	2.810	2.427	6.820	0.014	0.987
3	4.115	1.419	5.839	0.040	0.888
4	3.997	1.901	7.597	0.083	0.821
5	4.281	1.427	6.109	0.053	0.696
6	2.445	2.487	6.079	0.070	0.792
7	4.612	2.018	9.308	0.036	0.905
8	4.629	1.534	7.103	0.016	0.988
9	2.255	2.026	4.569	0.031	0.939
10	2.838	1.950	5.534	0.022	0.963
11	3.103	1.620	5.026	0.062	0.809
12	2.517	1.894	4.768	0.081	0.950
13	2.449	2.322	5.687	0.060	0.908
14	2.367	2.299	5.442	0.042	0.934
15	4.042	1.907	7.706	0.033	0.927
16	3.571	1.924	6.870	0.023	0.923
17	2.881	1.546	4.455	0.059	0.774
18	1.657	3.133	5.190	0.124	0.806
19	1.855	3.281	6.085	0.070	0.908
20	1.366	4.875	6.657	0.071	0.937
21	2.221	2.572	5.713	0.107	0.944
22	4.303	1.432	6.161	0.026	0.982

Table 6.3 R. Nenagh results for Nash cascade of n equal 1st order reservoirs

6.2 Initialised Fractional Order Linear Reservoir Results

6.2.1 Loss Model Testing

The results for the GA fitting of the parameters of an initialised, single, fractional-order, time-lagged, linear reservoir to the Flood Event Archive events subject to the use of the ϕ-index, percentage runoff (PR) and non-linear rainfall filter (RF) approaches in turn on the observed rain storm events for a sample catchment, the East Dart at Bellever (river gauge no. 46005) are shown in Tables 6.4 – 6.6. The K^{α} values for each event are calculated for dimensional consistency. The observed total event rainfall (R_T) in mm, observed peak streamflow (Q_P) in m^3/s and initial soil moisture deficit (SMD, supplied to the Flood Event Archive by the UK Meteorological Office from the nearest climate station records) in mm, for each event are also presented. K and T are stated in hours, ϕ is in mm.

Event	Date	R_T	Q_P	SMD	K	α	T	ϕ	K^α	NSE
1287	13-Nov-64	38.1	24.81	0	4.609	0.795	0.875	0.288	3.371	0.839
1289	28-Nov-65	39.9	38.15	0	2.920	0.753	1.997	0.913	2.242	0.969
1292	28-Dec-66	48.3	31.69	0	3.500	0.700	3.625	0.163	2.405	0.724
1297	21-Dec-68	34.4	30.38	0	2.250	0.893	3.317	1.406	2.063	0.915
1298	13-Dec-69	49.2	31.43	0	1.563	0.968	2.665	1.575	1.540	0.879
1299	08-Sep-70	32.6	38.34	0	1.500	0.820	0.906	0.415	1.394	0.936
1300	12-Nov-72	44.6	8.66	0	4.828	1.000	0.564	3.594	4.828	0.990
1301	04-Aug-73	109.9	50.79	50.8	1.875	0.706	2.910	0.226	1.559	0.878
1302	13-Sep-75	49.2	25.69	28.2	4.250	0.583	2.833	1.078	2.325	0.905
1303	10-Nov-74	48.5	43.92	0	2.281	0.885	2.250	0.563	2.075	0.966
1304	03-Aug-74	43.6	13.28	28.7	38.500	0.362	3.941	1.000	3.743	0.917
4351	12-Feb-76	51.4	23.35	0	2.582	0.725	2.390	0.088	1.989	0.899
4352	05-Oct-76	56.6	17.38	0.2	7.375	0.983	1.476	1.000	7.129	0.859
4353	14-Oct-76	104.1	17.73	0	7.688	1.000	0.771	1.566	7.683	0.903

Table 6.4 Catchment 46005 results for single fractional time-lagged reservoir using a ϕ-index loss model

Event	Date	R_T	Q_P	SMD	K	α	T	PR	K^α	NSE
1287	13-Nov-64	38.1	24.81	0	4.328	0.688	1.338	91.968	2.738	0.822
1289	28-Nov-65	39.9	38.15	0	2.000	0.895	2.000	68.571	1.859	0.932
1292	28-Dec-66	48.3	31.69	0	60.250	0.163	4.964	100.000	1.946	0.524
1297	21-Dec-68	34.4	30.38	0	1.750	0.897	3.500	76.812	1.652	0.922
1298	13-Dec-69	49.2	31.43	0	1.941	0.538	3.500	82.813	1.428	0.782
1299	08-Sep-70	32.6	38.34	0	1.719	0.763	0.891	100.000	1.512	0.924
1300	12-Nov-72	44.6	8.66	0	2.500	1.000	1.146	23.462	2.500	0.947
1301	04-Aug-73	109.9	50.79	50.8	2.000	0.625	3.000	98.112	1.542	0.867
1302	13-Sep-75	49.2	25.69	28.2	8.250	0.271	3.819	93.750	1.771	0.889
1303	10-Nov-74	48.5	43.92	0	2.000	0.799	2.363	96.875	1.740	0.959
1304	03-Aug-74	43.6	13.28	28.7	28.500	0.390	3.938	71.875	3.696	0.894
4351	12-Feb-76	51.4	23.35	0	46.500	0.163	2.944	100.000	1.866	0.608
4352	05-Oct-76	56.6	17.38	0.2	58.000	0.350	1.986	100.000	4.142	0.654
4353	14-Oct-76	104.1	17.73	0	6.817	0.839	1.500	63.281	5.005	0.887

Table 6.5 Catchment 46005 results for single fractional time-lagged reservoir using a *PR* loss model

Event	Date	R_T	Q_P	SMD	K	α	T	C	P	K^α	NSE
1287	13-Nov-64	38.1	24.81	0	10.390	0.597	0.429	0.873	0.485	4.049	0.964
1289	28-Nov-65	39.9	38.15	0	23.381	0.453	1.669	0.965	0.519	4.173	0.977
1292	28-Dec-66	48.3	31.69	0	31.577	0.109	3.778	0.692	0.890	1.456	0.832
1297	21-Dec-68	34.4	30.38	0	5.911	0.646	2.607	0.852	0.405	3.154	0.971
1298	13-Dec-69	49.2	31.43	0	25.790	0.519	1.249	0.929	0.611	5.402	0.954
1299	08-Sep-70	32.6	38.34	0	2.903	0.343	1.306	0.960	0.179	1.441	0.895
1300	12-Nov-72	44.6	8.66	0	36.627	0.341	1.528	0.569	0.364	3.408	0.974
1301	04-Aug-73	109.9	50.79	50.8	42.464	0.261	2.637	0.961	0.529	2.660	0.878
1302	13-Sep-75	49.2	25.69	28.2	49.098	0.254	2.775	0.911	0.436	2.693	0.960
1303	10-Nov-74	48.5	43.92	0	5.270	0.548	1.972	0.866	0.333	2.487	0.991
1304	03-Aug-74	43.6	13.28	28.7	40.966	0.488	2.365	0.817	0.432	6.126	0.948
4351	12-Feb-76	51.4	23.35	0	4.727	0.699	0.783	0.627	0.588	2.962	0.949
4352	05-Oct-76	56.6	17.38	0.2	22.495	0.586	1.223	0.890	0.558	6.202	0.919
4353	14-Oct-76	104.1	17.73	0	49.574	0.452	1.710	0.892	0.395	5.827	0.936

Table 6.6 Catchment 46005 results for single fractional time-lagged reservoir using a RF loss model

The following Figures 6.5 – 6.18 show the best fitting predicted streamflow hydrographs using the different loss models together with the observed total rainfall hyetograph and observed hydrograph for each event associated with Tables 6.4 – 6.6.

The following abbreviations are used on the Figures:

Phi-index - ϕ-index, equation (5.16)

PR – percentage runoff, equation (5.17)

RF – non-linear rainfall filter, equation (5.18)
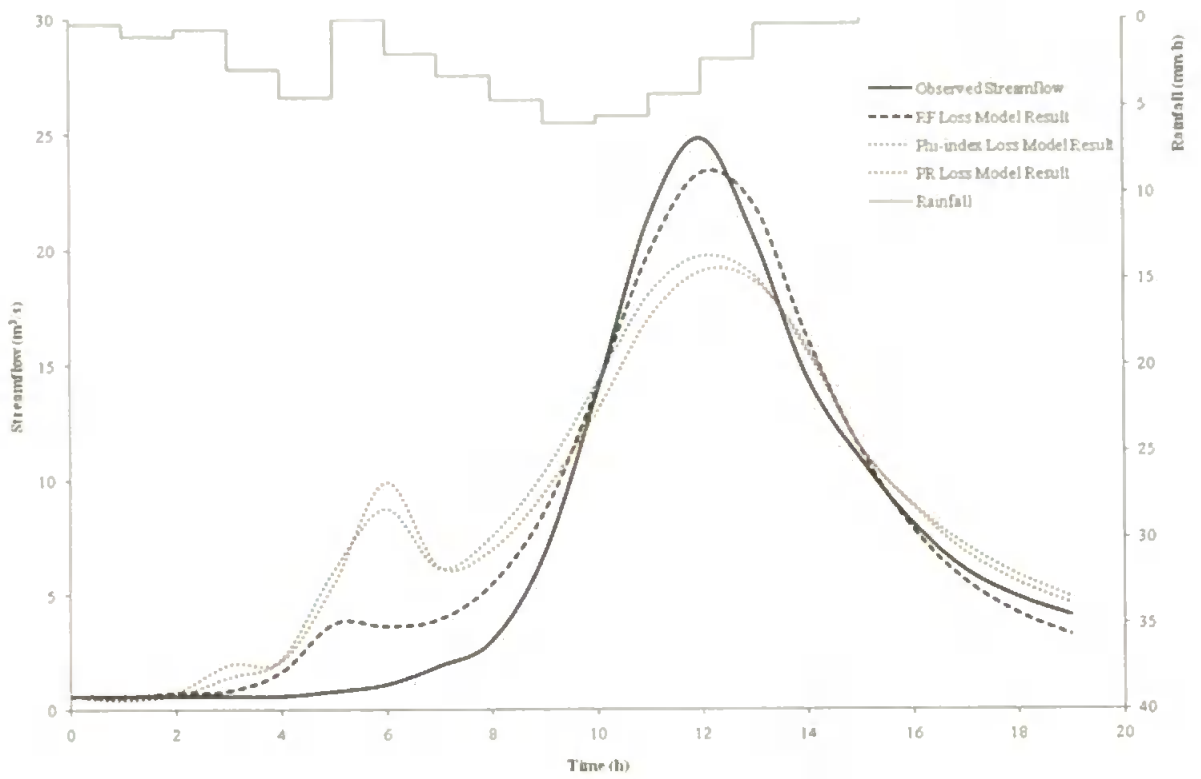
Figure 6.5 Predicted and observed results for event 1287
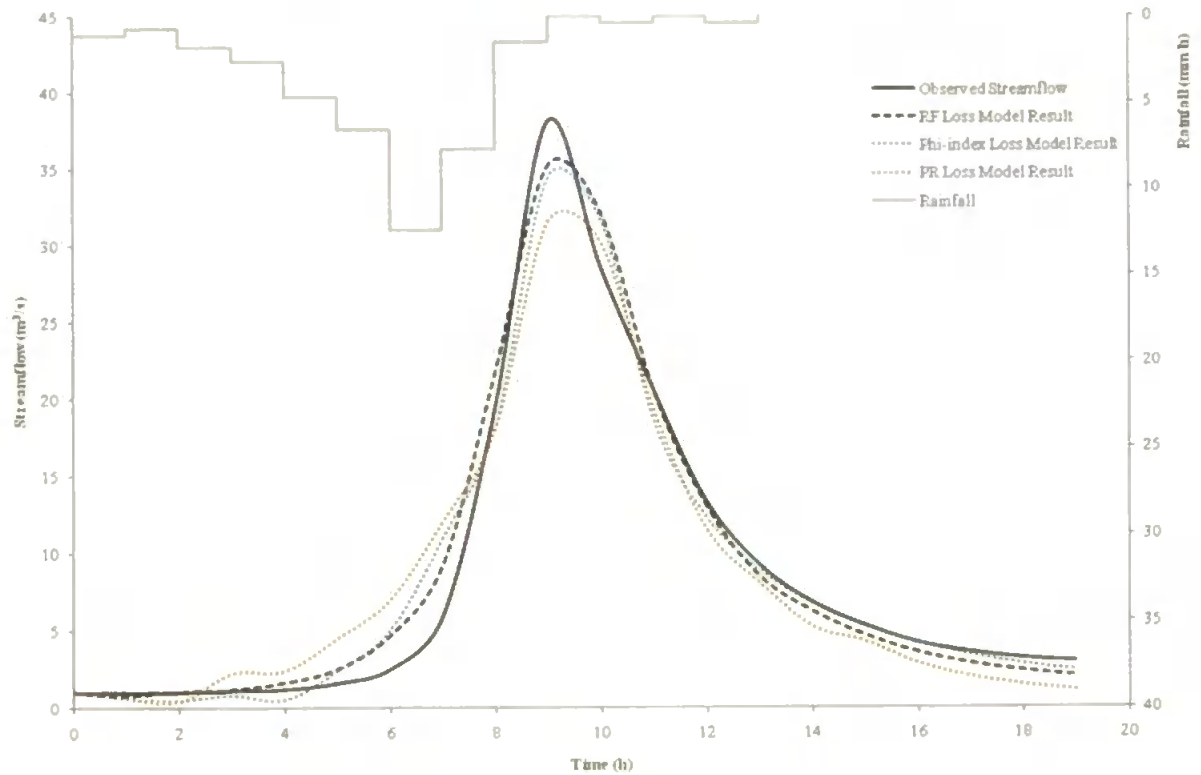
Figure 6.6 Predicted and observed results for event 1289

111
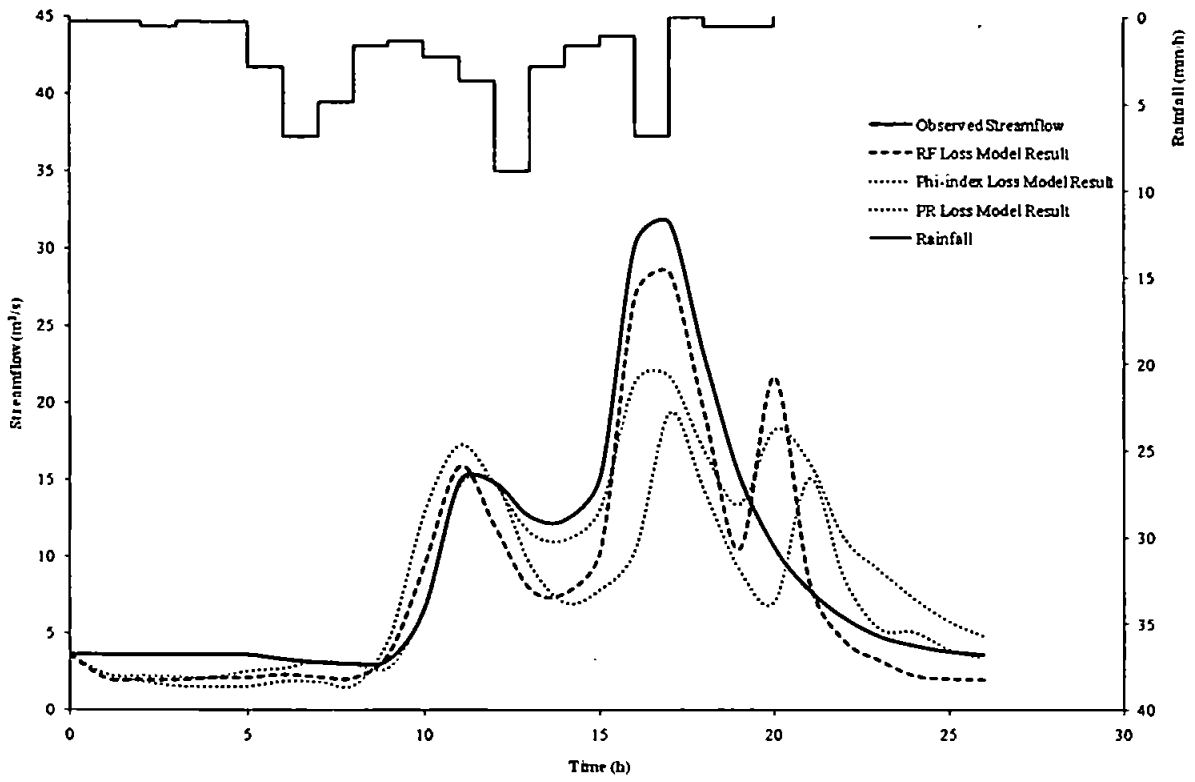
Figure 6.7 Predicted and observed results for event 1292
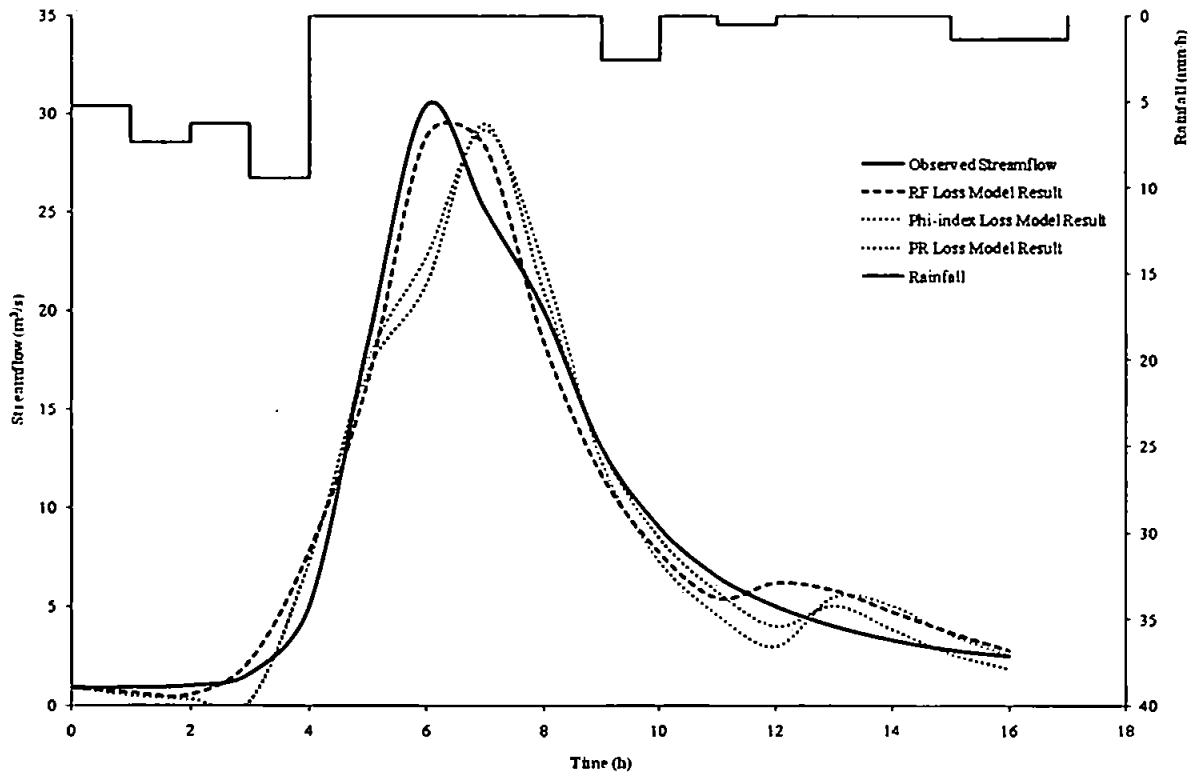
Figure 6.8 Predicted and observed results for event 1297

112
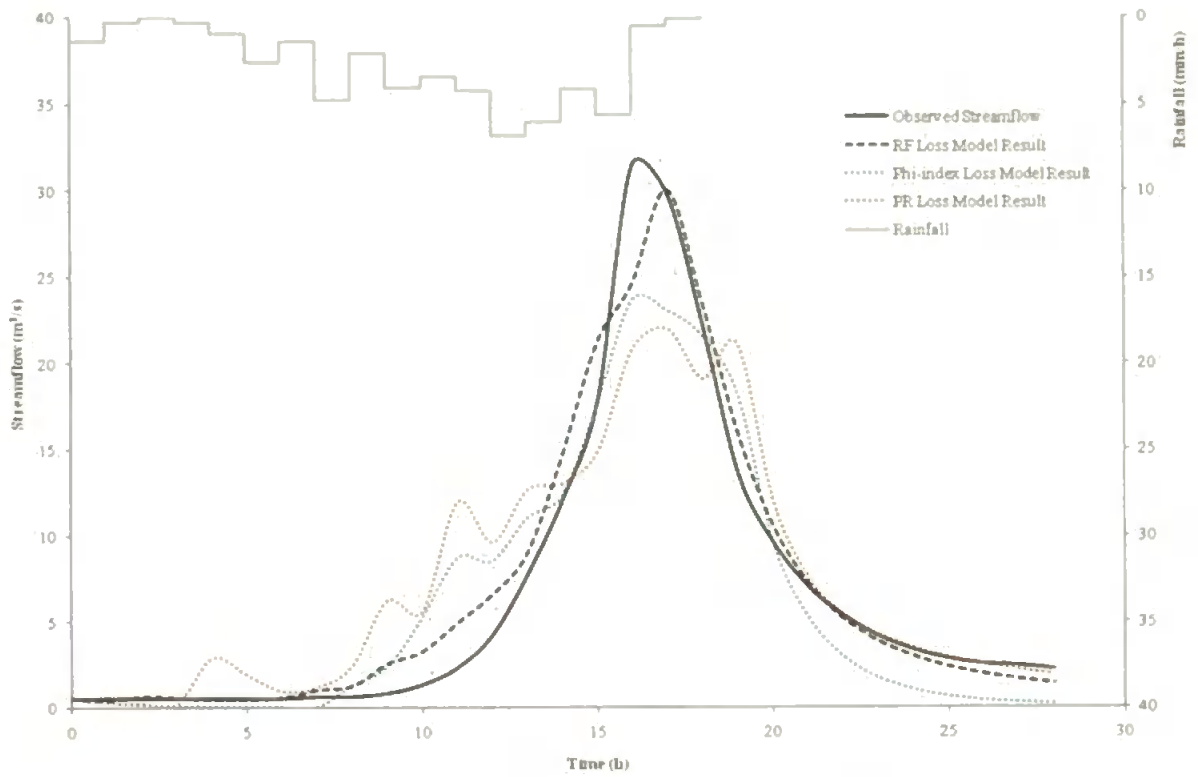
Figure 6.9 Predicted and observed results for event 1298
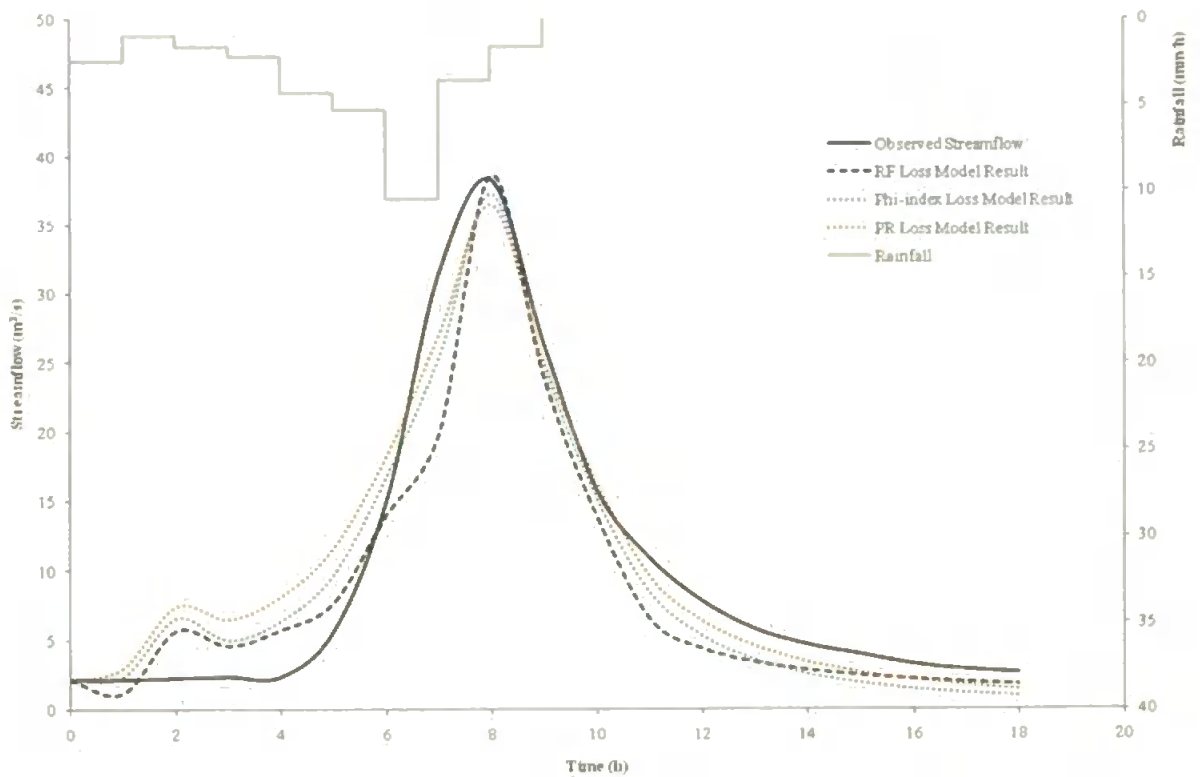
Figure 6.10 Predicted and observed results for event 1299

113
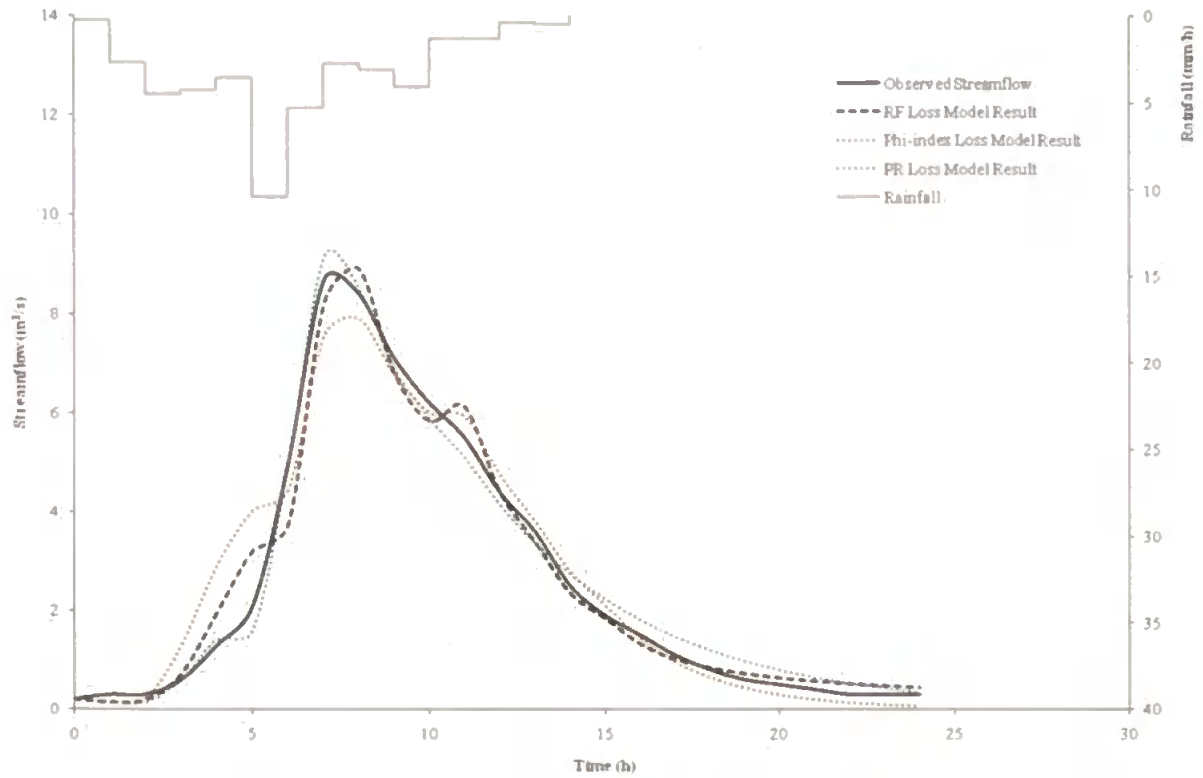
Figure 6.11 Predicted and observed results for event 1300
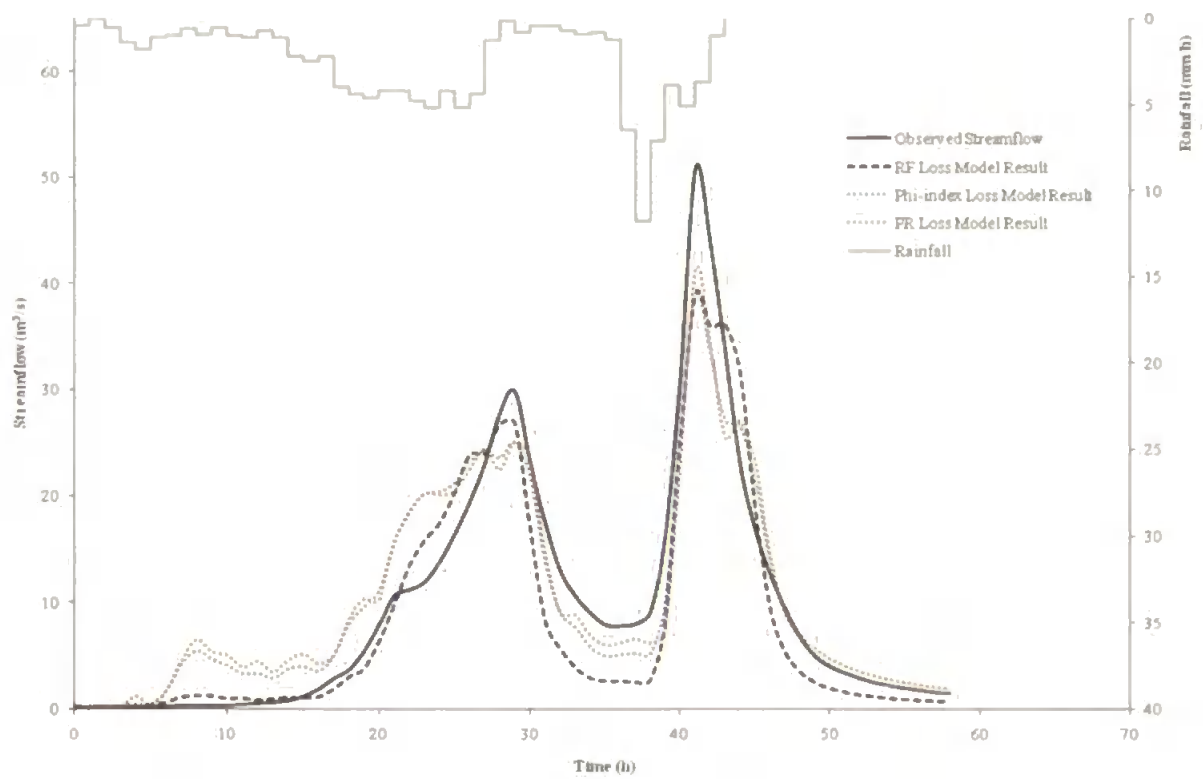
Figure 6.12 Predicted and observed results for event 1301

114
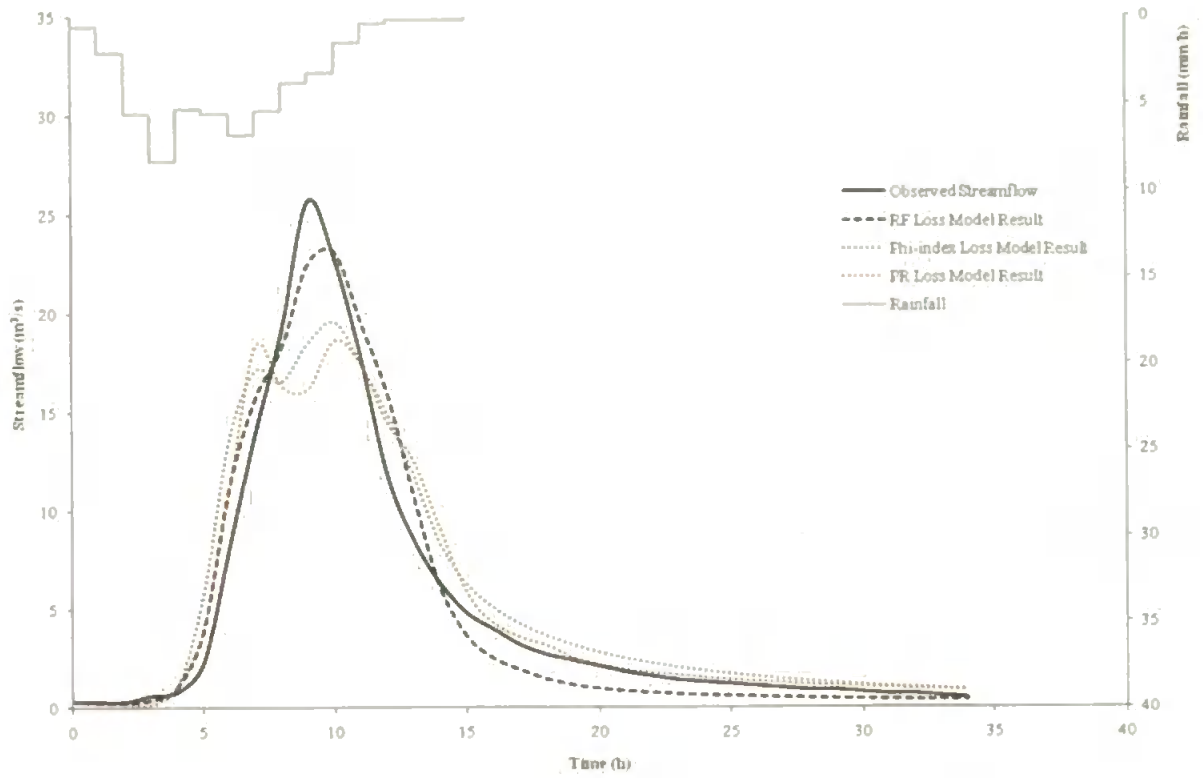
Figure 6.13 Predicted and observed results for event 1302
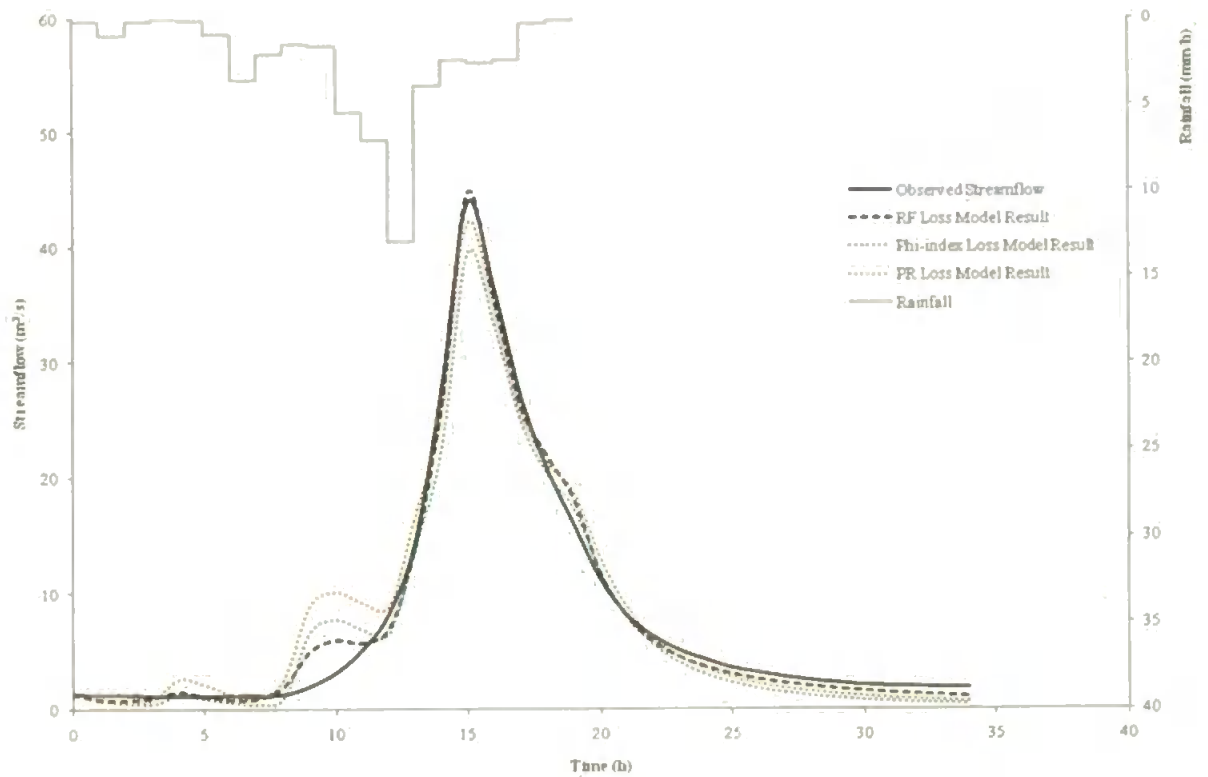
Figure 6.14 Predicted and observed results for event 1303
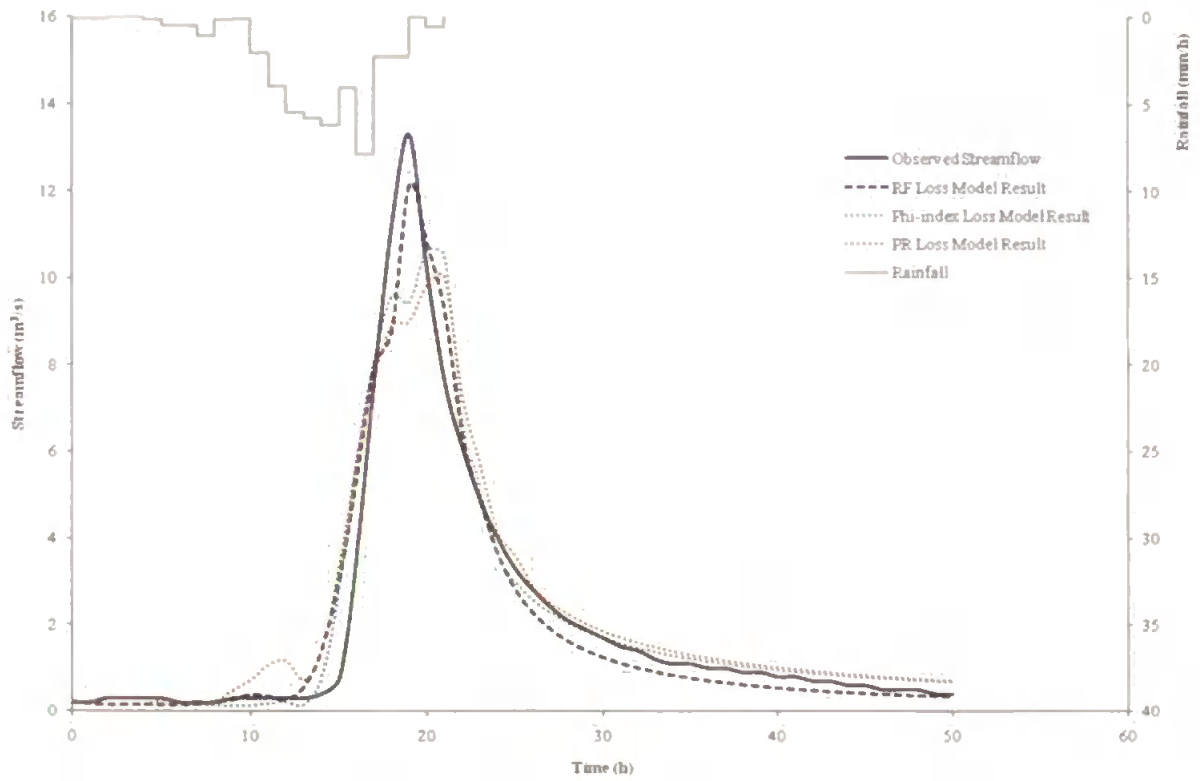
Figure 6.15 Predicted and observed results for event 1304
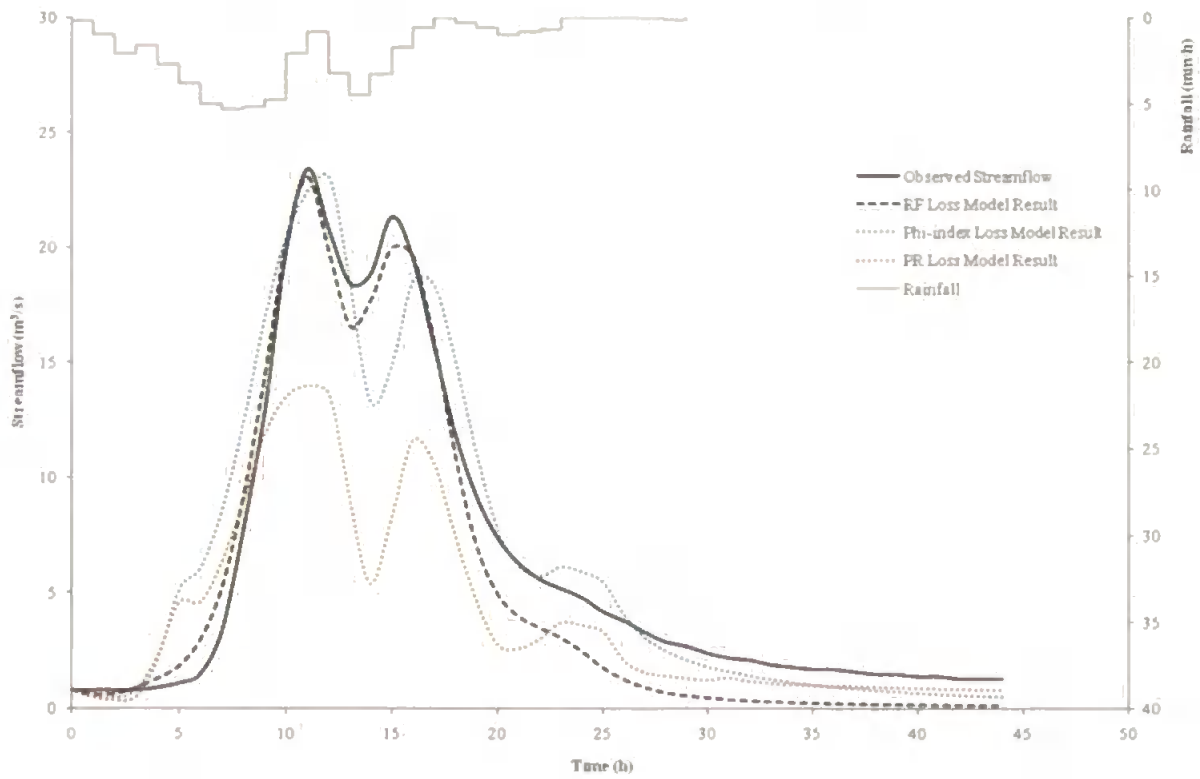
Figure 6.16 Predicted and observed results for event 4351

116
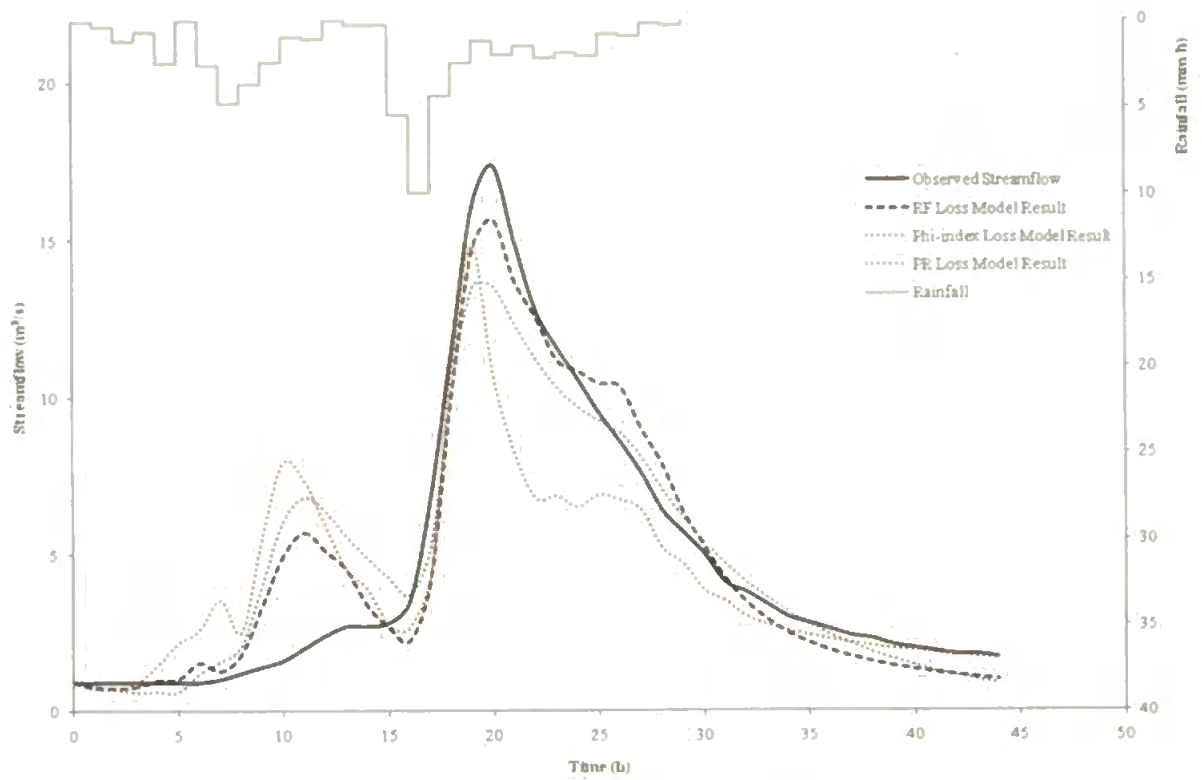
Figure 6.17 Predicted and observed results for event 4352
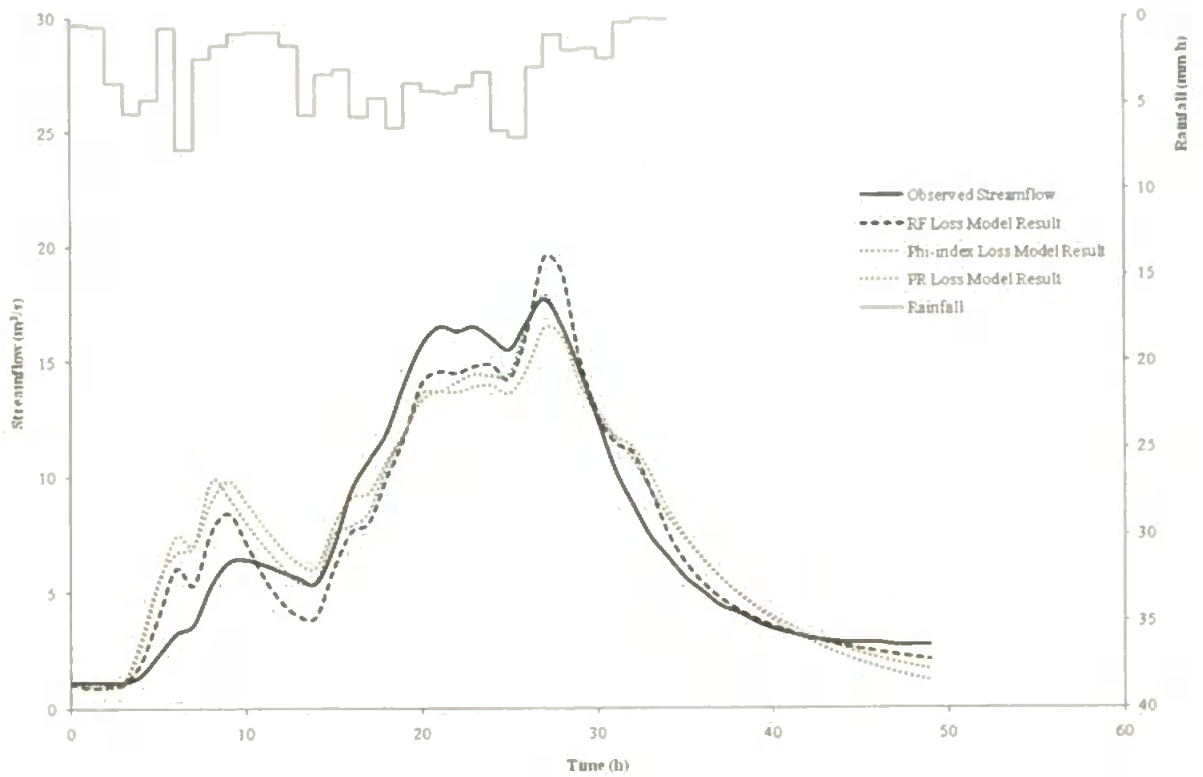
Figure 6.18 Predicted and observed results for event 4353

From Tables 6.4 – 6.6 and Figures 6.5 – 6.18 the non-linear rainfall filter (RF) model (equation (5.18)) was found to outperform the ϕ-index and *PR*. Consequently the RF loss model was selected for use in the subsequent event simulations for the Flood Event Archive catchments (re. section 6.2.3).

6.2.2   GA Parameter Selection

The results for different GA control parameters used for fitting an initialised, single, fractional-order, time-lagged, linear reservoir with a non-linear rainfall filter to a sample observed rain storm event (no. 1303, 10-Nov-74) for the East Dart at Bellever (river gauge no. 46005) are shown in Table 6.7 (and recall Figure 6.14 for a plot of the observed streamflow hydrograph and total rainfall hyetograph). *K* and *T* are stated in hours.

The abbreviations for the GA control parameters used in Table 6.7 are:

Pop. - population size

Gen. – number of generations

Tourn. – size of sample group in tournament selection

Cross. – probability of selection for crossover operator

Mut. - probability of selection for mutation operator

The weightings for the fitness function, equation (5.24) are:

w_1 – weighting applied to *RMSE*

w_2 - weighting applied to RMS_{slope}

such that $w_1 + w_2 = 1$.

GA Control Parameters					Fitness Weighting		Rainfall-Streamflow Model Parameters Fitted by GA						
Pop.	Gen.	Tourn.	Cross.	Mut.	w_1	w_2	K	α	T	C	P	K^α	NSE
25	50	4	0.6	0.2	0.6	0.4	1.270	0.579	2.779	0.980	0.020	1.149	0.960
75	50	4	0.6	0.2	0.6	0.4	62.461	0.129	2.991	0.985	0.395	1.707	0.919
100	50	4	0.6	0.2	0.6	0.4	4.446	0.581	1.911	0.784	0.375	2.381	0.992
50	25	4	0.6	0.2	0.6	0.4	131.415	0.185	1.844	0.820	0.840	2.465	0.930
50	75	4	0.6	0.2	0.6	0.4	5.561	0.387	2.713	0.991	0.272	1.942	0.981
50	100	4	0.6	0.2	0.6	0.4	4.169	0.464	2.527	0.919	0.260	1.940	0.982
50	50	2	0.6	0.2	0.6	0.4	28.538	0.364	1.833	0.935	0.595	3.392	0.982
50	50	3	0.6	0.2	0.6	0.4	7.096	0.477	2.278	0.989	0.289	2.545	0.982
50	50	5	0.6	0.2	0.6	0.4	157.432	0.179	1.714	0.824	0.854	2.472	0.926
50	50	6	0.6	0.2	0.6	0.4	9.702	0.397	2.456	0.993	0.346	2.464	0.980
50	50	4	0.4	0.2	0.6	0.4	5.880	0.538	1.863	0.812	0.414	2.596	0.992
50	50	4	0.5	0.2	0.6	0.4	8.884	0.403	2.534	0.984	0.344	2.409	0.979
50	50	4	0.7	0.2	0.6	0.4	22.413	0.271	2.720	0.987	0.426	2.324	0.960
50	50	4	0.6	0.05	0.6	0.4	3.649	0.656	1.941	0.850	0.254	2.337	0.987
50	50	4	0.6	0.10	0.6	0.4	19.084	0.338	2.102	0.903	0.497	2.706	0.954
50	50	4	0.6	0.25	0.6	0.4	32.933	0.333	1.918	0.946	0.588	3.197	0.982
50	50	4	0.6	0.30	0.6	0.4	7.094	0.467	2.275	0.947	0.315	2.495	0.981
50	50	4	0.6	0.2	1	0	9.232	0.392	2.472	0.992	0.333	2.389	0.980
50	50	4	0.6	0.2	0.5	0.5	10.937	0.447	1.940	0.917	0.442	2.911	0.994
50	50	4	0.6	0.2	0.4	0.6	9.076	0.241	1.797	0.657	0.760	1.701	0.931
50	50	4	0.6	0.2	0	1	73.411	0.188	2.290	0.803	0.579	2.245	0.827
50	50	4	0.6	0.2	0.6	0.4	5.270	0.548	1.972	0.866	0.333	2.487	0.991

Table 6.7 Influence of GA control parameters on fit for sample event 1303

From the results of the tests shown in Table 6.7, the following GA control parameters (Table 6.8) were selected as appropriate for producing effective parameter fitting for hourly flood event data together with computational efficiency (i.e. fewer function evaluations for a population of 50 rather than 100 individuals).

GA control parameter	Value used in Model Calibration
Population size	50
Number of generations	50
Selection method	Tournament size 4
Crossover probability	0.6
Mutation probability	0.2
Fitness weight w_1	0.6
Fitness weight w_2	0.2

Table 6.8 GA control parameters used for model calibration

6.2.3 Rainfall-Streamflow Model Results for the Flood Event Archive Data

The summary results for the GA fitting of the parameters of an initialised, single, fractional-order, time-lagged, linear reservoir to a range of the Flood Event Archive catchments, including the non-linear rainfall filter model (equation (5.18)) parameters (re. section 5.4.2 and 6.2.1), are shown in tables 6.9 – 6.19 (one for each catchment). The results with and without the rainfall loss model are listed for comparison. The K^{α} values for each event are calculated for dimensional consistency. The observed total event rainfall (R_T) in mm, observed peak streamflow (Q_P) in m³/s and initial soil moisture deficit (*SMD*, supplied to the Flood Event Archive by the UK Meteorological Office from the nearest climate station records) in mm, for each event are also presented. K and T are stated in hours.

Following each table are 4 figures showing the predicted and observed streamflow hydrographs together with the total event rainfall hyetograph for the best and worst cases for each catchment for the two models. Full sets of results plots are available in Appendices C and D. A summary of the composite K^{α} values for each catchment is given in Table 6.20.

Event	Date	R_T	Q_P	SMD	No loss model					With non-linear filter loss model						
					K	α	T	K^α	NSE	K	α	T	C	P	K^α	NSE
1287	13-Nov-64	38.1	24.81	0	6.086	0.724	0.899	3.697	0.811	10.390	0.597	0.429	0.873	0.485	4.045	0.964
1289	28-Nov-65	39.9	38.15	0	4.432	0.592	2.137	2.414	0.938	23.381	0.453	1.669	0.965	0.519	4.170	0.977
1292	28-Dec-66	48.3	31.69	0	2.781	0.569	3.856	1.790	0.734	31.577	0.109	3.778	0.692	0.890	1.457	0.832
1297	21-Dec-68	34.4	30.38	0	2.432	0.495	3.906	1.553	0.913	5.911	0.646	2.607	0.852	0.405	3.151	0.971
1298	13-Dec-69	49.2	31.43	0	4.227	0.451	2.974	1.916	0.787	25.790	0.519	1.249	0.929	0.611	5.402	0.954
1299	08-Sep-70	32.6	38.34	0	1.897	0.795	0.872	1.664	0.926	2.903	0.343	1.306	0.960	0.179	1.441	0.895
1300	12-Nov-72	44.6	8.66	0	681.821	0.321	1.670	8.121	0.863	36.627	0.341	1.528	0.569	0.364	3.414	0.974
1301	04-Aug-73	109.9	50.79	50.8	3.719	0.542	3.284	2.038	0.832	42.464	0.261	2.637	0.961	0.529	2.660	0.878
1302	13-Sep-75	49.2	25.69	28.2	12.021	0.223	3.948	1.741	0.895	49.098	0.254	2.775	0.911	0.436	2.689	0.960
1303	10-Nov-74	48.5	43.92	0	1.590	0.677	2.622	1.369	0.960	5.270	0.548	1.972	0.866	0.333	2.486	0.991
1304	03-Aug-74	43.6	13.28	28.7	176.706	0.319	3.930	5.210	0.889	40.966	0.488	2.365	0.817	0.432	6.122	0.948
4351	12-Feb-76	51.4	23.35	0	3.541	0.758	2.326	2.608	0.908	4.727	0.699	0.783	0.627	0.588	2.962	0.949
4352	05-Oct-76	56.6	17.38	0.2	20.074	0.587	1.882	5.816	0.749	22.495	0.586	1.223	0.890	0.558	6.199	0.919
4353	14-Oct-76	104.1	17.73	0	28.792	0.473	1.856	4.900	0.858	49.574	0.452	1.710	0.892	0.395	5.838	0.936

Table 6.9 Catchment 46005 results for single fractional time-lagged reservoir
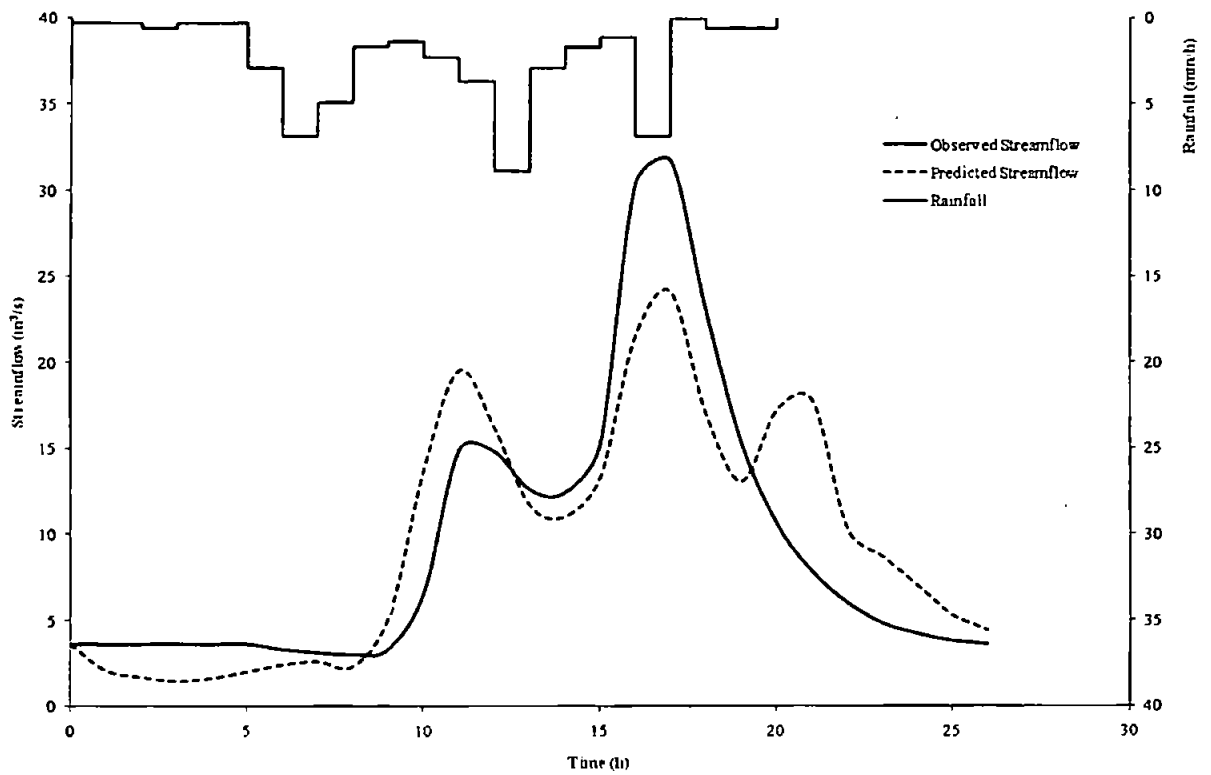
Figure 6.19 Results for event 1292 – without loss model
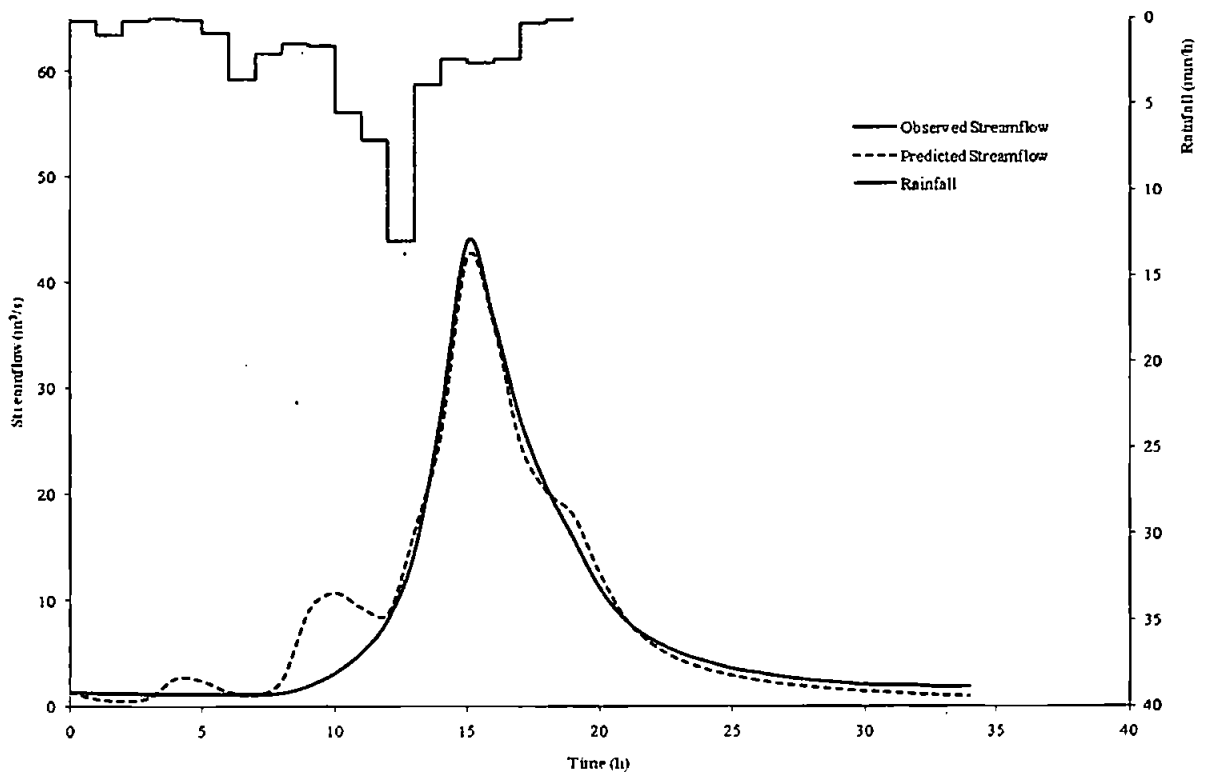
Figure 6.20 Results for event 1303 – without loss model

123
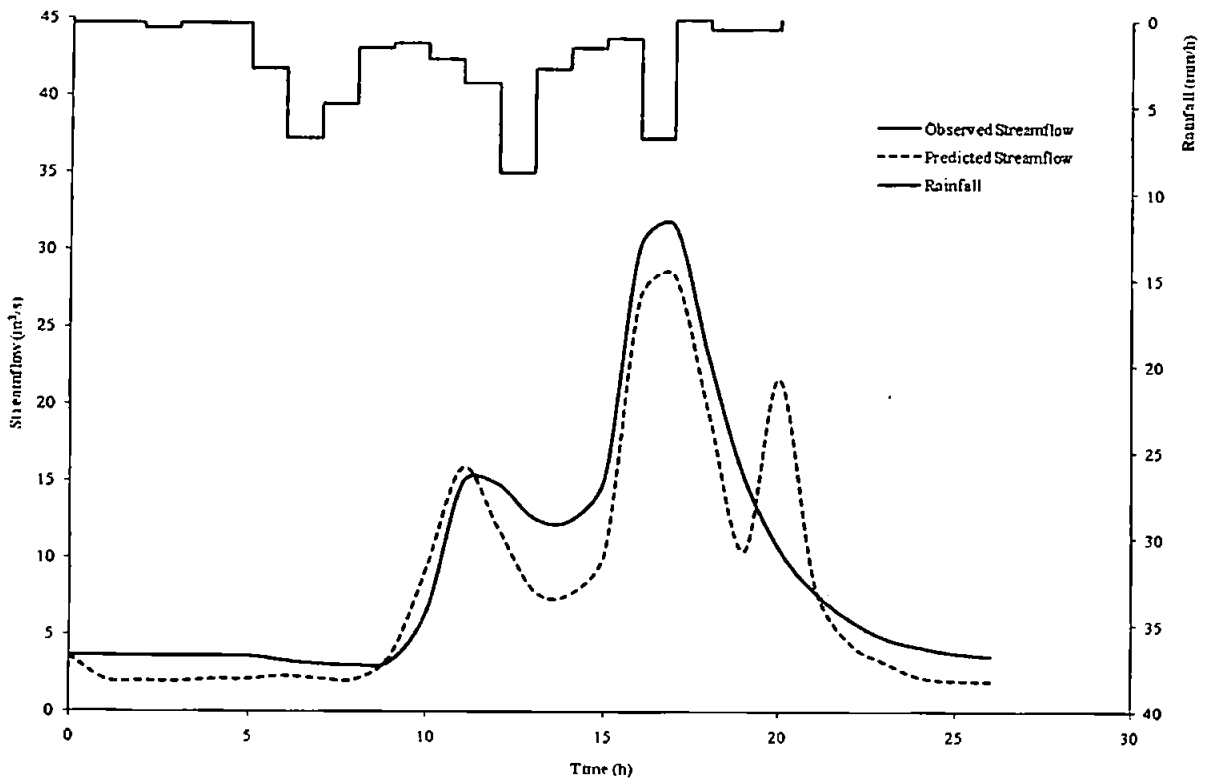
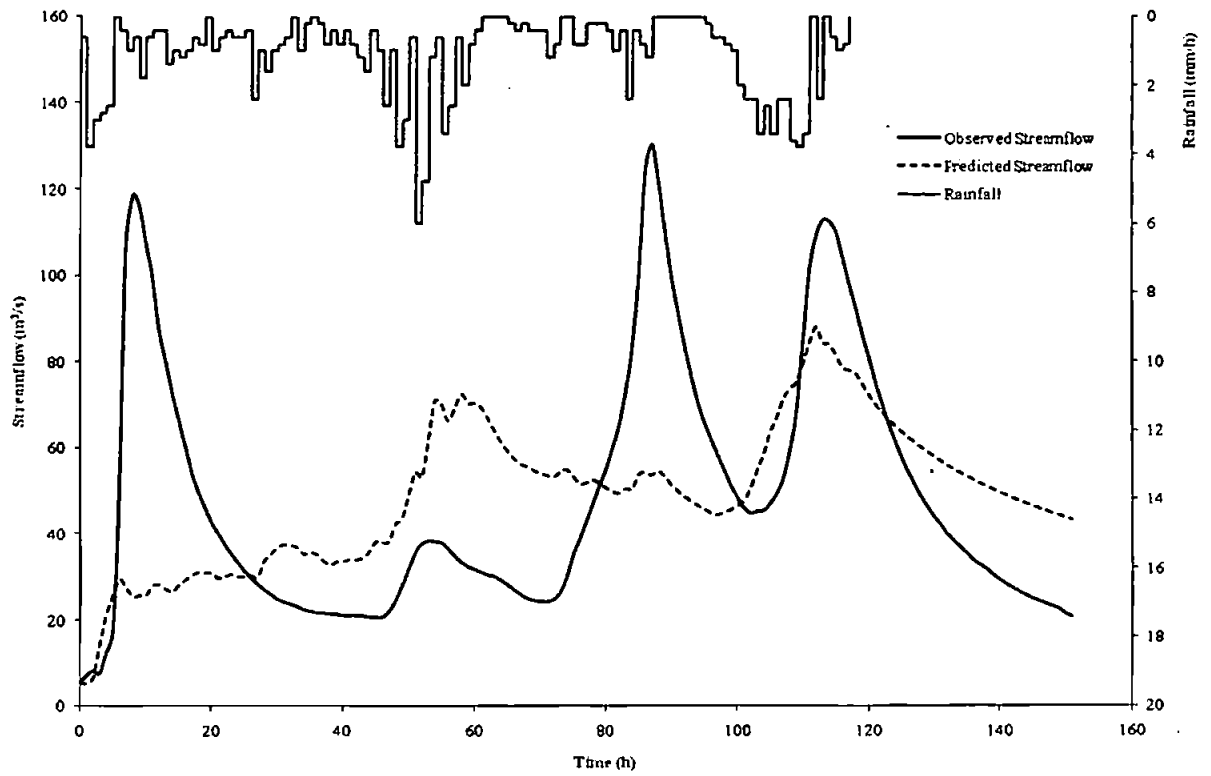**Figure 6.21 Results for event 1292 - with non-linear filter loss model**
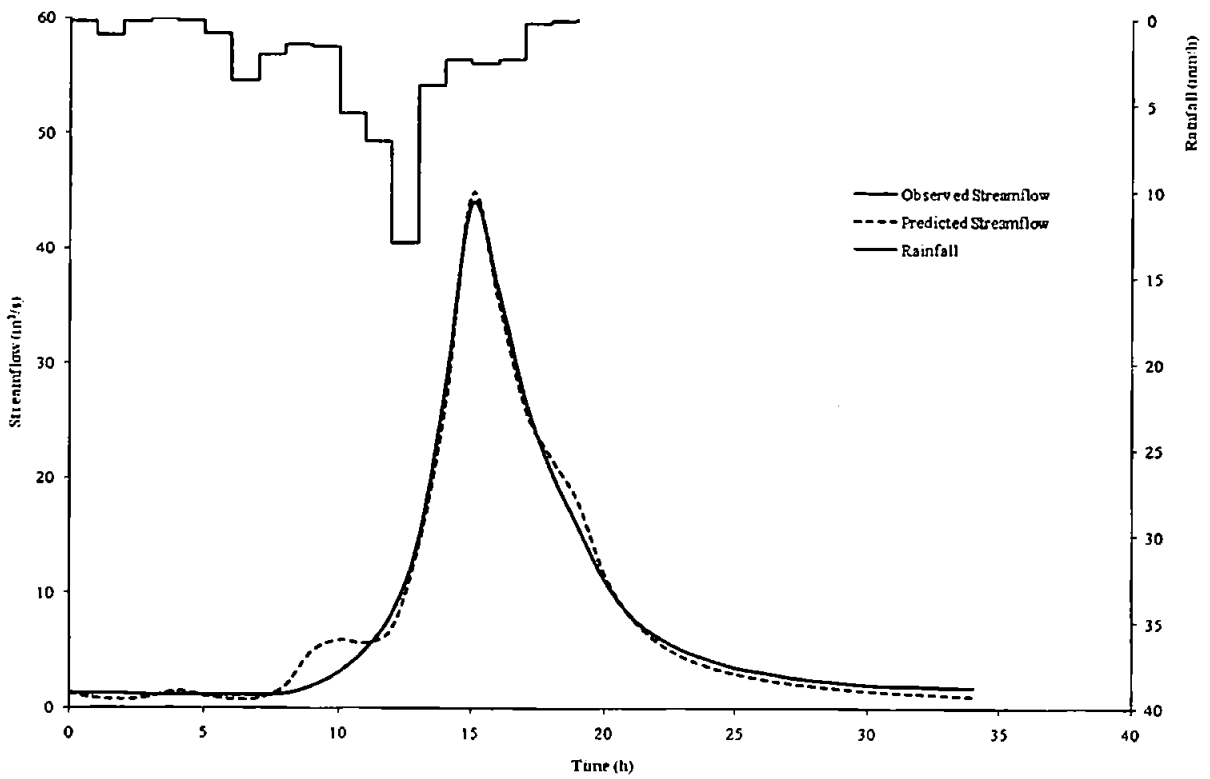
Figure 6.22 Results for event 1303 - with non-linear filter loss model

124

Event	Date	R_T	Q_P	SMD	No loss model					With non-linear filter loss model						
					K	α	T	K^α	NSE	K	α	T	C	P	K^α	NSE
492	05-Nov-67	15.2	3.72	9.9	682.461	0.464	8.808	20.654	0.891	95.986	0.568	8.628	0.679	0.064	13.363	0.945
495	15-Sep-68	30.1	6.58	2.8	634.500	0.424	6.855	15.425	0.923	32.289	0.860	3.199	0.802	0.419	19.851	0.956
496	01-Nov-68	48.7	10.17	0	495.552	0.429	7.855	14.328	0.949	62.036	0.610	6.699	0.699	0.224	12.403	0.978
3874	06-Mar-82	21.4	4.73	18.9	499.049	0.514	6.779	24.369	0.965	126.551	0.651	5.626	0.989	0.223	23.365	0.983
3877	25-Jun-82	23.2	5.86	46.8	286.622	0.644	3.782	38.239	0.930	145.446	0.698	3.531	0.975	0.177	32.327	0.934
3878	13-Nov-82	26.7	4.32	5.3	485.591	0.536	5.791	27.532	0.929	96.857	0.615	4.677	0.726	0.121	16.652	0.879
3880	01-May-83	21.2	5.02	4.1	634.246	0.466	5.755	20.223	0.849	52.188	0.726	4.592	0.644	0.119	17.659	0.936
3881	31-Jul-83	36	1.74	101.9	699.981	0.999	2.723	695.410	-1.807	172.950	0.681	3.986	0.615	0.519	33.421	0.936
3882	26-Nov-83	29.7	3.09	85.5	2998.022	0.490	5.708	50.542	0.943	49.333	0.666	5.312	0.230	0.002	13.416	0.991
3884	02-Aug-84	53	5.19	101.3	699.715	0.930	1.984	442.361	0.087	145.283	0.583	2.376	0.689	0.690	18.221	0.980
3890	29-Dec-86	29.5	7.61	4.9	351.564	0.455	9.883	14.402	0.899	26.351	0.910	5.512	0.792	0.448	19.630	0.971
3893	14-Oct-87	30.3	7.25	5.2	274.425	0.486	5.797	15.313	0.845	20.237	0.860	4.374	0.551	0.148	13.283	0.912
4166	13-Dec-79	27.6	8.41	9.5	255.538	0.511	4.766	16.991	0.890	41.462	0.684	4.418	0.733	0.156	12.778	0.931

Table 6.10 Catchment 30004 results for single fractional time-lagged reservoir
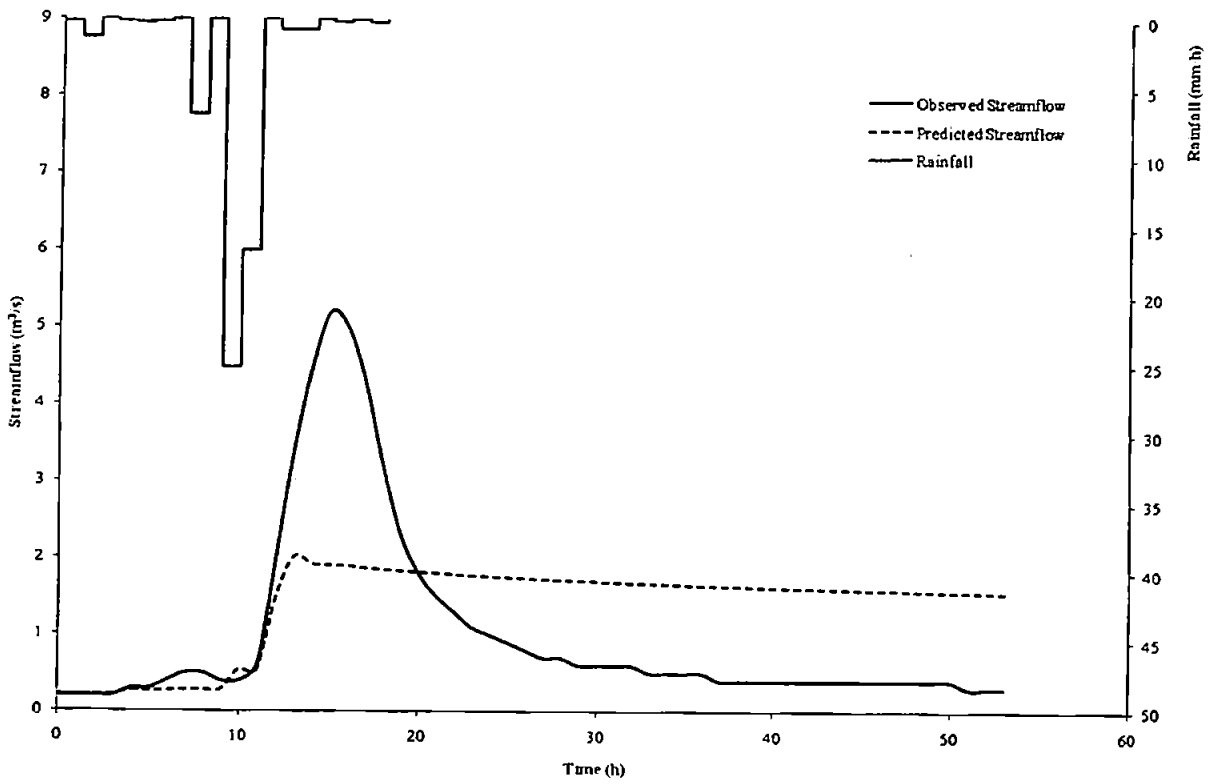
Figure 6.23 Results for event 3884 – without loss model
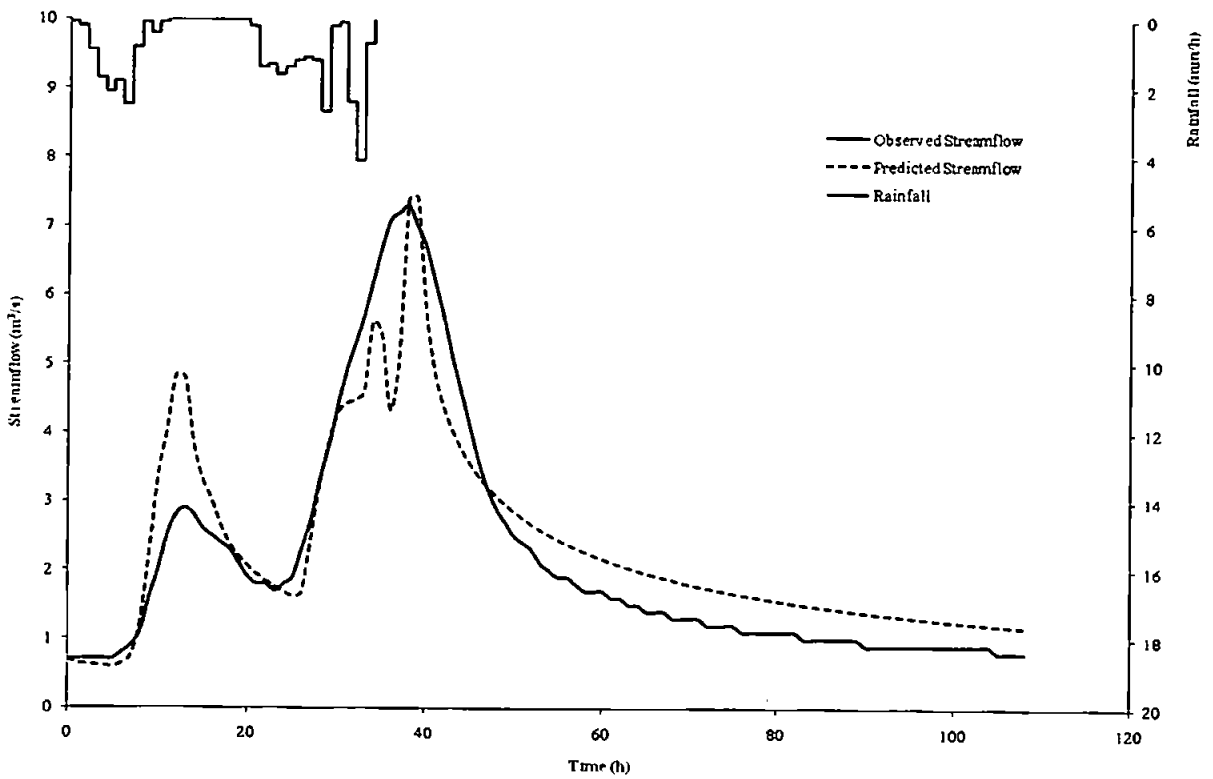
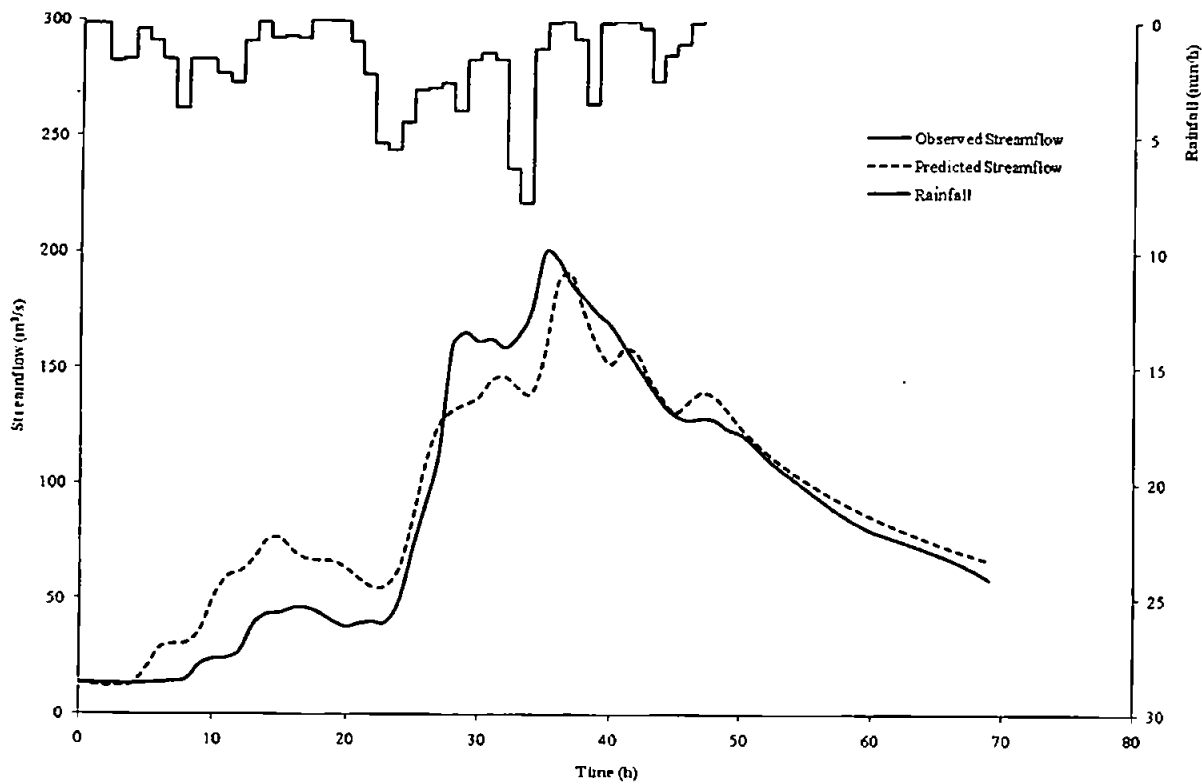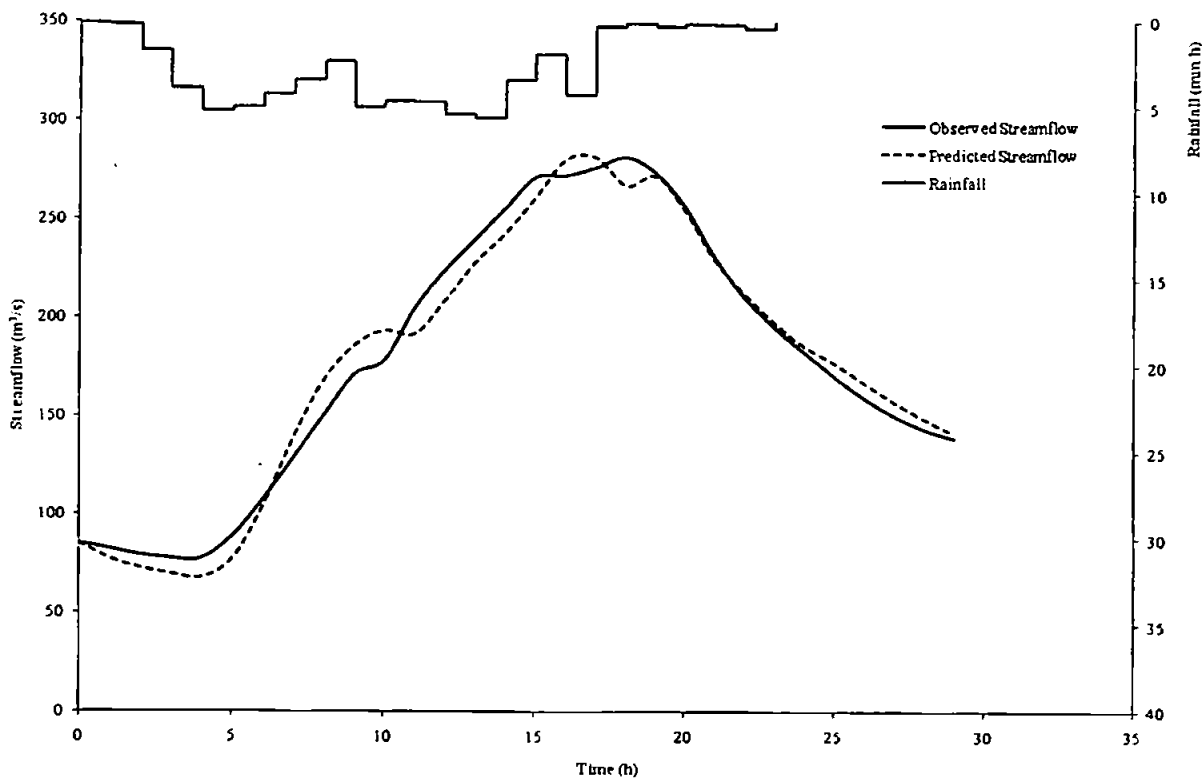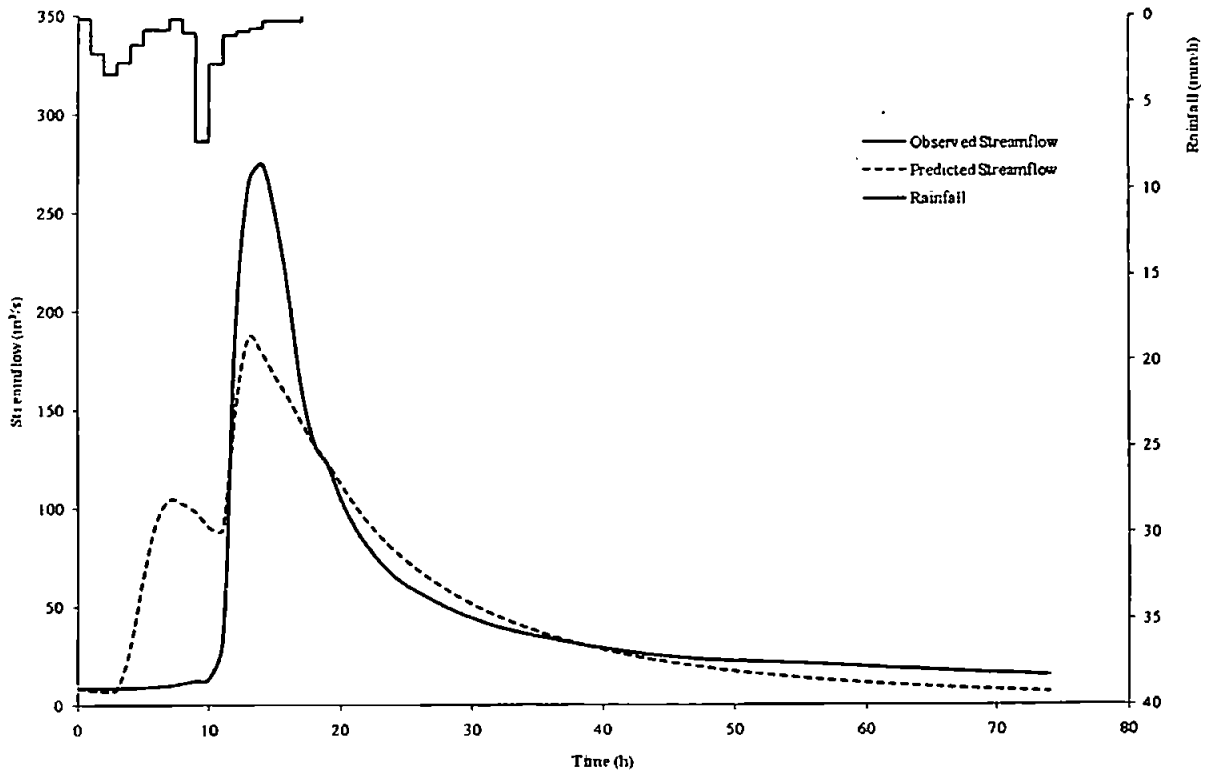**Figure 6.24 Results for event 3893 – without loss model**

126
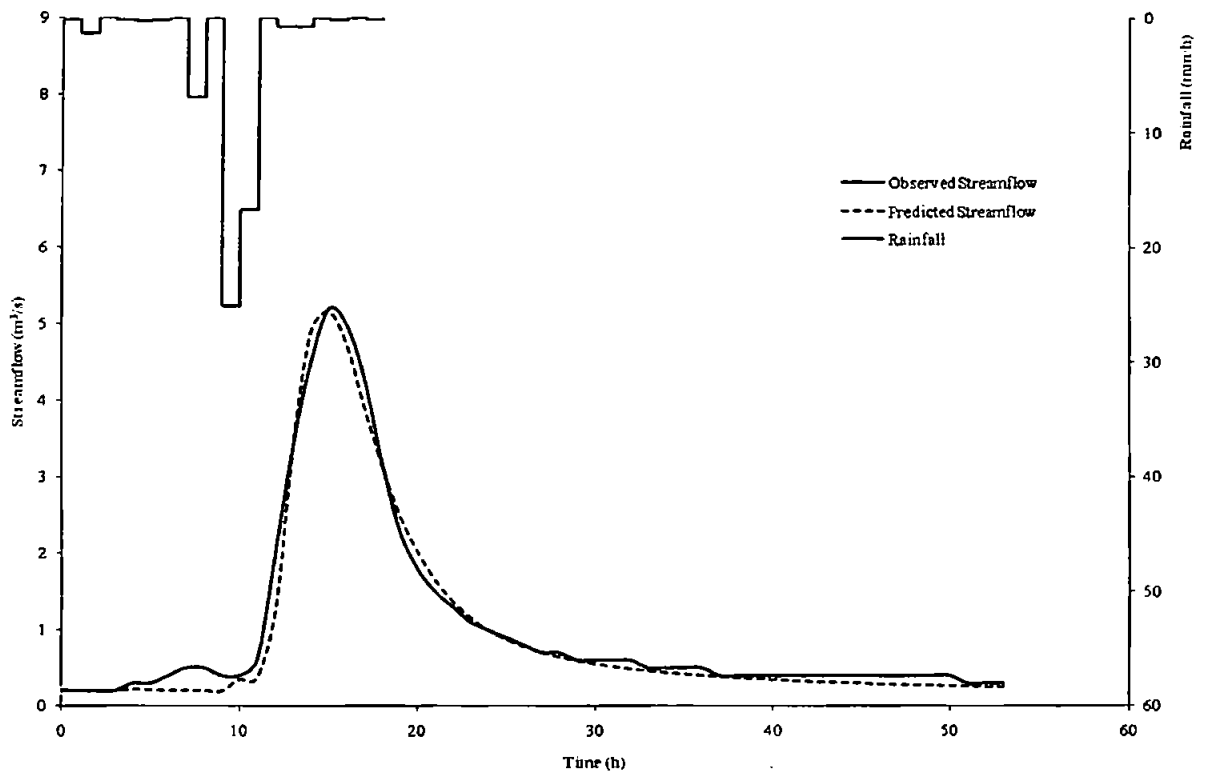
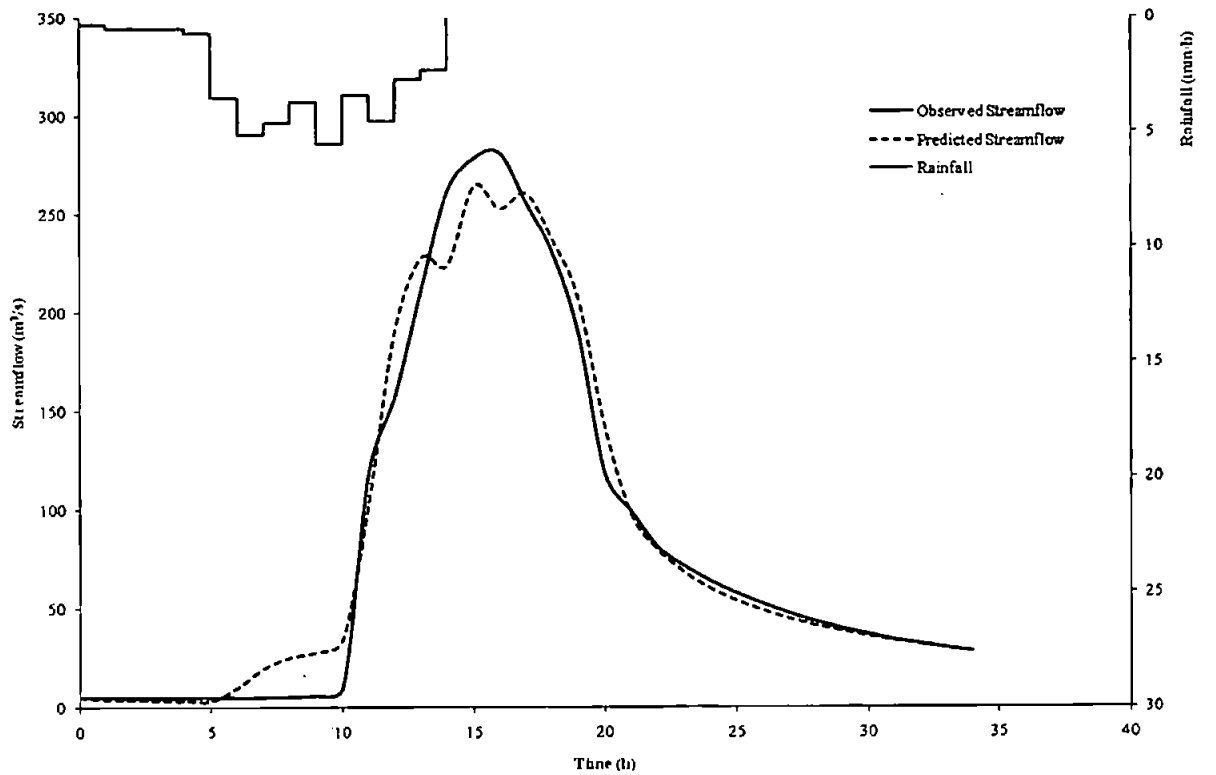**Figure 6.25 Results for event 3884 – with non-linear filter loss model**
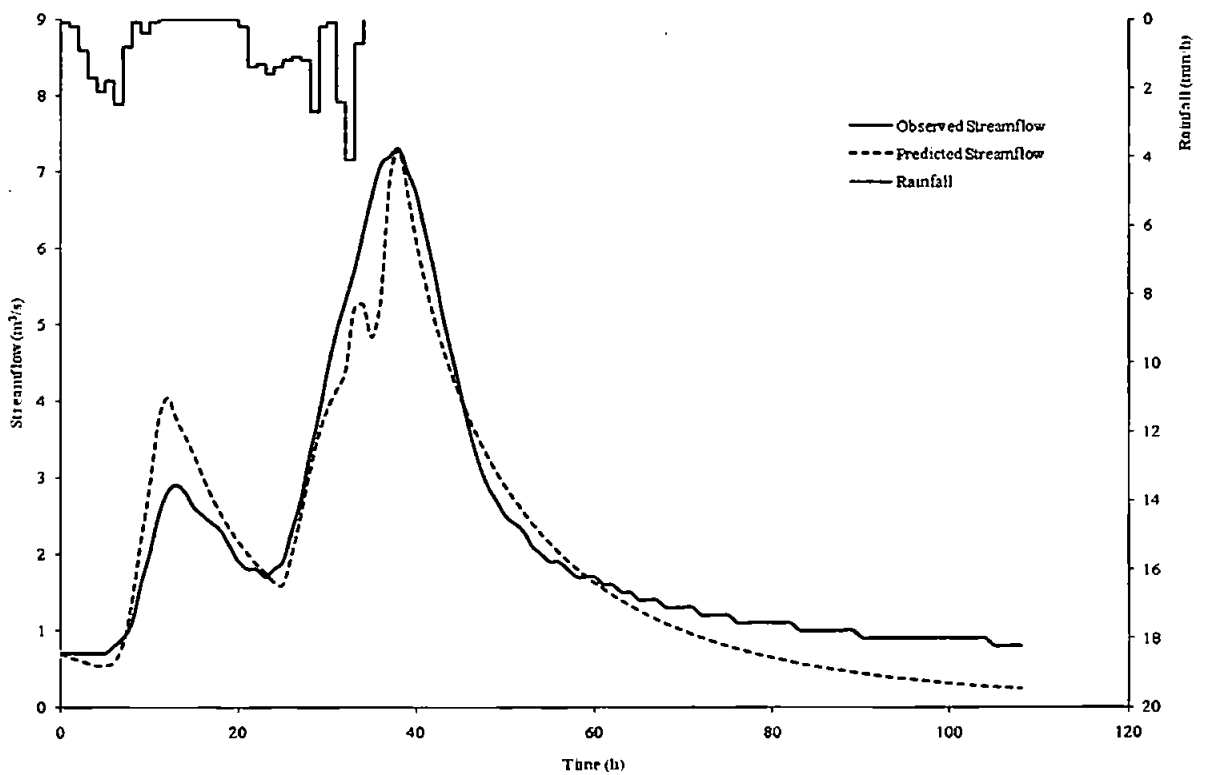
Figure 6.26 Results for event 3893 – with non-linear filter loss model

127

Event	Date	R_T	Q_P	SMD	No loss model					With non-linear filter loss model						
					K	α	T	K^α	NSE	K	α	T	C	P	K^α	NSE
2360	01-Jul-68	87.5	90.74	15.8	32.866	0.631	1.732	9.059	0.430	28.719	0.655	0.026	0.956	0.625	9.018	0.603
2361	19-Sep-68	77.4	47.68	6.3	30.507	0.871	1.539	19.630	0.827	22.288	0.965	1.263	0.821	0.065	19.993	0.847
2362	09-Oct-68	34.6	47.72	1.8	49.757	0.527	2.056	7.839	0.984	20.027	0.599	1.879	0.755	0.077	6.021	0.993
2363	23-Nov-68	30.6	48.79	0	18.873	0.535	3.947	4.815	0.972	10.875	0.661	3.554	0.825	0.154	4.843	0.967
2364	19-Dec-68	45.1	59.77	0	9.905	0.732	1.647	5.358	0.862	23.075	0.636	0.516	0.993	0.539	7.361	0.962
2365	20-Jan-69	85.6	119.12	0.2	5.179	0.731	2.561	3.327	0.896	12.667	0.682	1.654	0.753	0.517	5.650	0.887
2366	13-Dec-69	60.1	102.78	0.2	4.663	0.823	1.519	3.551	0.946	10.782	0.559	1.410	0.985	0.327	3.778	0.980
2367	18-Jan-72	55.7	154.82	0	2.423	0.592	3.754	1.689	0.849	23.114	0.334	2.820	0.913	0.505	2.855	0.926

Table 6.11 Catchment 74001 results for single fractional time-lagged reservoir
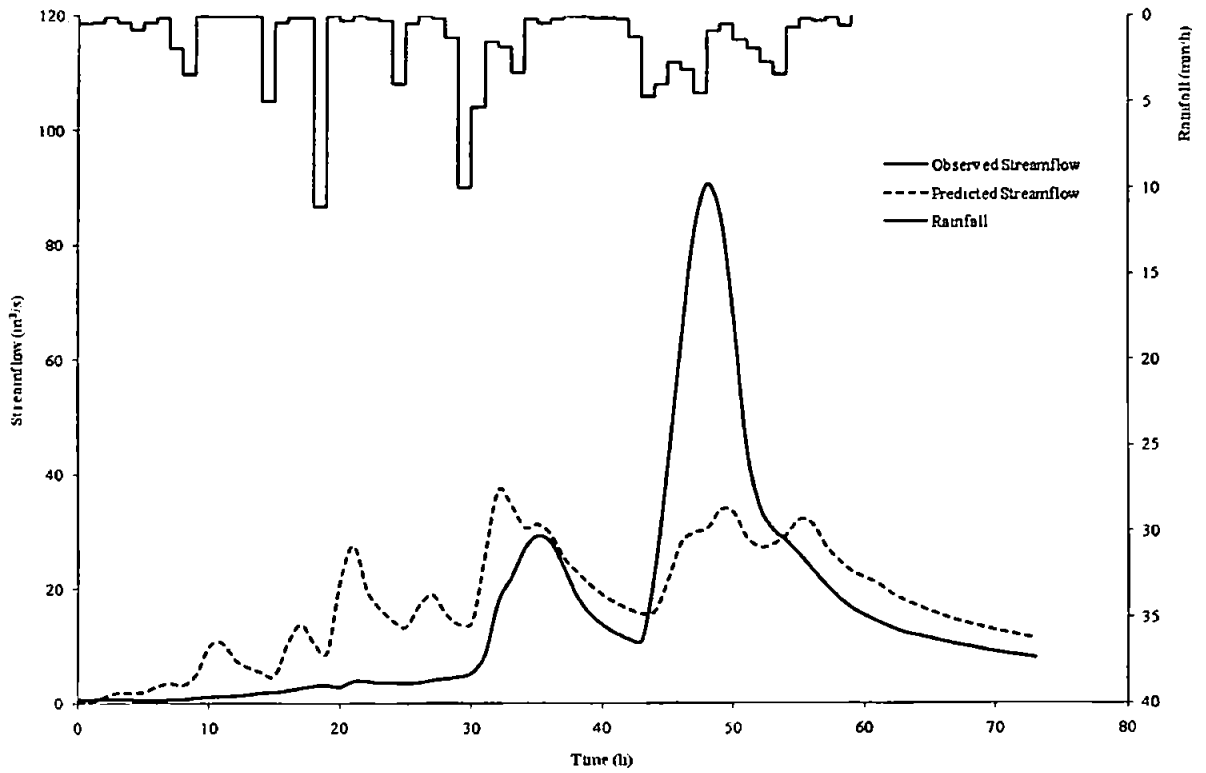
Figure 6.27 Results for event 2360 – without loss model
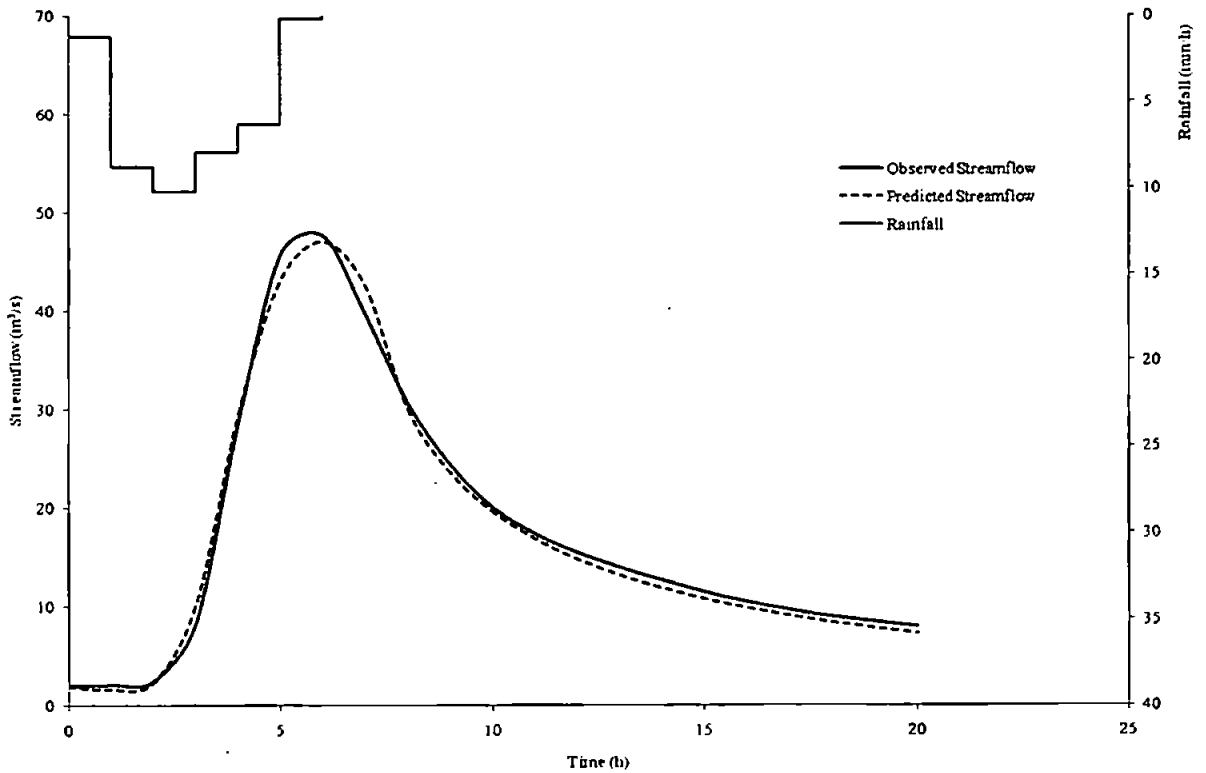

Figure 6.28 Results for event 2362 – without loss model

129
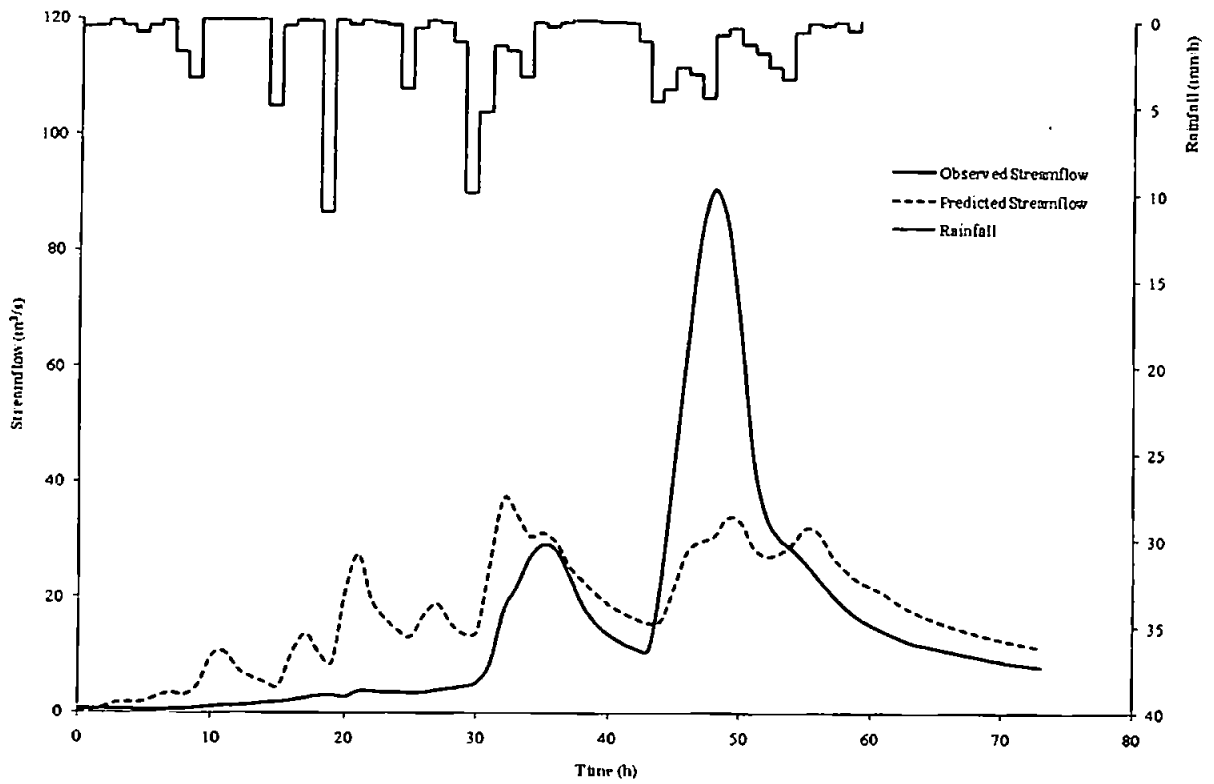
Figure 6.29 Results for event 2360 – with non-linear filter loss model
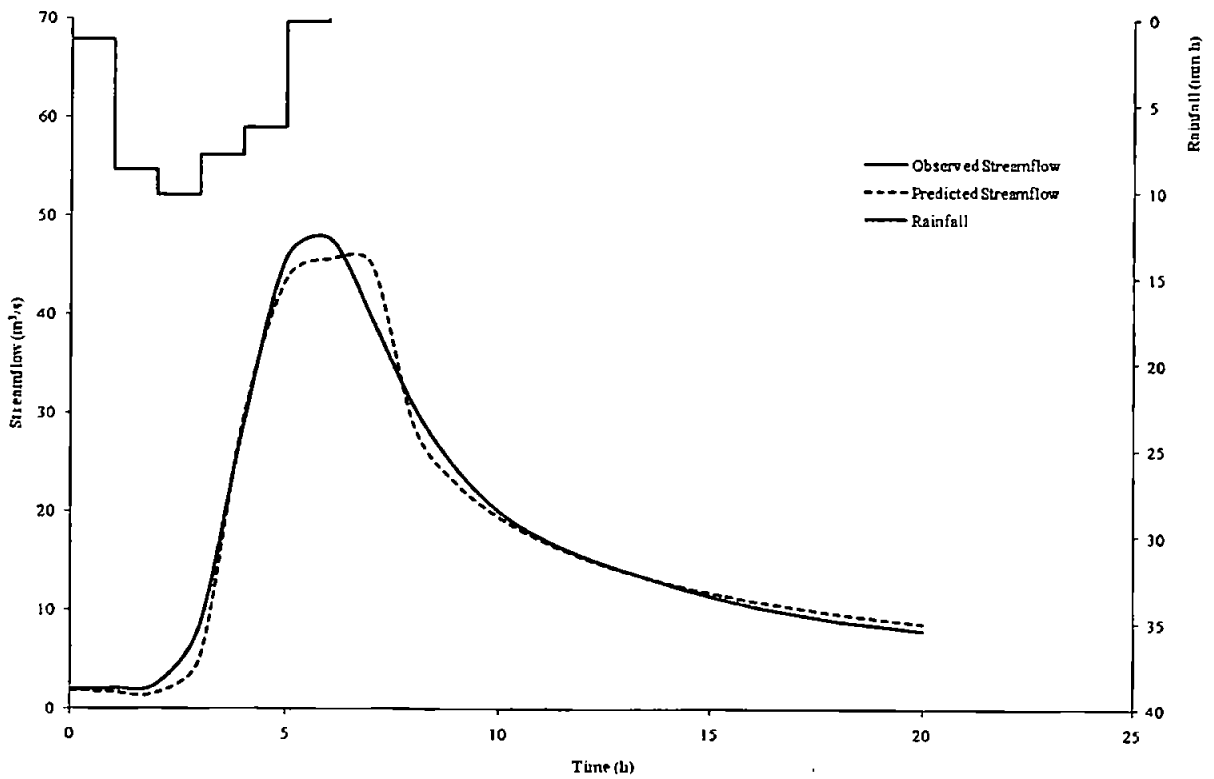
Figure 6.30 Results for event 2362 – with non-linear filter loss model

130

Event	Date	R_T	Q_P	SMD	No loss model					With non-linear filter loss model						
					K	α	T	K^α	NSE	K	α	T	C	P	K^α	NSE
3989	05-Aug-78	49.9	36.24	60.3	98.654	0.645	6.972	19.329	0.854	38.188	0.801	9.961	0.776	0.086	18.498	0.911
3990	07-Dec-78	19.1	17.16	55.9	86.037	0.663	7.630	19.173	0.894	54.145	0.731	7.643	0.918	0.081	18.503	0.916
3994	19-May-79	35.3	43.83	22.2	79.090	0.563	5.650	11.712	0.890	18.069	0.940	3.577	0.668	0.202	15.189	0.956
3995	29-May-79	28.3	57.52	3	38.976	0.755	2.693	15.887	0.844	24.768	0.999	0.289	0.996	0.437	24.689	0.939
3996	14-Nov-79	41.9	32.01	42.2	216.602	0.473	10.868	12.728	0.938	30.832	0.812	7.698	0.651	0.193	16.183	0.982
3997	11-Mar-80	13.3	17.49	0	75.121	0.599	8.787	13.292	0.958	39.129	0.707	8.613	0.995	0.128	13.363	0.975
3998	17-Mar-80	16.8	19.73	0.7	37.126	0.773	7.711	16.344	0.976	22.432	0.977	6.338	0.961	0.162	20.883	0.989
3999	29-Nov-81	14.7	21.72	49.5	64.094	0.628	9.604	13.636	0.962	36.138	0.709	9.501	0.884	0.064	12.723	0.979
4002	26-Apr-83	42.6	52.12	3.2	27.888	0.608	10.684	7.565	0.971	20.697	0.807	8.369	0.847	0.026	11.533	0.978
4004	08-Dec-83	41.4	43.32	49.1	138.155	0.473	10.811	10.289	0.921	36.775	0.933	4.689	0.983	0.483	28.884	0.980
4018	05-Jan-88	13	18.3	0	70.684	0.698	6.630	19.536	0.823	44.471	0.770	6.611	0.996	0.127	18.579	0.862
4393	03-Dec-81	10.7	15.16	42.1	69.360	0.688	8.713	18.479	0.969	48.146	0.751	8.660	0.996	0.075	18.349	0.977
4395	20-Apr-83	16.6	32.77	8.5	74.322	0.598	7.611	13.150	0.901	38.540	0.738	6.662	0.997	0.205	14.805	0.946
4399	01-Jun-83	15.2	21.51	7.1	68.576	0.731	6.530	21.991	0.911	29.351	0.905	5.623	0.994	0.279	21.302	0.975
4401	03-Feb-88	16.5	21.36	0.2	51.520	0.875	6.555	31.476	0.900	25.220	0.990	6.460	0.858	0.183	24.419	0.940

Table 6.12 Catchment 25005 results for single fractional time-lagged reservoir
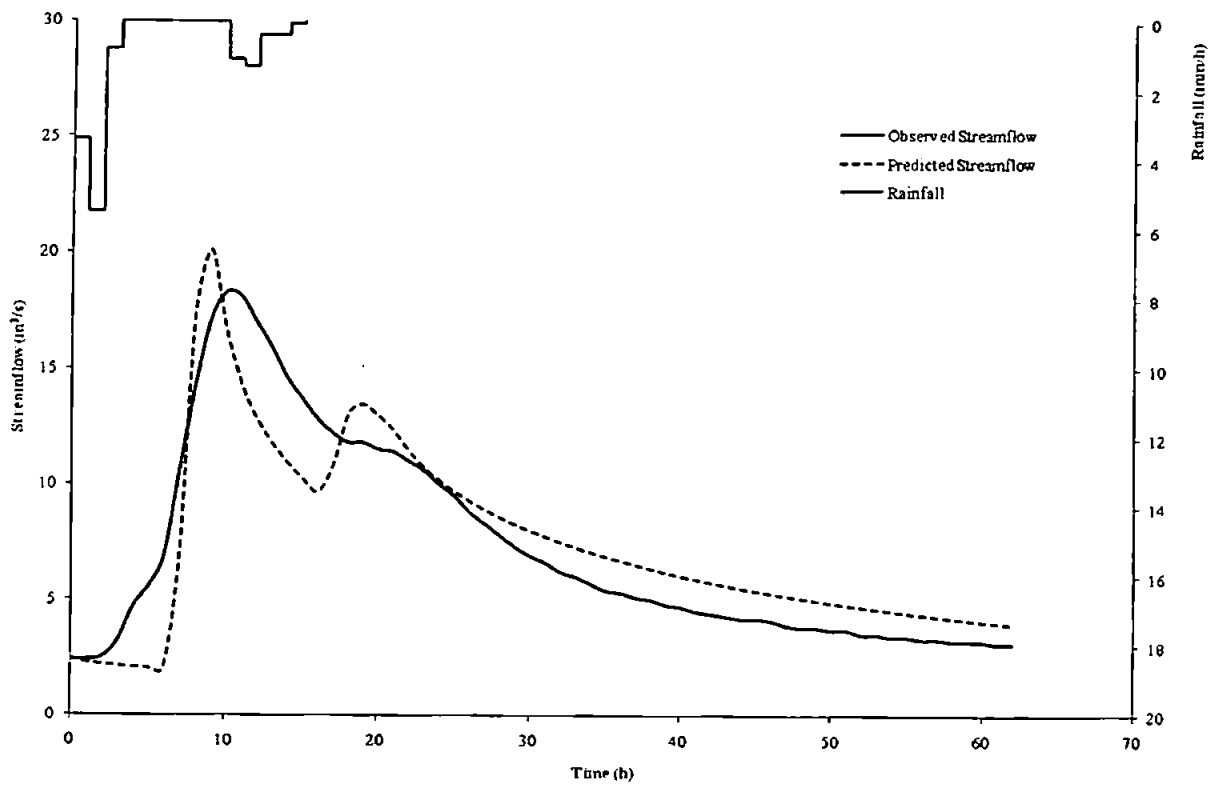
Figure 6.31 Results for event 4018 – without loss model
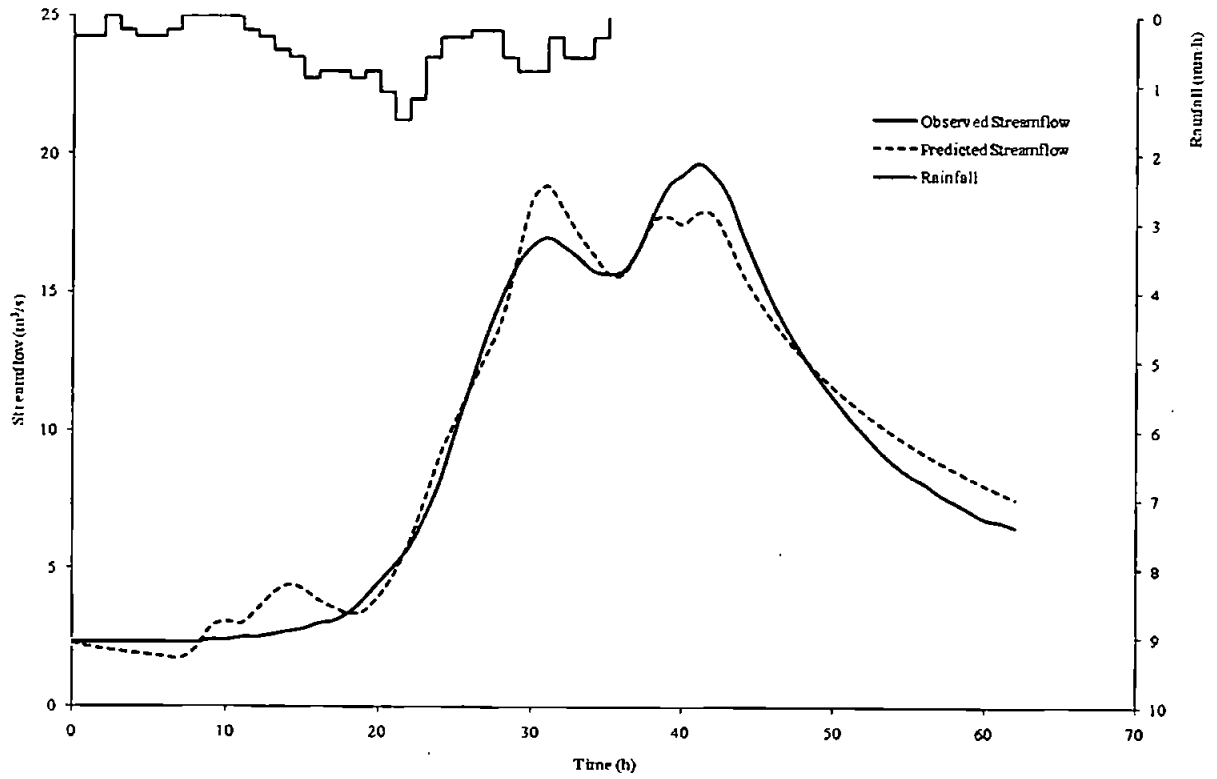
Figure 6.32 Results for event 3998 – without loss model

132
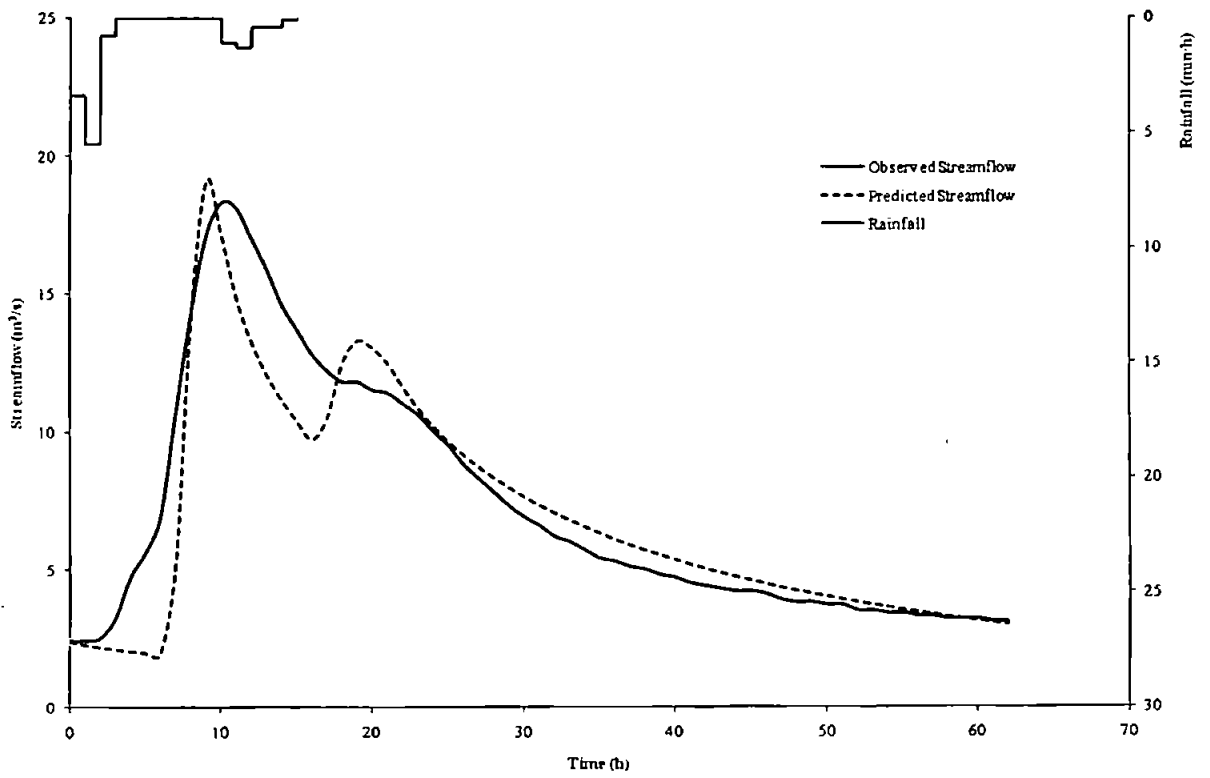
Figure 6.33 Results for event 4018 – with non-linear filter loss model
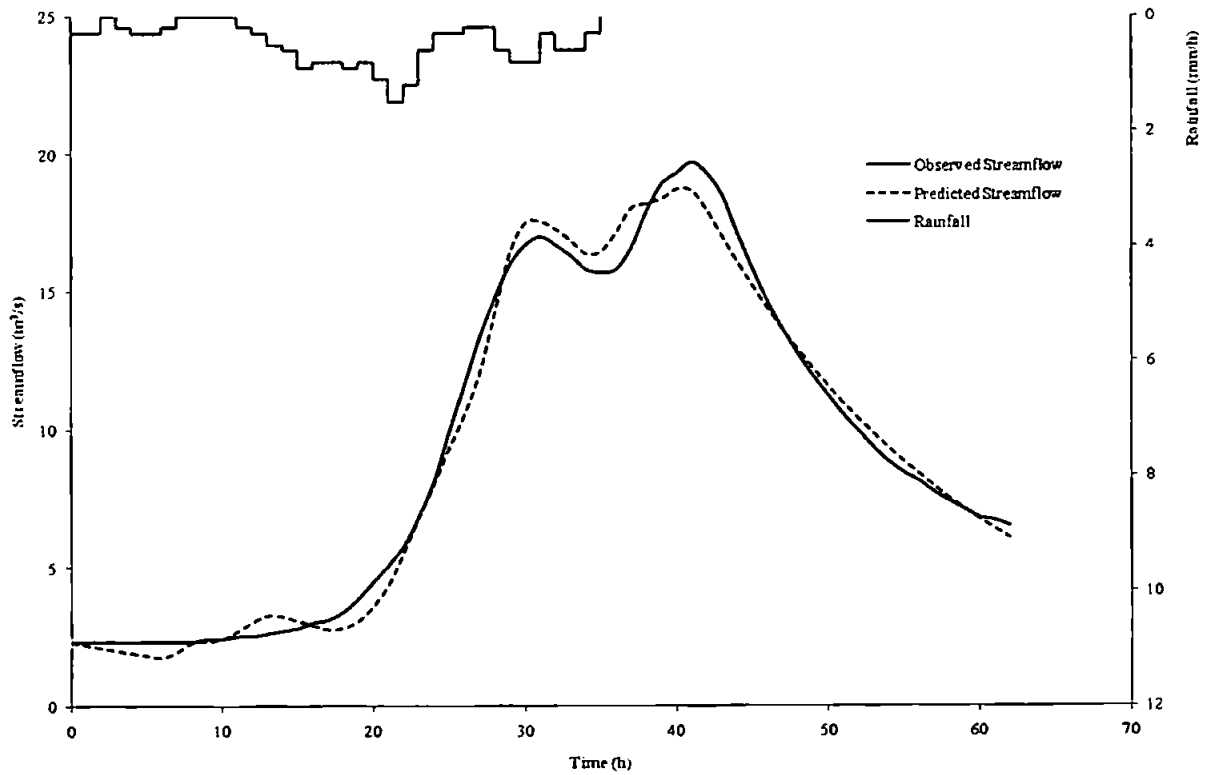
Figure 6.34 Results for event 3998 – with non-linear filter loss model

133

Event	Date	R_T	Q_P	SMD	No loss model					With non-linear filter loss model						
					K	α	T	K^{α}	NSE	K	α	T	C	P	K^{α}	NSE
1559	24-Jan-60	38.4	45.78	0	85.907	0.793	6.545	34.173	0.891	55.171	0.922	4.523	0.984	0.249	40.351	0.931
1560	27-Jan-60	32.1	38.09	0	62.750	0.922	2.365	45.436	0.868	41.305	0.999	1.431	0.975	0.246	41.152	0.923
1561	17-Nov-60	17.8	22.4	0	64.218	1.000	3.436	64.218	0.877	60.787	0.997	3.491	0.995	0.008	60.043	0.864
1562	03-Dec-60	34.7	45.36	0	58.237	0.774	8.616	23.241	0.915	29.858	0.997	6.580	0.786	0.126	29.555	0.948
1563	09-Dec-65	23.8	29.83	0	66.613	0.842	5.471	34.311	0.936	45.722	0.990	3.629	1.000	0.157	44.007	0.947
1564	22-Dec-65	20.1	23.65	0	64.141	0.956	4.128	53.410	0.971	49.081	0.994	3.701	0.980	0.088	47.948	0.973
1567	09-Dec-66	15.7	24.36	0	67.191	0.980	2.363	61.768	0.908	56.032	0.998	2.307	0.952	0.046	55.583	0.921
1568	08-Mar-67	23.8	22.88	0	94.546	0.854	2.330	48.663	0.913	54.874	0.981	1.348	0.966	0.184	50.853	0.958
1570	12-Mar-69	29.2	35.85	5	58.489	0.795	6.616	25.399	0.944	27.049	0.998	5.574	0.693	0.018	26.871	0.974
1571	05-May-69	36.2	34.19	20.4	109.201	0.810	4.609	44.768	0.807	64.141	0.942	2.558	0.861	0.146	50.387	0.841
1572	03-Aug-69	31.1	20.35	74.2	478.255	0.686	1.491	68.904	0.855	68.056	0.883	0.262	0.662	0.327	41.536	0.906

Table 6.13 Catchment 54004 results for single fractional time-lagged reservoir

134
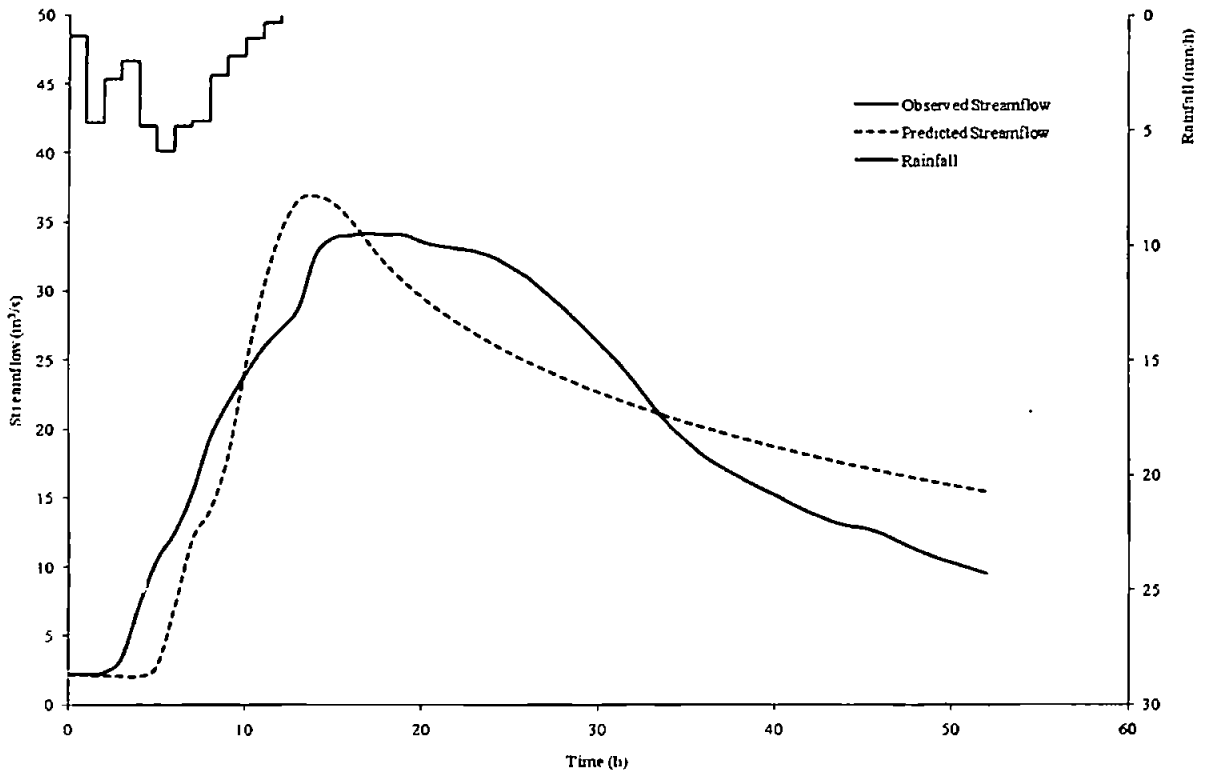
Figure 6.35 Results for event 1571 – without loss model
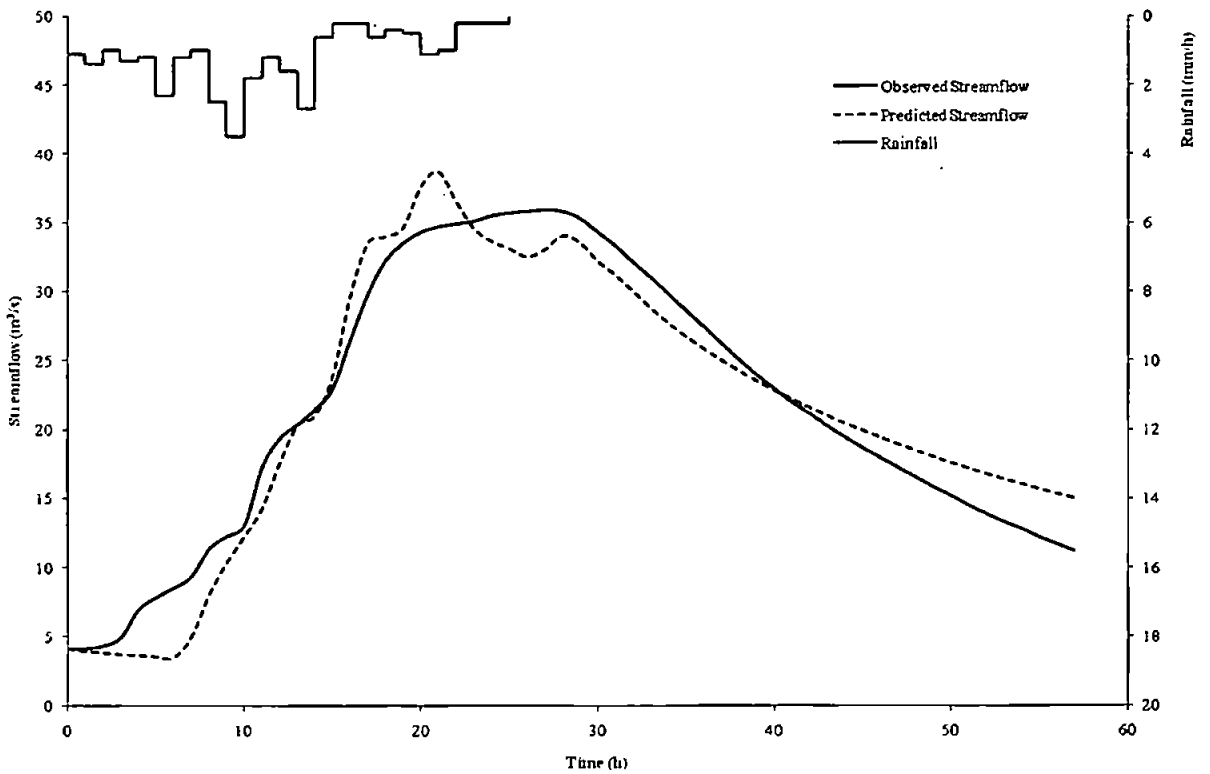
Figure 6.36 Results for event 1570 – without loss model

135
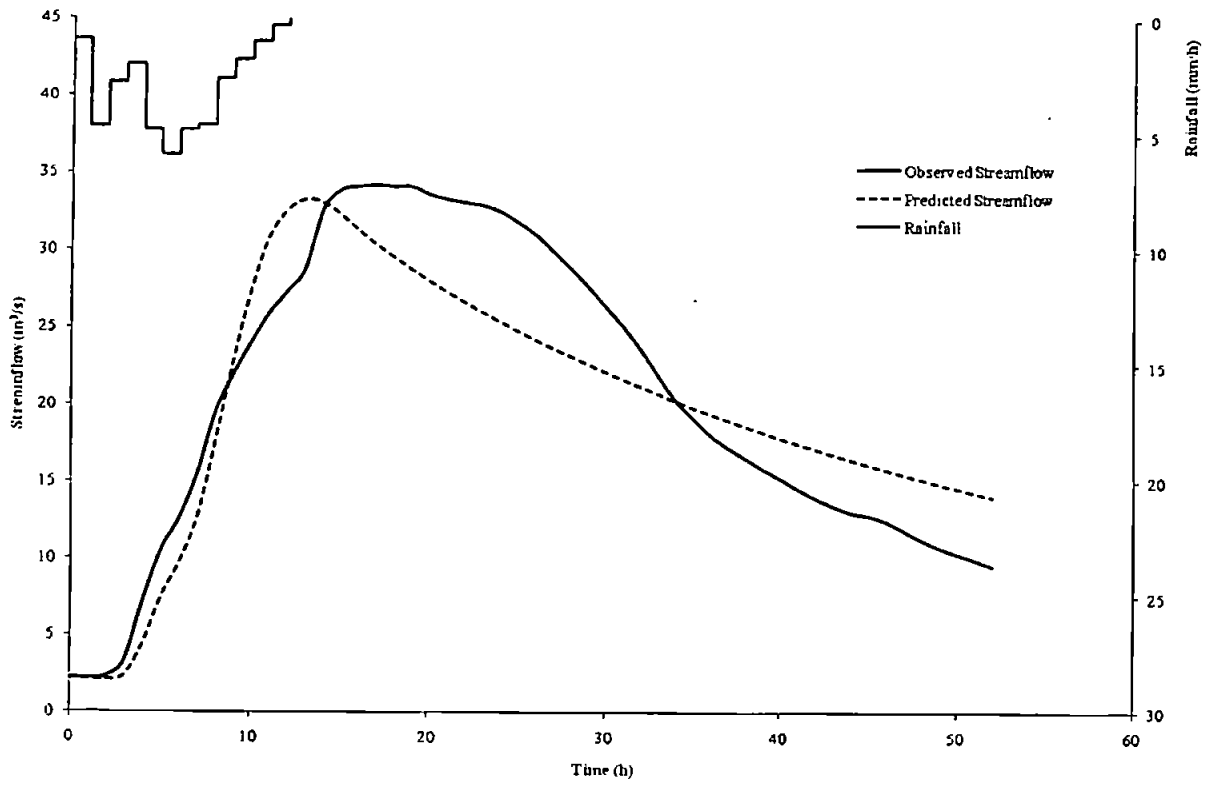
Figure 6.37 Results for event 1571 – with non-linear filter loss model
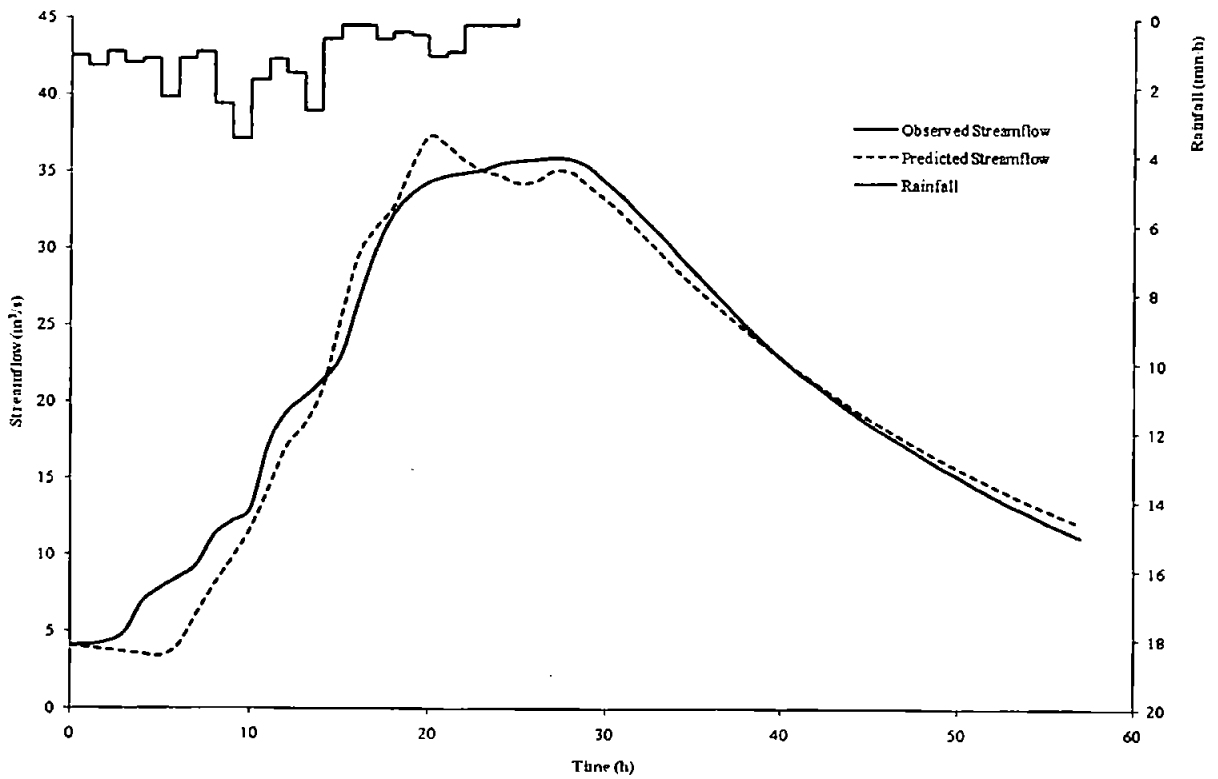
Figure 6.38 Results for event 1570 – with non-linear filter loss model

Event	Date	R_T	Q_P	SMD	No loss model					With non-linear filter loss model						
					K	α	T	K^α	NSE	K	α	T	C	P	K^α	NSE
650	03-Dec-60	22.9	37.25	0	63.655	0.823	19.668	30.518	0.700	61.145	0.995	9.860	0.964	0.020	59.900	0.592
651	27-Feb-61	21.1	20.12	0	100.021	0.985	4.385	93.345	0.744	75.626	0.999	4.499	0.959	0.081	75.300	0.769
653	08-Mar-63	11.6	13.46	7.5	82.585	1.000	13.525	82.585	0.889	77.089	0.994	9.896	0.975	0.038	75.105	0.753
656	02-Sep-65	37.8	8.21	84.4	637.367	0.952	0.757	467.497	0.813	145.634	0.995	0.173	0.391	0.115	142.052	0.785
657	08-Dec-65	21.9	24.49	0.2	89.594	0.999	4.542	89.192	0.703	88.991	0.994	4.519	0.994	0.007	86.626	0.695
658	18-Apr-66	27.8	23.12	3.1	101.791	0.927	5.580	72.635	0.748	61.865	0.999	5.485	0.944	0.131	61.610	0.791
659	27-Feb-67	15.6	20.33	0	69.024	0.999	4.676	68.732	0.662	66.125	0.997	4.688	0.983	0.004	65.299	0.657

Table 6.14 Catchment 37001 results for single fractional time-lagged reservoir
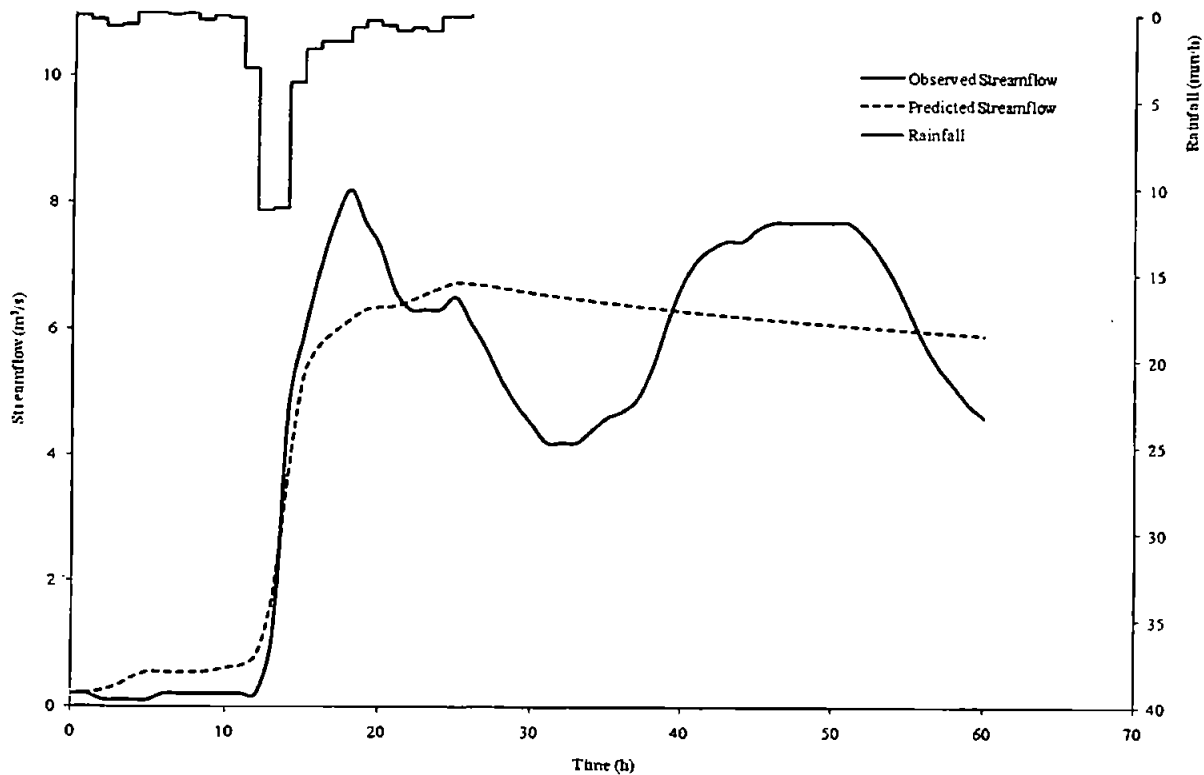
Figure 6.39 Results for event 656 – without loss model
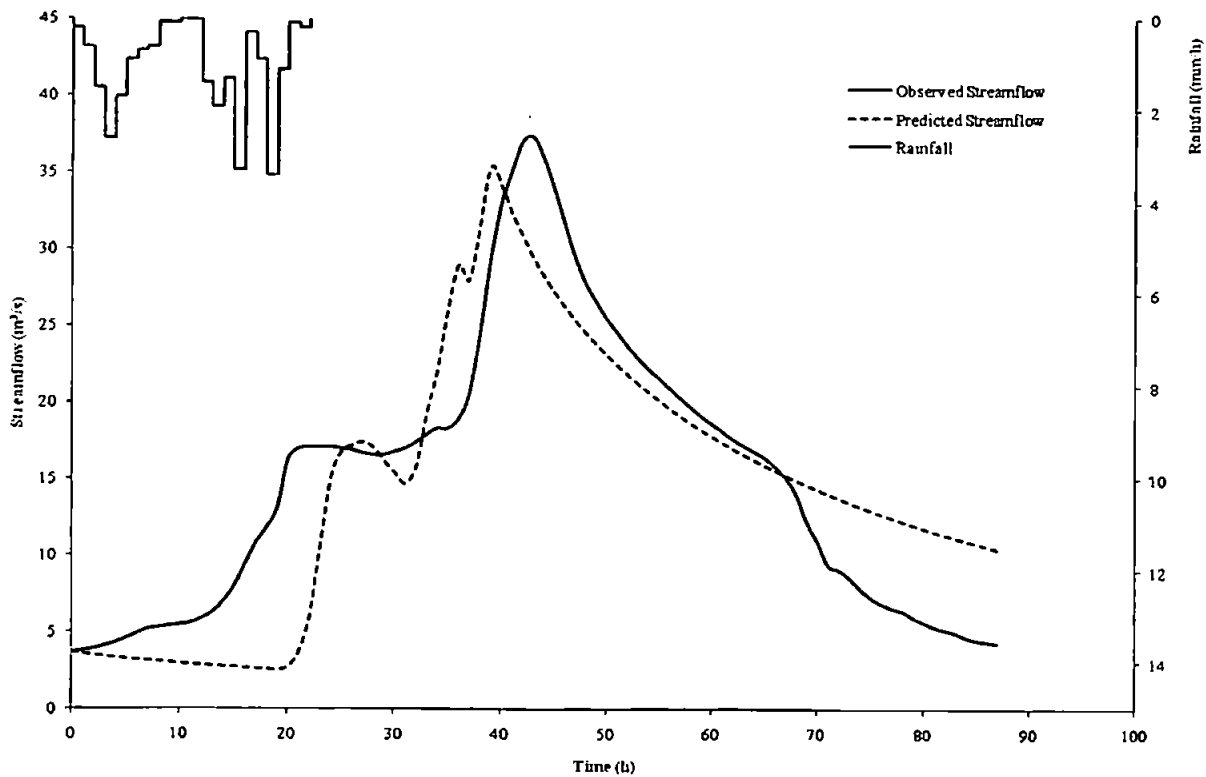
Figure 6.40 Results for event 650 – without loss model

138
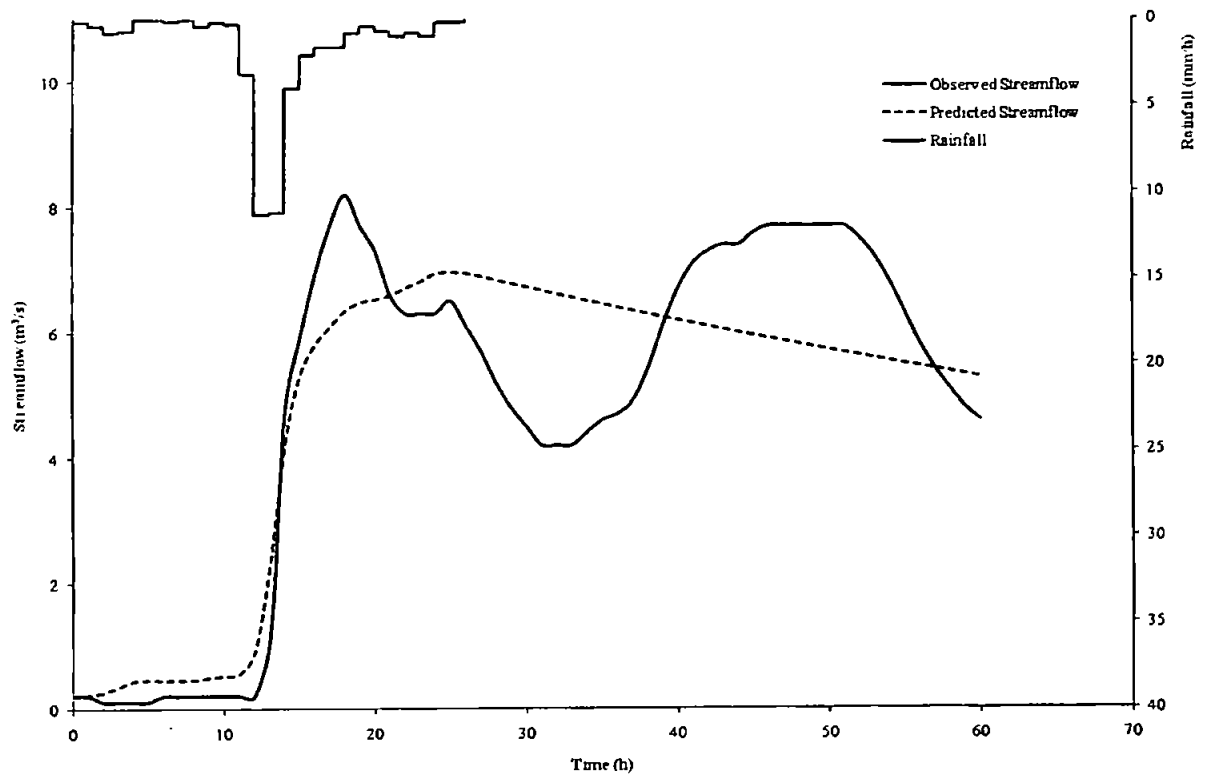
Figure 6.41 Results for event 656 – with non-linear filter loss model
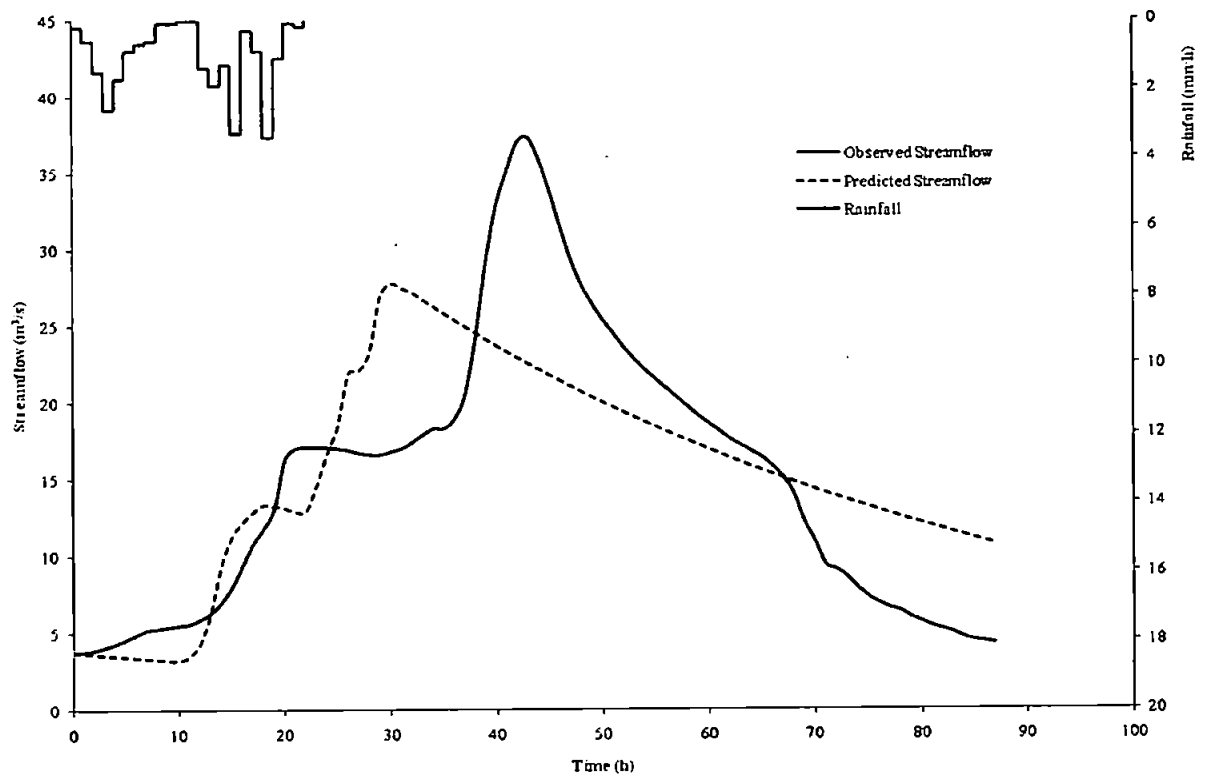
Figure 6.42 Results for event 650 – with non-linear filter loss model

139

Event	Date	R_T	Q_P	SMD	No loss model					With non-linear filter loss model						
					K	α	T	K^{α}	NSE	K	α	T	C	P	K^{α}	NSE
2072	06-Jul-64	71.6	236.74	44.4	289.574	0.321	4.859	6.169	0.907	121.104	0.401	3.746	0.780	0.456	6.845	0.962
2073	12-Nov-64	41.2	241.45	0	15.891	0.524	4.660	4.260	0.960	16.567	0.648	3.592	0.870	0.313	6.167	0.984
2074	11-Dec-64	191.5	535.23	0	7.160	0.753	1.850	4.403	0.937	6.308	0.947	1.594	0.749	0.109	5.721	0.950
2075	08-May-65	42.6	333.01	2	10.003	0.578	3.748	3.785	0.873	93.268	0.398	2.770	0.993	0.718	6.081	0.920
2076	14-Sep-66	40.6	301.86	0	10.378	0.585	2.639	3.930	0.973	8.903	0.766	1.730	0.855	0.160	5.338	0.988
2077	30-Nov-66	76.4	335.68	0	6.090	0.616	2.606	3.043	0.880	6.455	0.895	0.852	0.714	0.421	5.307	0.950
2078	22-Feb-67	61.8	399.48	0	2.973	0.363	3.541	1.485	0.922	18.854	0.234	3.564	0.976	0.272	1.988	0.939
2079	27-Feb-67	71.8	520.77	0	3.625	0.776	0.553	2.717	0.894	5.082	0.607	0.559	0.875	0.224	2.683	0.896
2080	01-Oct-67	56.8	442.82	0.3	4.580	0.569	2.485	2.377	0.968	24.839	0.498	1.807	0.996	0.365	4.952	0.938
2081	16-Oct-67	71.4	396.79	0.2	6.510	0.968	1.348	6.131	0.974	19.383	0.659	0.875	0.960	0.436	7.054	0.986
2082	22-Dec-67	57.9	376.91	0	6.220	0.873	1.513	4.931	0.966	6.940	0.828	1.589	0.968	0.056	4.973	0.962
2083	13-Jan-68	97.1	412.15	0.2	4.418	0.995	3.490	4.385	0.884	6.170	0.953	2.317	0.856	0.288	5.664	0.940
2084	22-Mar-68	122.9	449.58	0	7.546	0.997	0.111	7.500	0.944	10.376	0.659	0.626	0.996	0.172	4.673	0.929

Table 6.15 Catchment 66011 results for single fractional time-lagged reservoir
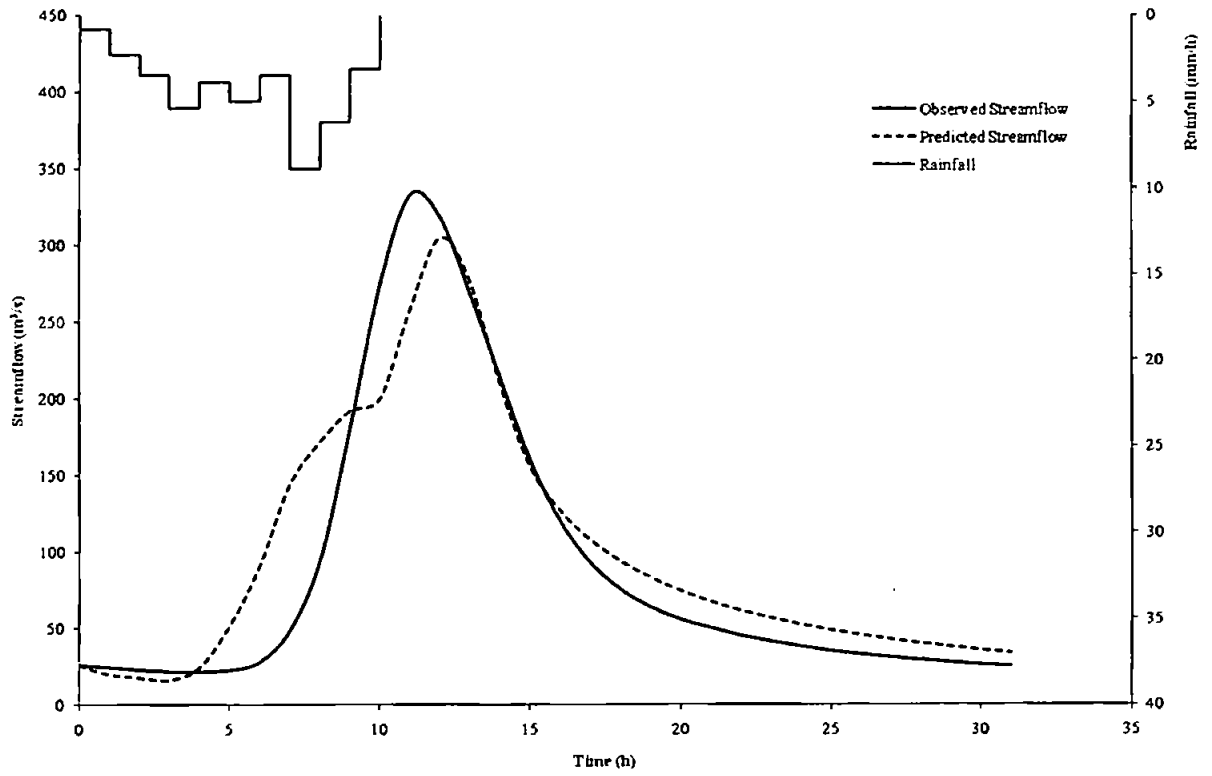
Figure 6.43 Results for event 2075 – without loss model
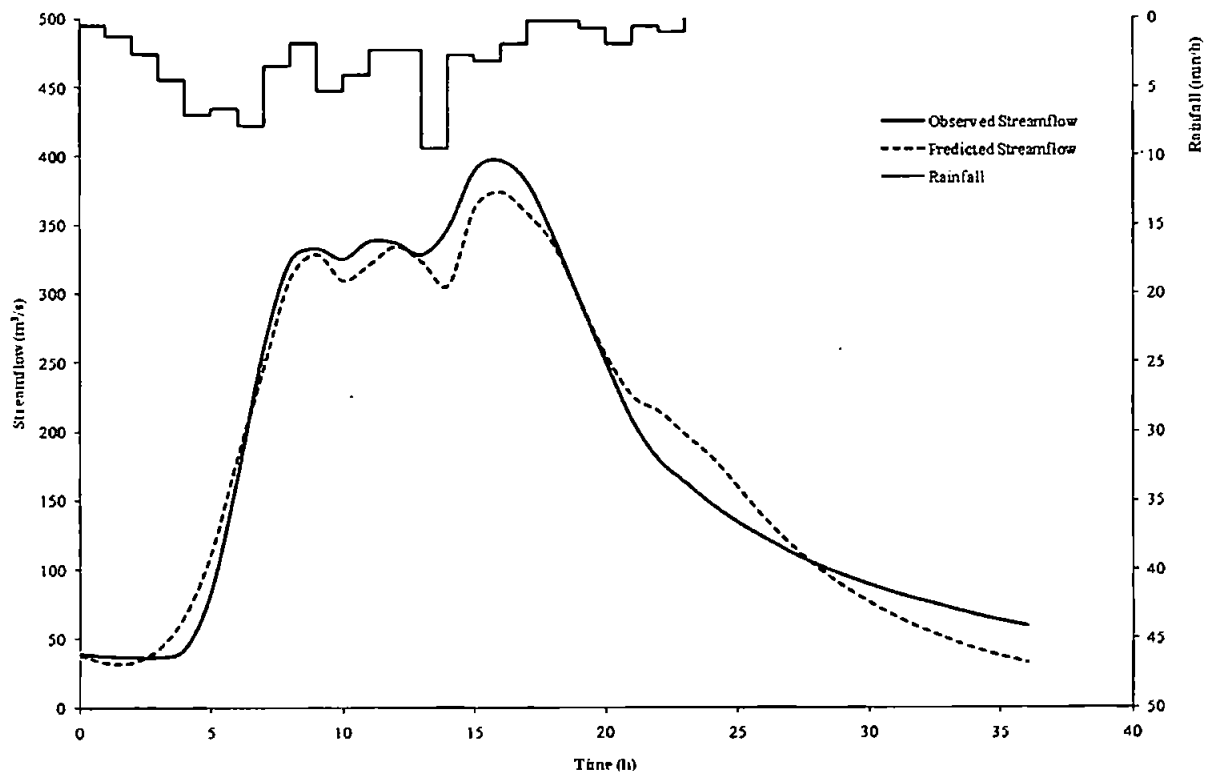
Figure 6.44 Results for event 2081 – without loss model

141
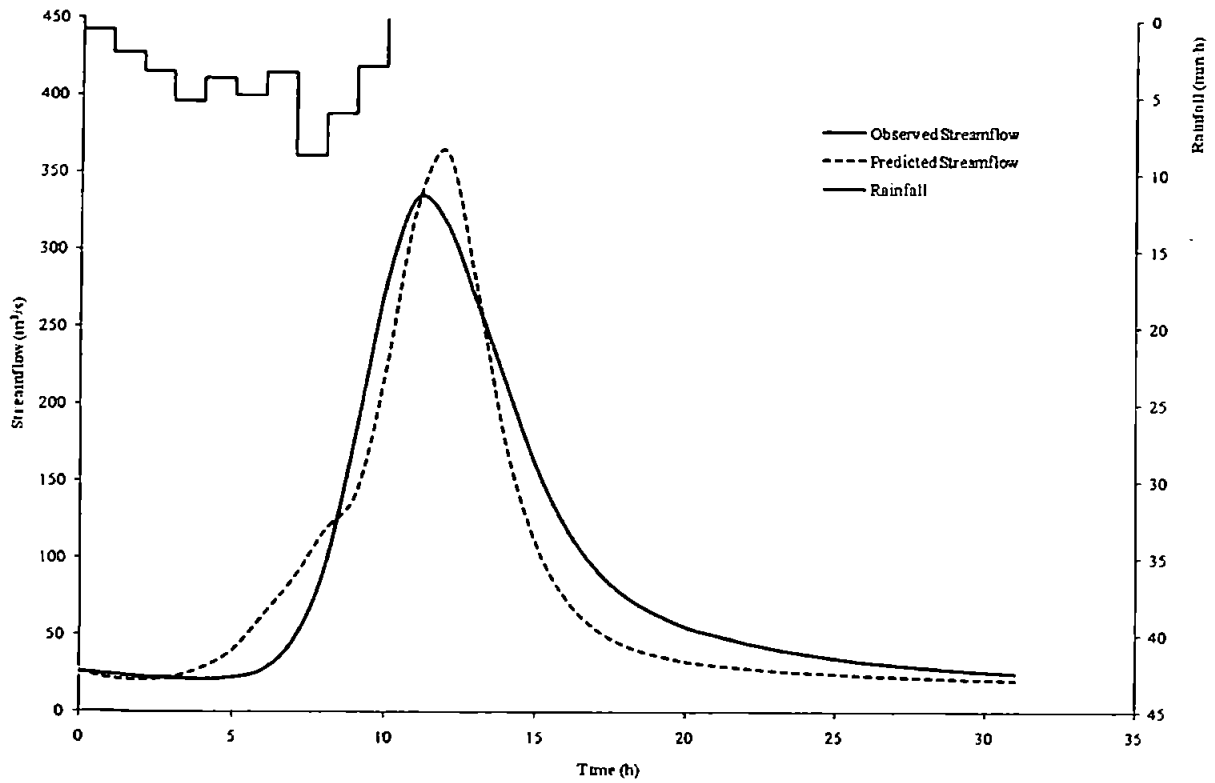
Figure 6.45 Results for event 2075 – with non-linear filter loss model
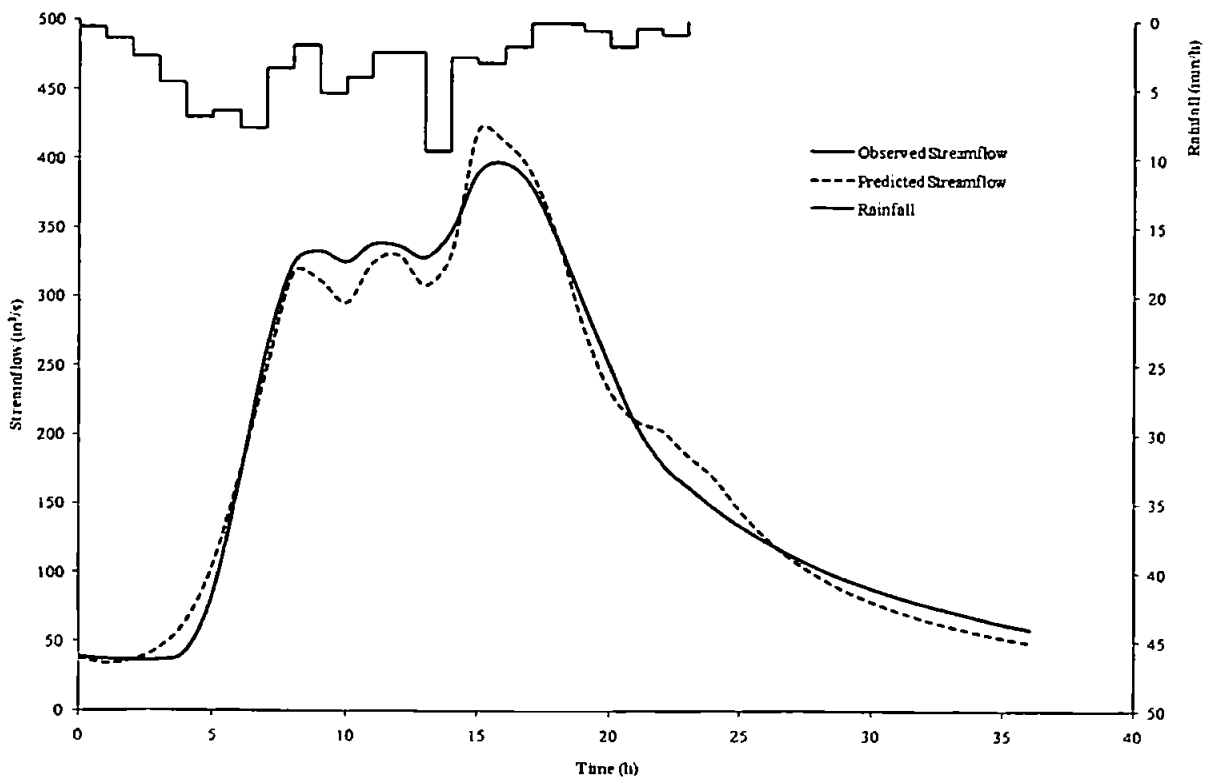
Figure 6.46 Results for event 2081 – with non-linear filter loss model

142

Event	Date	R_T	Q_P	SMD	No loss model					With non-linear filter loss model						
					K	α	T	K^α	NSE	K	α	T	C	P	K^α	NSE
409	04-Nov-67	24.2	40.02	0	61.251	0.863	13.591	34.856	0.895	48.901	0.994	9.993	0.996	0.105	47.773	0.893
410	10-Jul-68	51.2	56.87	19.5	134.559	0.783	19.525	46.445	0.735	79.084	0.997	9.782	0.884	0.148	78.054	0.704
411	01-Nov-68	26.1	43.99	0	88.606	0.783	17.590	33.486	0.676	56.744	0.999	9.942	0.998	0.172	56.515	0.696
412	12-Mar-69	27.9	36	4.1	101.506	0.712	14.716	26.830	0.881	48.185	0.990	9.461	0.991	0.245	46.354	0.914
413	05-May-69	36.3	56.63	12.9	108.992	0.720	12.680	29.304	0.782	42.841	0.999	9.513	0.979	0.409	42.680	0.884

Table 6.16 Catchment 28026 results for single fractional time-lagged reservoir
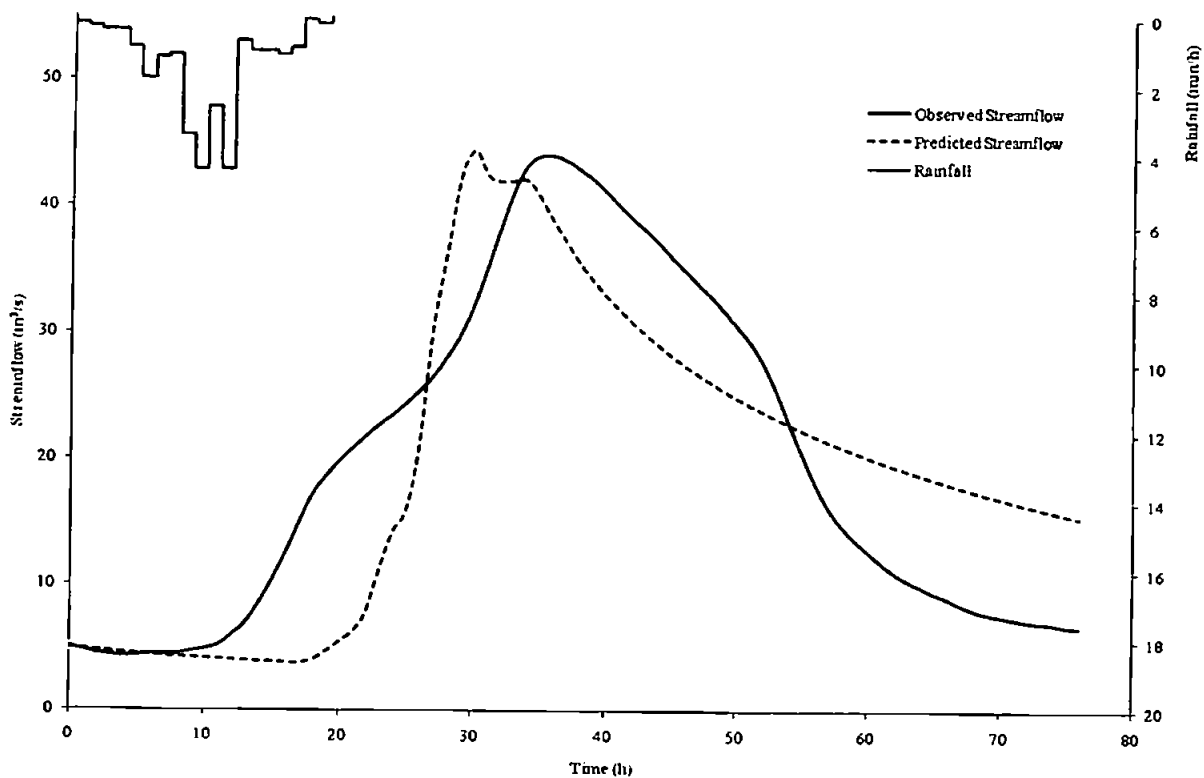
Figure 6.47 Results for event 411 – without loss model
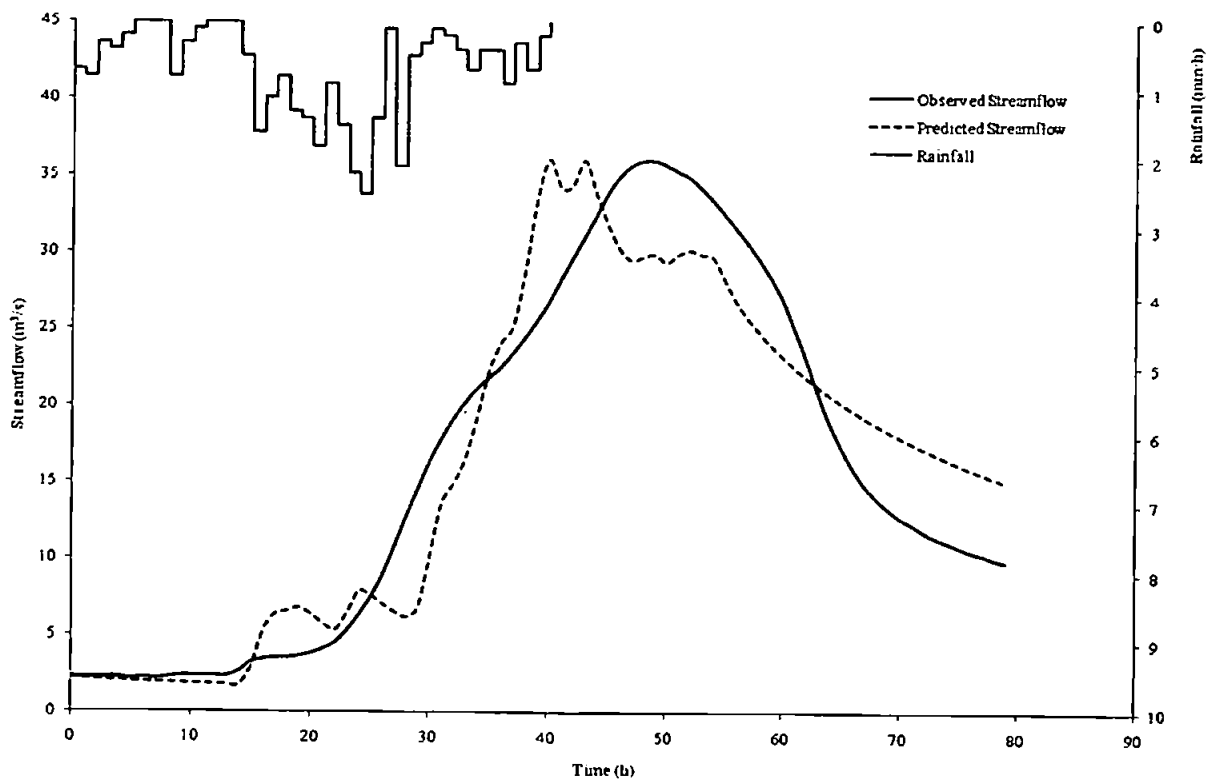
Figure 6.48 Results for event 412 – without loss model
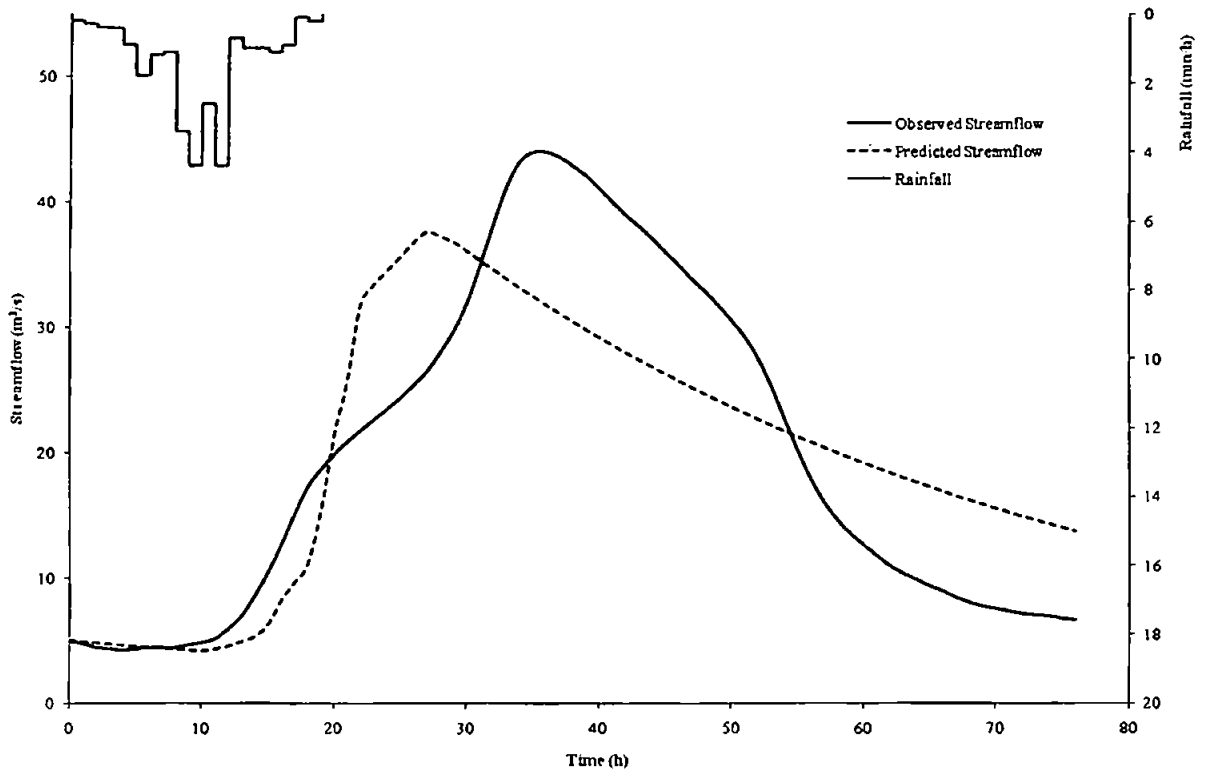
Figure 6.49 Results for event 411 – with non-linear filter loss model
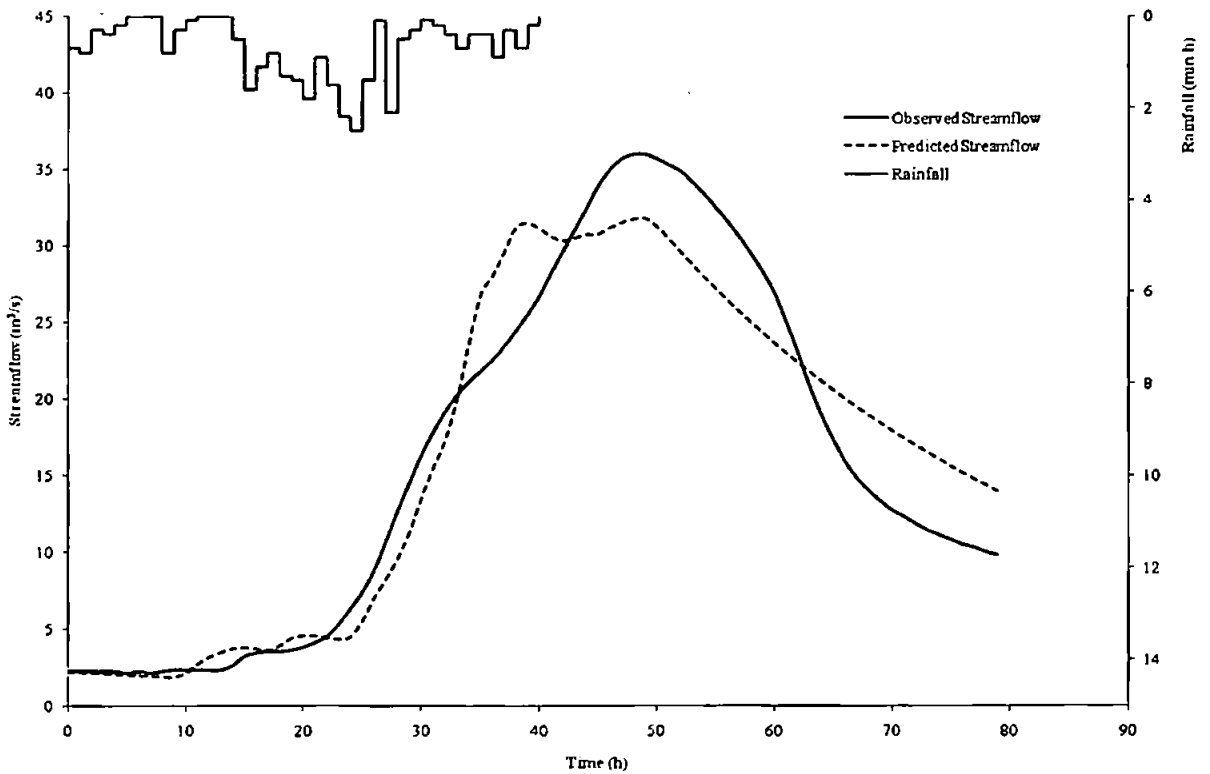
Figure 6.50 Results for event 412 – with non-linear filter loss model

145

Event	Date	R_T	Q_P	SMD	No loss model					With non-linear filter loss model						
					K	α	T	K^α	NSE	K	α	T	C	P	K^α	NSE
3671	02-Jul-78	70.4	155.59	77	219.109	0.483	5.662	13.506	0.829	104.886	0.422	5.607	0.881	0.265	7.124	0.920
3673	03-Oct-79	32.8	92.6	36.2	233.629	0.451	5.847	11.701	0.714	49.823	0.554	5.825	0.845	0.219	8.717	0.773
3675	24-Jul-80	77.9	275.97	72.5	65.252	0.473	3.779	7.216	0.665	13.821	0.608	3.657	0.669	0.089	4.937	0.706
3677	26-Oct-80	33.6	199.59	0	27.839	0.552	5.637	6.273	0.640	23.697	0.725	3.944	0.772	0.048	9.923	0.619
3678	23-Aug-85	41.7	192.28	10.8	29.329	0.653	3.328	9.081	0.481	9.491	0.841	1.605	0.776	0.003	6.636	0.631
3680	09-Jan-86	129.8	130.19	0	156.916	0.717	1.506	37.523	0.070	71.258	0.561	3.186	0.733	0.019	10.951	0.080
3682	19-Jan-86	27.1	87.19	0	49.716	0.600	1.591	10.421	0.661	21.862	0.829	0.151	0.939	0.262	12.900	0.703
3686	17-Jun-86	29.5	102.32	20	175.332	0.571	5.759	19.109	0.614	29.289	0.909	3.481	0.957	0.477	21.539	0.796
3687	30-Jul-86	34.5	163.76	69	61.843	0.539	3.575	9.236	0.698	21.561	0.670	2.269	0.952	0.571	7.826	0.920
3688	28-Oct-86	50.8	223.64	23.2	135.561	0.301	4.009	4.383	0.694	8.238	0.505	3.446	0.885	0.467	2.901	0.851
3691	02-Dec-86	25.3	134.02	3.3	11.213	0.737	3.842	5.938	0.805	20.227	0.316	5.729	0.943	0.013	2.586	0.679
3697	09-Jul-87	23.7	106.79	6.1	299.070	0.457	5.366	13.534	0.925	39.829	0.606	4.685	0.722	0.219	9.327	0.961
3698	14-Mar-88	30.9	50.18	0	398.613	0.565	4.832	29.465	0.748	46.445	0.698	3.582	0.917	0.508	14.572	0.897
3704	22-Sep-84	94.3	321.8	12.9	27.319	0.289	4.874	2.601	0.933	62.808	0.364	3.833	0.967	0.327	4.513	0.938
3705	07-Sep-83	101.9	268.29	49.9	52.875	0.495	5.413	7.129	0.830	46.961	0.650	2.486	0.948	0.584	12.208	0.922

Table 6.17 Catchment 7001 results for single fractional time-lagged reservoir

Figure 6.51 Results for event 3680 – without loss model
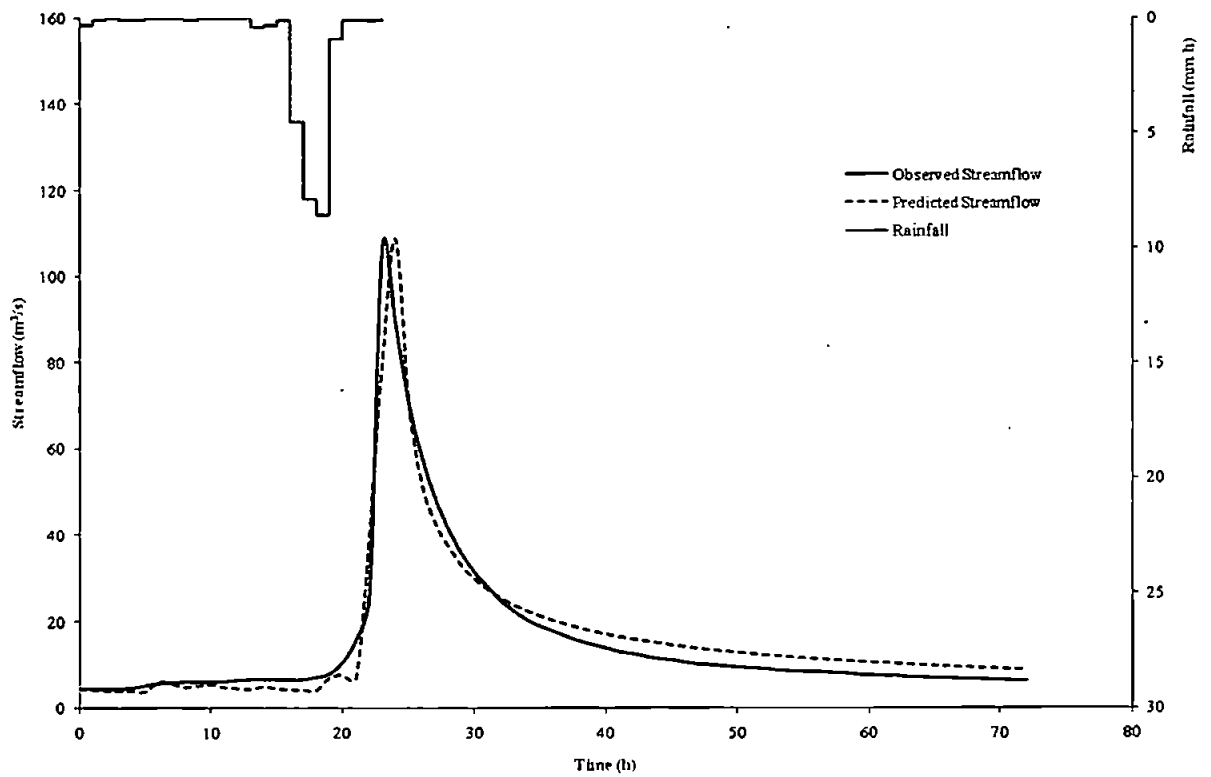
Figure 6.52 Results for event 3697 – without loss model
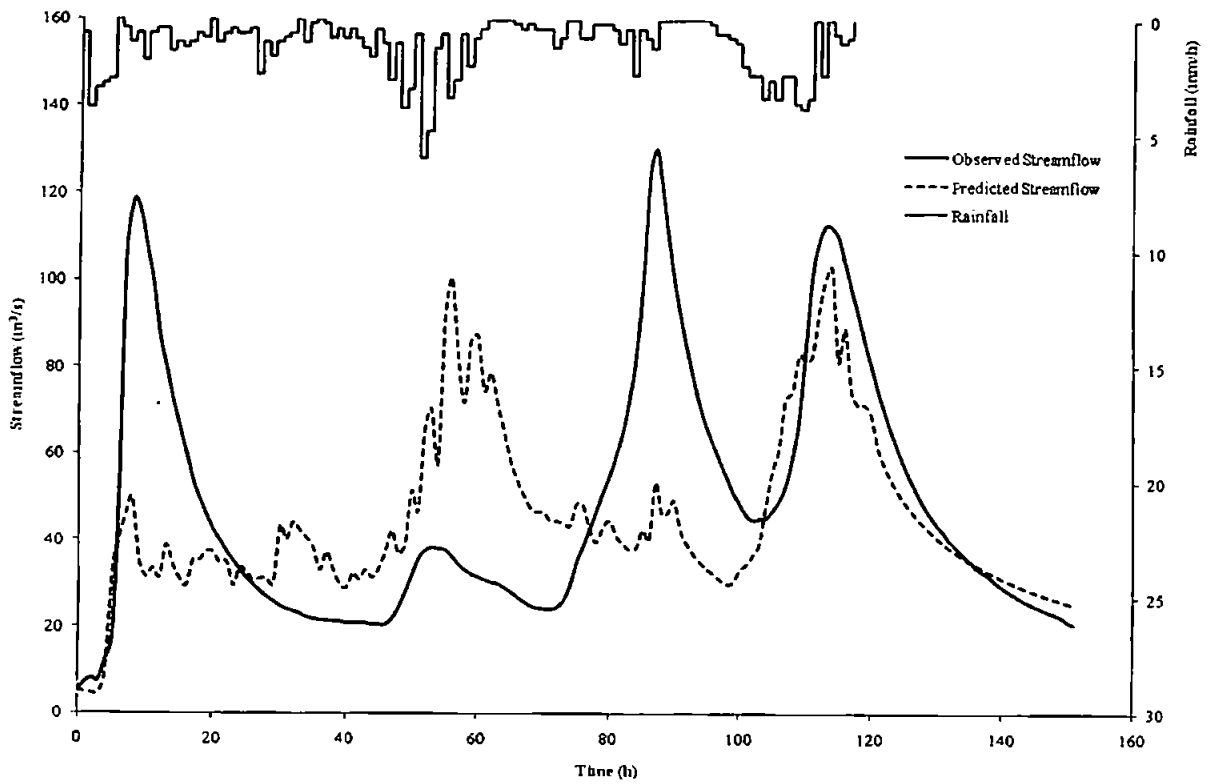
Figure 6.53 Results for event 3680 – with non-linear filter loss model
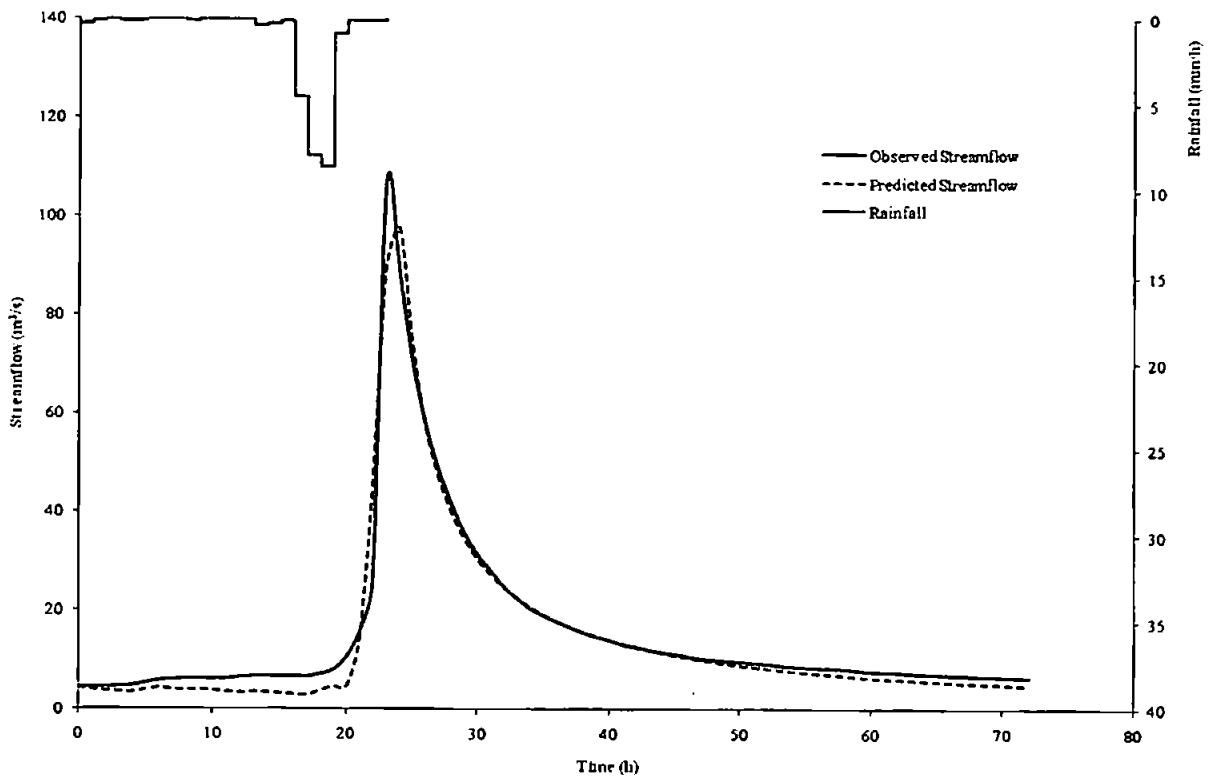
Figure 6.54 Results for event 3697 – with non-linear filter loss model

148

Event	Date	R_T	Q_P	SMD	No loss model					With non-linear filter loss model						
					K	α	T	K^α	NSE	K	α	T	C	P	K^α	NSE
1836	22-Mar-68	97.9	218.87	0	40.934	0.753	3.381	16.364	0.975	37.726	0.804	2.245	0.894	0.250	18.519	0.985
1837	12-May-68	33.1	120.8	2.4	95.945	0.533	4.787	11.387	0.981	51.899	0.583	4.738	0.864	0.092	9.999	0.987
1838	26-Jun-68	39.1	142.59	1.4	47.341	0.677	2.636	13.619	0.931	24.005	0.891	0.907	0.828	0.391	16.977	0.983
1840	10-Oct-68	49.1	159.05	0	43.909	0.635	3.691	11.041	0.972	24.665	0.733	3.440	0.828	0.063	10.481	0.974
1841	26-Oct-68	83.8	199.89	1.6	46.834	0.755	2.587	18.250	0.910	29.383	0.785	1.467	0.811	0.376	14.205	0.905
1842	17-Jan-69	42.7	155.6	0	23.055	0.743	4.618	10.293	0.916	21.456	0.932	2.422	0.962	0.337	17.418	0.957
1843	11-Nov-69	40.7	154.03	0	104.293	0.525	2.702	11.471	0.973	18.851	0.807	1.496	0.598	0.144	10.695	0.986
1844	15-Jan-70	53.2	217.51	0	26.535	0.706	4.806	10.121	0.944	19.068	0.904	3.209	0.823	0.245	14.368	0.969
1845	01-Nov-70	51.1	224.03	0	30.674	0.649	3.605	9.224	0.985	26.342	0.748	2.648	0.891	0.212	11.552	0.986
1846	18-Oct-71	64.7	236.23	0	46.903	0.561	3.772	8.661	0.924	49.469	0.678	2.406	0.968	0.398	14.085	0.978
1847	05-Dec-72	62.3	281.29	0	27.407	0.721	2.520	10.882	0.981	29.090	0.780	1.787	0.892	0.261	13.859	0.987

Table 6.18 Catchment 57005 results for single fractional time-lagged reservoir

Figure 6.55 Results for event 1841 – without loss model

Figure 6.56 Results for event 1847 – without loss model

150
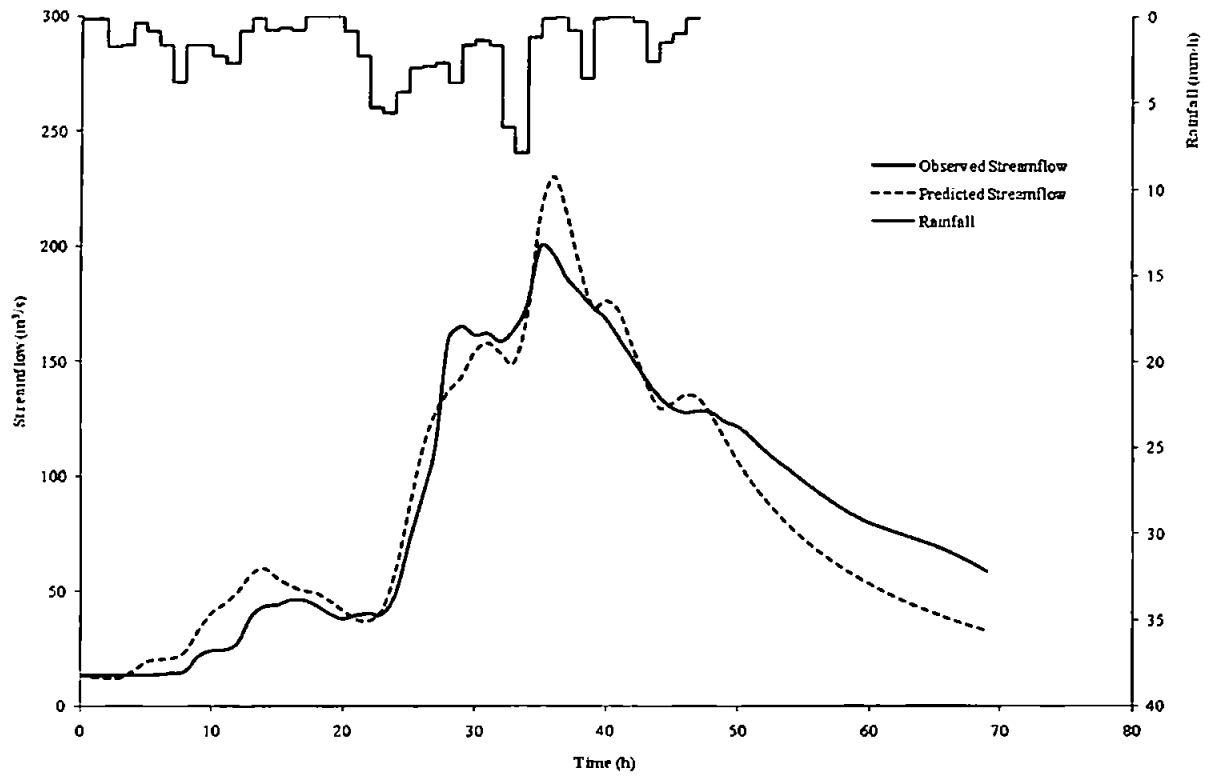
Figure 6.57 Results for event 1841 – with non-linear filter loss model
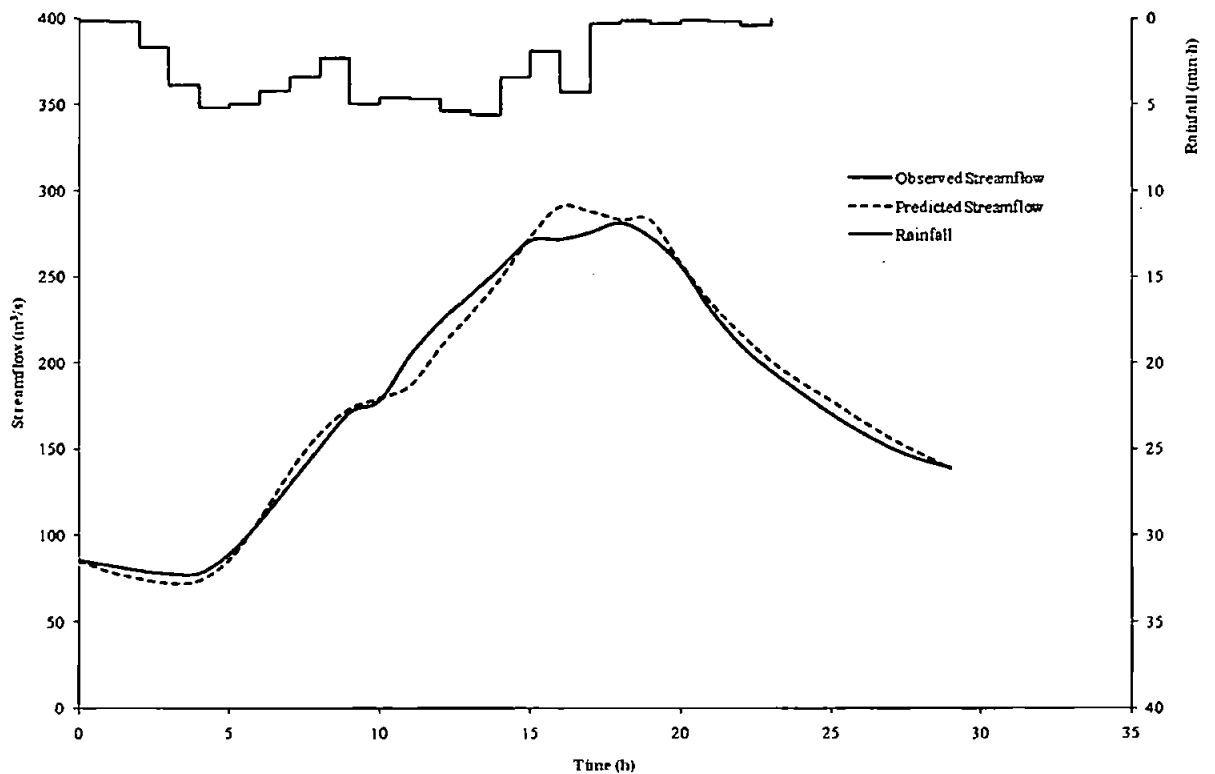
Figure 6.58 Results for event 1847 – with non-linear filter loss model

151

Event	Date	R_T	Q_P	SMD	No loss model					With non-linear filter loss model						
					K	α	T	K^α	NSE	K	α	T	C	P	K^α	NSE
2282	16-Sep-70	37.8	280.68	20.4	24.419	0.356	5.835	3.119	0.976	13.792	0.492	4.914	0.854	0.176	3.637	0.986
2283	31-Oct-70	15	258.9	0	7.480	0.856	5.735	5.598	0.938	7.683	0.817	5.771	0.988	0.020	5.290	0.926
2284	11-Feb-71	51.6	285.25	0.8	17.284	0.538	5.911	4.633	0.885	20.880	0.708	3.133	0.930	0.480	8.597	0.969
2285	20-Nov-71	25.5	181.98	0.3	26.310	0.722	3.864	10.601	0.718	15.183	0.943	2.262	0.998	0.511	13.002	0.832
2286	18-Jan-72	26.7	274.96	0	14.428	0.830	2.474	9.165	0.718	11.502	0.826	1.995	0.993	0.496	7.520	0.802
2287	03-Jul-72	54.2	207.83	8.6	22.611	0.573	3.660	5.971	0.909	25.135	0.768	0.828	0.994	0.386	11.896	0.962
2288	11-Feb-73	17.8	152.69	0	10.305	0.936	5.343	8.876	0.818	10.317	0.975	4.832	0.995	0.009	9.732	0.807
2289	15-Dec-73	24.7	182.58	0	7.934	0.530	9.170	2.997	0.846	7.935	0.677	6.837	0.954	0.050	4.064	0.828
2290	30-Apr-75	19.9	162.83	0.9	14.615	0.762	5.910	7.719	0.930	13.837	0.857	5.448	0.993	0.031	9.503	0.918
2291	24-Sep-75	64.6	492.98	0.7	6.782	0.772	4.421	4.383	0.902	10.823	0.739	3.586	0.985	0.214	5.813	0.914

Table 6.19 Catchment 72006 results for single fractional time-lagged reservoir

Figure 6.59 Results for event 2286 – without loss model

Figure 6.60 Results for event 2282 – without loss model

153
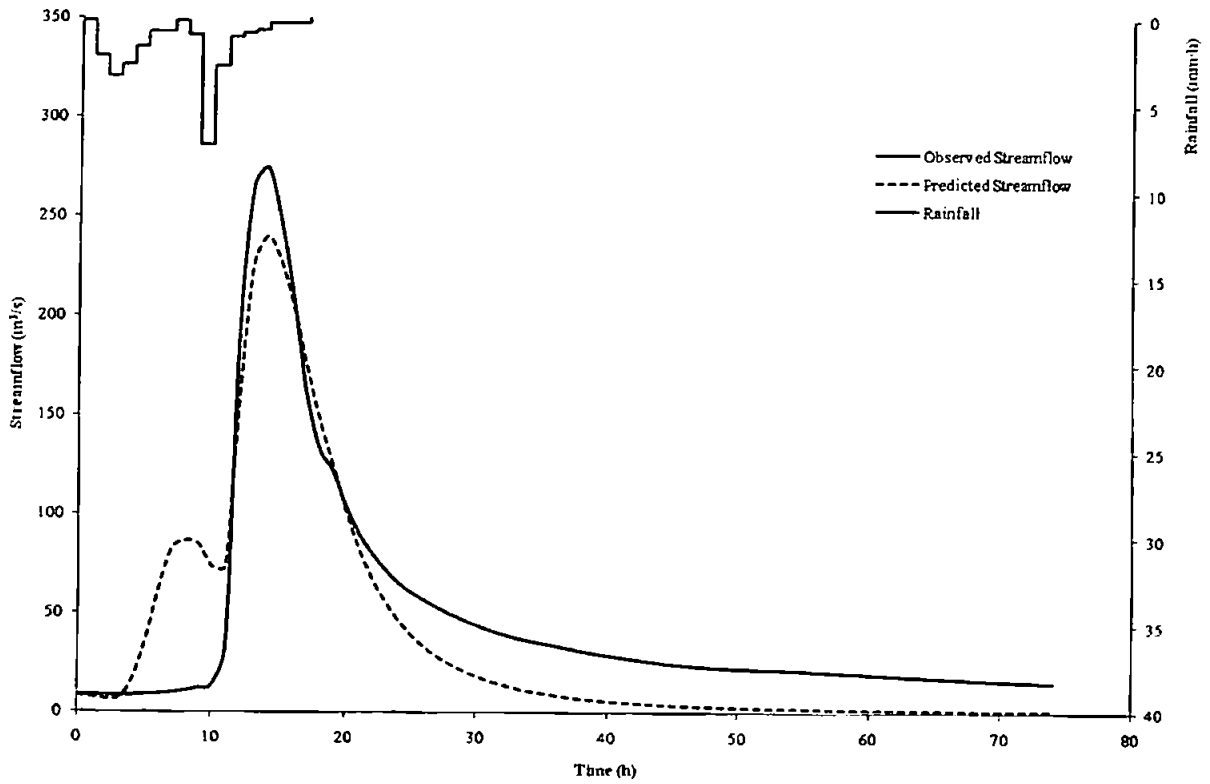
Figure 6.61 Results for event 2286 – with non-linear filter loss model
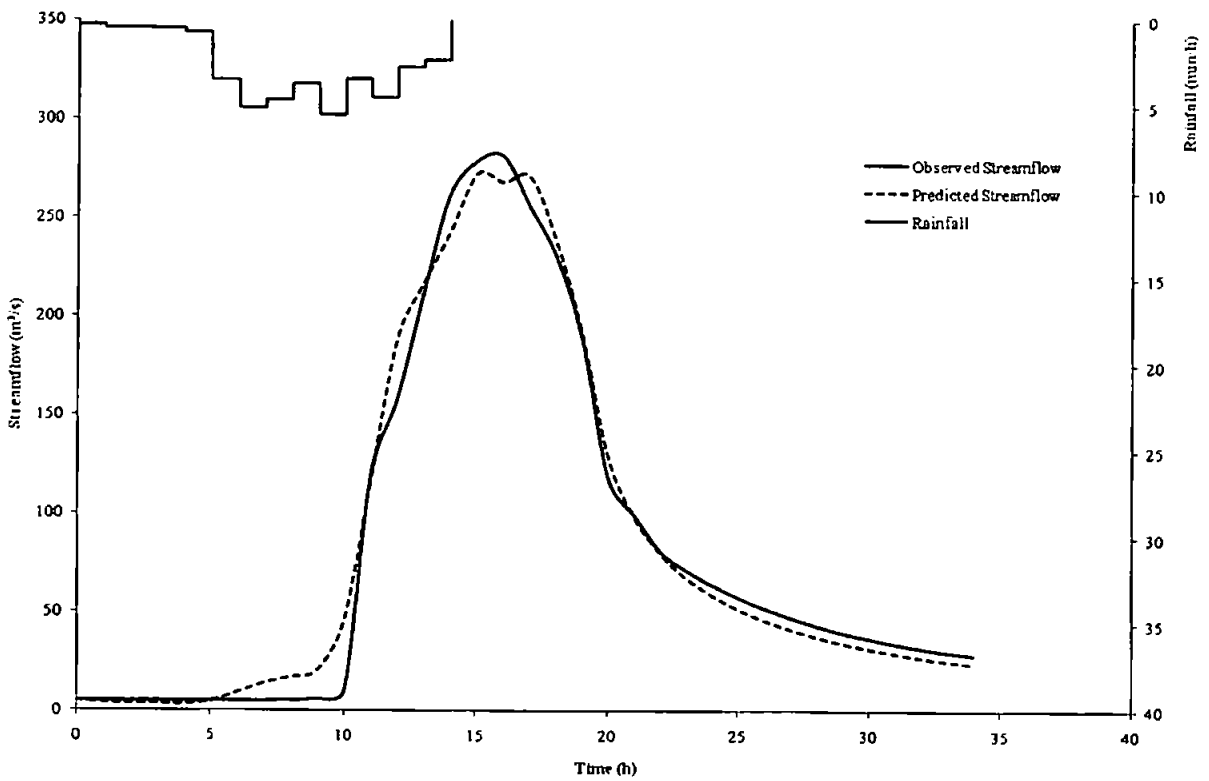
Figure 6.62 Results for event 2282 – with non-linear filter loss model

154

Catchment No:		46005	30004	74001	25005	54004	37001	66011	28026	7001	57005	72006
No loss model	Min.	1.369	14.328	1.689	7.565	13.000	30.518	1.485	26.830	2.601	8.661	2.997
	Max.	8.121	695.410	19.630	31.476	478.255	467.497	7.500	46.445	37.523	18.250	10.601
	Range	6.752	681.082	17.941	23.911	465.255	436.979	6.015	19.615	34.922	9.589	7.604
	Average	3.203	107.368	6.909	16.306	140.641	129.215	4.240	34.184	12.474	11.938	6.306
With RF loss model	Min.	1.441	12.403	2.855	11.533	26.871	59.900	1.988	42.680	2.586	9.999	3.637
	Max.	6.199	33.421	19.993	28.884	60.043	142.052	7.054	78.054	21.539	18.519	13.002
	Range	4.758	21.018	17.138	17.351	33.172	82.152	5.066	35.374	18.953	8.520	9.365
	Average	3.717	18.951	7.440	18.527	44.390	80.842	5.188	54.275	9.111	13.833	7.905

Table 6.20 Summary of K^α results for each catchment

6.2.4 Model Parameter Space Investigation

The *NSE* results of tests of alternative parameter sets (calibrated for different events) on the model performance for the events on a sample catchment are shown in Table 6.20. In this case the initialised, single, fractional-order, time-lagged, linear reservoir with a non-linear rainfall filter has been used for the observed storm events for the East Dart at Bellever (river gauge no. 46005). The calibrated parameter sets are those taken from Table 6.9 and are numbered in Table 6.21 as follows.

1   calibrated using GA on event 1287

2   calibrated using GA on event 1289

3   calibrated using GA on event 1292

4   calibrated using GA on event 1297

5   calibrated using GA on event 1298

6   calibrated using GA on event 1299

7   calibrated using GA on event 1300

8   calibrated using GA on event 1301

9   calibrated using GA on event 1302

10   calibrated using GA on event 1303

11   calibrated using GA on event 1304

12   calibrated using GA on event 4351

13   calibrated using GA on event 4352

14   calibrated using GA on event 4353

Event	Calibration Set Used													
	1	2	3	4	5	6	7	8	9	10	11	12	13	14
1287	0.964	0.794	-0.227	0.336	0.690	0.763	0.106	0.602	0.595	0.748	0.208	0.885	0.633	0.408
1289	0.586	0.977	-0.447	0.441	0.973	0.222	0.276	0.752	0.866	0.855	0.492	0.828	0.904	0.612
1292	0.520	0.577	0.832	0.683	0.607	-0.145	-0.066	0.542	0.469	0.494	0.329	0.626	0.597	0.324
1297	0.013	0.550	0.225	0.971	0.487	-0.858	-0.243	0.673	0.586	0.668	0.243	0.409	0.449	0.164
1298	0.631	0.923	0.190	0.637	0.954	0.387	0.241	0.909	0.843	0.789	0.546	0.721	0.920	0.594
1299	0.888	0.573	-0.517	0.046	0.512	0.896	0.105	0.288	0.310	0.505	0.038	0.730	0.426	0.265
1300	-9.797	-5.528	-1.108	-16.425	-4.243	-10.066	0.974	-6.031	-2.417	-11.539	0.155	-11.545	-2.835	0.337
1301	0.683	0.913	-0.262	0.763	0.848	-0.268	0.089	0.878	0.754	0.895	0.506	0.728	0.905	0.543
1302	0.338	0.790	-0.527	-0.102	0.775	0.138	0.463	0.741	0.960	0.453	0.710	0.079	0.884	0.796
1303	0.854	0.964	0.226	0.793	0.935	0.573	0.240	0.938	0.840	0.991	0.470	0.943	0.853	0.546
1304	-2.815	-0.759	0.260	-3.757	-0.131	-3.634	0.579	-0.987	0.150	-2.792	0.948	-2.825	0.326	0.834
4351	0.918	0.910	0.370	0.877	0.877	0.689	0.092	0.810	0.679	0.935	0.382	0.949	0.810	0.469
4352	0.498	0.846	0.055	0.117	0.911	-0.360	0.229	0.693	0.686	0.341	0.618	0.750	0.919	0.704
4353	-3.673	-1.683	-32.981	-3.554	-4.440	-0.611	0.410	-0.565	0.659	-1.283	0.857	-5.457	-1.847	0.936

Table 6.21 *NSE* results for alternative calibrated parameter sets for events on catchment 46005

From Table 6.21 the most consistent best performing calibration set for all the events is set 14. Plots of the predicted and observed hydrographs using calibration set 14 are available in Appendix E.

The inter-relationship between the parameters is visualised using the interactive calibration-support system developed by Packham *et al* (2005) in Figure 6.63. This shows a parallel coordinates plot of the best fitting parameter sets from the GA calibration for a typical single-peak flow event on the same catchment (no. 1303, 10-Nov-74). Recall Table 6.9 for the best set of parameter values found using the GA.

N.B. On the visualisation plots a represents α, and Ka represents K^{α}.
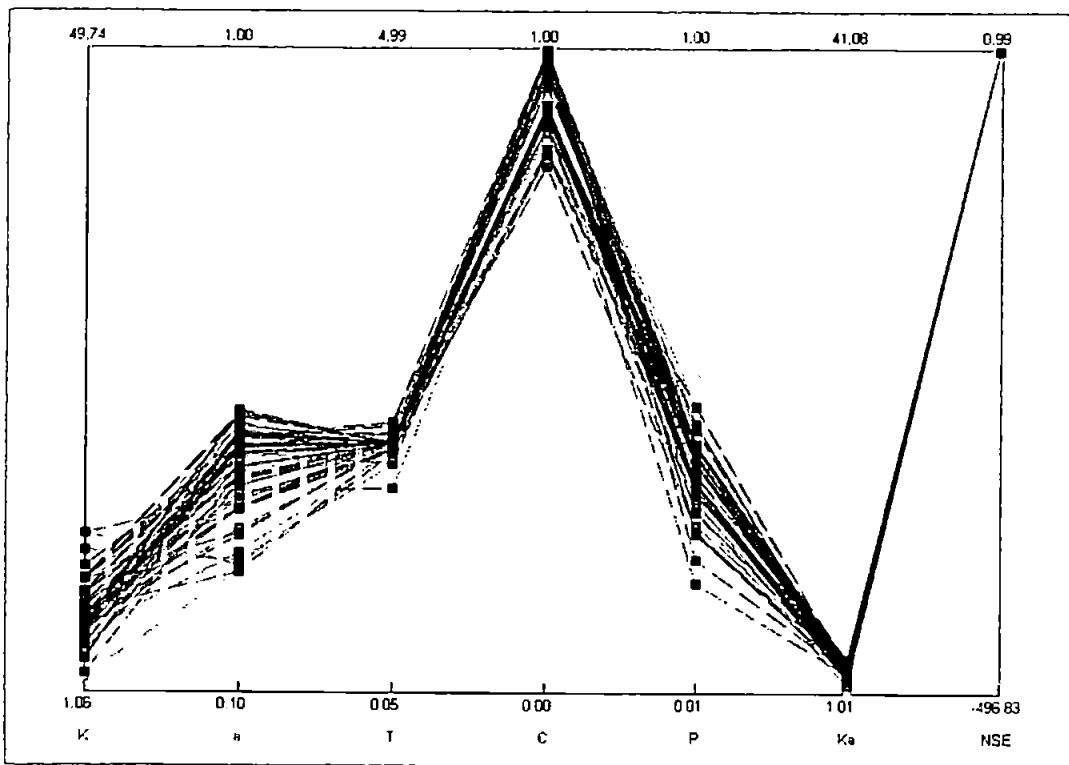
Figure 6.63 Parallel coordinates plot of parameters of best cluster for event 1303

The parallel coordinates plot shows all the sets of parameter values for the best fitting models in a single picture. The parameters are arranged in parallel with lines joining the

values (i.e coordinates) of an individual model solution. The better solutions are shown in the darker hue. Figure 6.64 shows a scatter plot of the composite K^α and T parameters with NSE indicating that there is a cluster of good solutions for a relatively narrow band of T and K^α values in spite of the wide range of individual K and α values evident in Figure 6.64.
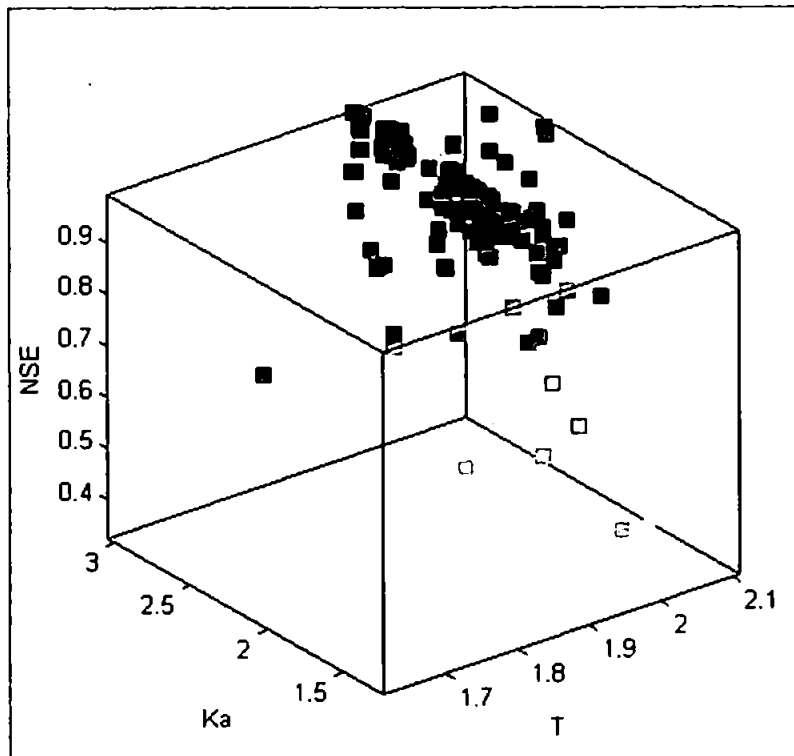
Figure 6.64 Scatter plot of lagged reservoir parameters of best cluster for event 1303

For the associated loss model Figure 6.65 shows that the range of C and P values is relatively small for the better (darker hue) solutions, suggesting convergence.
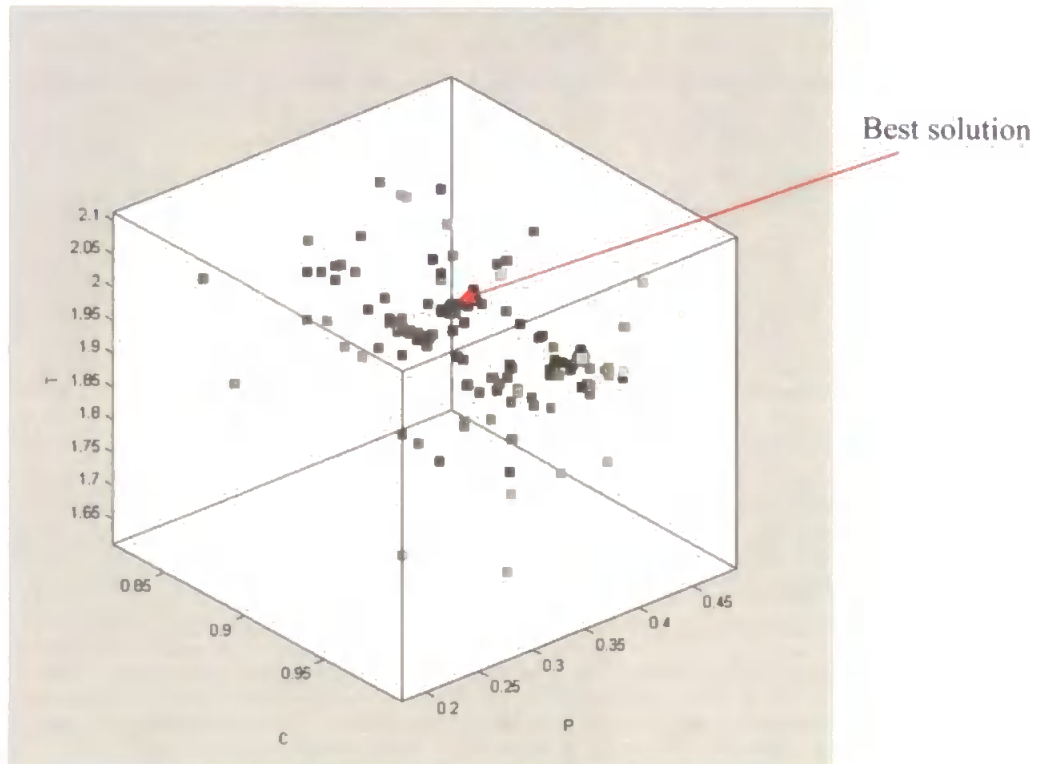
Figure 6.65 Scatter plot of loss model parameters of best cluster for event 1303

From the results presented in section 6.2.3 event 3884 (re. Figure 6.23) and event 656 (re. Figure 6.39) exhibit anomalous calibration behaviour. The search spaces for these models have been visualised using the interactive calibration-support system developed by Packham *et al* (2005) and are given in Figures 6.66 – 6.68. Again, the better solutions are shown in a darker hue and Ka represents K^α.

For the flow event 3884 (02-Aug-84) for the River Lymn at Partney Mill (river gauge no. 30004) Figure 6.66 shows a scatter plot of the best fitting parameter sets from the GA calibration. Recall Figure 6.23 showing the anomalous model fit. The initialised, single, fractional-order, time-lagged, linear reservoir without a loss model has been used for this observed storm event.
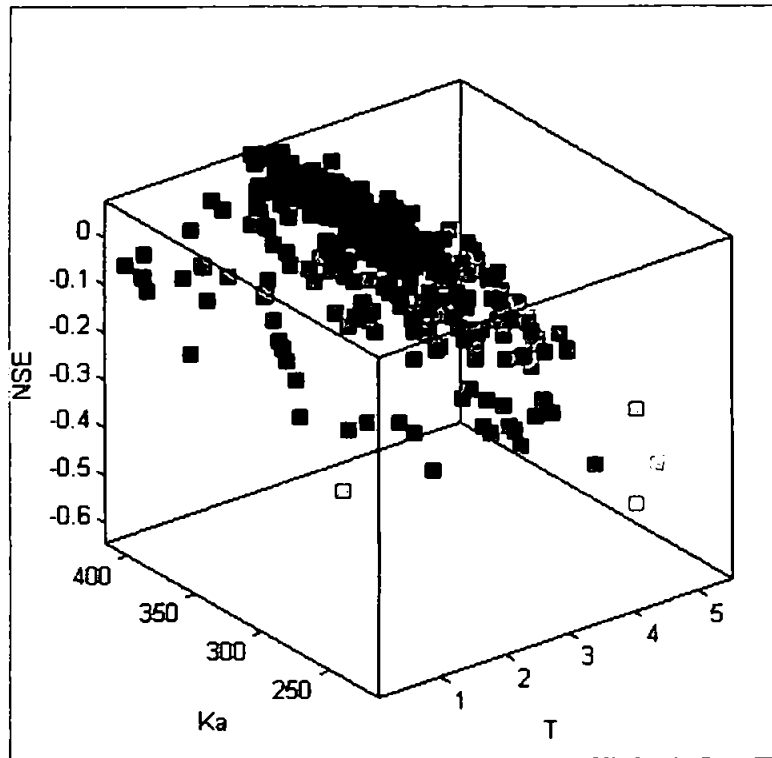
Figure 6.66 Scatter plot of parameters of best cluster for event 3884

The plot indicates a wide range of K^α and T values leading to solutions of similar (although not very good) fitness. However, the plot should be compared with Figure 6.25 where the inclusion of the non-linear rainfall filter loss model has resulted in a good fit to the observed streamflow hydrograph.

For the flow event on the catchment 656 (02-Sep-65) for the River Roding at Redbridge (river gauge no. 37001) Figures 6.67 and 6.68 show scatter plots of the best fitting parameter sets from the GA calibration. Recall Figure 6.39 showing the anomalous model fit. The initialised, single, fractional-order, time-lagged, linear reservoir with and without the non-linear rainfall filter loss model has been used for this observed storm event.
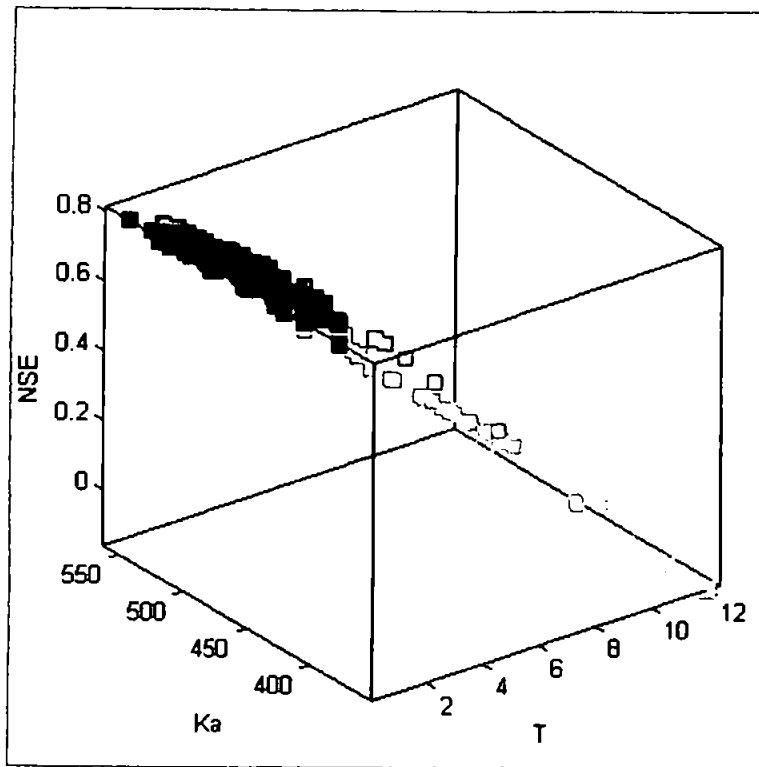
Figure 6.67 Scatter plot of parameters of best cluster for event 656 – without loss model
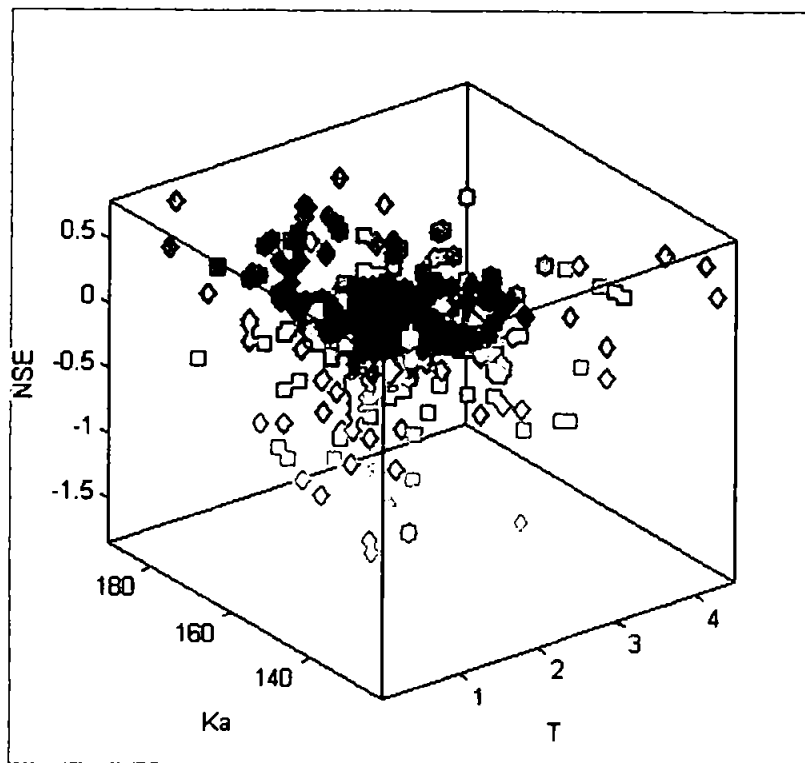
Figure 6.68 Scatter plot of parameters of best cluster for event 656 – with rainfall loss model

162

In a similar manner to the results for event 3884, Figures 6.67 and 6.68 demonstrate that the inclusion of the loss model has a constraining effect on the feasible K^α and T spaces, but the K^α range is still wide in Figure 6.68 indicating the poor convergence. However, the rainfall hyetograph in Figure 6.39 covers the period 0 – 26 hours, peaking at 12 hours and leading to a peak streamflow at 18 hours. The later streamflow peak at 48 hours is likely to be because of a lack of available rainfall data leading to this second event.

Chapter 7 Discussion

7.1 Theoretical Development

In the light of field evidence (Kirchner 2003) that the travel times of conservative tracers in rainfall show a long-memory effect indicating that "old" (pre-storm event) water released from prior storage in the catchment dominates the streamflow response to a rain storm (i.e. water appears to be stored over a long time period but is discharged in a relatively short period) then the premise of runoff (rapid response) as distinct from baseflow (slow response) in natural (rural) catchments has been brought into question. The separation of runoff from baseflow in computational streamflow modelling, particularly for flood prediction, is the basis of the classical unit hydrograph approach. However, if the mixing of water within the surface/subsurface storage component of the catchment is to be represented, then a different model is necessary. A candidate approach has been identified in this study on the basis of the power-law asymptotic behaviour of fractional-order systems. The fractional calculus provides relaxation equations in the form of ordinary linear differential equations of non-integer order. The convolution kernel of the fractional-order integral exhibits long term memory loss (i.e. the system is dominated by more recent states as the independent variable, e.g. time, increases). This integral is part of the differ-integral composition (sequence) that defines the fractional derivative. Consequently, the assumption has been made that the rate of change of volume with time of a conceptual (virtual) reservoir representing the catchment behaviour can be expressed by a fractional-order time derivative of the outflow rate. This assumption has only been tested in so far as the resulting models have been successfully fitted to observed events. It is recommended that this assumption be tested by field observation (e.g. through the use of tracers on experimental catchments). In the light of such field evidence Zoch's (1934) assumption of a linear reservoir may prove to be restrictive and the use of the non-linear form given by equation (2.6) may be required in order to represent the catchment drainage

166

behaviour more closely. However, a non-linear model would involve an additional parameter and require an iterative solution scheme.

A further advantage of the fractional-order differential equations derived in this theory is their linearity so that the principles of superposition and proportionality can be utilised in their solution. Applying the constraint that the order of the fractional derivative, α, is $0 < \alpha \leq 1$ has been shown to represent the heavily damped response of a system over the duration of the input event (i.e. it is non-oscillatory). This is typical of flood events in rivers.

The merit of the use of the fractional derivative in the Caputo sense is that the initial conditions are incorporated as the traditional integer-order values. It is accepted that the Caputo definition is restrictive in that this infers a constant initialisation function. However, given the earlier discussion regarding the difficulty in defining the surface-subsurface storage-flux history then the same is true of the actual initialisation function, again requiring further field studies of the interaction between the "old" and "new" water in the generation of total streamflow. In the meantime the Caputo derivative formulation has enabled useful model equations to be derived and tested in this study.

The theory treats the catchment system as having spatially averaged (lumped) behaviour so that it is represented by an ordinary fractional order differential equation. This limits the applicability of the equation to flood forecasting applications, rather than the modelling scenarios of land use change, etc. The model could be extended to incorporate spatial variation (e.g. in land cover) by dividing into subcatchments or by incorporating a spatial derivative term. In addition this distributed form of model would permit the input of rainfall from multiple gauges (or radar data) to capture the effect of

moving storms across the catchment. Alternatively lateral inflows from subcatchments could be used as inputs rather than a single upstream input rainfall.

The catchment characteristics were assumed constant over the total duration of the streamflow event (i.e. time-invariant) so that the coefficients of the differential equations are constants. There is no field evidence to suggest that this is not true, but it has yet to be verified. Future work could include time-varying parameters, although this would increase the model complexity and make parameter identification much more difficult.

The general theory developed in this study was based on the foregoing assumptions resulting in the following ordinary $\beta n\alpha$-order linear differential equation with constant coefficients, a_j.

$$\left[a_n {}_0^C D_t^{n\beta\alpha} + a_{(n-1)} {}_0^C D_t^{(n-1)\beta\alpha} + \cdots + a_0\right] q(t) = i(t) \quad t \geq 0 \tag{7.1}$$

where ${}_0^C D_t^{j\beta\alpha} q(t)$ is the sequential Caputo fractional derivative defined as

$$_0^C D_t^{j\beta\alpha} q(t) = \underbrace{_0^C D_t^\beta {}_0^C D_t^\beta \cdots {}_0^C D_t^\beta}_{j\text{-times}} {}_0^C D_t^\alpha q(t) \tag{7.2}$$

It was shown that the generalised cascade model was still achieved by using a single composite fractional order α in place of $\alpha\beta$ in equation (7.1). In this way the conceptualisation of the catchment using a physically-intuitive integer number of reservoirs (i.e. with $\beta = 1$) is adequate. This formulation was shown to be a fractional order form of Chow and Kulandaiswamy's (1971) general storage equation. The properties of cascades with equal and unequal storage characteristics and varying numbers of reservoirs have been investigated and, in particular, the implications of the initial conditions required. Consequently, the classical Nash (1957; 1960) cascade of n reservoirs has been corrected and reinterpreted for fractional n.

The convolution formulation traditionally used in the solution for the forced response component of the solution of equation (7.1) was found to be unbounded at time zero. It was found that the solution could only be found by utilising the Laplace transform of the pulse rainfall hyetograph (Wang and Wu 1983) and recasting as equation (7.3). This solution technique overcomes Cavallini's (2006) problem for the cascade of 2 unequal reservoirs.

$$q(t) = \frac{1}{K^{n\alpha}} \sum_{j=0}^{m} w_j U(t - nT - j\Delta t)(t - nT - j\Delta t)^{n\alpha} E_{\alpha, n\alpha+1}^n \left[-\left(\frac{(t-nT-j\Delta t)}{K} \right)^{\alpha} \right] + q_0 E_\alpha \left[-\left(\frac{t}{K} \right)^{\alpha} \right] \quad (7.3)$$

The other cascade models can be obtained as particular cases as follows:

- $n = 1$ gives the single reservoir models

- $\alpha = 1$ gives the classical integer order reservoir models

- $T = 0$ gives the unlagged models

For example when $\alpha = 1$ and the system is initially relaxed (i.e. the second term of equation (7.3) is zero) then the basis of Dooge's (1959) general instantaneous unit hydrograph theory is obtained.

The absence of the need for a cascade of reservoirs is a significant result (particularly for model parsimony) and this opens the way for potential future development of a lumped catchment model theory. A recommendation for future work is to investigate potential relationships between the parameters and physically measurable catchment descriptors (e.g. through the use of multiple regression analysis for a larger dataset than used in this study). This could prove valuable in the search for reliable models for ungauged catchments. In addition, in this lumped form, the fractional order

169

instantaneous unit hydrograph concept could be applied to the geomorphological IUH to investigate modelling drainage channel network evolution.

7.2   Rainfall-Runoff Modelling

For the particular case of the effective (net) rainfall to stormflow (runoff) transformation uninitialized (i.e. initially relaxed) cascade models were tested against the classical Nash cascade using the River Nenagh events. The model parameters were successfully fitted using the genetic algorithm. The results (Tables 6.1 – 6.3 and the associated plots in Appendices A and B) show good agreement with the observed runoff hydrographs.

For the cascade of equal-K, fractional-order reservoirs, Table 6.1 shows that the storage delay times, K, lie in the range 1.37 – 7.90 hours (with an average of 3.72 hours). This range is similar to that for the cascade of 2 unequal-K, fractional-order reservoir (Table 6.2 has a range of 1.00 – 8.28 hours for K_1 and K_2, with an average of 3.26 hours) and to that for the Nash cascade (Table 6.3 has a range of 1.37 – 6.09 hours for K, with an average of 3.20 hours). However, in general, the cascade of equal-K, fractional-order reservoirs produced better fits than the unequal-K reservoirs and the Nash cascade to the observed runoff hydrographs for the events tested (shown by the *NSE* values in the Tables 6.1 – 6.3 and the plots in Appendices A and B). This suggests that the use of the α-order derivative and the lag parameter, T, improve the rainfall-runoff model over that for the classical Nash cascade. The values of T range between 0.31 and 1.82 hours (with an average of 1.03 hours) indicating that the lag parameter has significance.

The range of n for the α-order cascade (1.04 – 3.32, with an average of 1.49) supports the use of a low number of reservoirs in the fractional-order cascade for adequate fitting, whereas the Nash cascade covers a larger range up to 4.88. The alternative form

of fractional order model using unequal-K reservoirs confirmed this in that the minimum size series of 2 reservoirs produced similar results to the equal-K cascade. This also fits with the findings of Chow and Kulandaiswamy (1971) for cascades of unequal integer-order reservoirs. Furthermore, the parameter fitting for the cascade of 2 unequal-K fractional order reservoirs appears to converge to the integer order form (the α values are between 0.88 and 1.00, with an average of 0.98) which would appear to indicate that the unequal reservoir cascade does not improve the classical integer-order model for runoff prediction.

The α values for the cascade of equal-K reservoirs are close to 1 (i.e. the integer order - Nash - cascade) but cover a small but significant range 0.7 – 1.0 (with an average of 0.87). However, this variation may be a consequence of the modelling of net (effective) rainfall to runoff which is somewhat artificial since it requires pre-processing of the observed streamflow to separate the baseflow and subsequent subtraction of the losses from the observed rainfall. The techniques for doing so are subjective (refer to the review in section 2.2.1). Bree's (1978) presentation of the River Nenagh data set uses only a single autographic rain gauge record to represent the areal rainfall for the catchment which does not take account of storm movement across the catchment. The quality of the rating curve used to convert the observed river stage measurements to streamflow was not assessed. The subsequent processing of the streamflow data at 3 hourly intervals assuming a constant baseflow to separate the runoff so that the percentage runoff could be derived from the rainfall data has, therefore, introduced some uncertainty.

Overall the composite model parameter nK^{α} values for the equal-K fractional order cascade (2.23 – 8.69, with an average of 4.56) are close to the nK values for the Nash

171

cascade (4.46 − 9.31, with an average of 6.25). For the unequal-K fractional order cascade the composite model parameter takes a slightly different form, $K_1^\alpha + K_2^\alpha$, although the range 3.8 − 9.4, with an average of 6.36, is similar. It would appear that for the closed case of effective (net) rainfall to stormflow (runoff) the application of the fractional order system converges to the classical integer order unit hydrograph, which is to be expected for a system that conserves mass. This mass conservation is forced by the loss model in the pre-processing such that the volume of effective rainfall equals the volume of runoff.

7.3 Rainfall-Streamflow Modelling

7.3.1 Cascades of Reservoirs

The sequential Caputo derivative used in the derivation of (7.1) requires a substantial number of initial conditions expressed as functions of the Caputo derivatives evaluated at $t = 0^+$. This raises the issue of the complexity of the generalised cascade model with multiple reservoirs for practical application where the system is not initially at rest (unlike the rainfall-runoff transformation system assumption). Furthermore, if Lorenzo and Hartley's (2008) approach is taken to overcome the restriction of using constant initialisation with the Caputo derivative and time varying initialisation functions are introduced then each derivative term requires an associated initialisation function. This would add substantially to the model complexity. The implications for the development of parsimonious fractional order cascade models are significant. Consequently, a single fractional-order, time-lagged, linear reservoir subject to a single initial condition was used to test the viability of the new theory for modelling the rainfall-streamflow transformation.

7.3.2   Rainfall Loss Models

A further assumption was made in order to consider the influence of infiltration and evapotranspiration losses from the observed rainfall, and so derive the effective rainfall as the input to the fractional-order reservoir system.   Of the rainfall loss models reviewed (re. section 2.2.1) the ϕ-index, *PR*, and non-linear rainfall filter (RF) based on Young and Beven (1994) were tested. It was not possible to test an infiltration equation approach because no infiltration capacity data was available for the Flood Event Archive catchments, although this could be tested in a future study for catchments with such data. Similarly, the lack of available antecedent daily rainfall time series data for the Flood Event Archive events prevented testing of the PDM model used in the revitalised FSR/FEH rainfall-runoff method. Again, future work could include testing the PDM model where the data is available.

The results for a sample catchment in Tables 6.4 – 6.6 and Figures 6.5 – 6.18 show the consistently superior performance of the non-linear rainfall filter (RF) model over the ϕ-index and *PR.*. Consequently the RF loss model was selected for use in the simulations for the Flood Event Archive catchments. .However, the loss model has not been validated in the field, and it remains an open problem. Conceptually, in many cases, loss models have been proposed on the basis of equating the volume of stormflow to that of the effective rainfall. In the open system of streamflow generation such volume conservation does not necessarily hold because of mixing of event and pre-event water. The concept of baseflow as distinct from stormflow and its separation, therefore, is unclear. Because the "memory" effect is represented in the fractional order approach this renders the modelled system non-conservative where pre-event infiltrated water has a contributory effect on the subsequent streamflow output. Consequently, this may have a compensatory effect which requires a revised form of loss model to that used.

173

Conceptually, the observed rain storm is a source of energy to a system containing stored energy (see also (Tessier *et al.* 1996)). This highlights the need to encapsulate the initialisation history correctly, and is an area for future investigation. In order to compare the influence of the loss model, the fractional-order reservoir system was run also without a loss function. Significantly, in many cases, the results of the calibrations with and without the loss model shown in Tables 6.9 – 6.19 (and in the plots in Appendices C and D) showed that the inclusion of a rainfall loss model only made modest improvements to the accuracy of the predictions. These results are considered further in section 7.3.3.

7.3.3   Flood Event Archive Modelling

For the general case of the effective (net) rainfall to streamflow transformation the initialised, single fractional order lagged reservoir model was tested for storms observed across a range of UK catchment scales ($22km^2$ to $510km^2$) using the UK Flood Event Archive events. The model parameters (including those of the RF loss function used to derive the effective rainfall input) were fitted using the genetic algorithm. Generally, the results (Tables 6.9 – 6.19 and the associated plots in Appendices C and D) show a acceptable agreement with the observed runoff hydrographs for most catchments, but with some notable exceptions.

Comparing the sample plots in Figures 6.19 – 6.62 the fitted hydrographs are closer to the observed streamflow when the RF loss function is included (and with smoother hydrograph shapes) although the results with no loss function were often acceptable. However, the 2 types of model (with and without loss model) are fitted with distinctly different parameter values. The most striking difference is in the very wide range of storage delay times, K, (1.6 – 2998 hours) when no loss model is used compared with

the closer range (2.9 – 173 hours) when the loss model is included. There is a question of whether very high storage delay times for a catchment have a physical meaning for the model without a loss function. In contrast Table 6.20 shows that the ranges of the composite K^α values are closer for the 2 types of model (1.4 – 695.4 without the loss function and 1.4 – 142.1 with the loss function). The results on an event by event basis in Tables 6.9 – 6.19 show greater agreement in the fitted K^α values for particular events. This suggests that the K^α parameter is more characteristic of the catchment and event. A notable example of the improved effect of the RF loss function on the performance of the fractional order model is illustrated in the results for event 3884 on catchment number 30004 (the River Lymn at Partney Mill) where Figure 6.25 shows the improved fit over that in Figure 6.23 (without the loss function). Consequently the following discussion is focussed on the results for the fractional order model with the RF loss function included. An area for future investigation of the nature of the K^α parameter on an event by event basis would be to compare the observed (total) rainfall volume with the observed streamflow volume to see whether K^α is correlated with volume difference.

Generally the sample plots in Figures 6.19 – 6.62 (see Appendix C for the full set of results) show a good fit of the model predicted hydrograph to the shape of the observed streamflow, especially the recession. Furthermore the better fits are for single peaked events. The model tends to be responsive to low rainfall or rainless periods in the event hyetograph resulting in relatively steep recessions between peaks (i.e. less damping) which does not always match the observed streamflow well. In addition the model appears to be applicable over a range of scales in terms of area (22 – 510 km^2) and average annual rainfall (607 – 2265 mm), as well as for catchments including some urbanisation (up to 13% of area). No discernable pattern in parameter values with

catchment size was detected. Similarly, the model fit was not influenced by initial *SMD*, except that larger *K* values were required. This would appear to support the importance of the initialisation on the performance of the fractional order model.

However, there are catchment specific features and data quality issues which may introduce some uncertainty into the model performance. For example Table 6.14 (and the associated plots in Appendix C) for catchment number 37001 (the River Roding at Redbridge) show poor fits to the observed streamflow. The peak flows are underestimated, too early and with poorly fitting recessions. However this may be due to the storage effect of artificial reservoirs on this catchment (Environment Agency 2009). In particular, for event 656 (Figure 6.39) which has a very poor fit, there may be missing rainfall data after the initial streamflow peak (recall the observations in section 6.2.4). Furthermore the derivation of the Catchment Average Rainfall Profile used in compiling the Flood Event Archive data set used few (often just one) autographic rain gauges adjusted so that the centroids of the observed hyetographs were matched (re. section 5.4.2). This introduces uncertainty as to whether the archived rainfall represents the areal rainfall correctly. Similarly the quality of the rating curves used to convert the observed river stage measurements to streamflows for each catchment is subject to uncertainty (e.g. in the number and range of field calibration measurements, stage recorder errors, and incidences of channel by-passing and channel instability at high flows). It is recommended, therefore, that the fractional-order model be tested on a broader set of catchments with a greater density of gauges.

Overall the results across the range of UK catchment scales tested ($22km^2$ to $510km^2$) showed that, generally, the single fractional order lagged reservoir model was

successful in predicting the total streamflow, with reasonably consistent K^{α} values for the majority of events for a given catchment.

7.3.4 Model Parameter Characteristics

Whilst the use of the GA in fitting the parameters to the model has produced acceptable streamflow hydrographs in many cases, the intercomparison tests for the East Dart River at Bellever (river gauge no. 46005) in Table 6.21 illustrate the uncertainty in defining a set of parameters for a particular catchment. The GA fitted parameters for calibration on an event by event basis in Table 6.9 show considerable variation. The results of the tests using calibration set 14 from Table 6.21 (and see the plots in Appendix E) confirm the issue of lack of unique identifiability. Furthermore, whilst outline testing of the key control parameters of the GA has been undertaken to determine working values for the purposes of calibrating the fractional order model, it cannot be taken for granted that the GA has converged on a global optimum (or, even that one exists). This is compounded by the uncertainties in the initialisation function, the loss model formulation as well as the quality of the data used. However, the visualisation of the clustering of good (high fitness) parameter sets identified by the GA for the sample event 1303 (Figures 6.63 – 6.65) indicates a relatively narrow band of T and K^{α} values in spite of the wide range of individual K and α values evident in Table 6.9. This suggests that convergence to an acceptable fit is possible with the fractional order model using the GA but the parameters are event-specific. A further constraint is necessary in order to improve the identifiability of the model at a catchment level. Again this raises the issue of the adequacy of the initialisation used and this is discussed further in section 7.3.5.

The characteristic behaviour of the fractional order model (including loss function) for different K and α values can be seen in the sample plots in Figures 6.19 – 6.62 (and see Appendix C for the full set of results). Typically the low α-order models generate steeper peaks with a long tail recession. Conversely, higher α-order models result in a broader peak shape and a shorter recession. The α ranges fitted by the GA across the different events was 0.11 – 1.0, but varied between 0.45 and 1.0 using the averages for each catchment. Typically the low K reservoirs produce higher, narrower peaks, whereas the high K reservoirs generate lower, broader peaks. The K and K^{α} ranges are discussed in section 7.3.3. Similar to the rainfall-runoff model results the inclusion of a time lag is important with the values of T ranging between 0.03 and 10 hours on an event by event basis (but ranging between 1.8 – 6.7 hours using the averages for each catchment). Figures 6.19 – 6.62 also show another feature of the fractional-order model response. For events with relatively low or zero rainfall at the start of the event the predicted hydrographs show a decay in streamflow from the initial flow condition until the rainfall commences, often below that of the observed hydrograph. This suggests that the assumed catchment history (the single constant initial condition, q_0, when using the Caputo fractional derivative) is too simplistic. This is coupled with the uncertainty over the choice of q_0 having been specified at $t = 0$ of the hyetograph.

For the RF loss function the 2 parameters take values across most of the available range for each event, but, typically, using the averages for each catchment $C > 0.7$ and $P < 0.5$ The implications of the loss model on the results are discussed in section 7.3.2.

7.3.5 Initialisation History

As discussed in sections 7.3.3 and 7.3.4, some of the cases of poor fit of the fractional order reservoir model to the observed data and the substantial variation in parameter

values for a given catchment may well be a consequence of the restricted initialisation used for the Caputo derivative. In particular it is evident that there can be a number of different catchment storage/flux histories that pass through a common single initial condition at $t = 0$ and result in different subsequent streamflow events. However, only one such history will give rise to the observed streamflow event for $t > 0$. This implies that each event is likely to have a different (but unique to that event) set of α, K, T values which are defined by the initialisation history, which explains the variation in the K^α values fitted to the different events for the same catchments. This approach to initialisation may supersede the use of single-valued antecedent conditions such as initial soil moisture deficit or antecedent precipitation index commonly used in streamflow modelling. However, the true initialisation representing the surface-subsurface water mixing history for an event is not easily defined. The antecedent catchment state (given by the degree of soil water saturation and the recent passage of water through the catchment) may need to be captured as a time-history which will vary on an event-by-event basis. The form of such an initialisation function and over what pre-event timescale it should be evaluated is a subject of future research. A potential approach is to assume that the baseflow recession of the antecedent streamflow event characterises the surface-subsurface storage-flux history of a river. This may be modelled by the free response solution to the fractional order differential equation describing the single fractional order lagged reservoir. The identification of the K and α parameters can be undertaken by fitting this term to the observed antecedent streamflow recession data. This could be undertaken for several sets of data to obtain catchment averaged values. However, the consequent adoption of a time-varying initialisation function requires the reformulation of the fractional differential equation since the Caputo derivative implies a constant initial condition. Lorenzo and Hartley (2008) have proposed a mathematical framework for this but the required Laplace transforms are not

always available in closed form. Furthermore, this approach is likely to be subject to the difficulties of an objective baseflow separation. This, therefore, also supports the need for future field investigation to identify a correct initialisation function.

Chapter 8 Conclusions and Recommendations

8.1 Conclusions

The following have been developed in this study:

1. A new general theory for the lumped rainfall-streamflow transformation using a fractional order linear deterministic systems approach subject to an initial condition.

2. A general equation for the cascade of initialised time-lagged linear reservoirs of fractional order that further generalises Dooge's (1959) general theory of the instantaneous unit hydrograph and generalises the general storage equation of Chow and Kulandaiswamy (1971).

3. The necessary conditions for the initialisation of cascade models resulting in a corrected differential equation form of the classical Nash (1957; 1960) cascade.

4. A bounded solution technique using the unit step response function fitted using the genetic algorithm.

5. A finite series expansion of the binomial function for fractional powers.

6. The Laplace transform of the Caputo sequential derivative.

The new model has been successfully applied to the classical closed system of effective rainfall to stormflow (runoff) modelling using a set of 22 pre-processed events for the River Nenagh. The cascade of 2 unequal fractional-order reservoirs was shown to converge to that of the integer order case, as did the cascade of equal reservoirs (but with some small differences), which is to be expected for a system that conserves mass. The single fractional order, lagged reservoir model with a constant initialisation function was successfully applied to the general open system of total rainfall to streamflow transformation for a selection of events from a range of UK catchment scales in terms of area ($22km^2$ to $510km^2$), and average annual rainfall ($607 - 2265$ mm), as well as for catchments including some urbanisation (up to 13% of area).

The assumption that the time-history of water storage/flow states in the surface/subsurface catchment system can be represented by a fractional-order time derivative of the outflow rate of a linear reservoir has been shown to be feasible. However, this assumption has only been tested in so far as the resulting models have been fitted to observed events.

The second assumption made in the models presented, that the mixing effect observed between "old" and "new" water in the generation of total streamflow is represented by a constant initial condition (a consequence of the Caputo definition of a fractional derivative) appears to be restrictive. The results showed that the model was successful in predicting the total streamflow with reasonably consistent K^{α} values for the majority of events, but the individual K and α values showed a wide variation. In addition, events with an initial SMD required larger K values. The parameter fitting using the GA for different storm events on the same catchment demonstrated that convergence to an acceptable fit is possible but that the parameters are event-specific. However, the true initialisation representing the surface-subsurface water mixing history is unlikely to be a constant. The antecedent catchment state (given by the degree of soil water saturation and the recent passage of water through the catchment) may need to be captured as a time-history which will vary on an event-by-event basis and should, therefore, improve the identifiability of the model at a catchment level.

The non-linear rainfall filter (RF) loss function to represent the infiltration and evapotranspiration losses from the observed rainfall was found to improve the model fit over the ϕ-index and PR approaches. However, for several events, the inclusion of a rainfall loss function only made modest improvements to the accuracy of the model output. Because pre-event infiltrated water has a contributory effect on the subsequent

streamflow output and this "memory" effect is represented in the fractional order approach then this may have a compensatory effect which requires a revised form of loss model to be developed (i.e. the system is non-conservative).

The results show that the new approach is viable for modelling the rainfall-streamflow transformation at the lumped catchment scale without the need for cascades of reservoirs, which reduces the number of model parameters required.

8.2   Recommendations

The non-constant K^{α} parameter values for each catchment appear to indicate that the correct representation of the catchment storage/flux history is necessary on an event-by-event basis. A potential approach would be to test the assumption that the recession curve of the antecedent streamflow event characterises the recent surface-subsurface storage-flux history of a river. This may be modelled by the free response solution to the fractional order differential equation reformulated in accordance with Lorenzo and Harley's (2008) approach. The identification of the K and α parameters can be undertaken by fitting this term to the observed antecedent streamflow recession data. Similarly, further insight into the K^{α} parameter may be obtained by comparing the observed (total) rainfall volume with the observed streamflow volume to see whether K^{α} is correlated with volume difference on an event by event basis. Further work is also recommended on determining the nature of the initialisation function through the use of field tracer studies.

The assumption of a linear relationship between outflow and storage for the fractional-order reservoir has been shown to be viable for the range of events tested in this study. However, the use of a non-linear form may improve the representation of catchment

drainage behaviour more closely. However, a non-linear model would involve an additional parameter and require an iterative solution scheme, thus increasing the computational overhead. Similarly the validity of the assumed constant catchment parameters could be tested by allowing them to vary with time, although this would increase the model complexity and make parameter identification much more difficult.

In order to incorporate spatial variation (e.g. in land cover) and the effect of moving storms across the catchment a distributed model can be derived by dividing into subcatchments or by incorporating a spatial derivative term. Alternatively lateral inflows from subcatchments could be used as inputs to a river routing model. In addition, the fractional order instantaneous unit hydrograph concept could be extended to the geomorphological IUH to investigate modelling drainage channel network evolution.

The potential application of the fractional-order reservoir model to predicting streamflow in ungauged catchments using only observed rainfall requires the identification of relationships between the parameters and physically measurable catchment descriptors. One approach proposed is to use multiple regression analysis of the model parameters and catchment descriptors for a larger dataset than that used in this study. It is important, however, that high quality observations of event rainfall and streamflow are selected with a view to reducing the uncertainty inherent in measured and derived input data.

Appendix A: R. Nenagh Results – Equal Casacade

The following Figures show the predicted and observed runoff hydrographs together with the net (effective) event rainfall hyetograph for the River Nenagh. The predictions were made with the cascade of n equal-K fractional linear reservoirs subject to a time lag, T.
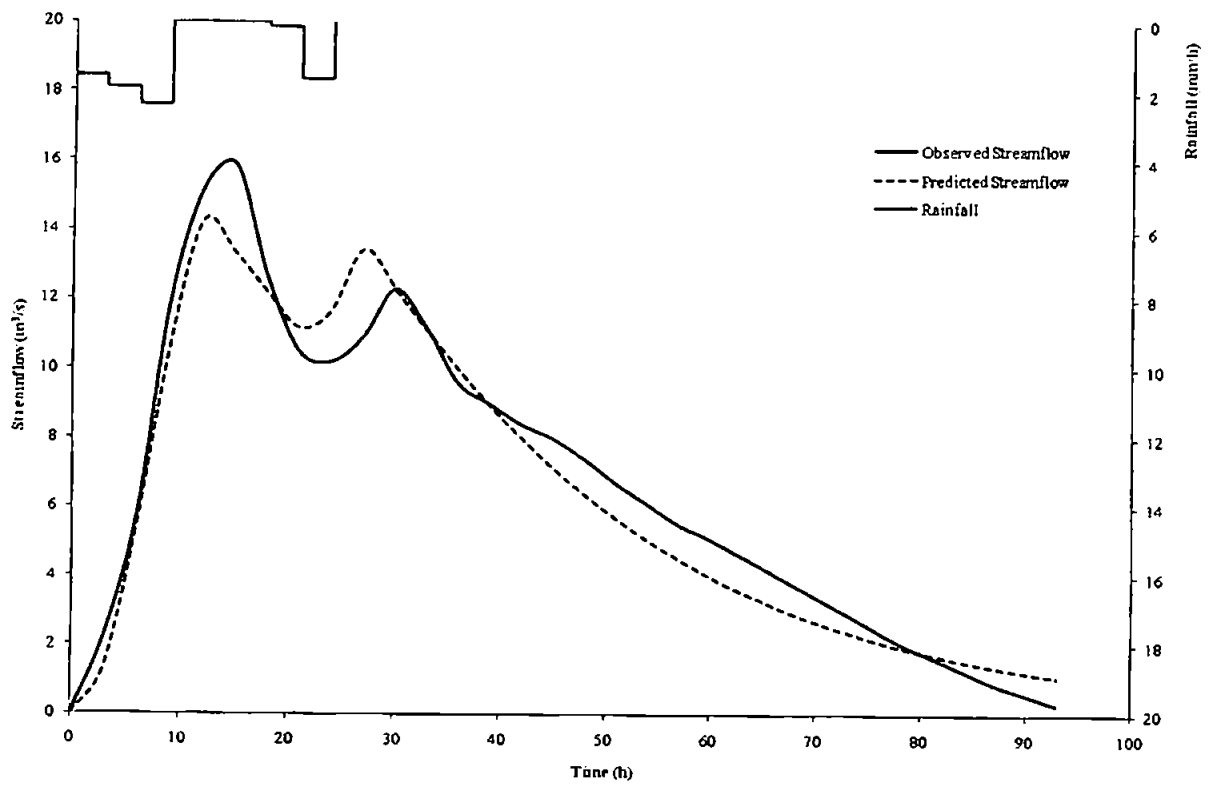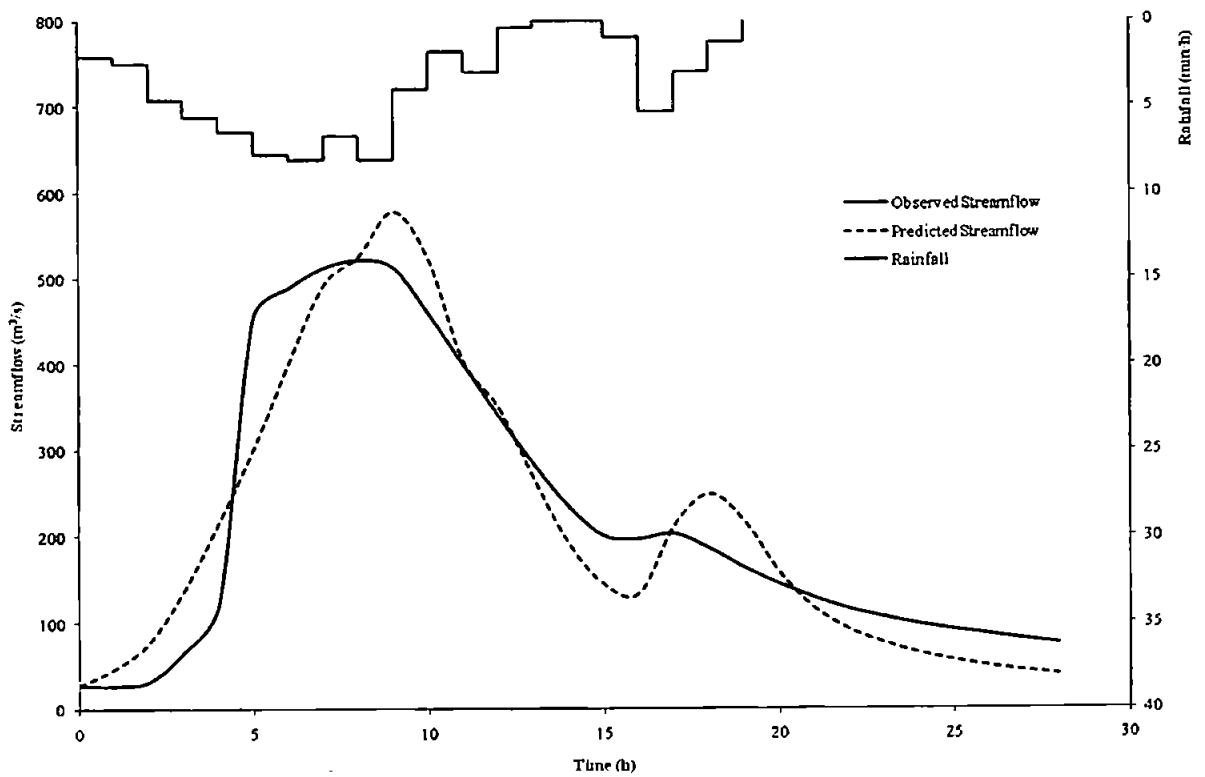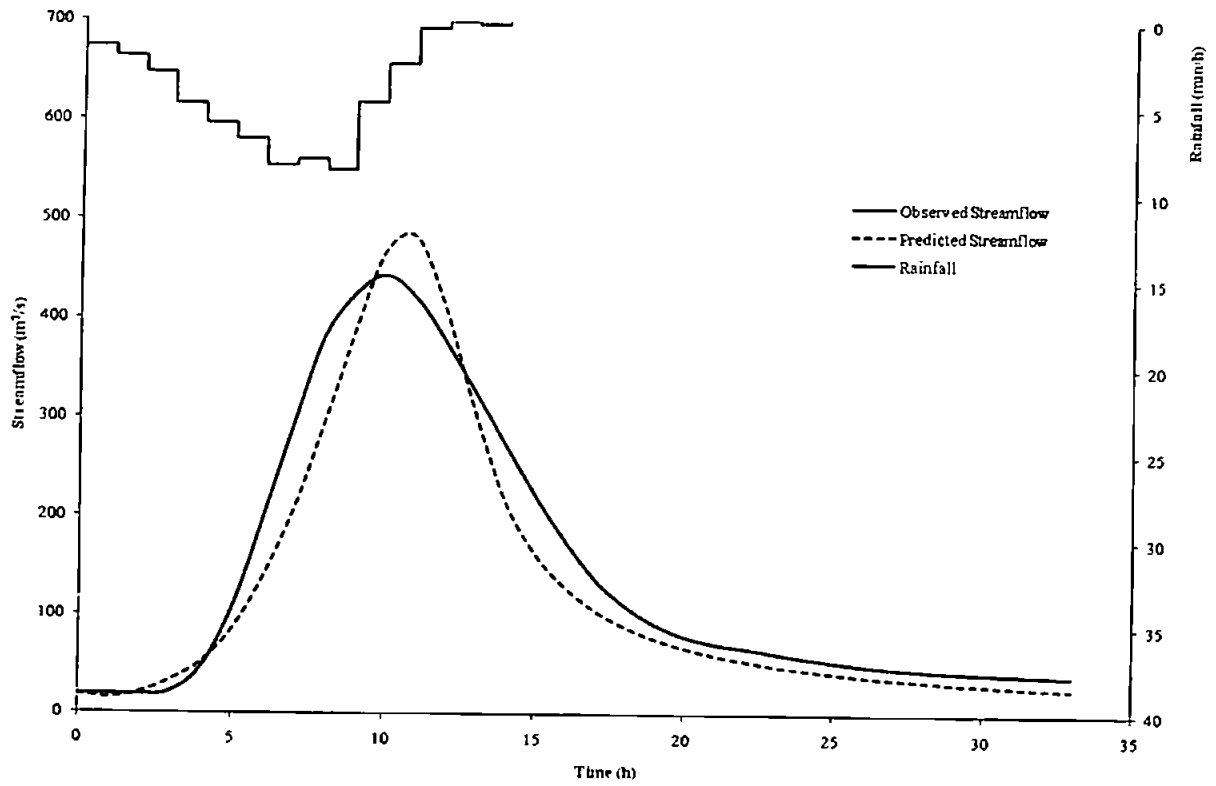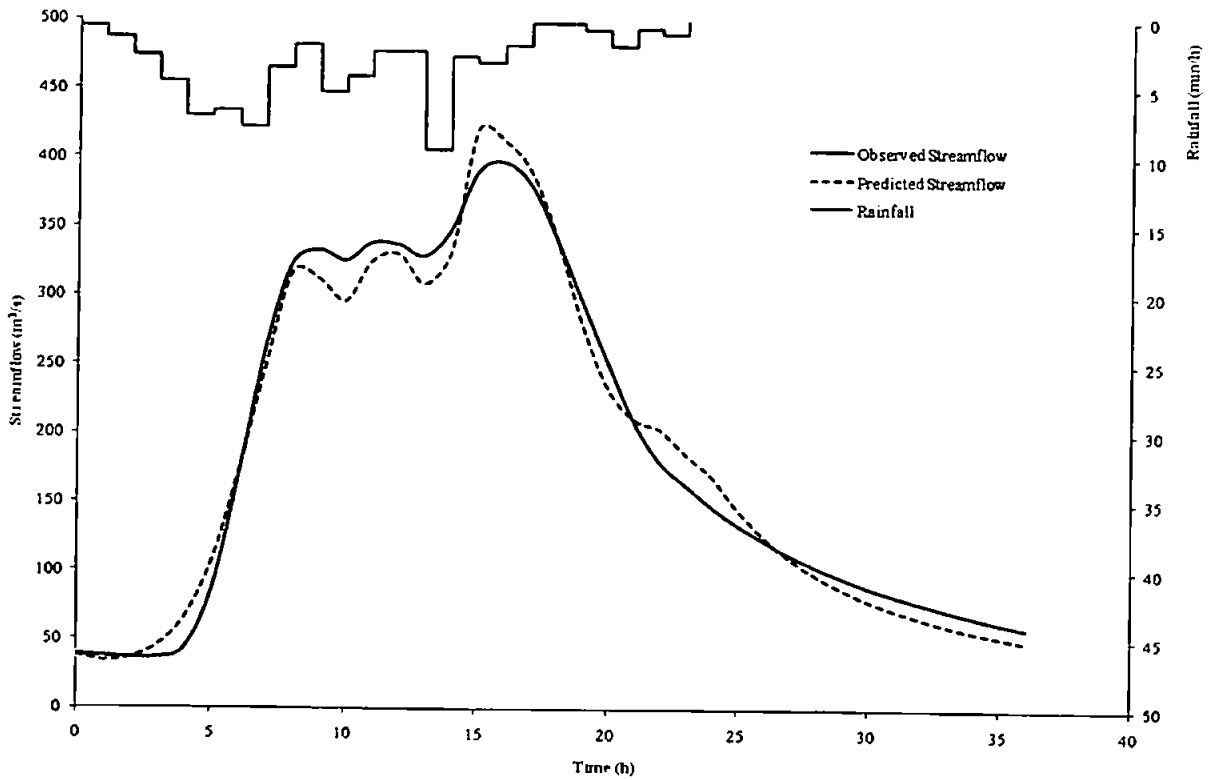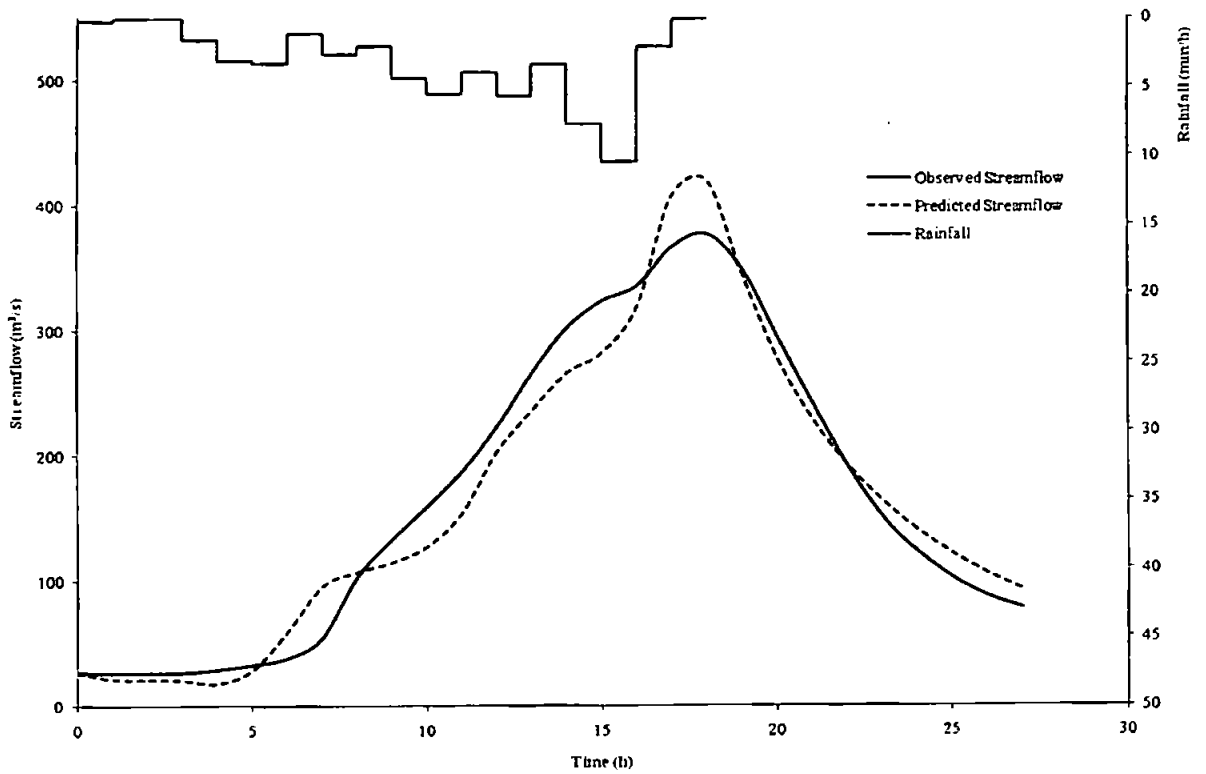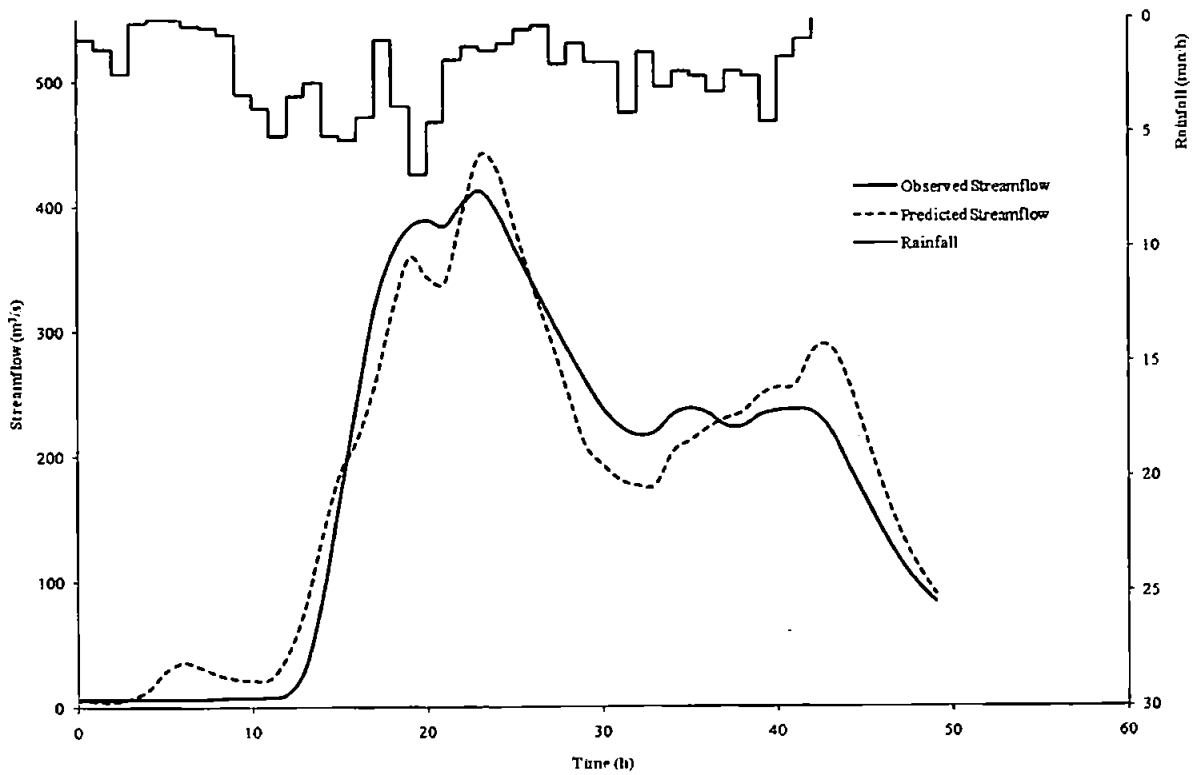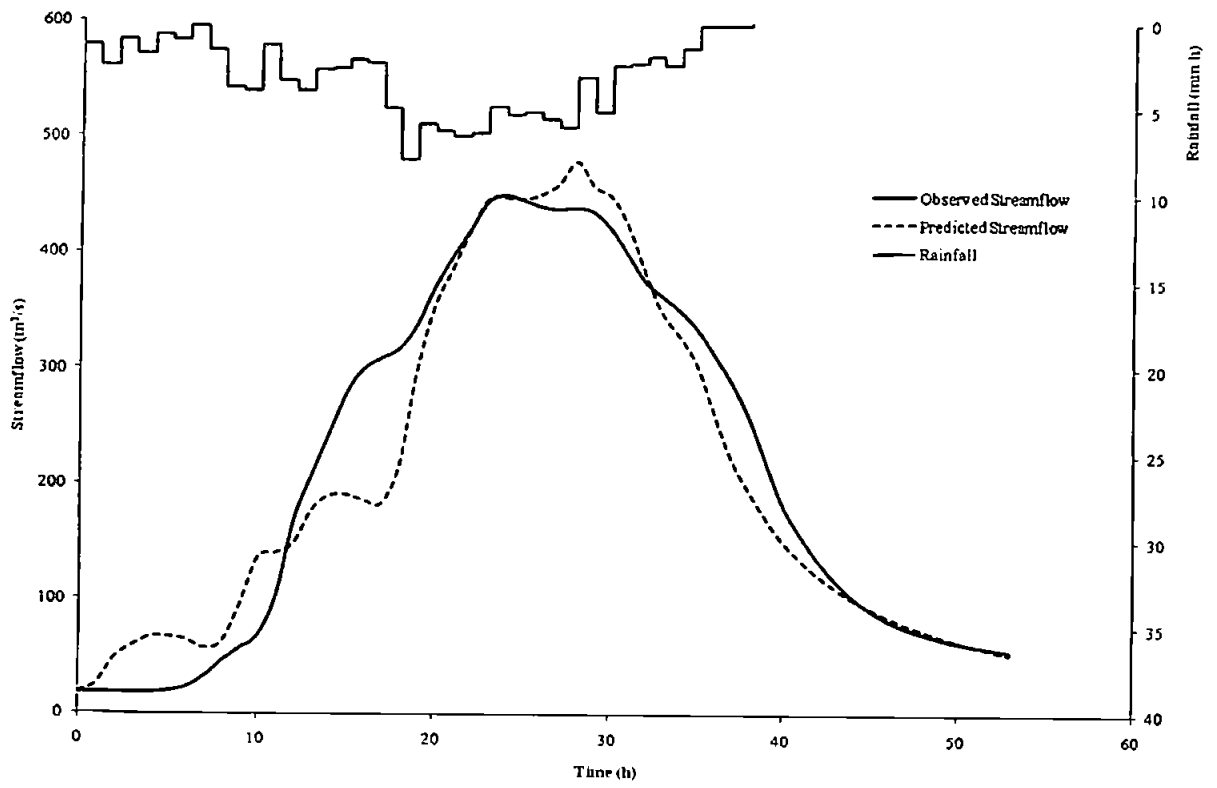
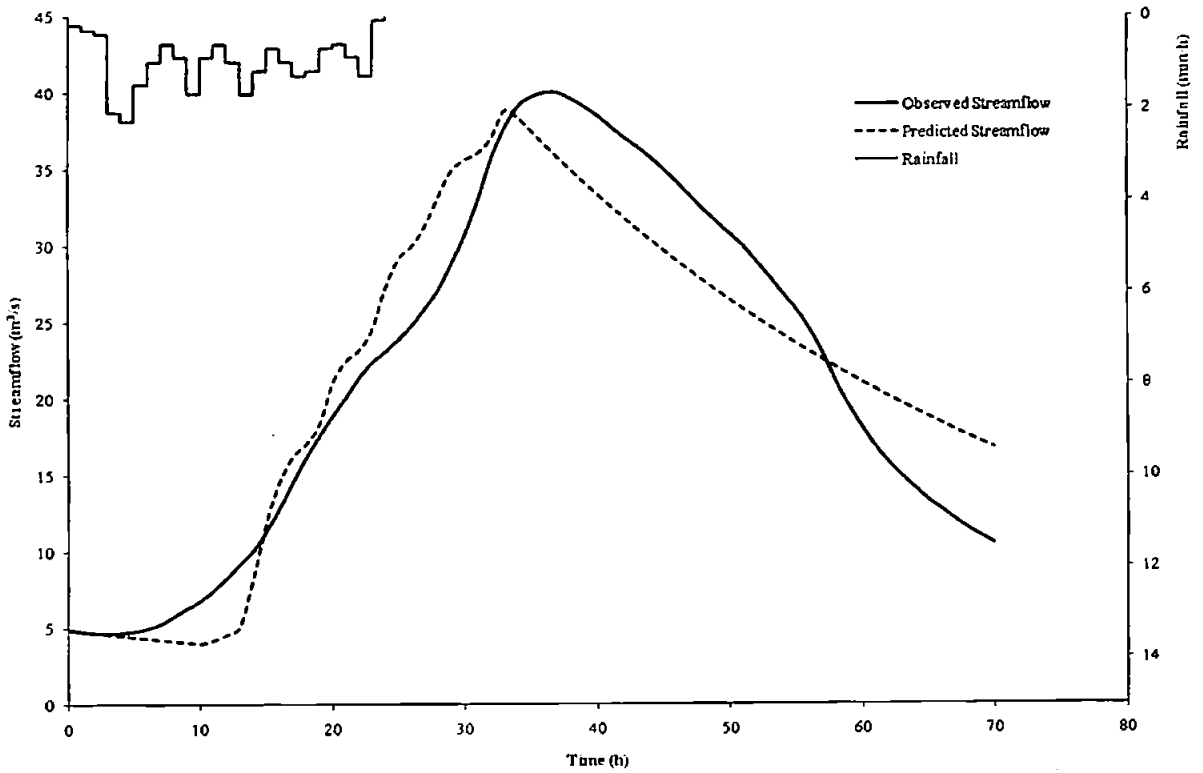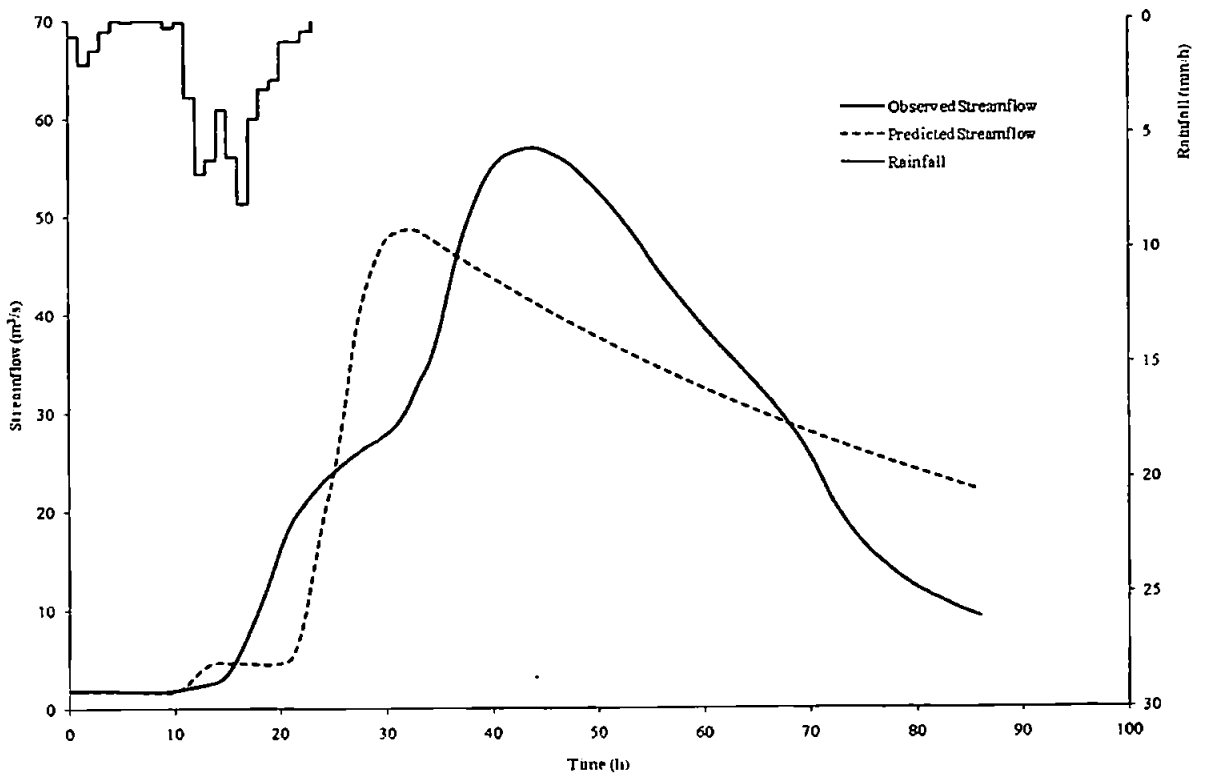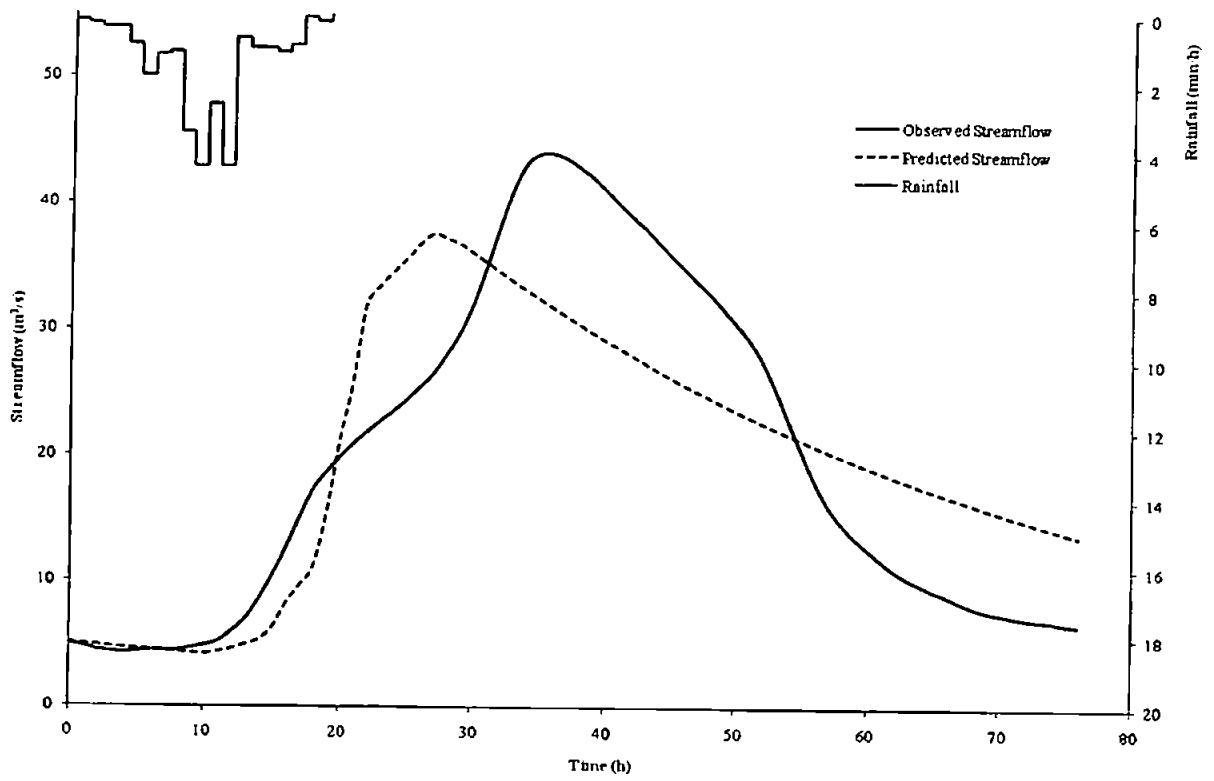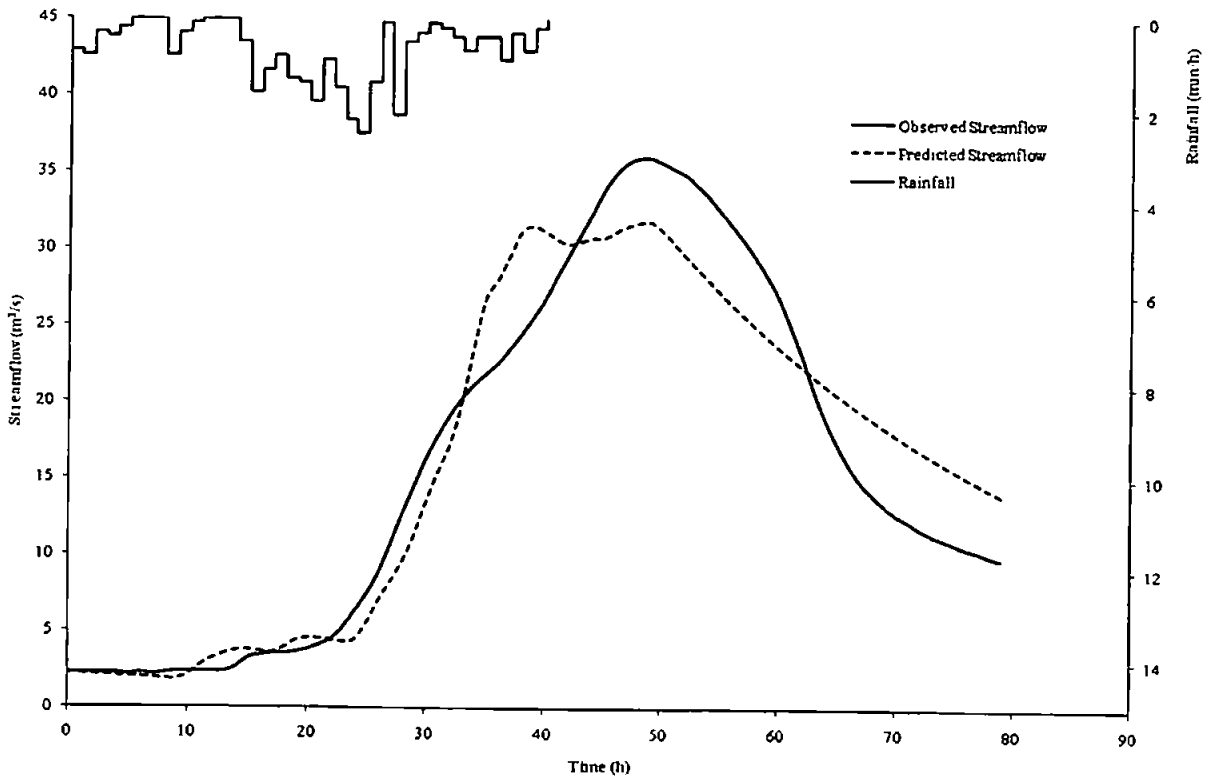**Figure A1 Predicted and observed results for event 01**
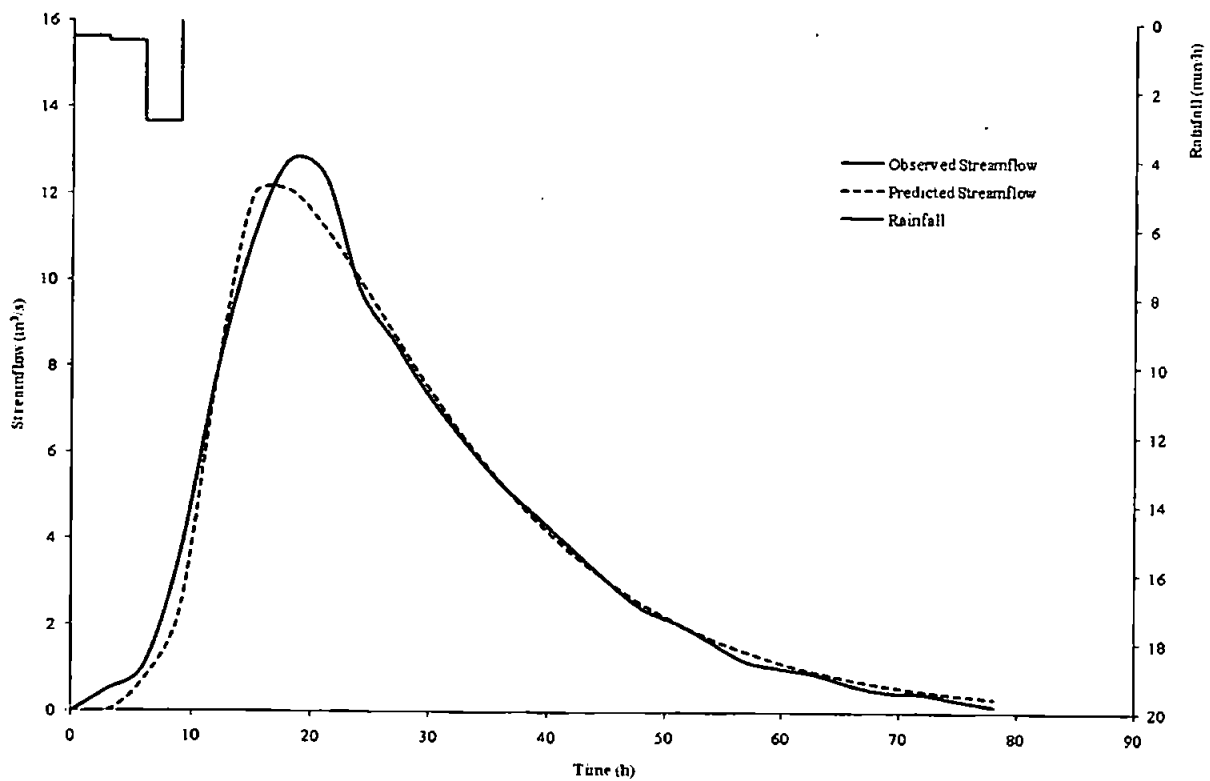
Figure A2 Predicted and observed results for event 02

188
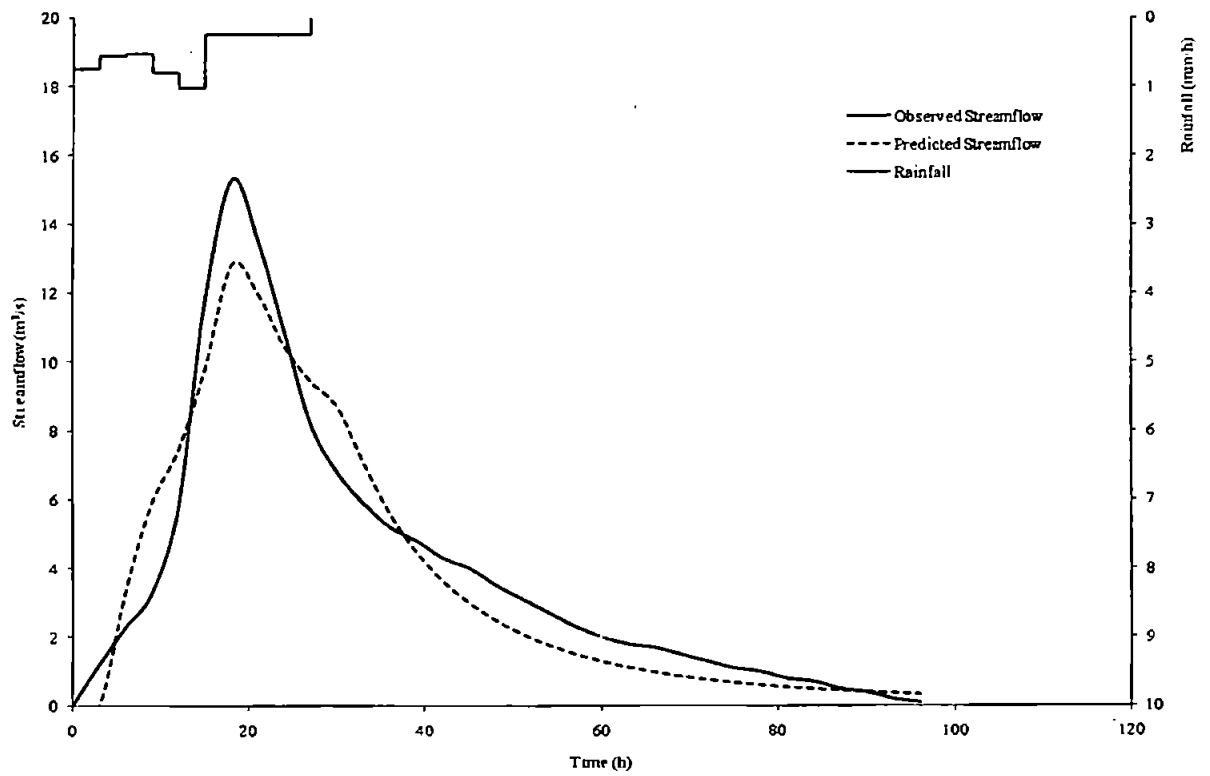
Figure A3 Predicted and observed results for event 03
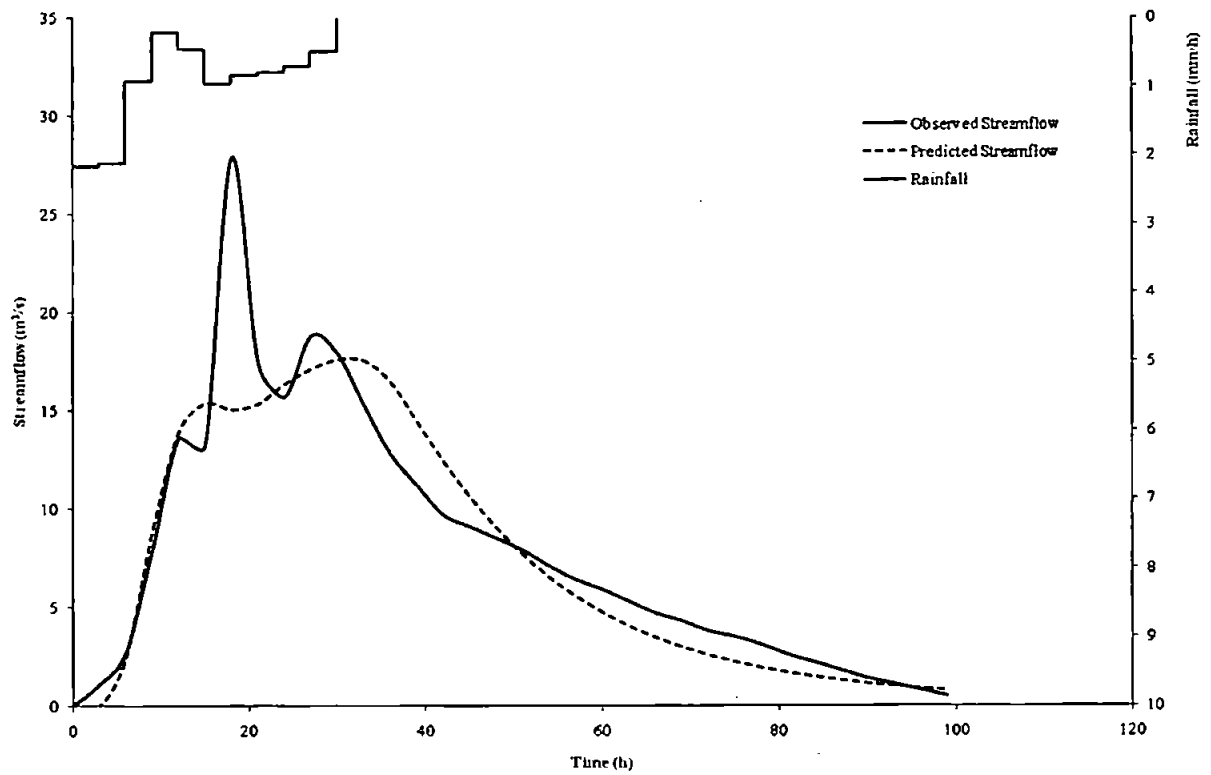
Figure A4 Predicted and observed results for event 04

189
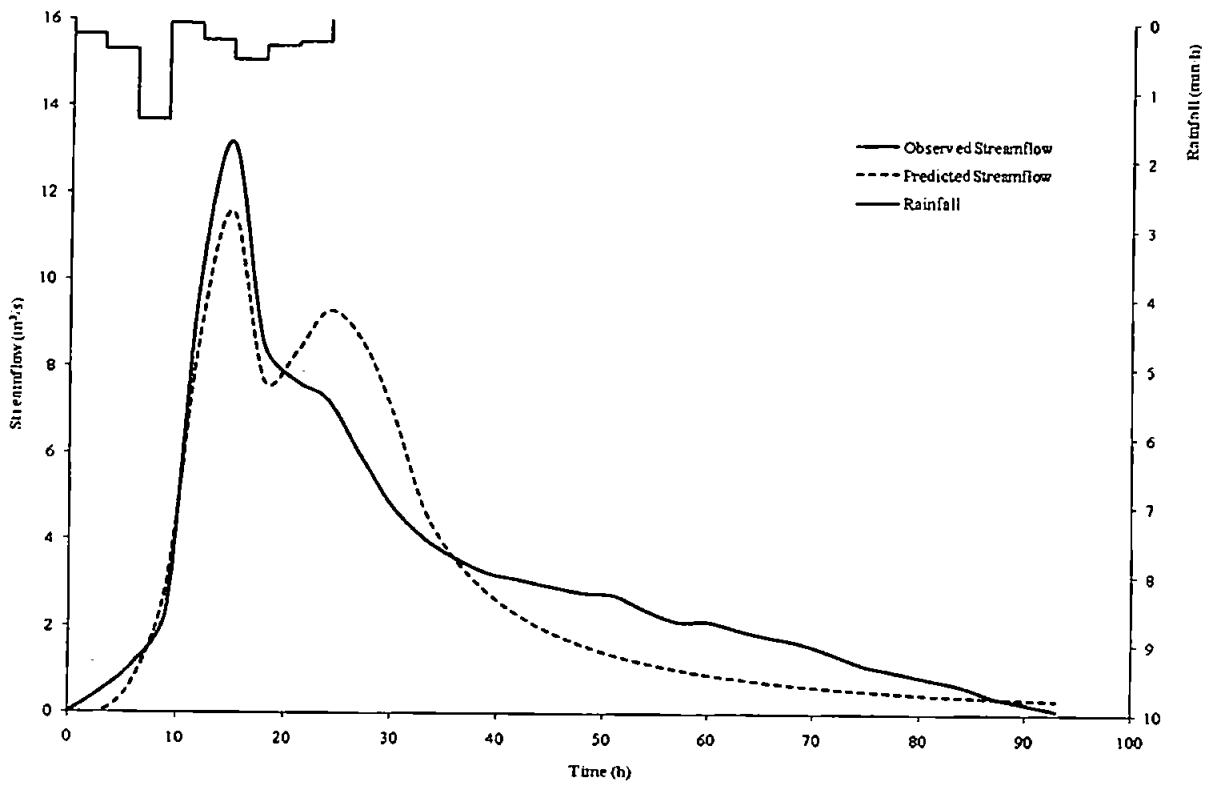
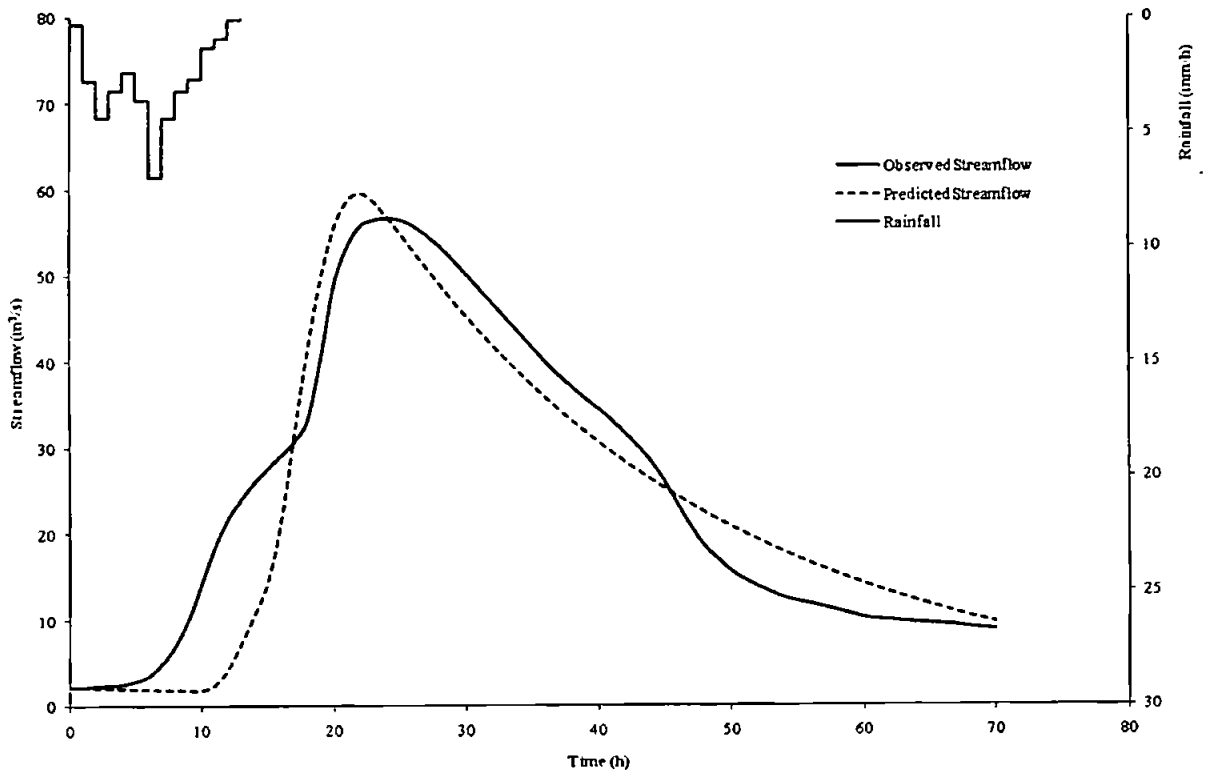**Figure A5 Predicted and observed results for event 05**
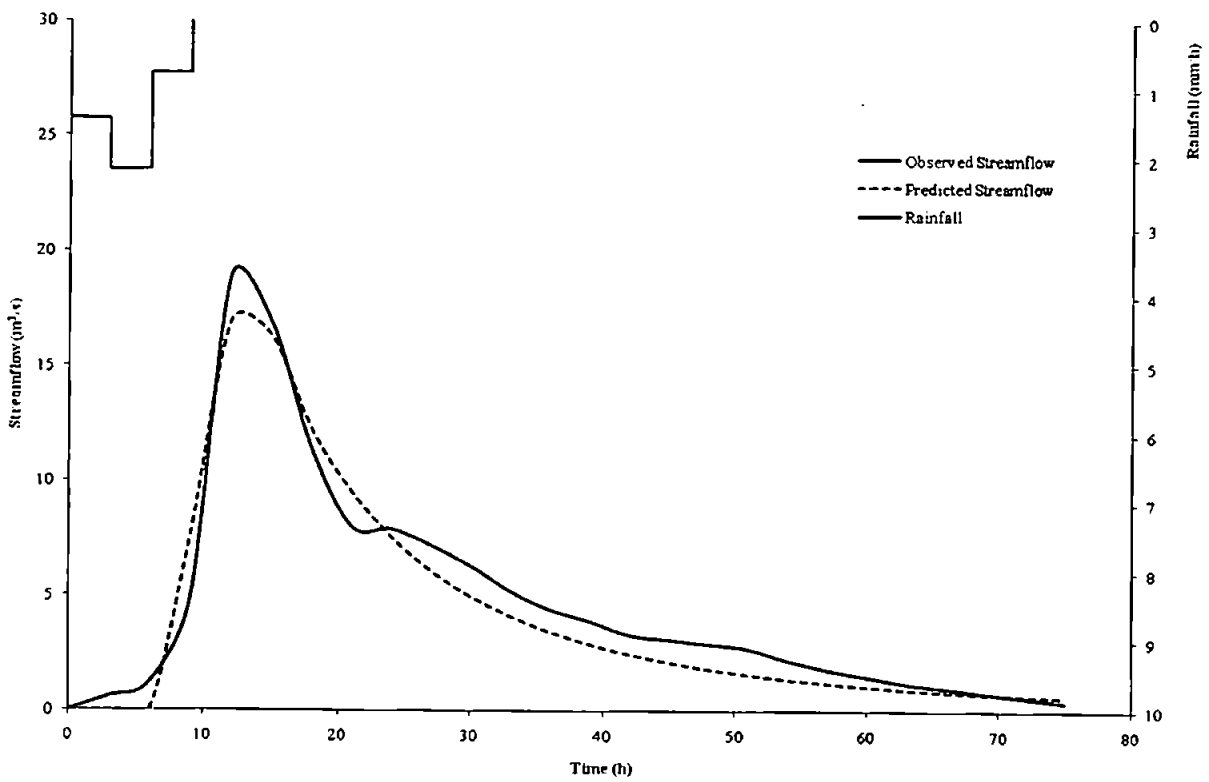
Figure A6 Predicted and observed results for event 06

190
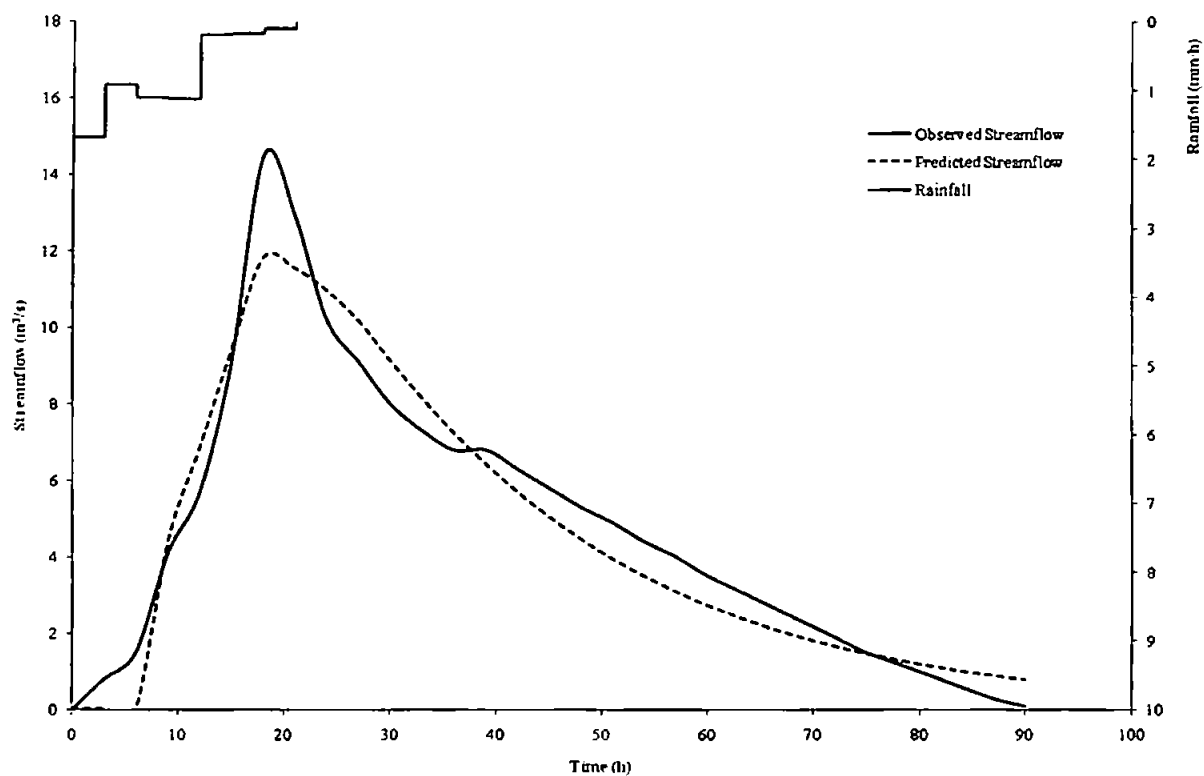
Figure A7 Predicted and observed results for event 07
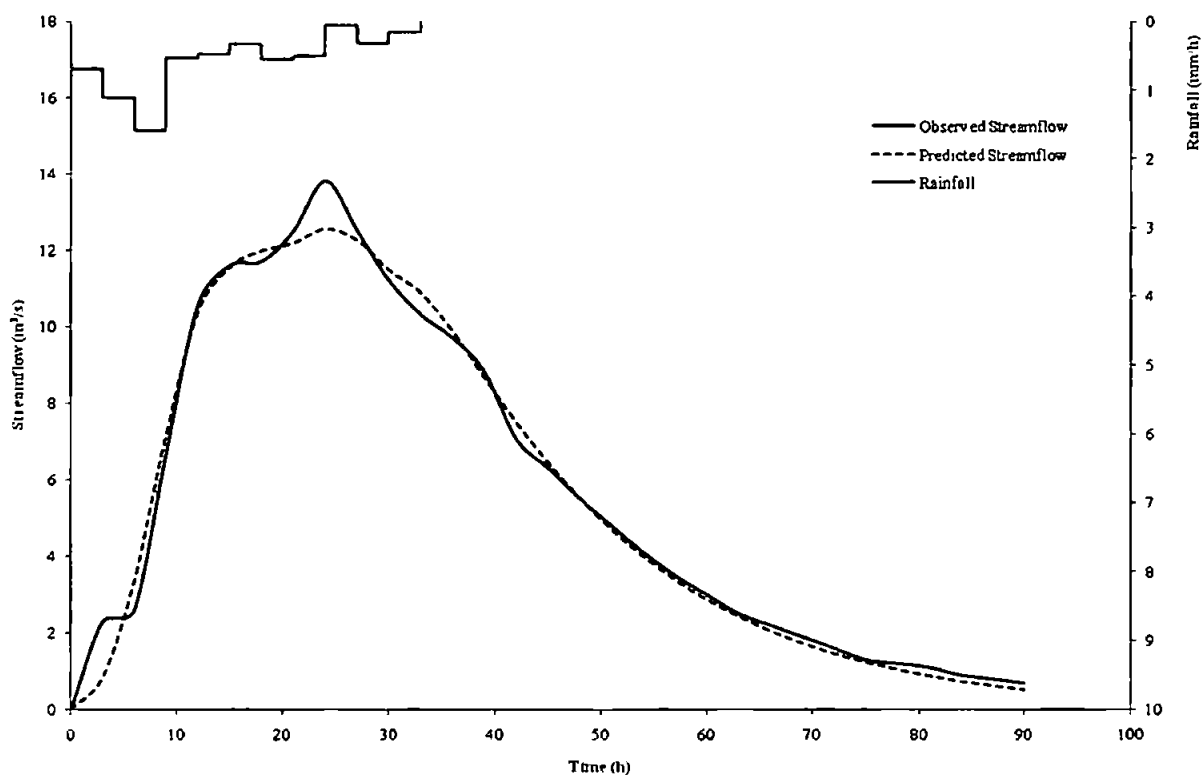
Figure A8 Predicted and observed results for event 08
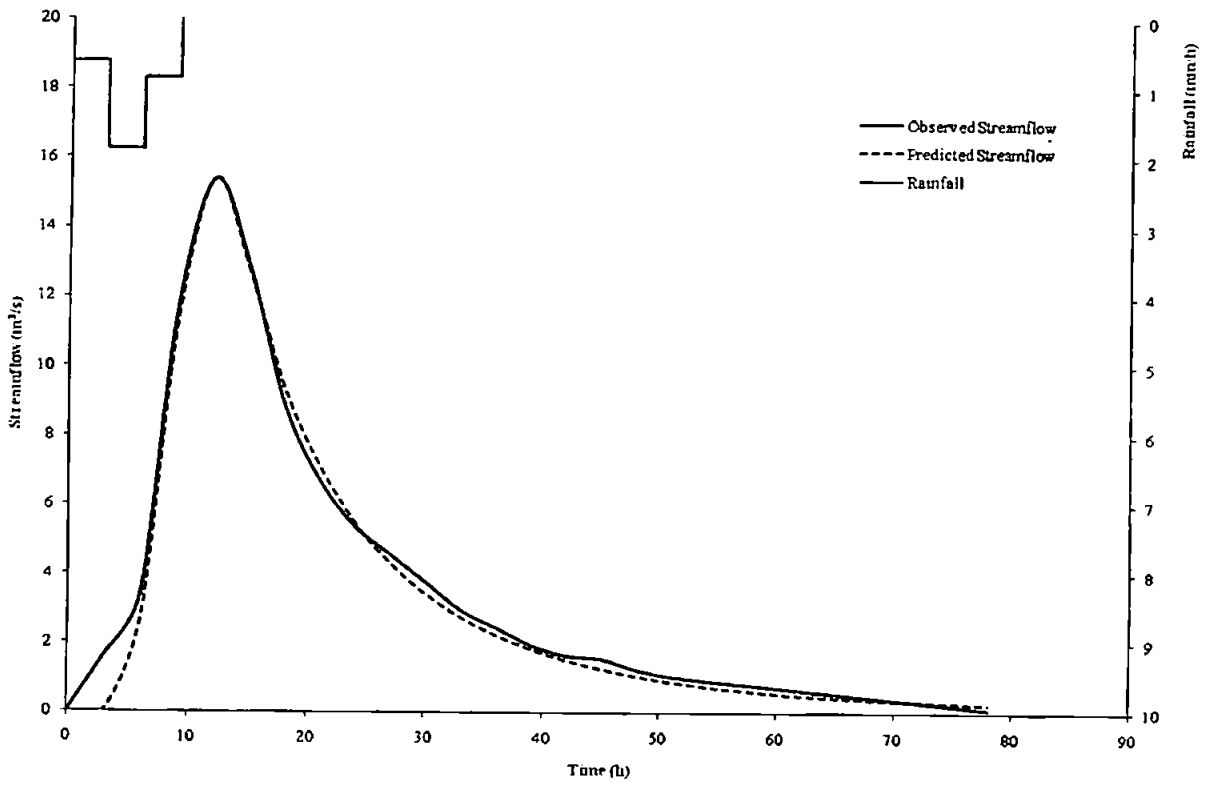
Figure A9 Predicted and observed results for event 09
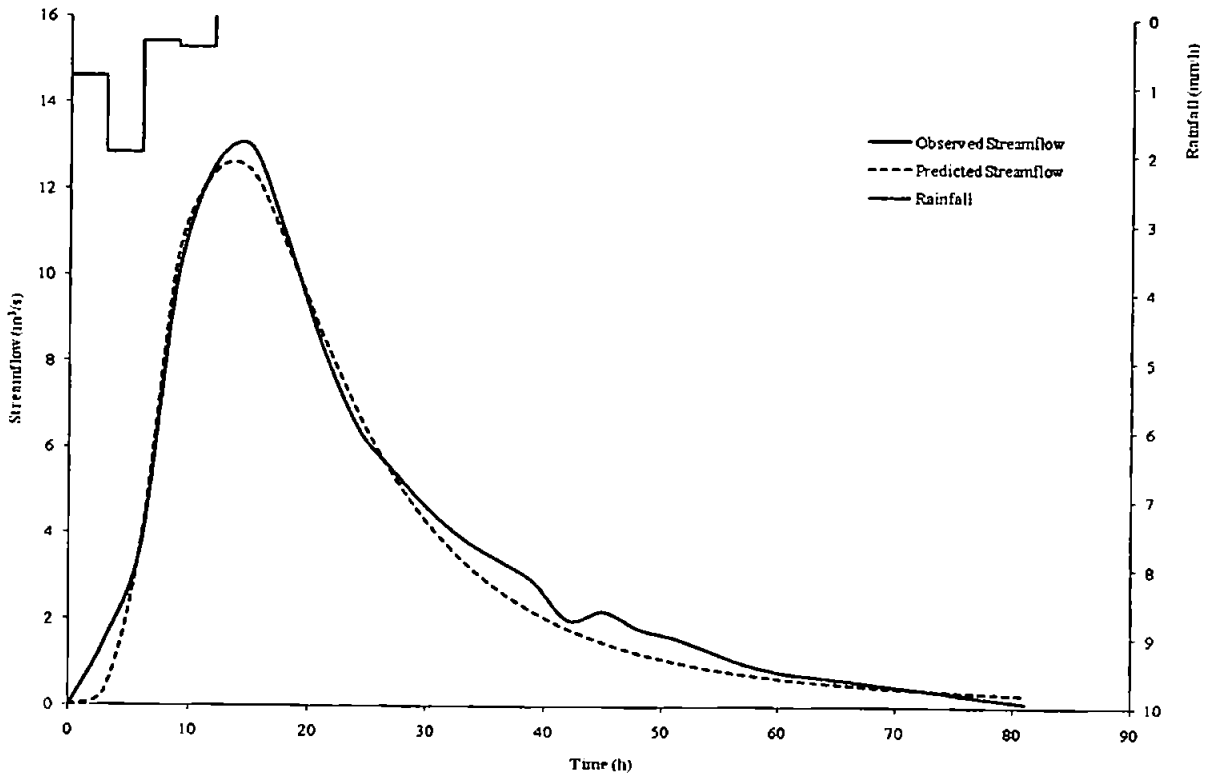
Figure A10 Predicted and observed results for event 10
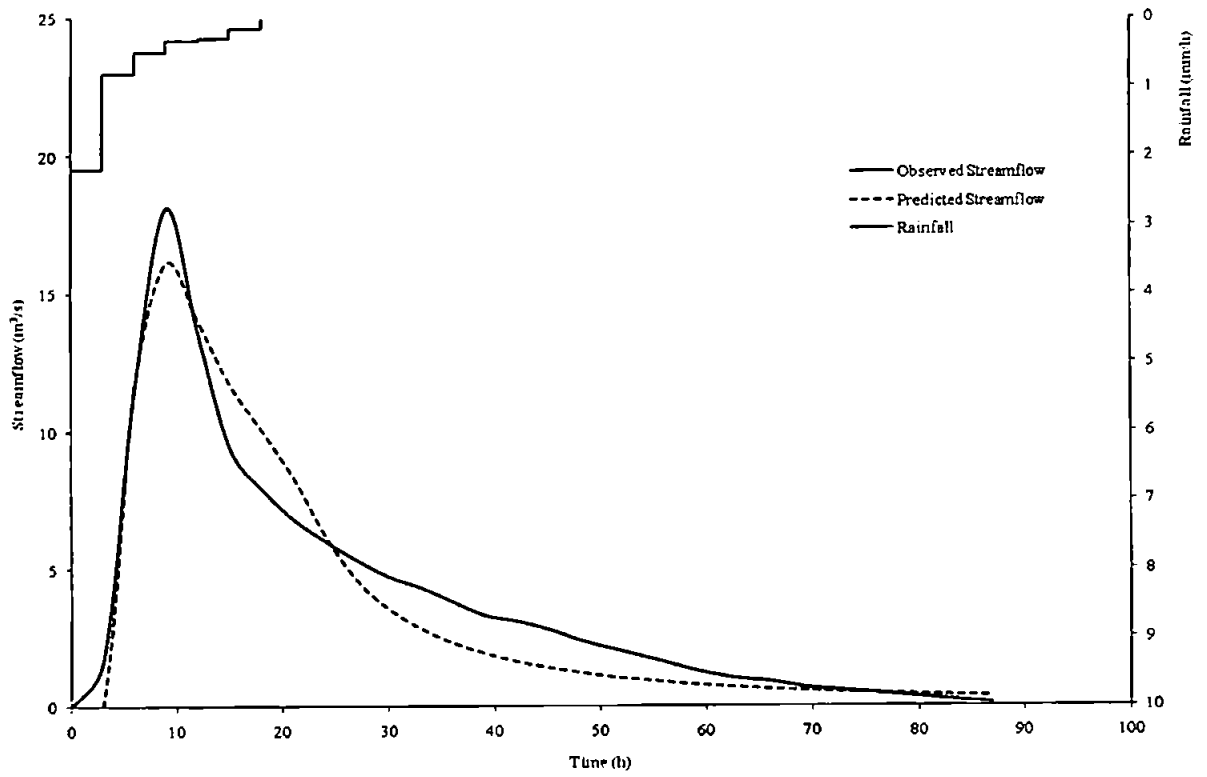
Figure A11 Predicted and observed results for event 11
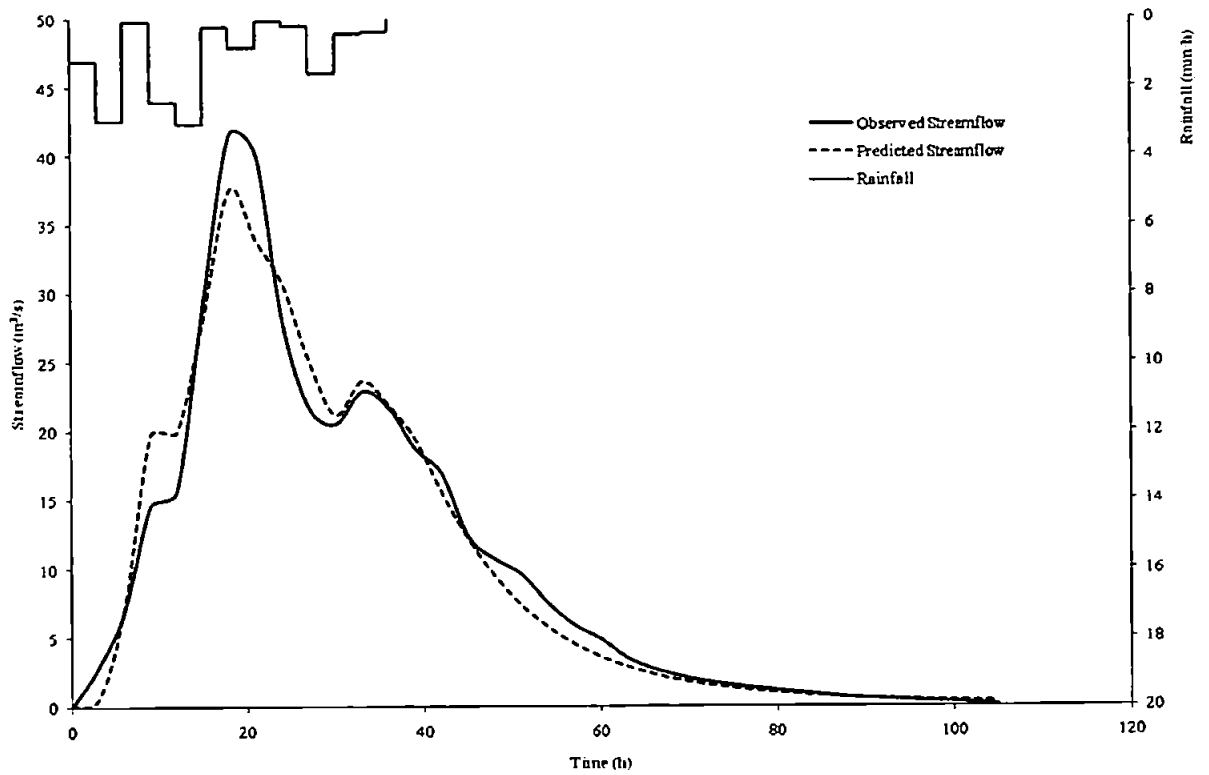
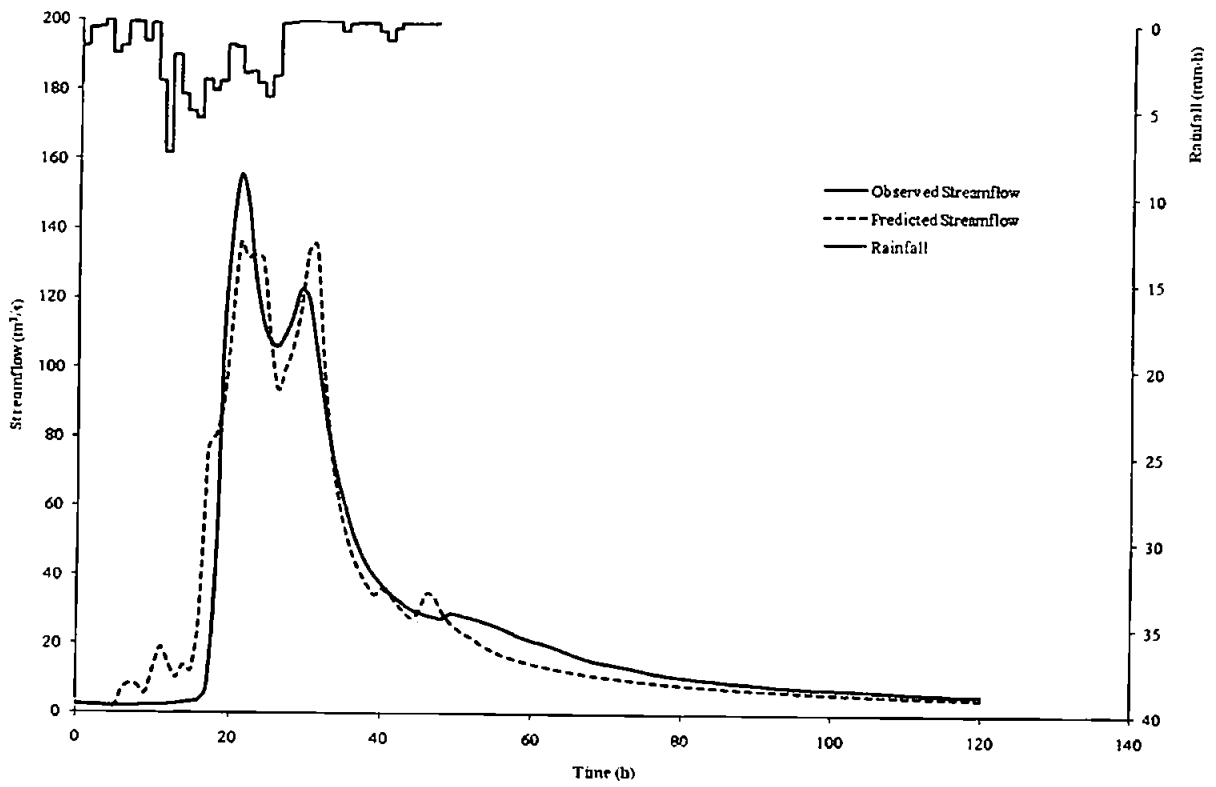**Figure A12 Predicted and observed results for event 12**
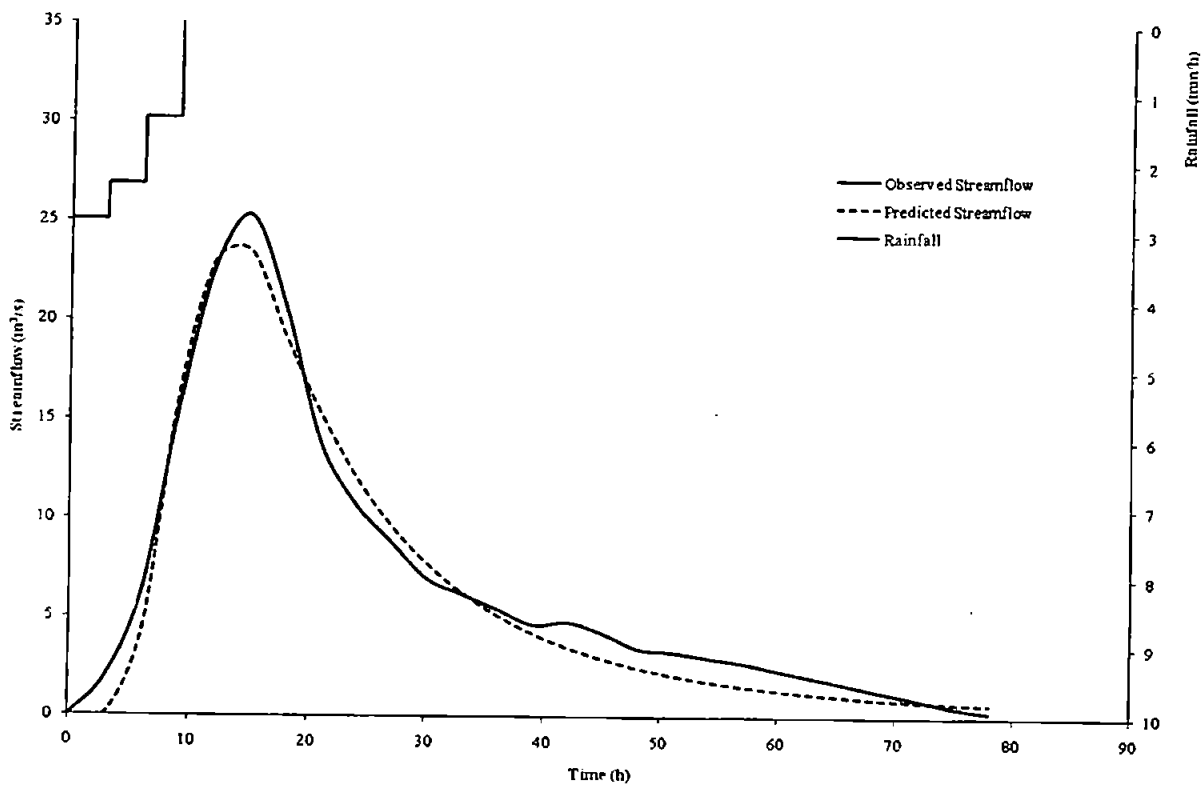
Figure A13 Predicted and observed results for event 13
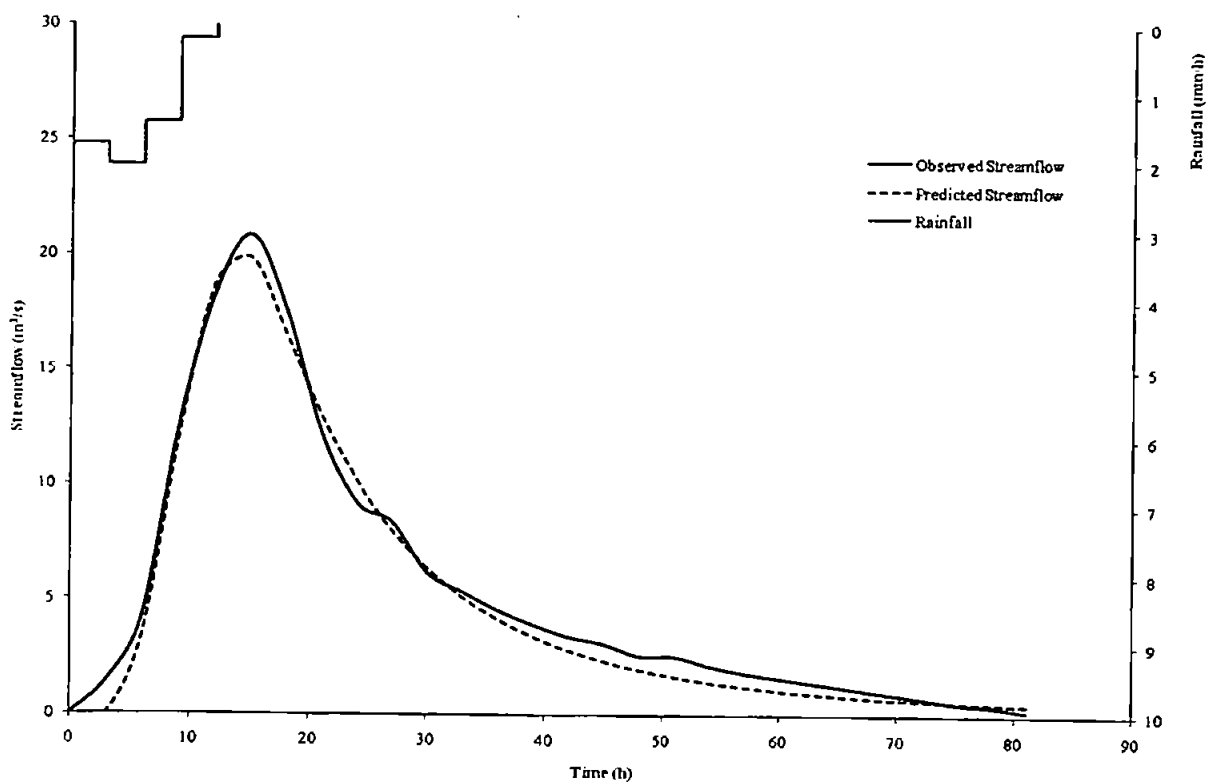
Figure A14 Predicted and observed results for event 14
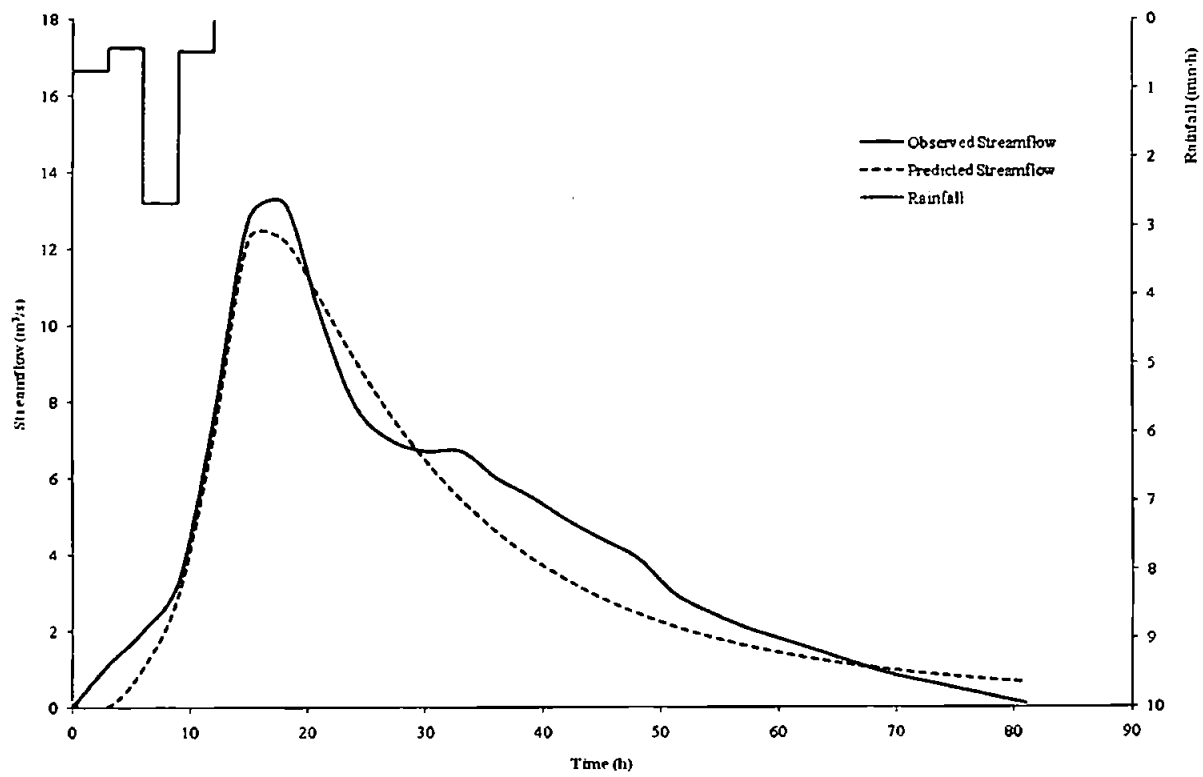
Figure A15 Predicted and observed results for event 15
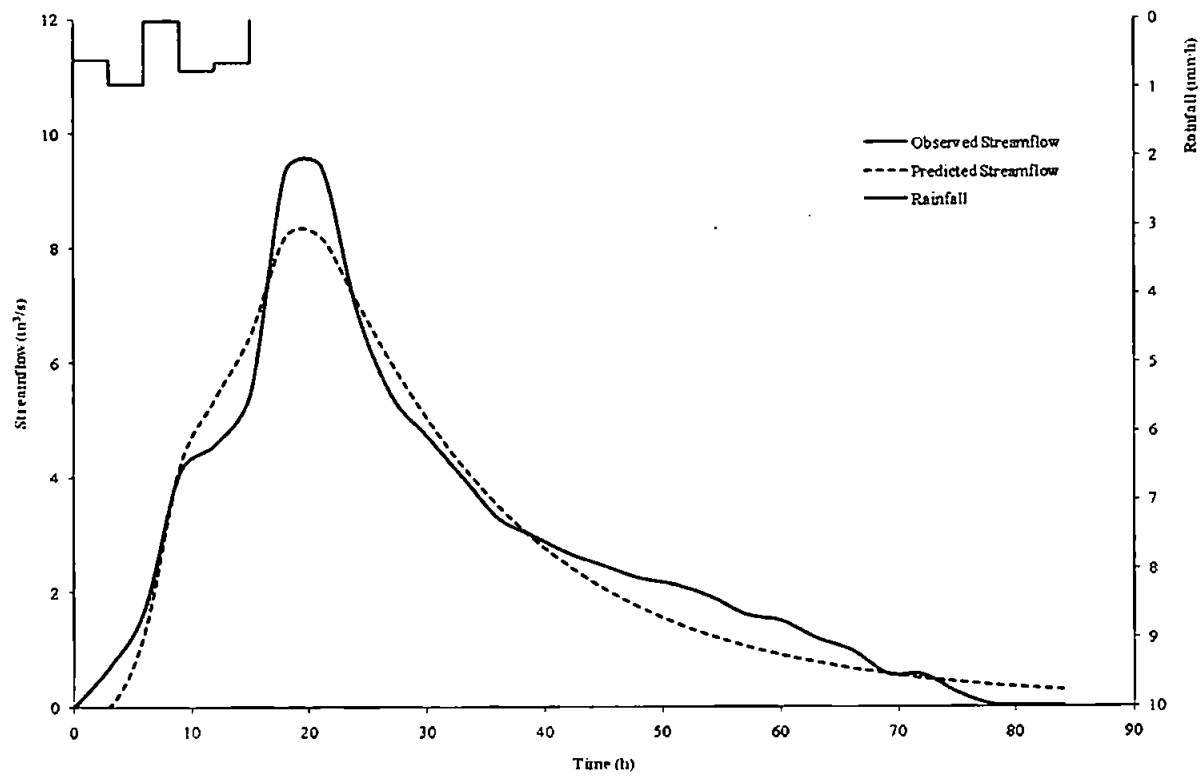
Figure A16 Predicted and observed results for event 16
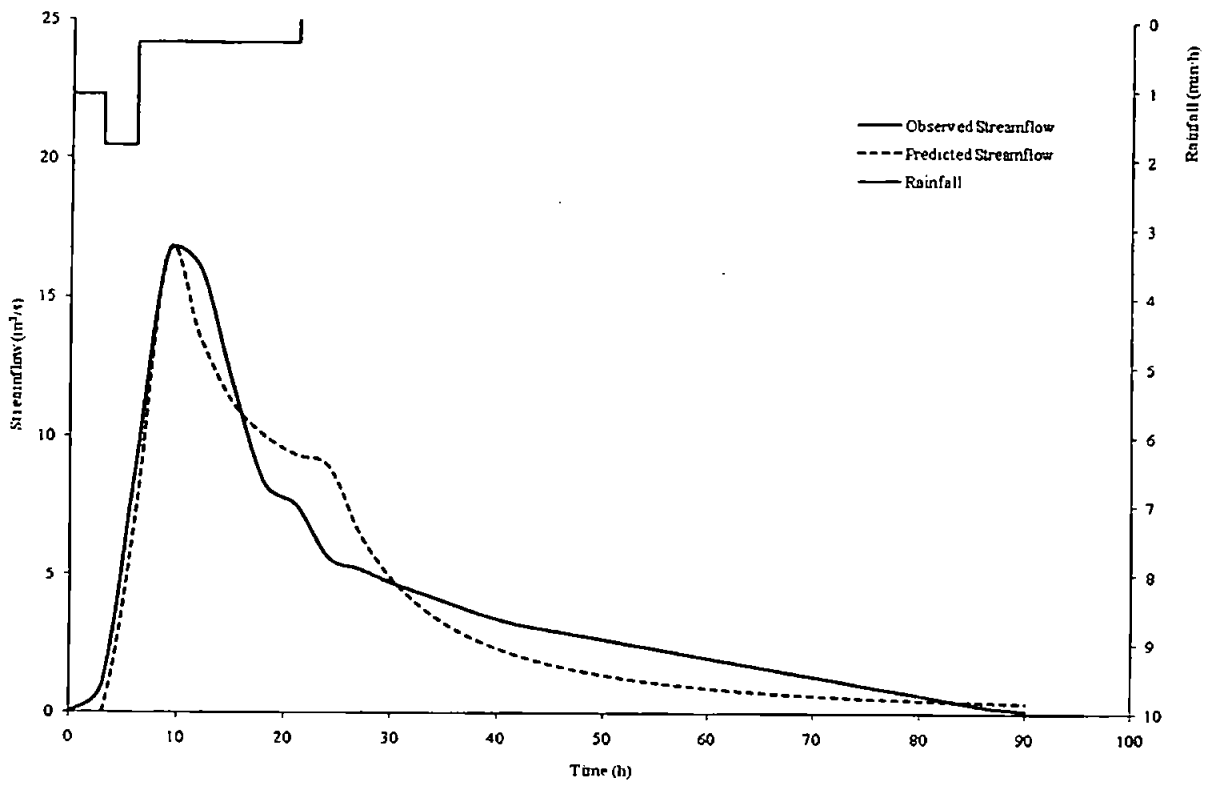
Figure A17 Predicted and observed results for event 17
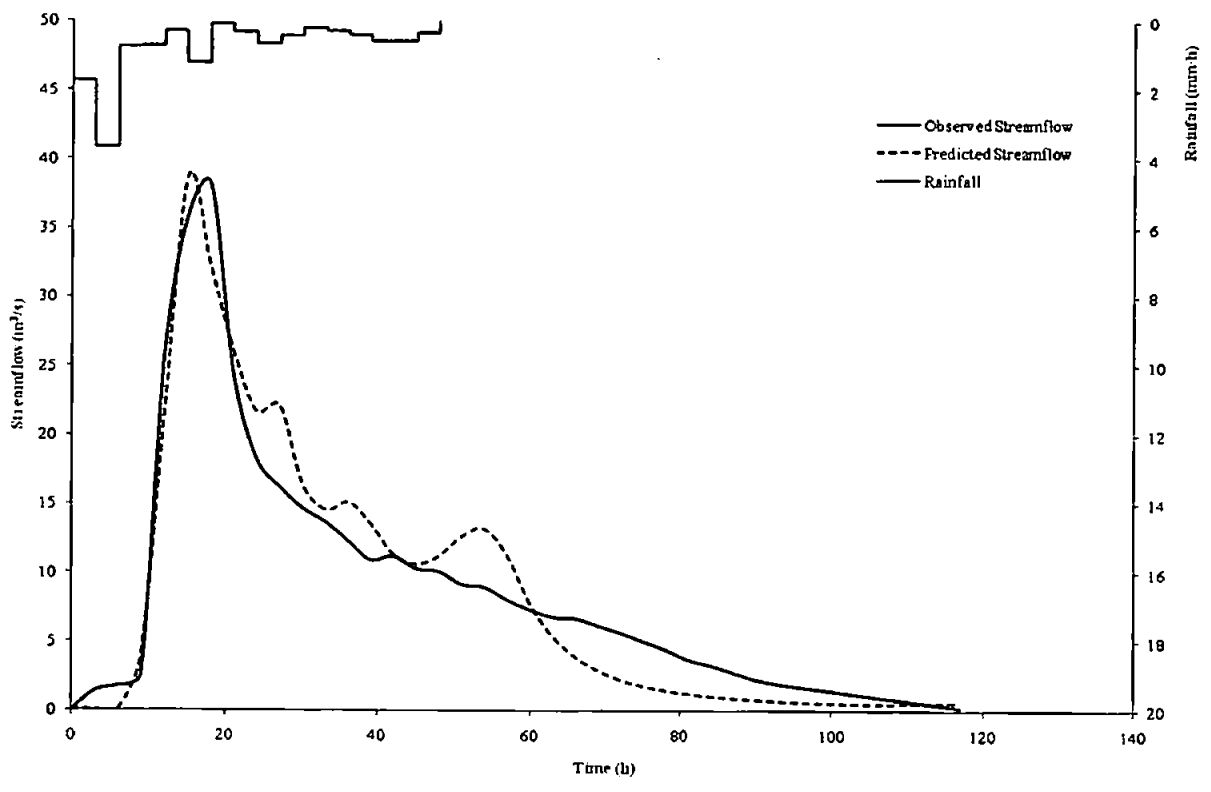
Figure A18 Predicted and observed results for event 18
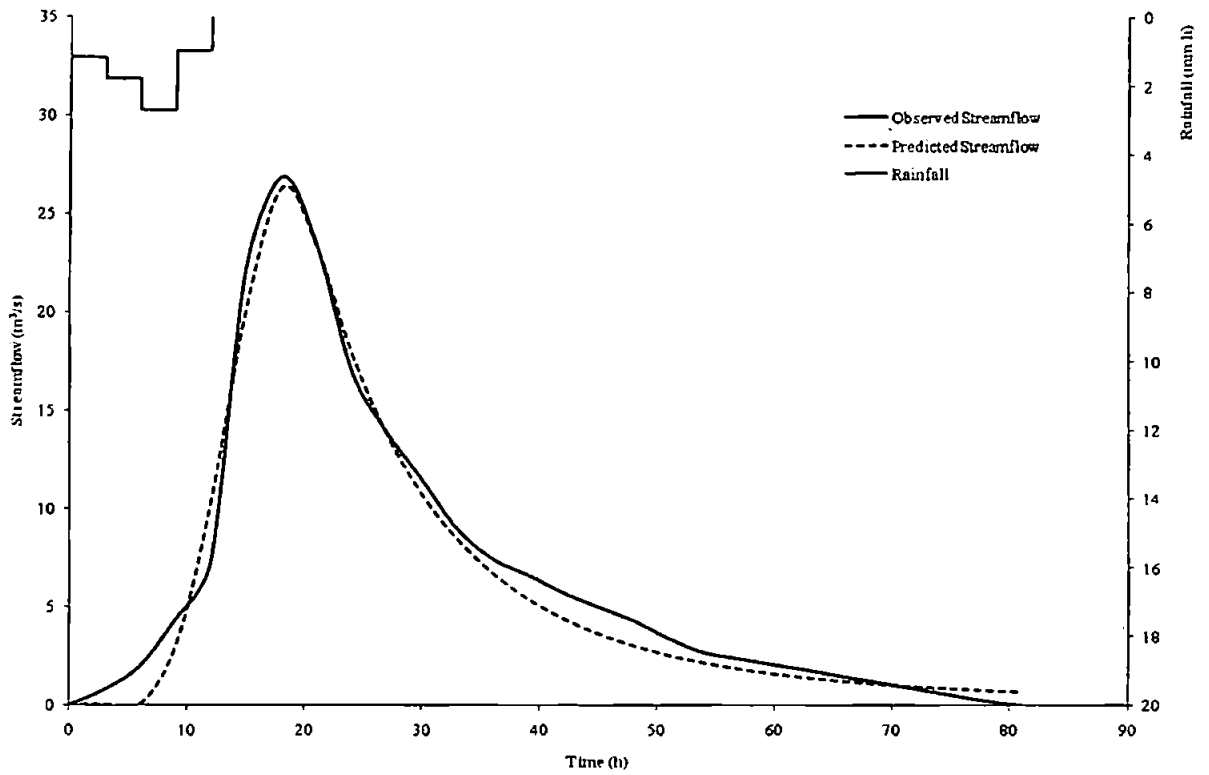
Figure A19 Predicted and observed results for event 19
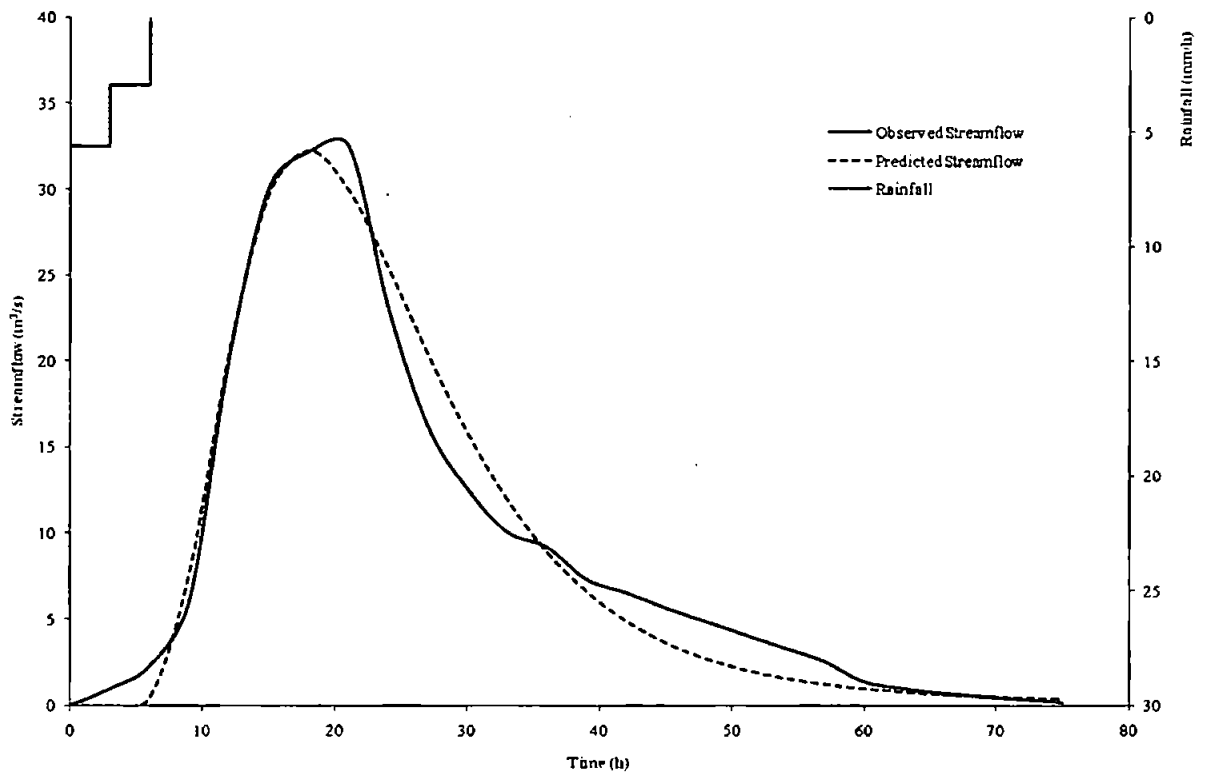
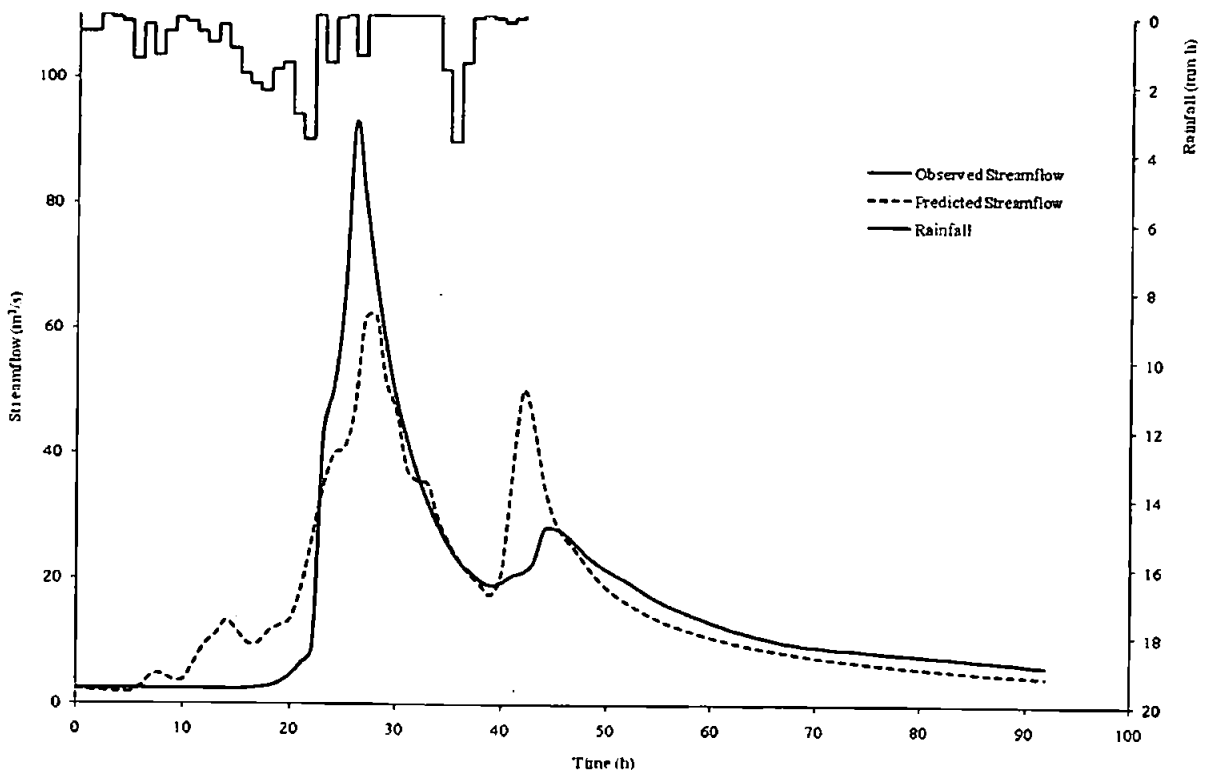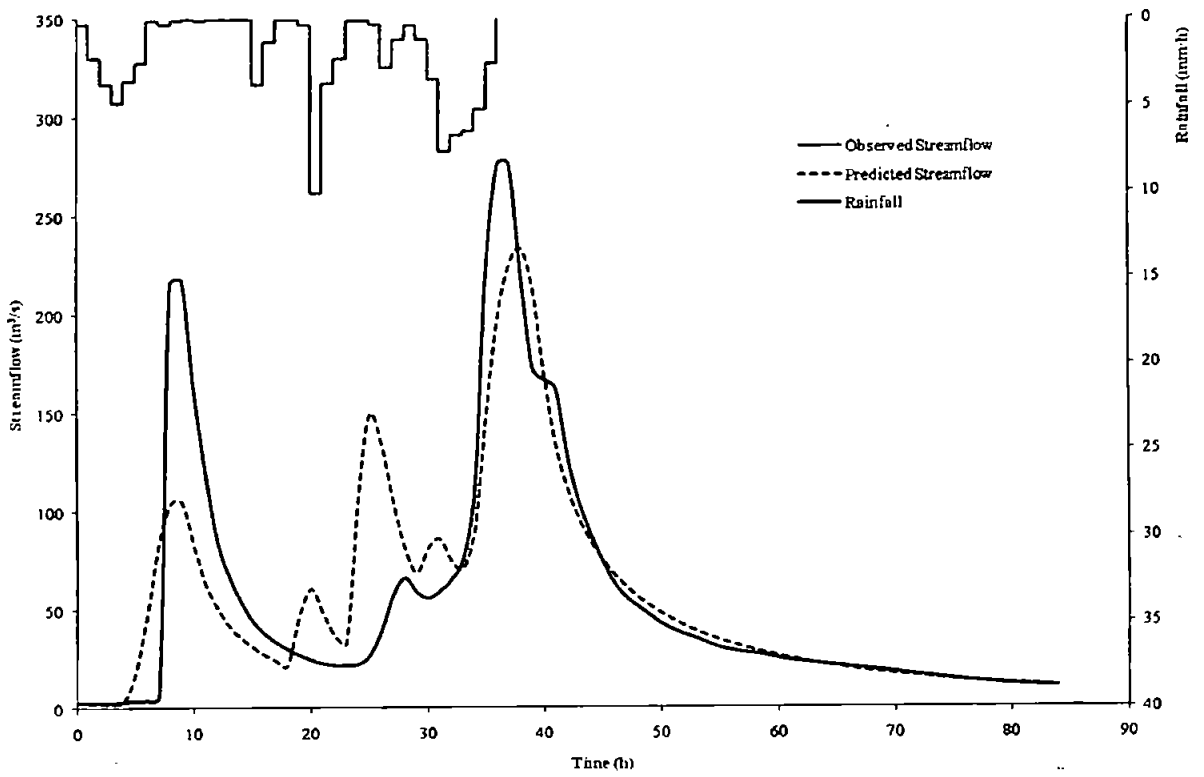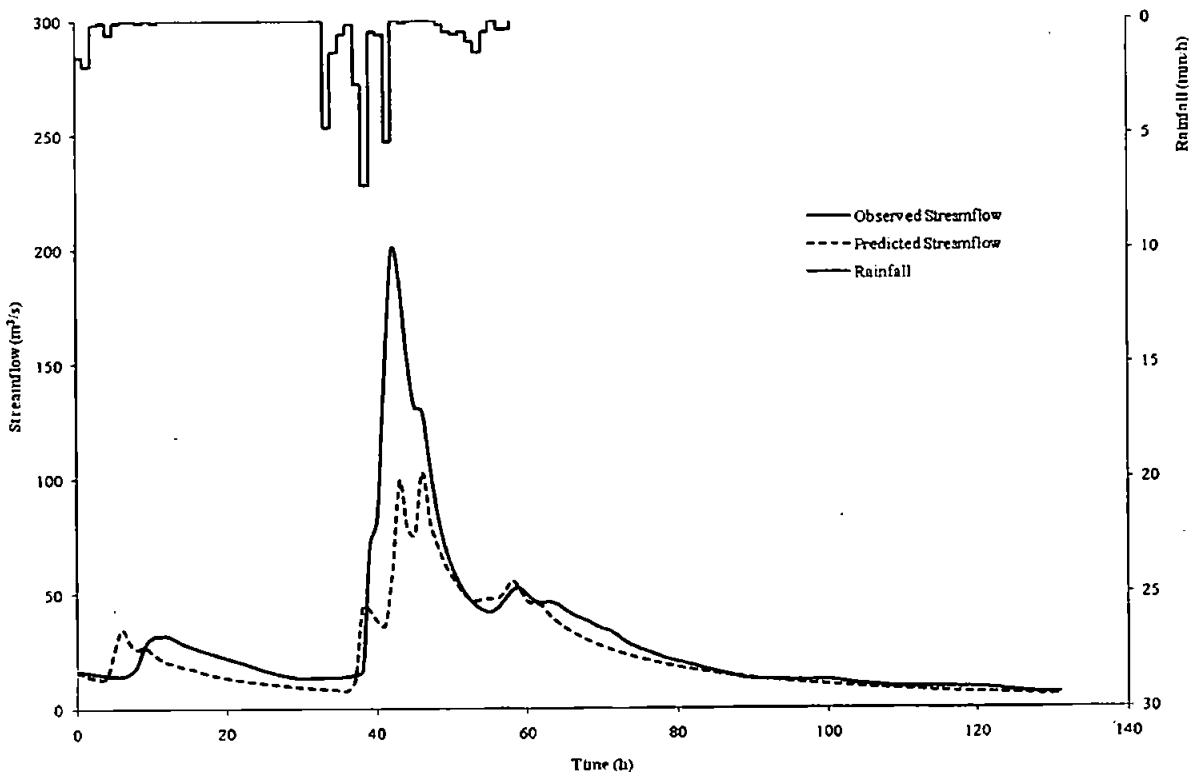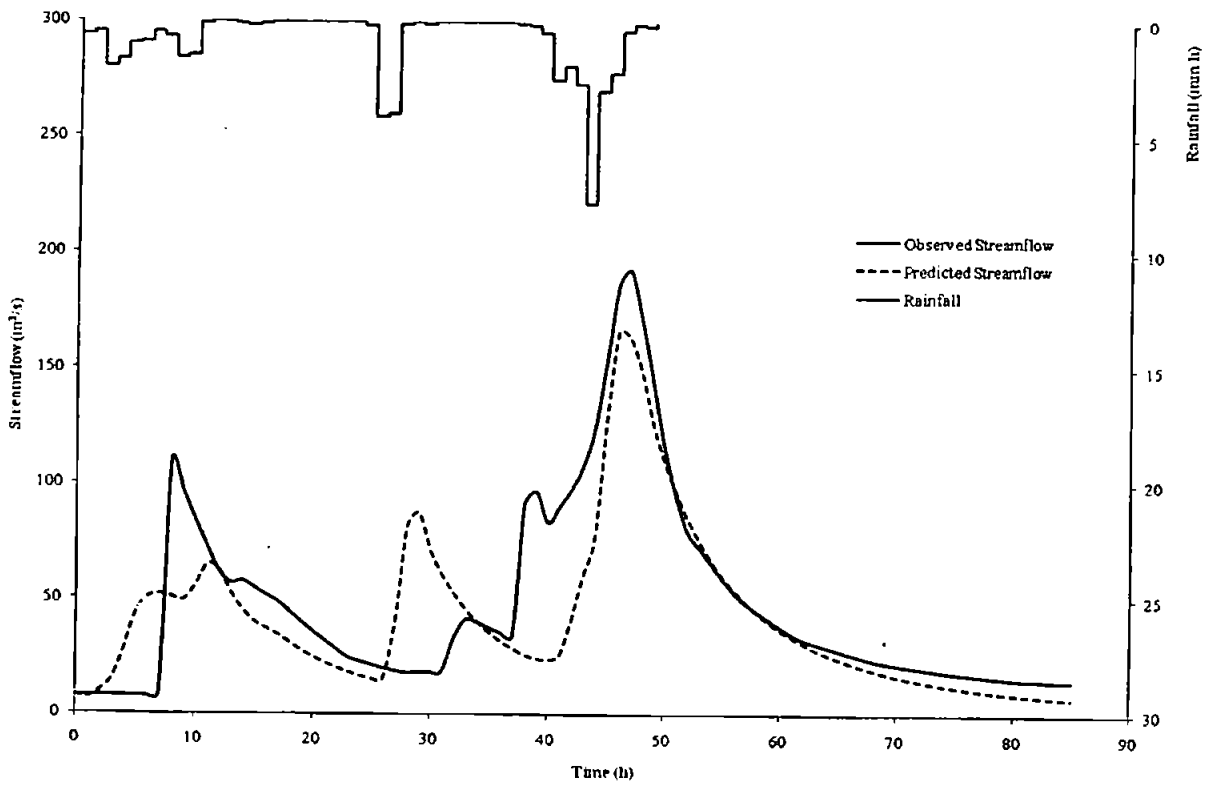**Figure A20 Predicted and observed results for event 20**

197
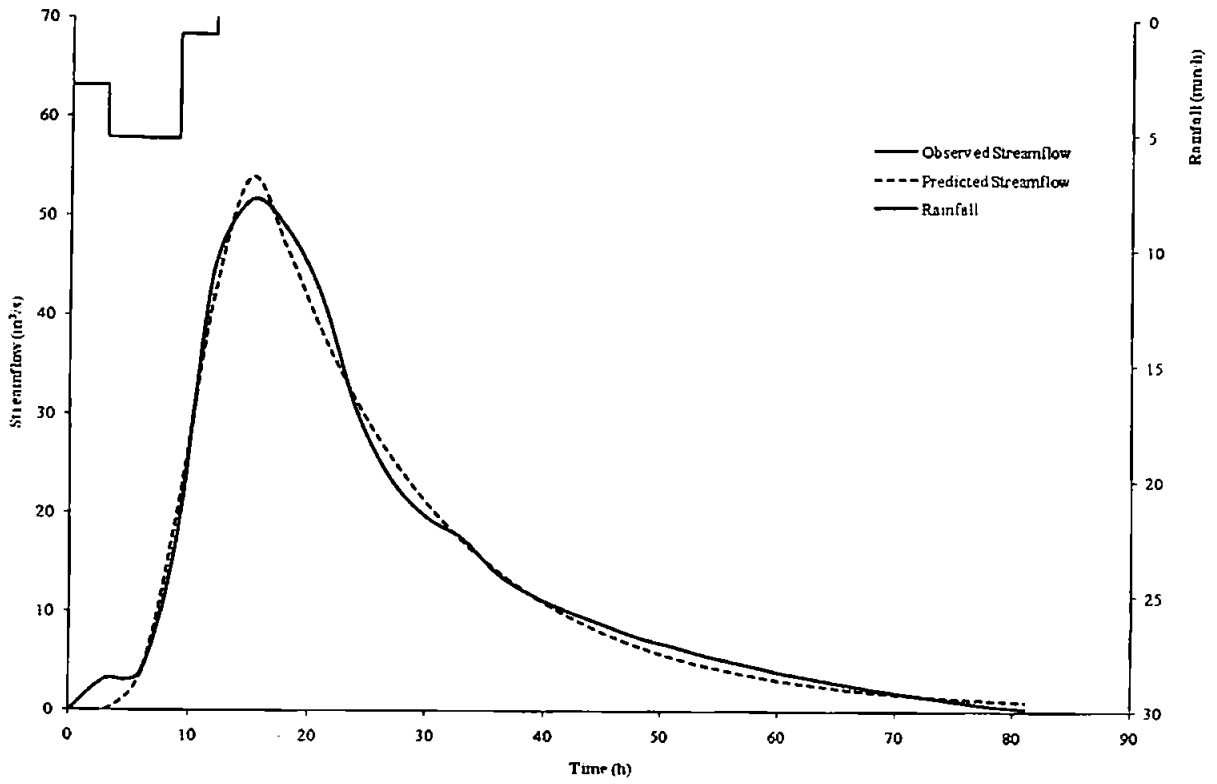
Figure A21 Predicted and observed results for event 21
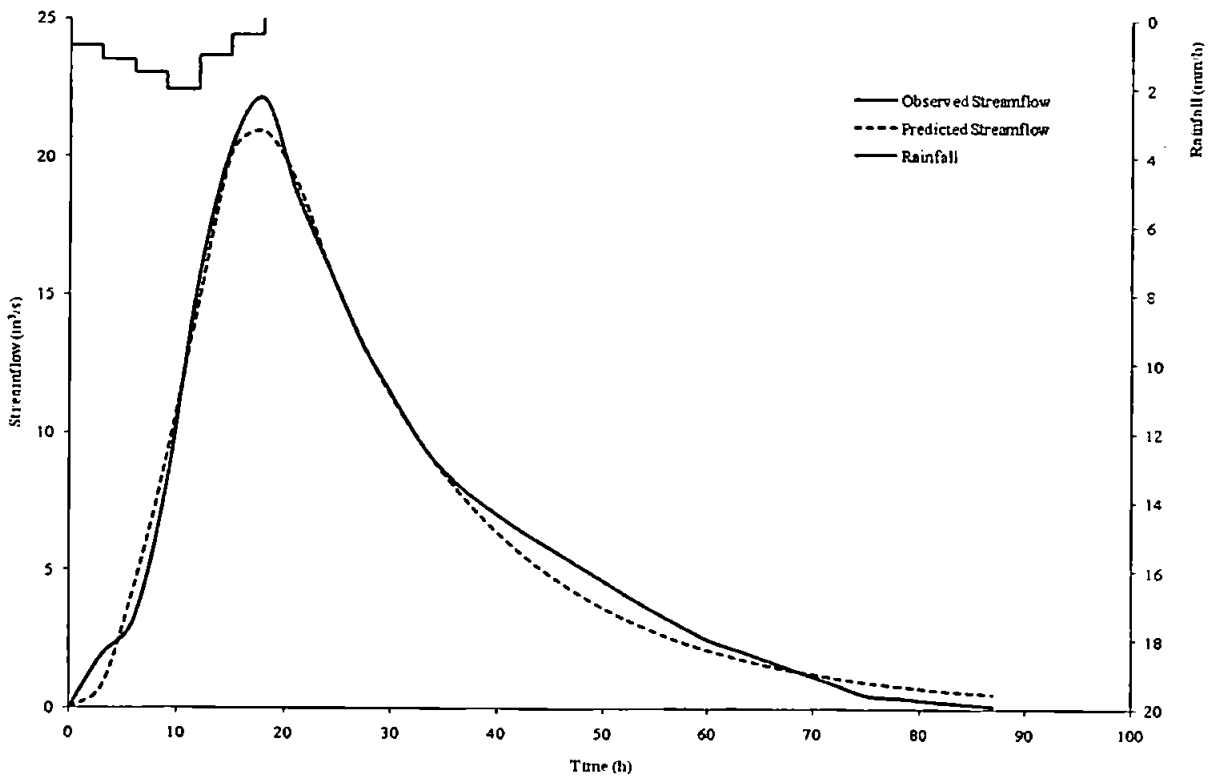
Figure A22 Predicted and observed results for event 22

Appendix B: R. Nenagh Results – Unequal Casacade

The following Figures show the predicted and observed runoff hydrographs together with the net (effective) event rainfall hyetograph for the River Nenagh. The predictions were made with the cascade of two unequal-K fractional linear reservoirs.
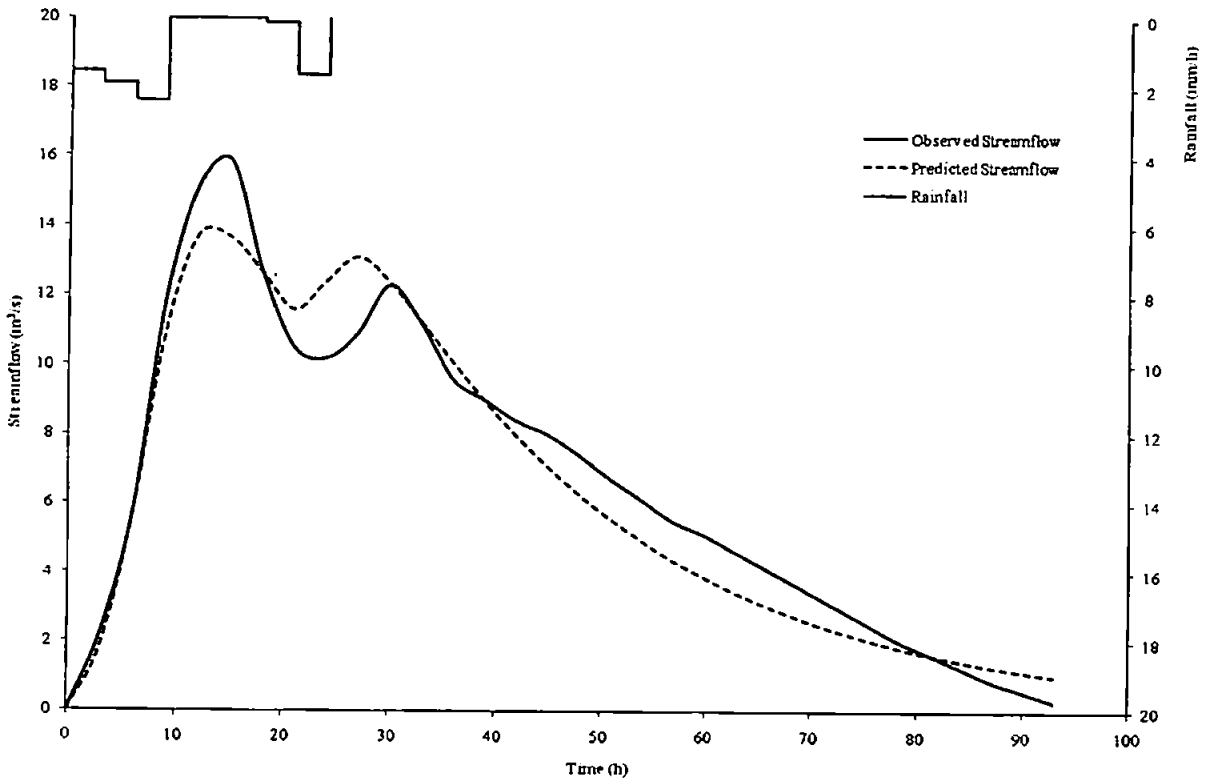
Figure B1 Predicted and observed results for event 01
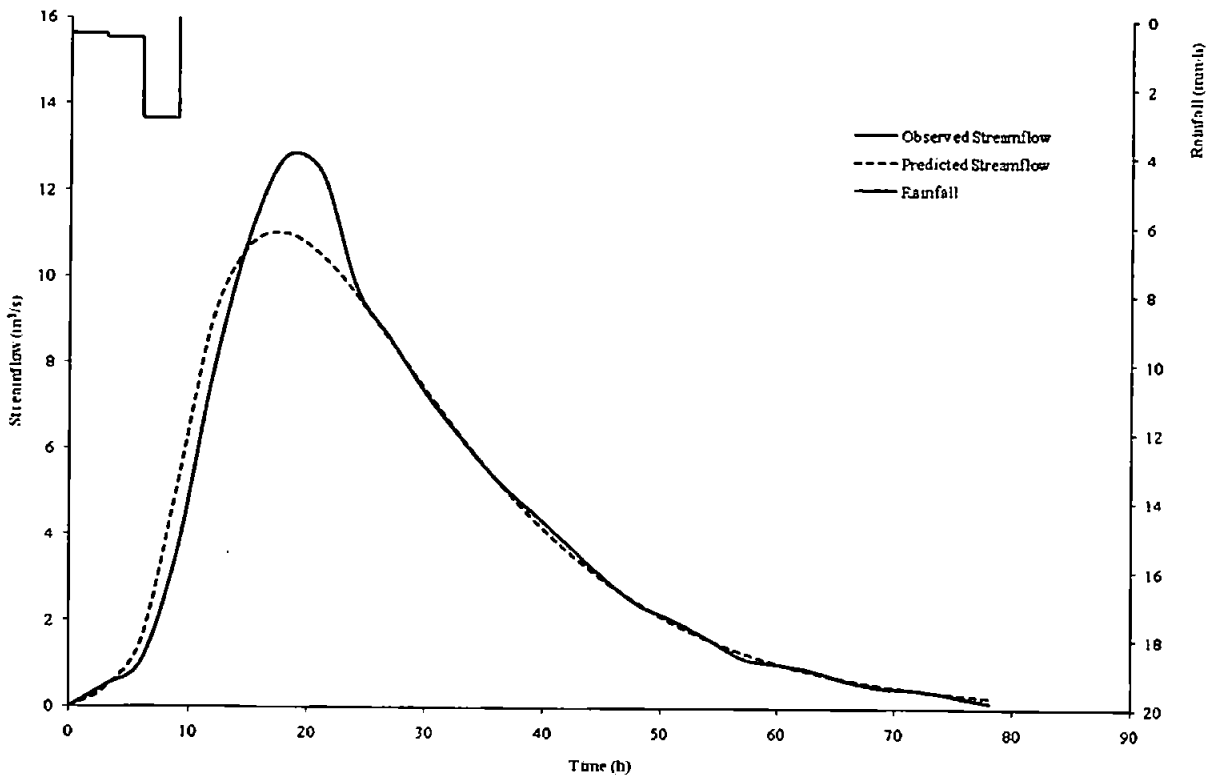
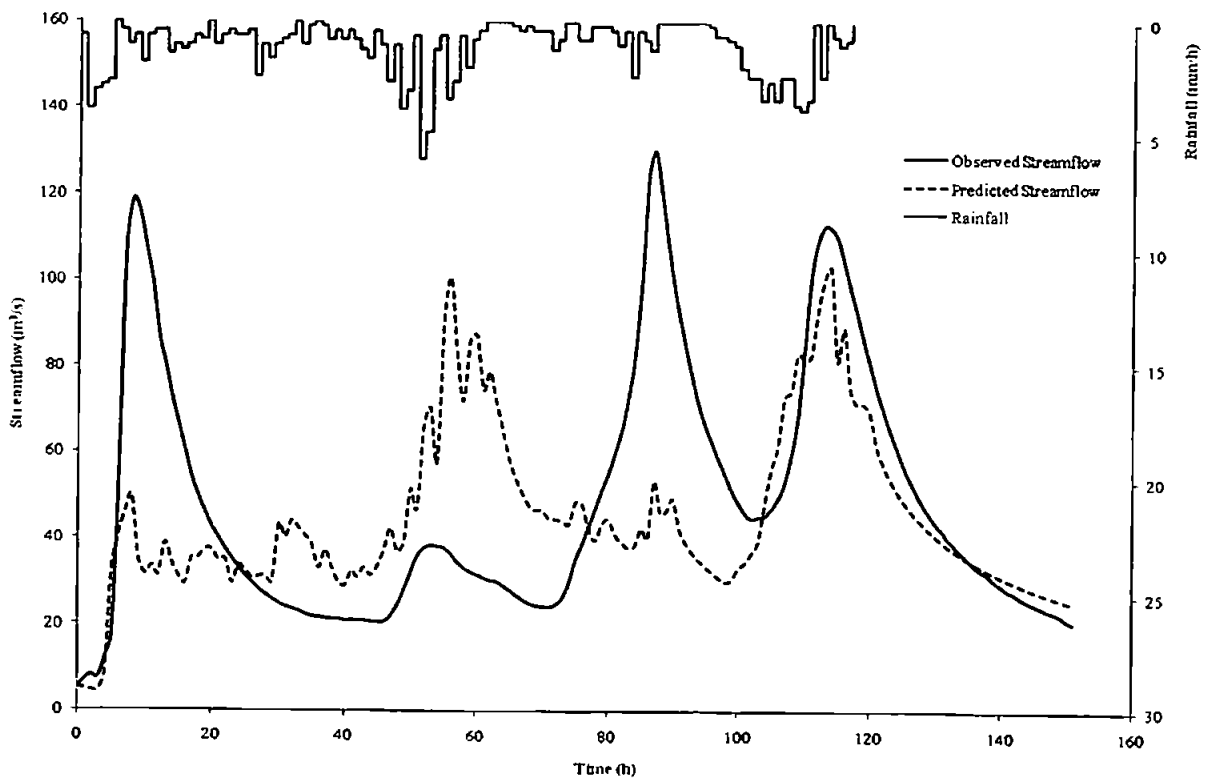
Figure B2 Predicted and observed results for event 02

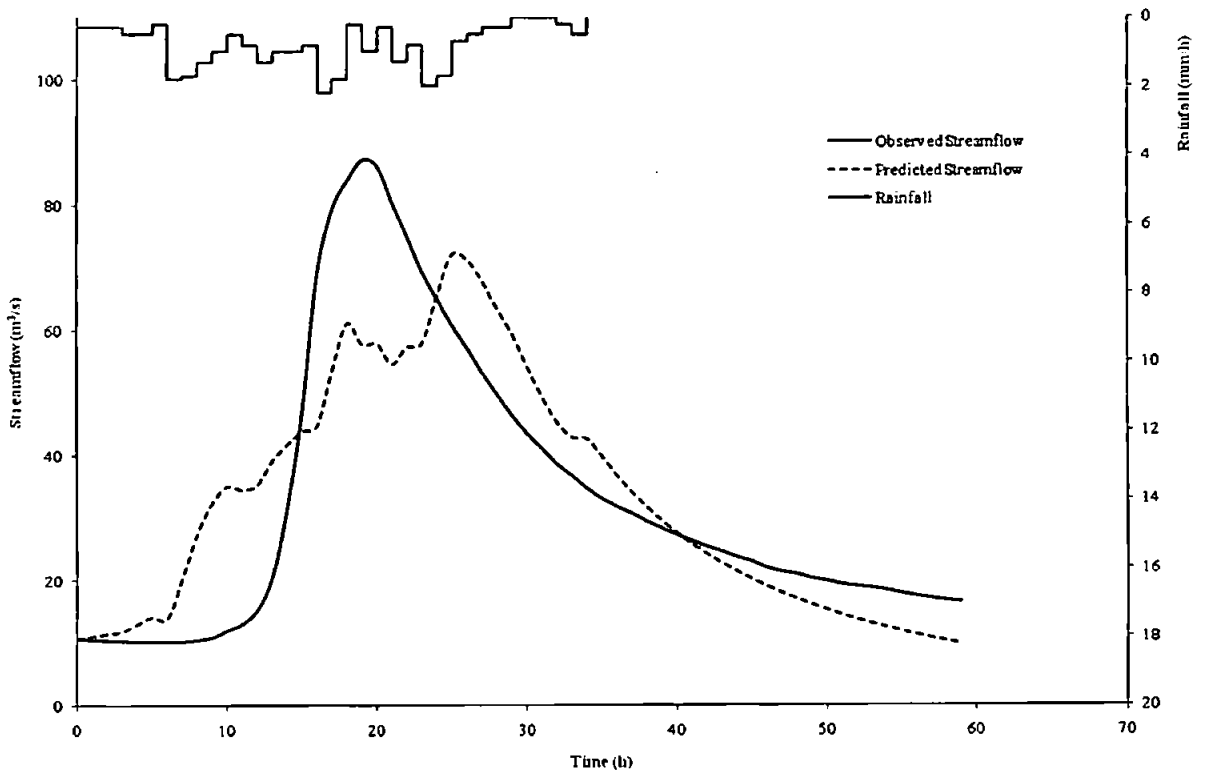200
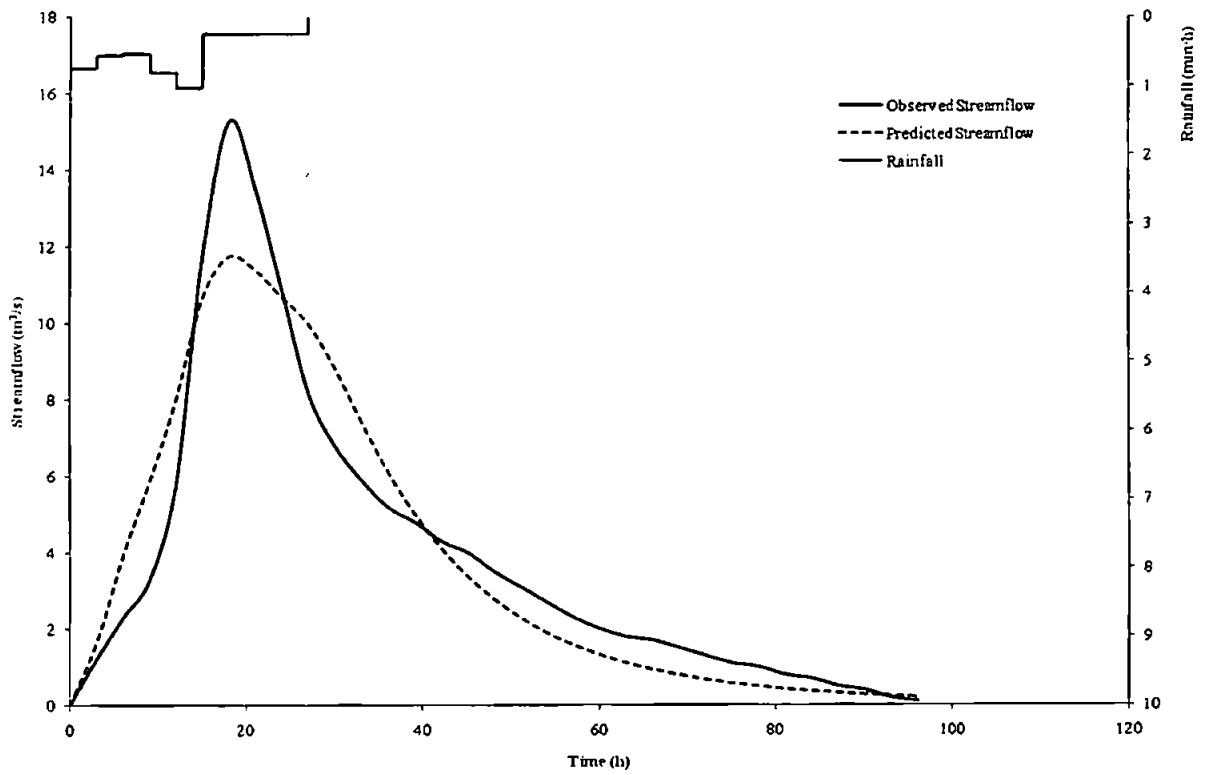
Figure B3 Predicted and observed results for event 03
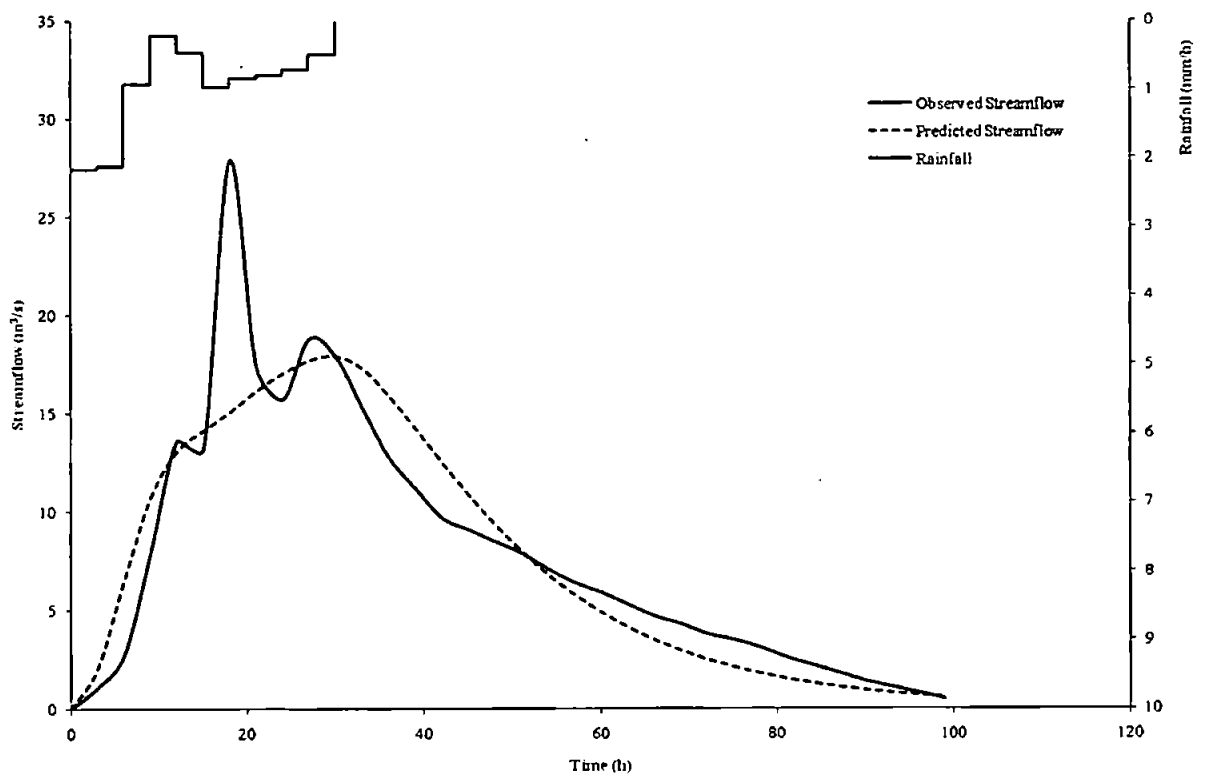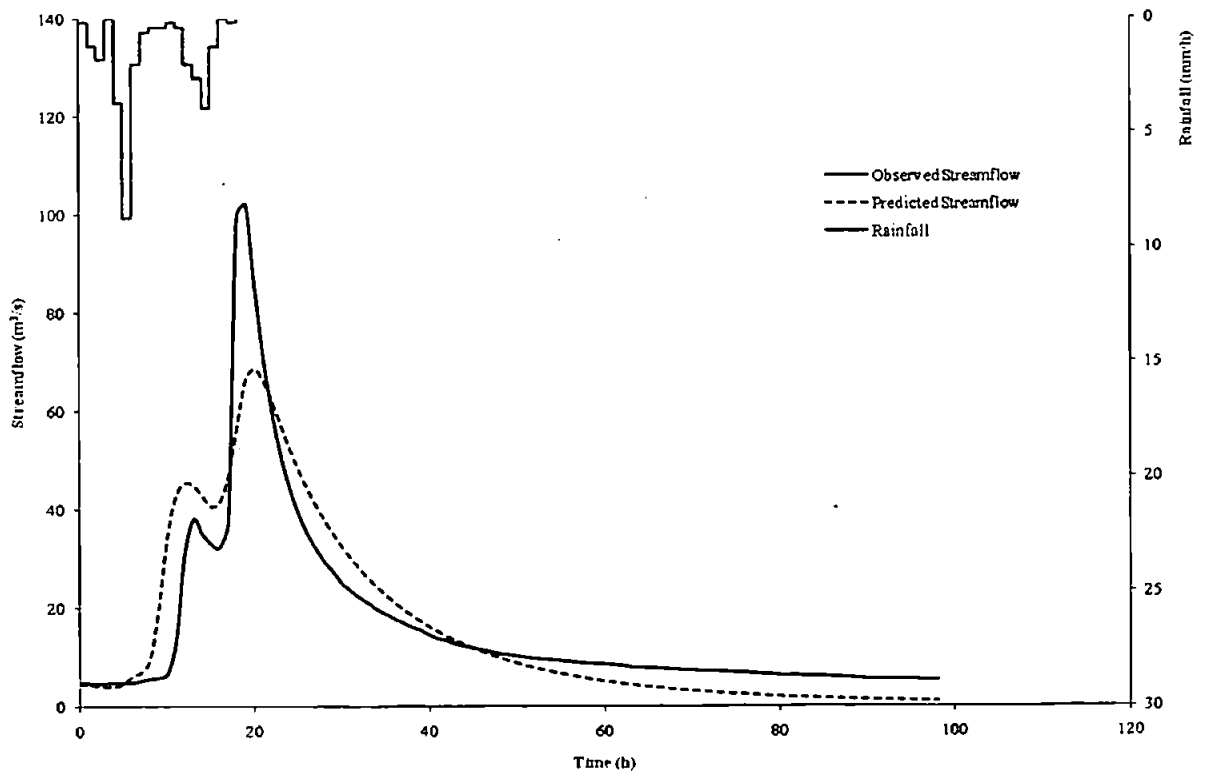

Figure B4 Predicted and observed results for event 04
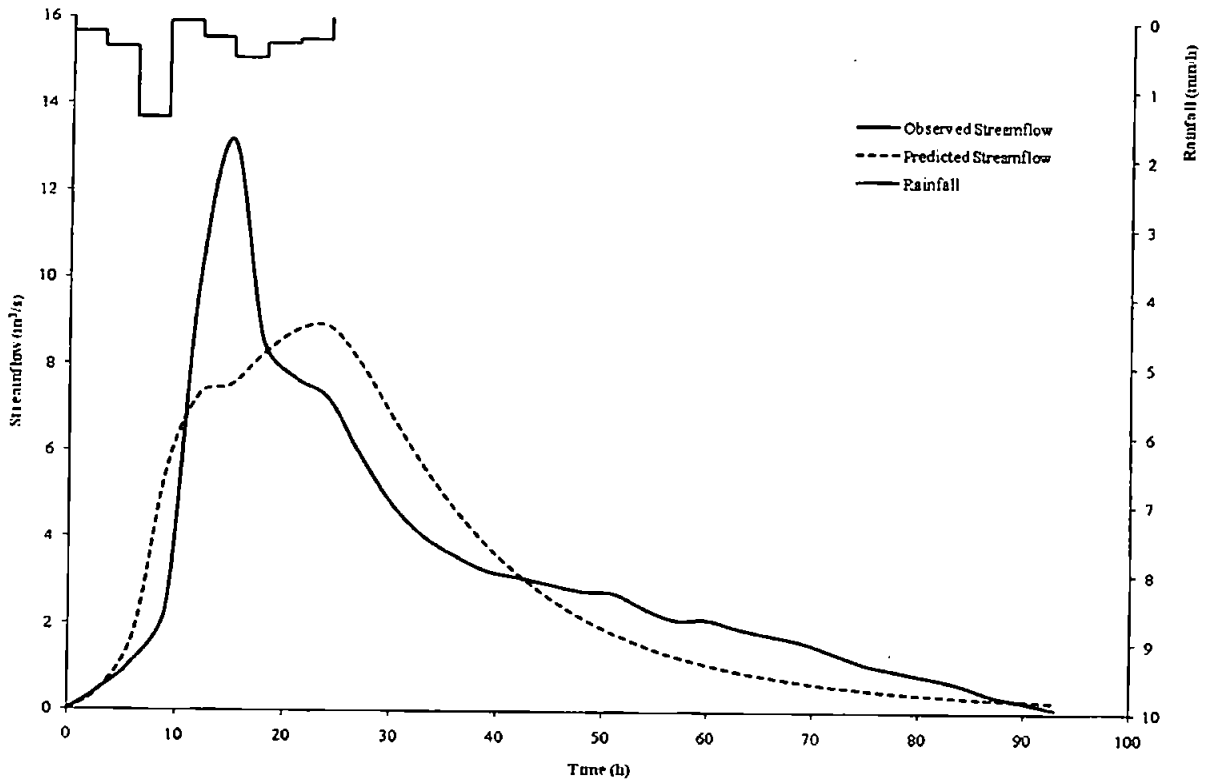
Figure B5 Predicted and observed results for event 05
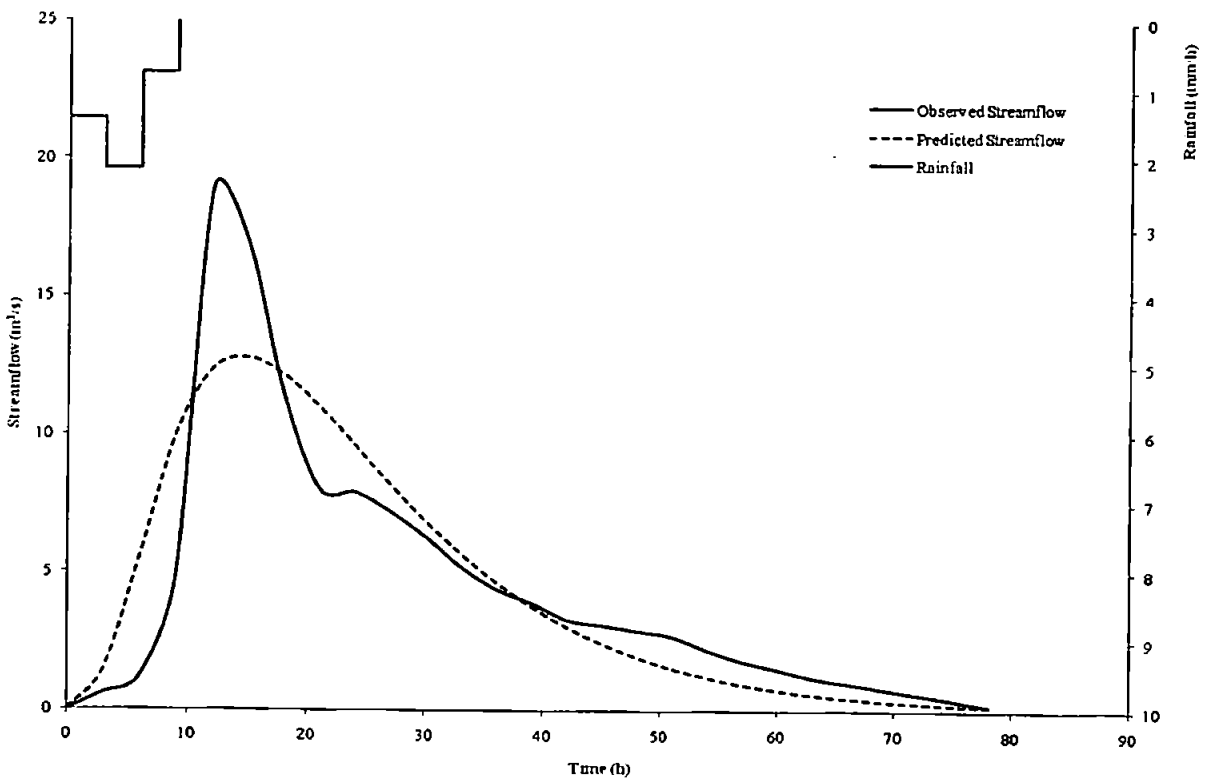
Figure B6 Predicted and observed results for event 06
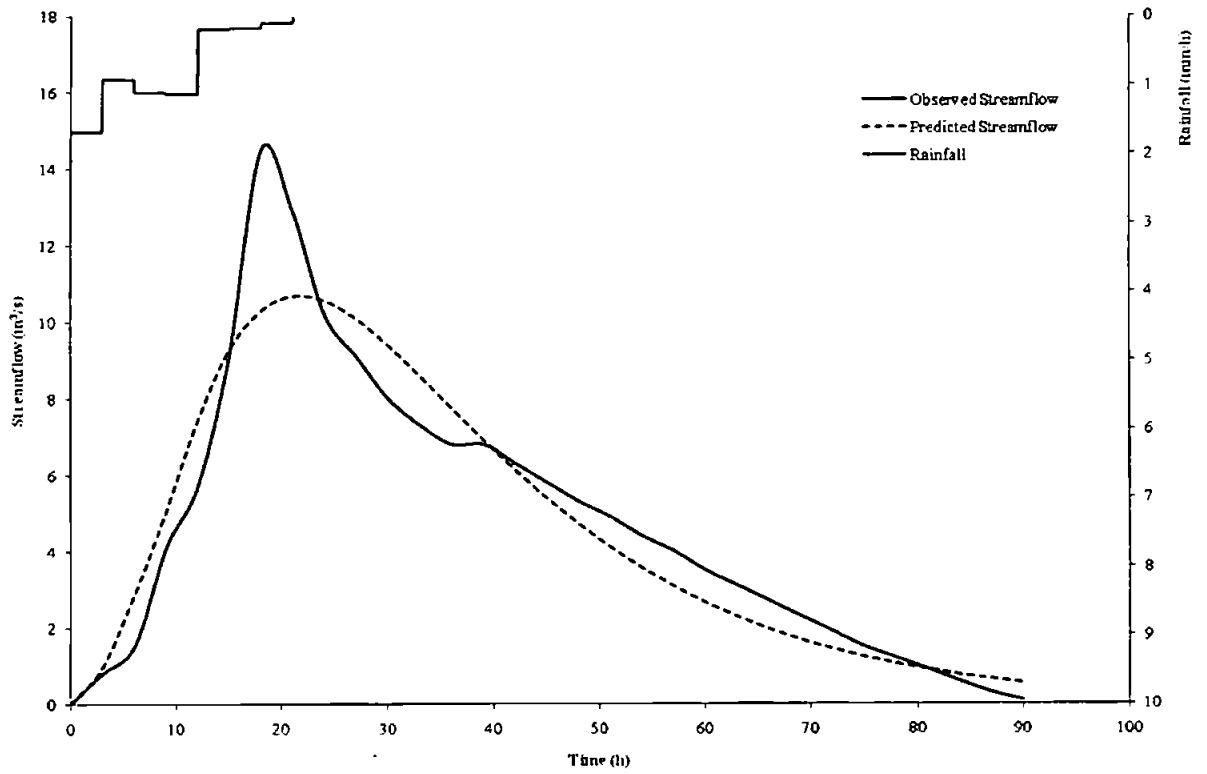
Figure B7 Predicted and observed results for event 07
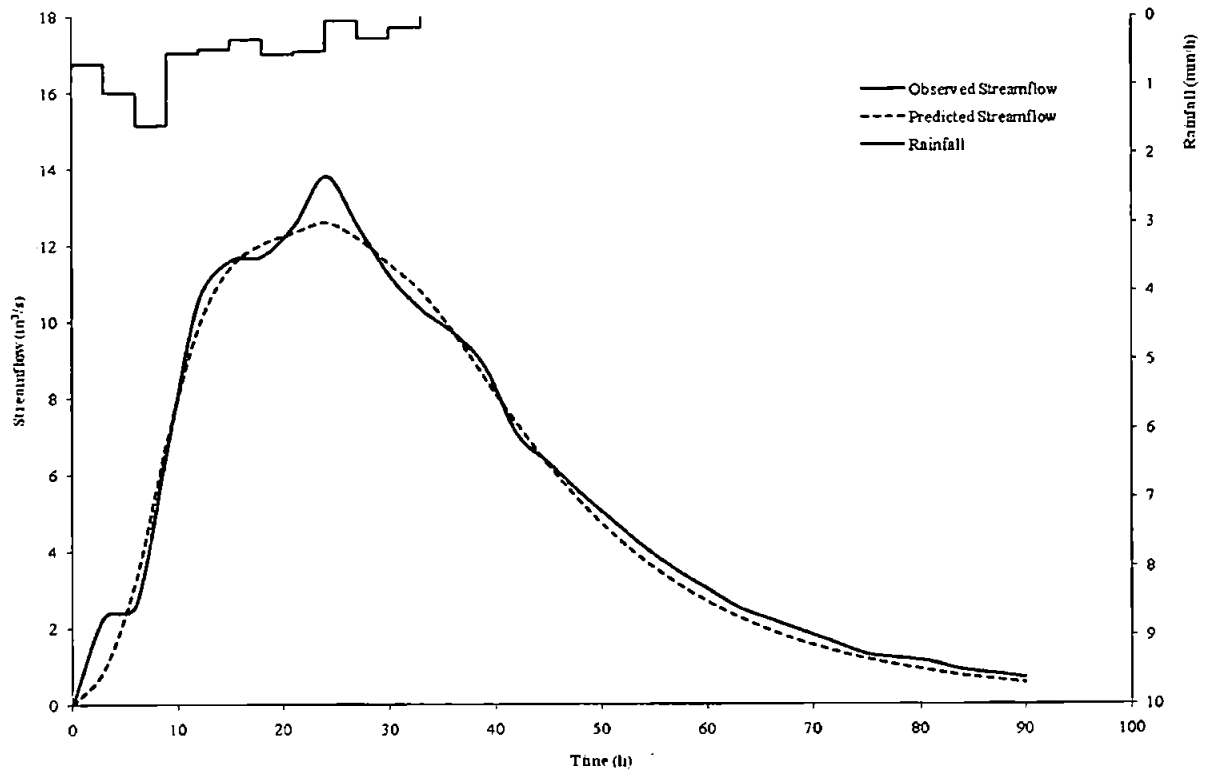
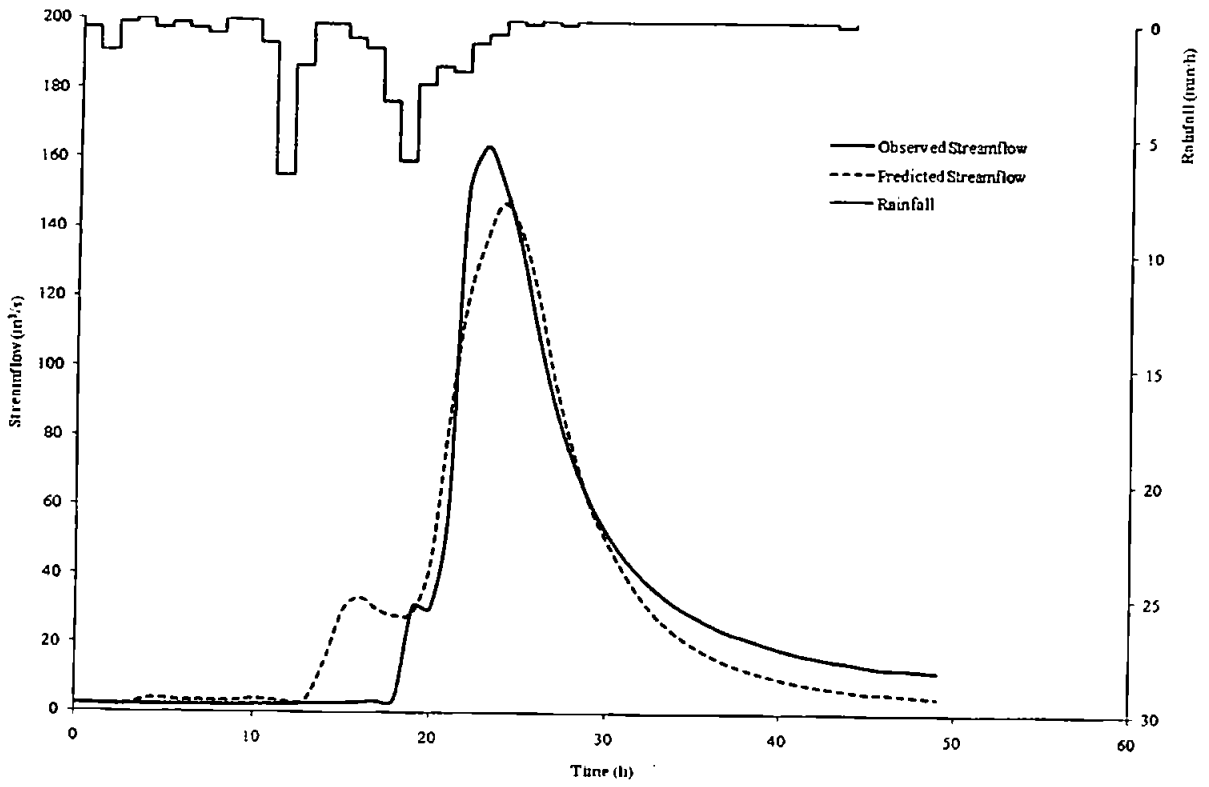

Figure B8 Predicted and observed results for event 08

203
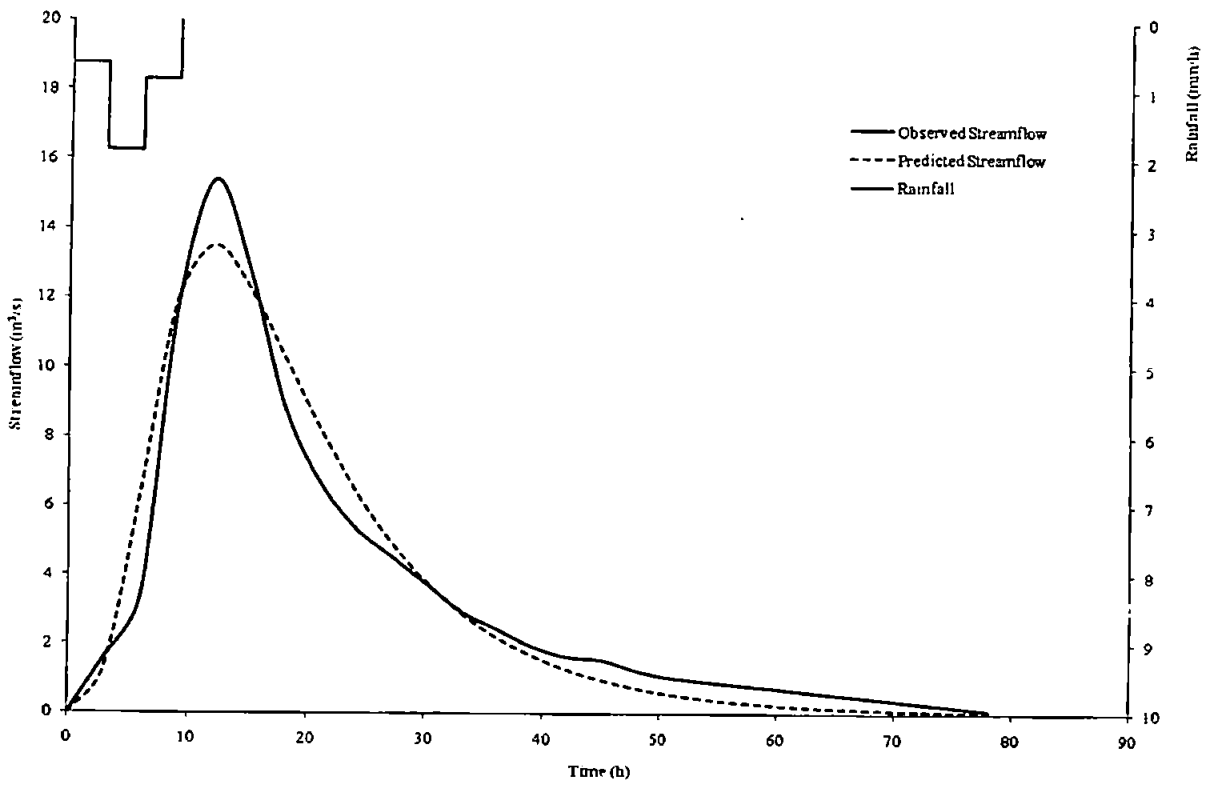
Figure B9 Predicted and observed results for event 09
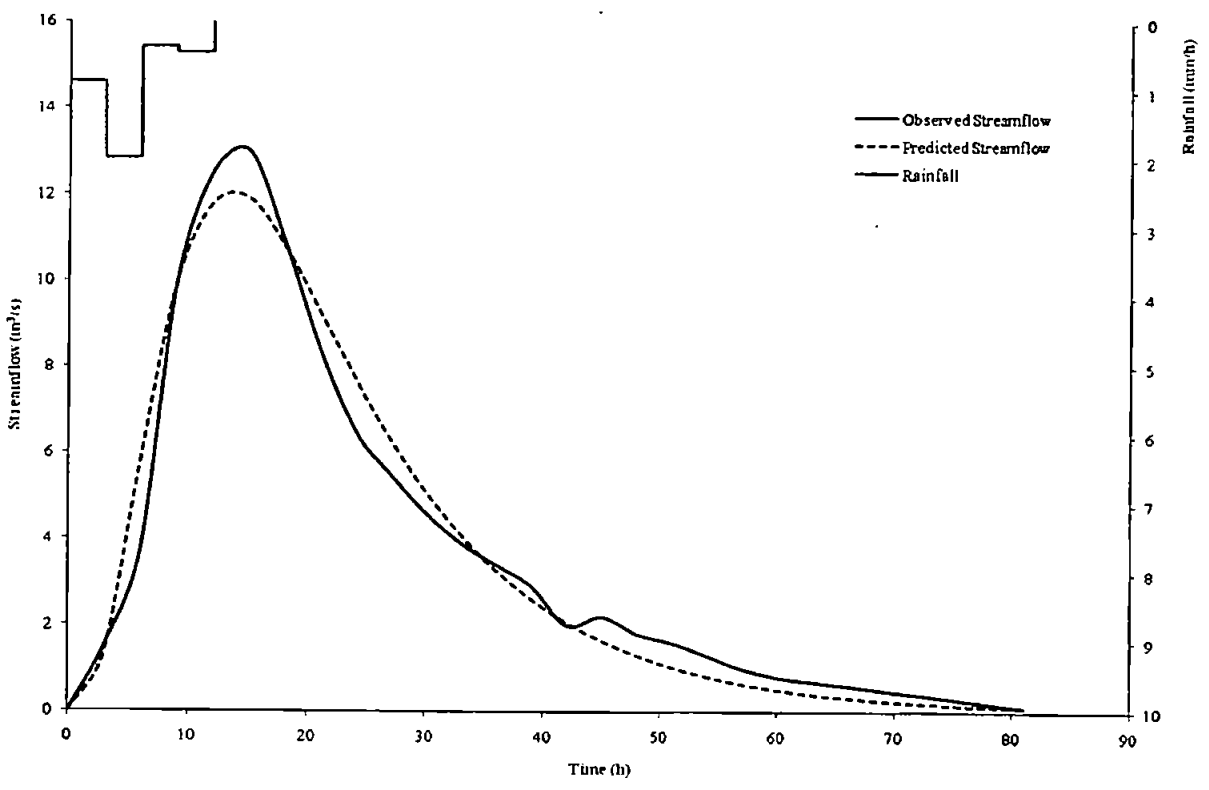
Figure B10 Predicted and observed results for event 10
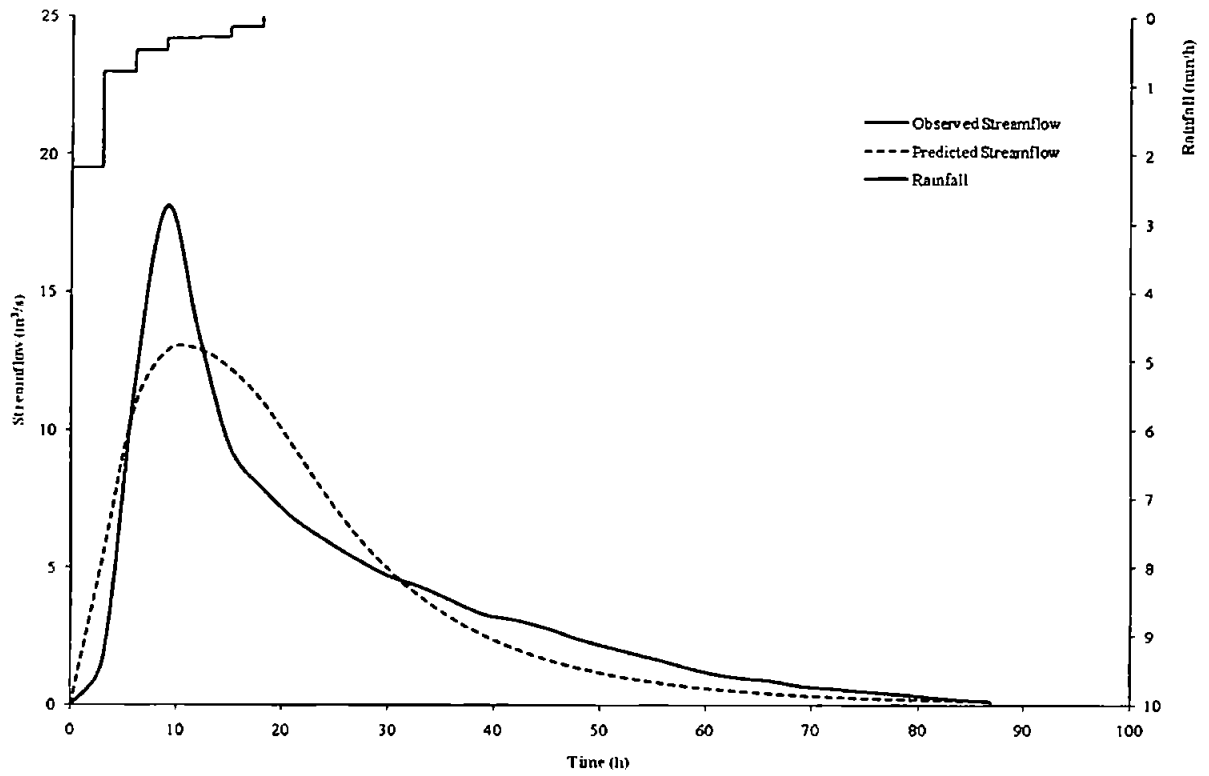
Figure B11 Predicted and observed results for event 11
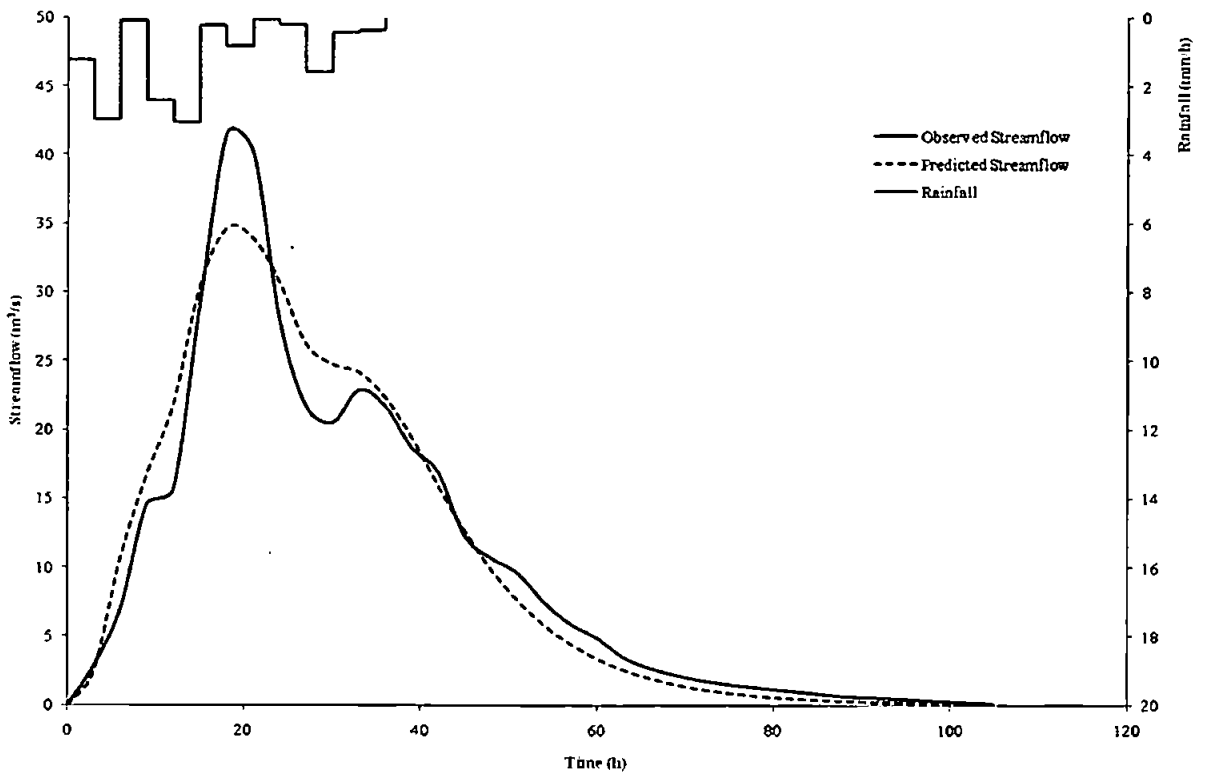
Figure B12 Predicted and observed results for event 12

205
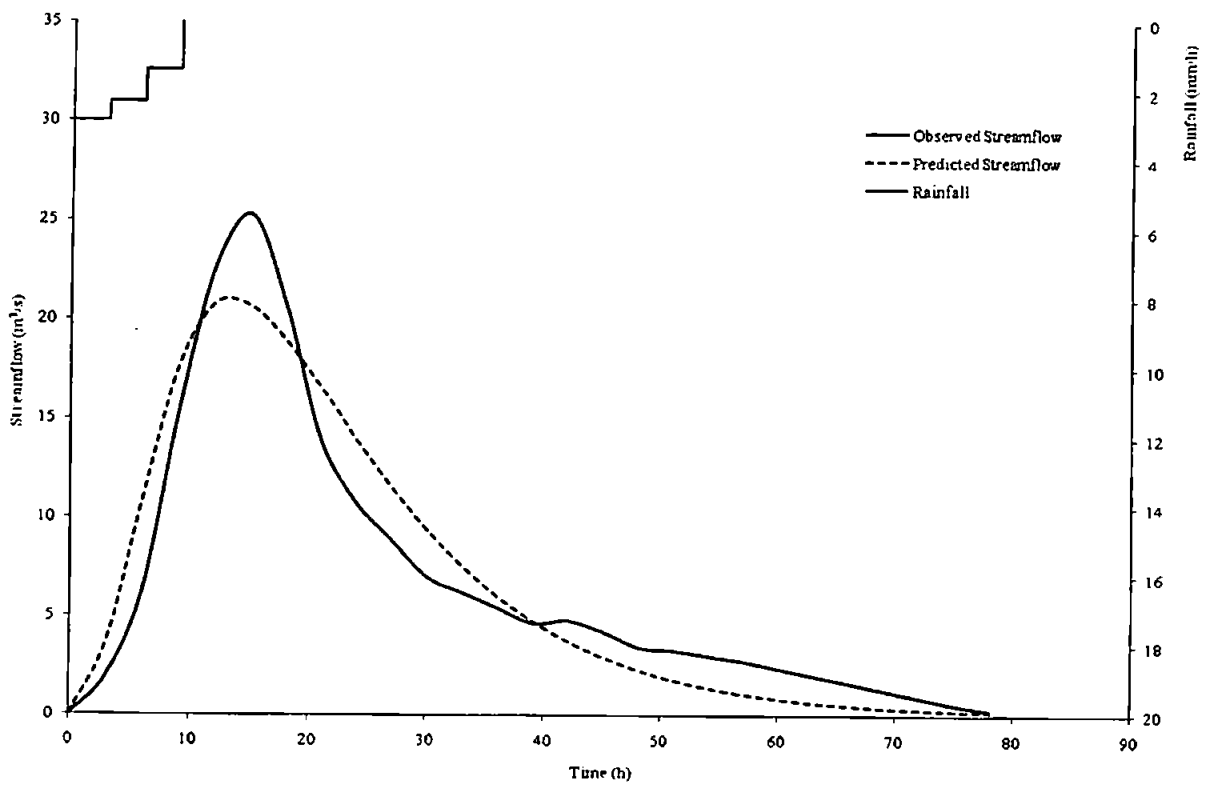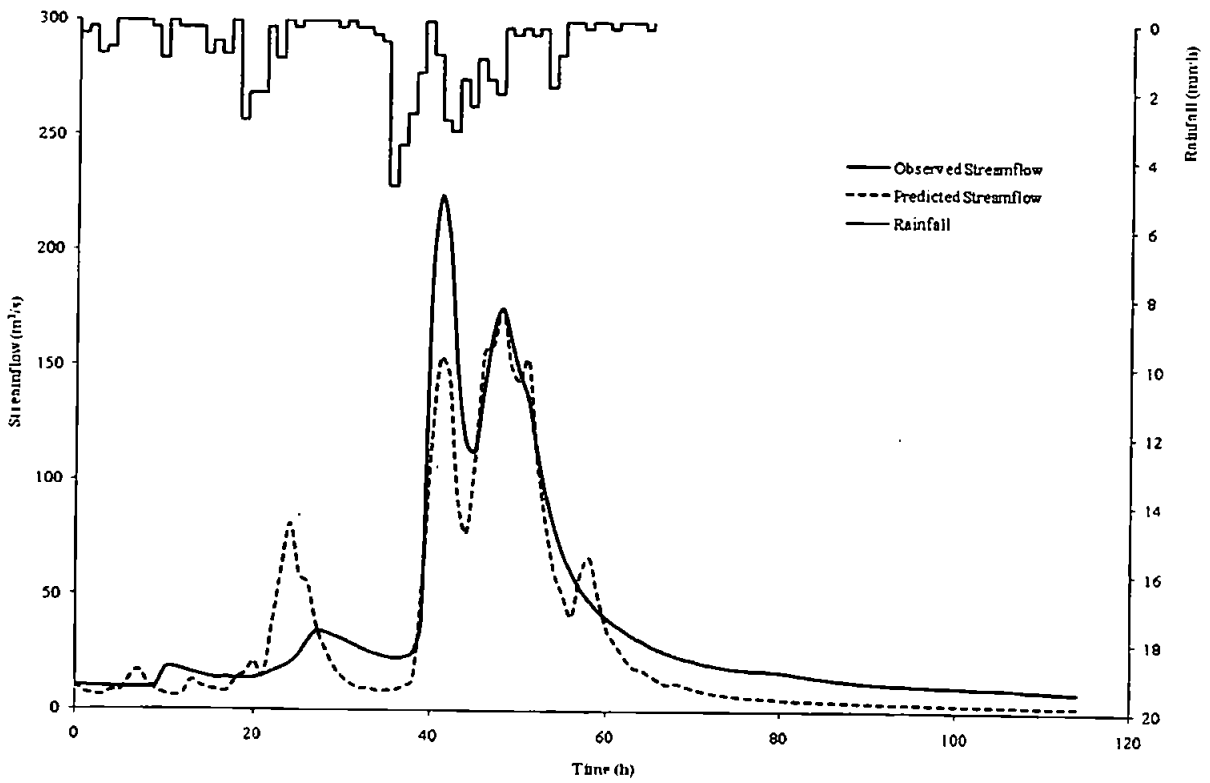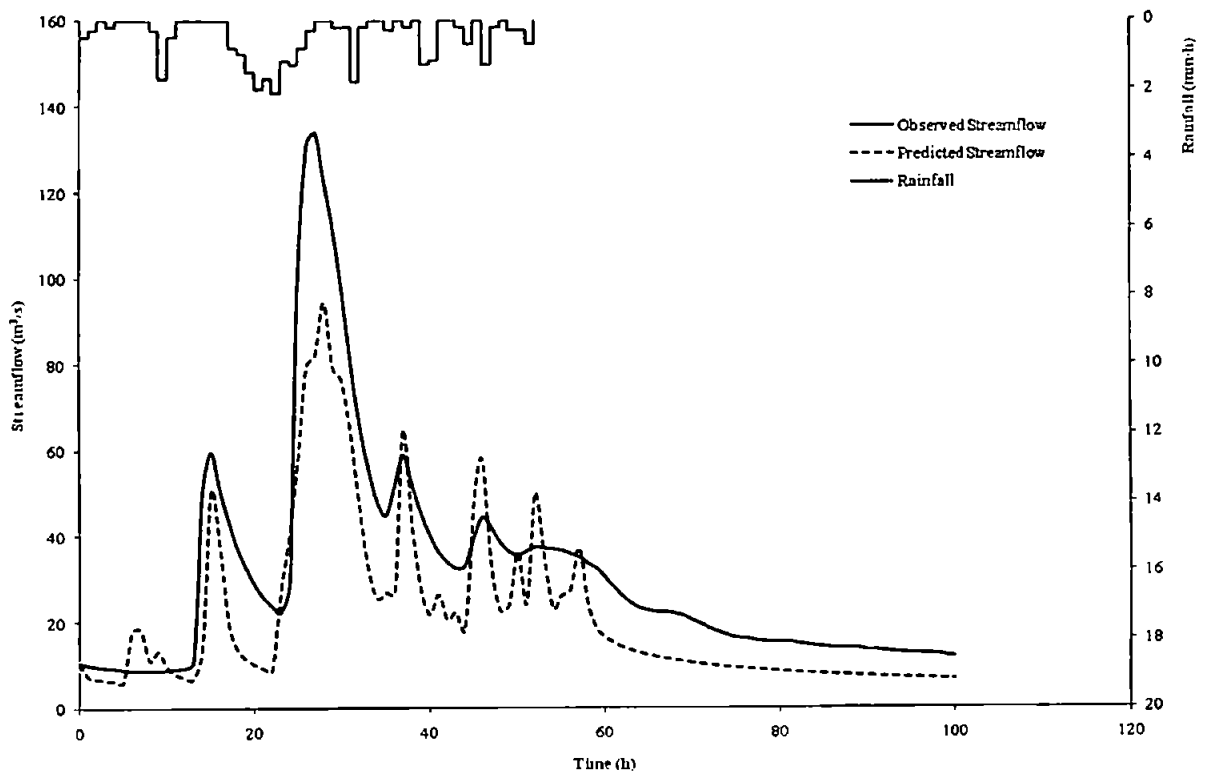
Figure B13 Predicted and observed results for event 13
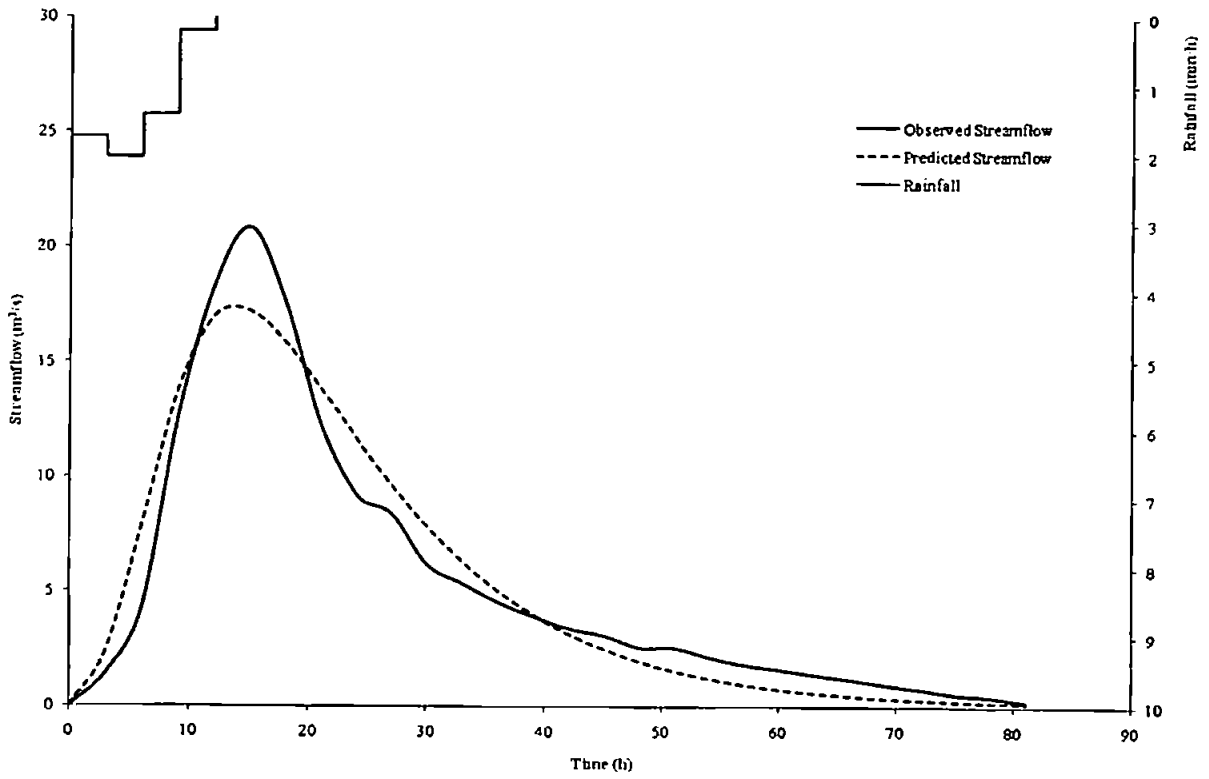
Figure B14 Predicted and observed results for event 14

206
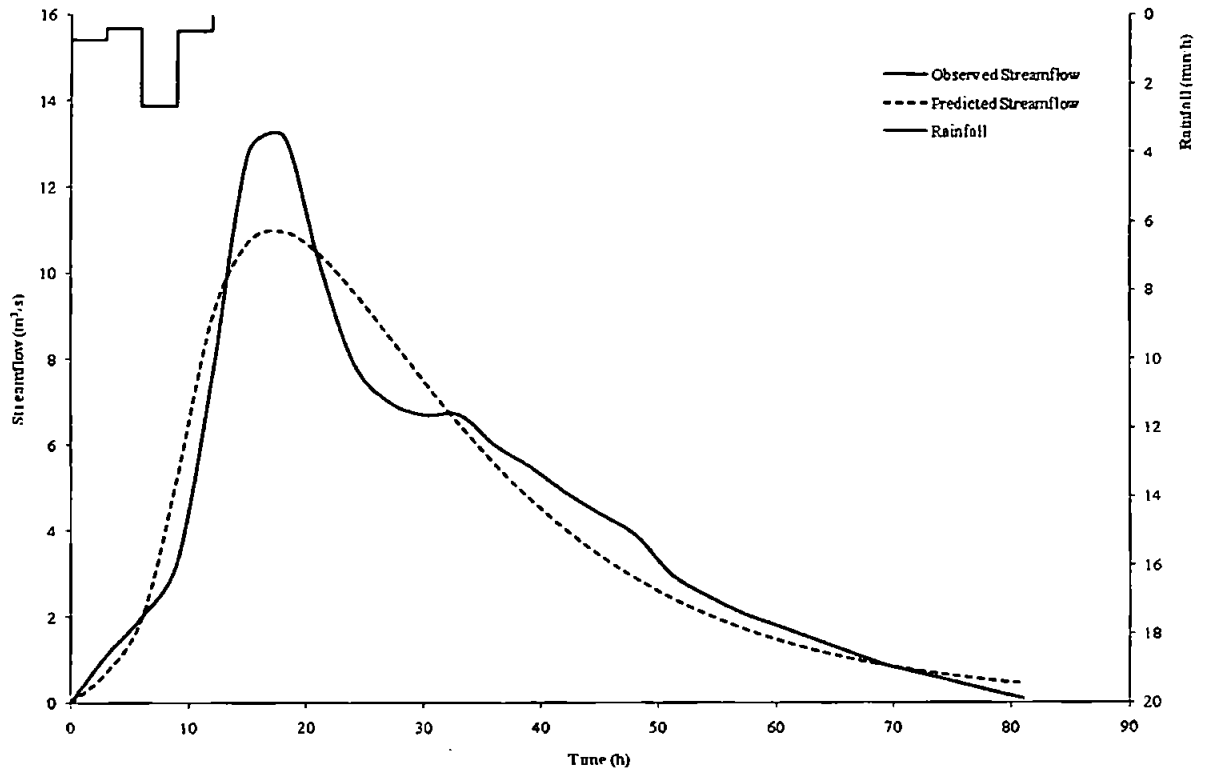
Figure B15 Predicted and observed results for event 15
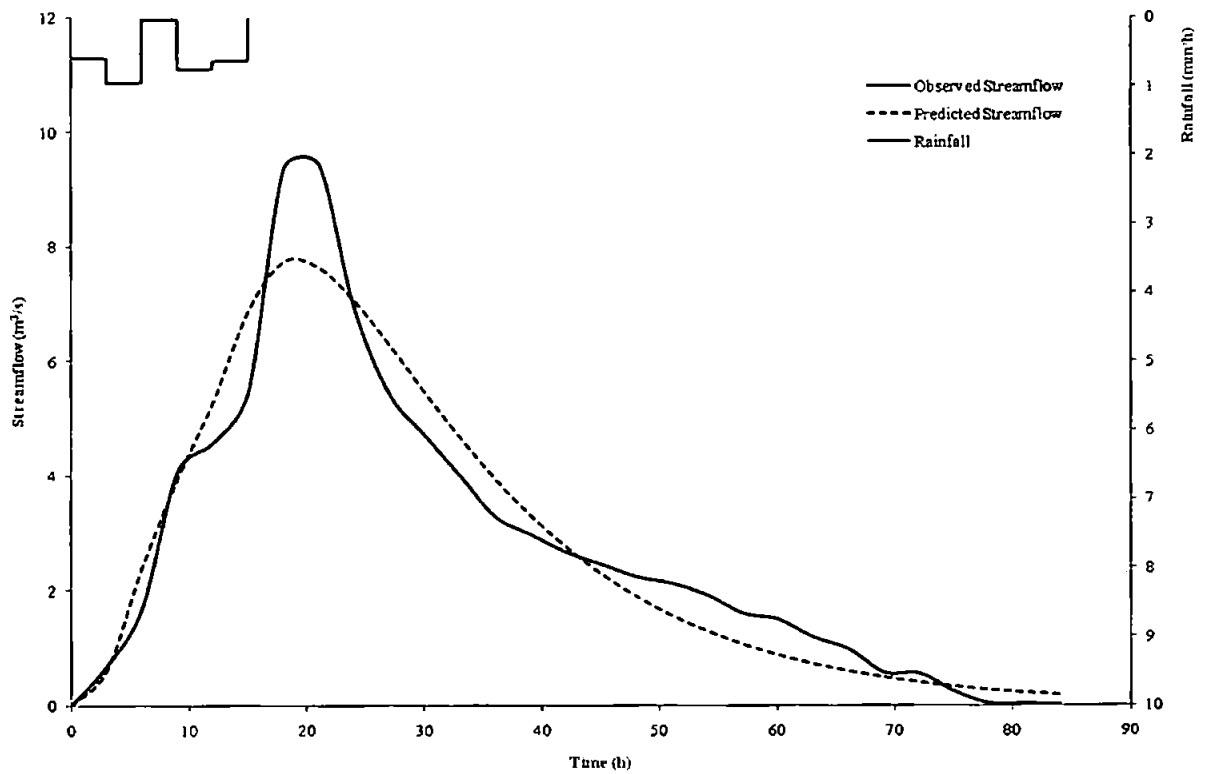
Figure B16 Predicted and observed results for event 16

207
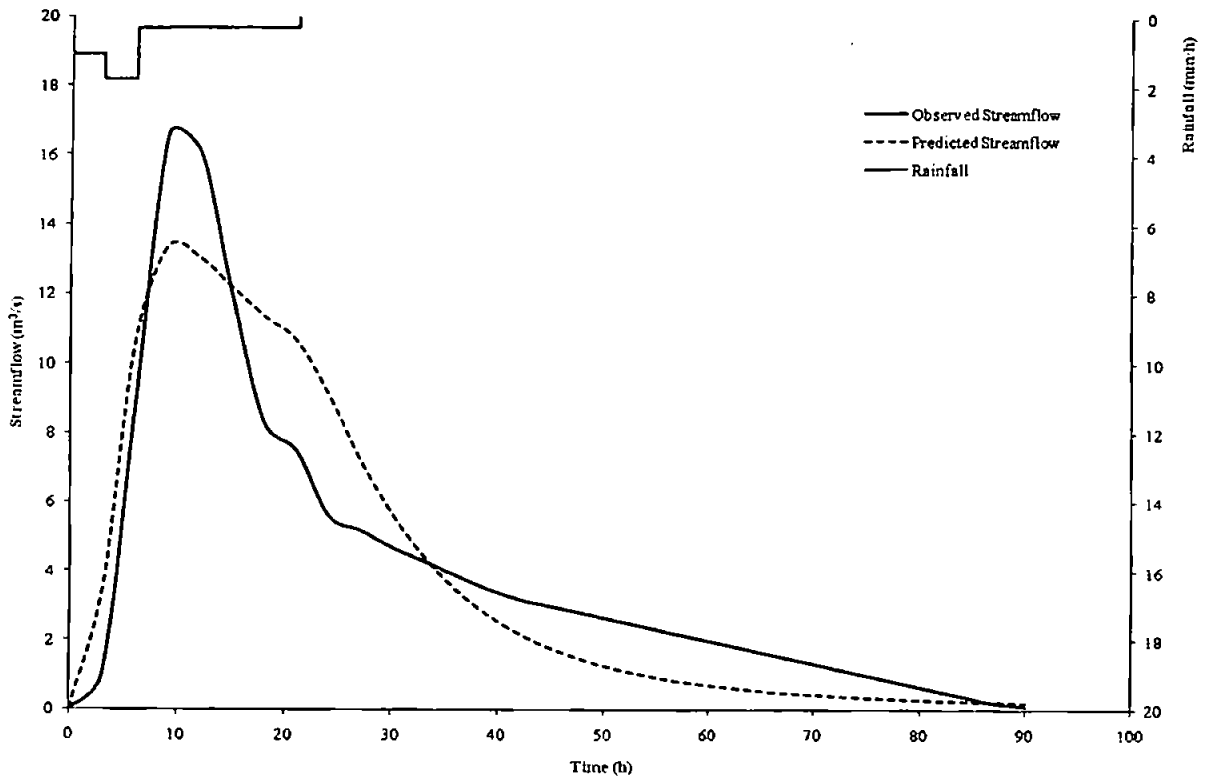
Figure B17 Predicted and observed results for event 17
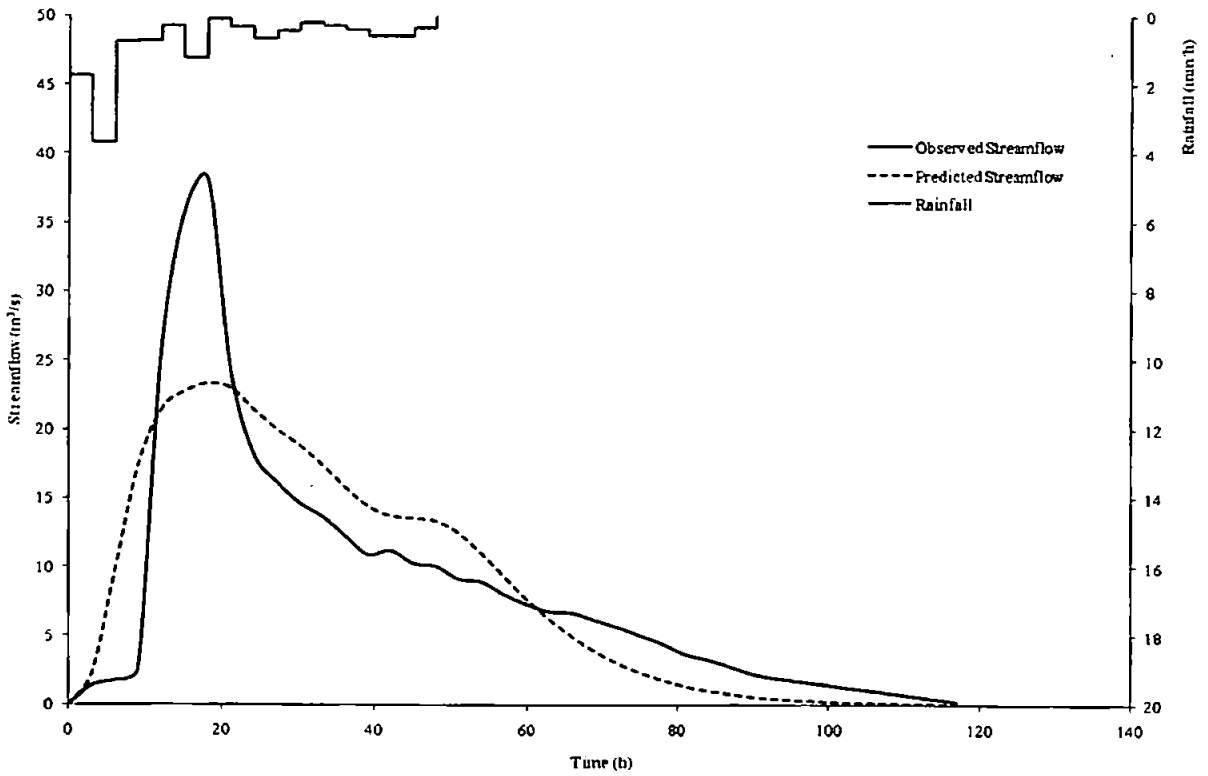
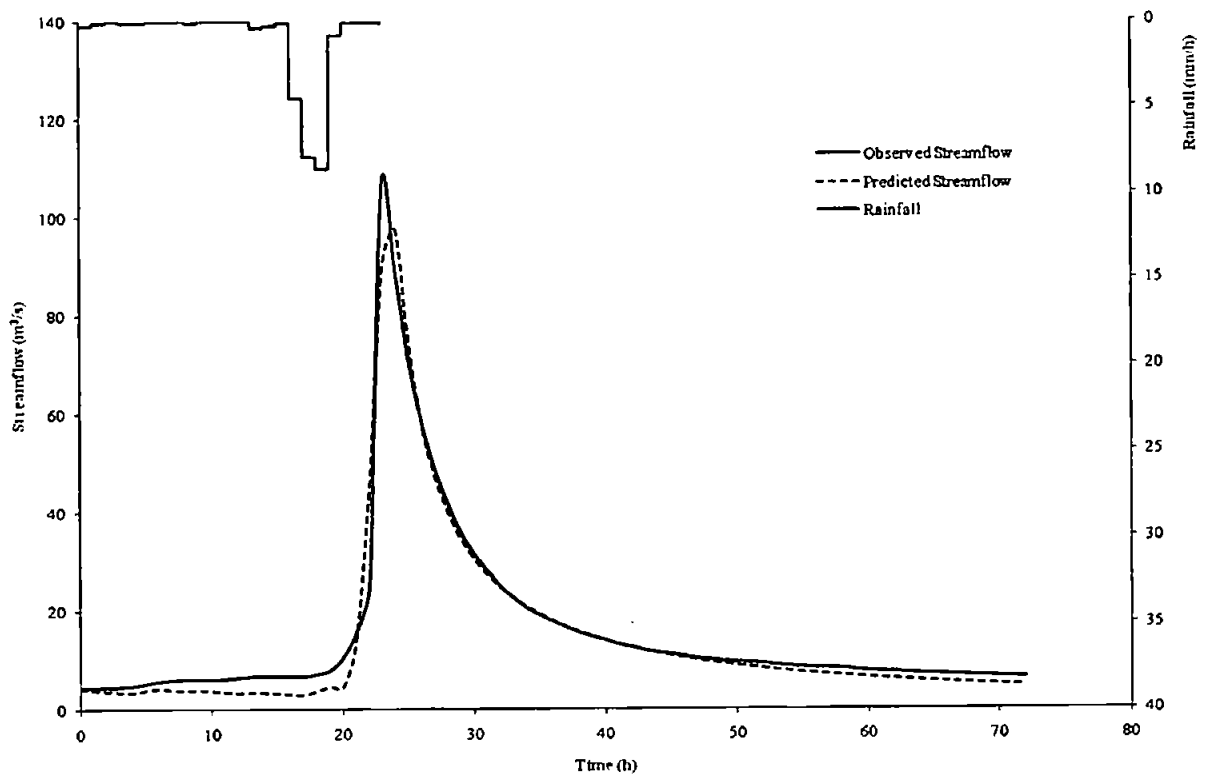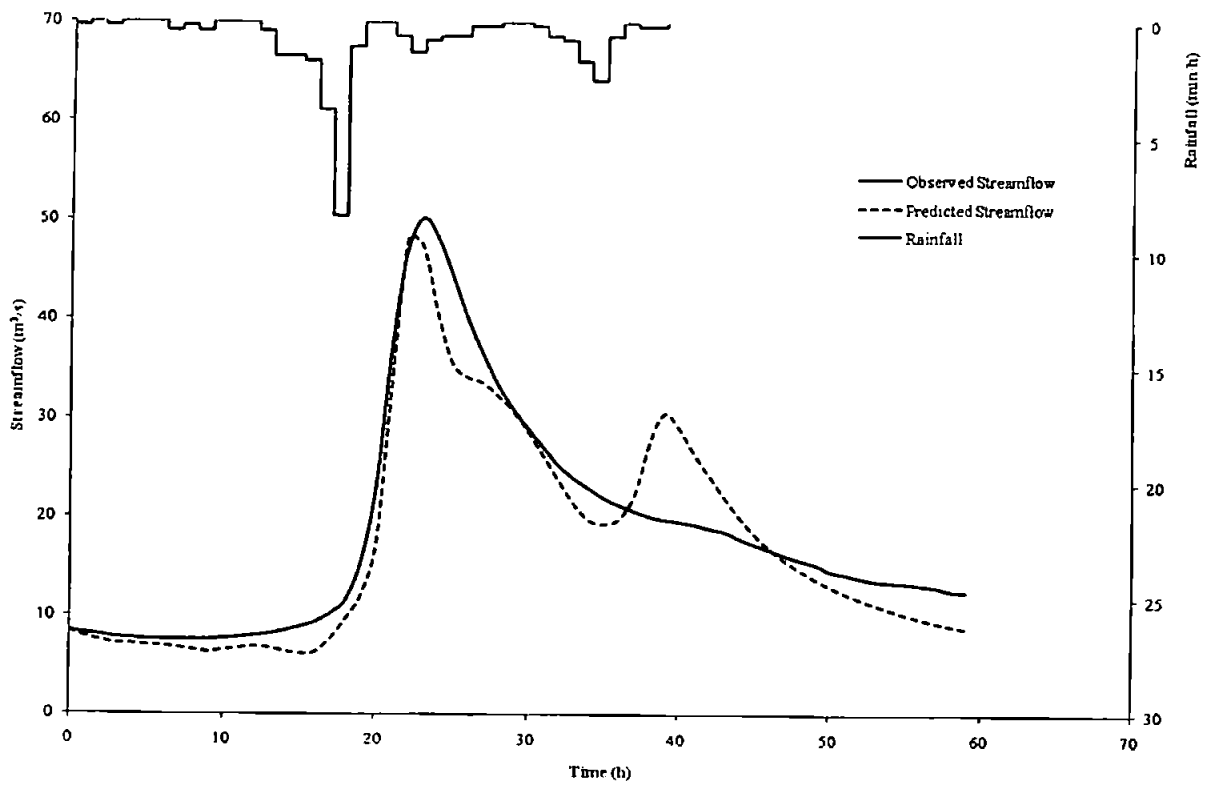
Figure B18 Predicted and observed results for event 18

208
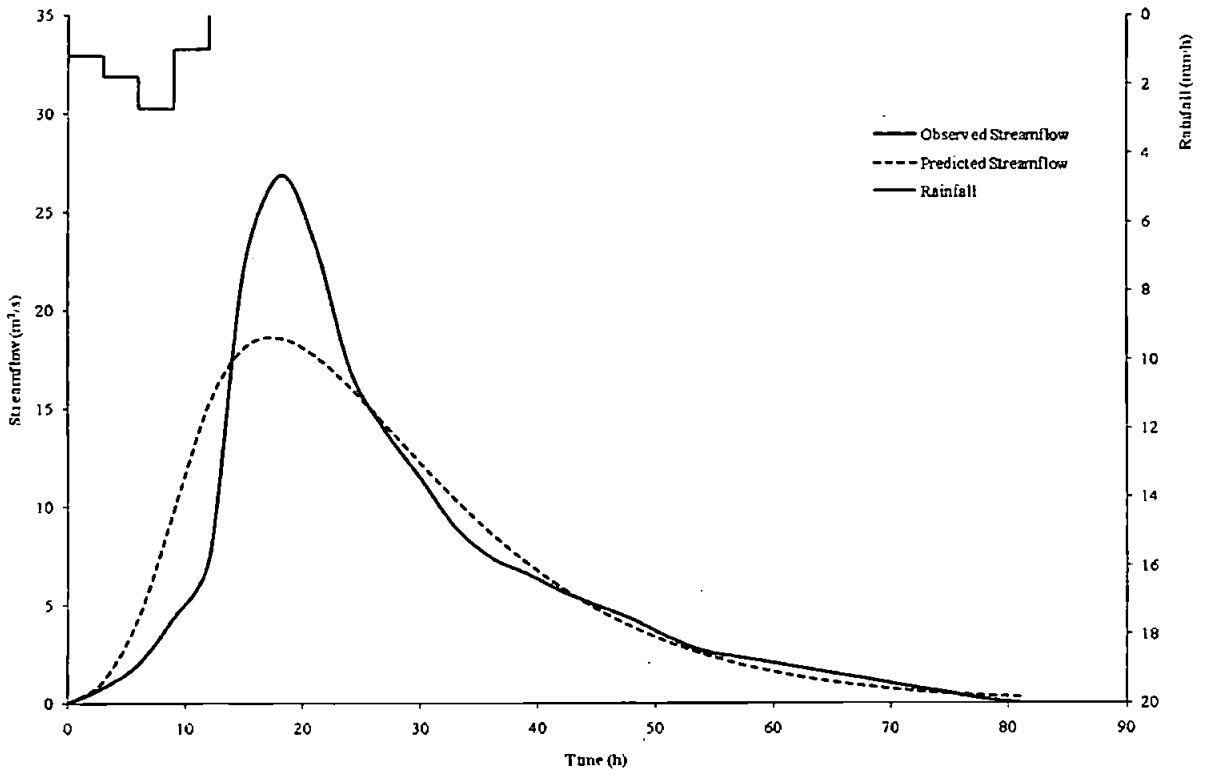
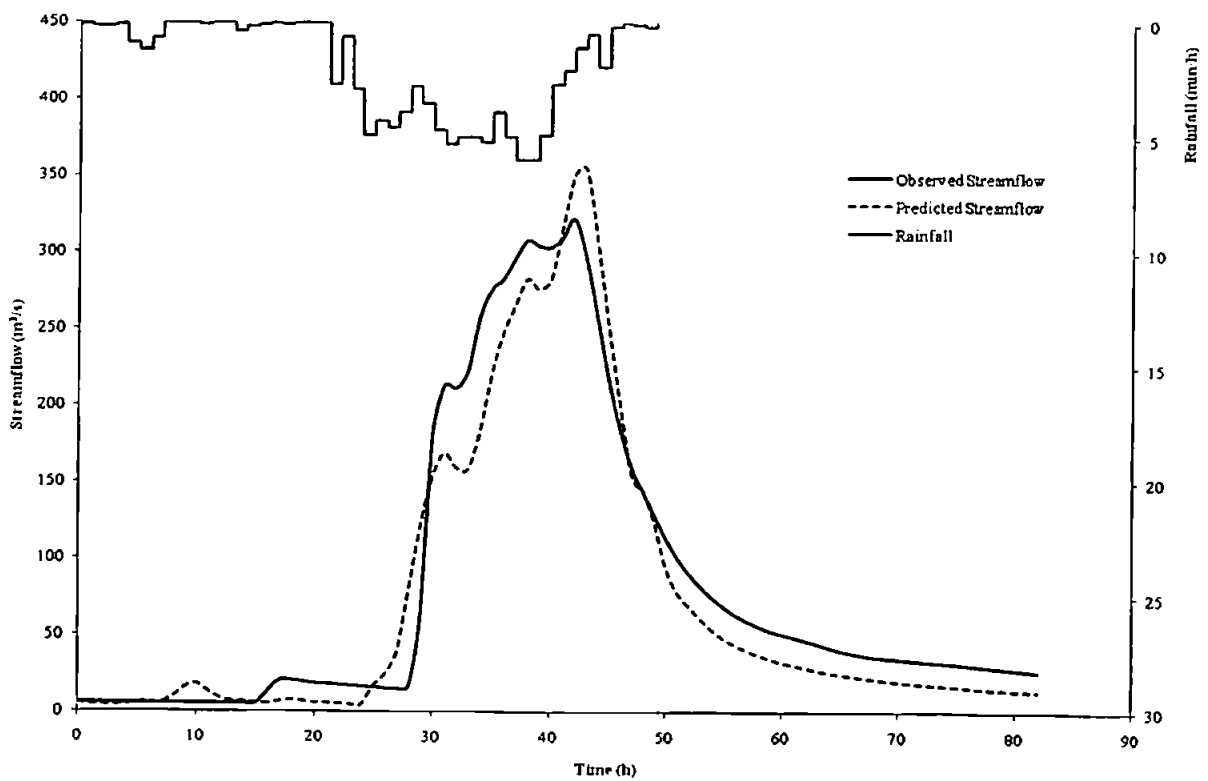**Figure B19 Predicted and observed results for event 19**
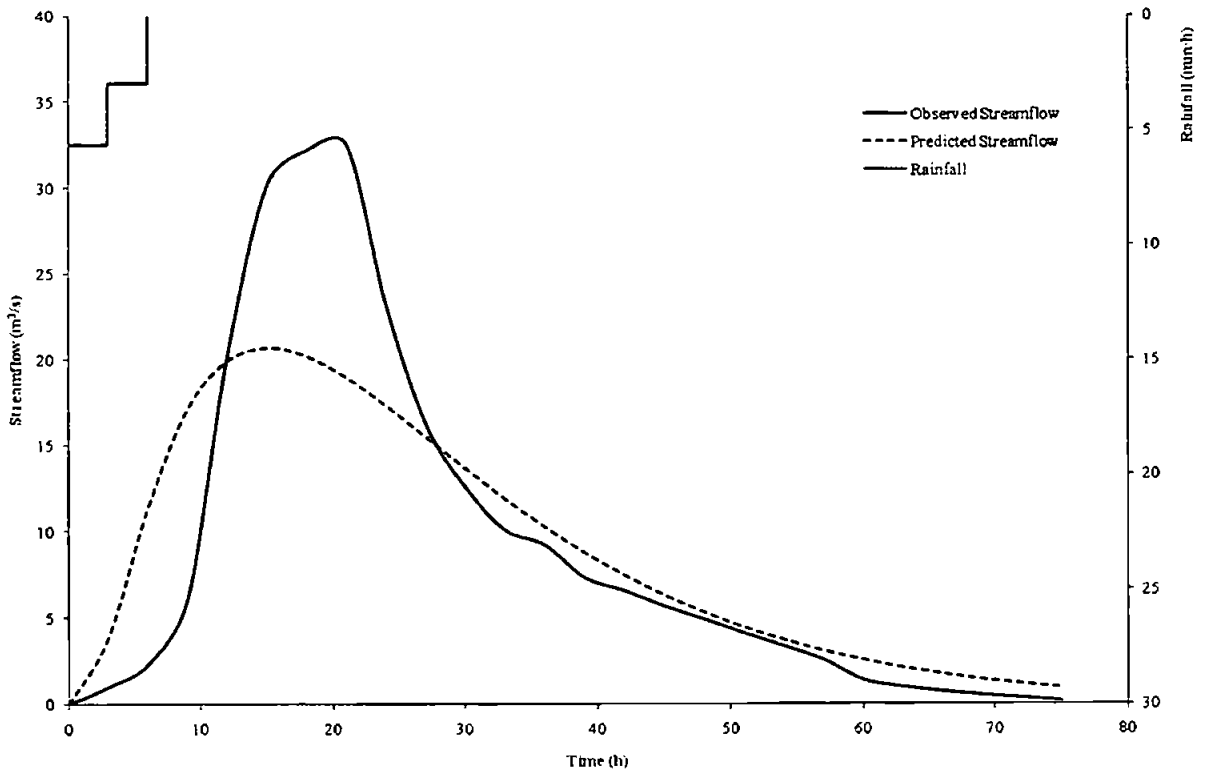
Figure B20 Predicted and observed results for event 20
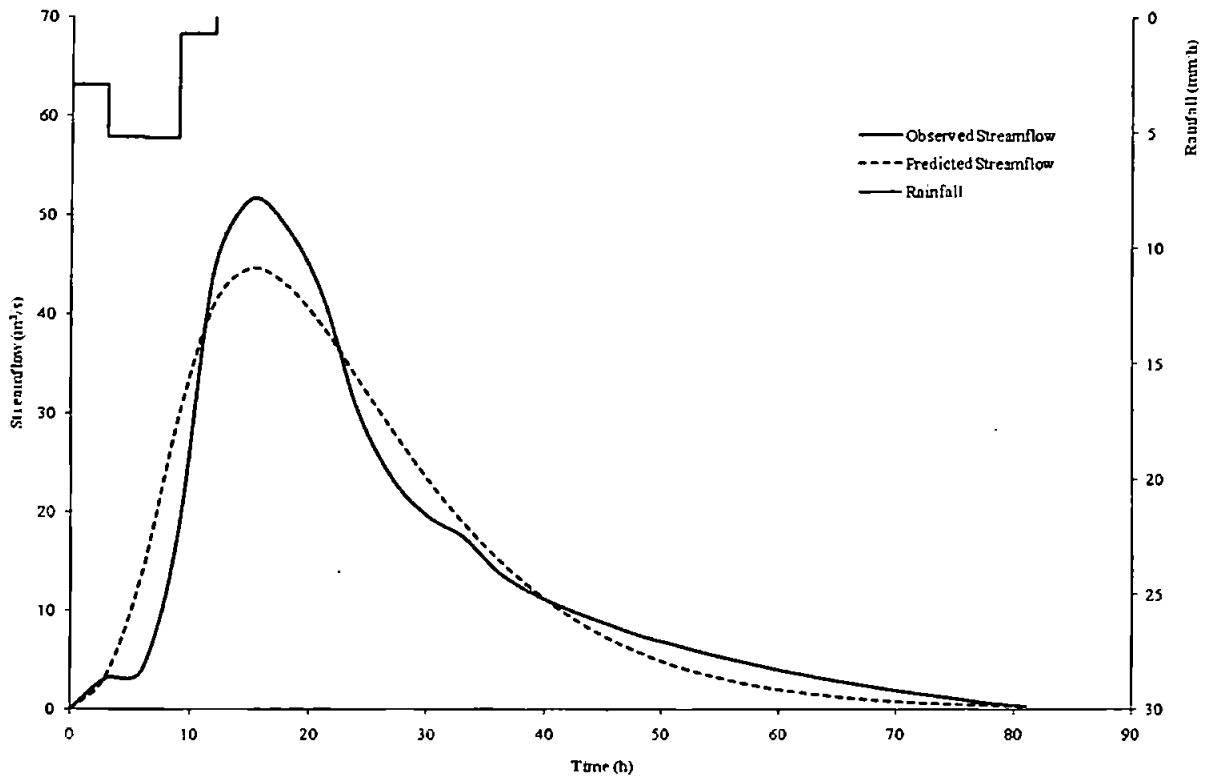
Figure B21 Predicted and observed results for event 21
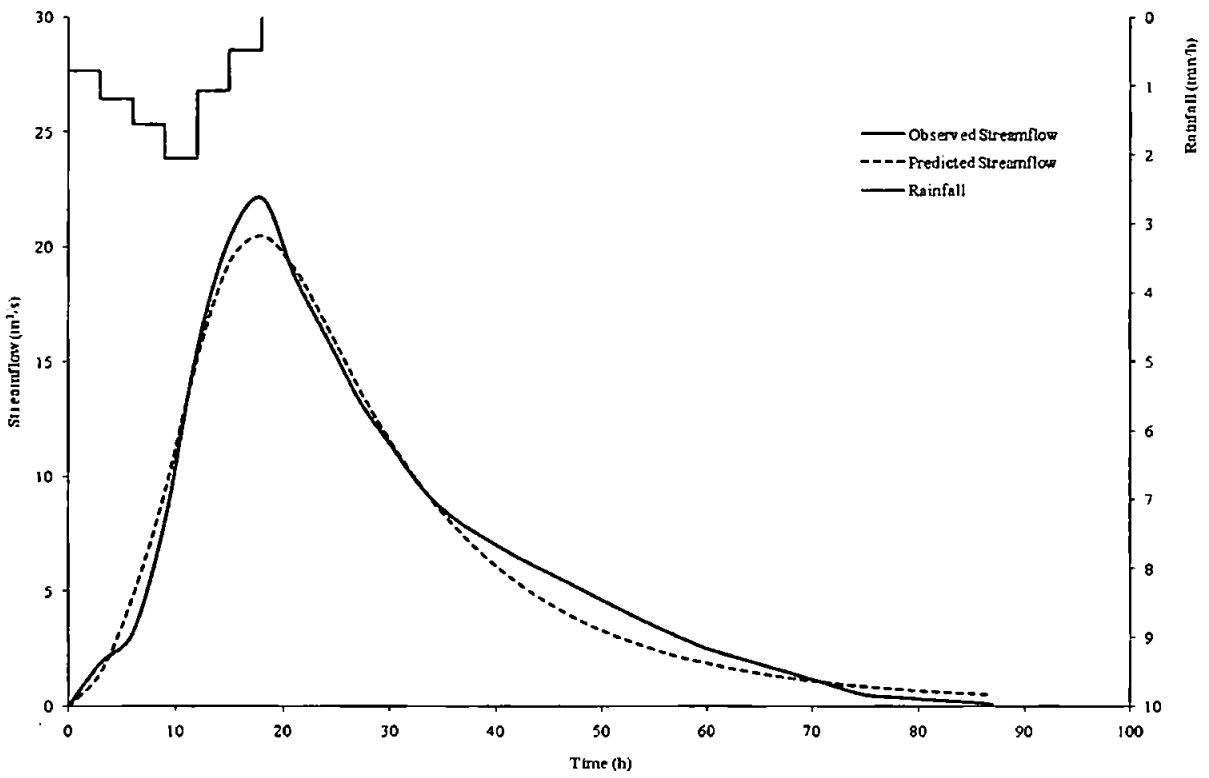
Figure B22 Predicted and observed results for event 22

210

Appendix C: Single Fractional Reservoir Results With Non-Linear Loss Model

The following Figures show the predicted and observed streamflow hydrographs together with the observed event rainfall hyetograph for the selected catchments from the UK Flood Event Archive. The predictions were made with the initialised, single, fractional-order, time-lagged, linear reservoir, subject to a non-linear rainfall filter loss model - equation (5.18).

C1: Catchment 46005 – East Dart River at Bellever
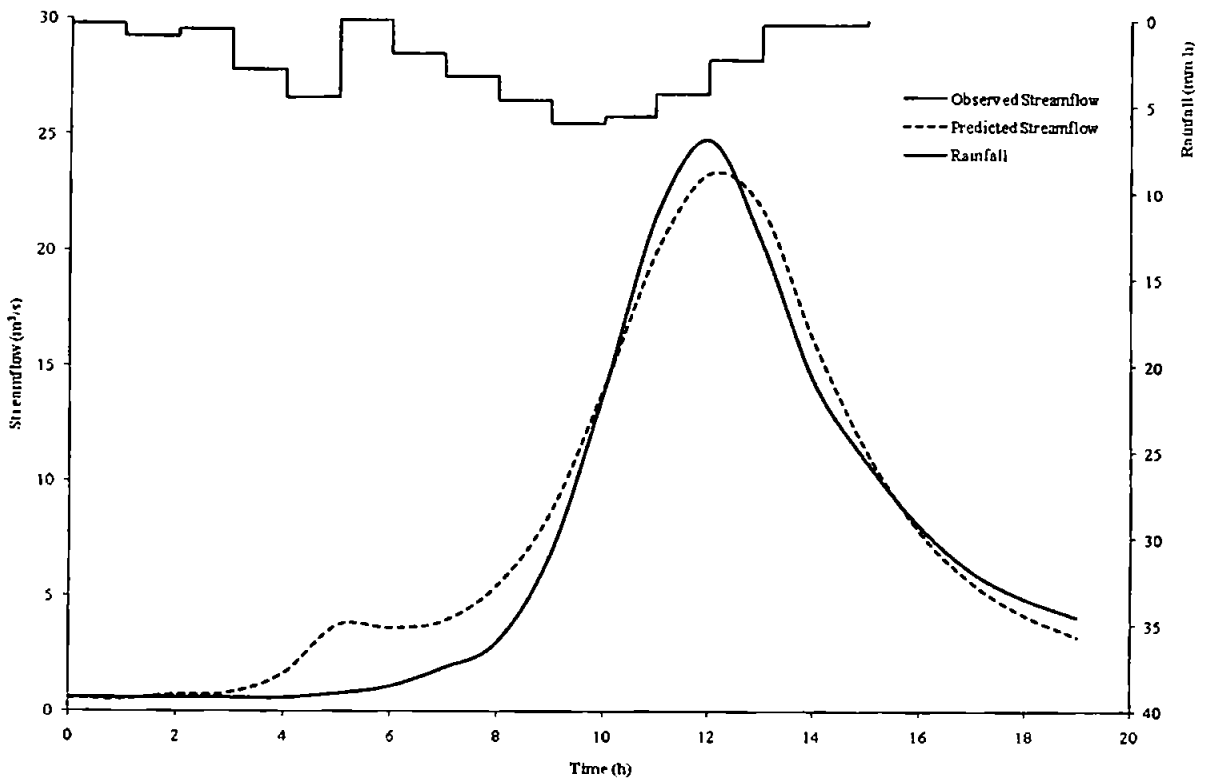
Figure C1.1 Predicted and observed results for event 1287
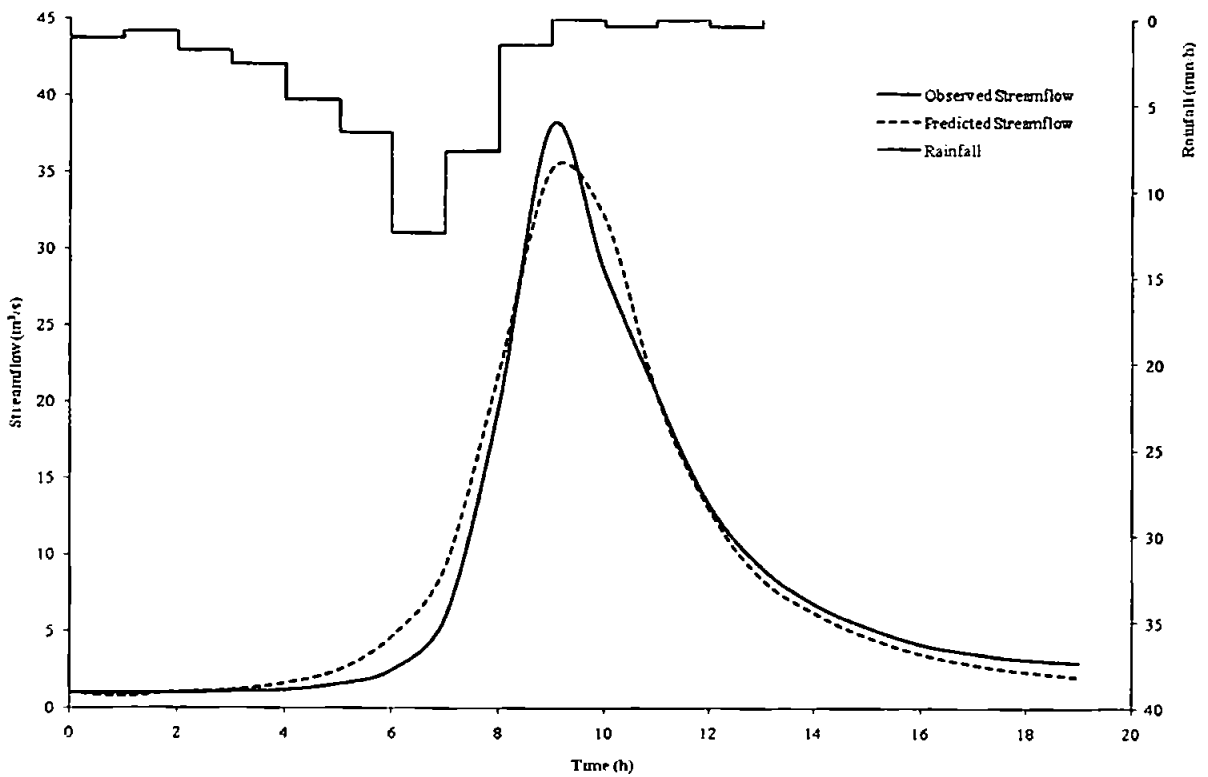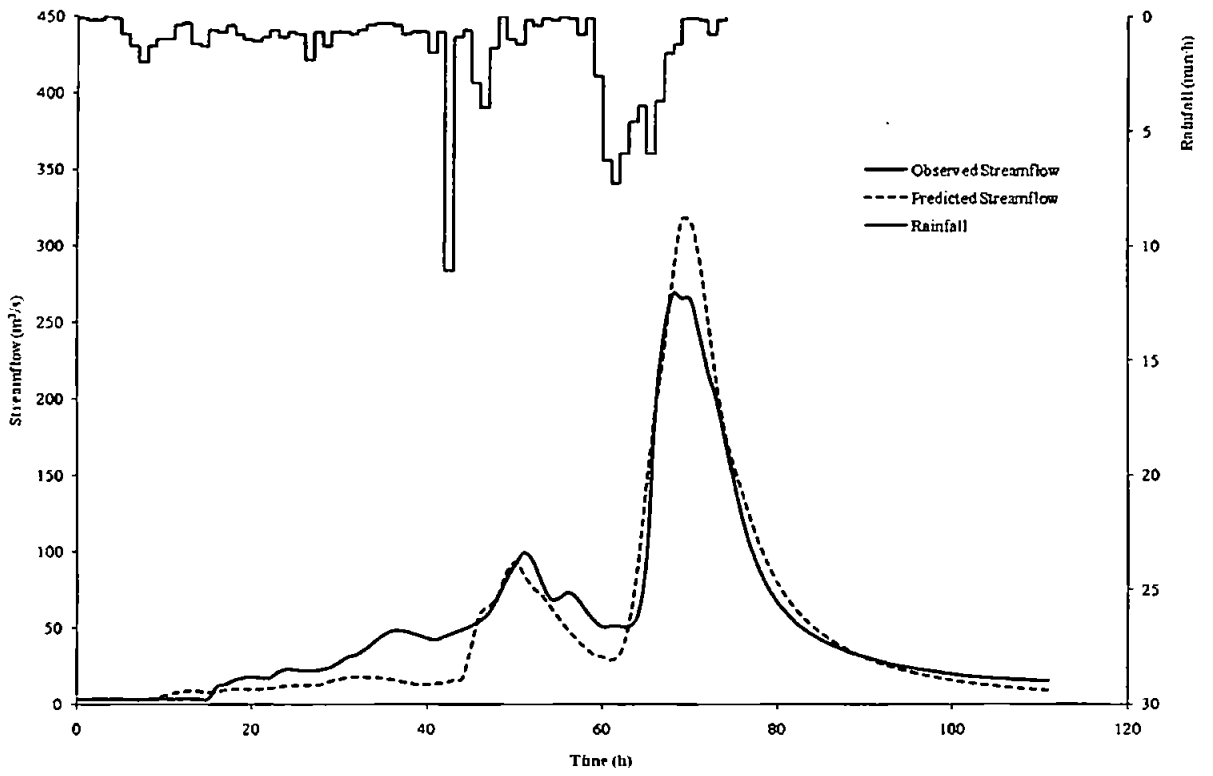

Figure C1.2 Predicted and observed results for event 1289
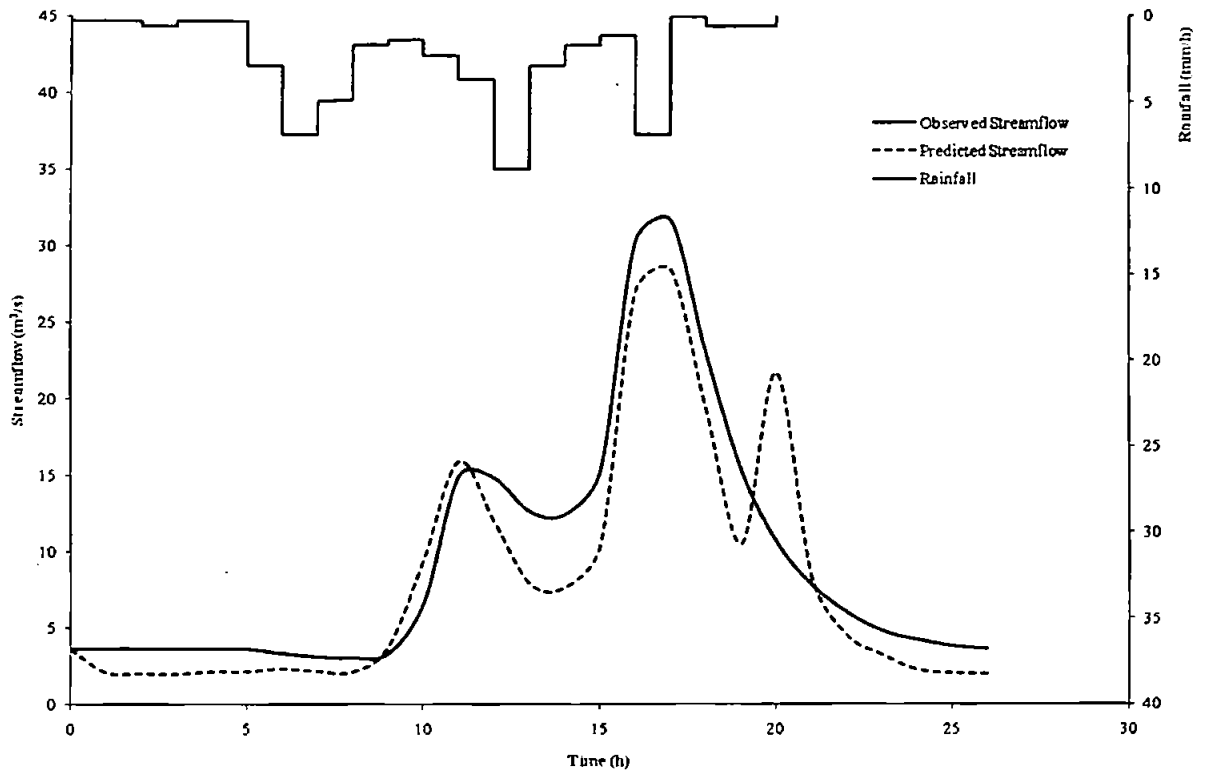
Figure C1.3 Predicted and observed results for event 1292
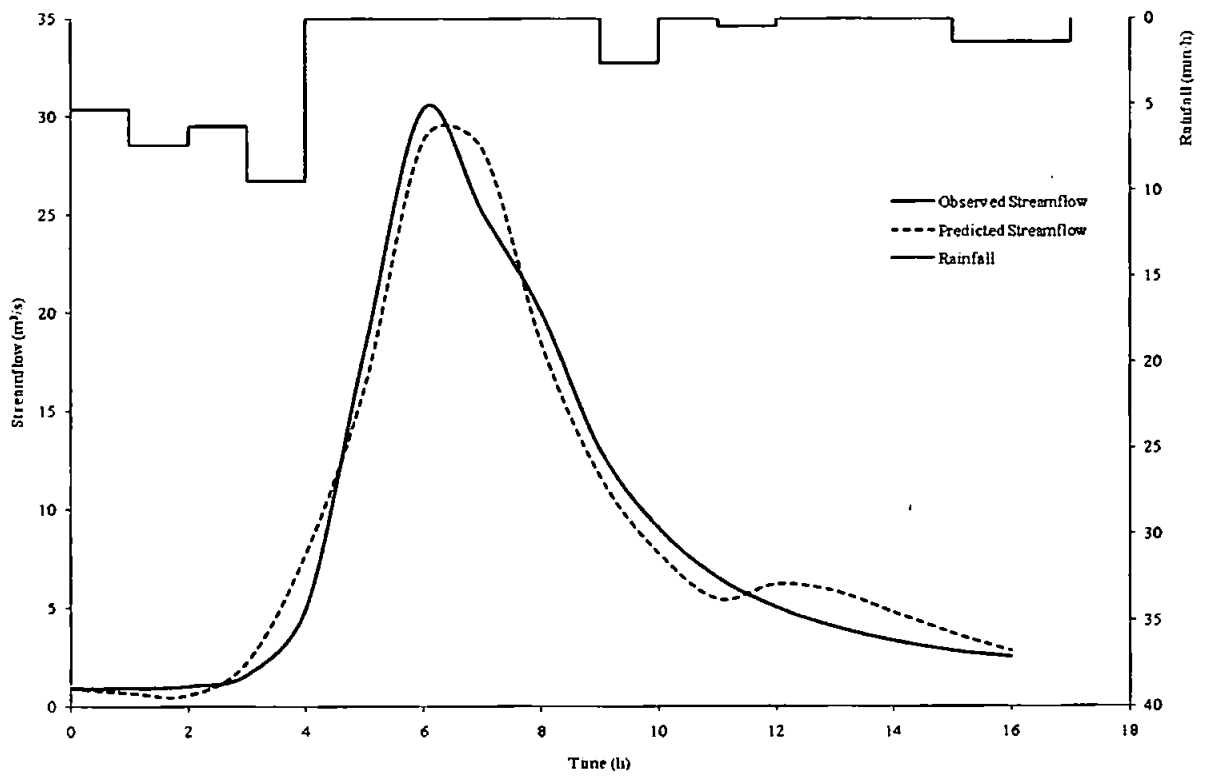
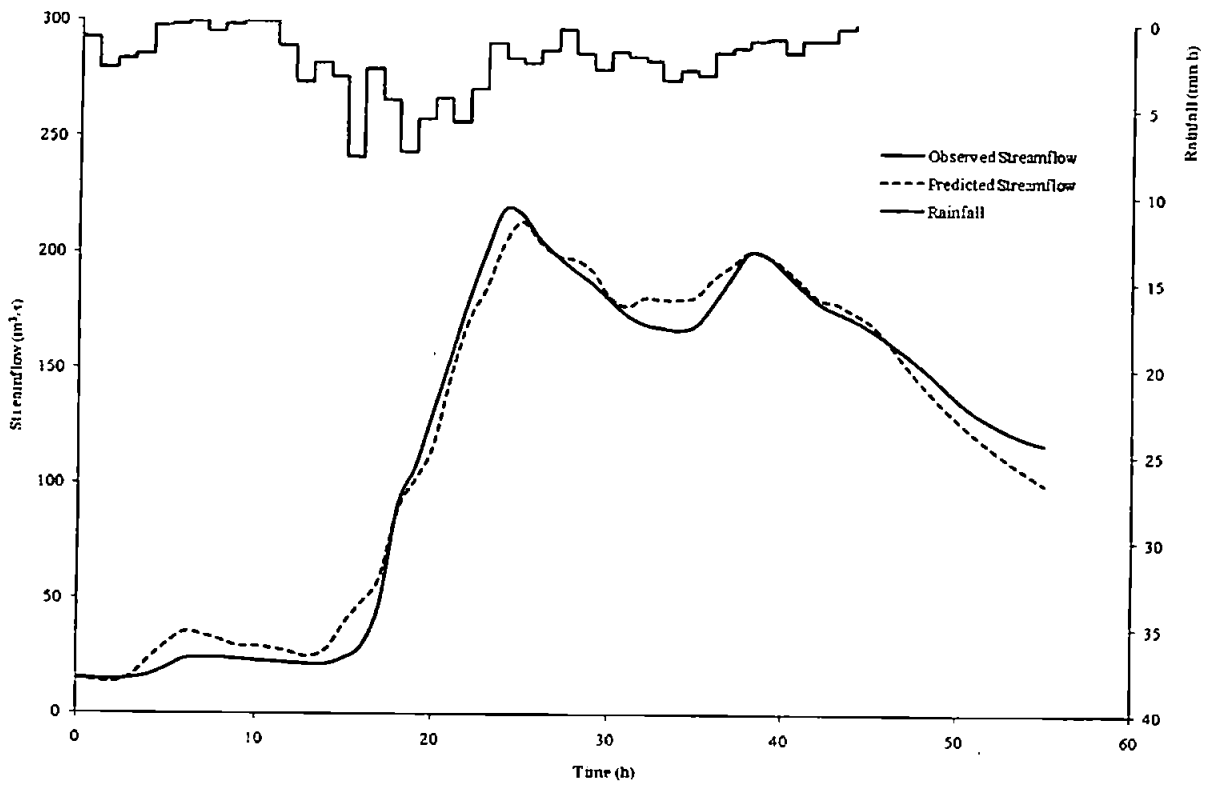**Figure C1.4 Predicted and observed results for event 1297**

213
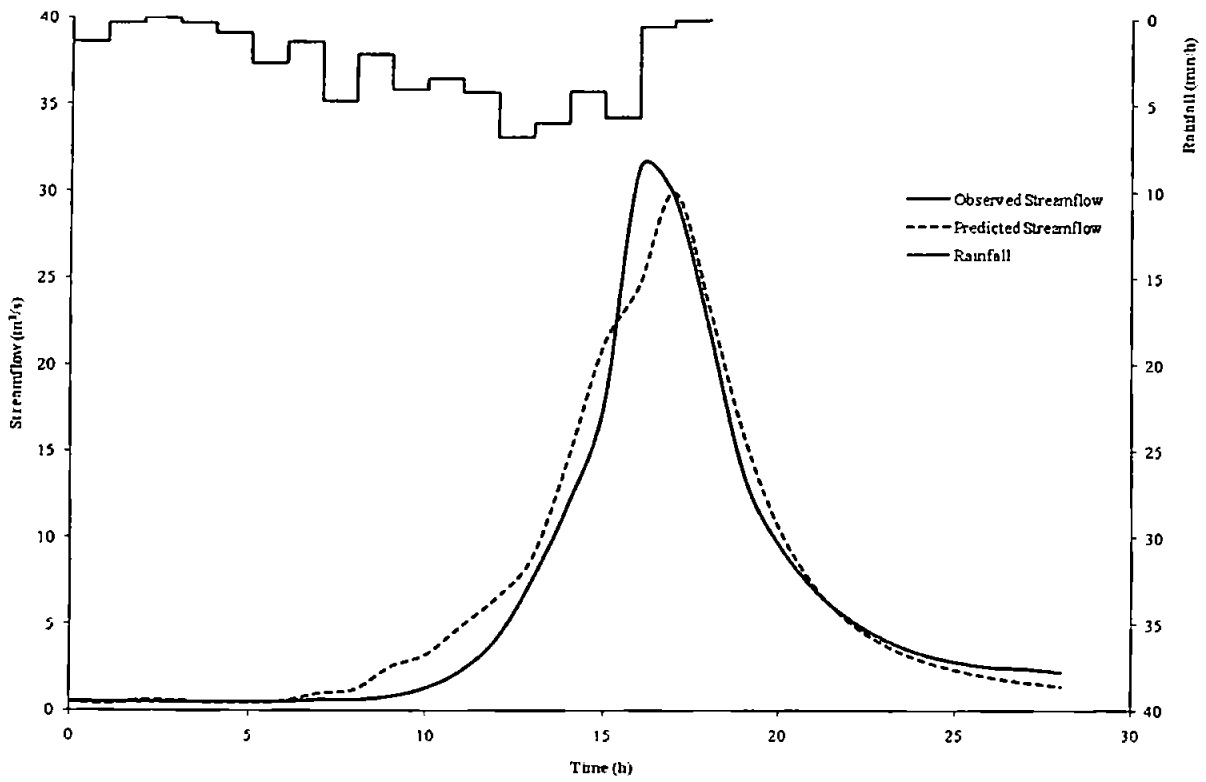
Figure C1.5 Predicted and observed results for event 1298
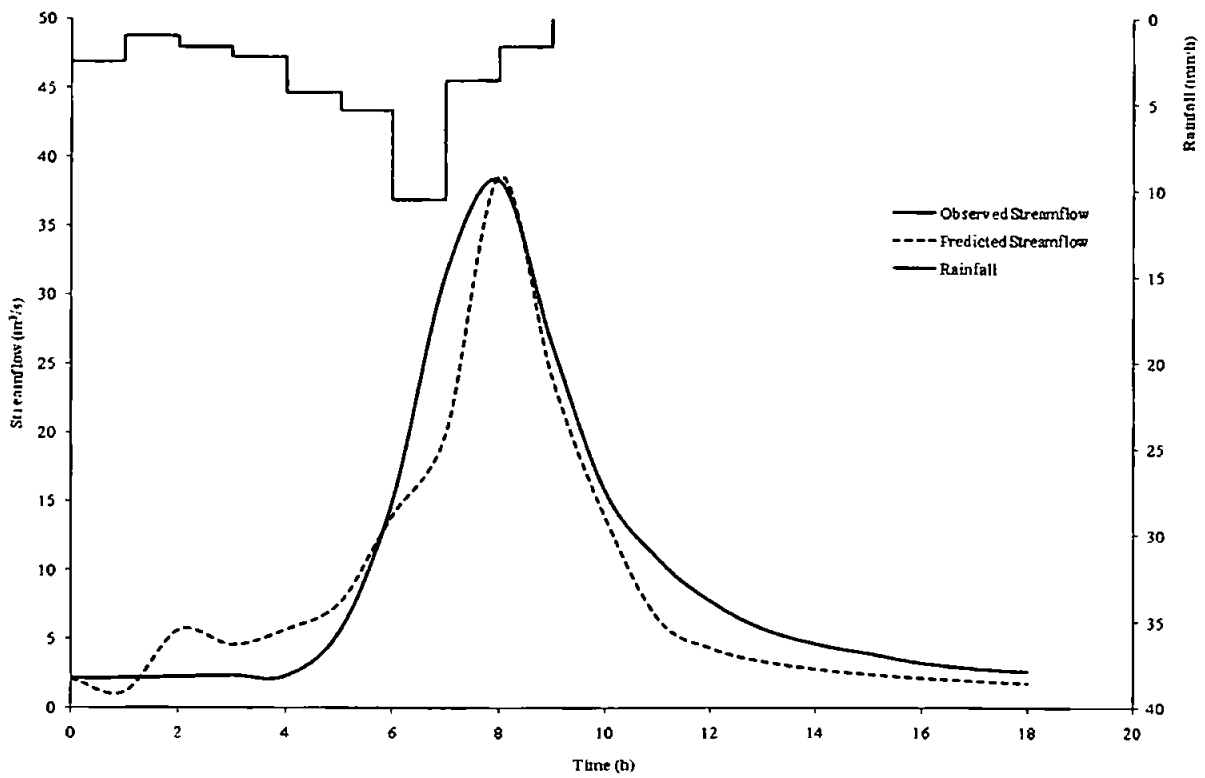
Figure C1.6 Predicted and observed results for event 1299
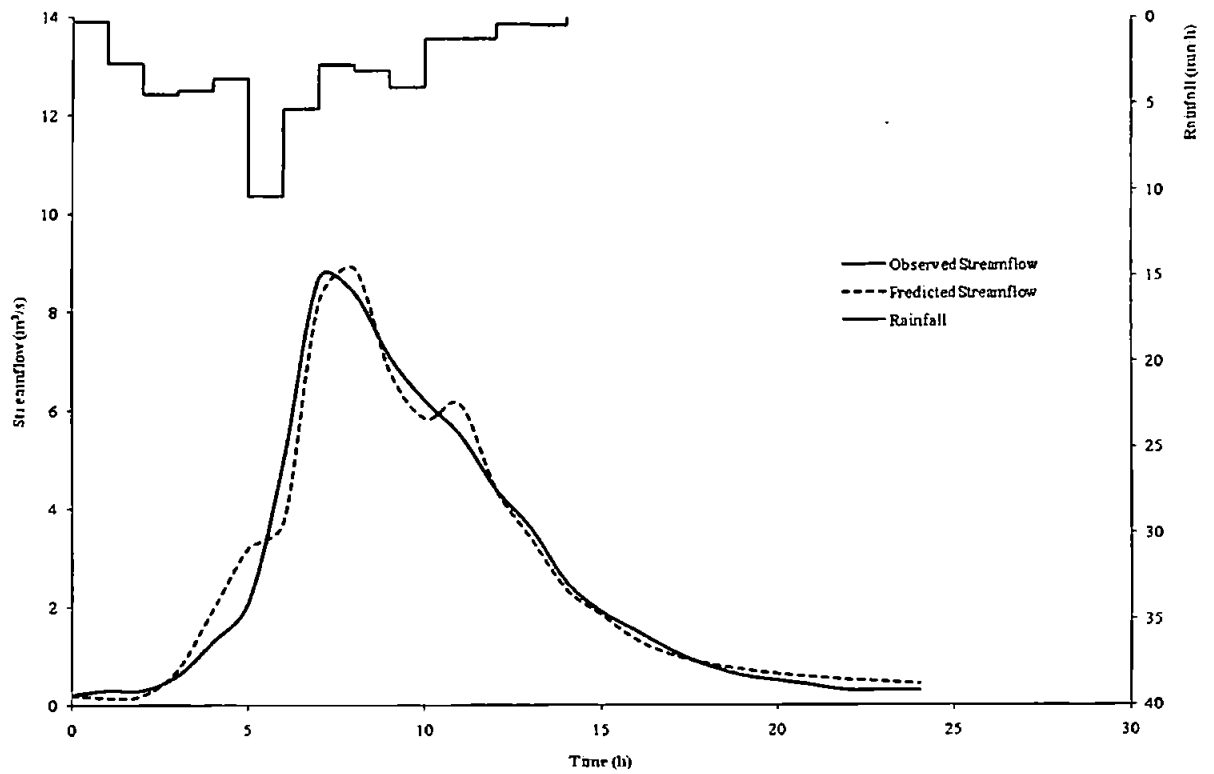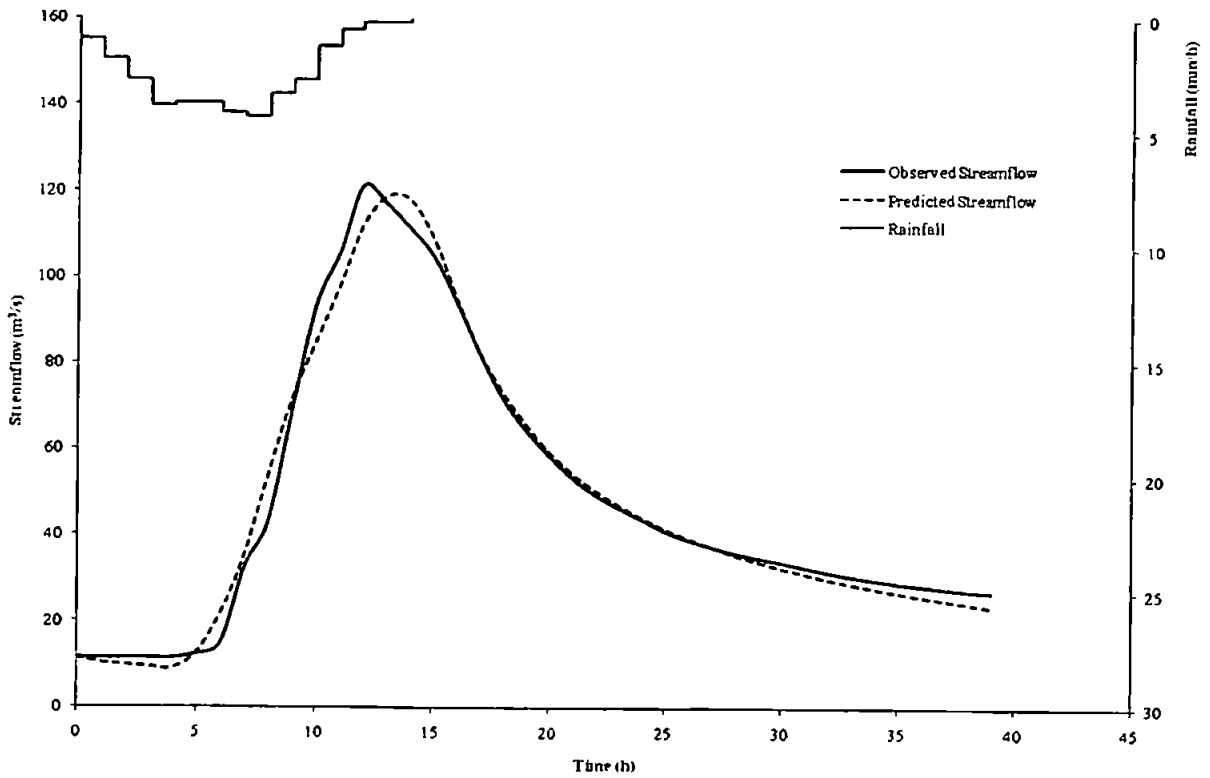
Figure C1.7 Predicted and observed results for event 1300
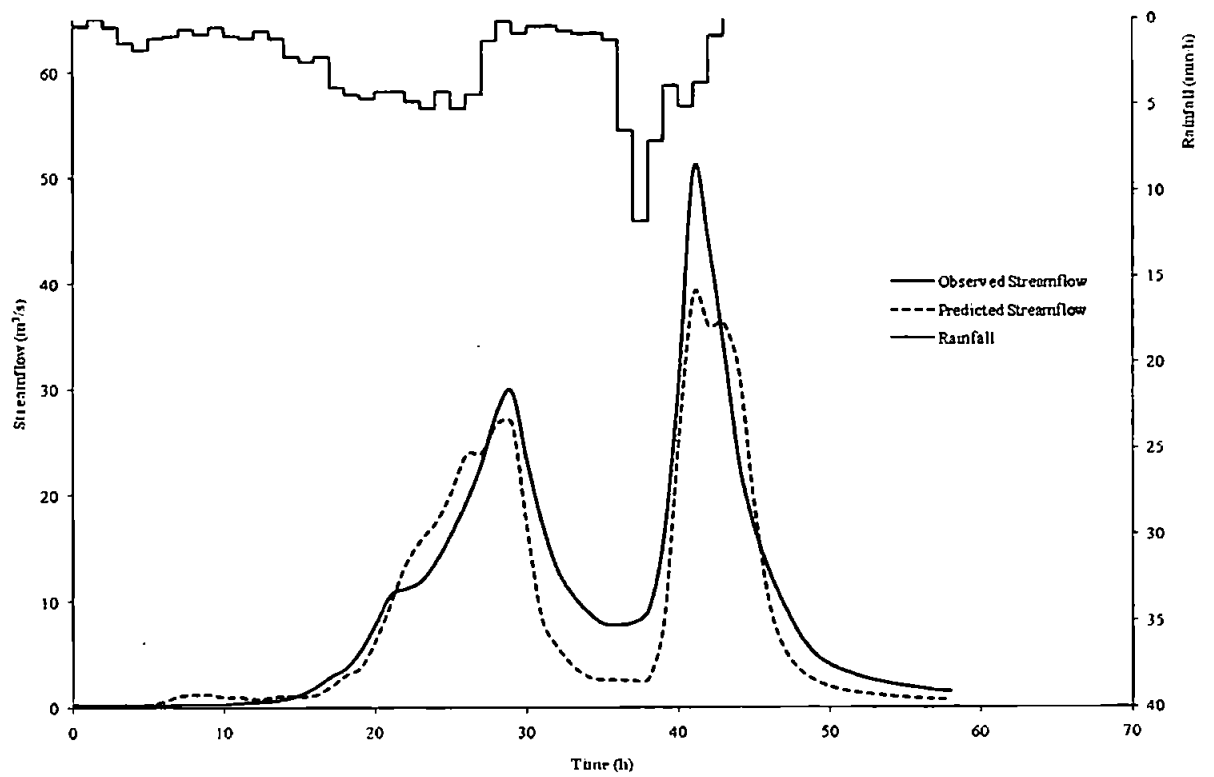
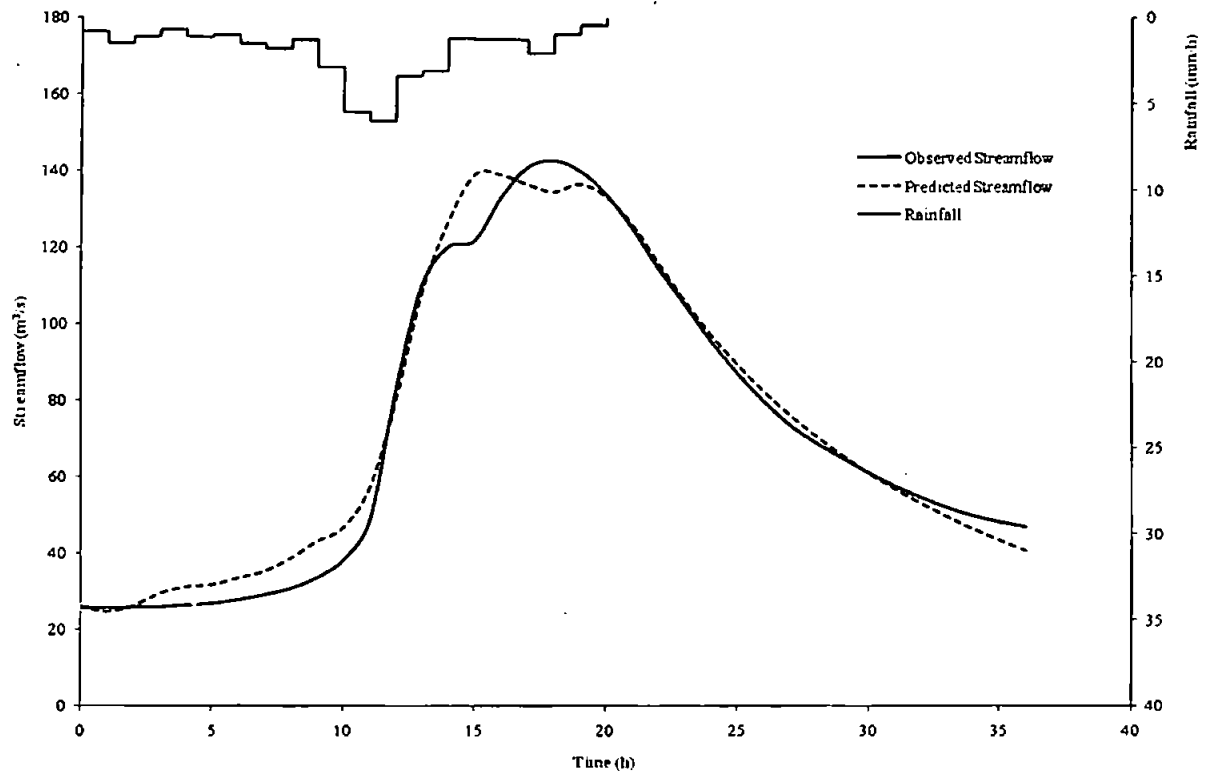**Figure C1.8 Predicted and observed results for event 1301**

215
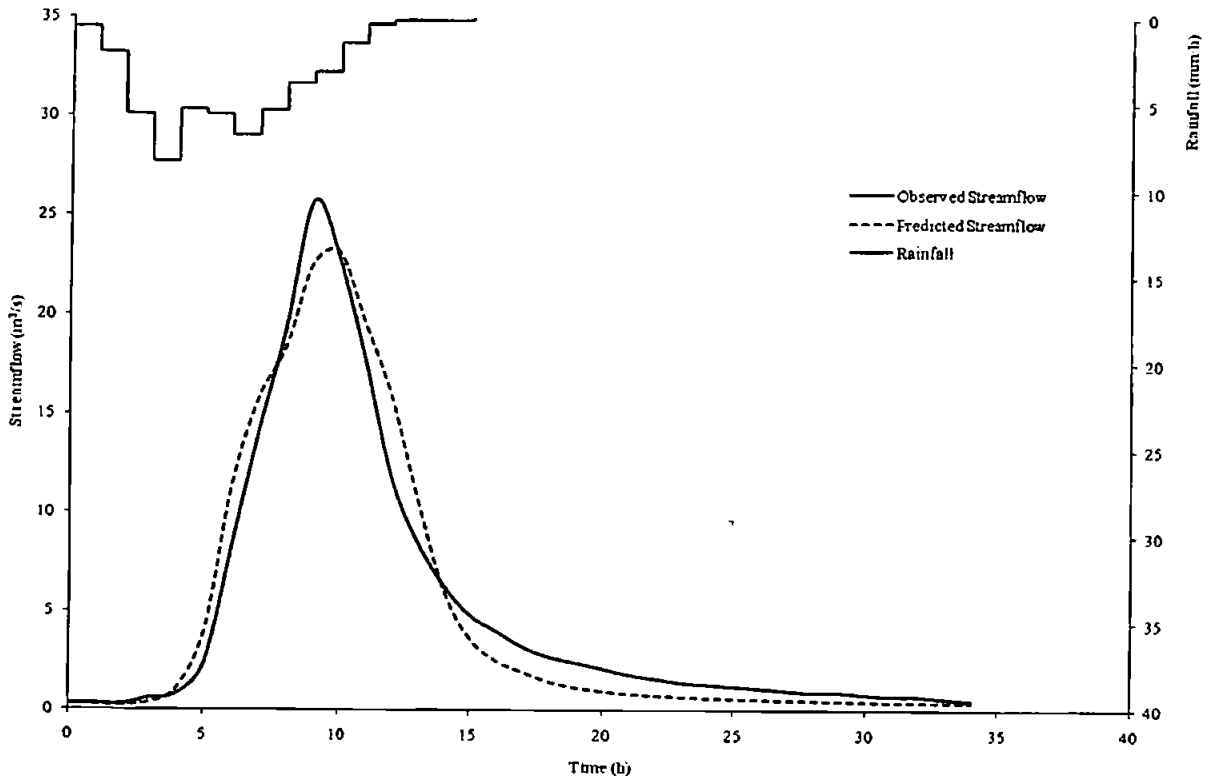
Figure C1.9 Predicted and observed results for event 1302
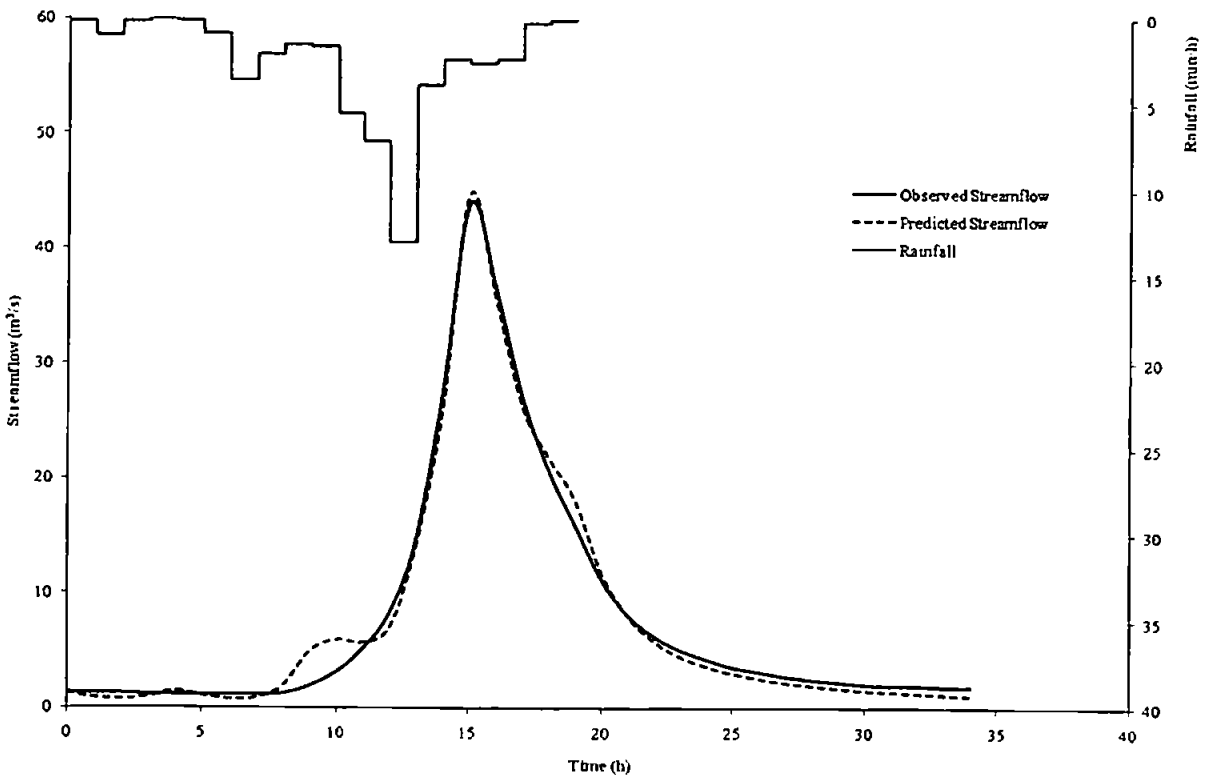
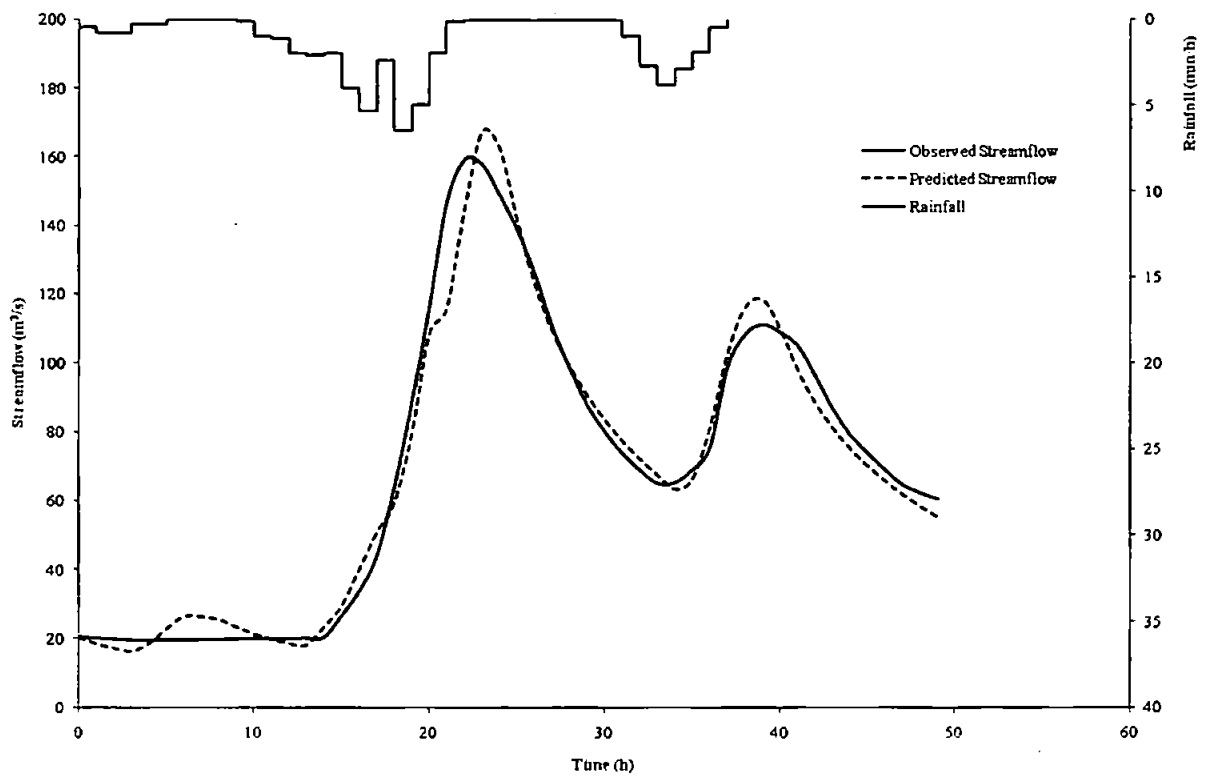**Figure C1.10 Predicted and observed results for event 1303**
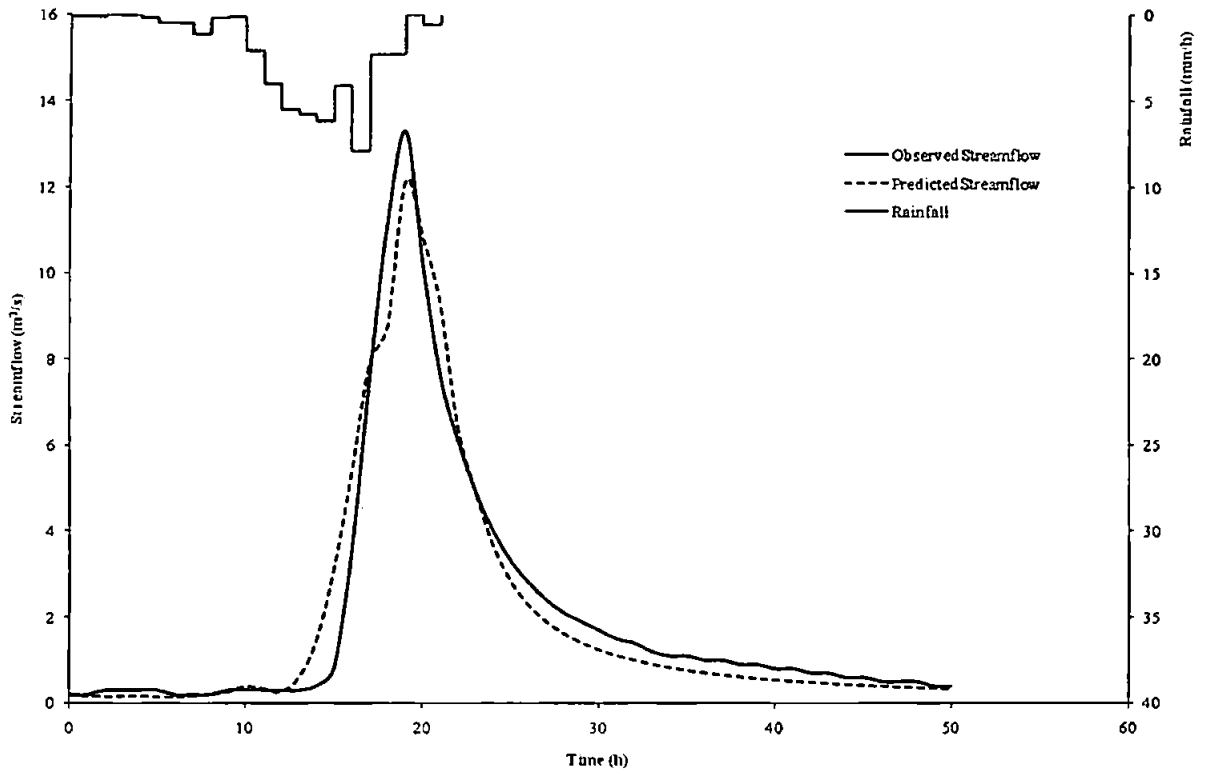
Figure C1.11 Predicted and observed results for event 1304
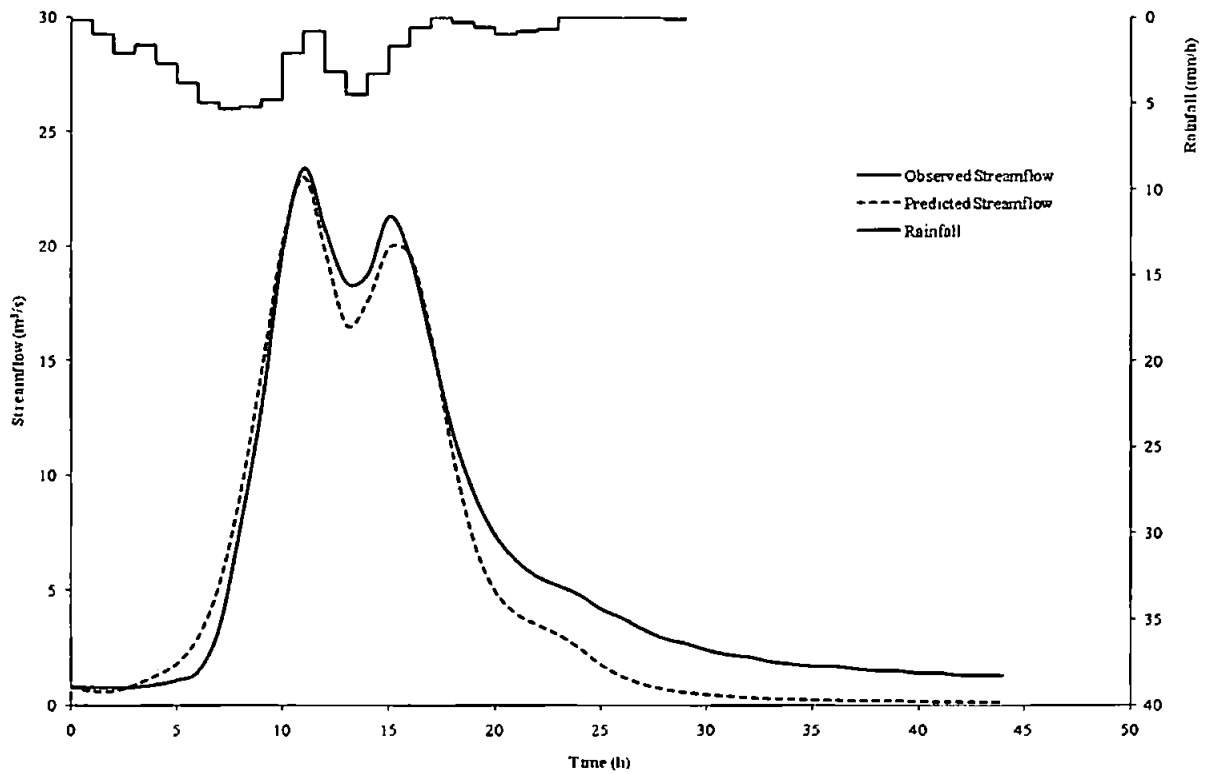
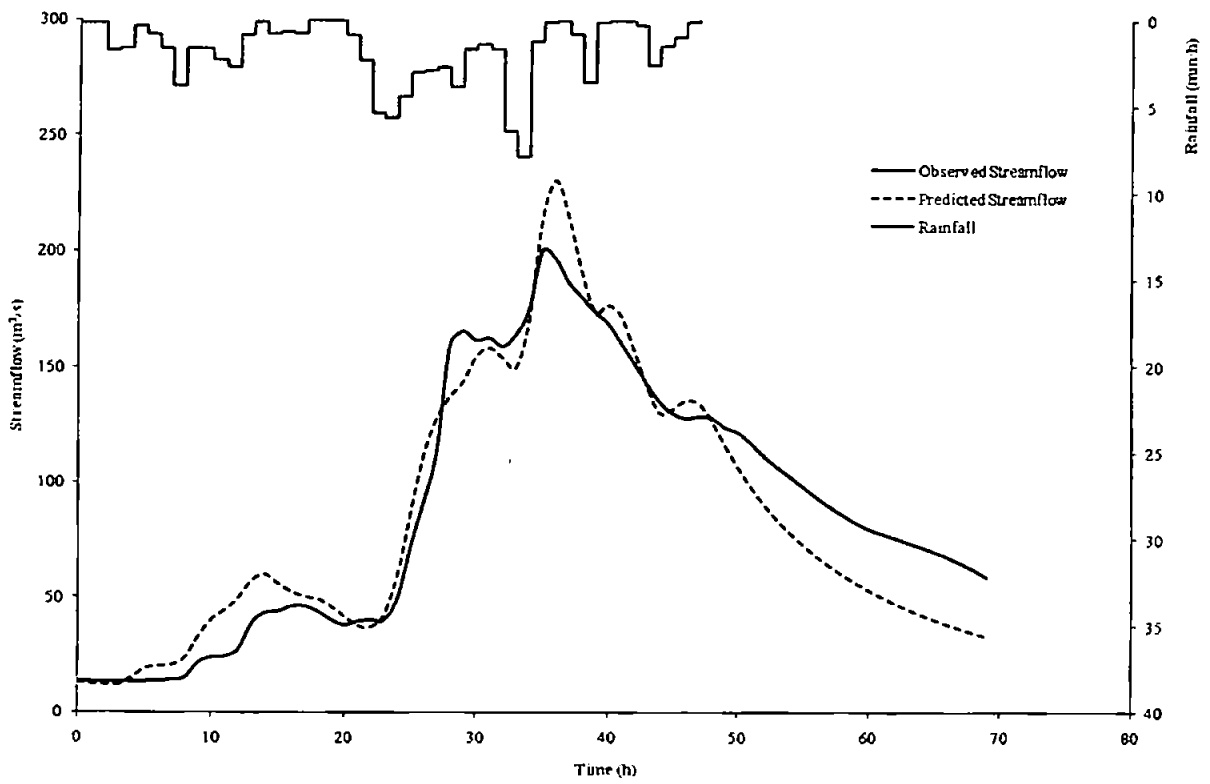**Figure C1.12 Predicted and observed results for event 4351**

217
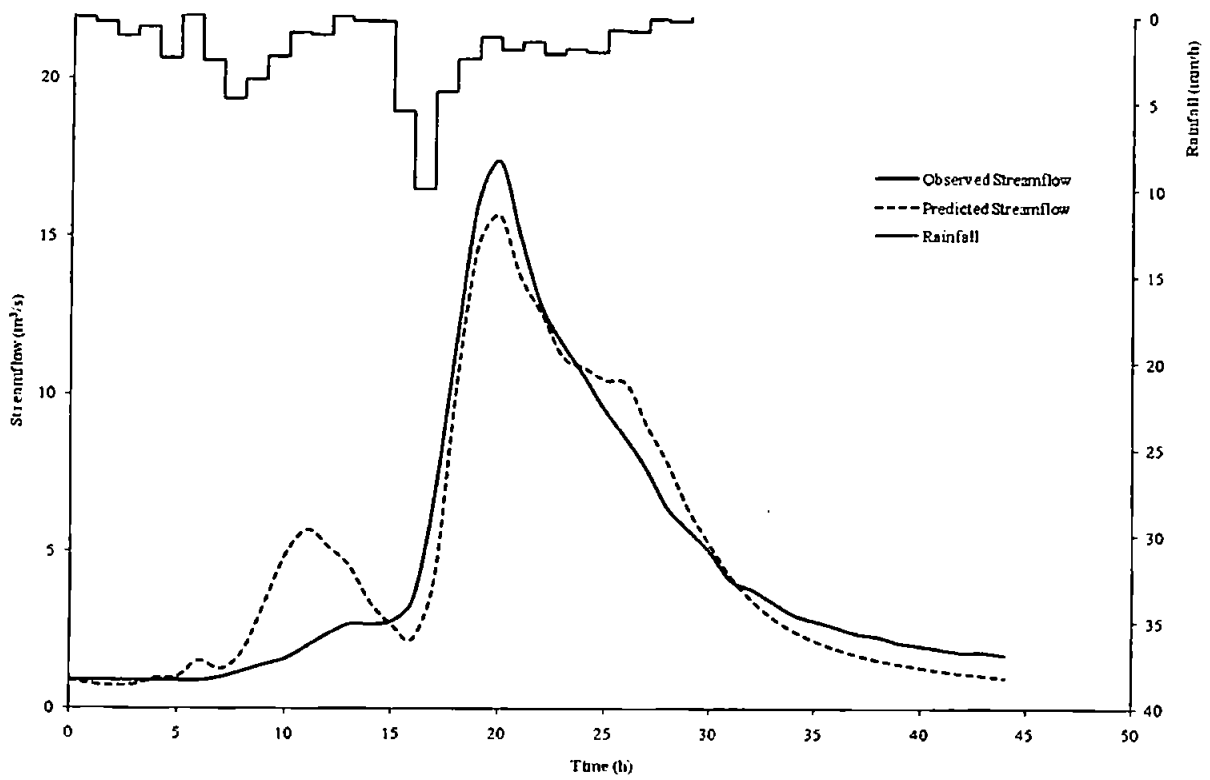
Figure C1.13 Predicted and observed results for event 4352

Figure C1.14 Predicted and observed results for event 4353

218
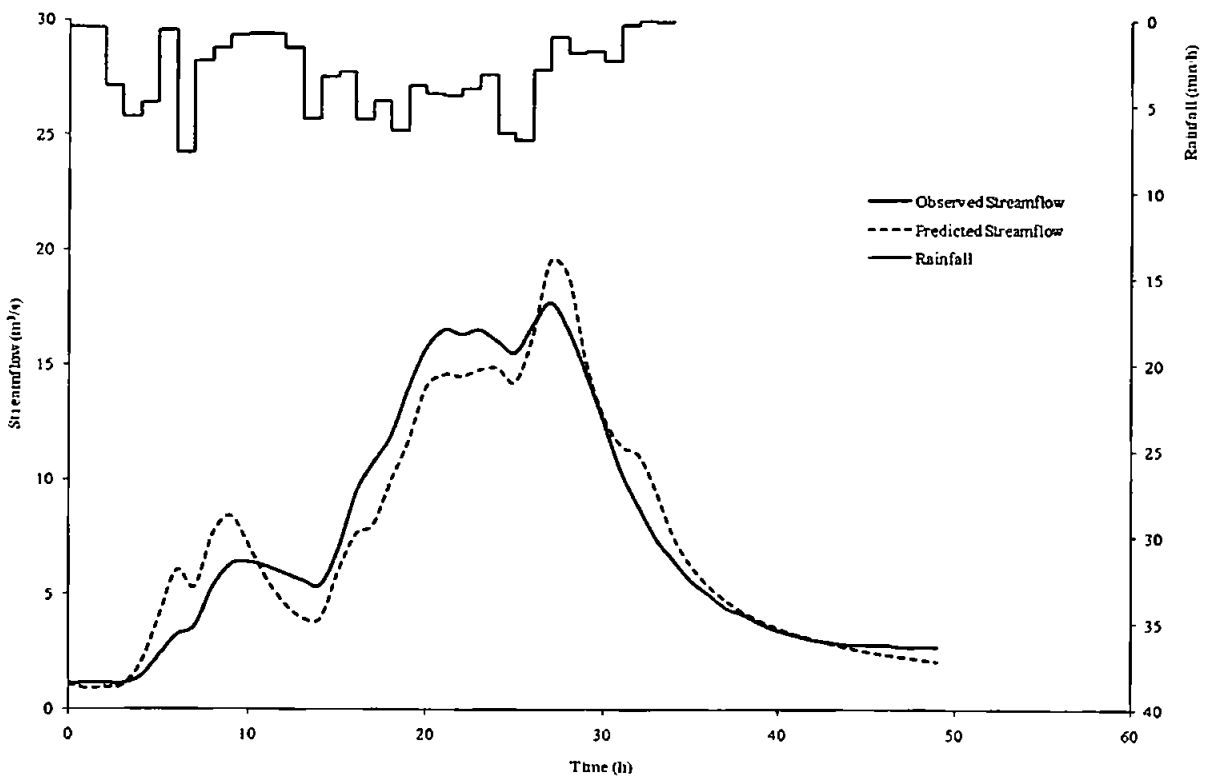
C2: Catchment 30004 – River Lymn at Partney Mill
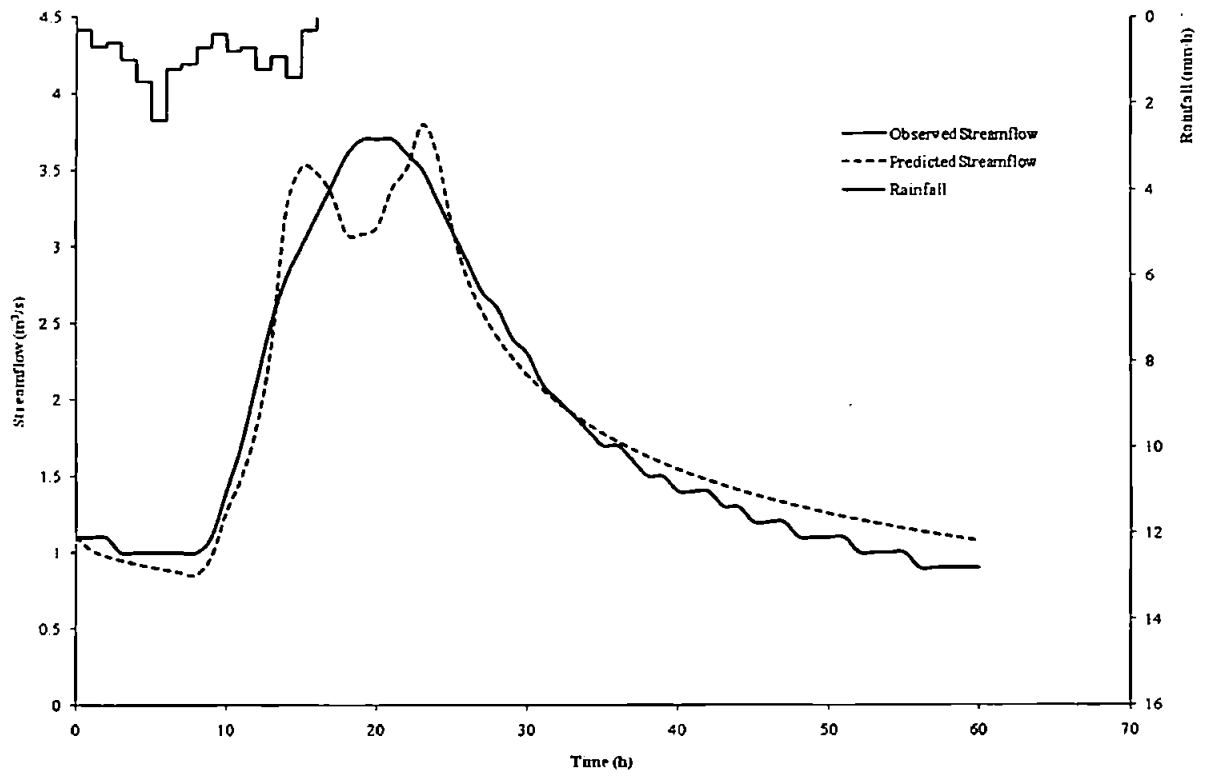
Figure C2.1 Predicted and observed results for event 492
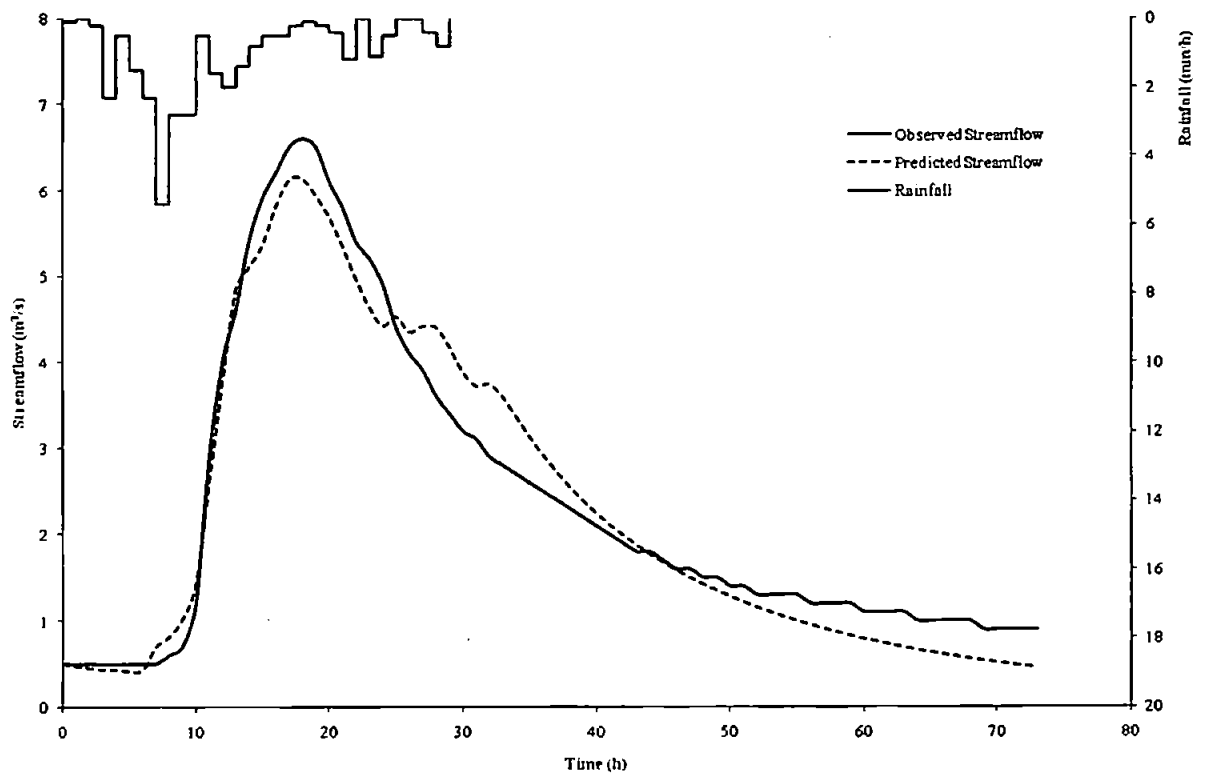
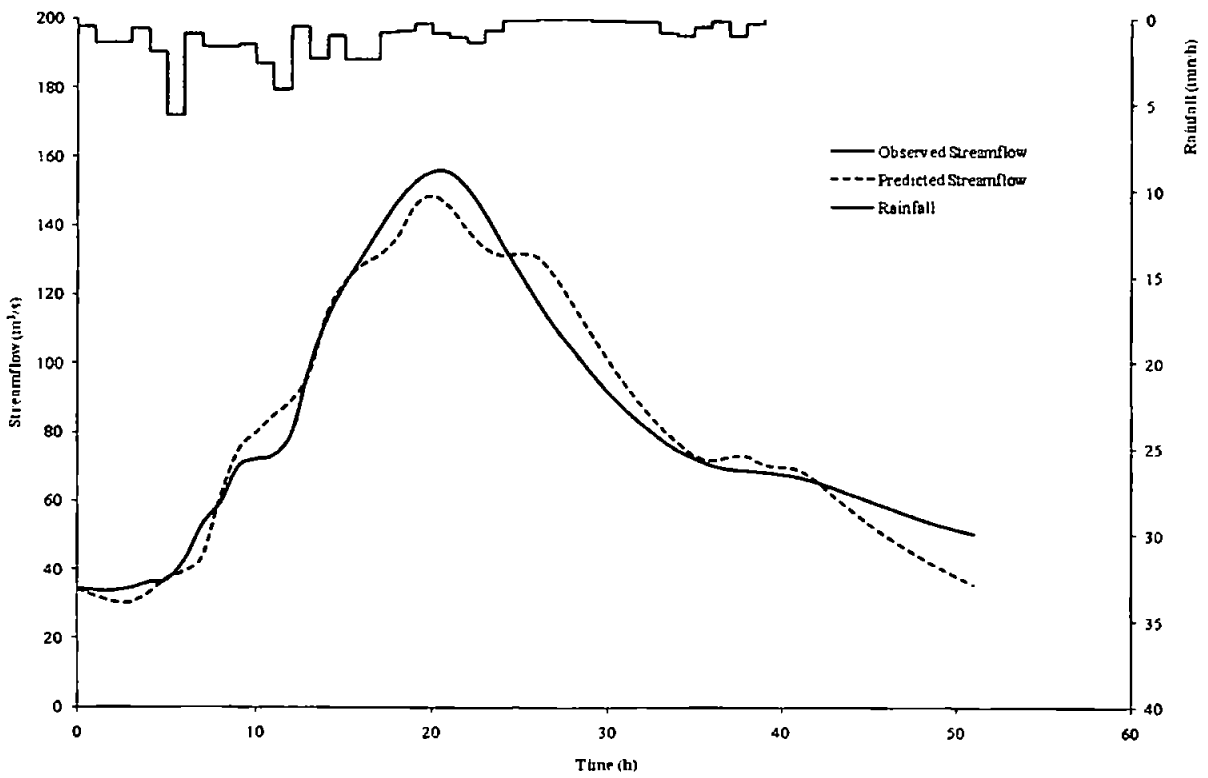**Figure C2.2 Predicted and observed results for event 495**
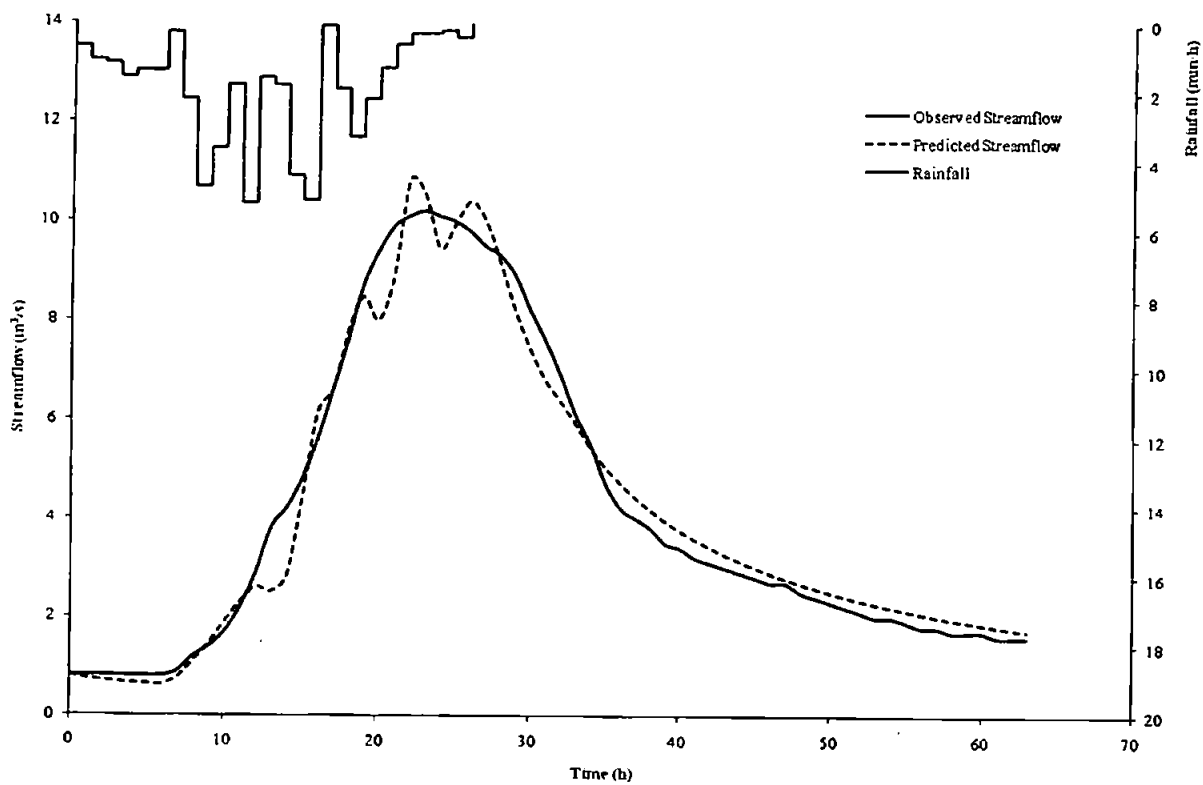
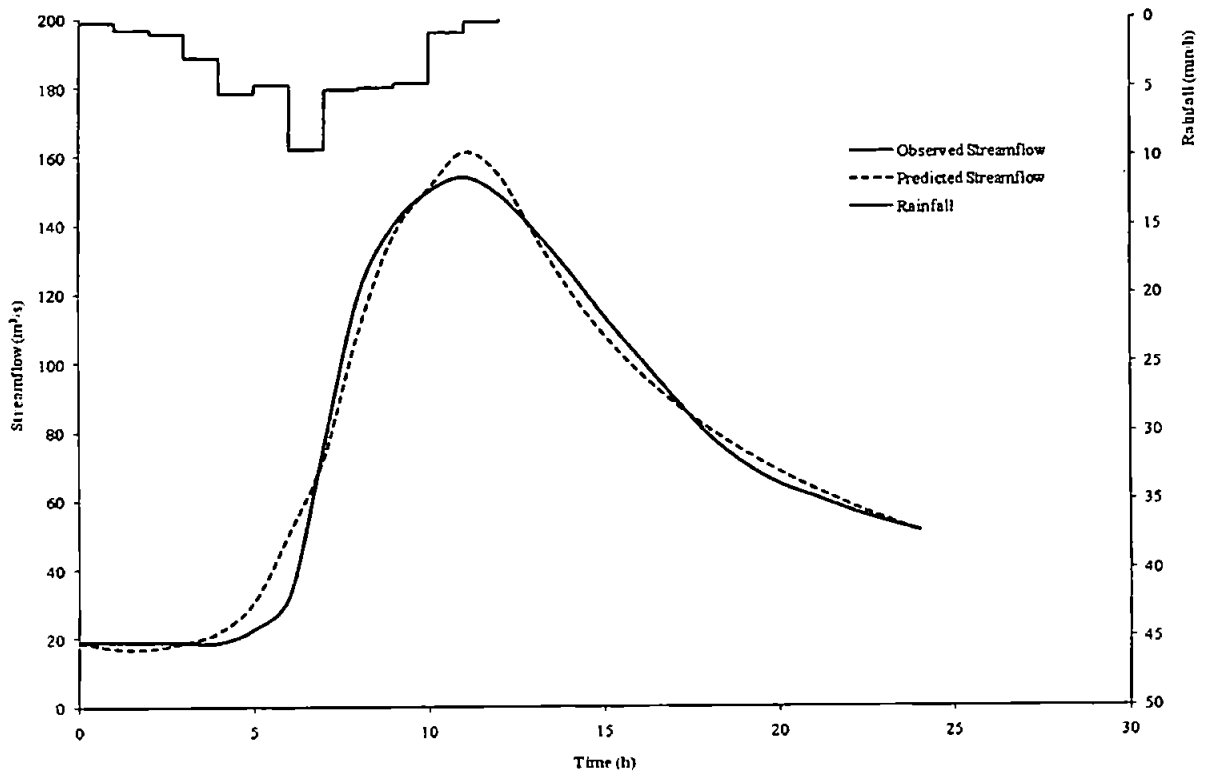**Figure C2.3 Predicted and observed results for event 496**
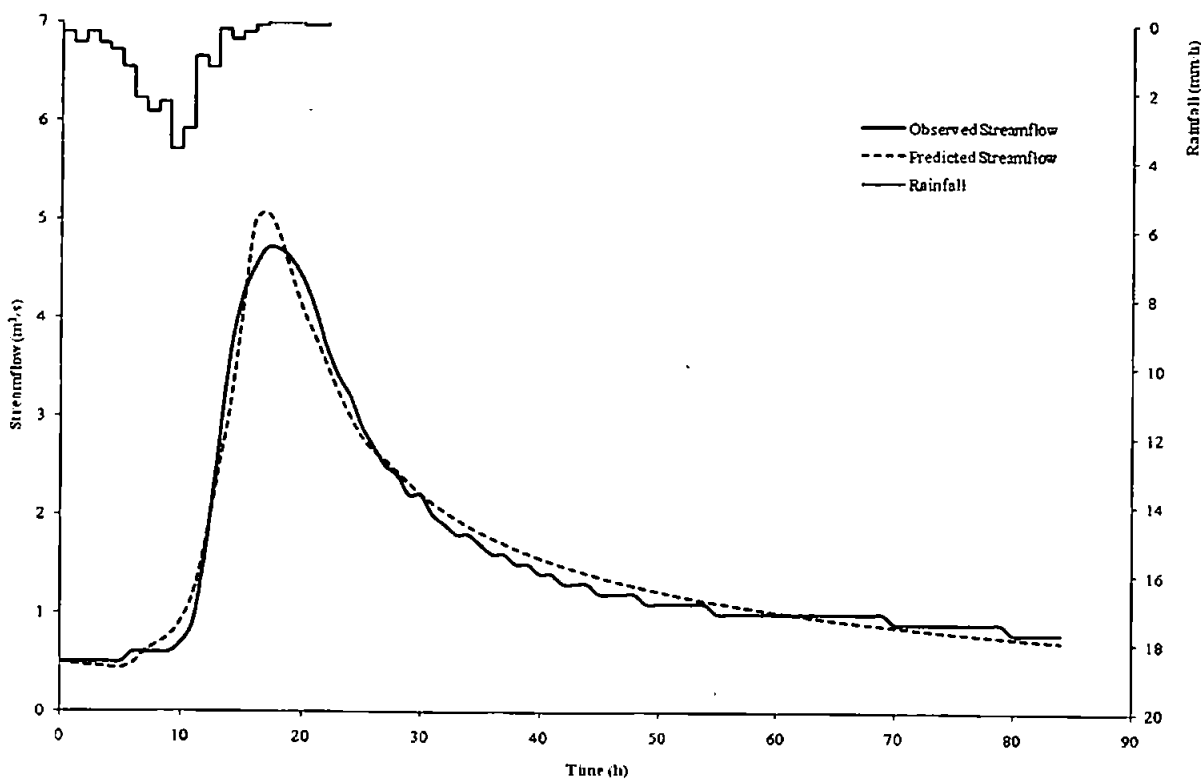
Figure C2.4 Predicted and observed results for event 3874

220
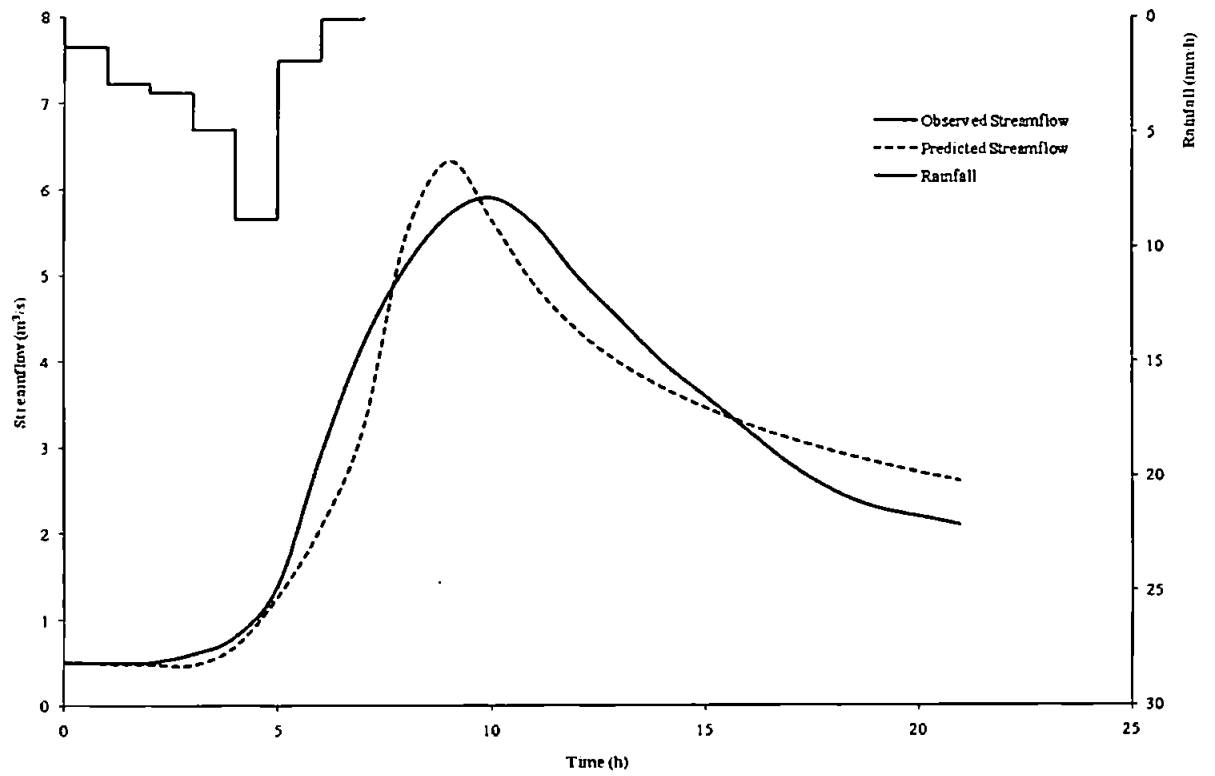
Figure C2.5 Predicted and observed results for event 3877
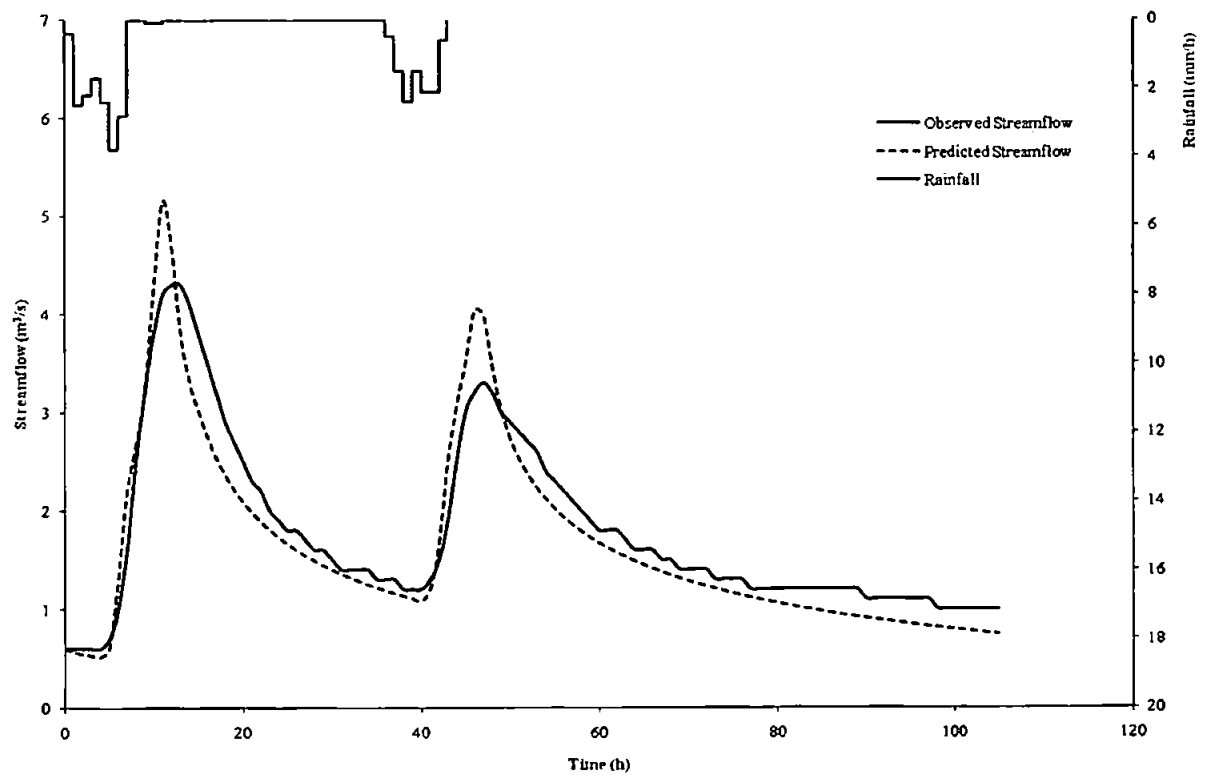
Figure C2.6 Predicted and observed results for event 3878

221
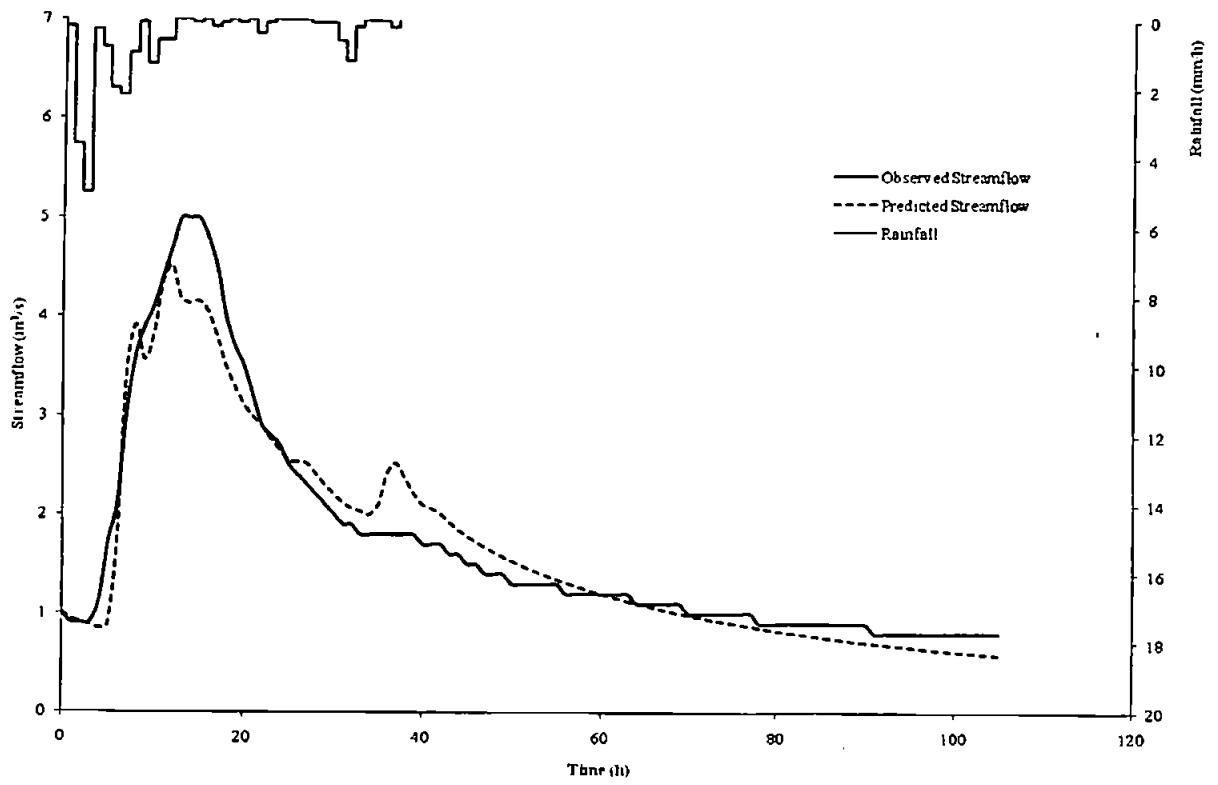
Figure C2.7 Predicted and observed results for event 3880
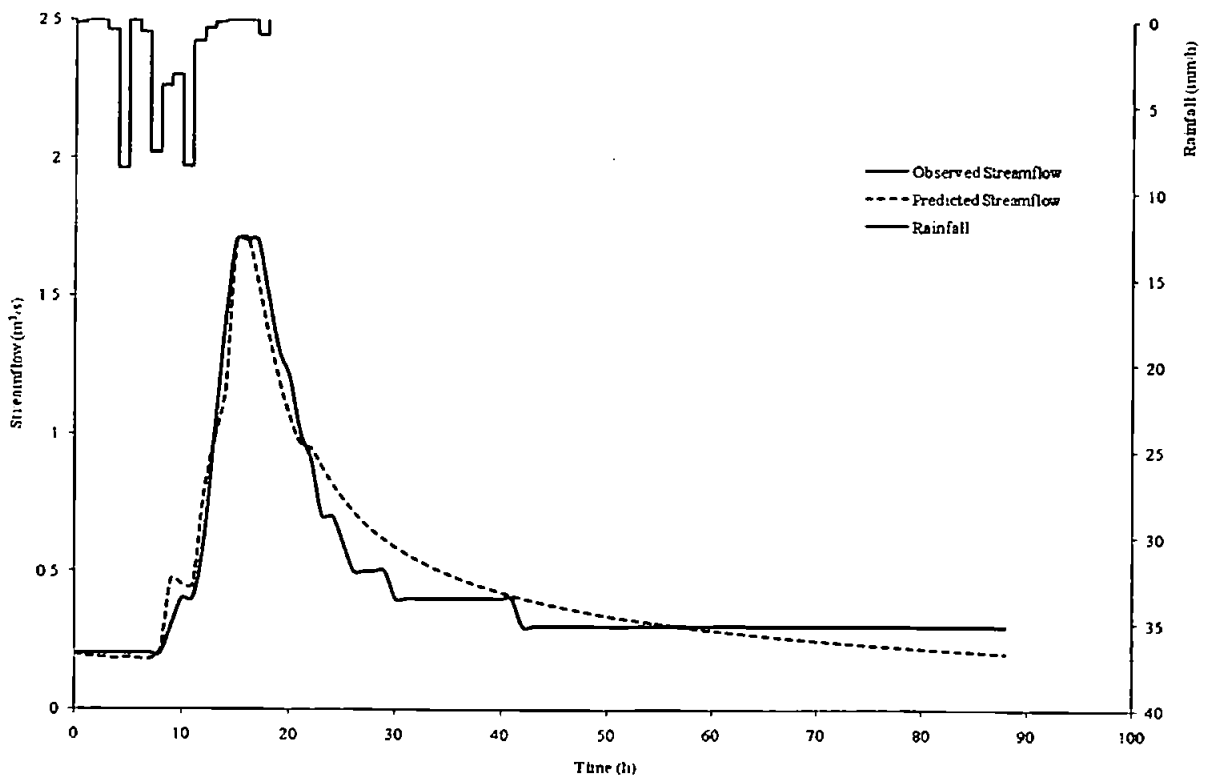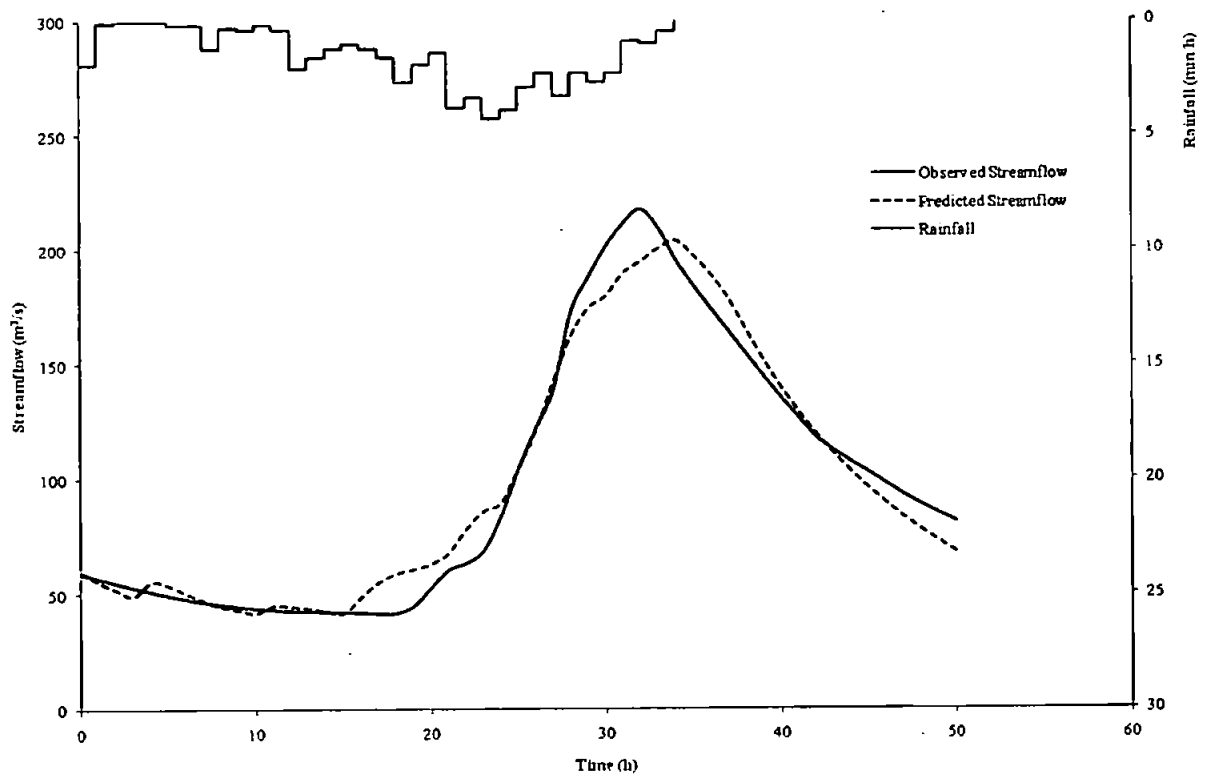

Figure C2.8 Predicted and observed results for event 3881

222
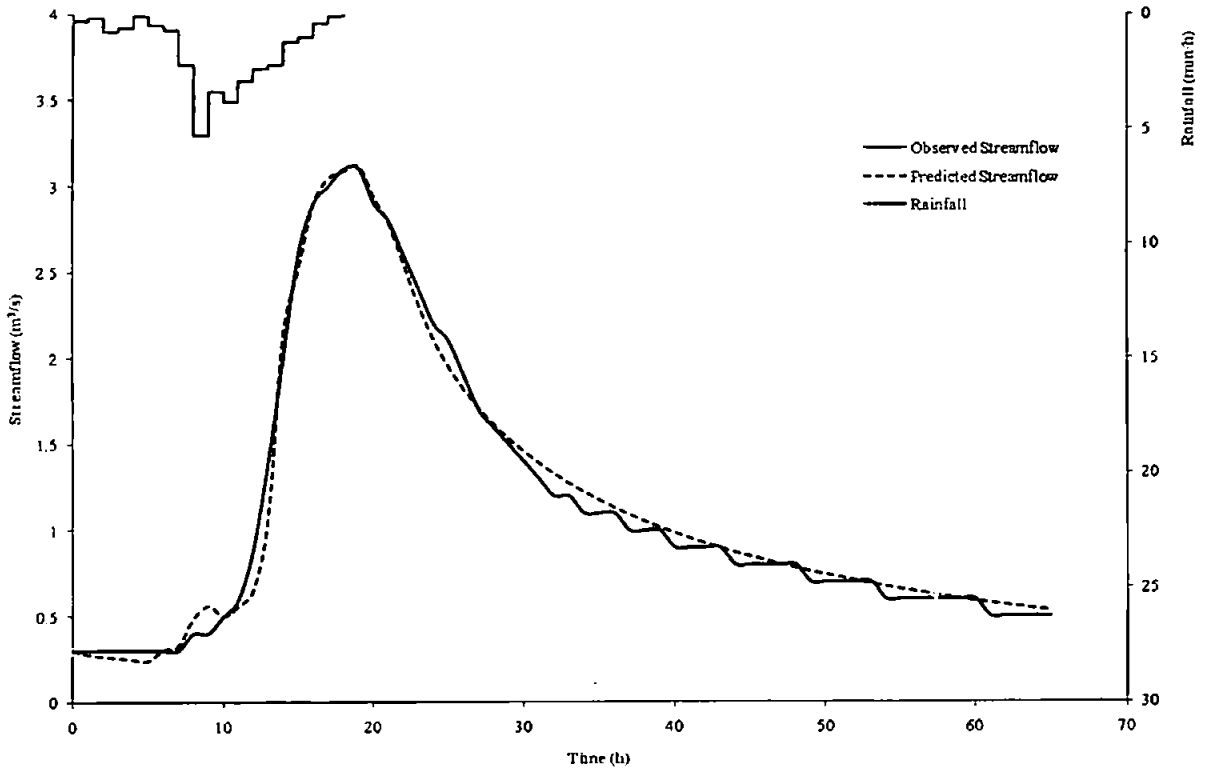
Figure C2.9 Predicted and observed results for event 3882
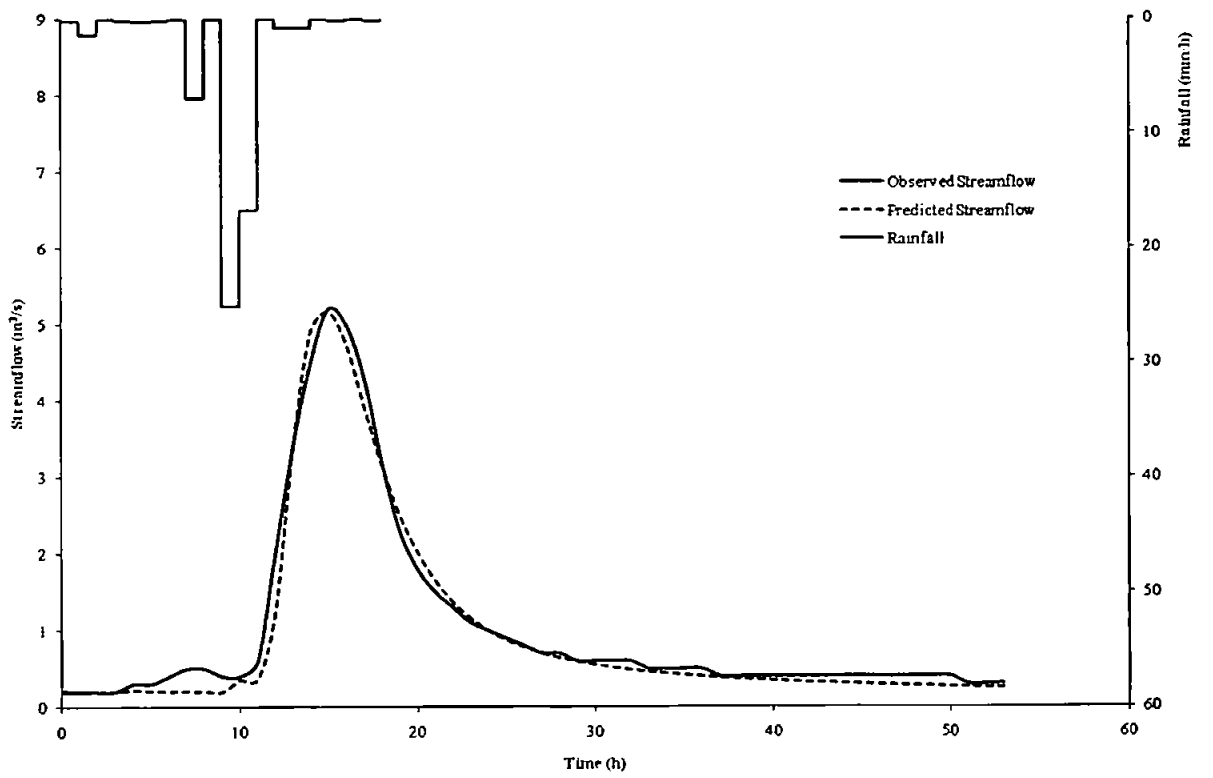
Figure C2.10 Predicted and observed results for event 3884

223
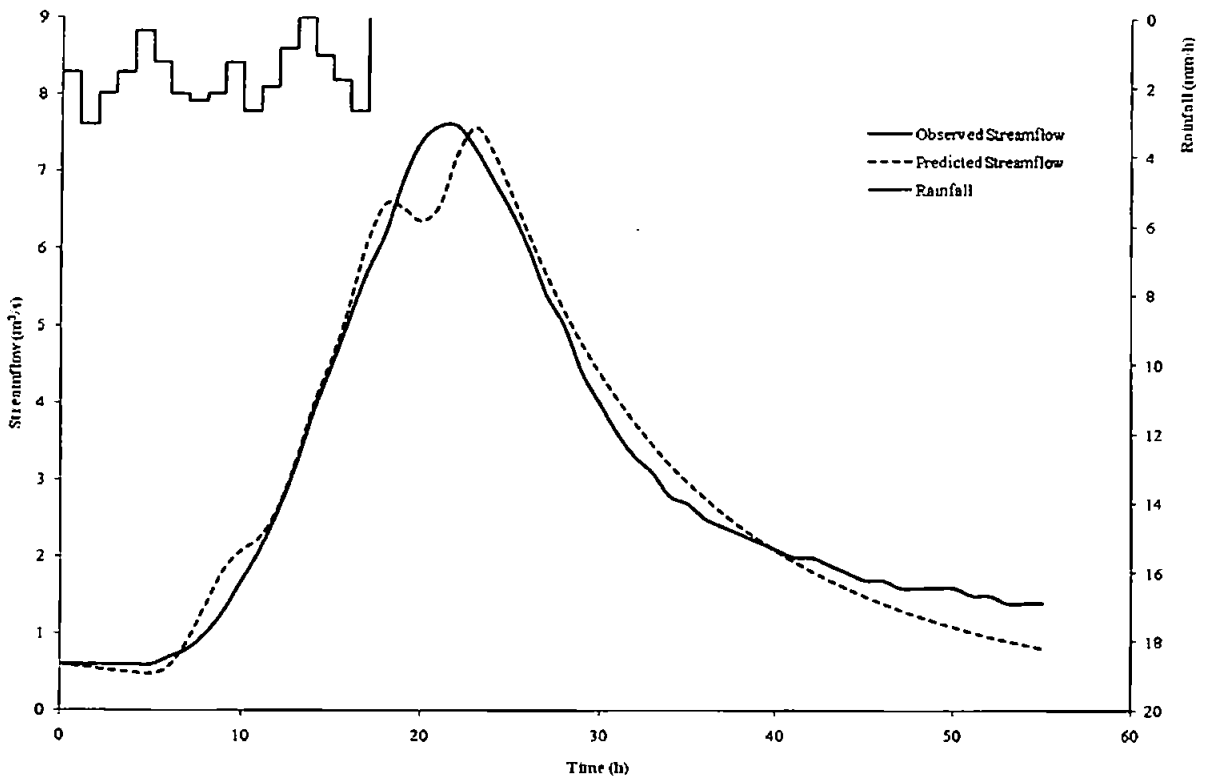
Figure C2.11 Predicted and observed results for event 3890
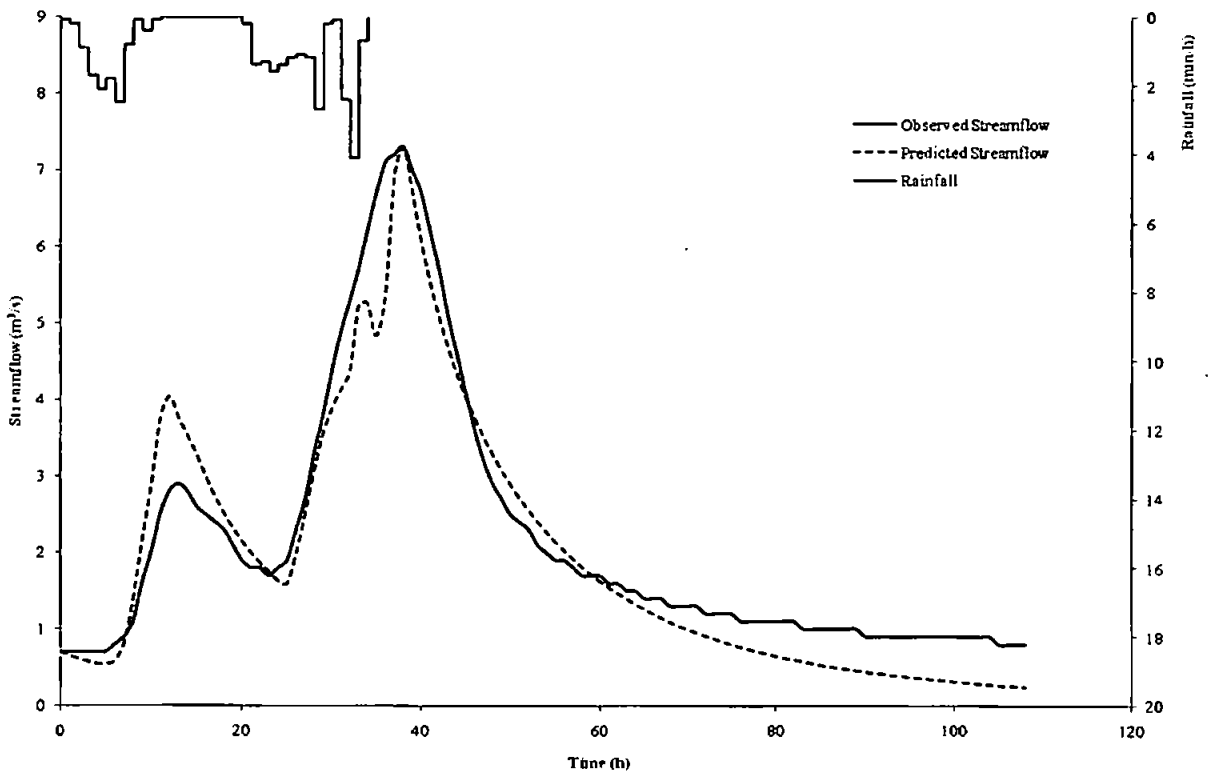
Figure C2.12 Predicted and observed results for event 3893
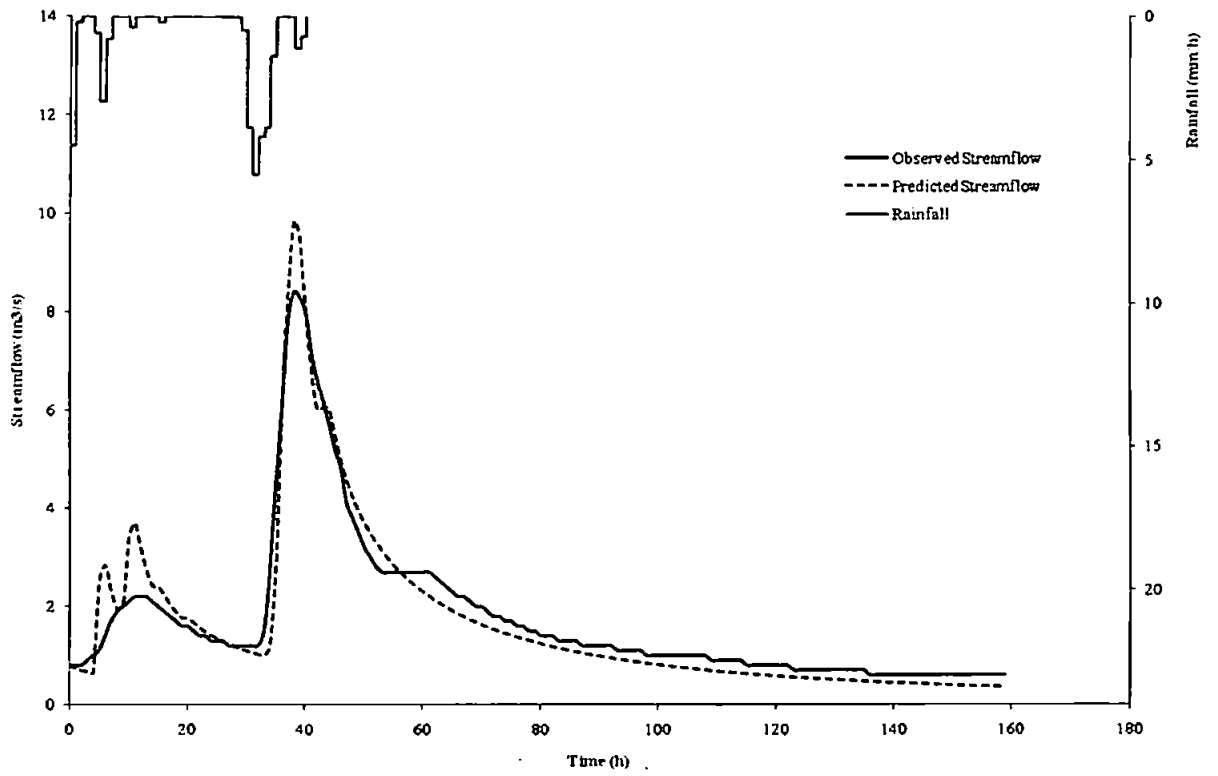
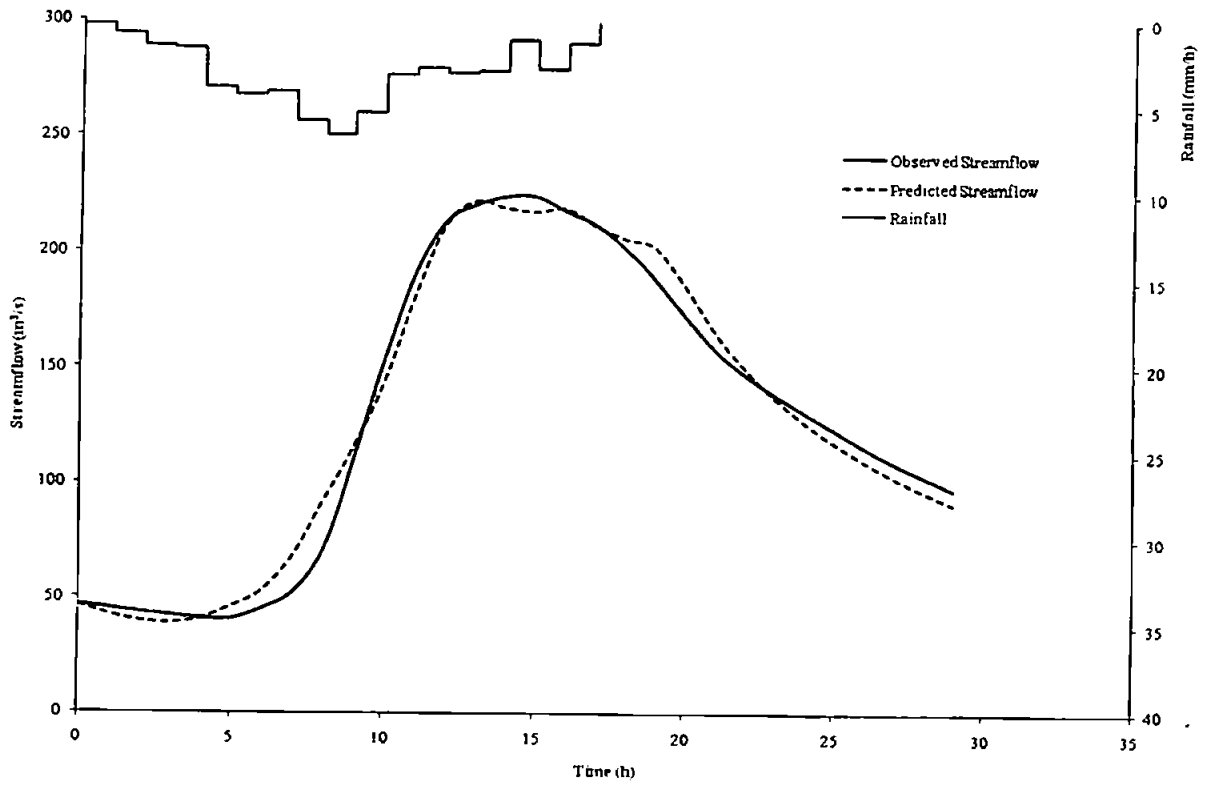**Figure C2.13 Predicted and observed results for event 4166**

C3: Catchment 74001 – River Duddon at Duddon Hall
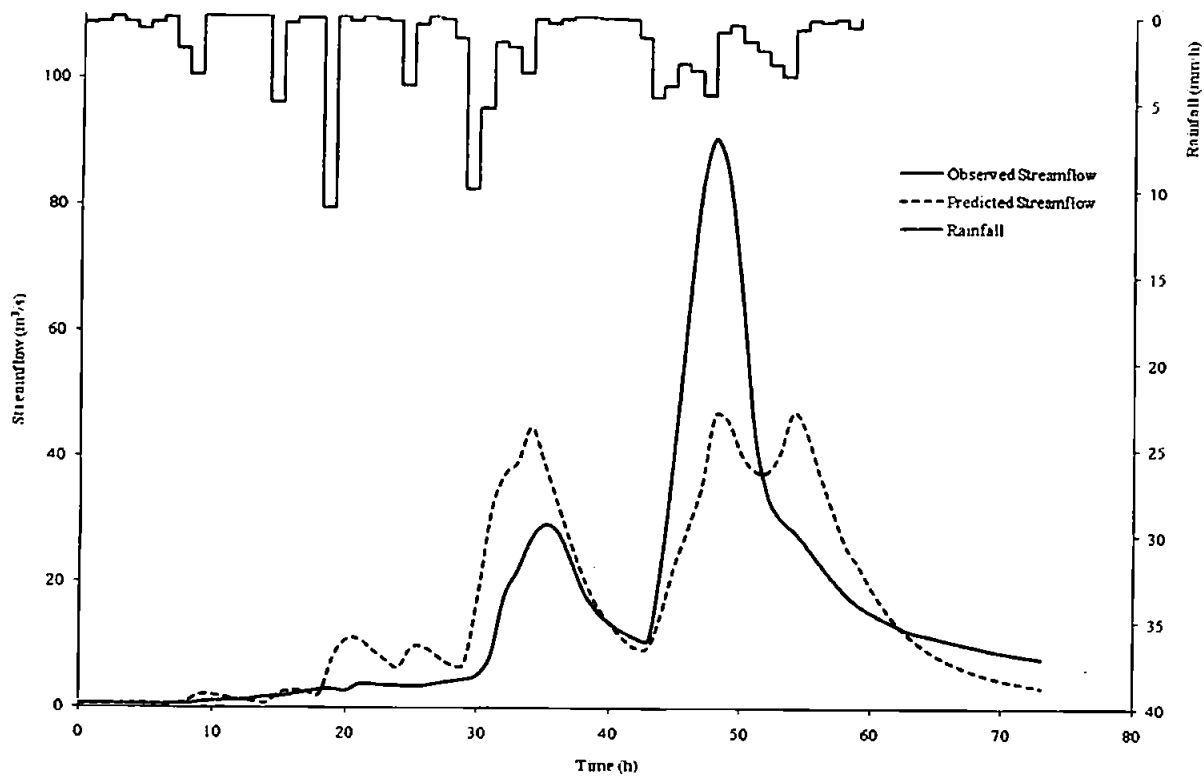
Figure C3.1 Predicted and observed results for event 2360
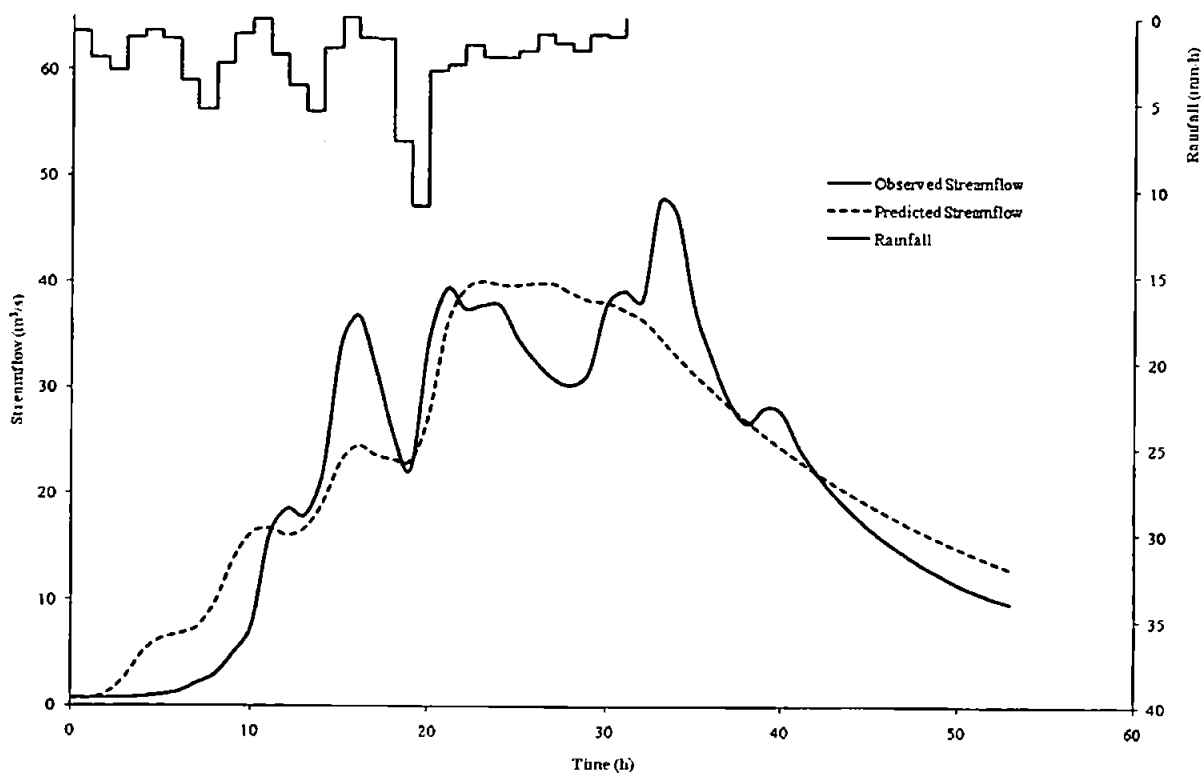
Figure C3.2 Predicted and observed results for event 2361
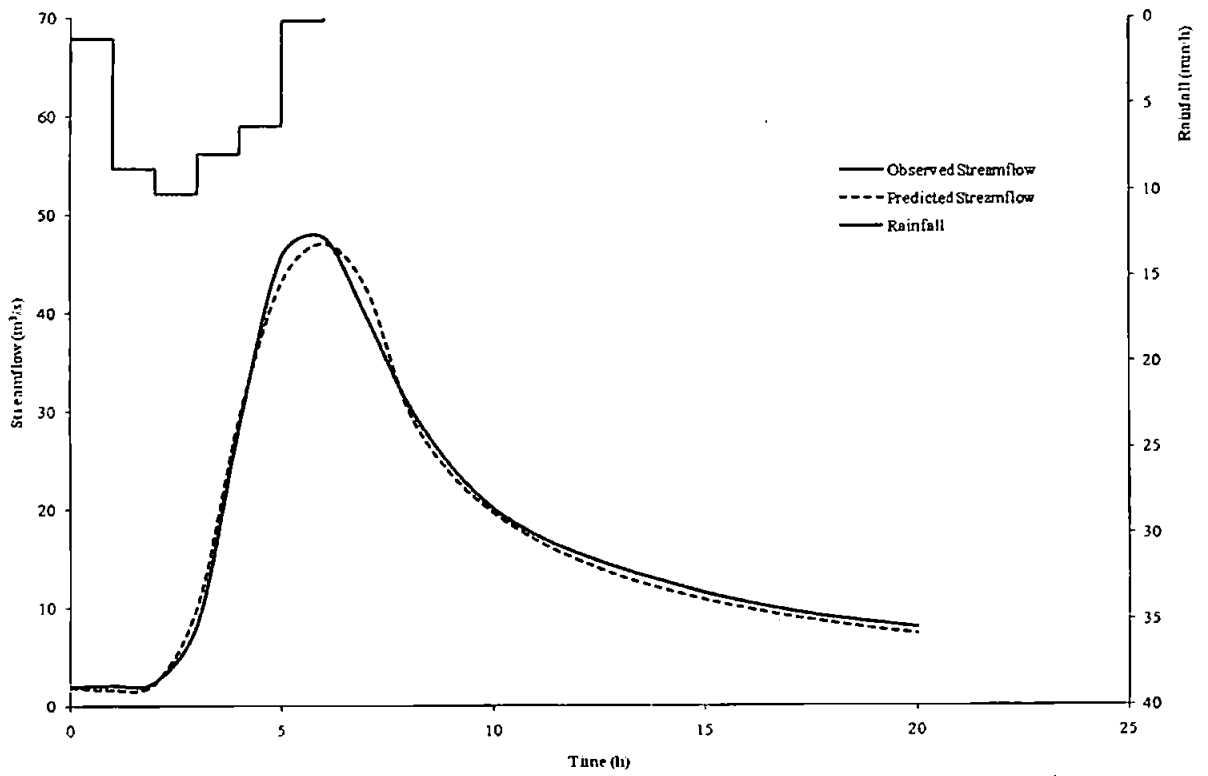
Figure C3.3 Predicted and observed results for event 2362
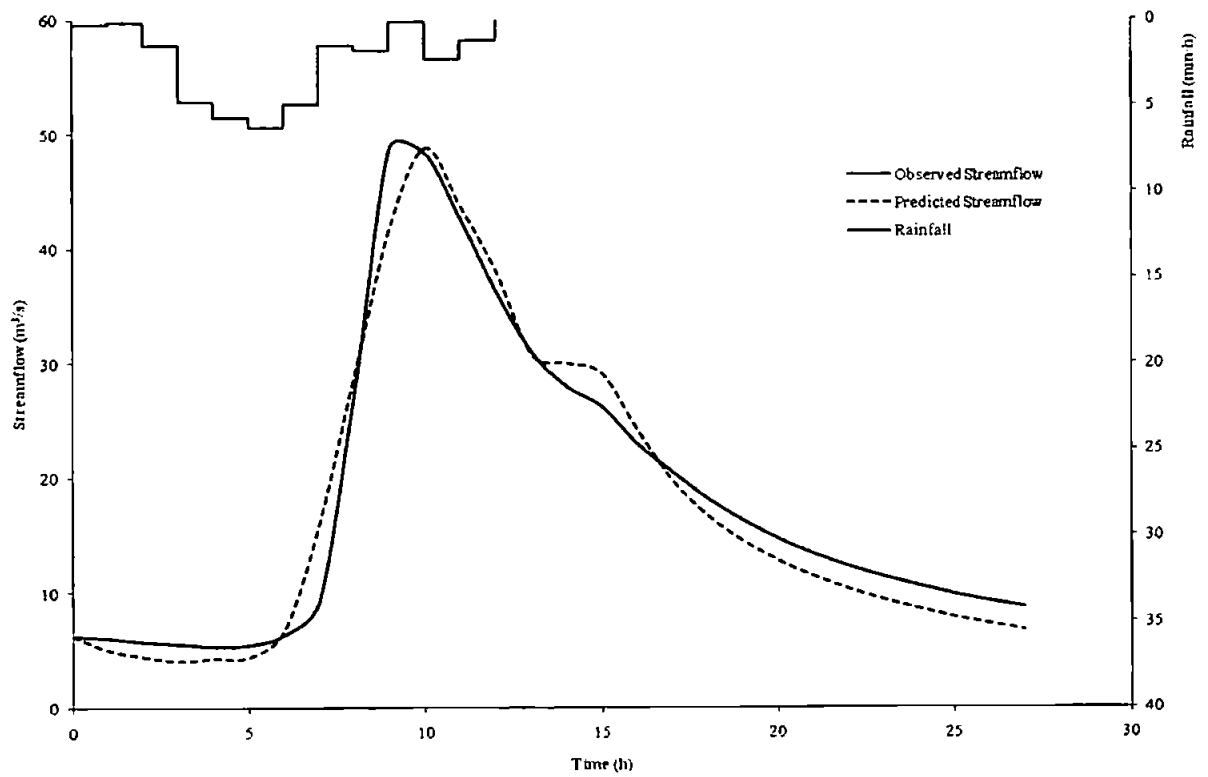
Figure C3.4 Predicted and observed results for event 2363
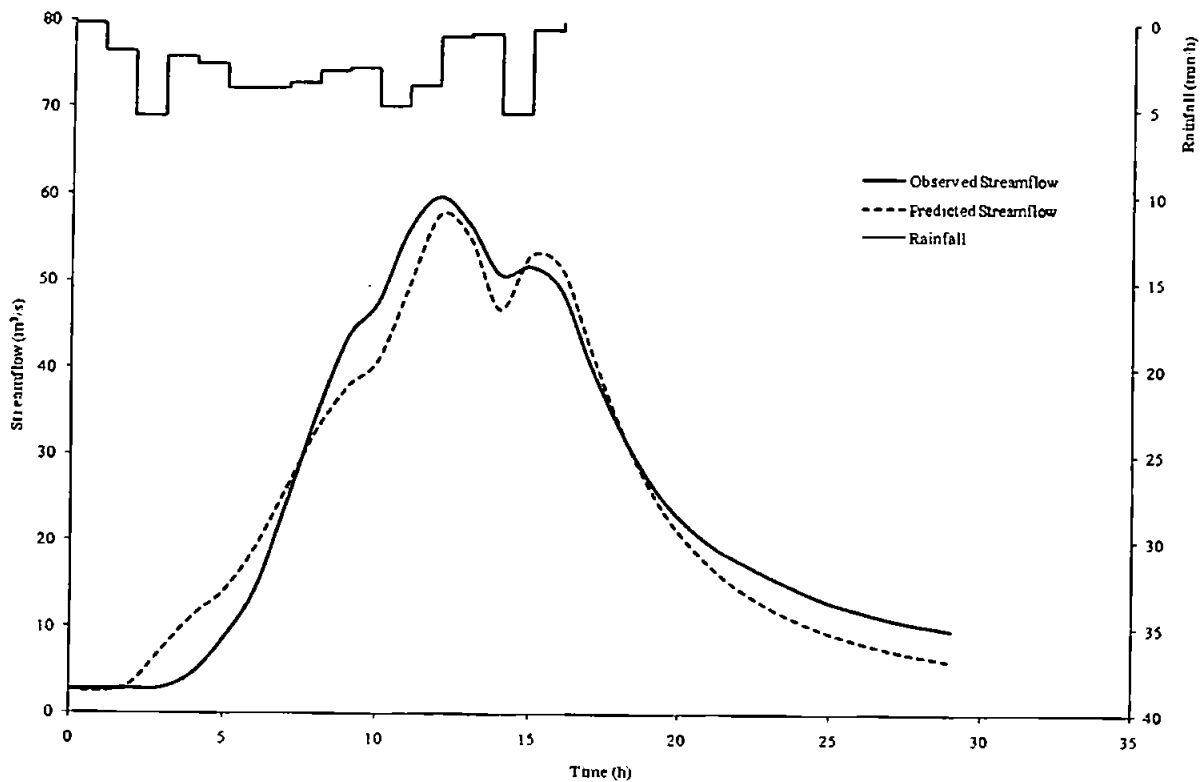
Figure C3.5 Predicted and observed results for event 2364
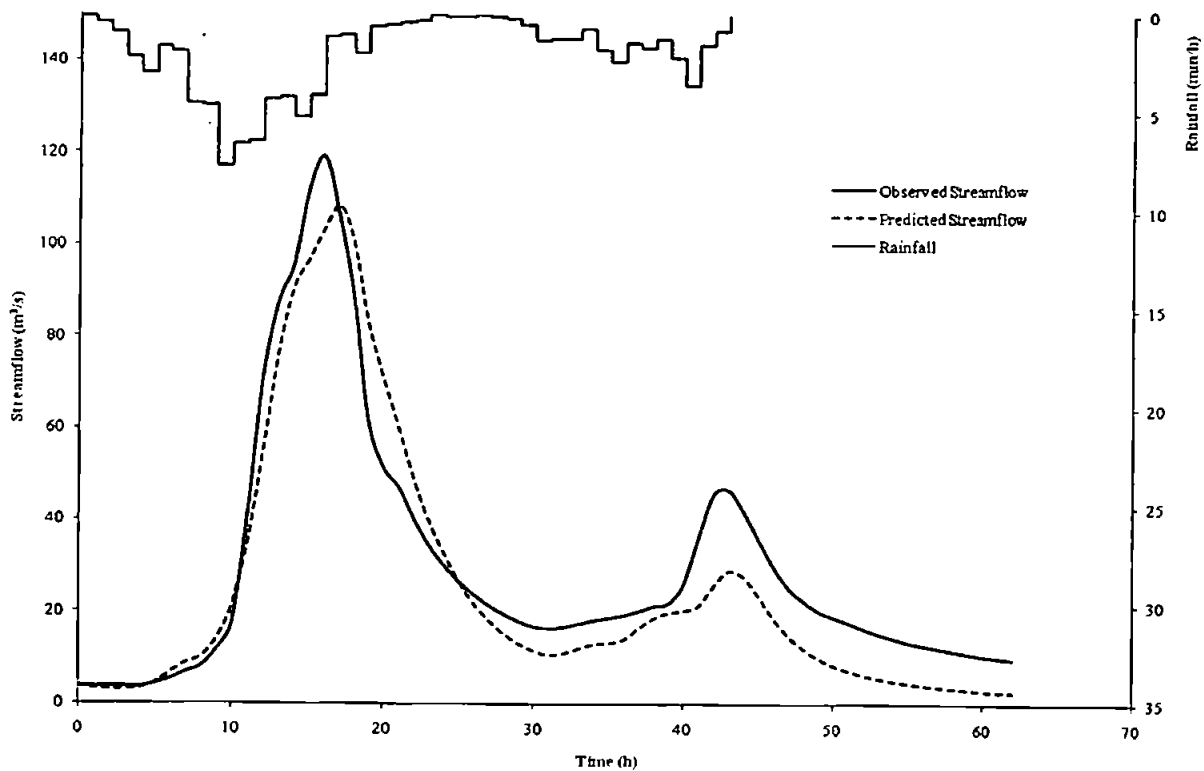
Figure C3.6 Predicted and observed results for event 2365
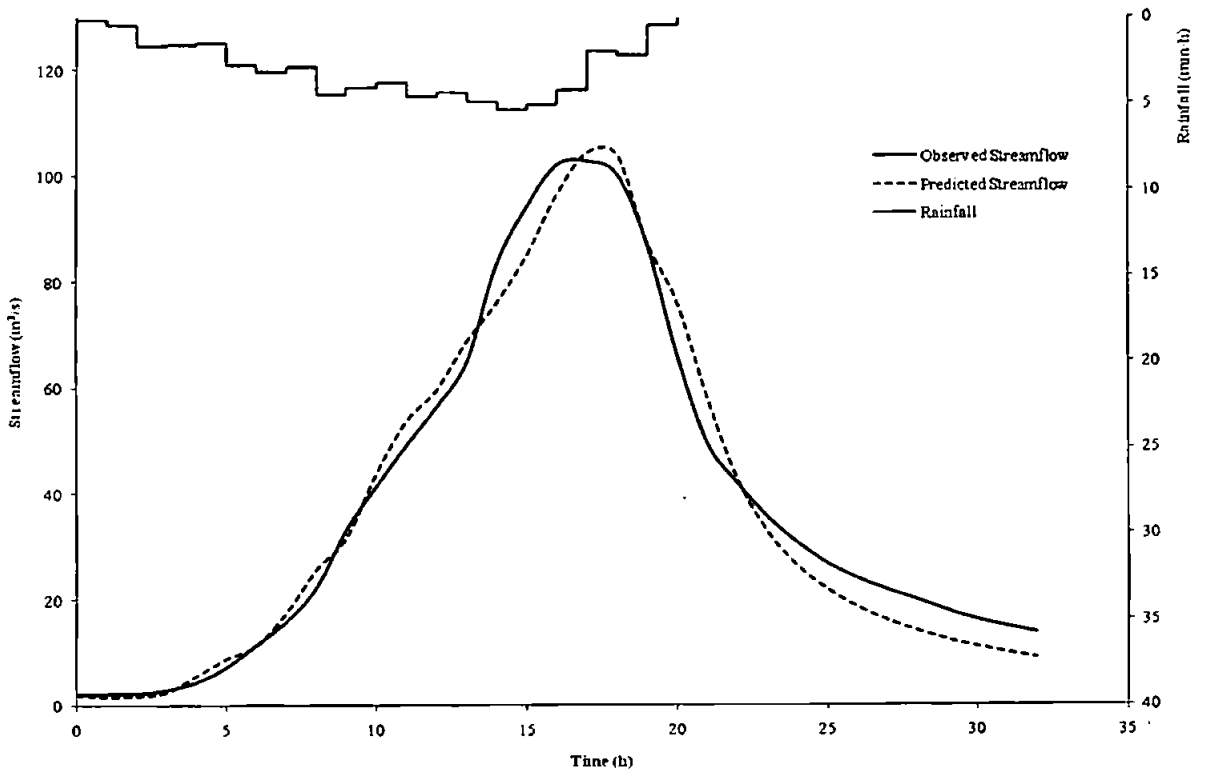
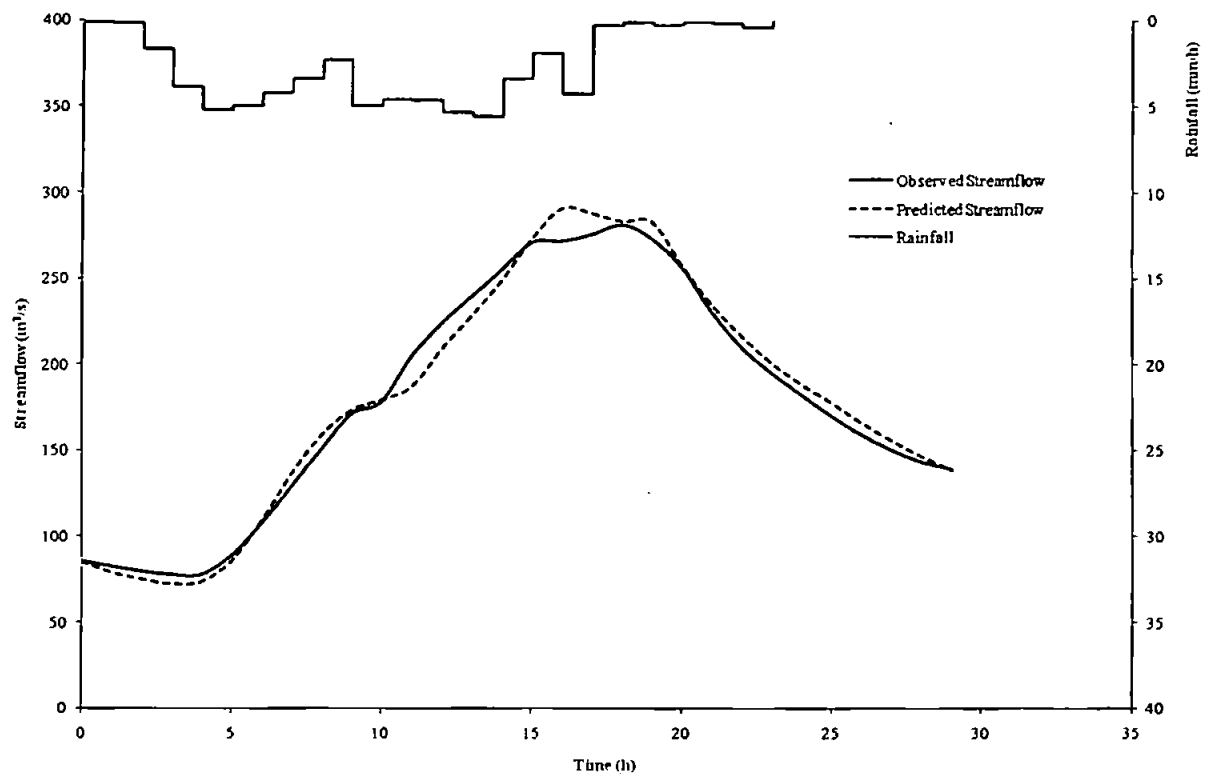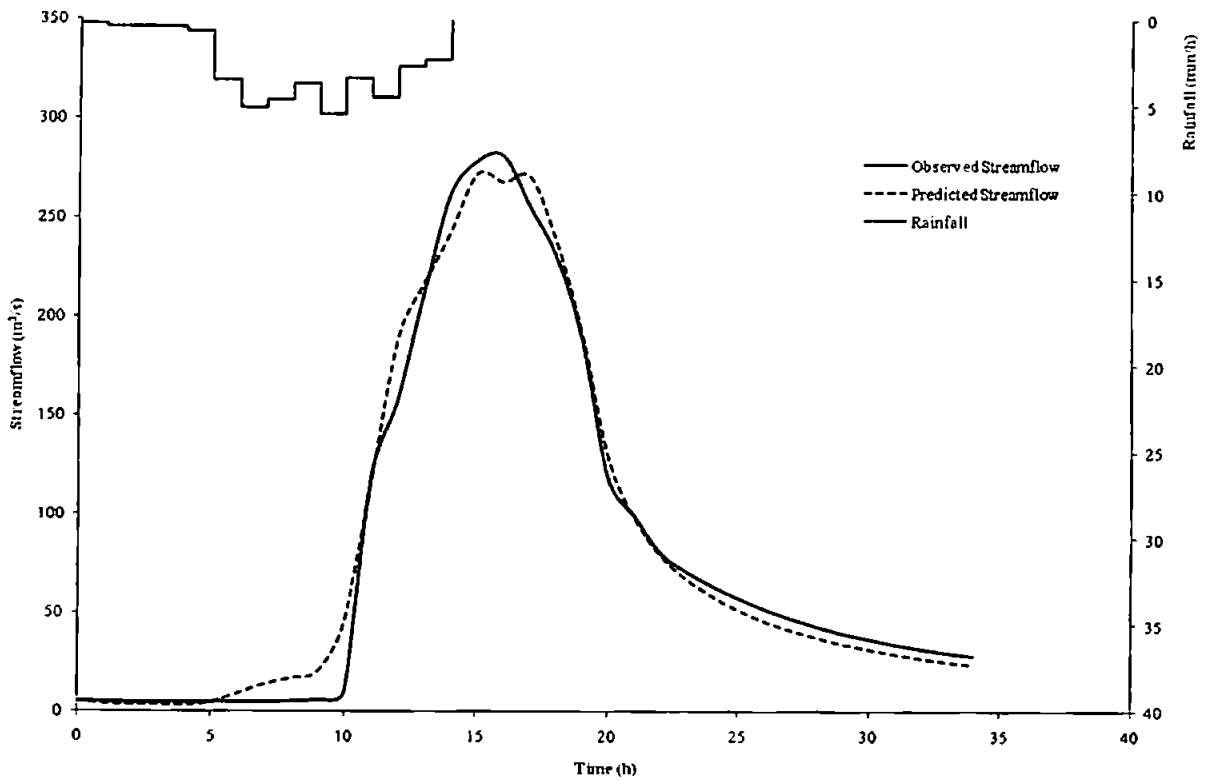**Figure C3.7 Predicted and observed results for event 2366**
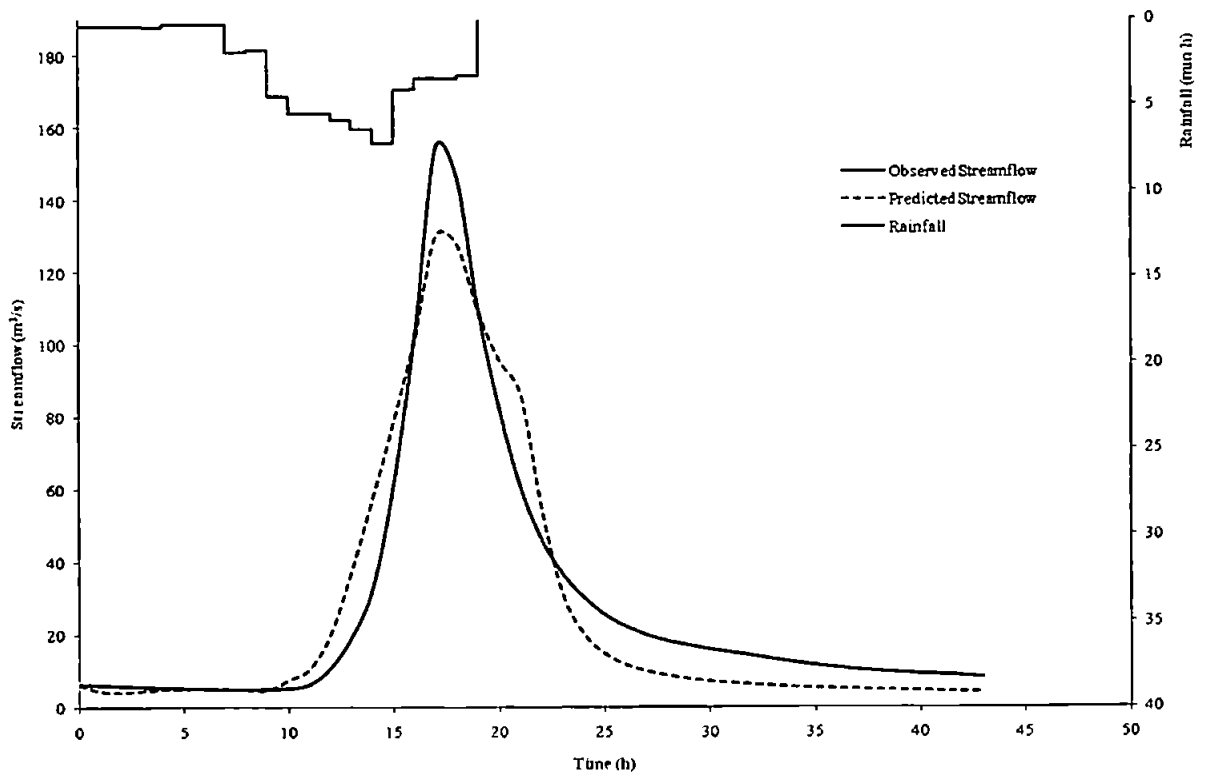
Figure C3.8 Predicted and observed results for event 2367

229

C4: Catchment 25005 – River Leven at Leven Bridge
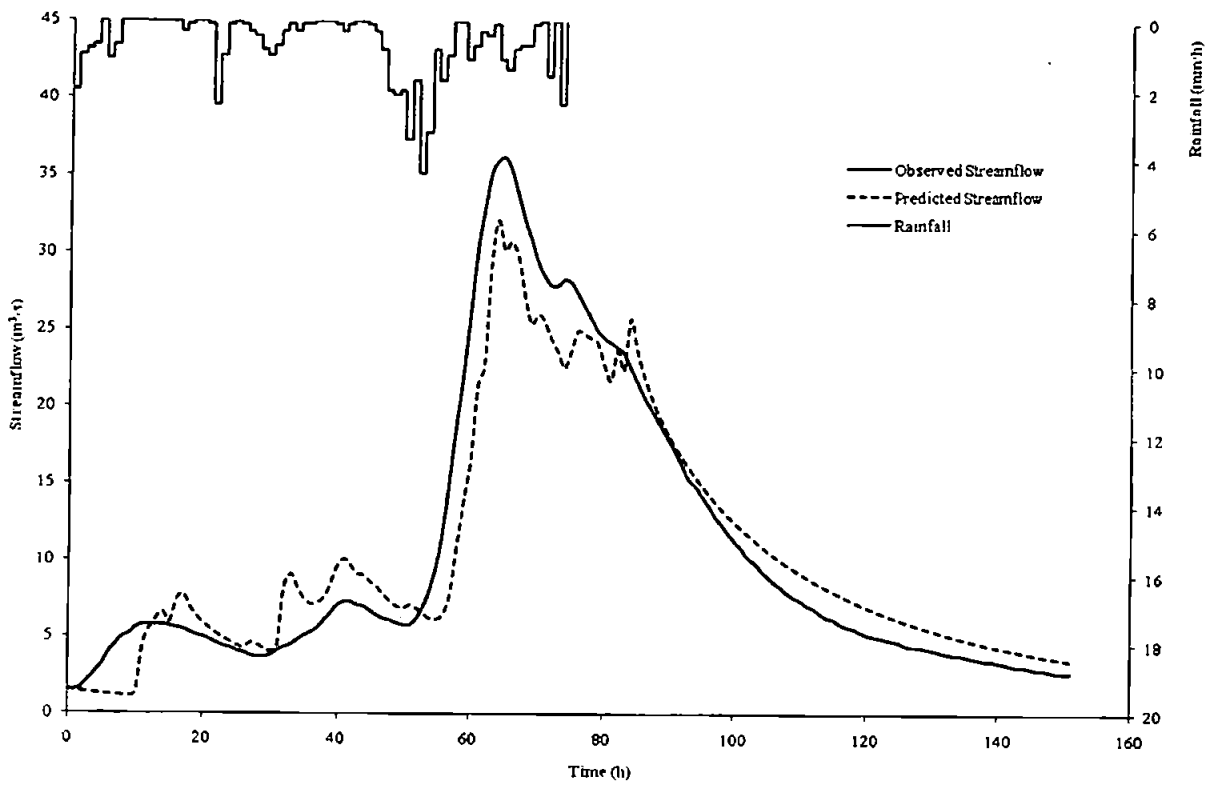
Figure C4.1 Predicted and observed results for event 3989
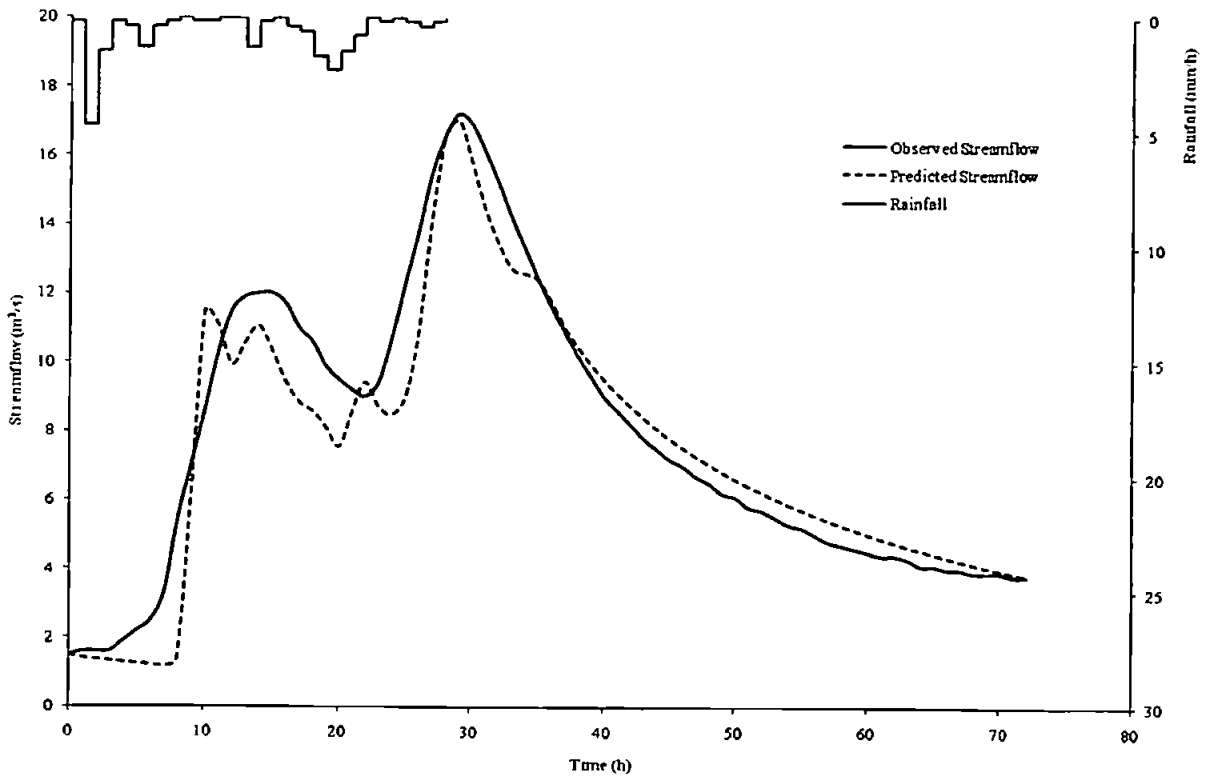
Figure C4.2 Predicted and observed results for event 3990
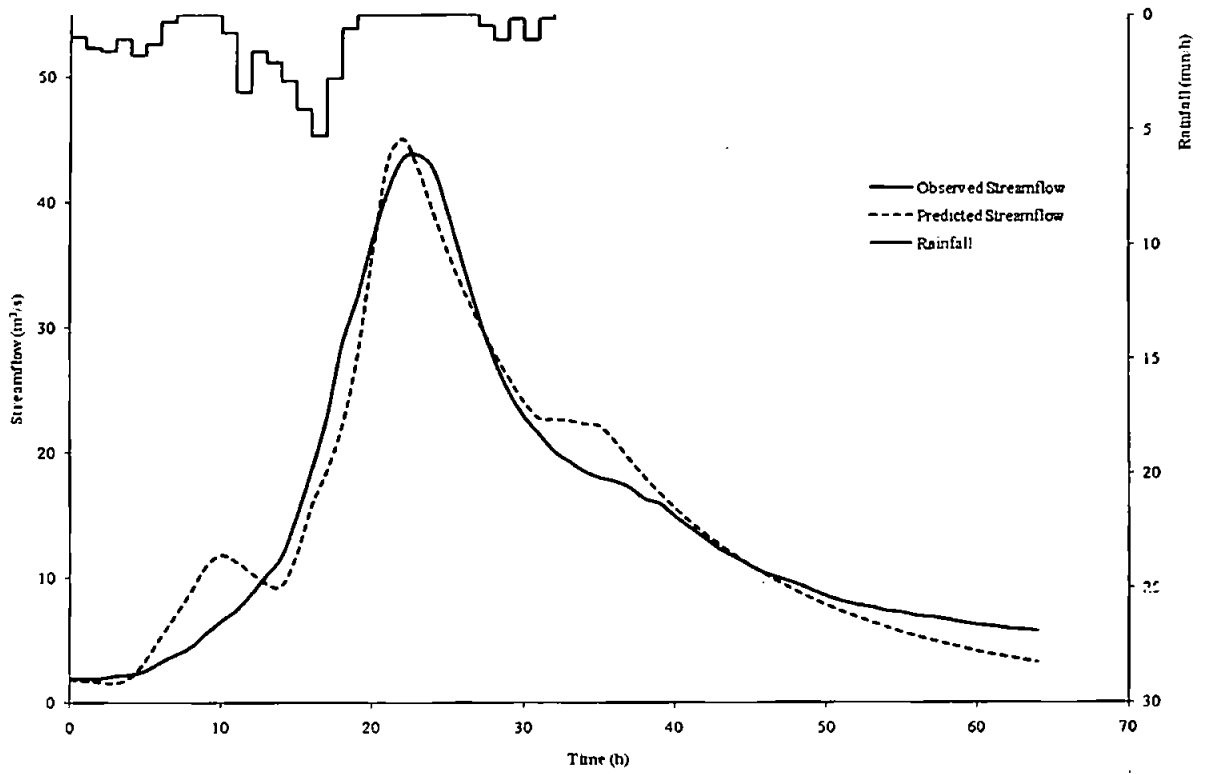
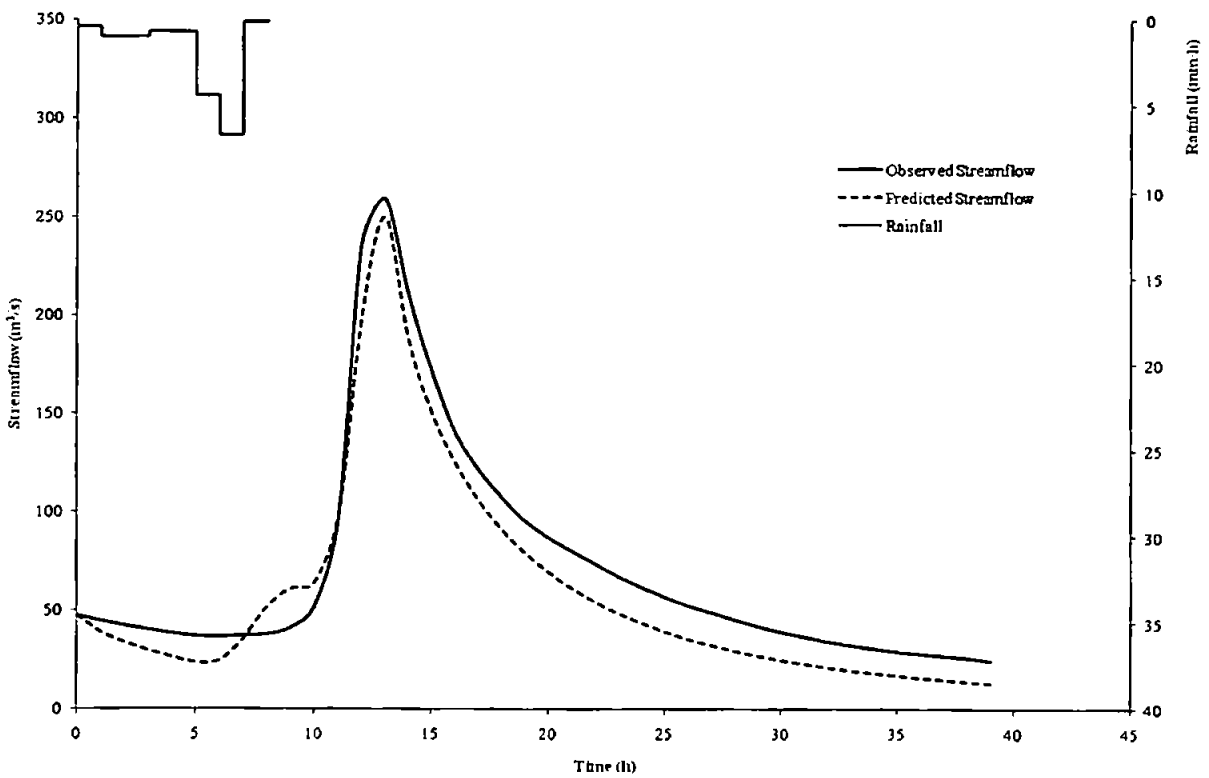**Figure C4.3 Predicted and observed results for event 3994**
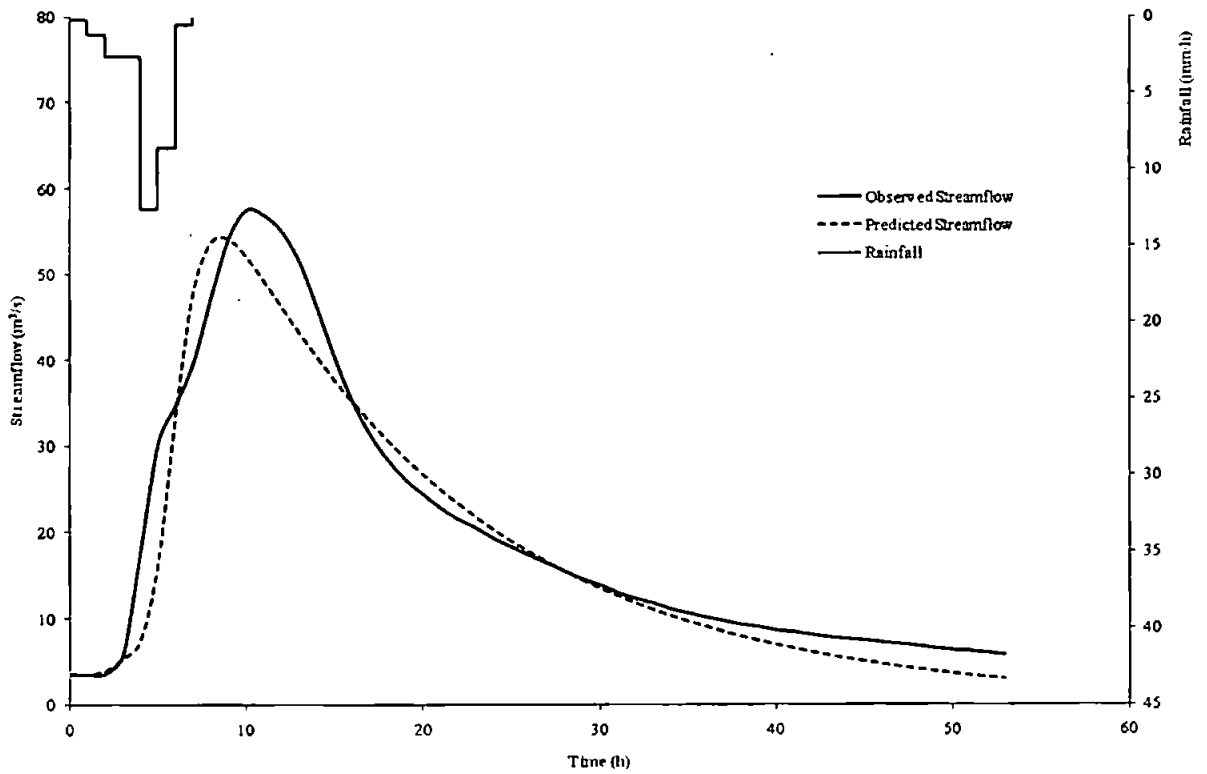
Figure C4.4 Predicted and observed results for event 3995

231
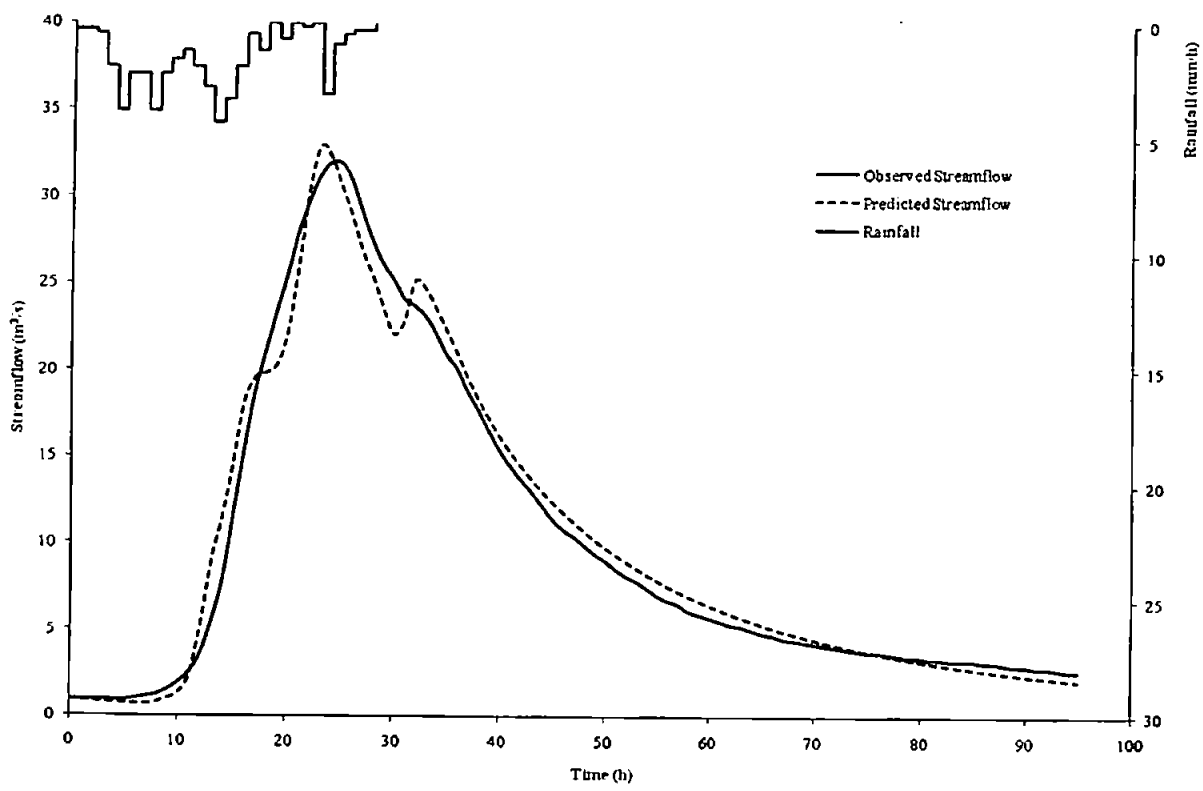
Figure C4.5 Predicted and observed results for event 3996
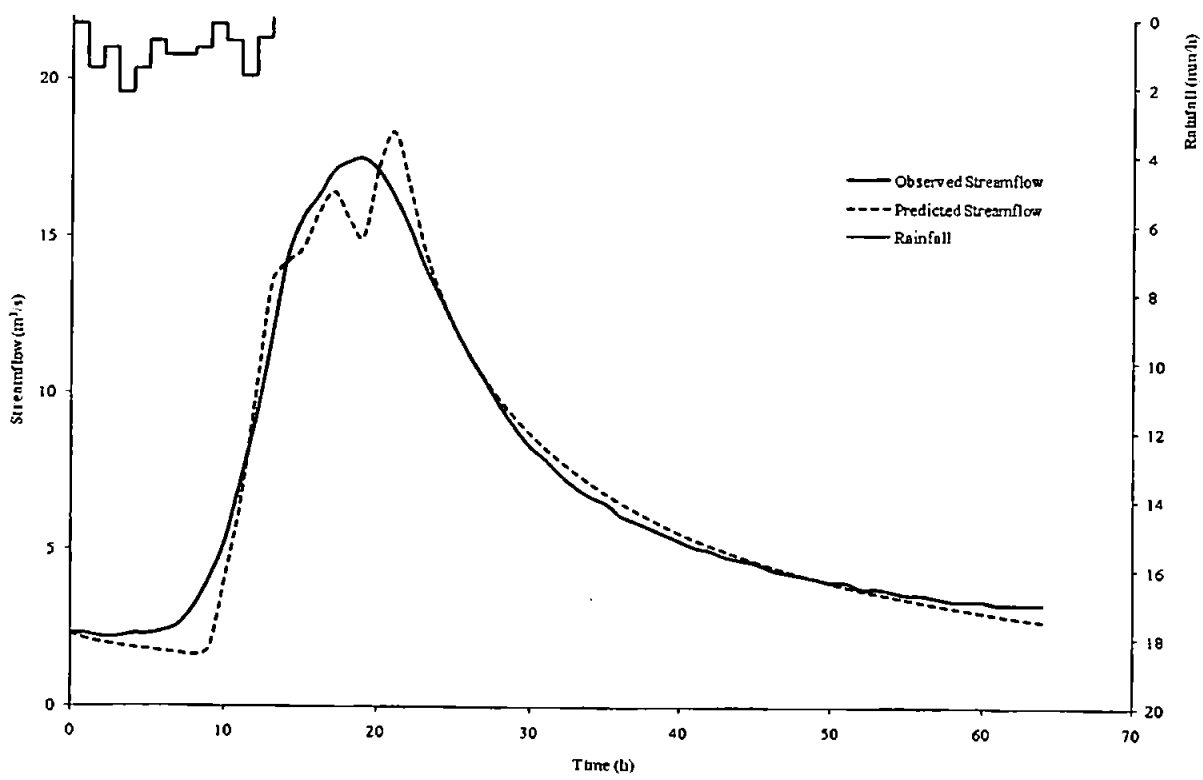
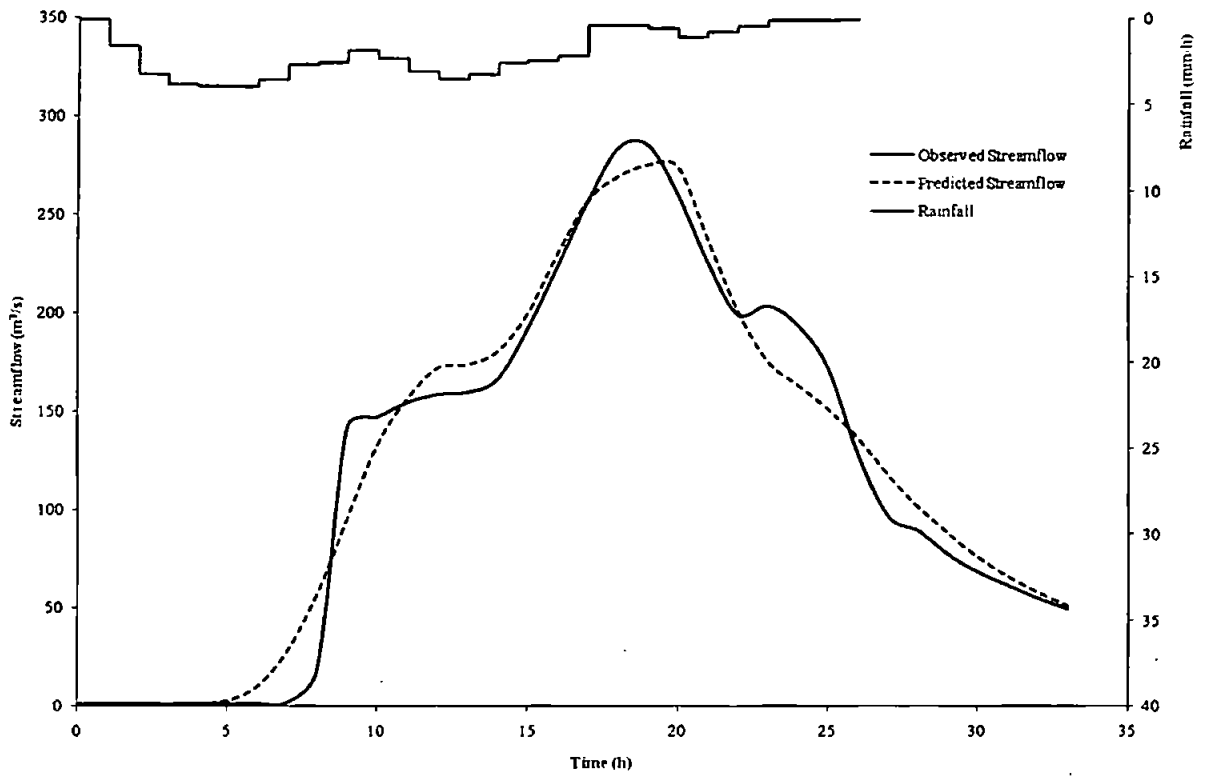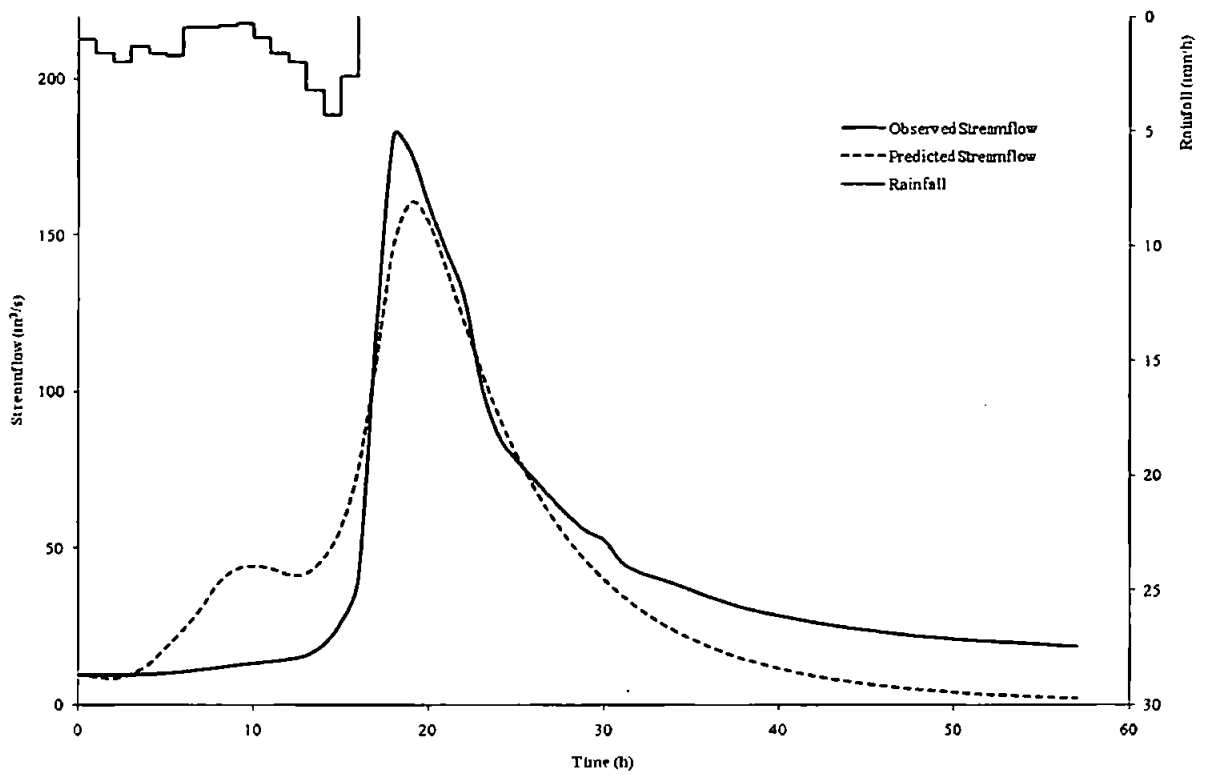**Figure C4.6 Predicted and observed results for event 3997**
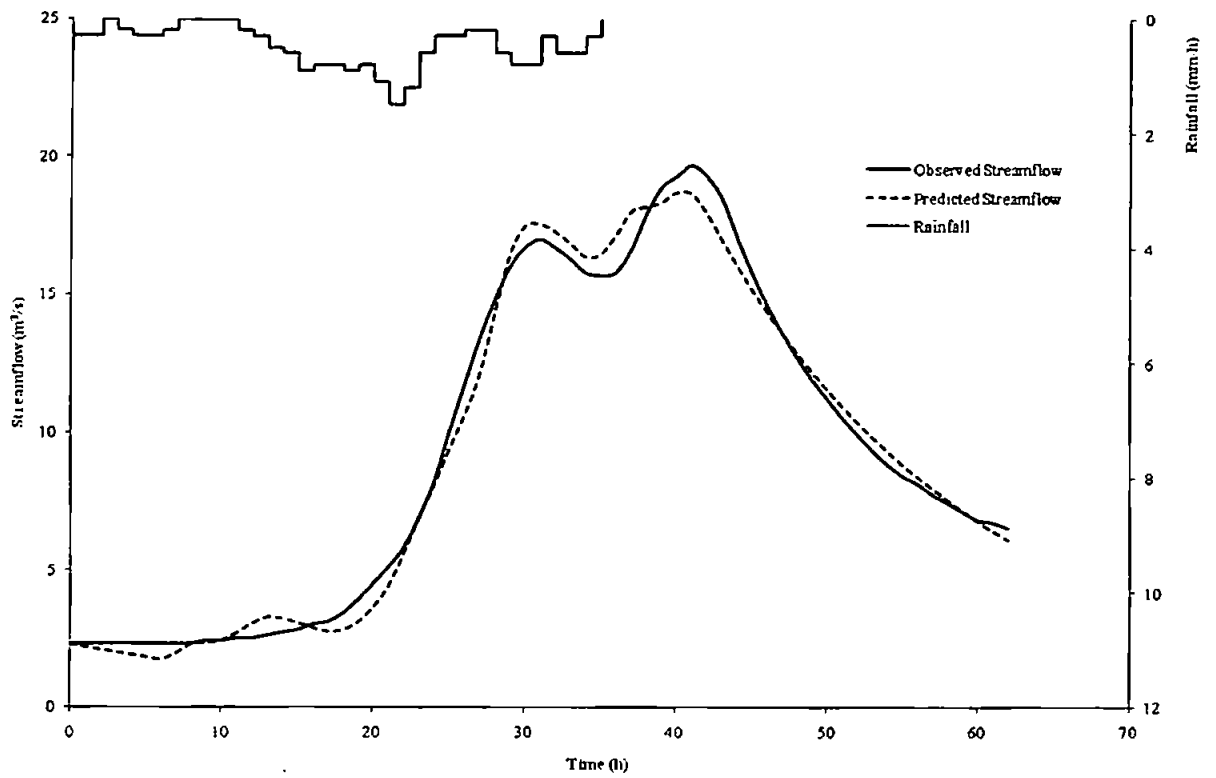
Figure C4.7 Predicted and observed results for event 3998
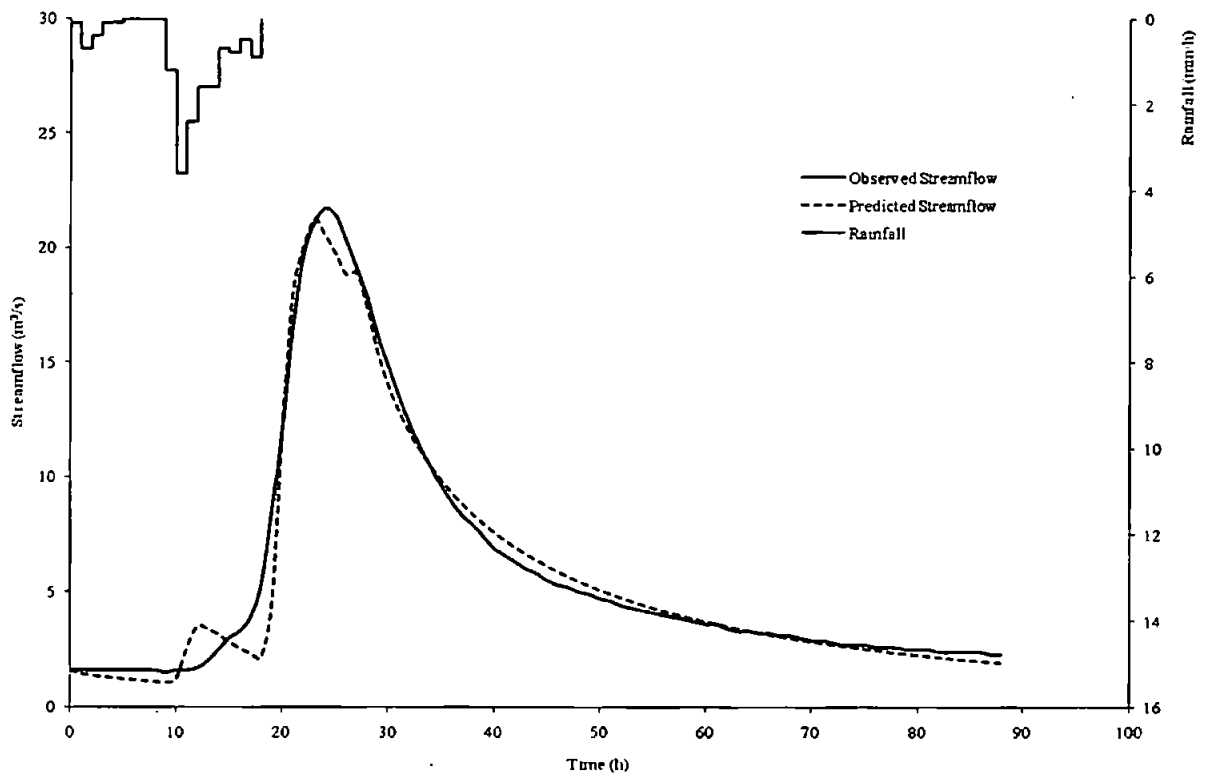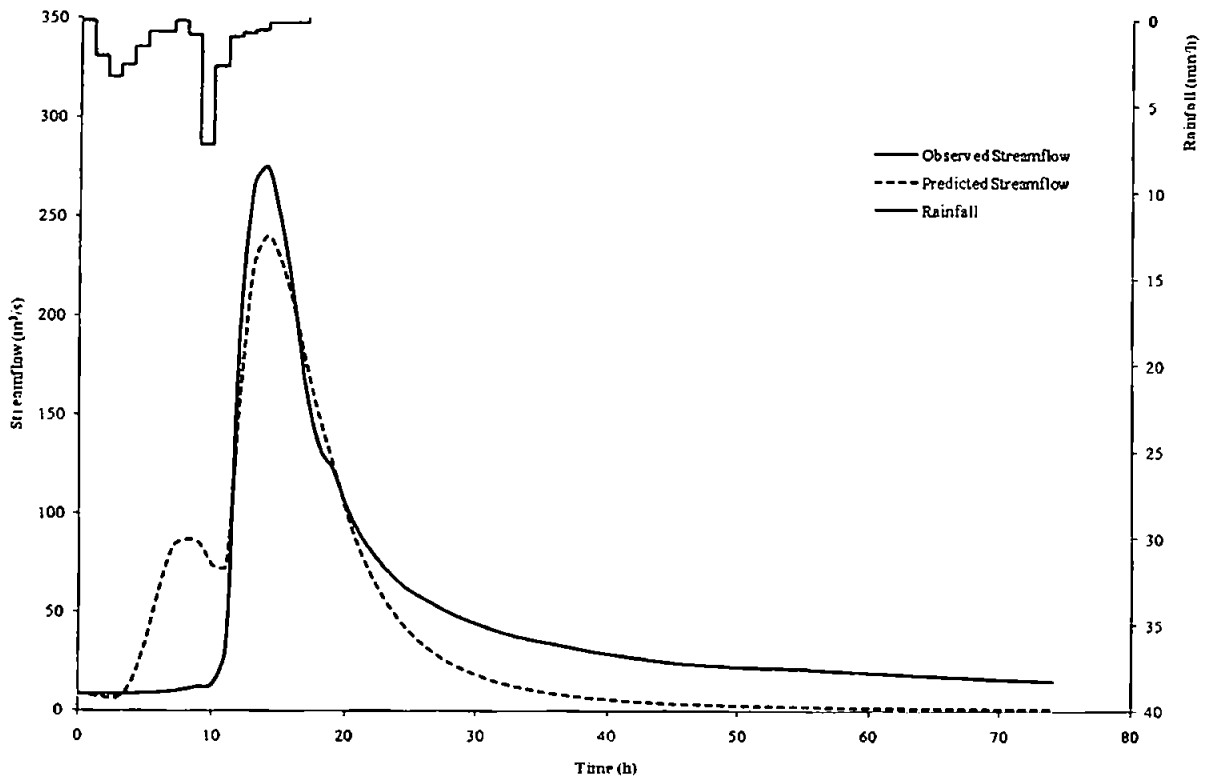

Figure C4.8 Predicted and observed results for event 3999
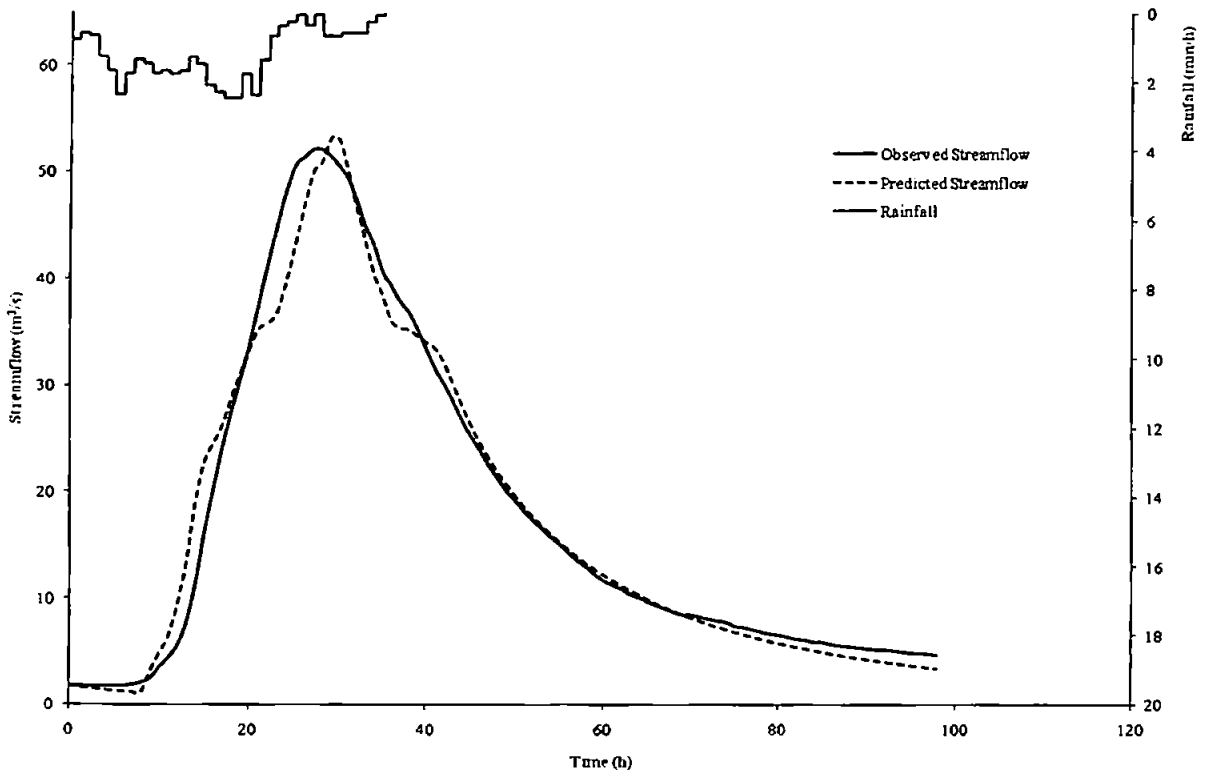
Figure C4.9 Predicted and observed results for event 4002
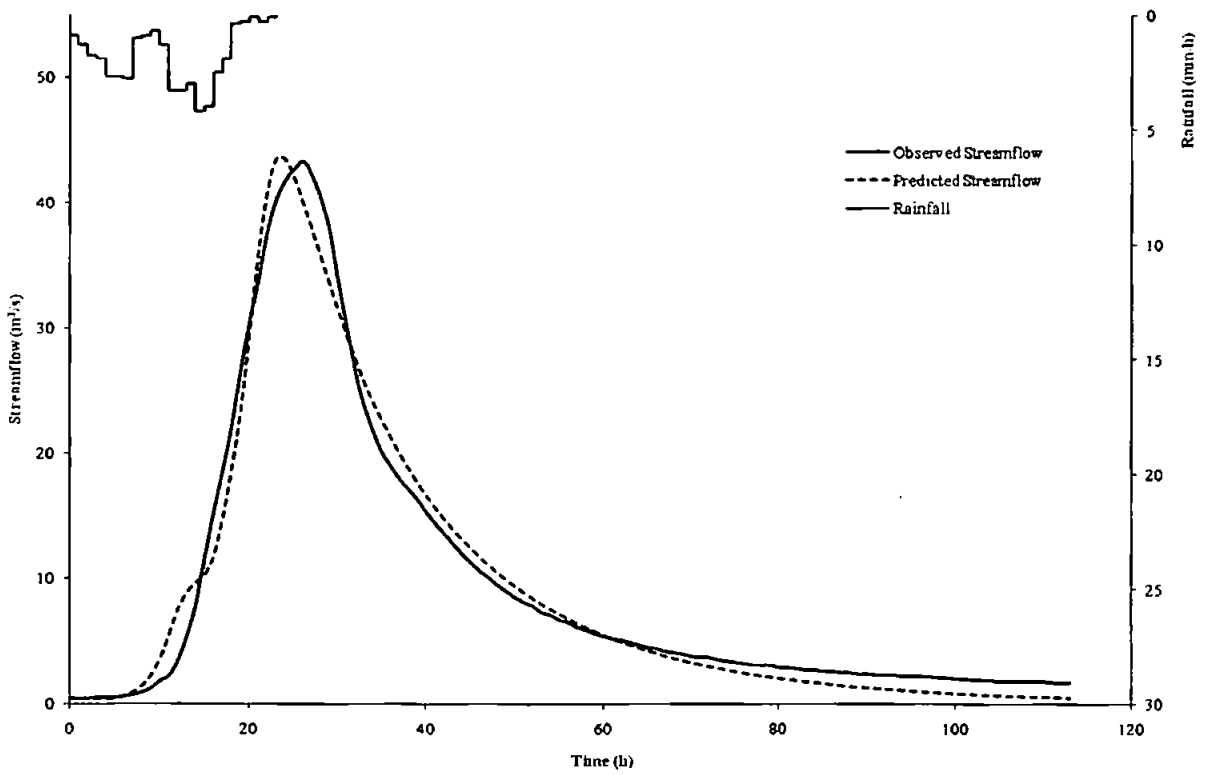
Figure C4.10 Predicted and observed results for event 4004

234
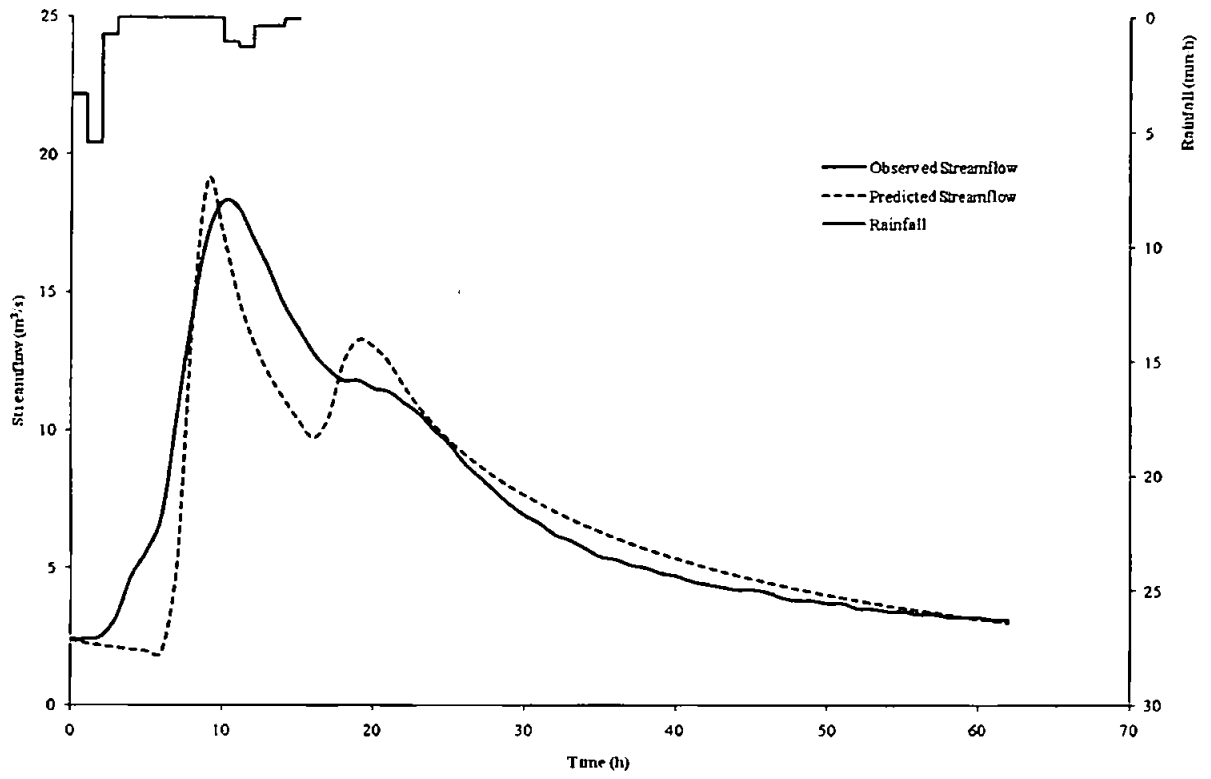
Figure C4.11 Predicted and observed results for event 4018
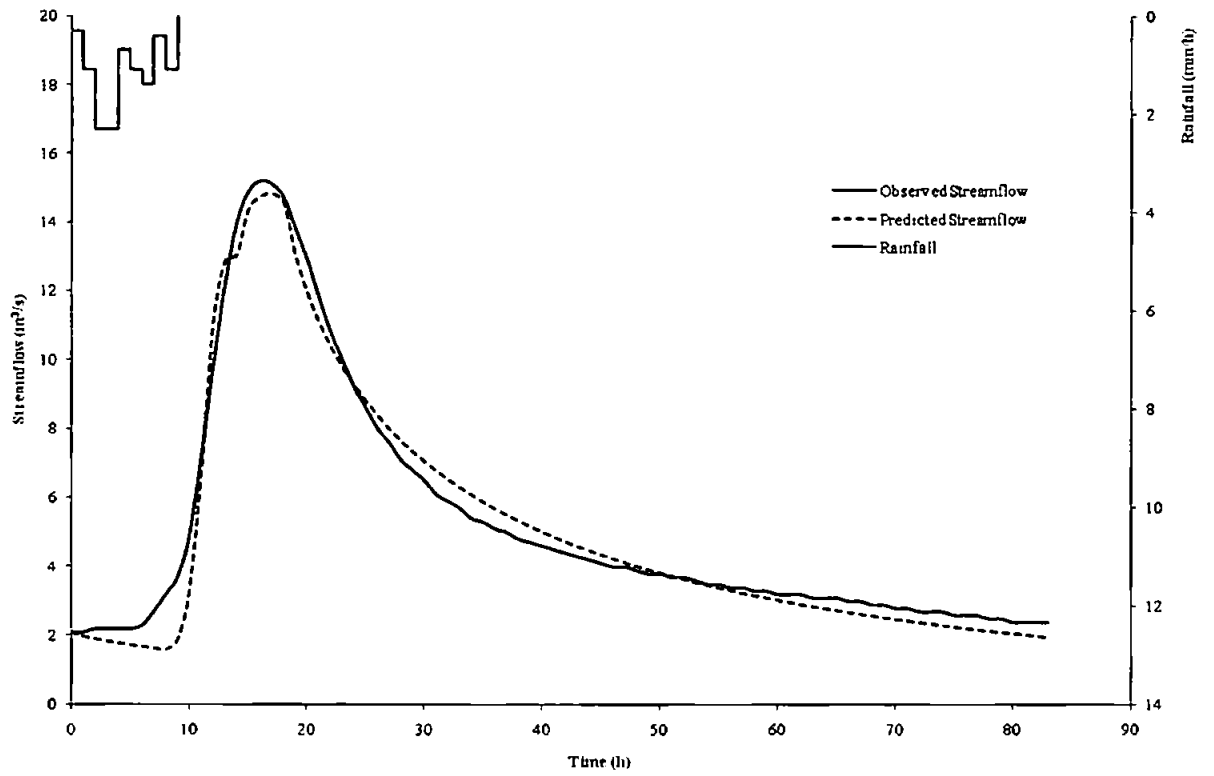
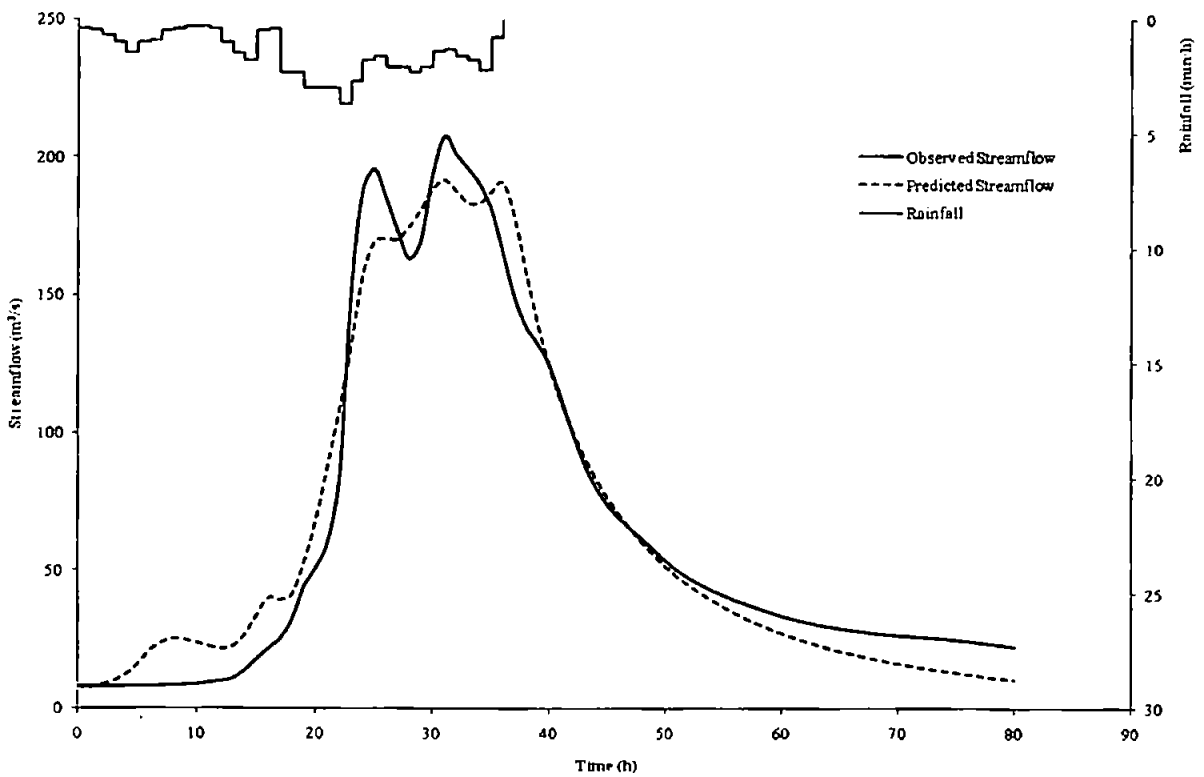**Figure C4.12 Predicted and observed results for event 4393**

235
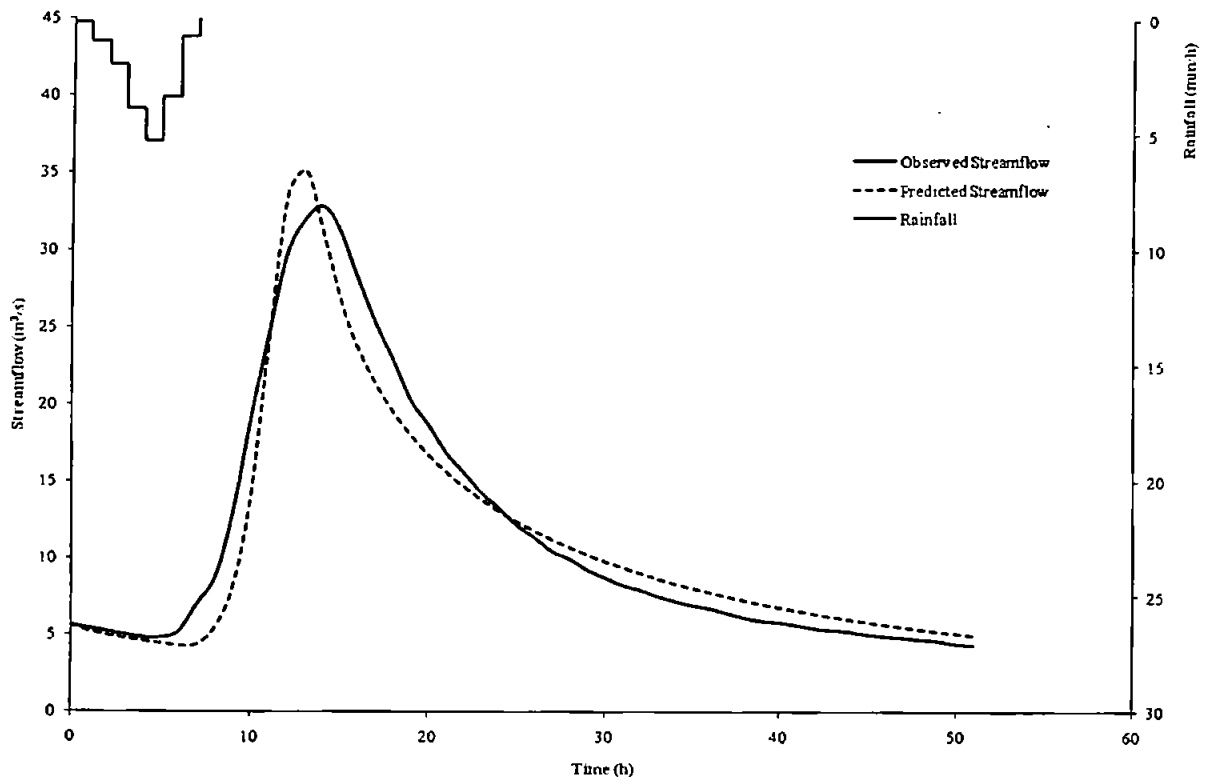
Figure C4.13 Predicted and observed results for event 4395
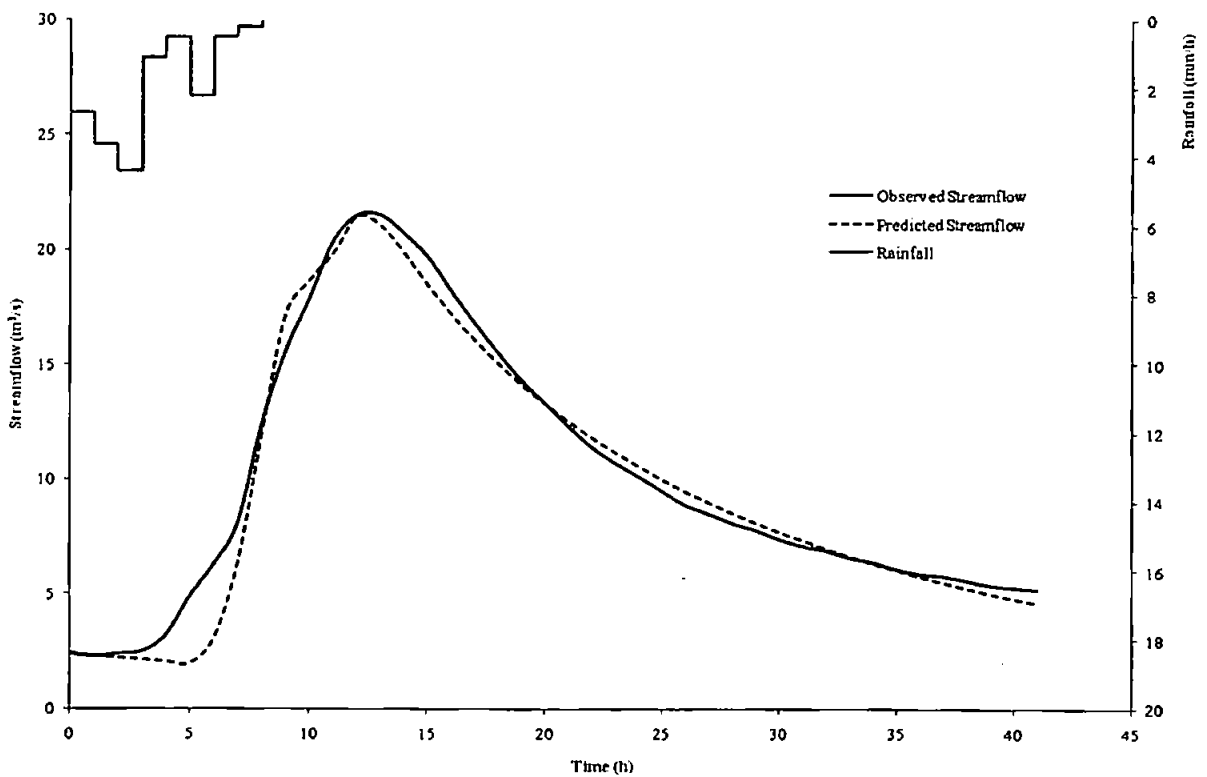
Figure C4.14 Predicted and observed results for event 4399
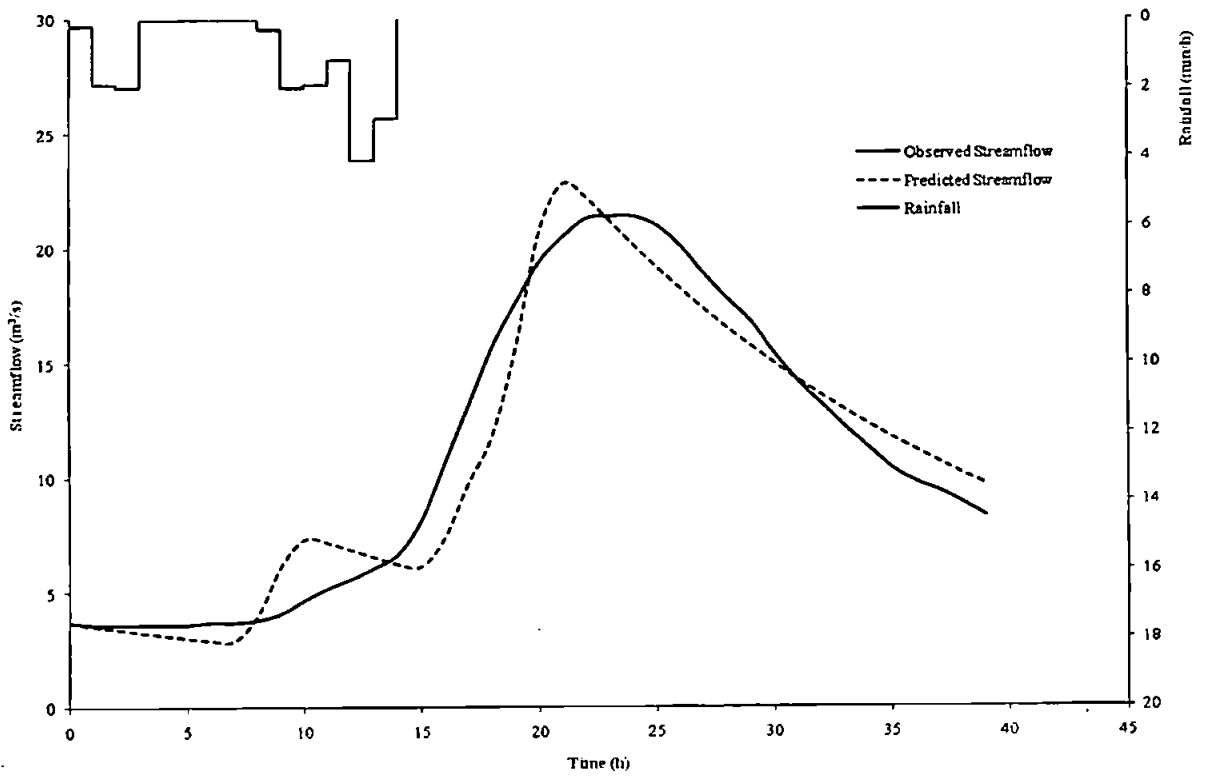
Figure C4.15 Predicted and observed results for event 4401

C5: Catchment 54004 – River Sowe at Stoneleigh
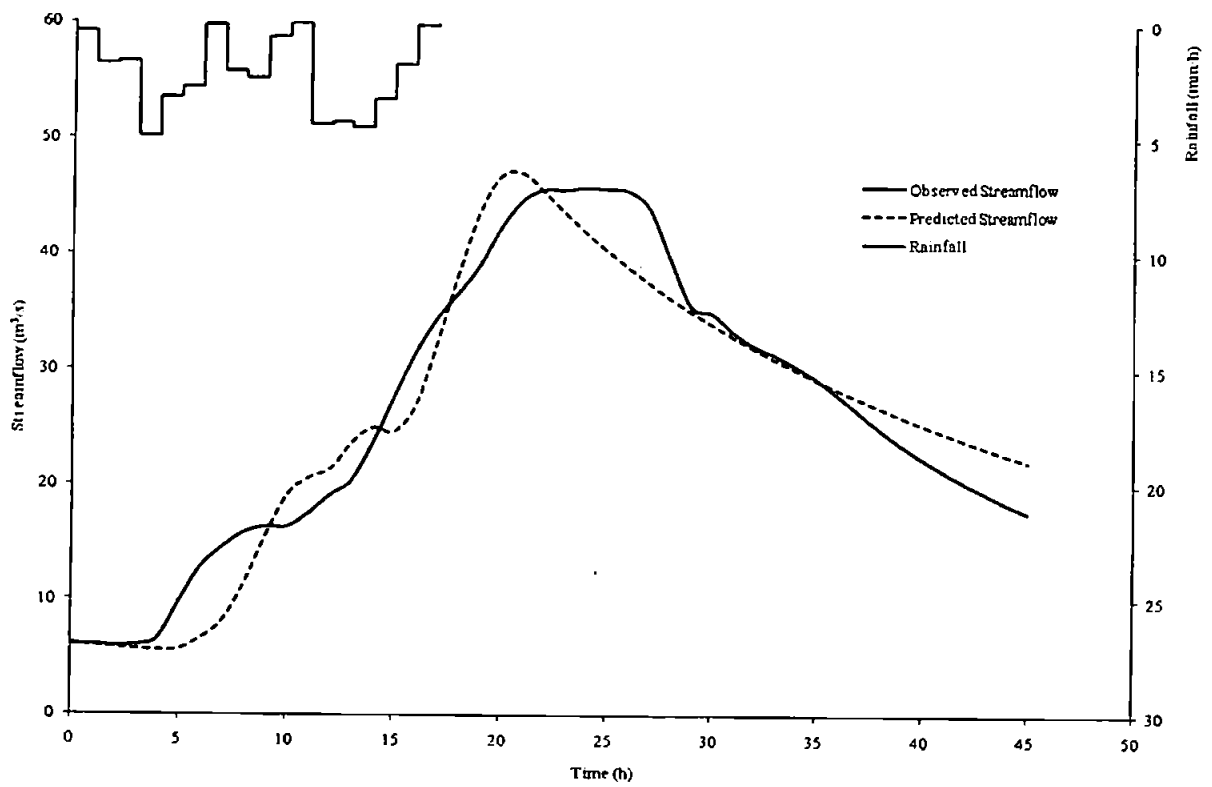
Figure C5.1 Predicted and observed results for event 1559
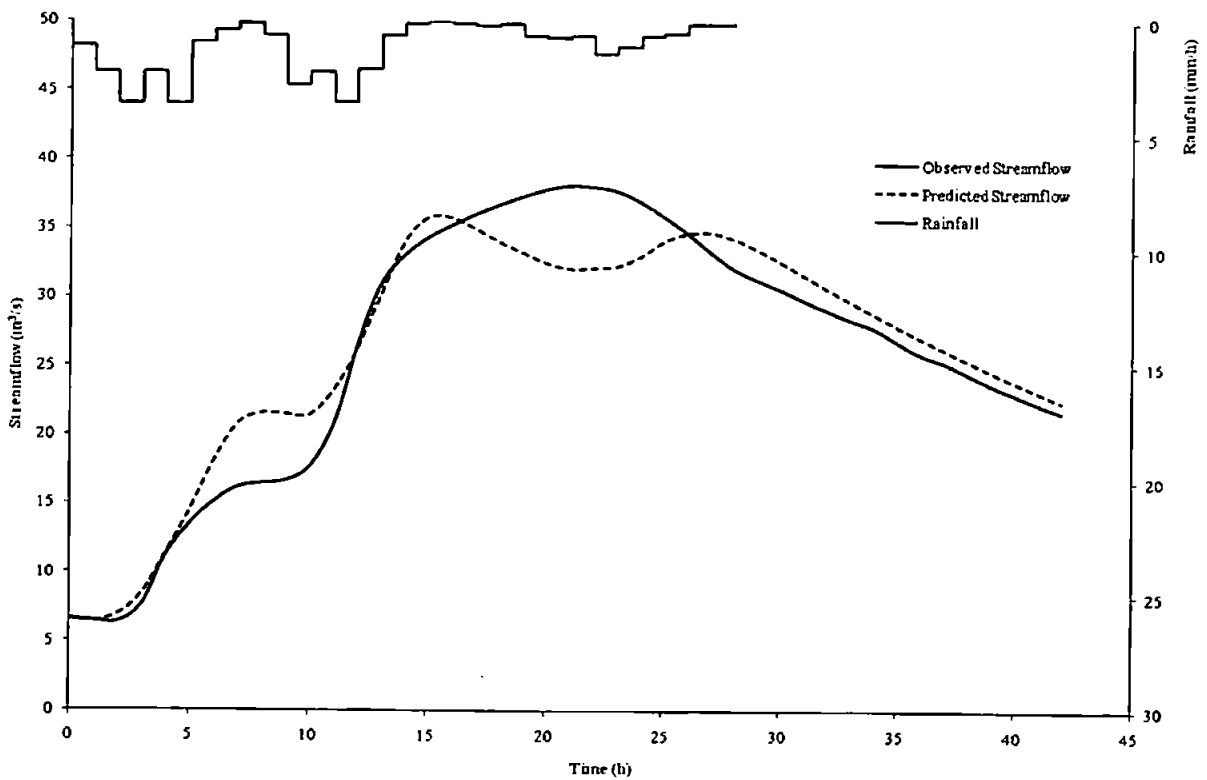
Figure C5.2 Predicted and observed results for event 1560

238
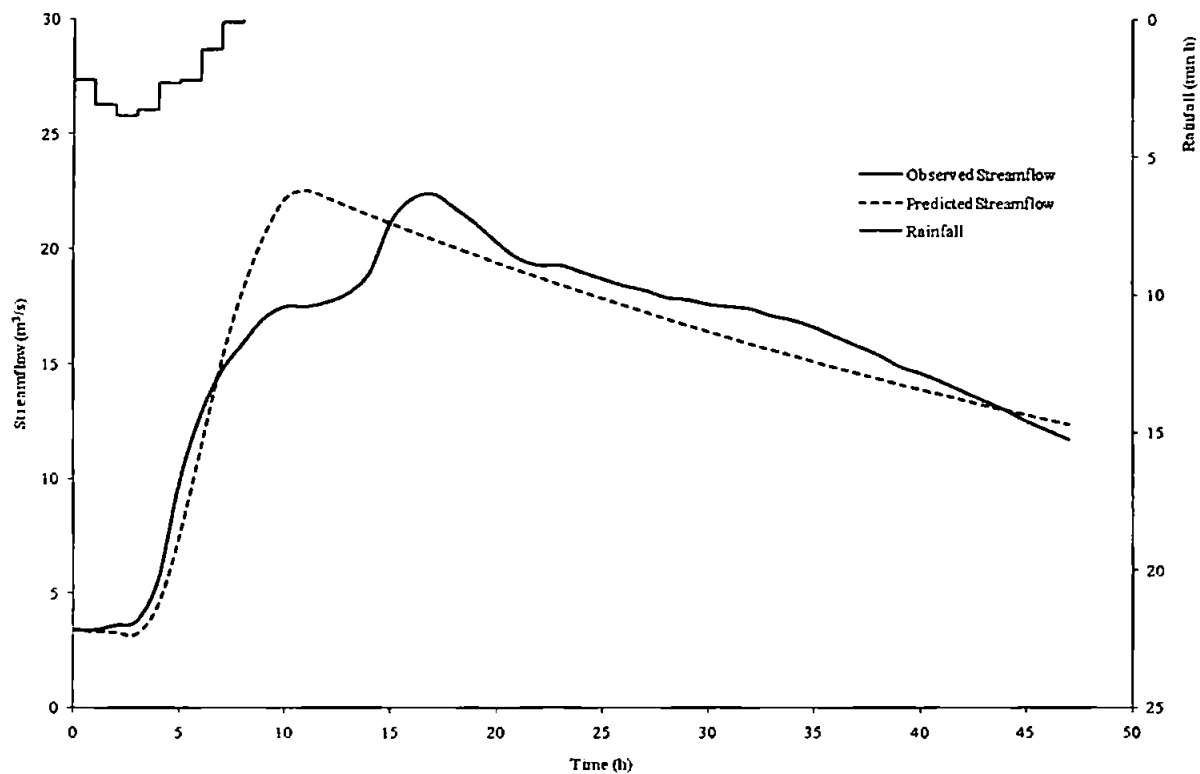
Figure C5.3 Predicted and observed results for event 1561
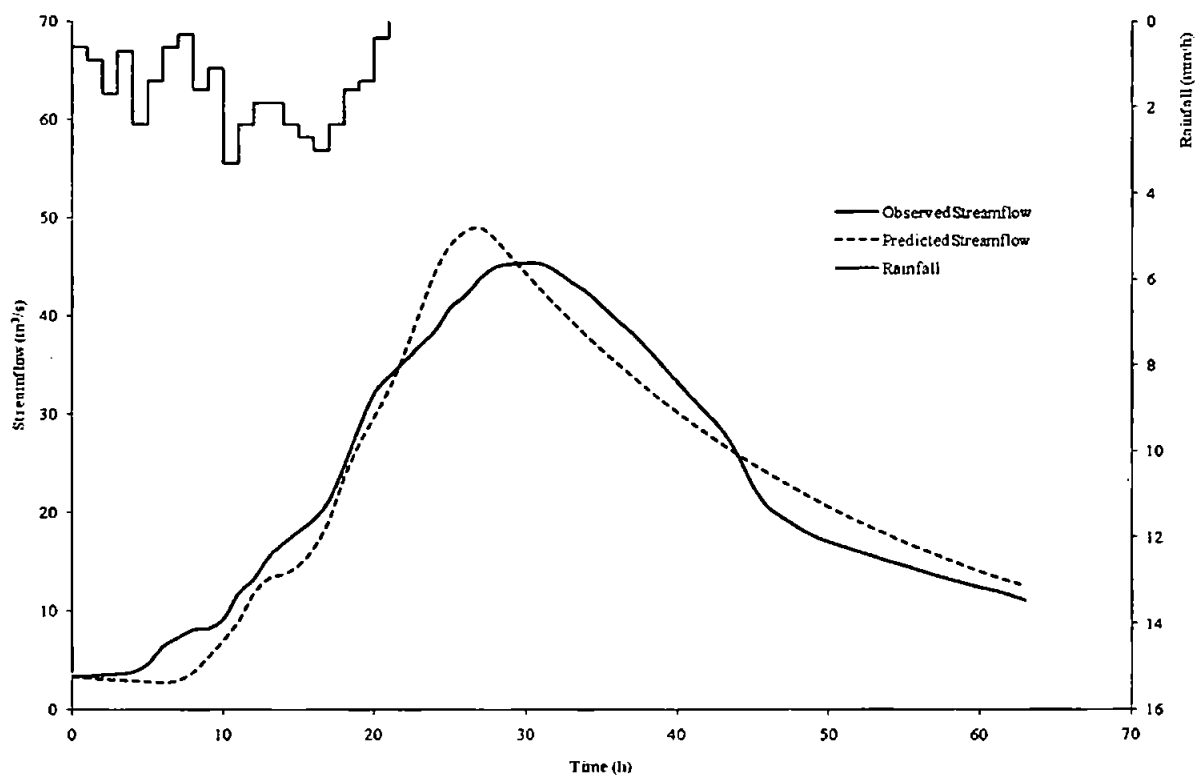
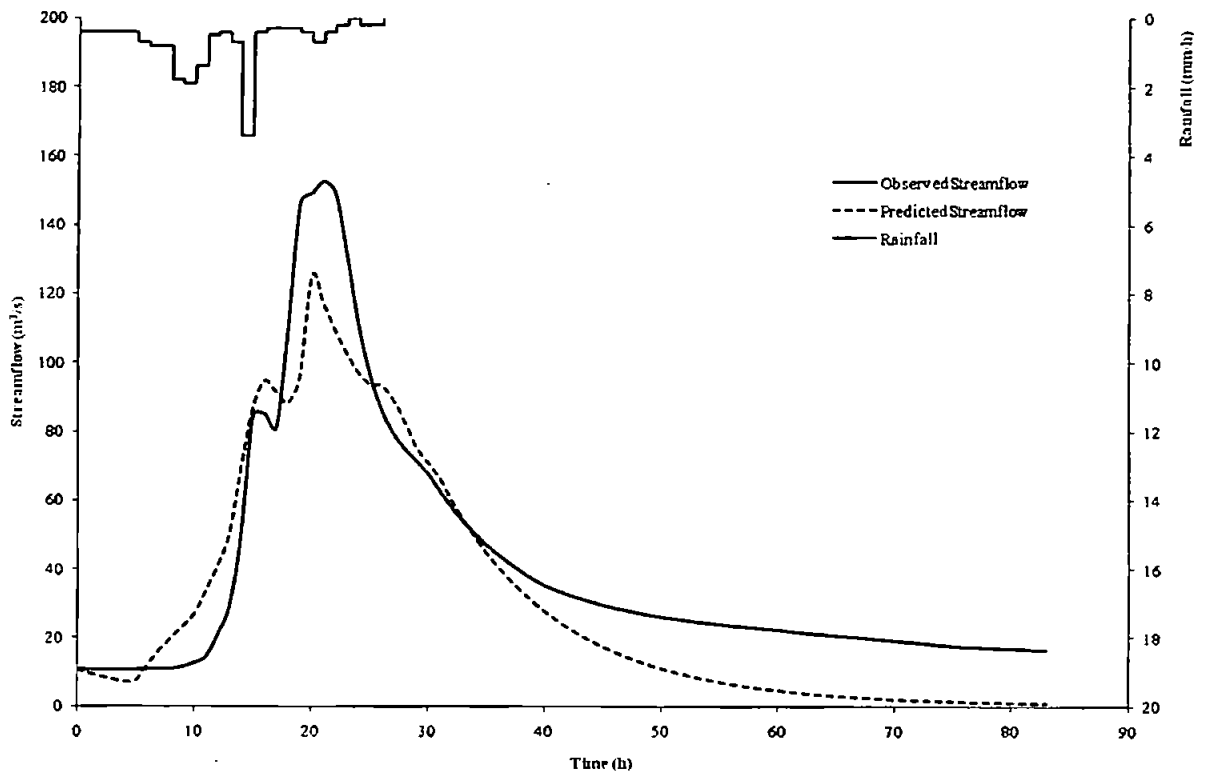**Figure C5.4 Predicted and observed results for event 1562**

239
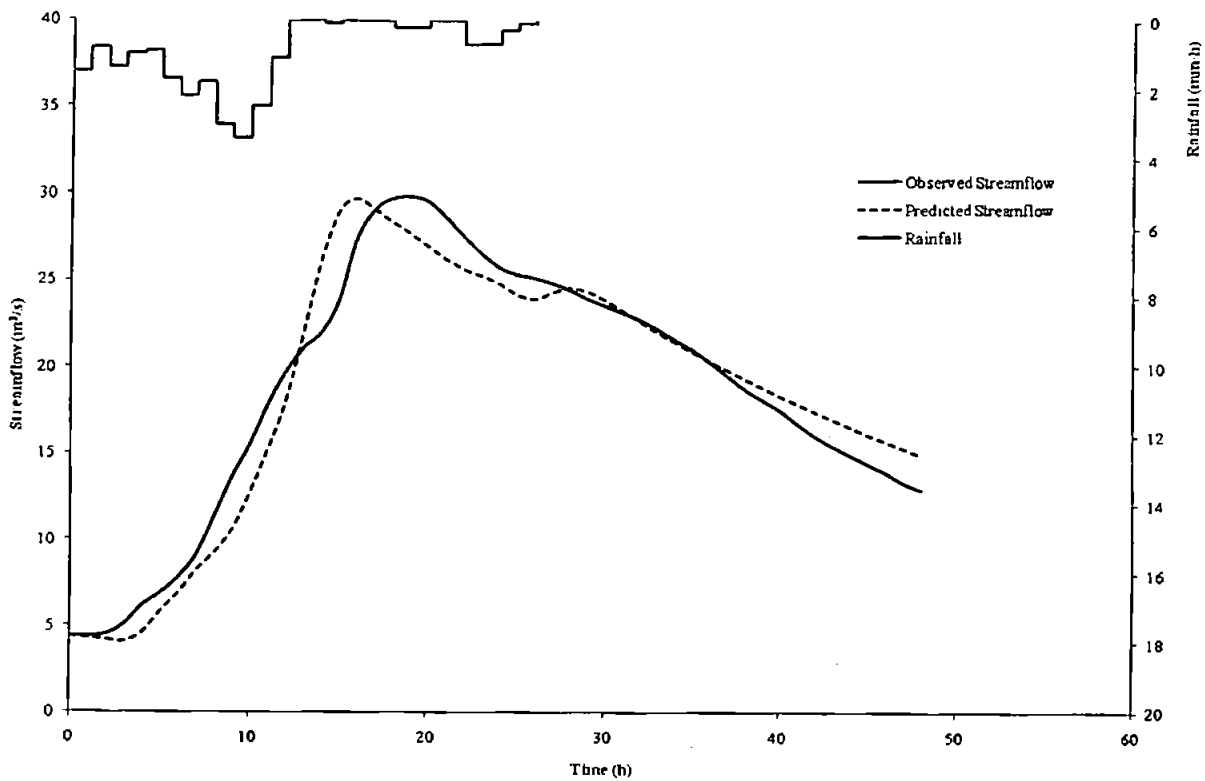
Figure C5.5 Predicted and observed results for event 1563
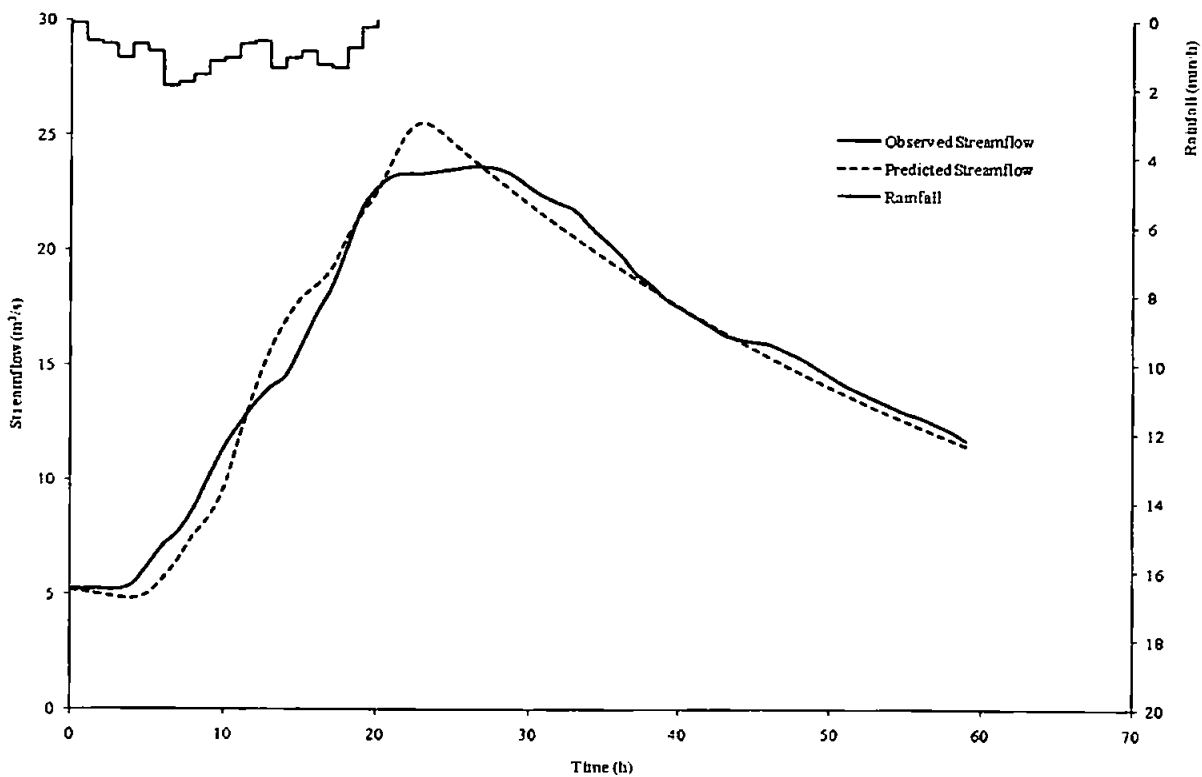
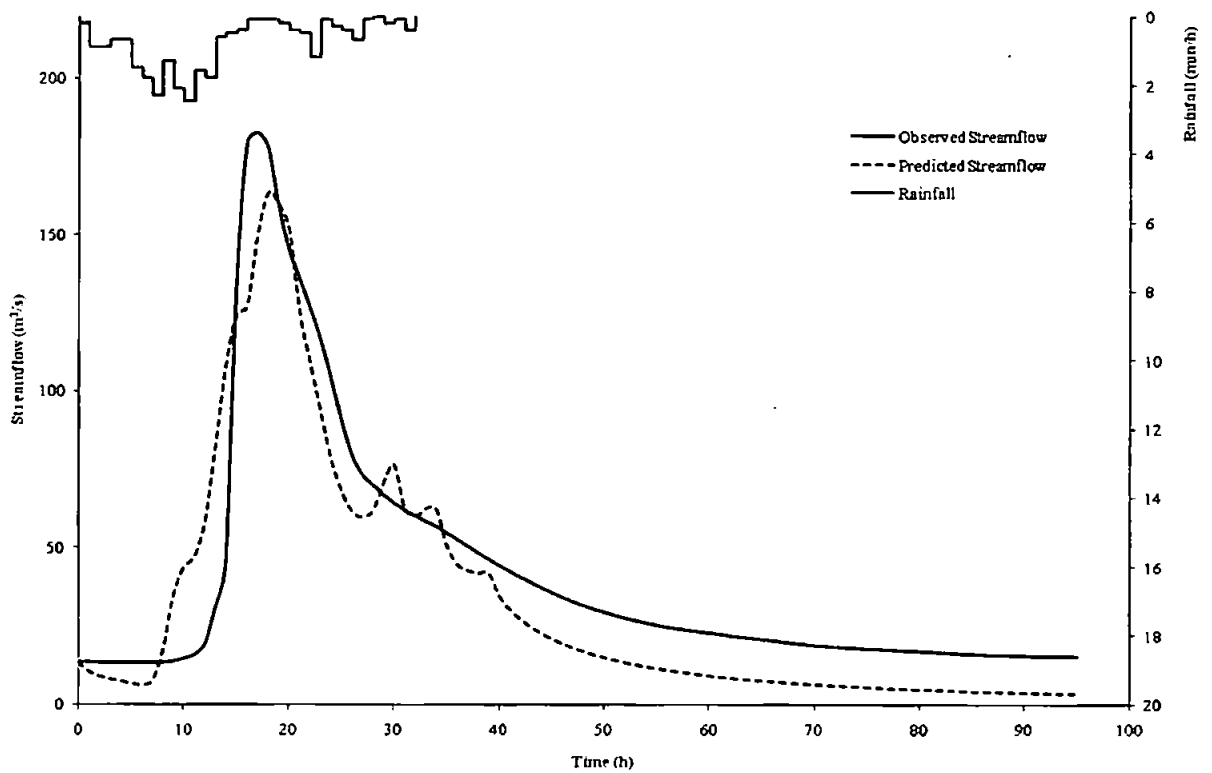

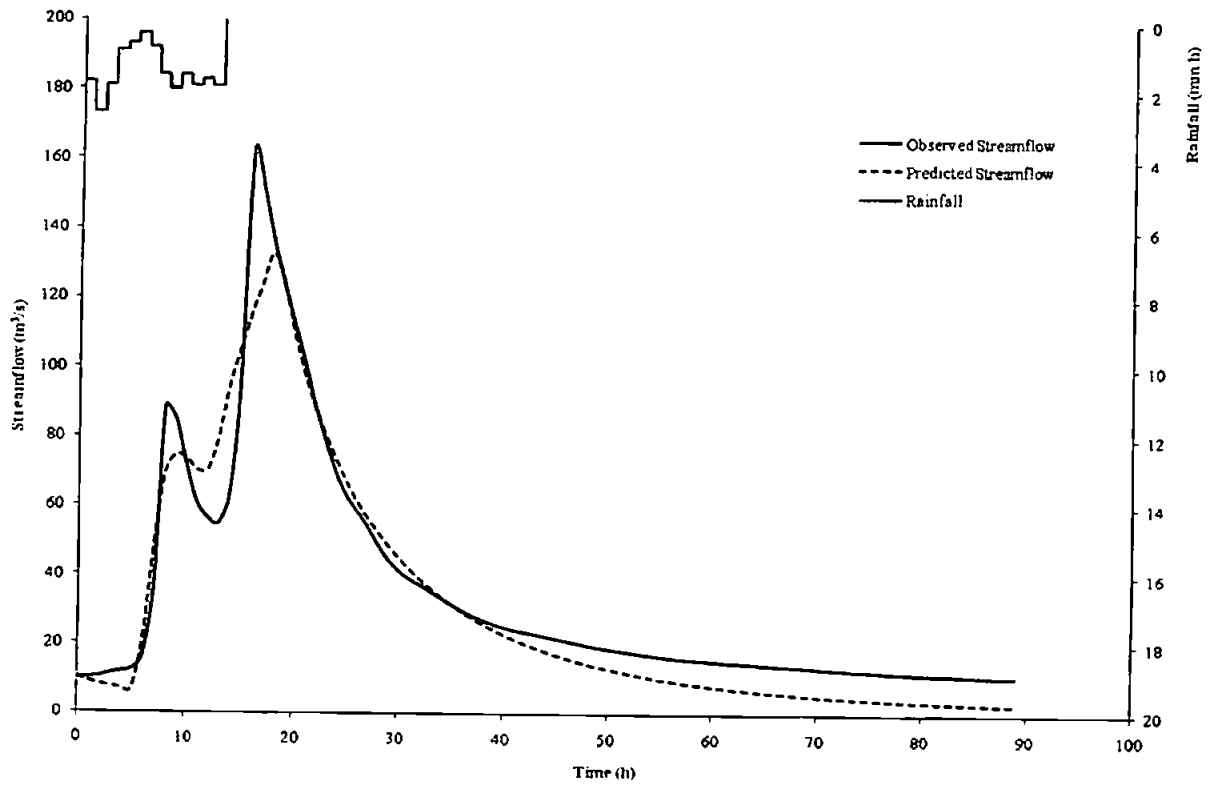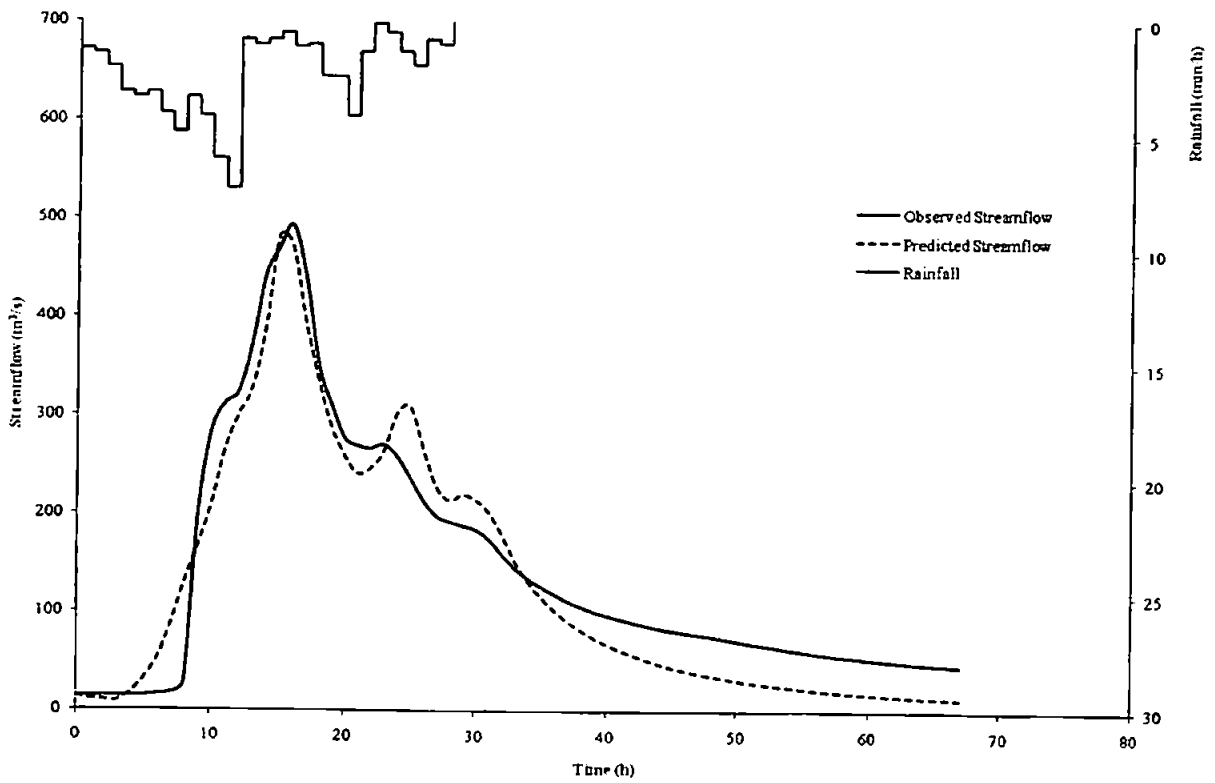**Figure C5.6 Predicted and observed results for event 1564**
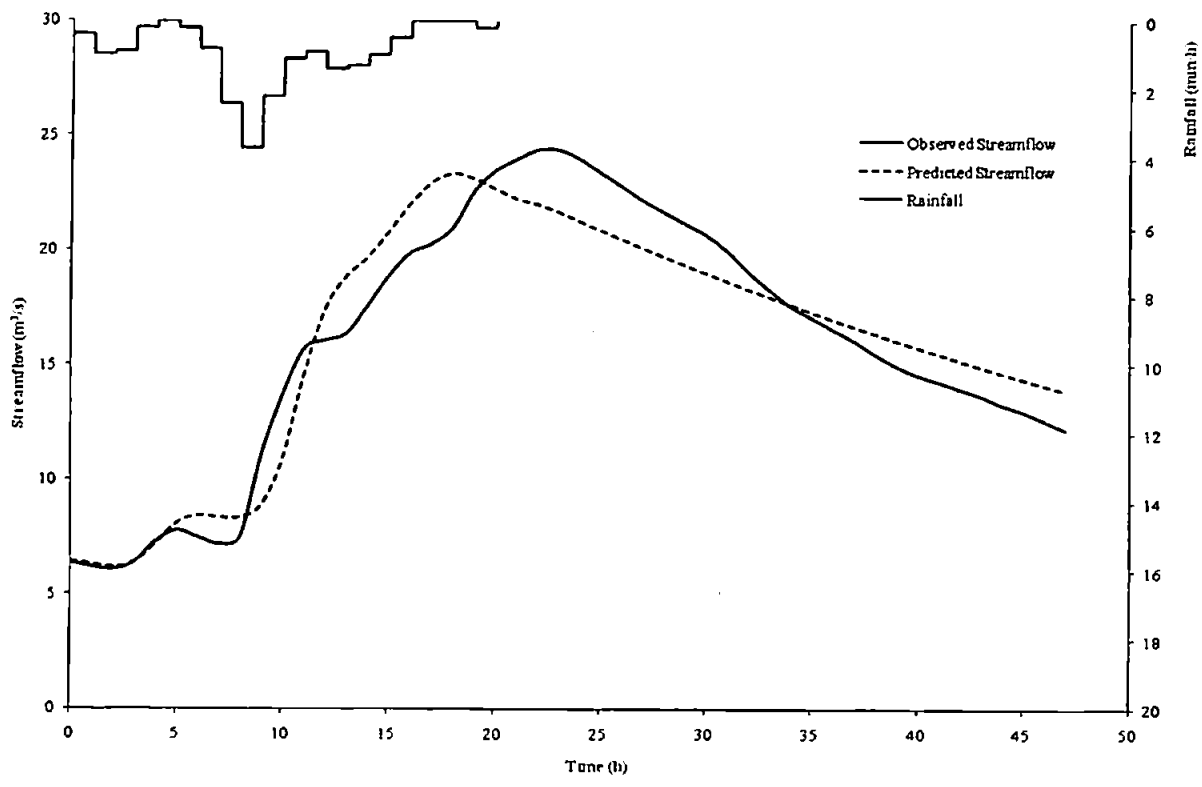
Figure C5.7 Predicted and observed results for event 1567
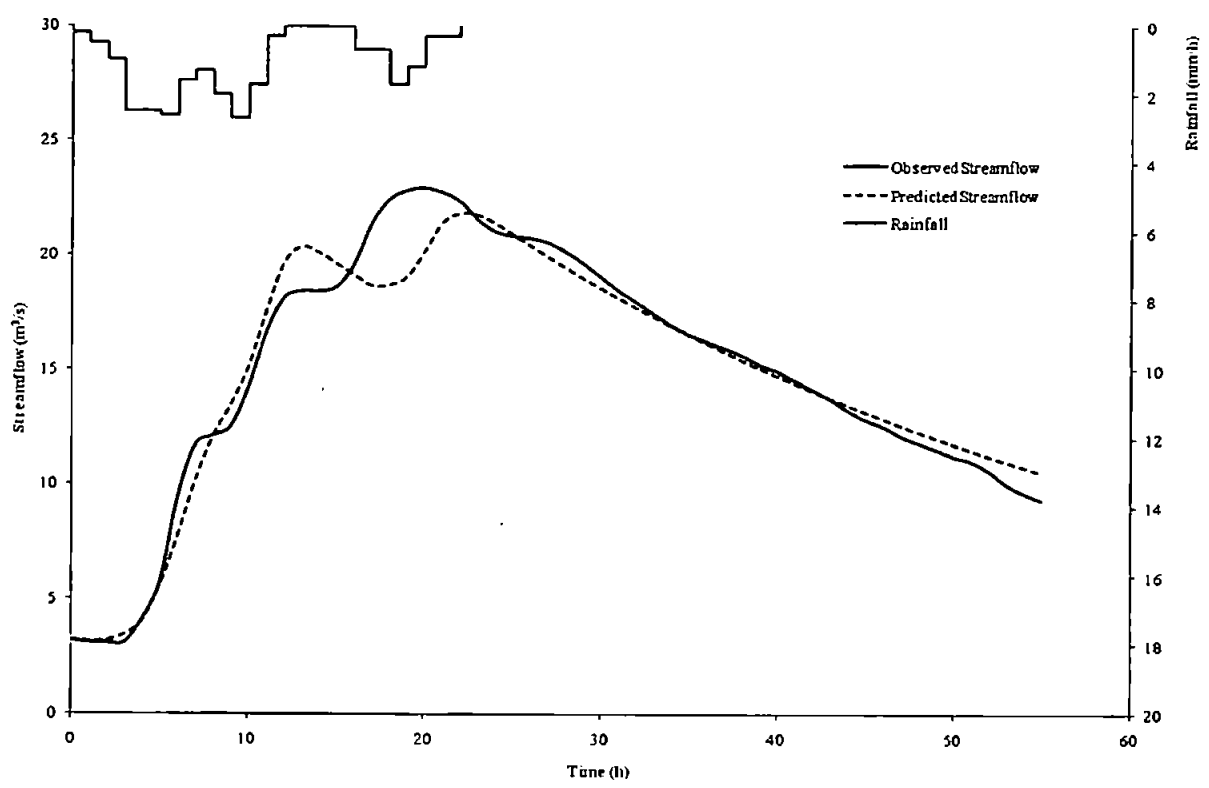
Figure C5.8 Predicted and observed results for event 1568

241
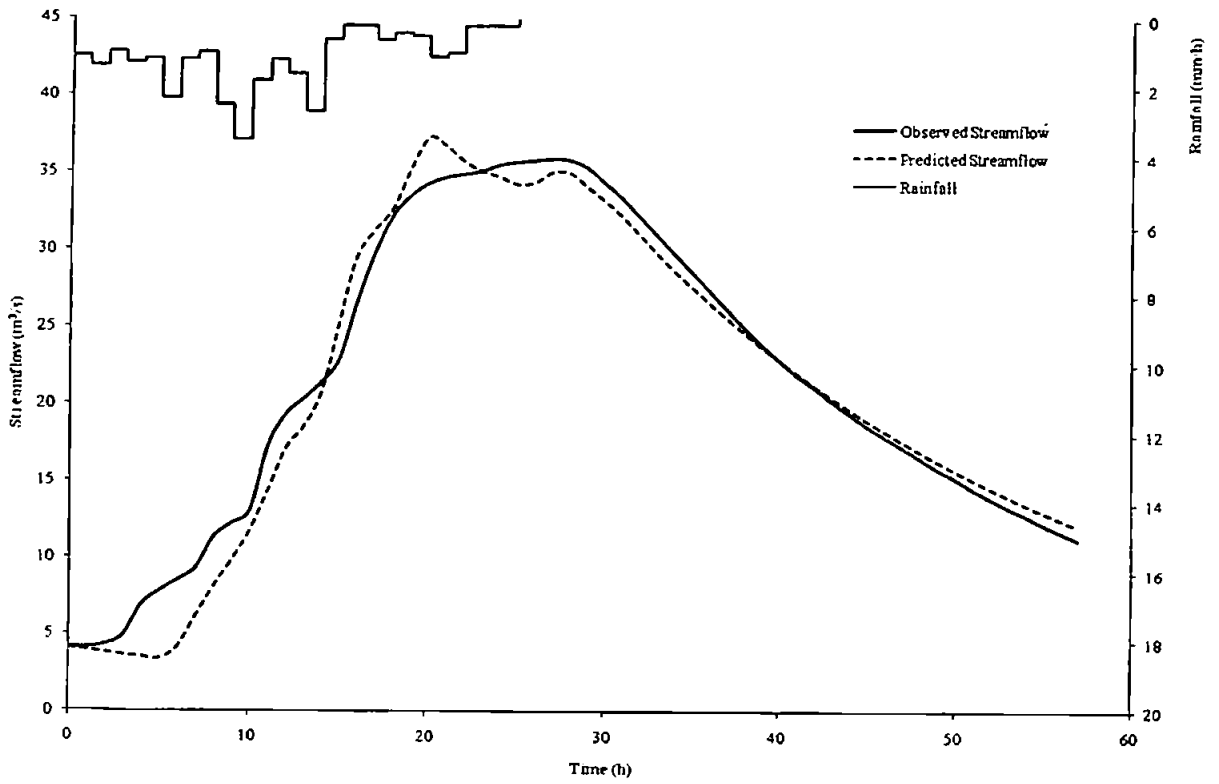
Figure C5.9 Predicted and observed results for event 1570
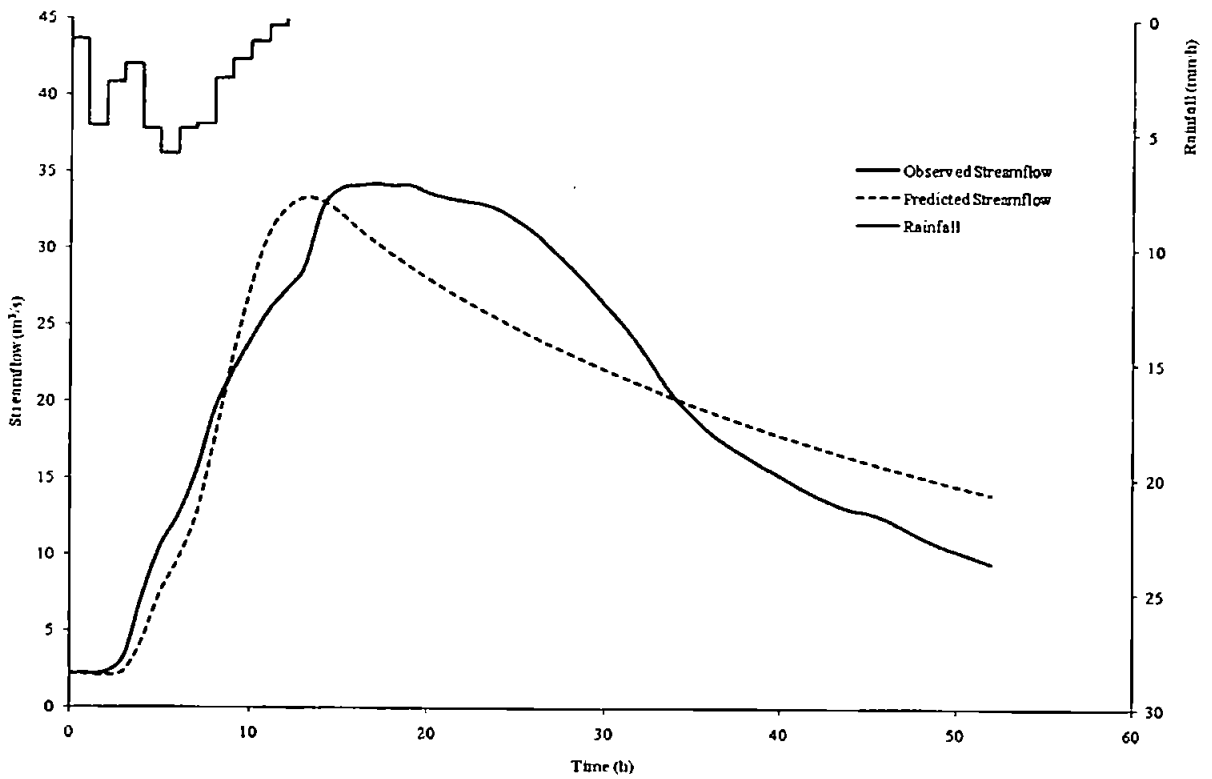
Figure C5.10 Predicted and observed results for event 1571
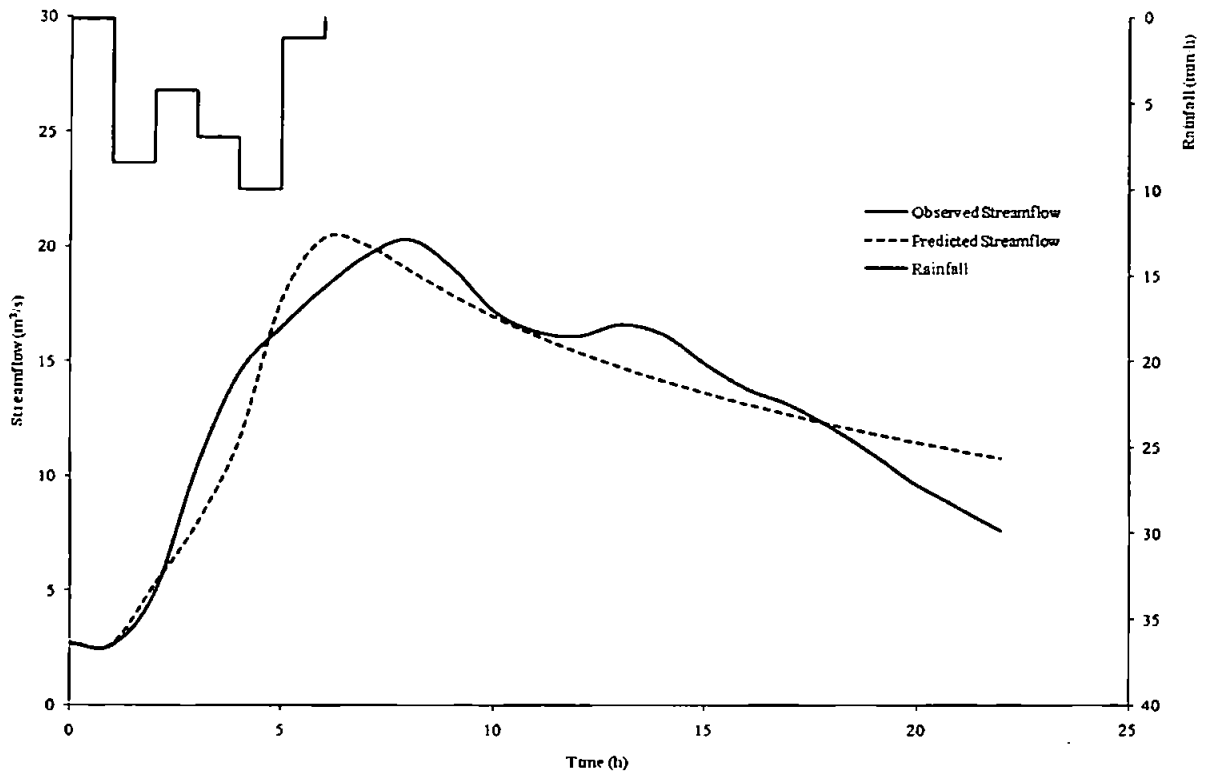
Figure C5.11 Predicted and observed results for event 1572

C6: Catchment 37001 – River Roding at Redbridge
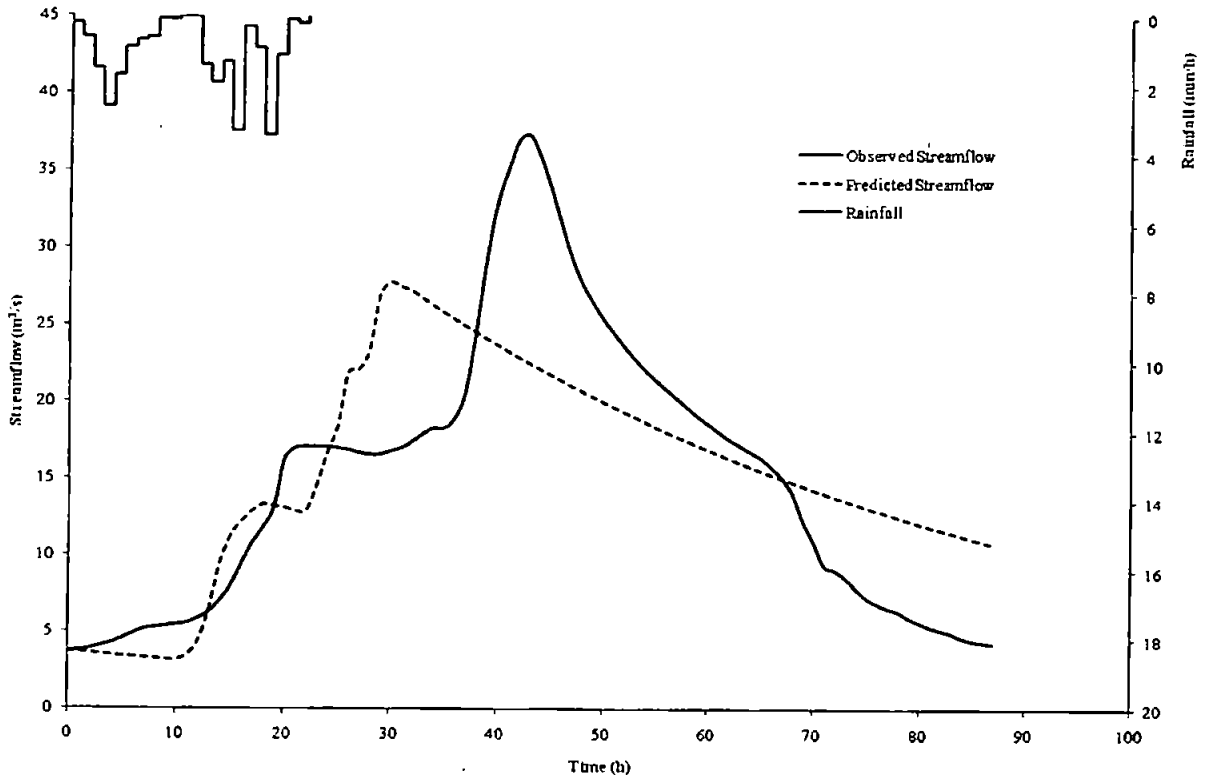
Figure C6.1 Predicted and observed results for event 650
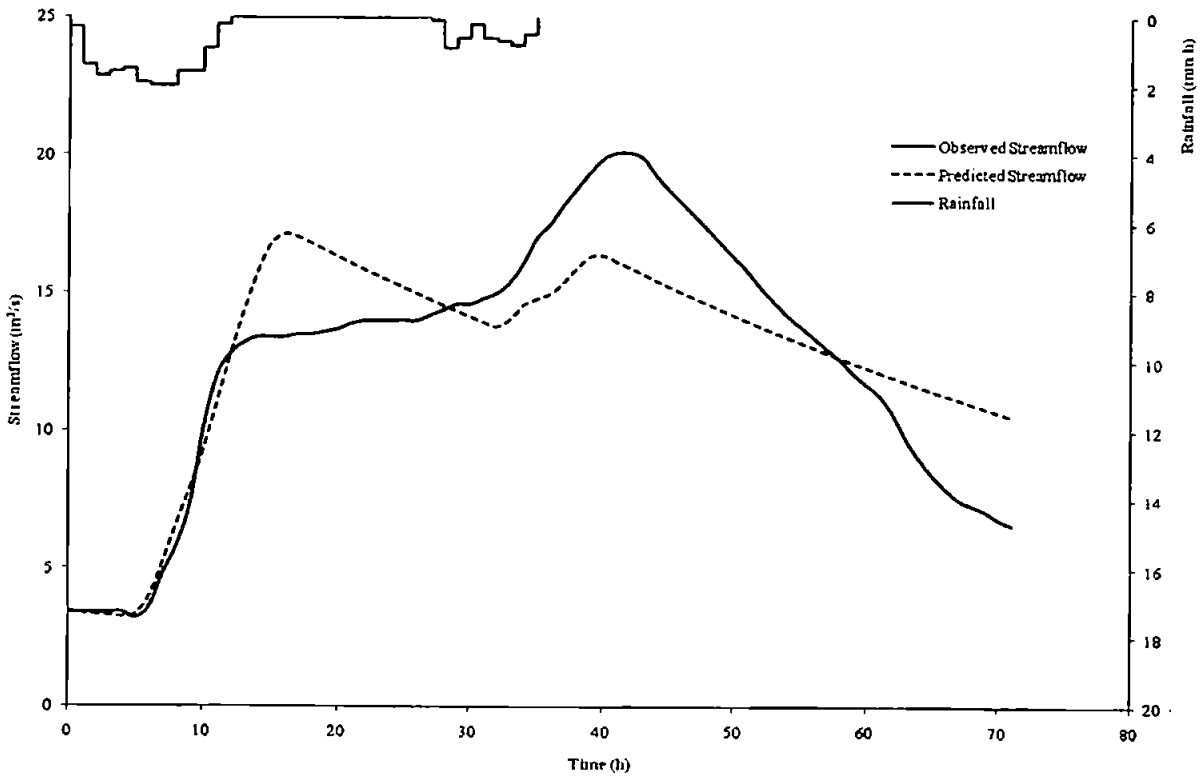
Figure C6.2 Predicted and observed results for event 651
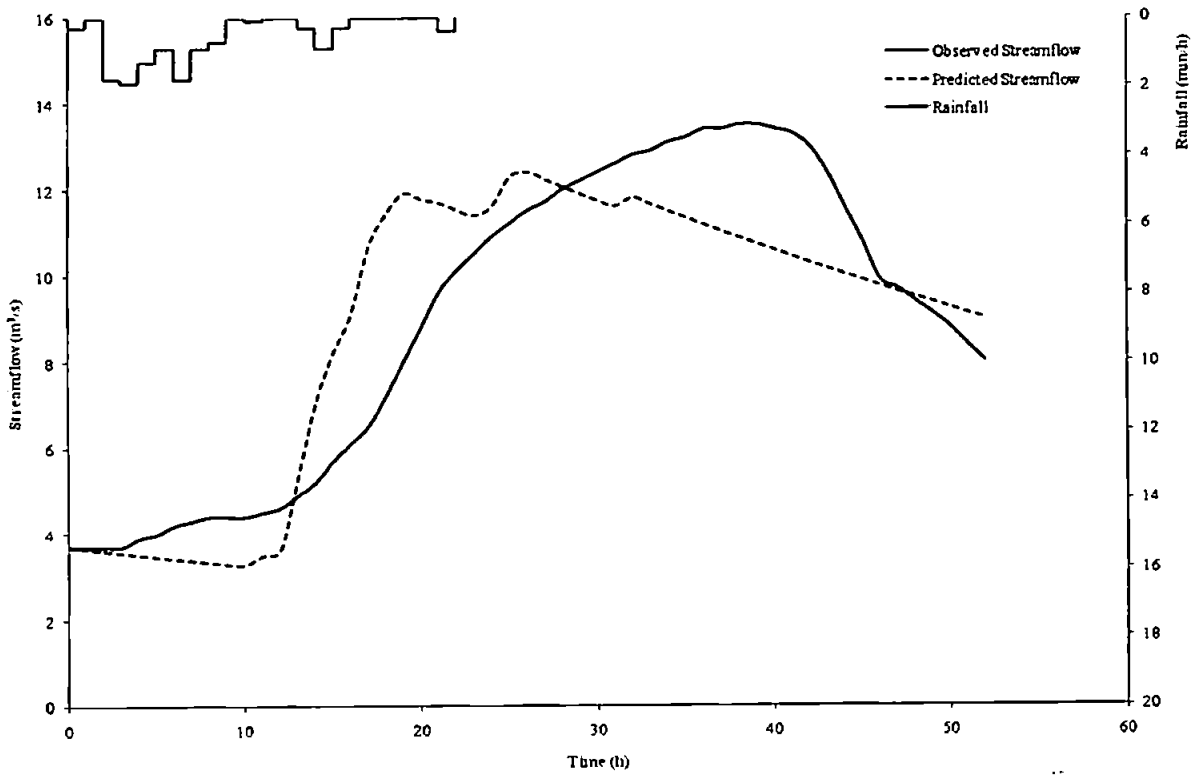
Figure C6.3 Predicted and observed results for event 653
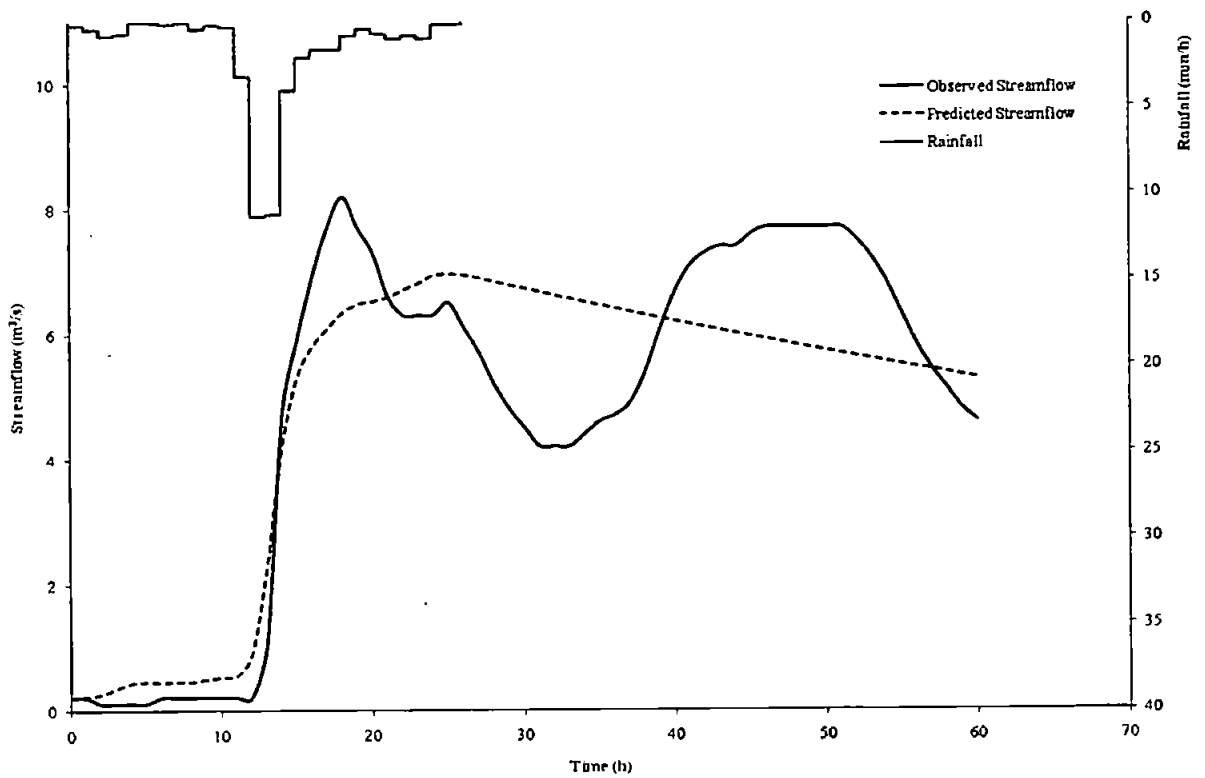
Figure C6.4 Predicted and observed results for event 656
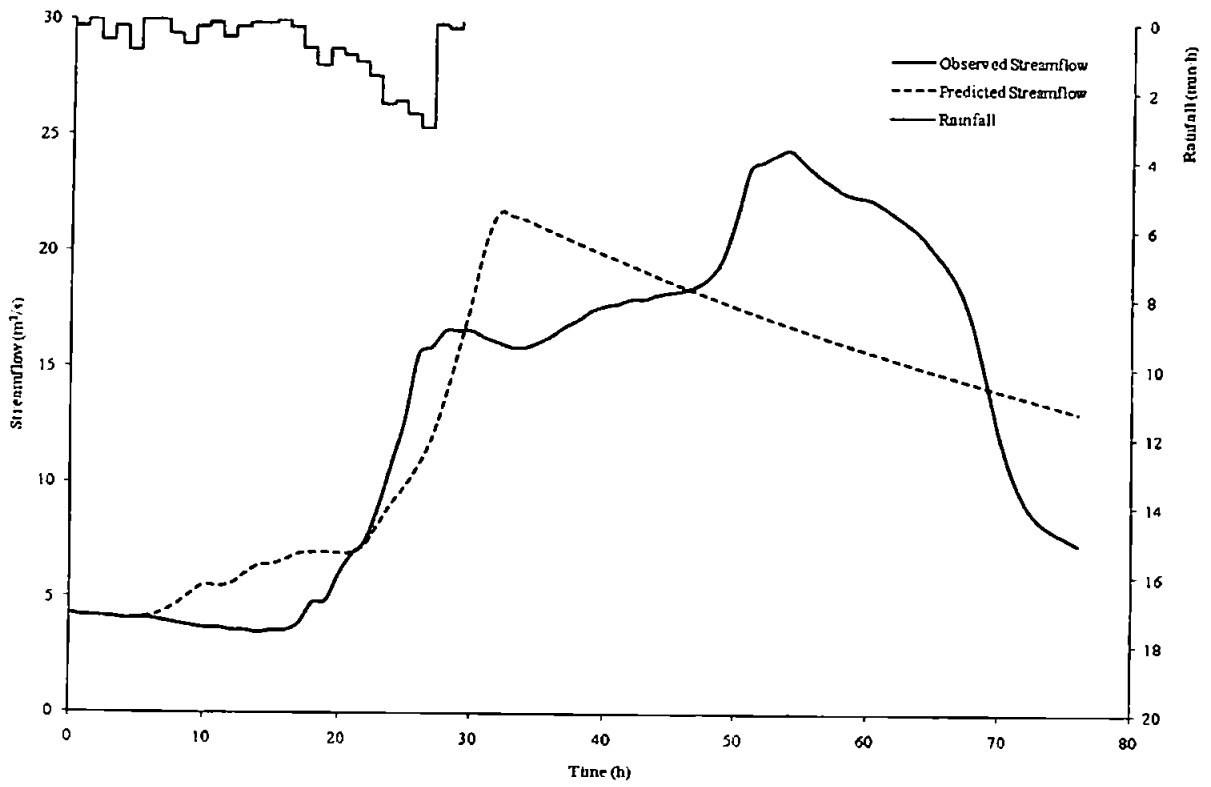
Figure C6.5 Predicted and observed results for event 657
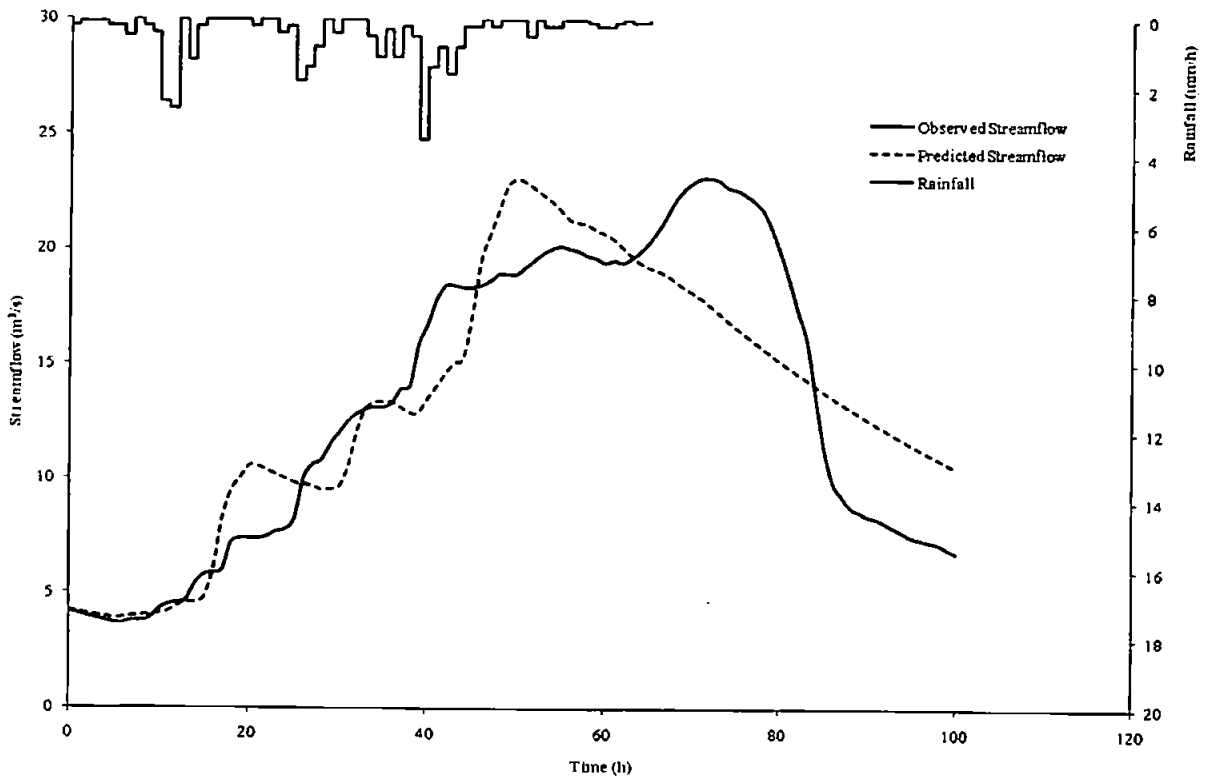
Figure C6.6 Predicted and observed results for event 658

246
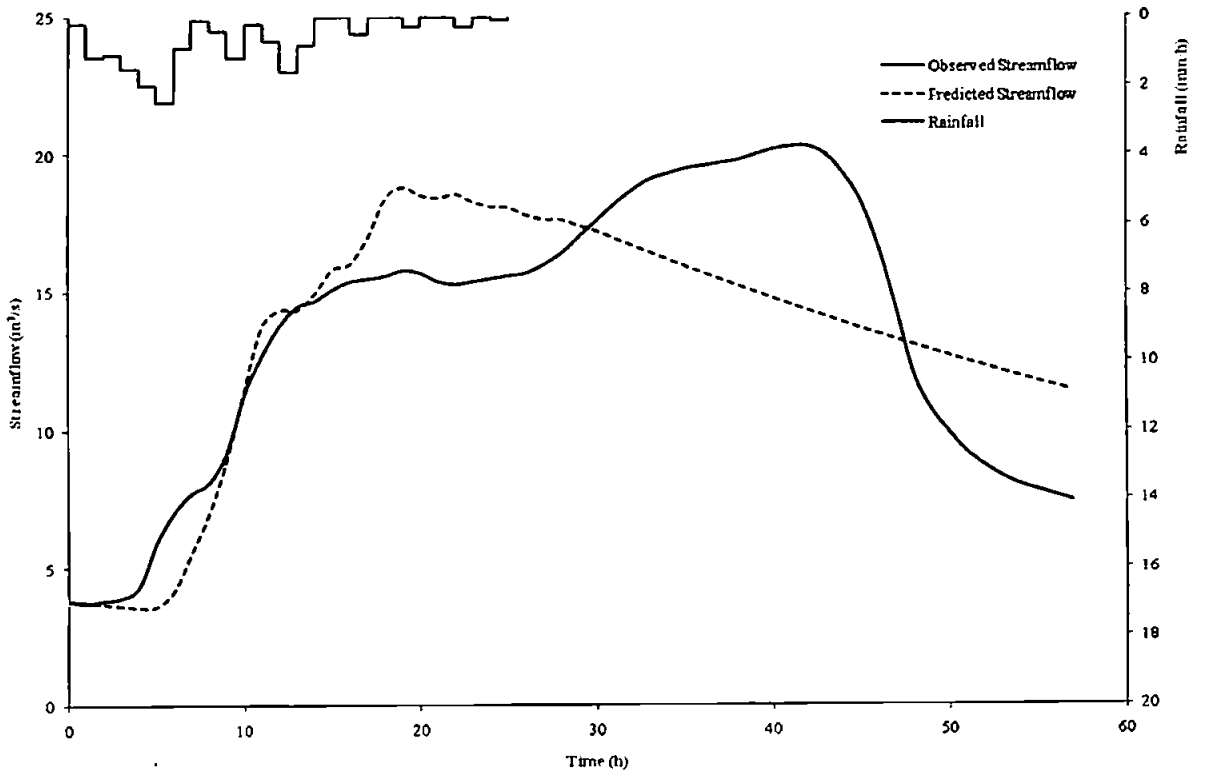
Figure C6.7 Predicted and observed results for event 659

C7: Catchment 66011 – River Conwy at Cwm Llanerch
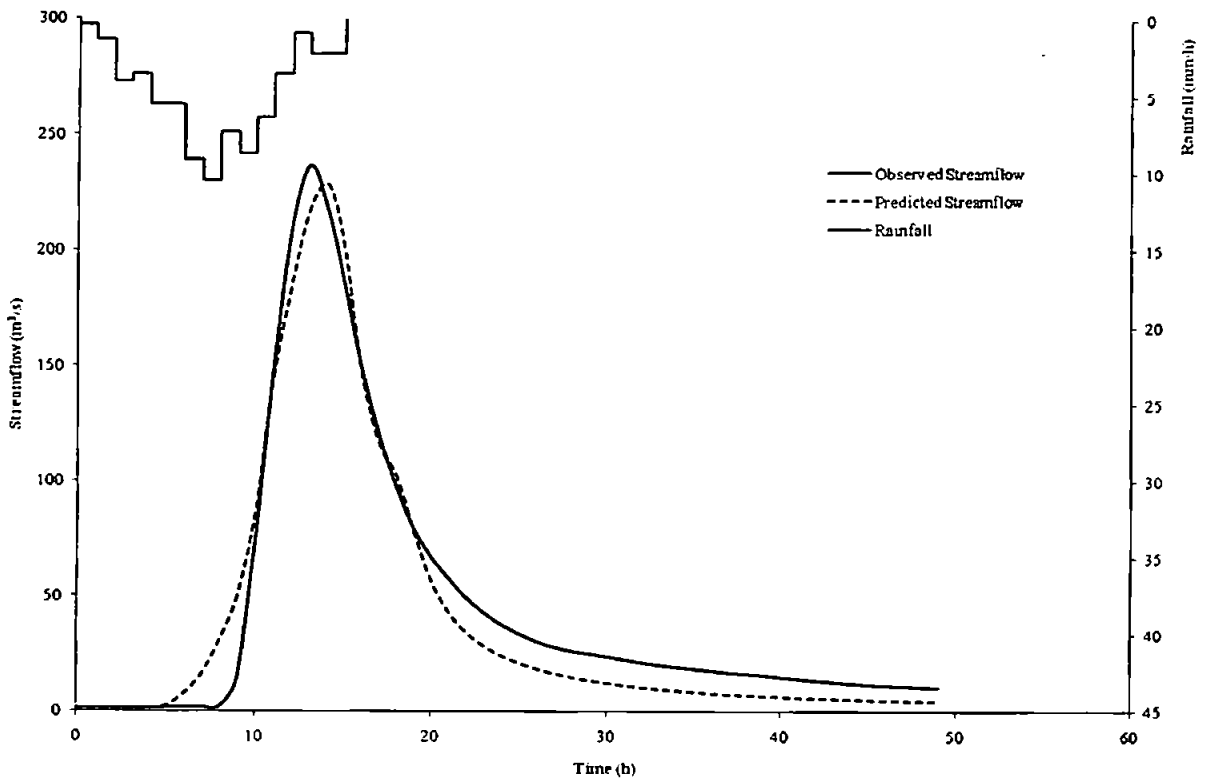
Figure C7.1 Predicted and observed results for event 2072
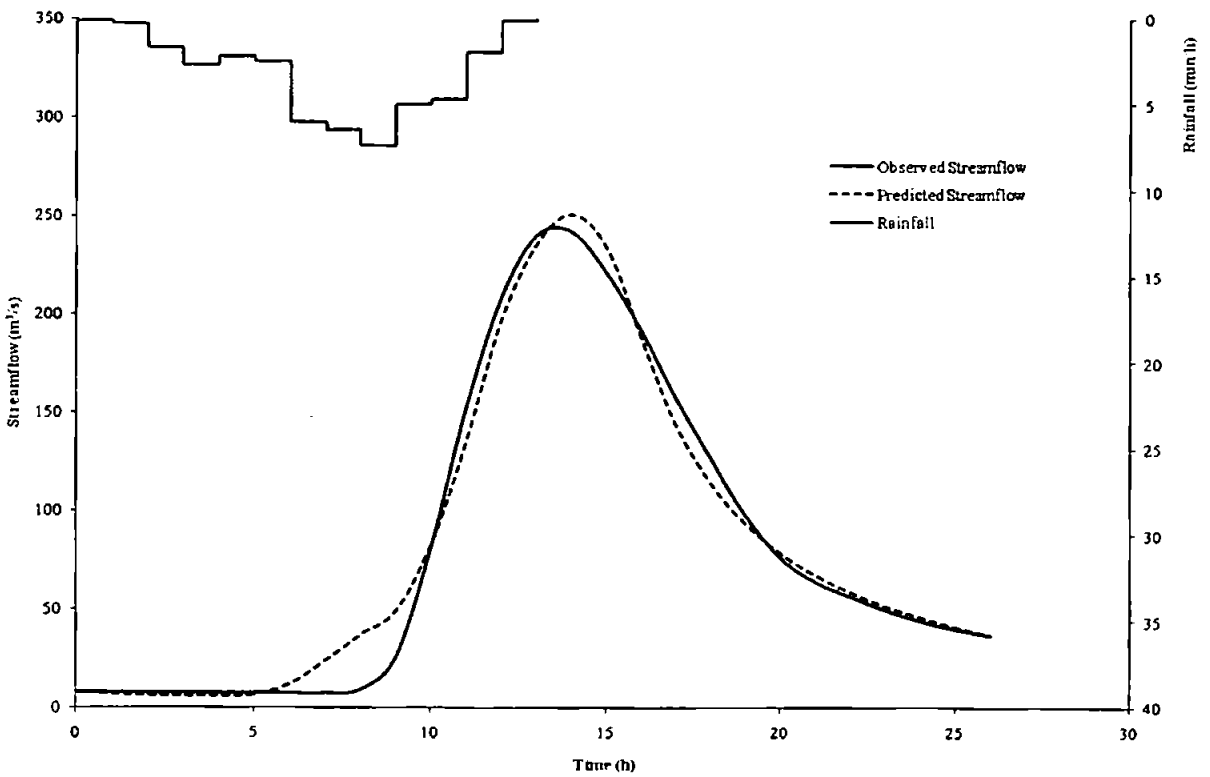
Figure C7.2 Predicted and observed results for event 2073
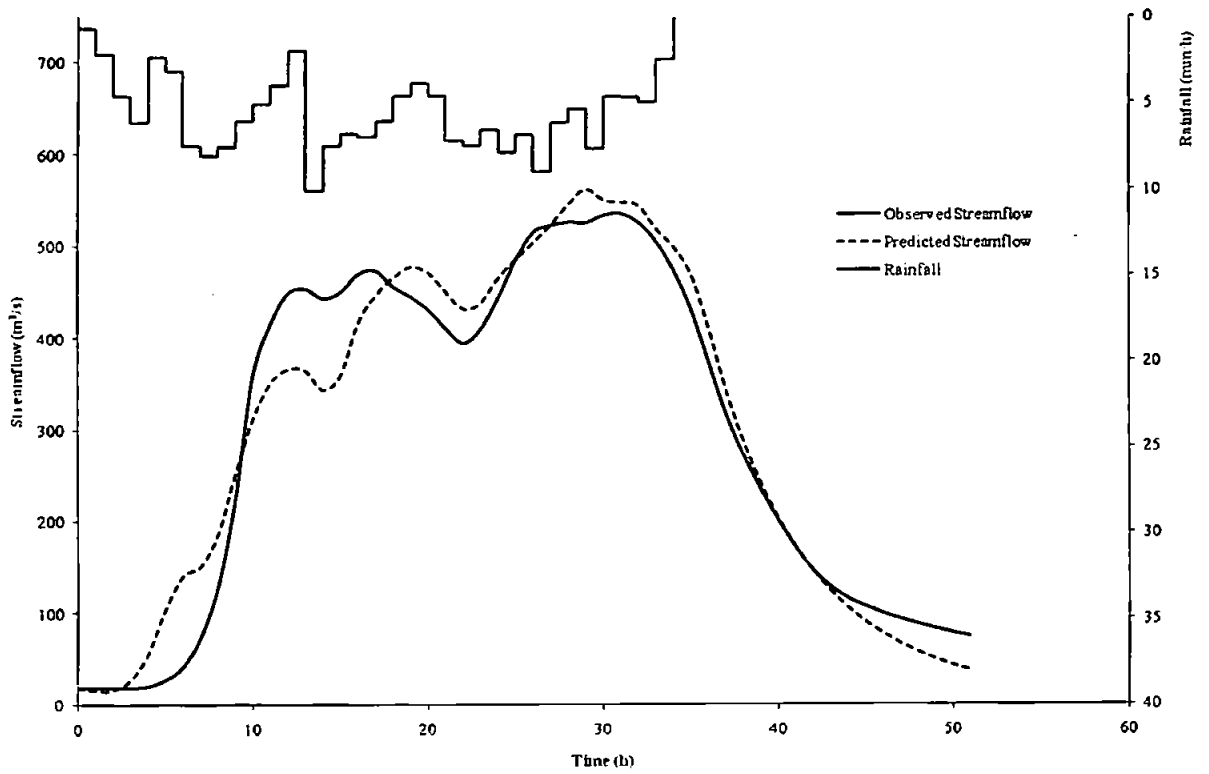
Figure C7.3 Predicted and observed results for event 2074
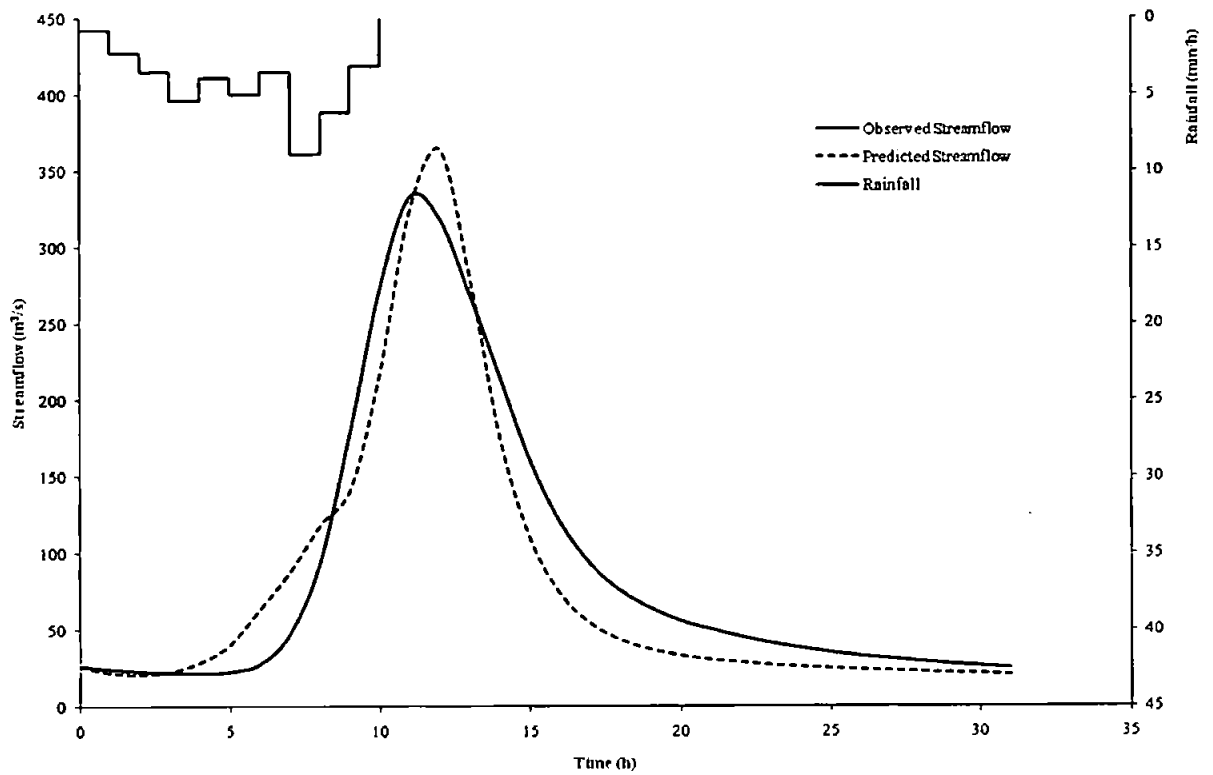
Figure C7.4 Predicted and observed results for event 2075
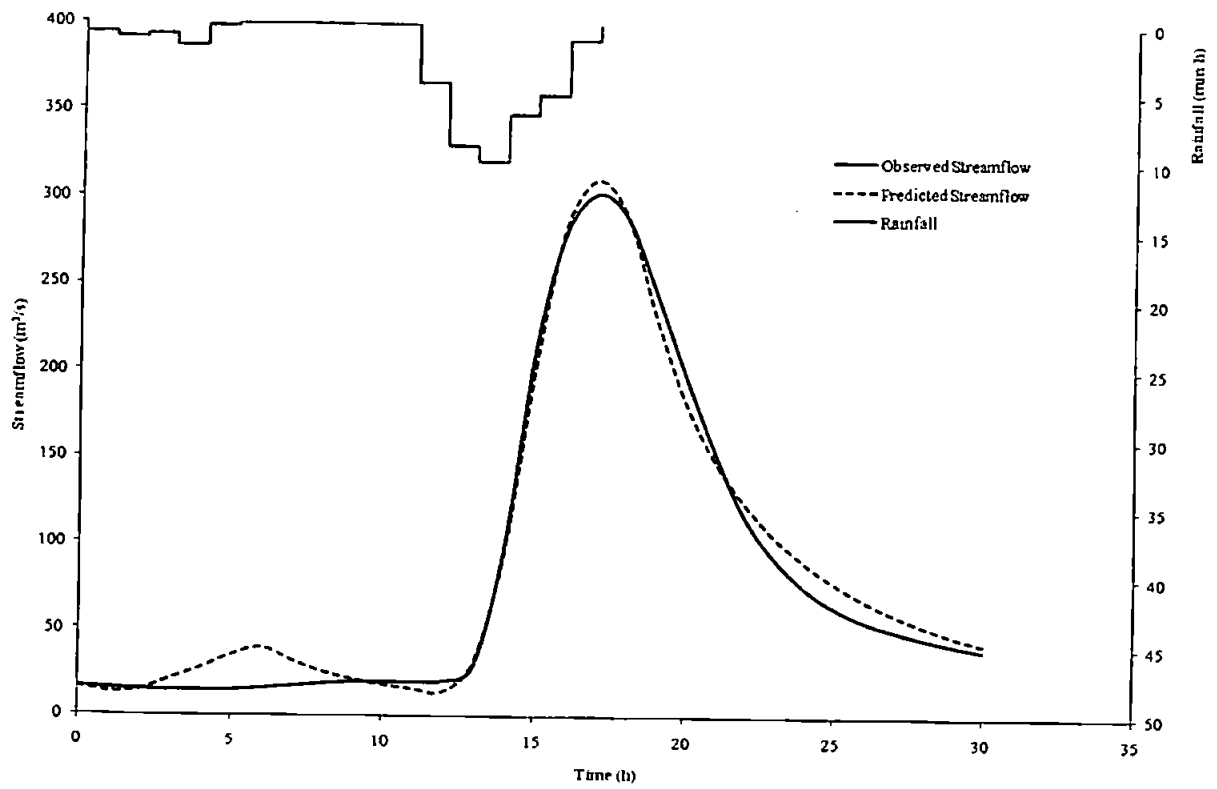
Figure C7.5 Predicted and observed results for event 2076
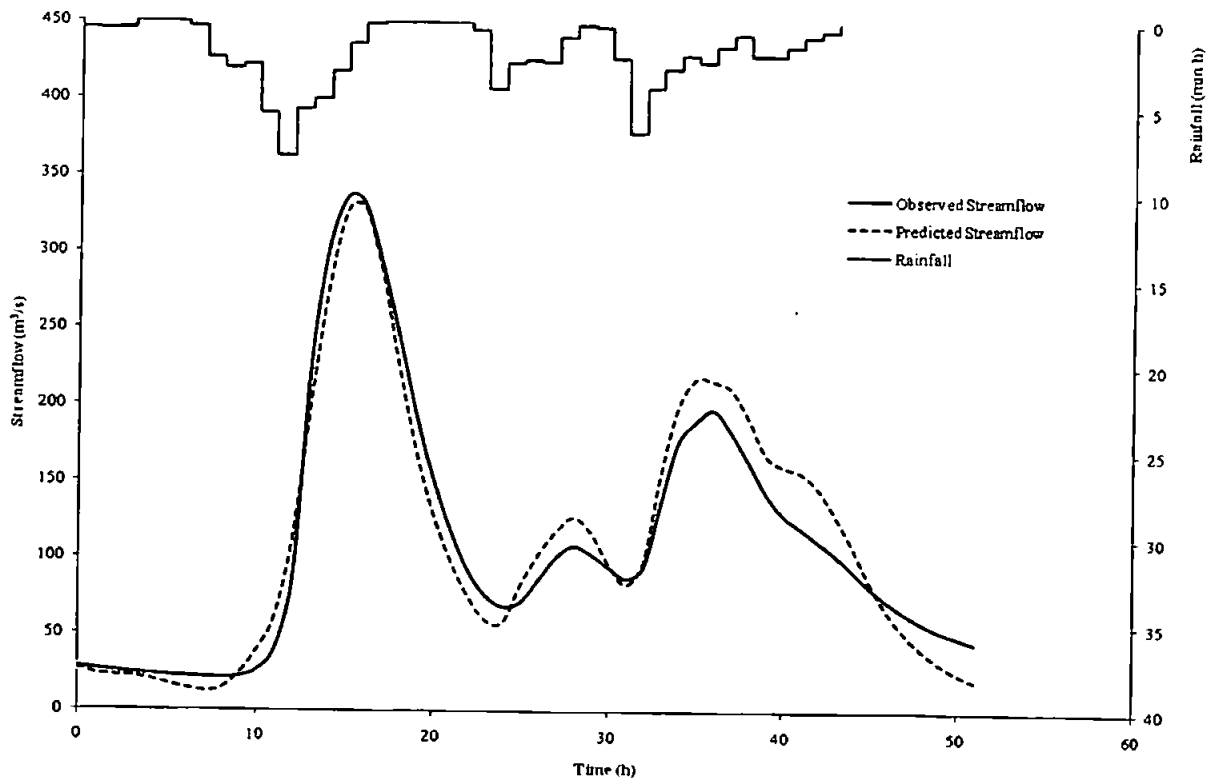
Figure C7.6 Predicted and observed results for event 2077
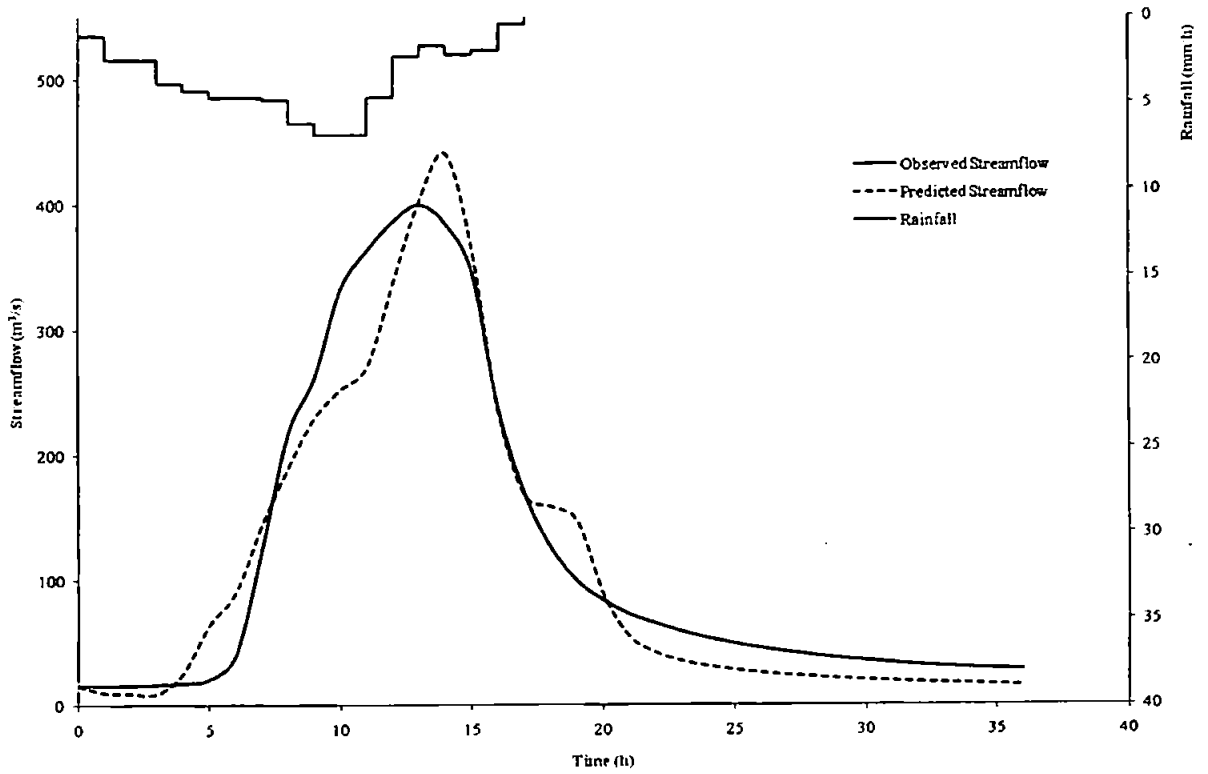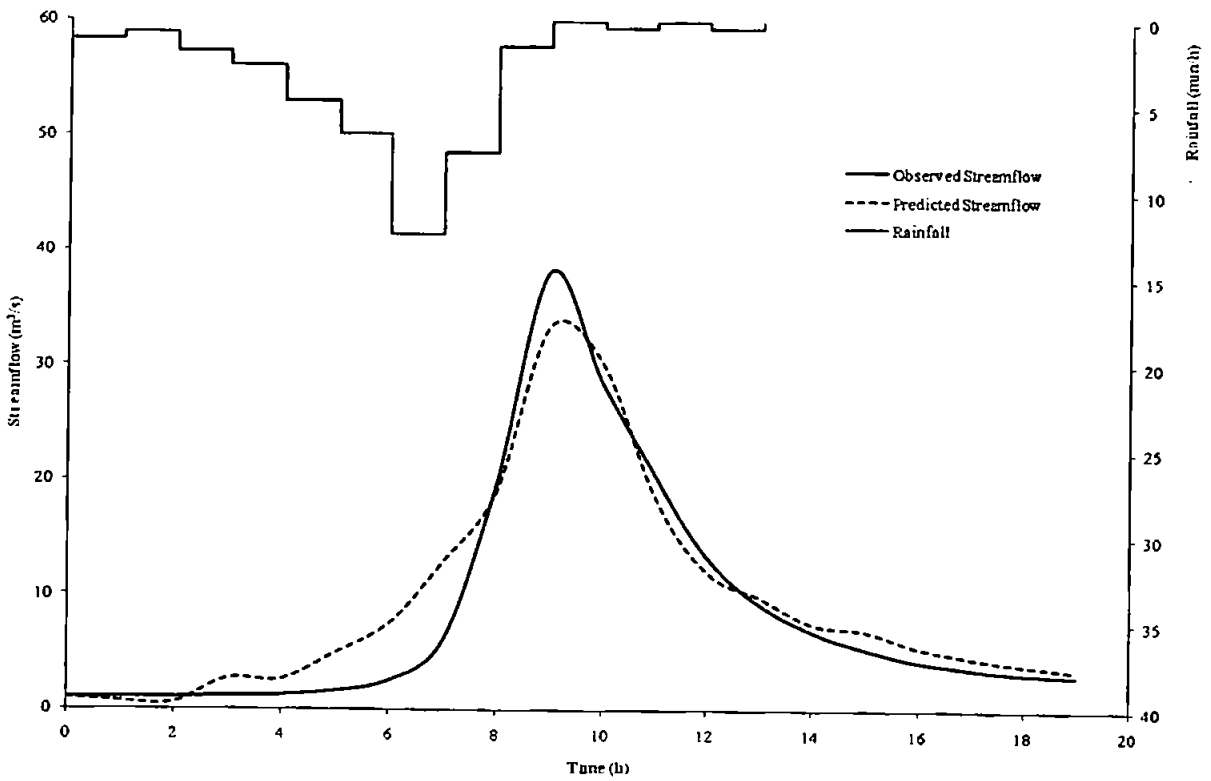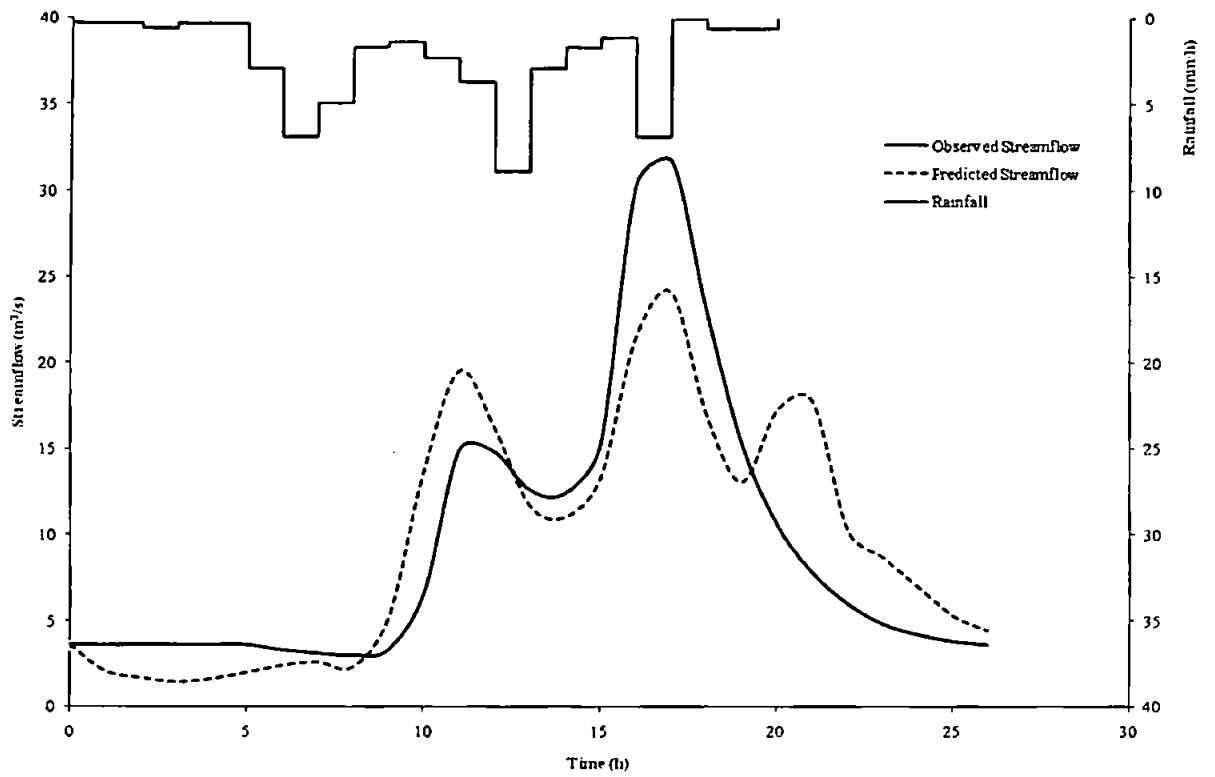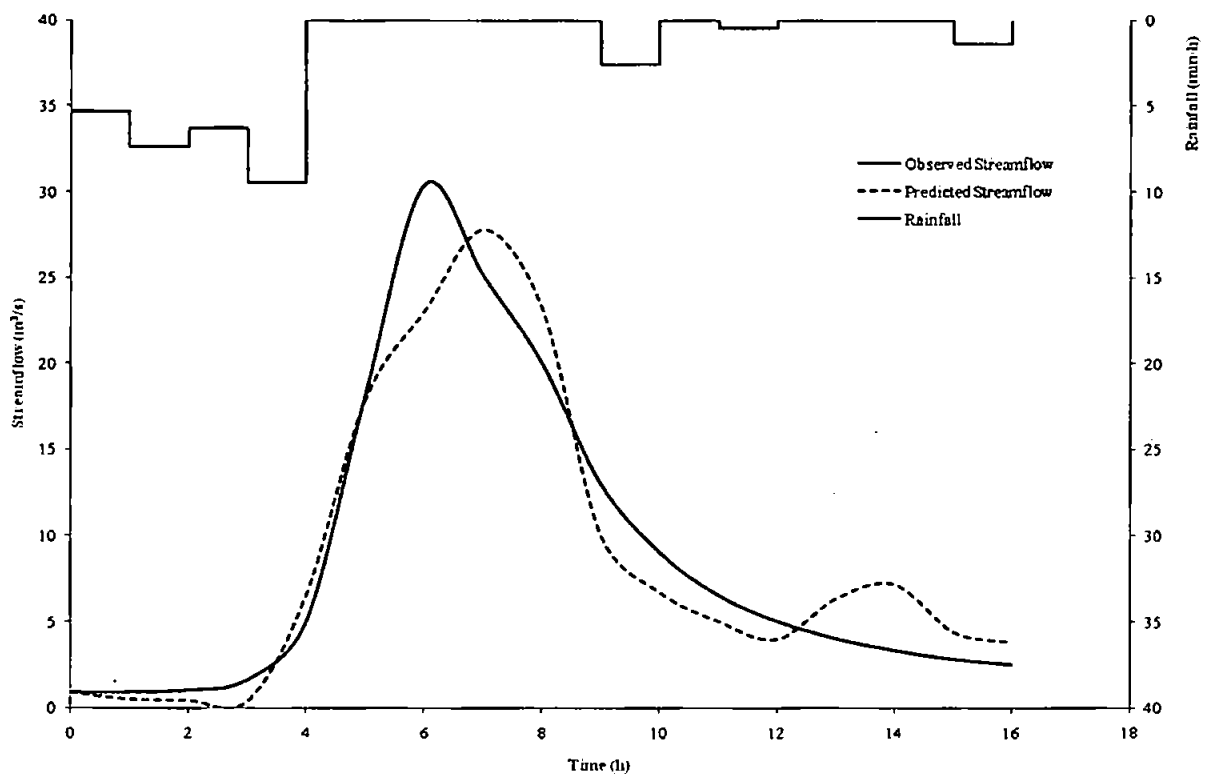
Figure C7.7 Predicted and observed results for event 2078

Figure C7.8 Predicted and observed results for event 2079

Figure C7.9 Predicted and observed results for event 2080

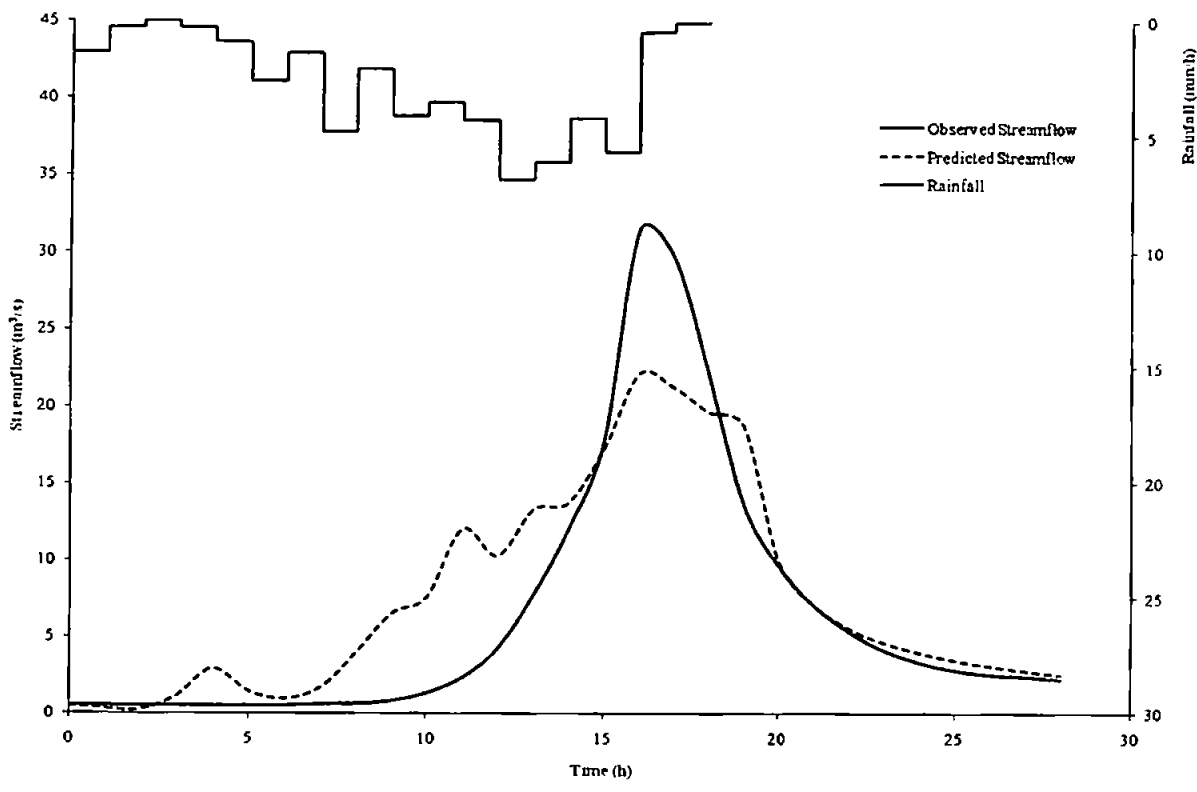**Figure C7.10 Predicted and observed results for event 2081**

Figure C7.11 Predicted and observed results for event 2082

Figure C7.12 Predicted and observed results for event 2083

253

Figure C7.13 Predicted and observed results for event 2084

C8: Catchment 28026 – River Anker at Polesworth

Figure C8.1 Predicted and observed results for event 409

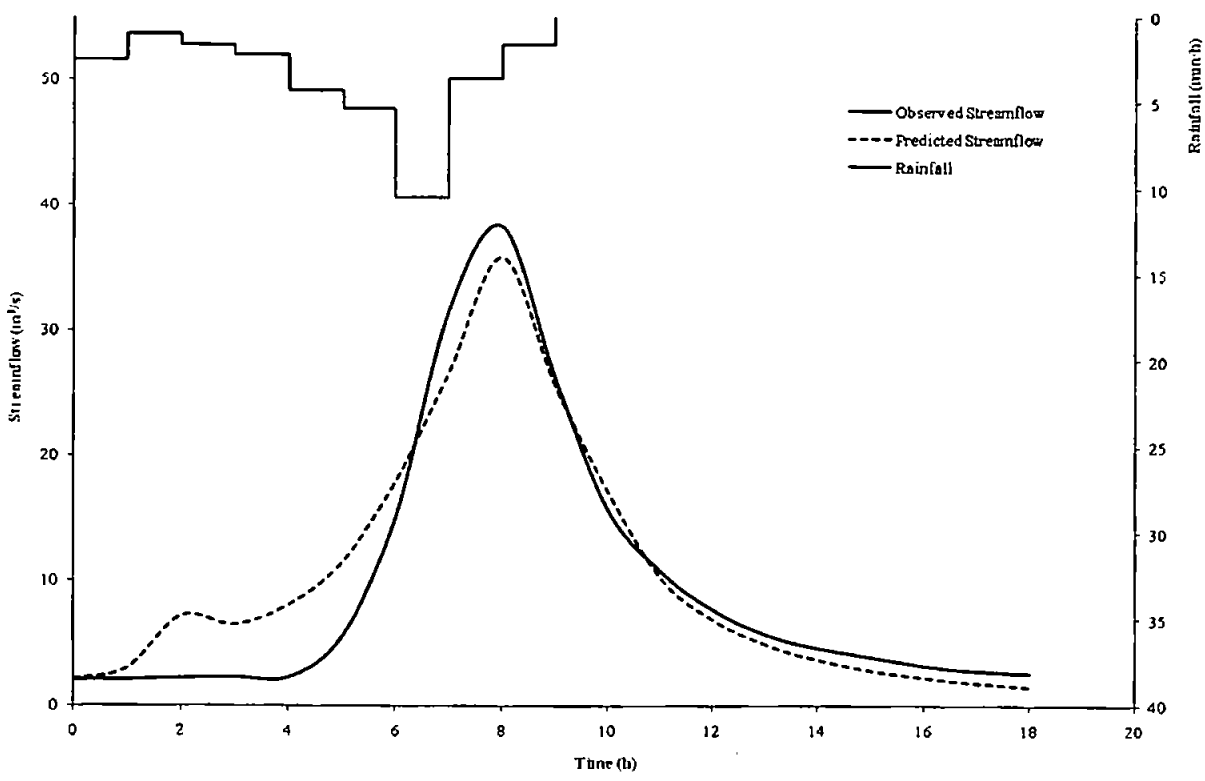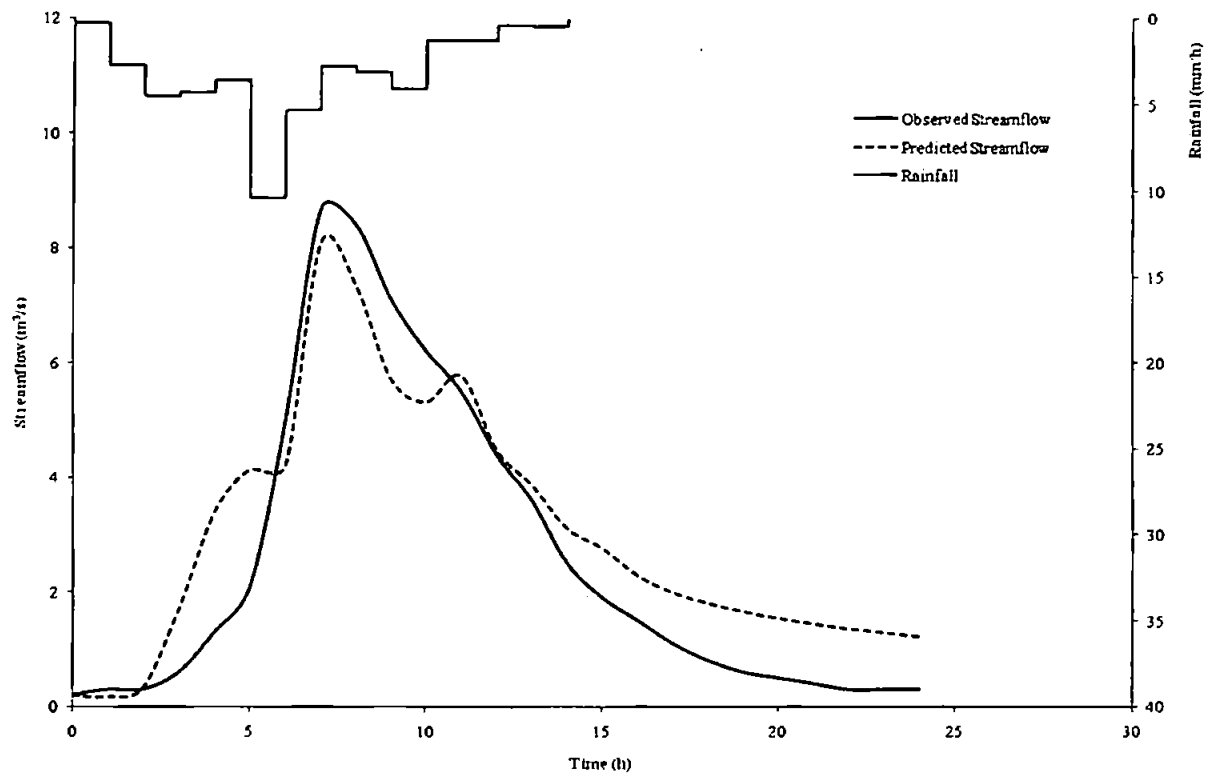**Figure C8.2 Predicted and observed results for event 410**

255

Figure C8.3 Predicted and observed results for event 411

Figure C8.4 Predicted and observed results for event 412

Figure C8.5 Predicted and observed results for event 413

# C9: Catchment 7001 – River Findhorn at Shenachie

Figure C9.1 Predicted and observed results for event 3671

Figure C9.2 Predicted and observed results for event 3673

Figure C9.3 Predicted and observed results for event 3675

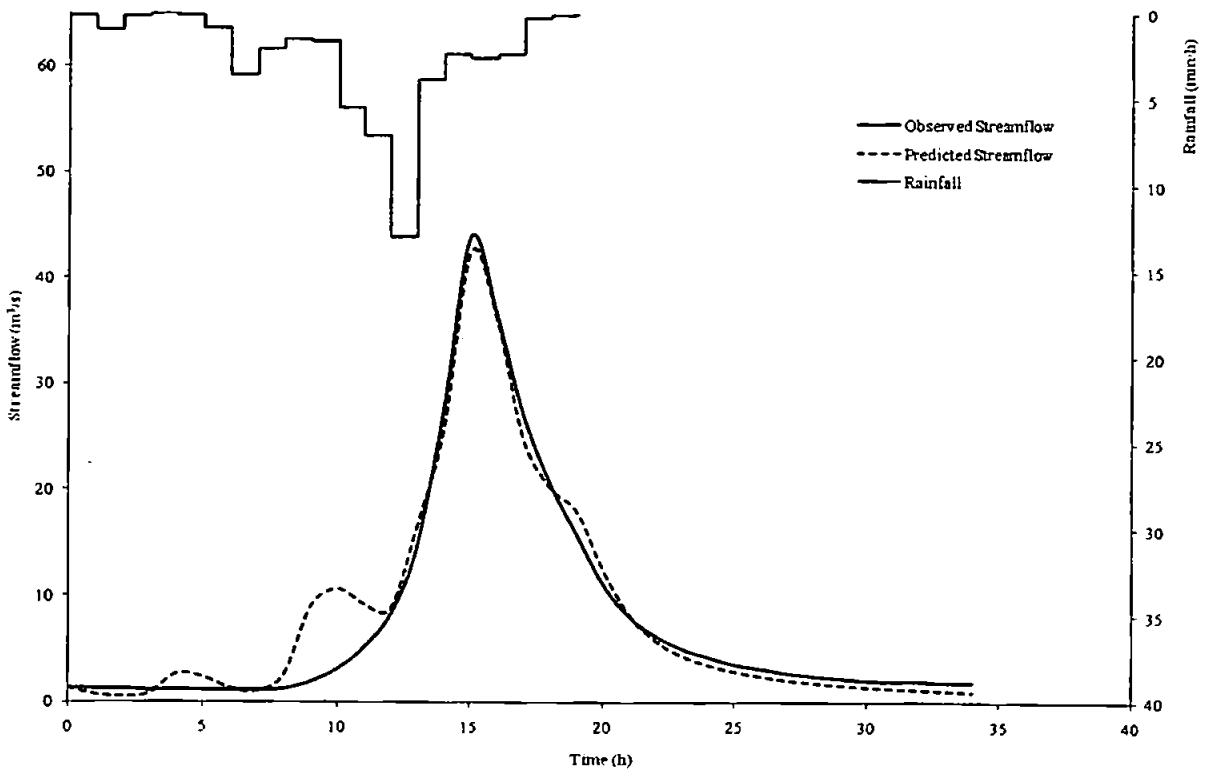**Figure C9.4 Predicted and observed results for event 3677**

259

Figure C9.5 Predicted and observed results for event 3678

Figure C9.6 Predicted and observed results for event 3680

Figure C9.7 Predicted and observed results for event 3682

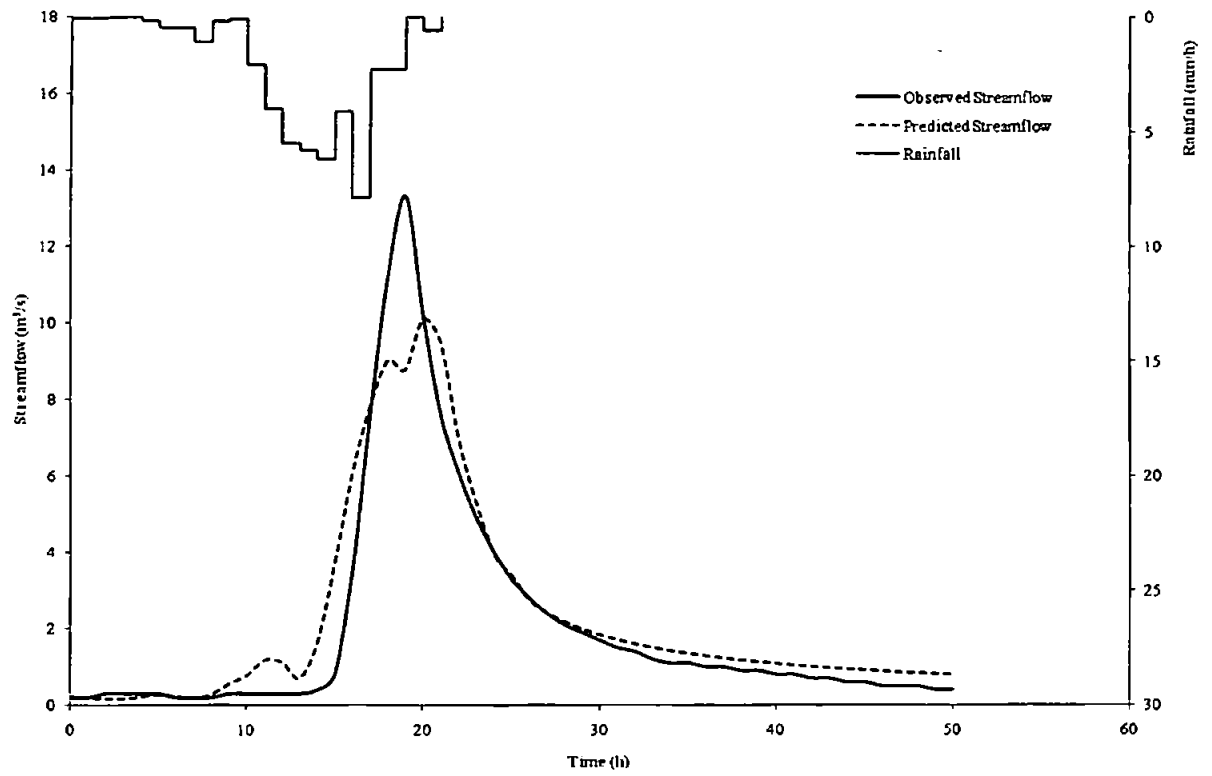**Figure C9.8 Predicted and observed results for event 3686**

261

Figure C9.9 Predicted and observed results for event 3687

Figure C9.10 Predicted and observed results for event 3688

Figure C9.11 Predicted and observed results for event 3691

Figure C9.12 Predicted and observed results for event 3697
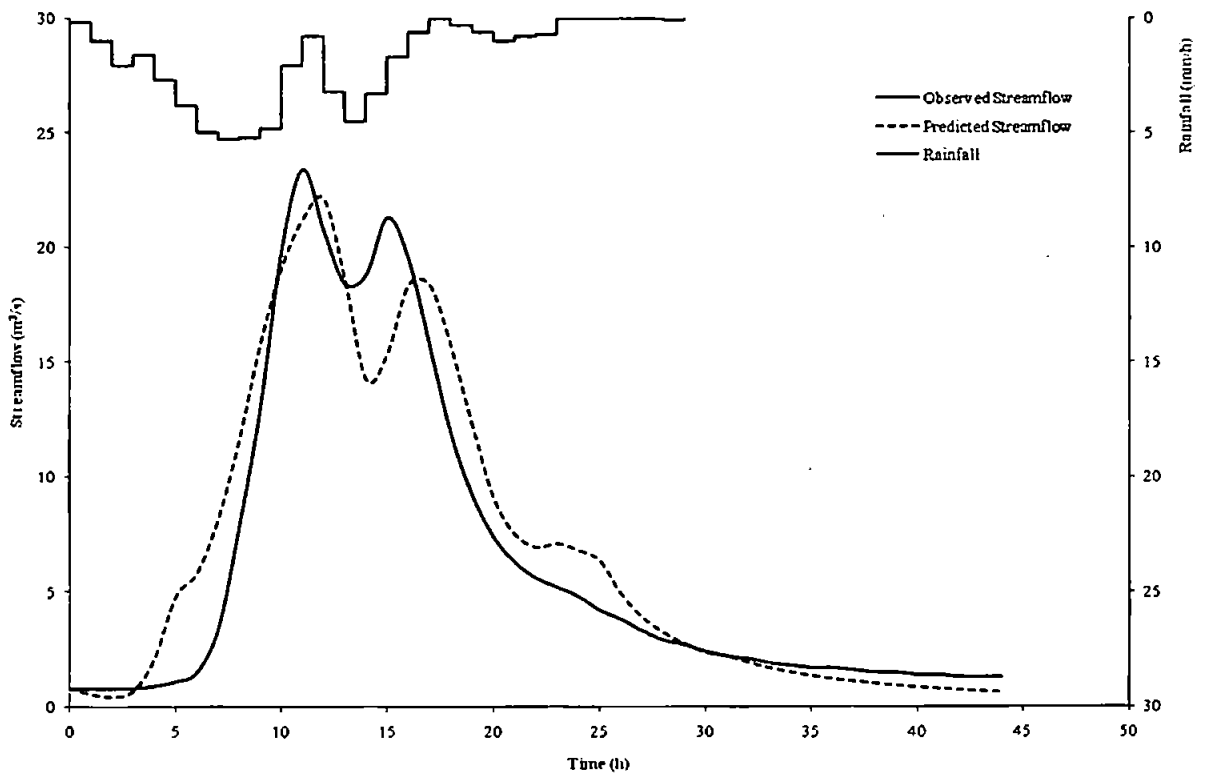
263

Figure C9.13 Predicted and observed results for event 3698

Figure C9.14 Predicted and observed results for event 3704

Figure C9.15 Predicted and observed results for event 3705

# C10: Catchment 57005 – River Taff at Pontypridd

Figure C10.1 Predicted and observed results for event 1836

Figure C10.2 Predicted and observed results for event 1837

Figure C10.3 Predicted and observed results for event 1838

Figure C10.4 Predicted and observed results for event 1840

267

Figure C10.5 Predicted and observed results for event 1841

Figure C10.6 Predicted and observed results for event 1842

Figure C10.7 Predicted and observed results for event 1843

Figure C10.8 Predicted and observed results for event 1844

269

Figure C10.9 Predicted and observed results for event 1845
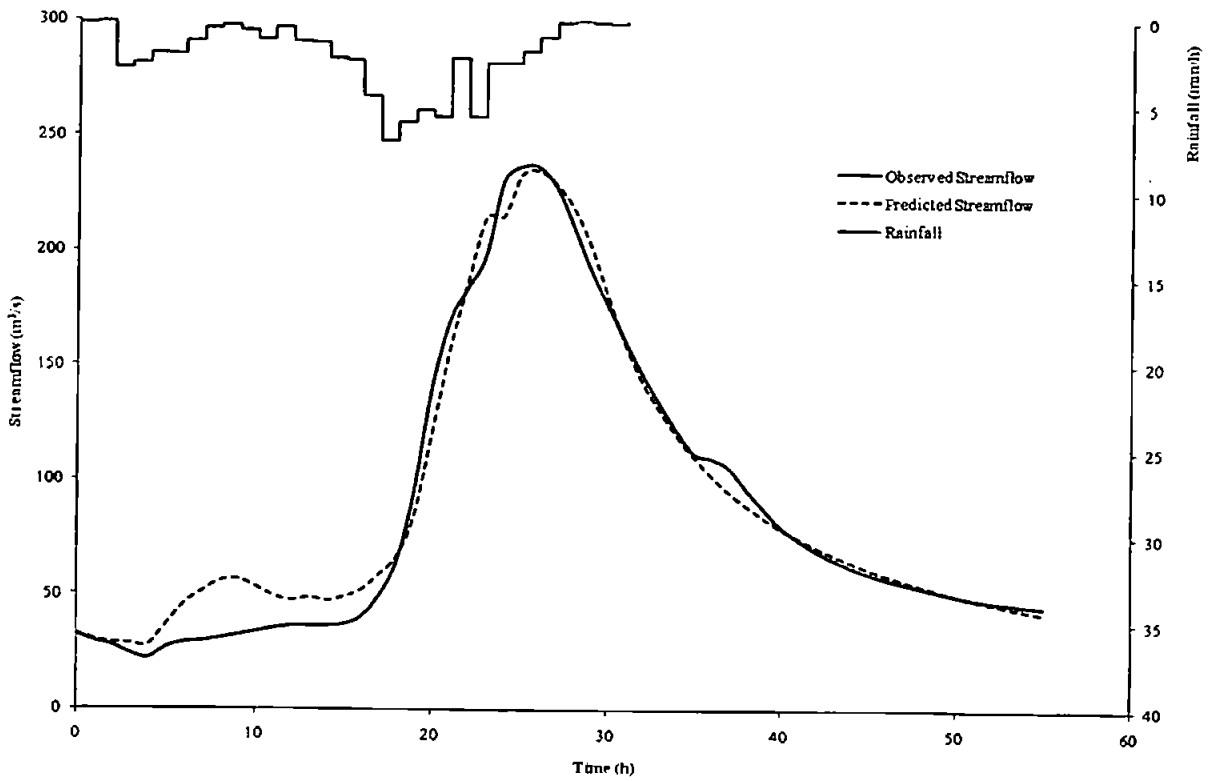
Figure C10.10 Predicted and observed results for event 1846

Figure C10.11 Predicted and observed results for event 1847

C11: Catchment 72006 – River Lune at Kirkby Lonsdale

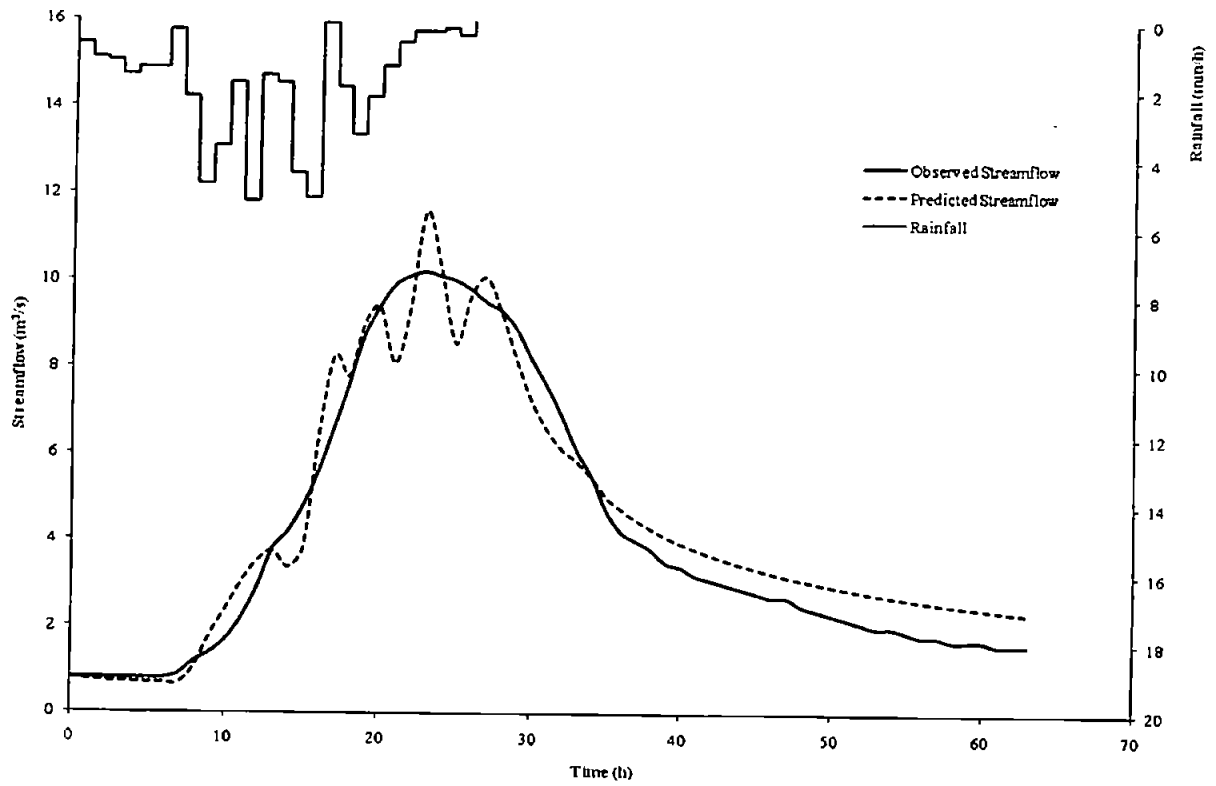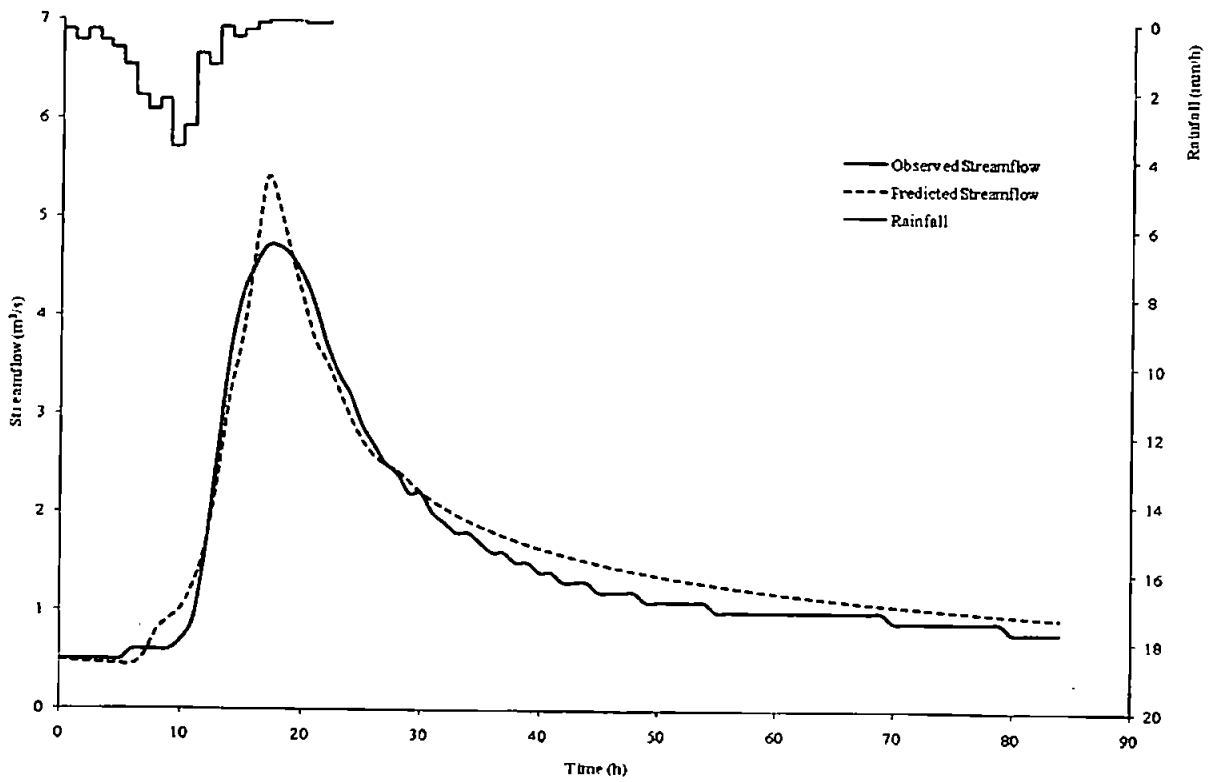**Figure C11.1 Predicted and observed results for event 2282**

Figure C11.2 Predicted and observed results for event 2283

Figure C11.3 Predicted and observed results for event 2284

Figure C11.4 Predicted and observed results for event 2285

273

Figure C11.5 Predicted and observed results for event 2286

Figure C11.6 Predicted and observed results for event 2287

Figure C11.7 Predicted and observed results for event 2288
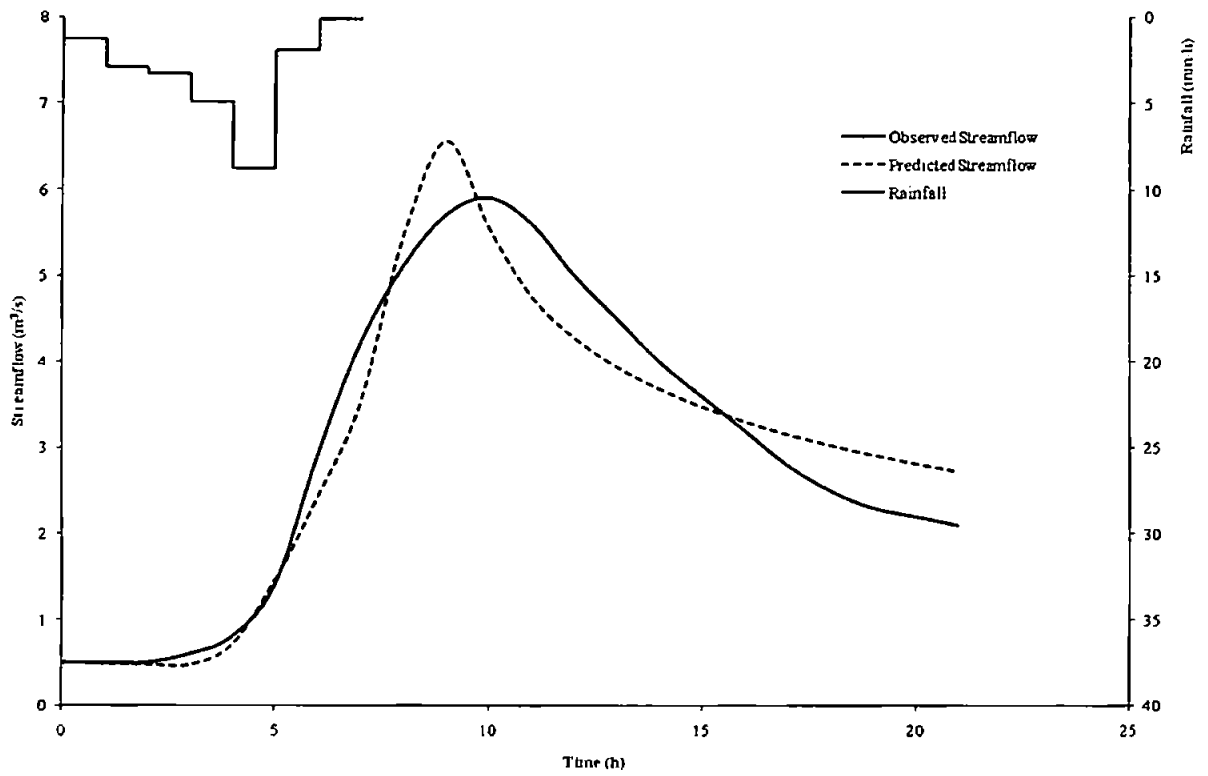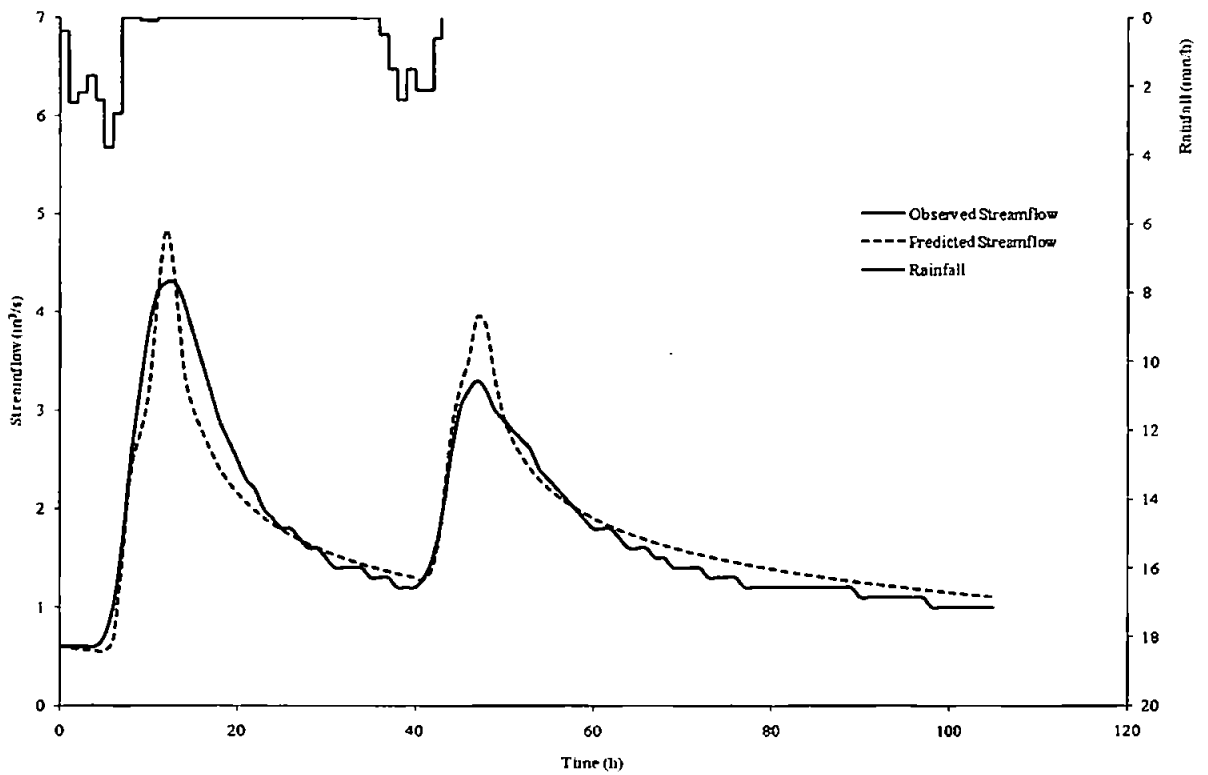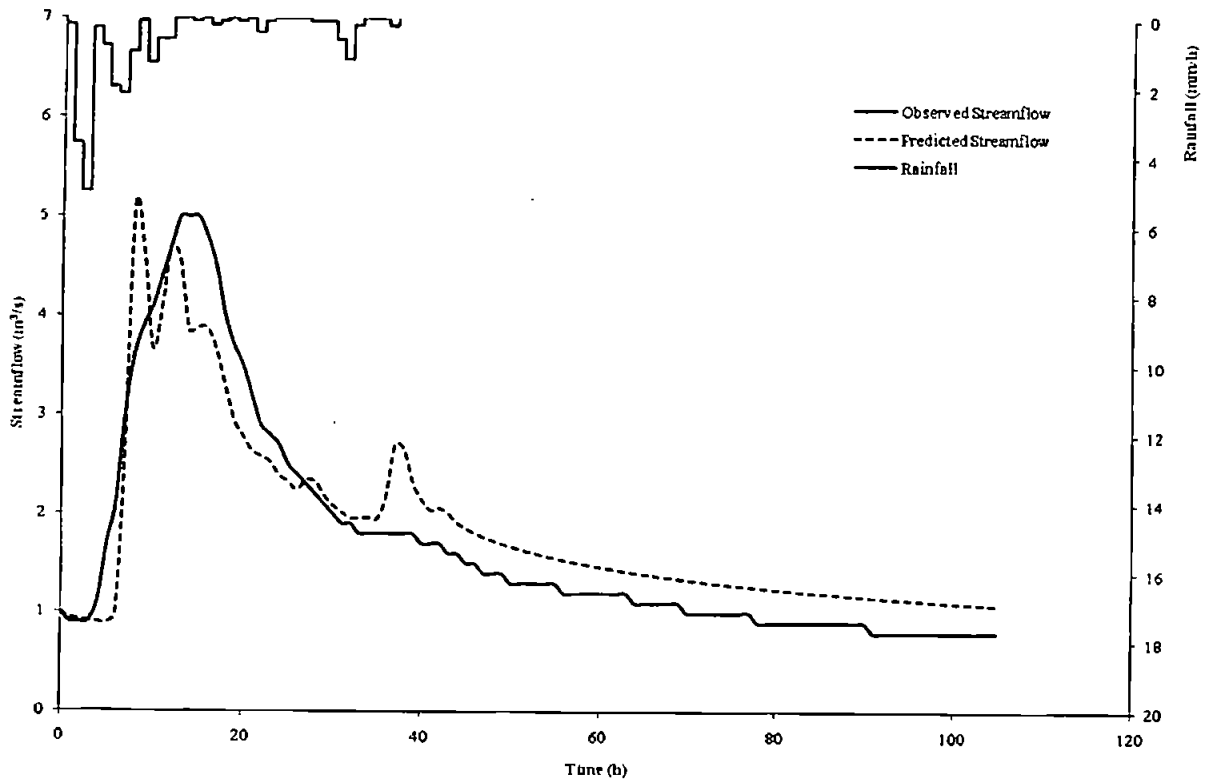

Figure C11.8 Predicted and observed results for event 2289

275

Figure C11.9 Predicted and observed results for event 2290

Figure C11.10 Predicted and observed results for event 2291

276

Appendix D: Single Fractional Reservoir Results Without Loss Model

The following Figures show the predicted and observed streamflow hydrographs together with the observed event rainfall hyetograph for the selected catchments from the UK Flood Event Archive. The predictions were made with the initialised, single, fractional-order, time-lagged, linear reservoir, without using a rainfall loss model.

# D1: Catchment 46005 – East Dart River at Bellever
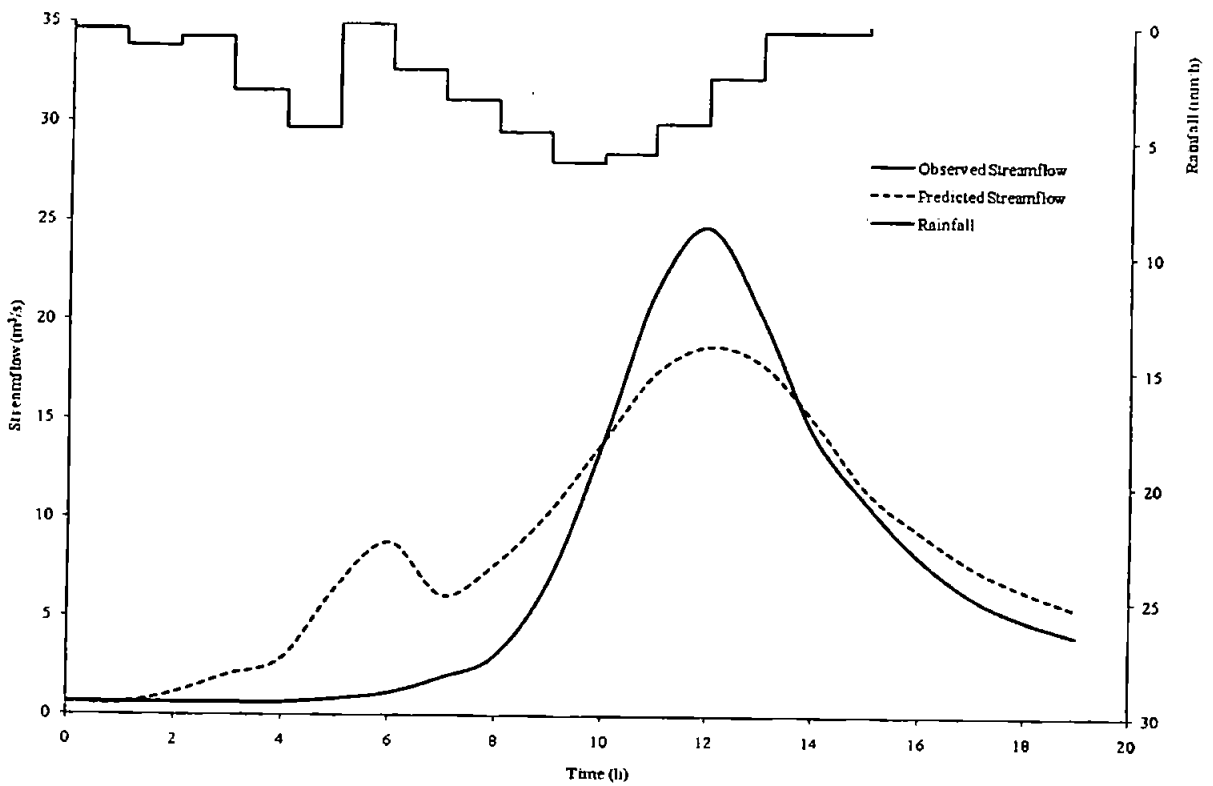
Figure D1.1 Predicted and observed results for event 1287

Figure D1.2 Predicted and observed results for event 1289

Figure D1.3 Predicted and observed results for event 1292

Figure D1.4 Predicted and observed results for event 1297

279

Figure D1.5 Predicted and observed results for event 1298

Figure D1.6 Predicted and observed results for event 1299

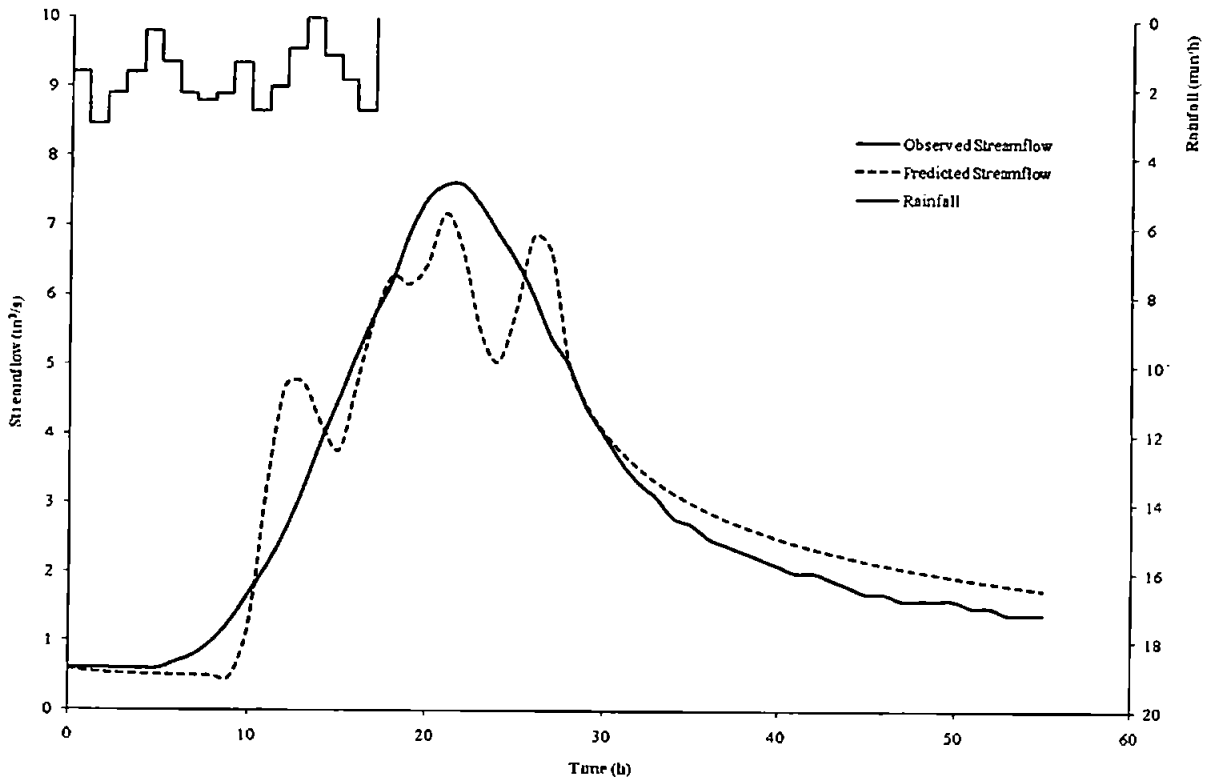**Figure D1.7 Predicted and observed results for event 1300**
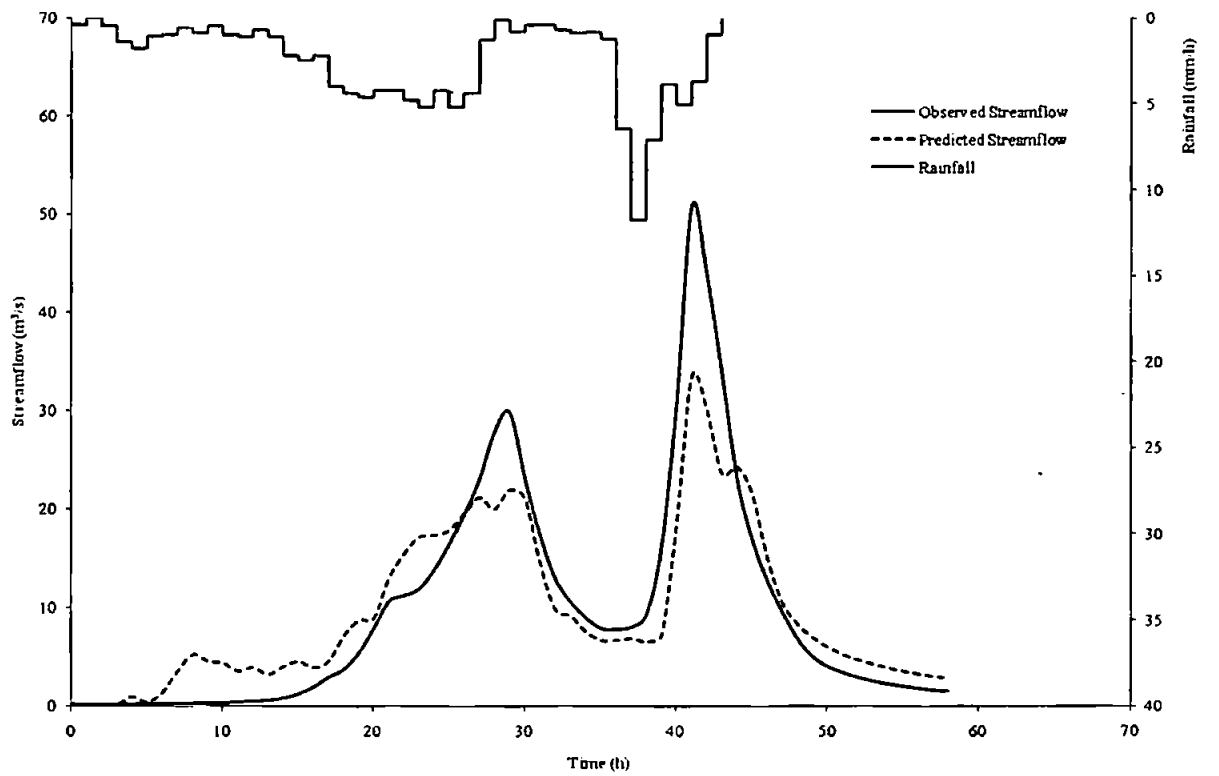
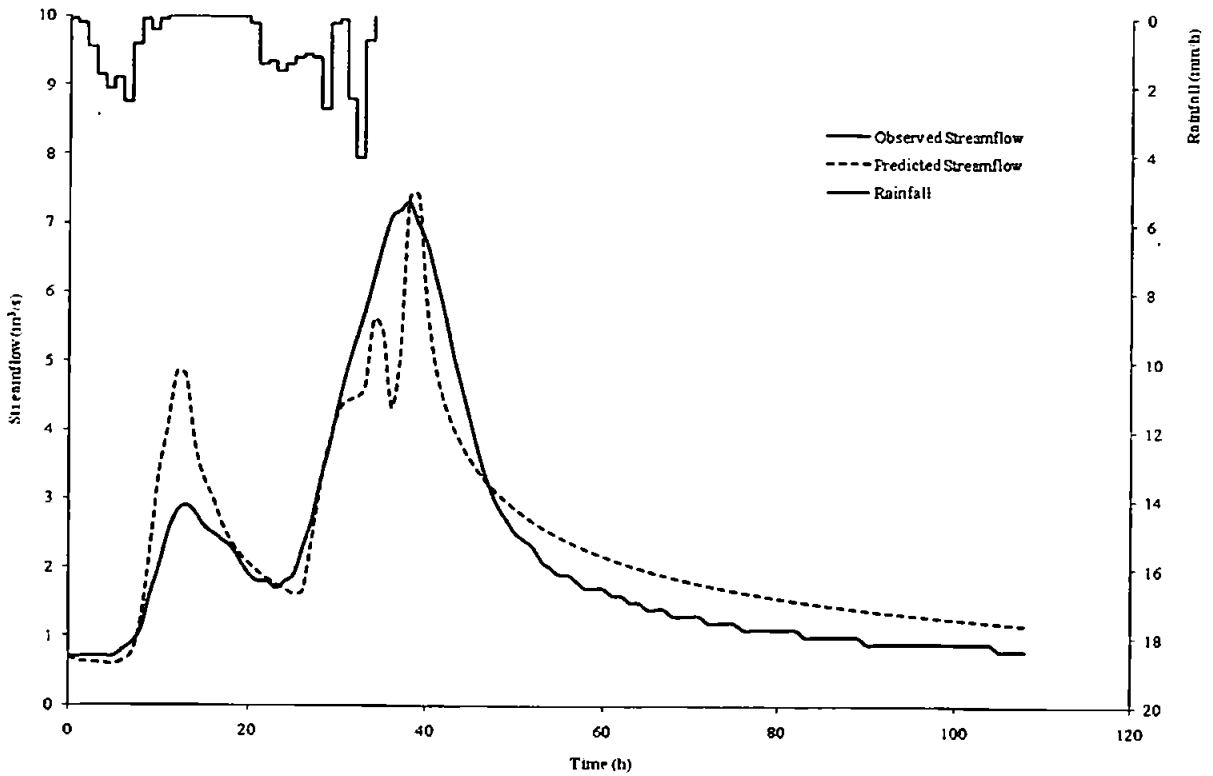**Figure D1.8 Predicted and observed results for event 1301**

281
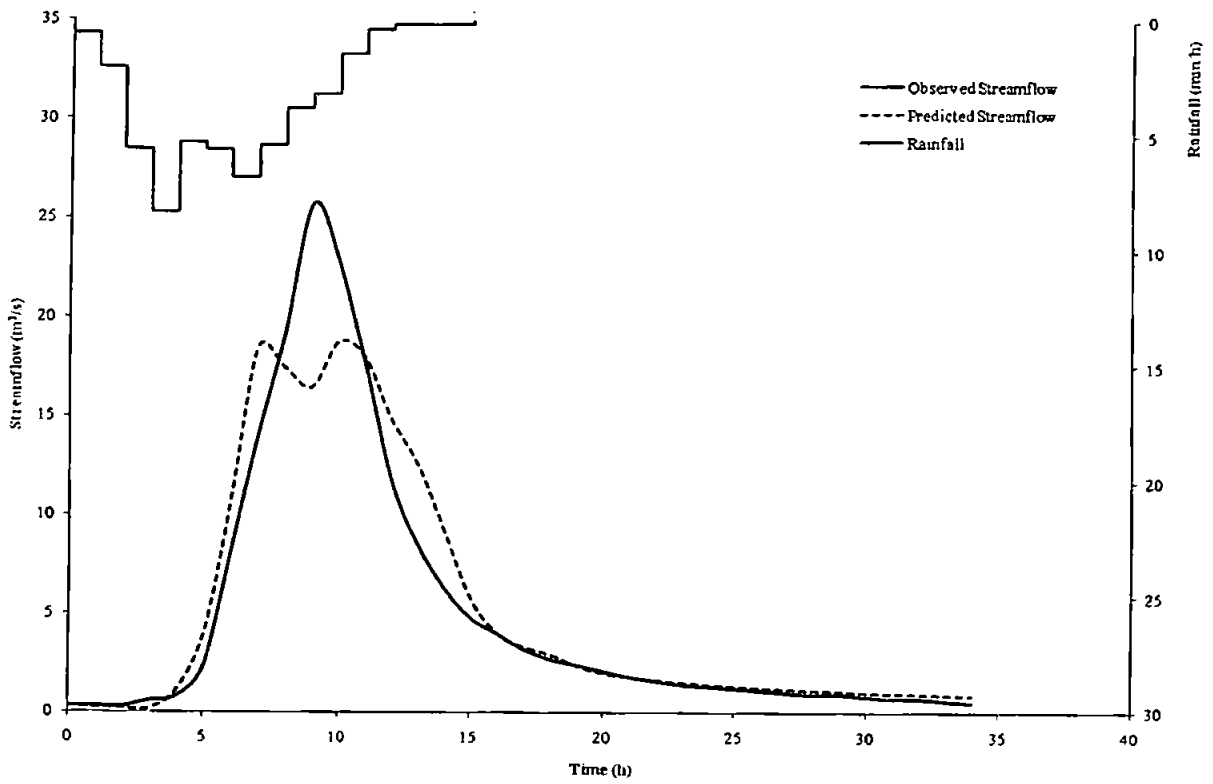
Figure D1.9 Predicted and observed results for event 1302

Figure D1.10 Predicted and observed results for event 1303

Figure D1.11 Predicted and observed results for event 1304

Figure D1.12 Predicted and observed results for event 4351

283
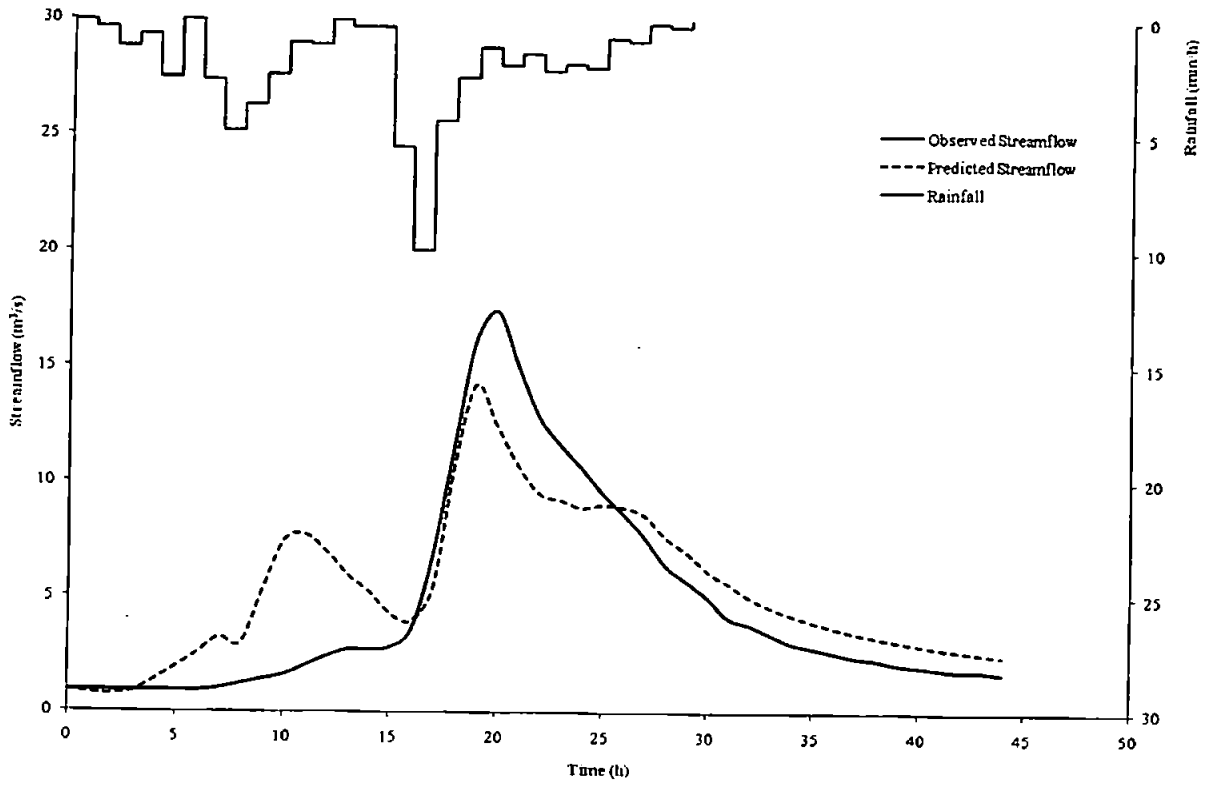
Figure D1.13 Predicted and observed results for event 4352
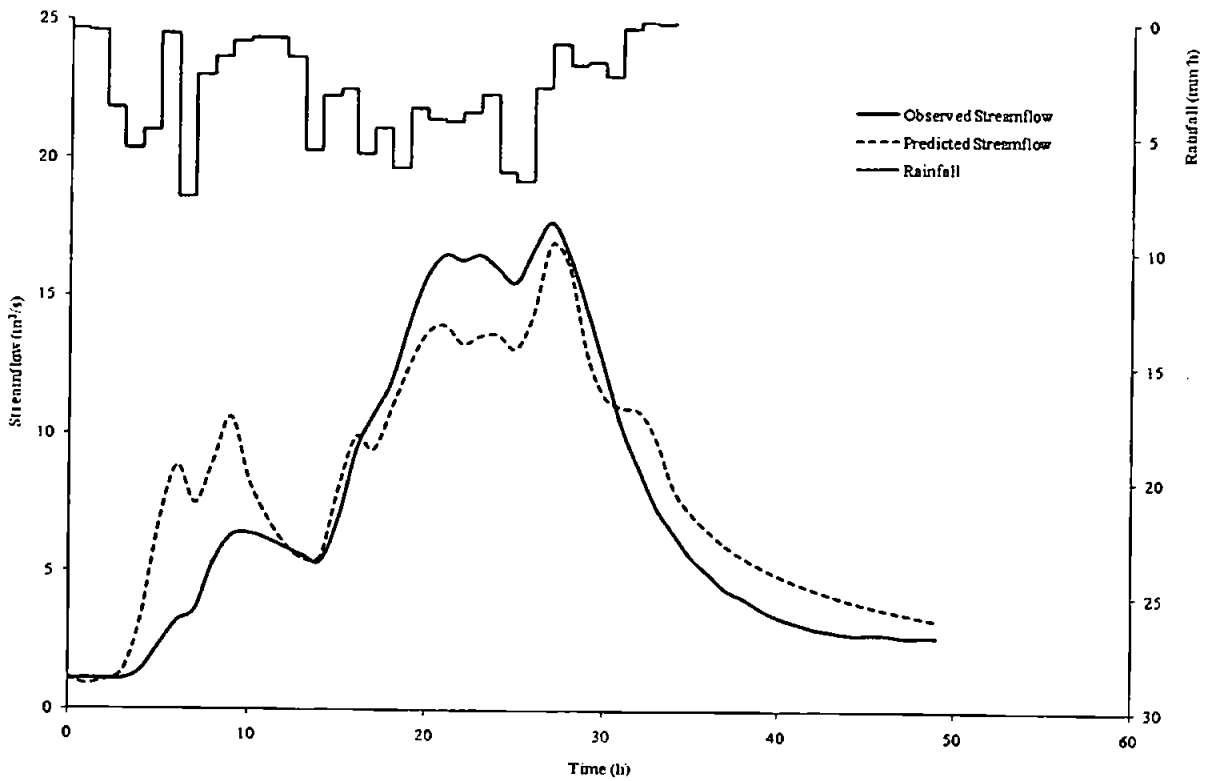
Figure D1.14 Predicted and observed results for event 4353

D2: Catchment 30004 – River Lymn at Partney Mill
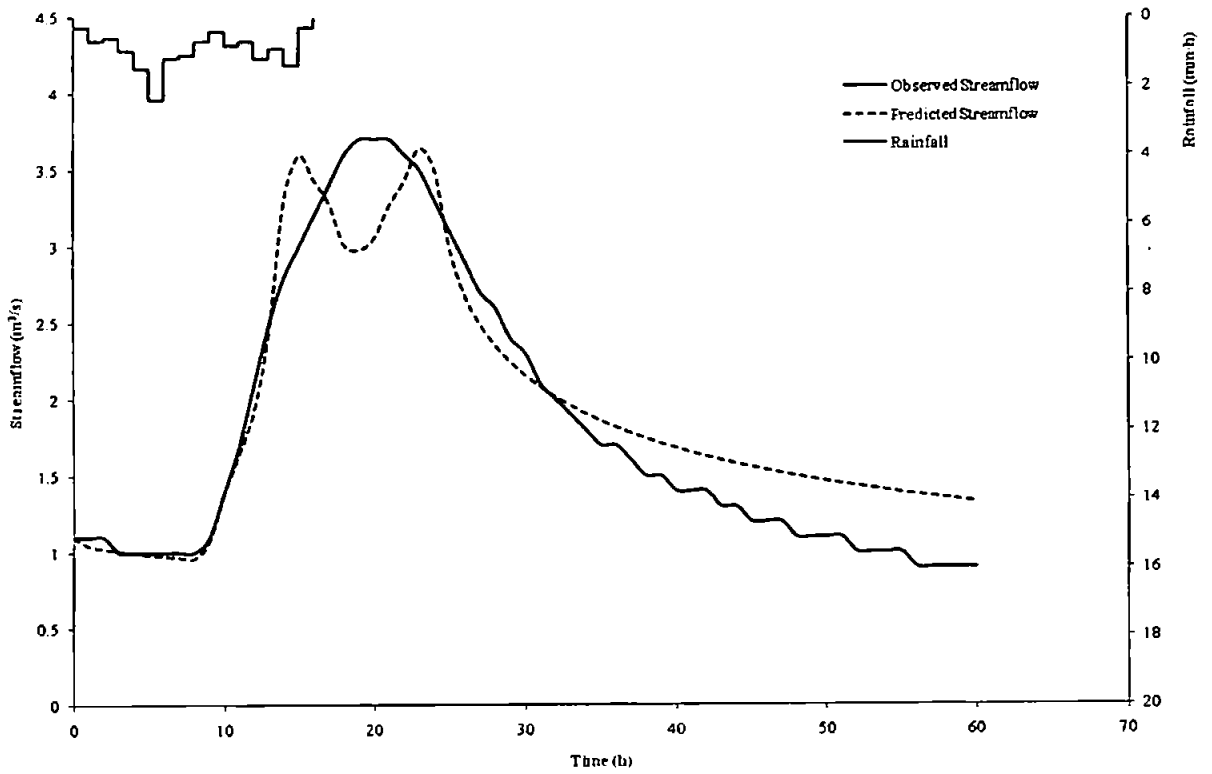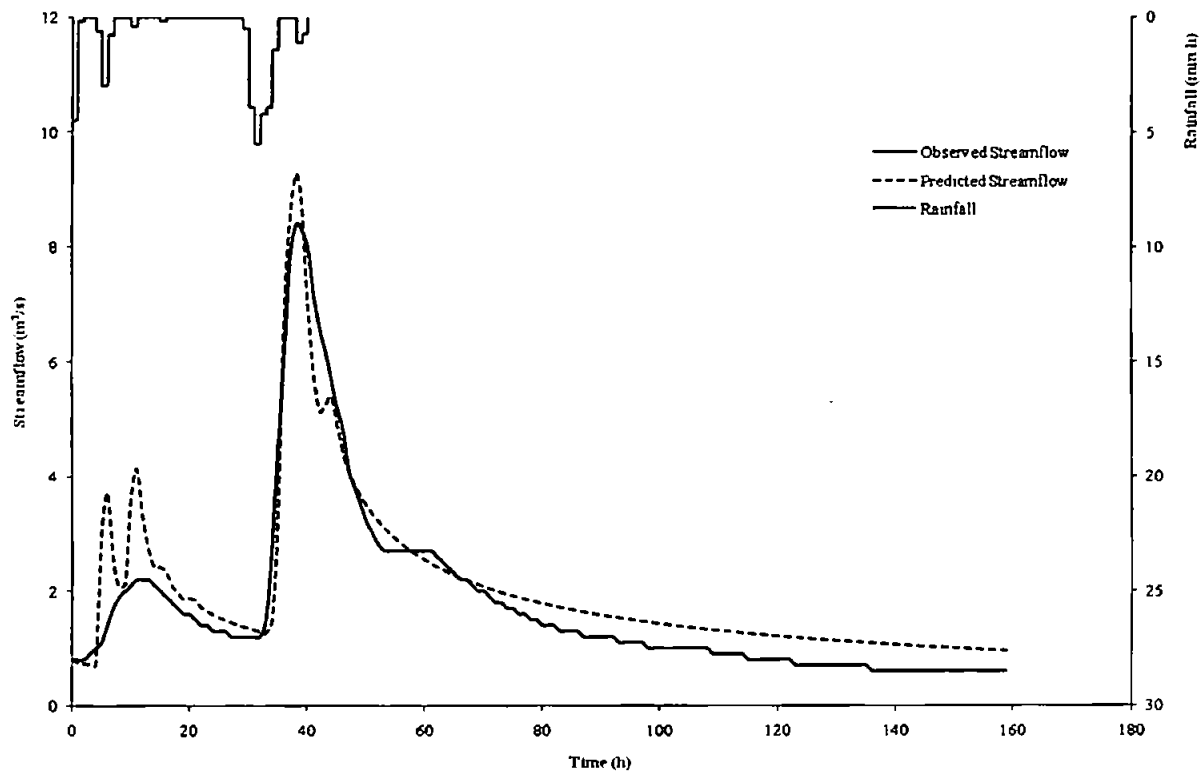

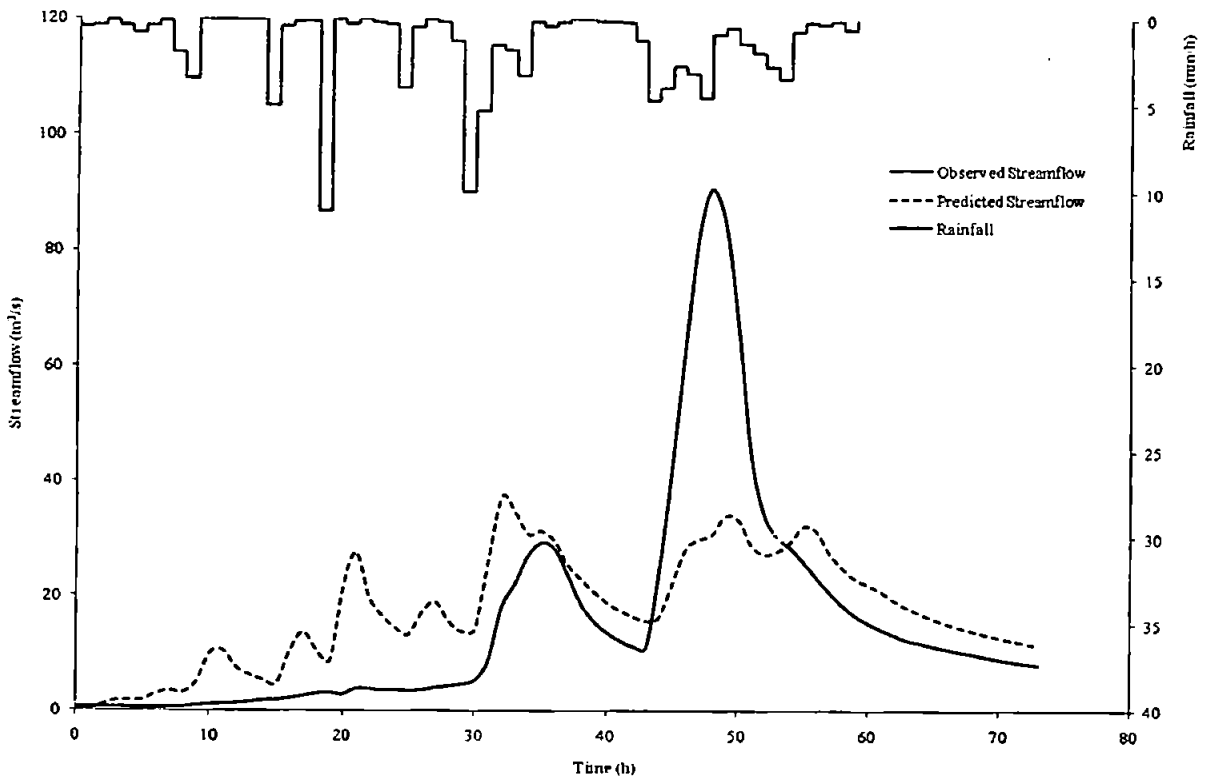**Figure D2.1 Predicted and observed results for event 492**
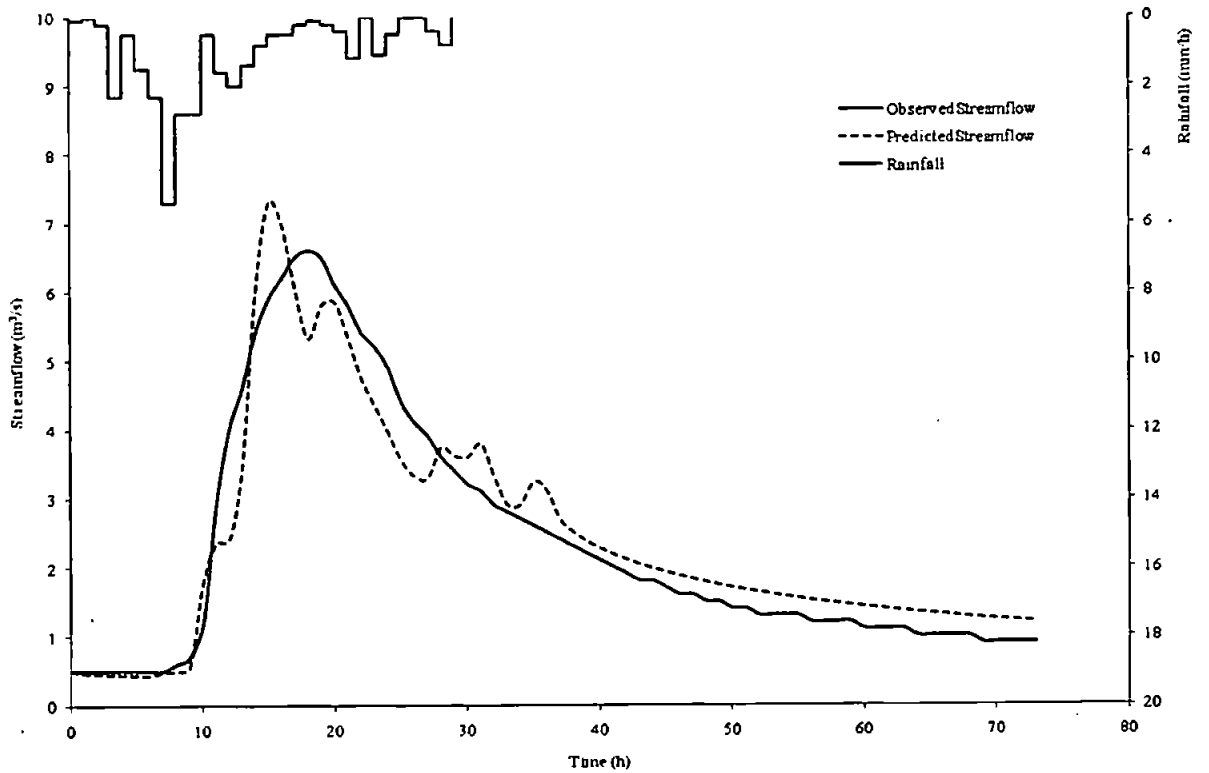
Figure D2.2 Predicted and observed results for event 495

Figure D2.3 Predicted and observed results for event 496

Figure D2.4 Predicted and observed results for event 3874

286

Figure D2.5 Predicted and observed results for event 3877

Figure D2.6 Predicted and observed results for event 3878

287

Figure D2.7 Predicted and observed results for event 3880
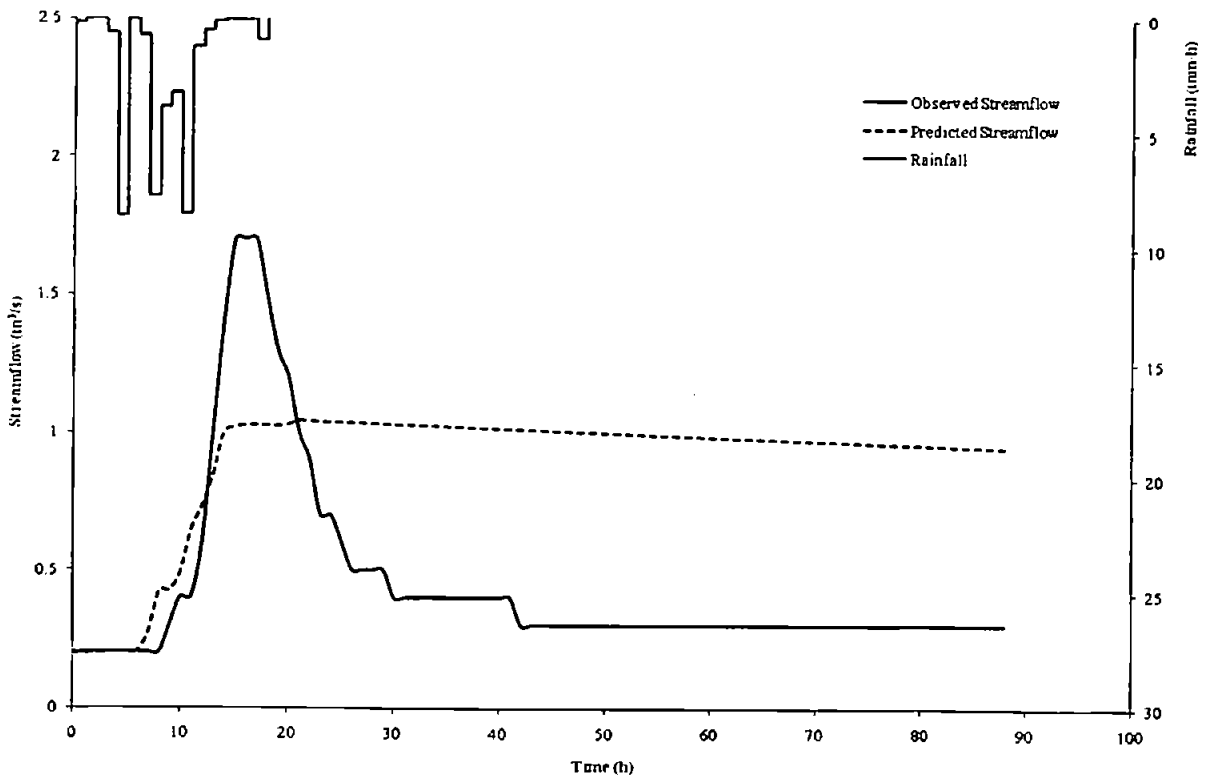
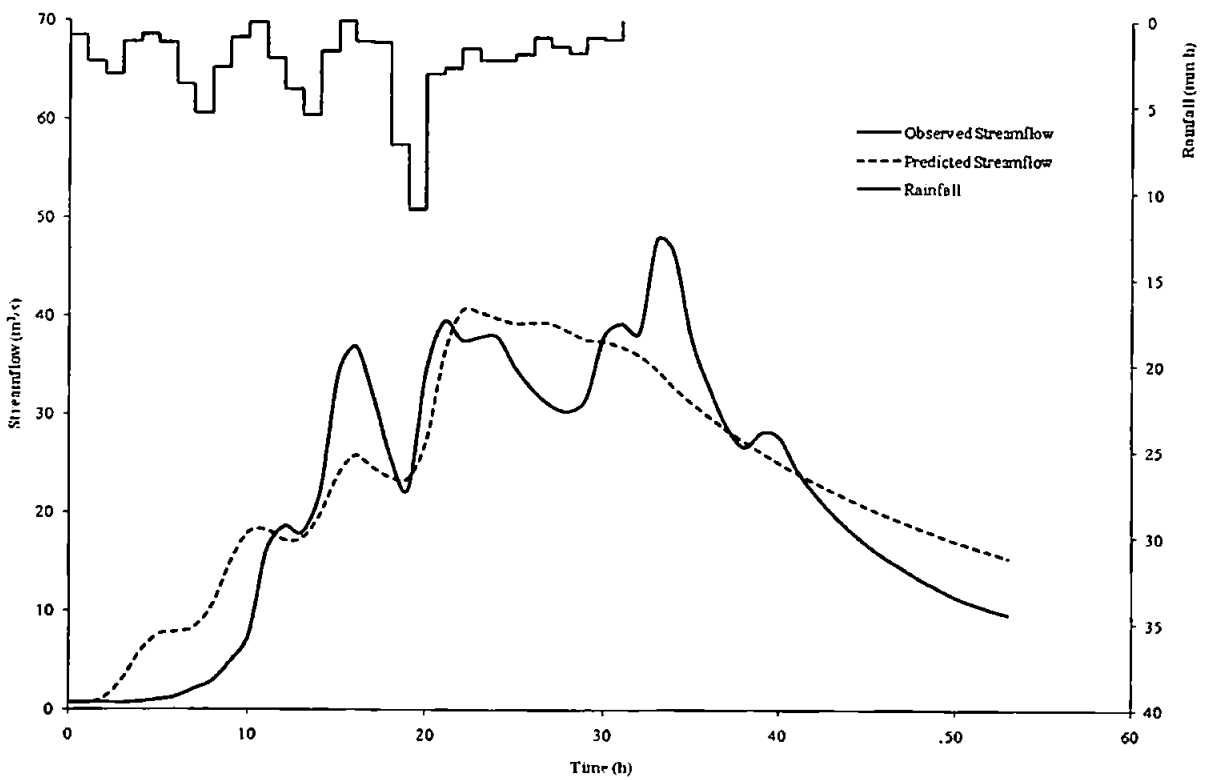**Figure D2.8 Predicted and observed results for event 3881**

288
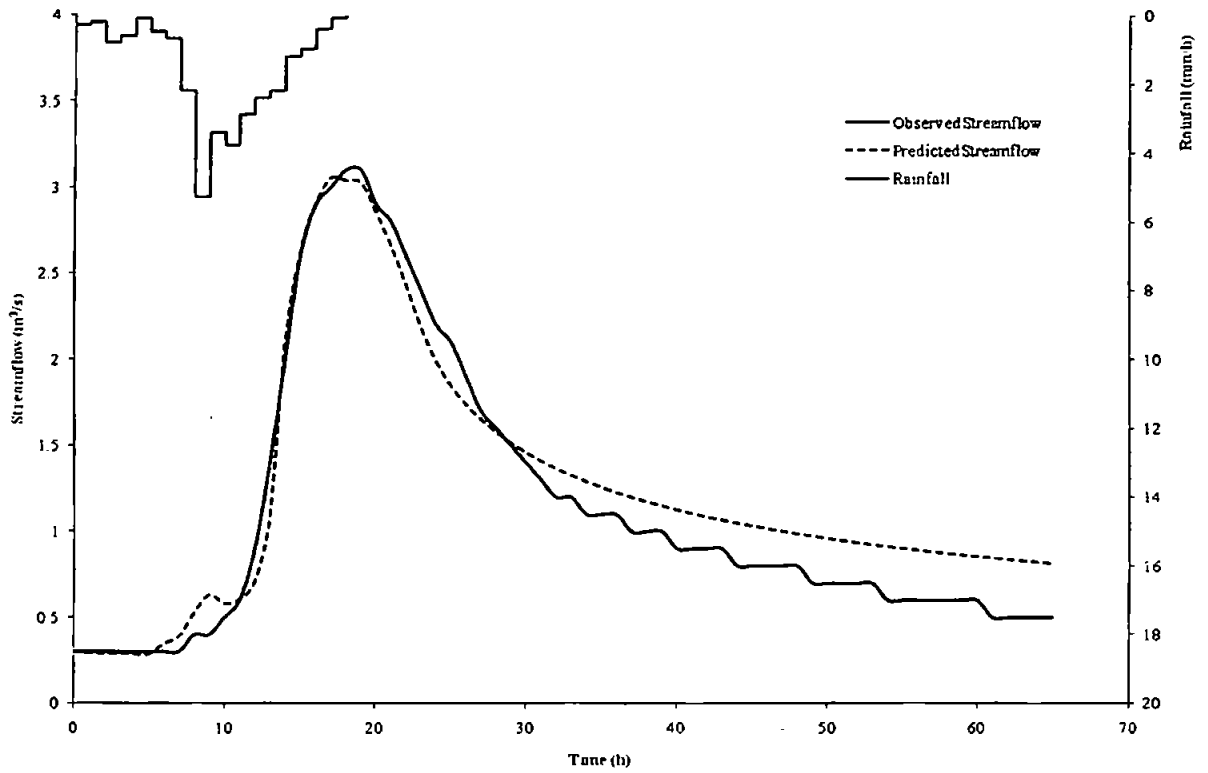
Figure D2.9 Predicted and observed results for event 3882
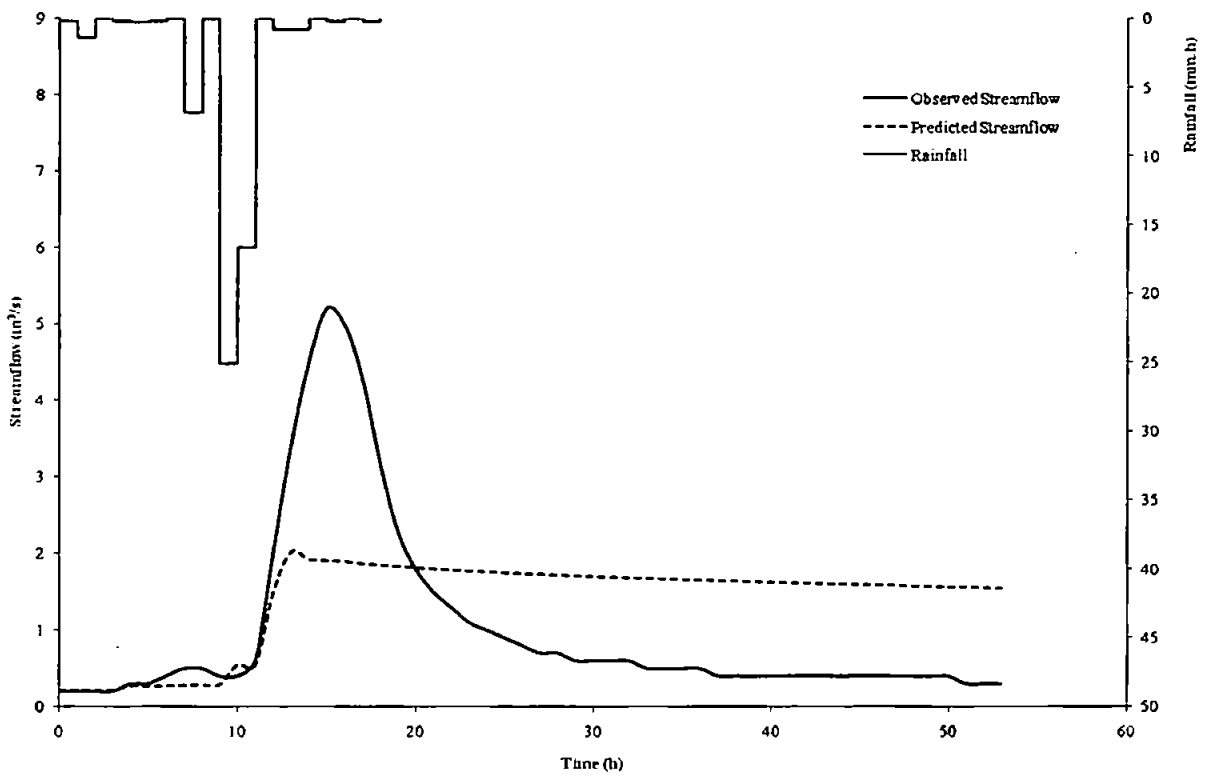
Figure D2.10 Predicted and observed results for event 3884

289

Figure D2.11 Predicted and observed results for event 3890

Figure D2.12 Predicted and observed results for event 3893

290

Figure D2.13 Predicted and observed results for event 4166

D3: Catchment 74001 – River Duddon at Duddon Hall

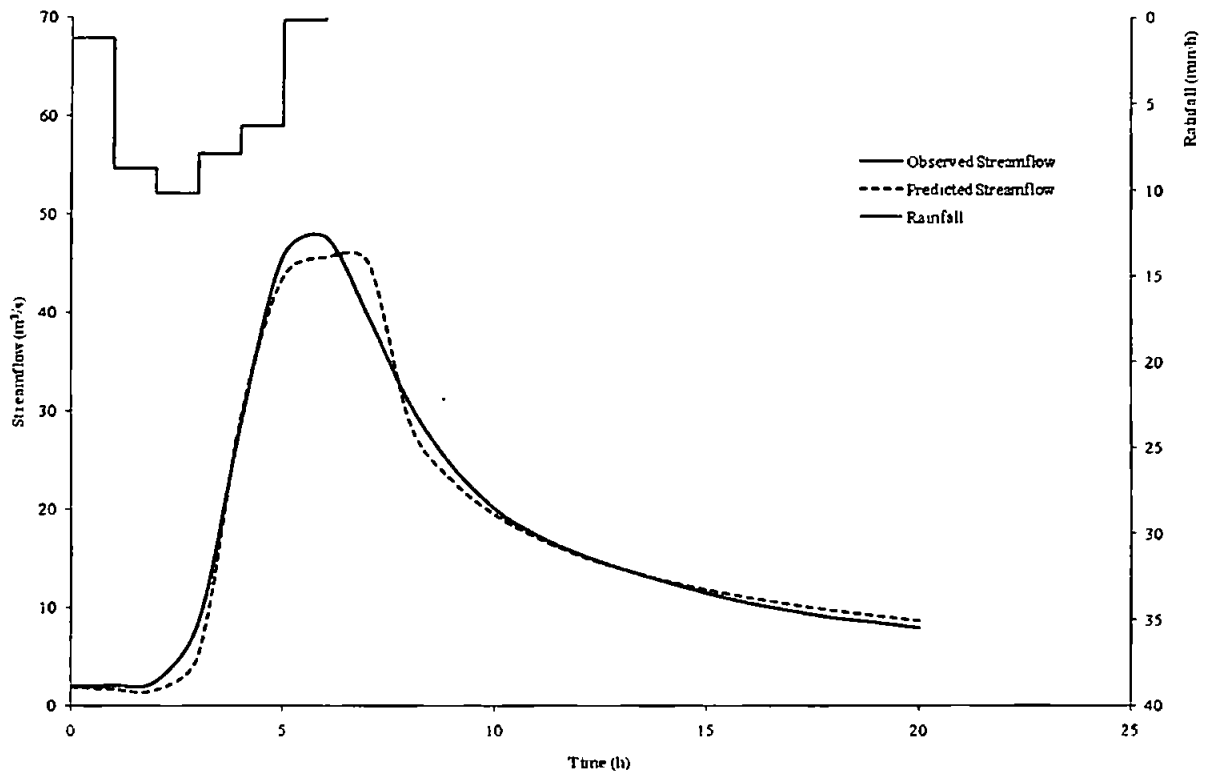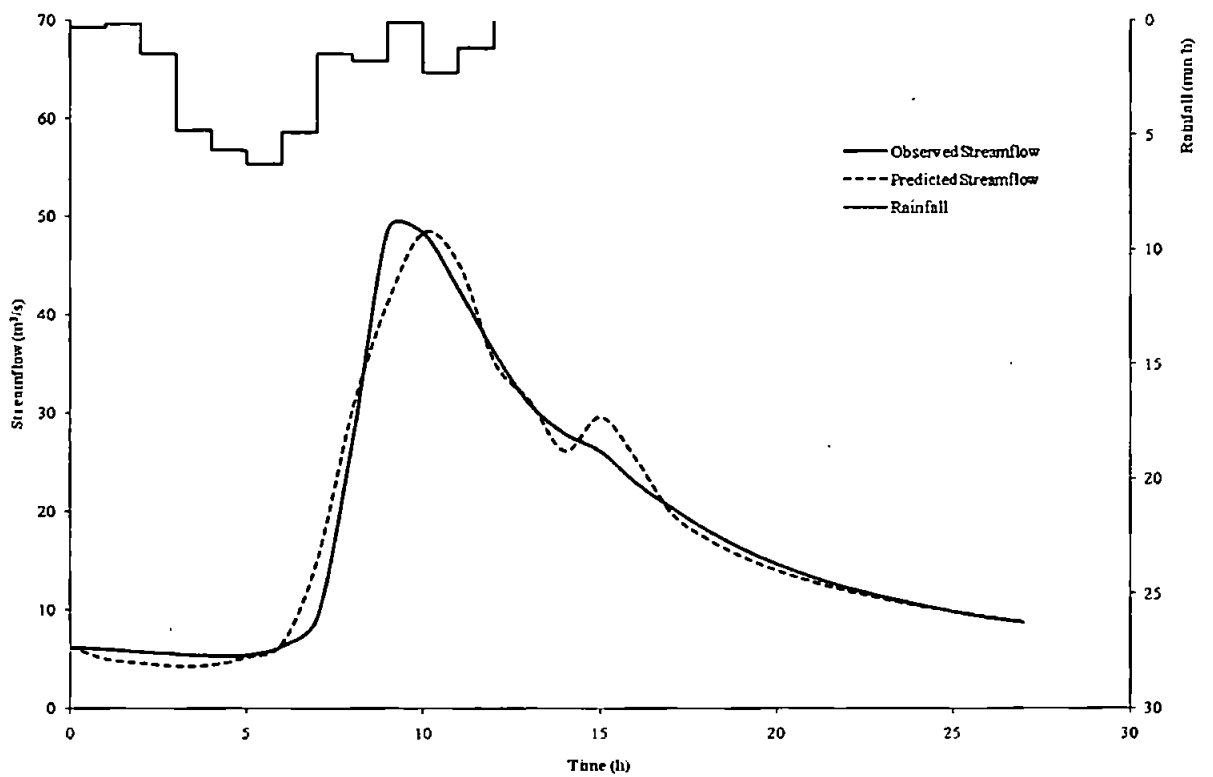**Figure D3.1 Predicted and observed results for event 2360**
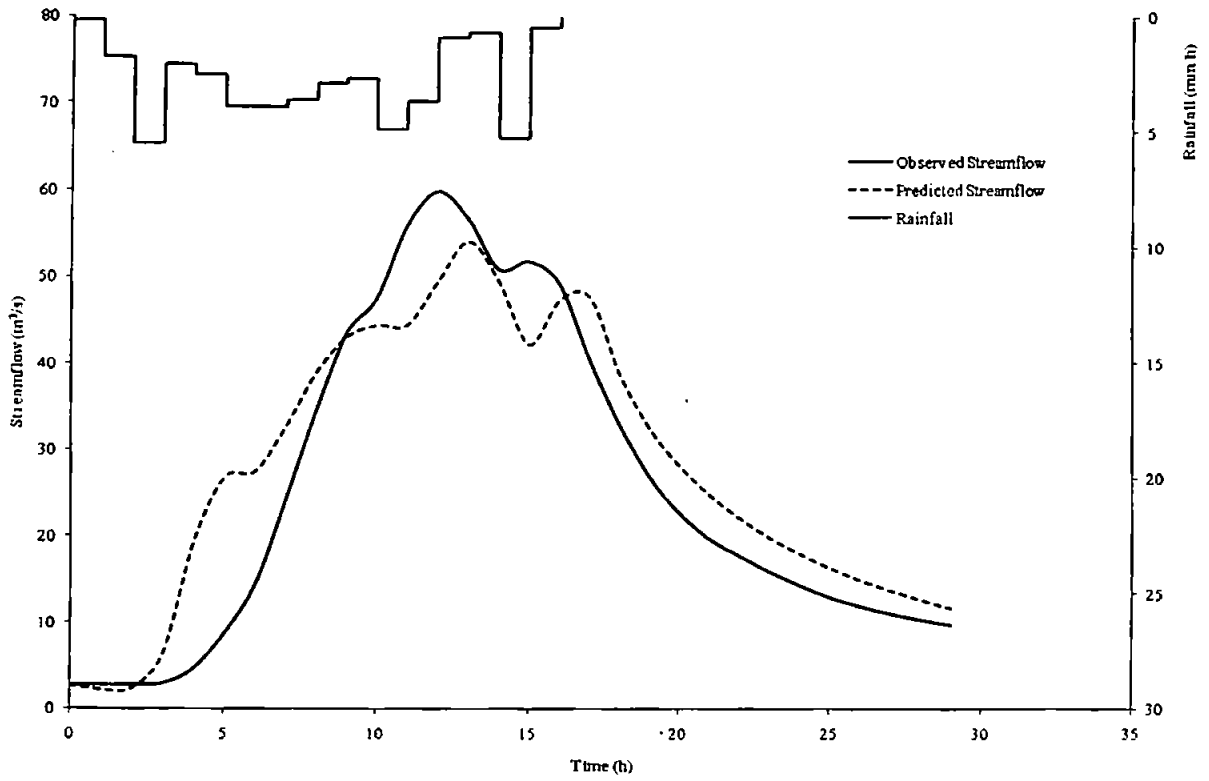

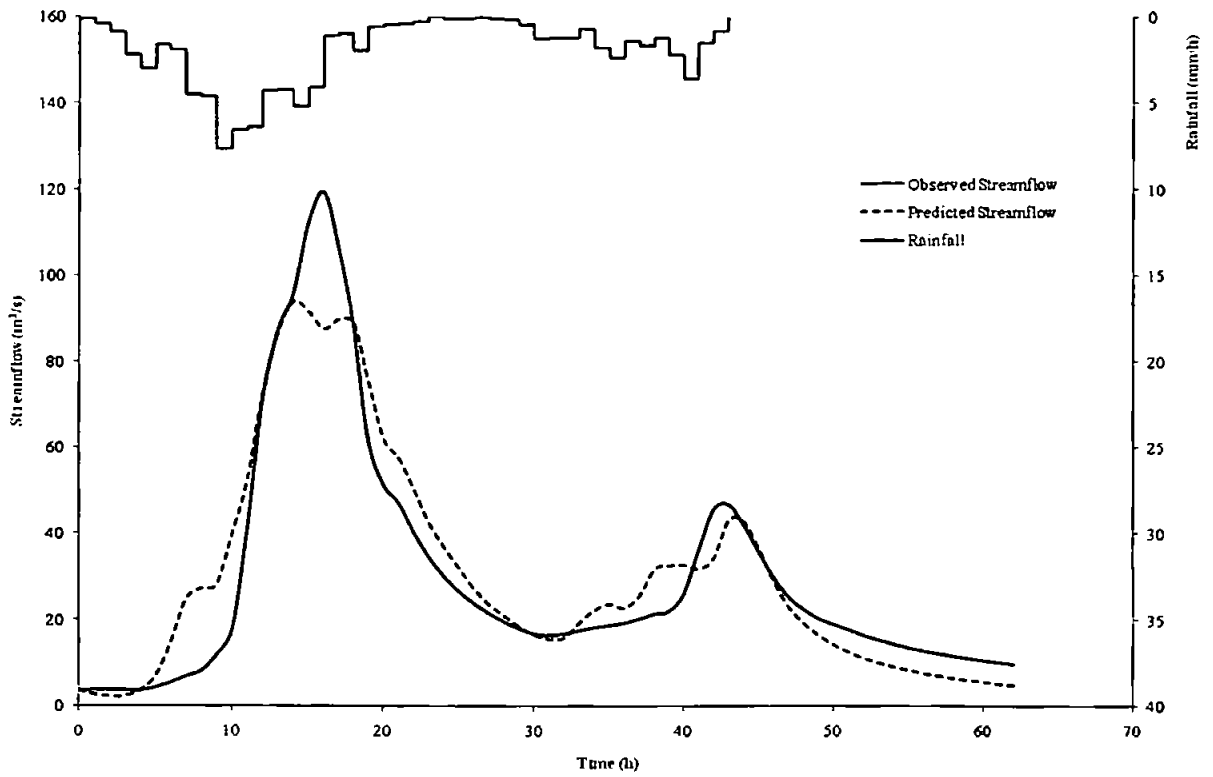**Figure D3.2 Predicted and observed results for event 2361**

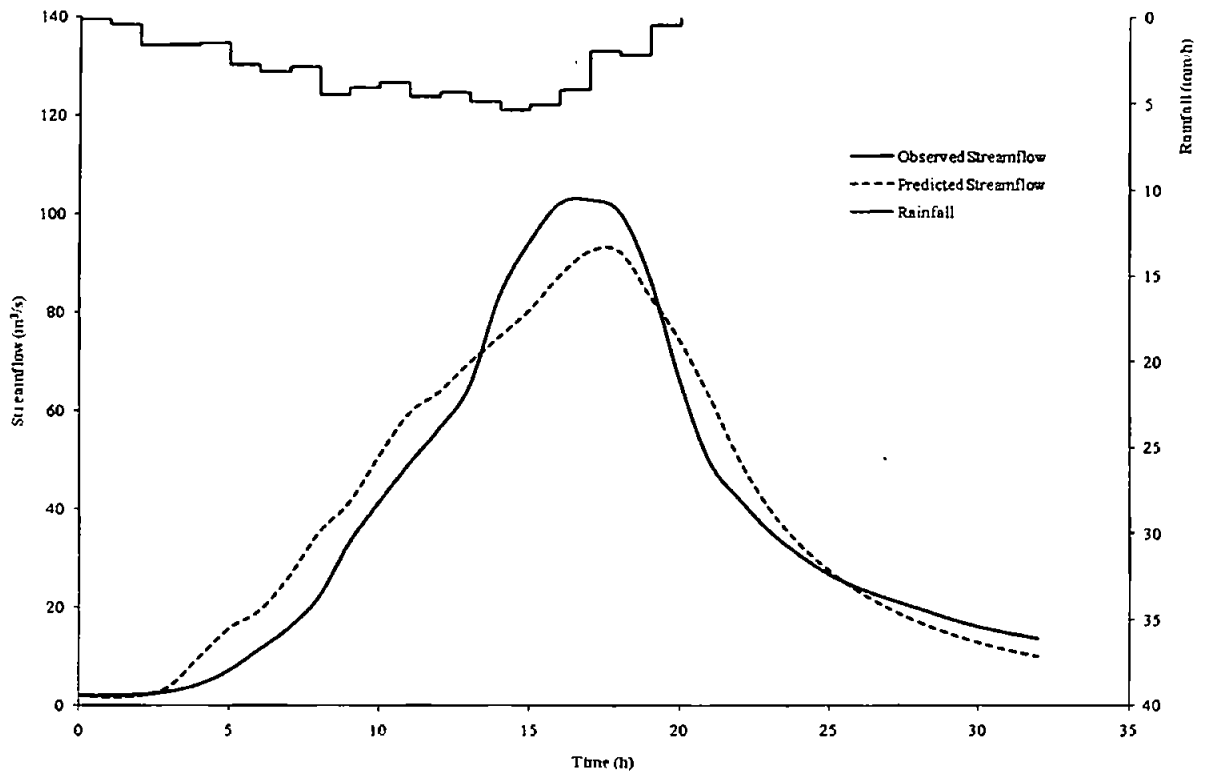**Figure D3.3 Predicted and observed results for event 2362**

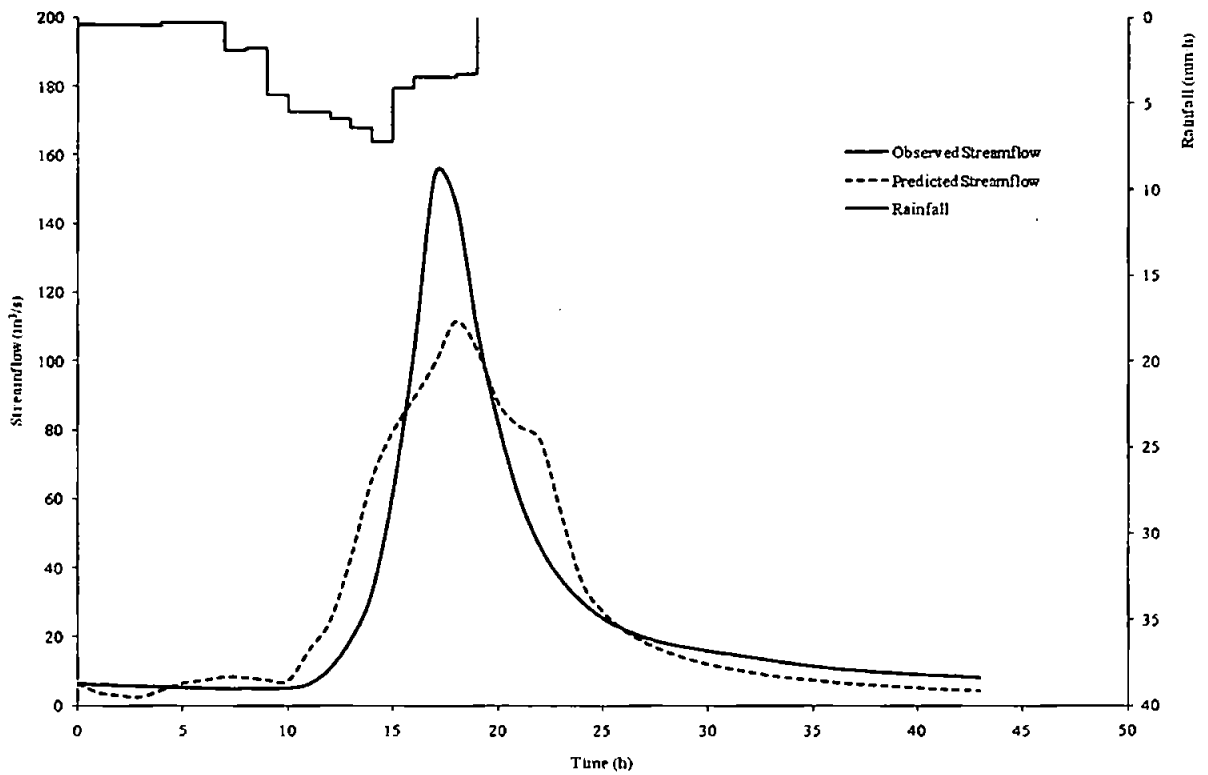**Figure D3.4 Predicted and observed results for event 2363**

Figure D3.5 Predicted and observed results for event 2364

Figure D3.6 Predicted and observed results for event 2365

294

Figure D3.7 Predicted and observed results for event 2366

Figure D3.8 Predicted and observed results for event 2367

D4: Catchment 25005 – River Leven at Leven Bridge

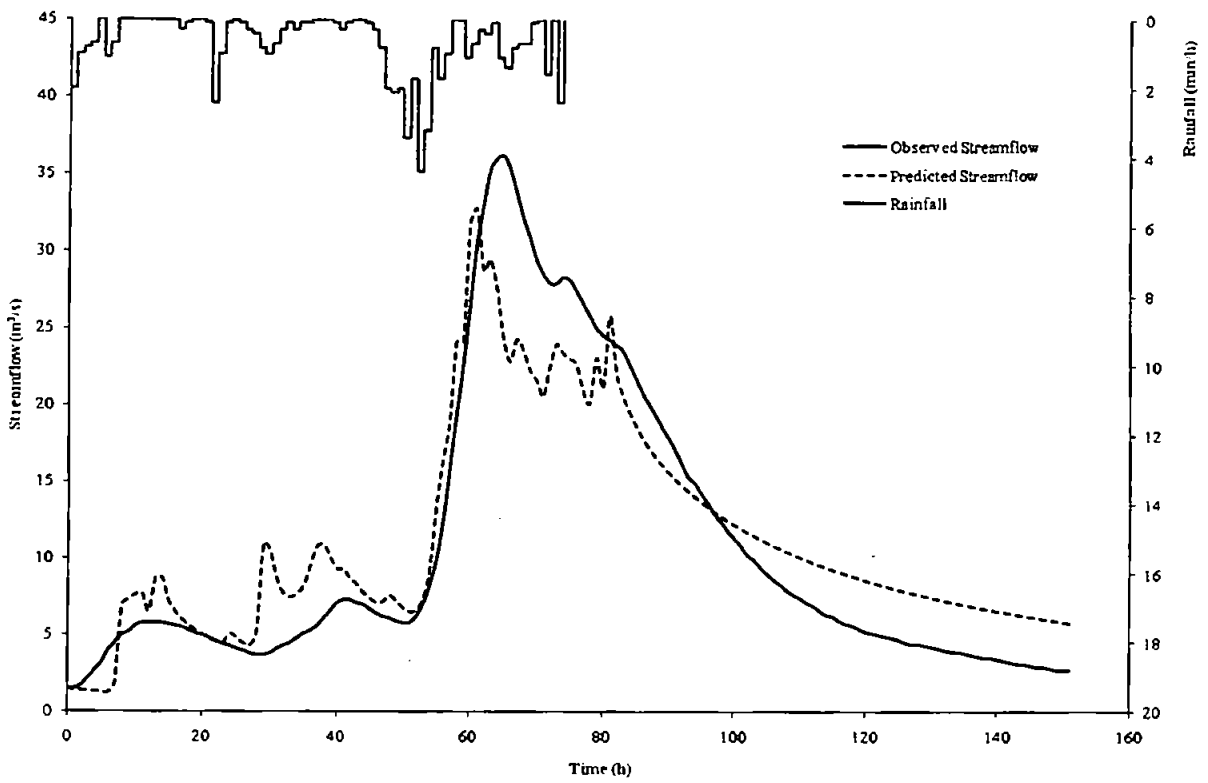**Figure D4.1 Predicted and observed results for event 3989**

Figure D4.2 Predicted and observed results for event 3990

Figure D4.3 Predicted and observed results for event 3994

Figure D4.4 Predicted and observed results for event 3995
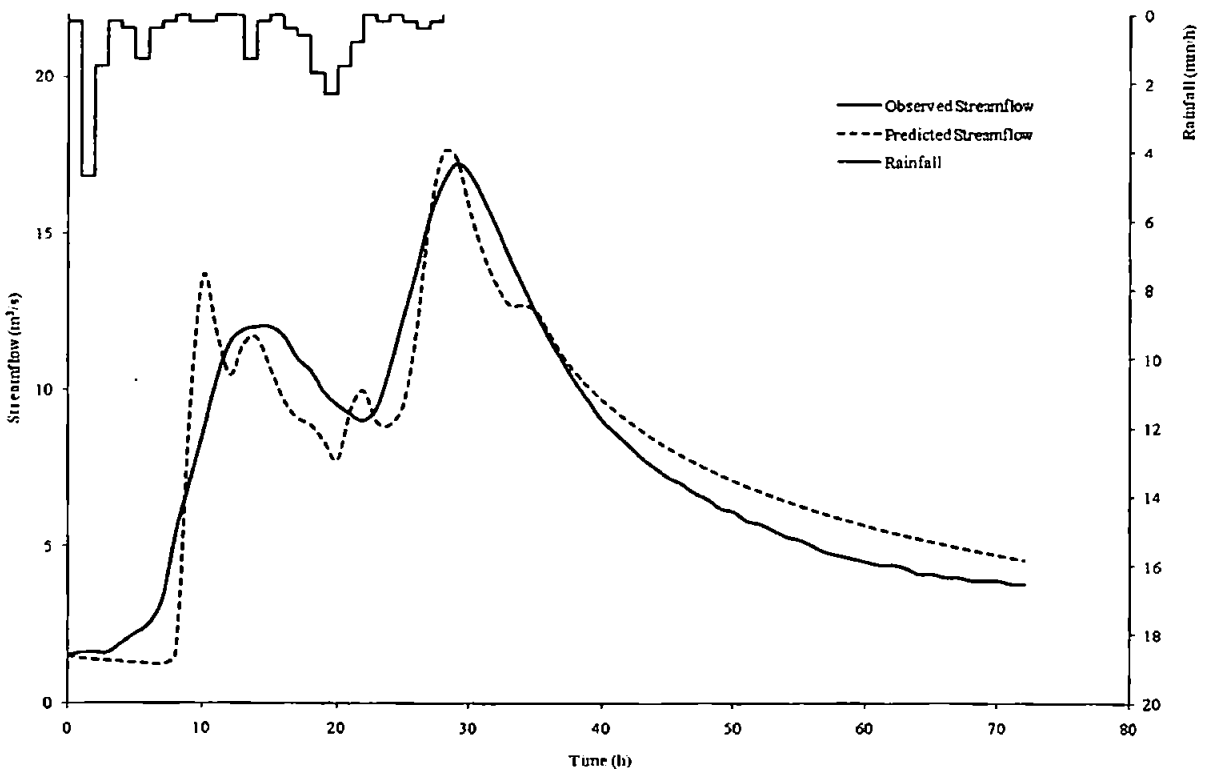
297

Figure D4.5 Predicted and observed results for event 3996

Figure D4.6 Predicted and observed results for event 3997

298

Figure D4.7 Predicted and observed results for event 3998

Figure D4.8 Predicted and observed results for event 3999

Figure D4.9 Predicted and observed results for event 4002

Figure D4.10 Predicted and observed results for event 4004

Figure D4.11 Predicted and observed results for event 4018
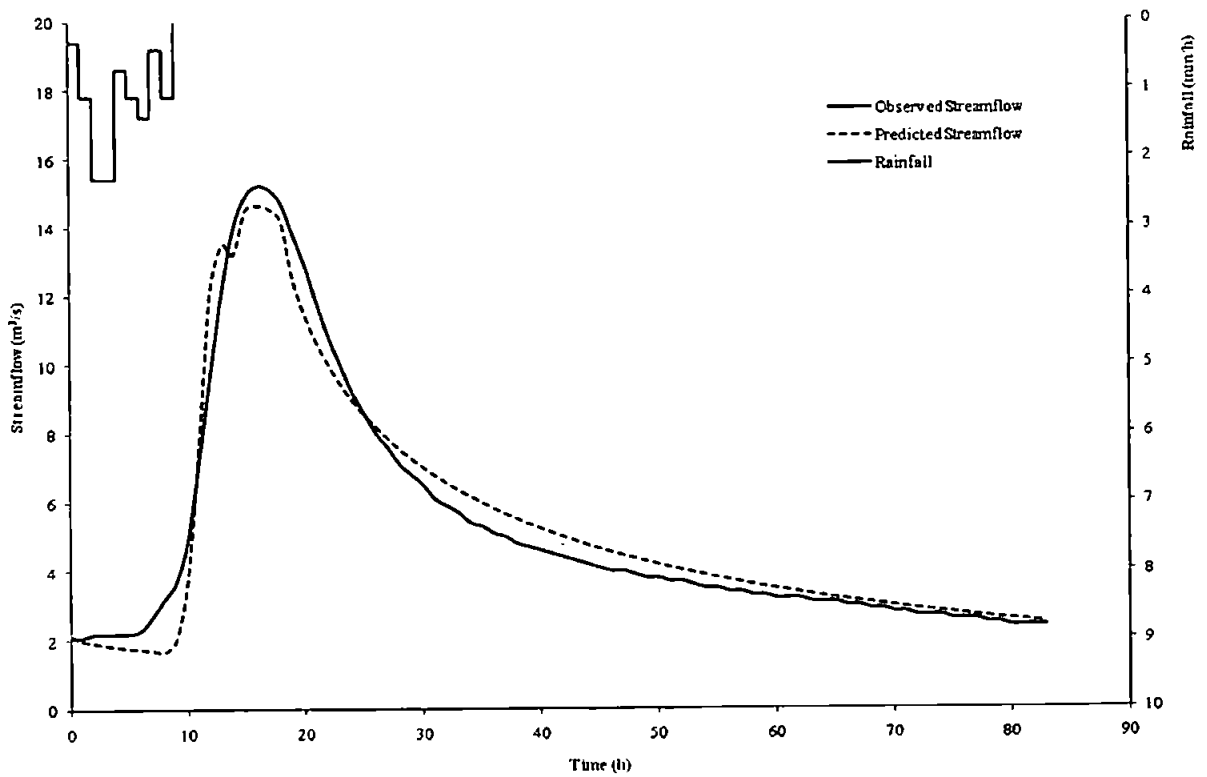
Figure D4.12 Predicted and observed results for event 4393

301
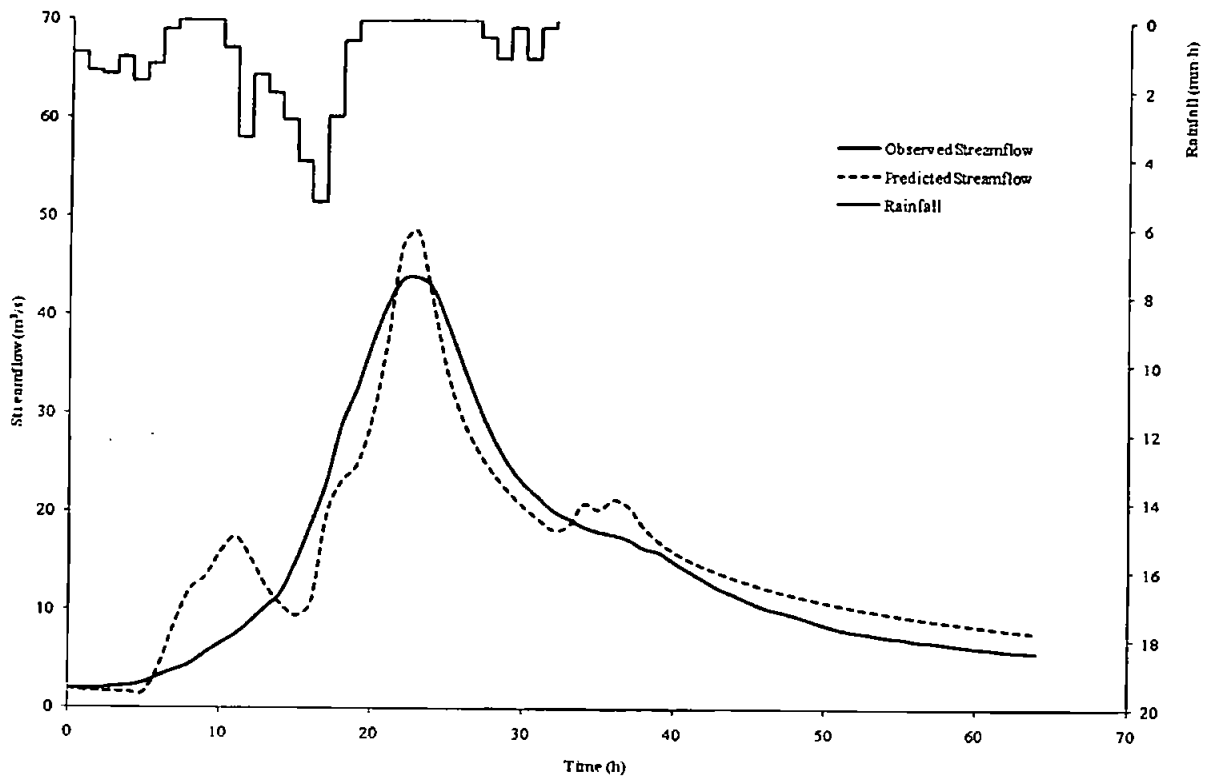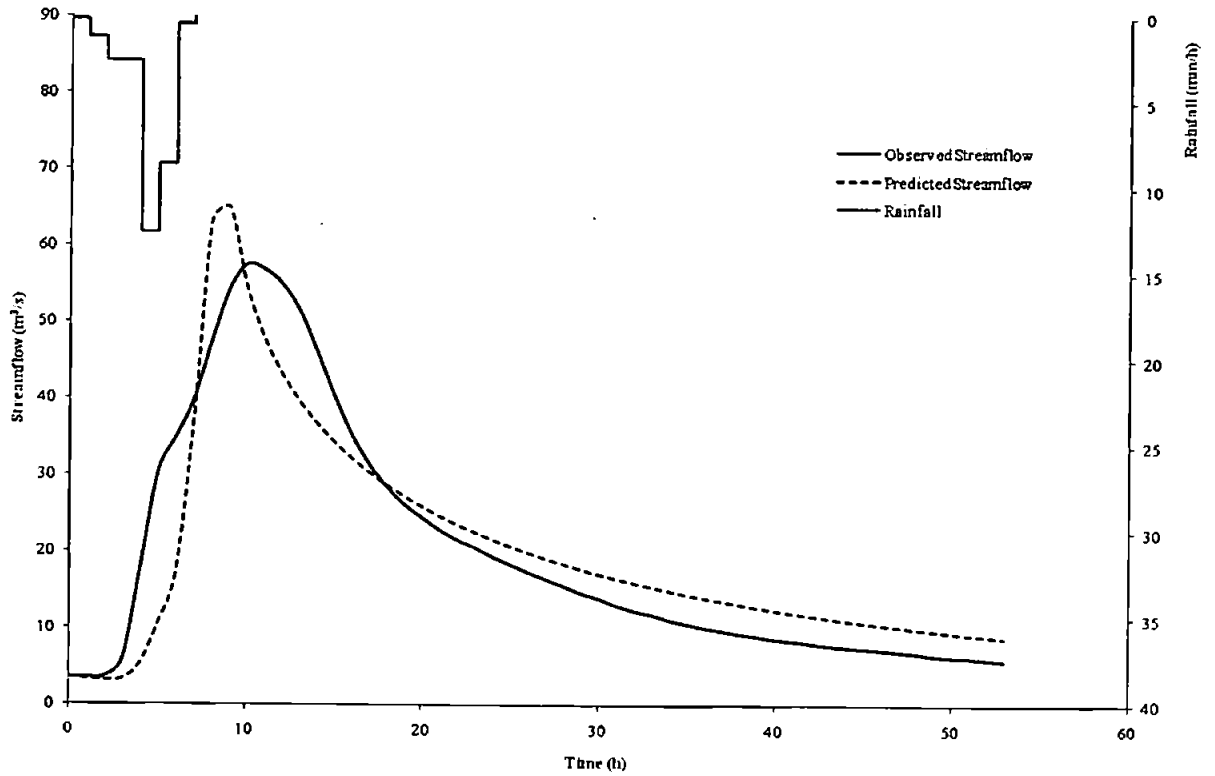
Figure D4.13 Predicted and observed results for event 4395

Figure D4.14 Predicted and observed results for event 4399

Figure D4.15 Predicted and observed results for event 4401

D5: Catchment 54004 – River Sowe at Stoneleigh

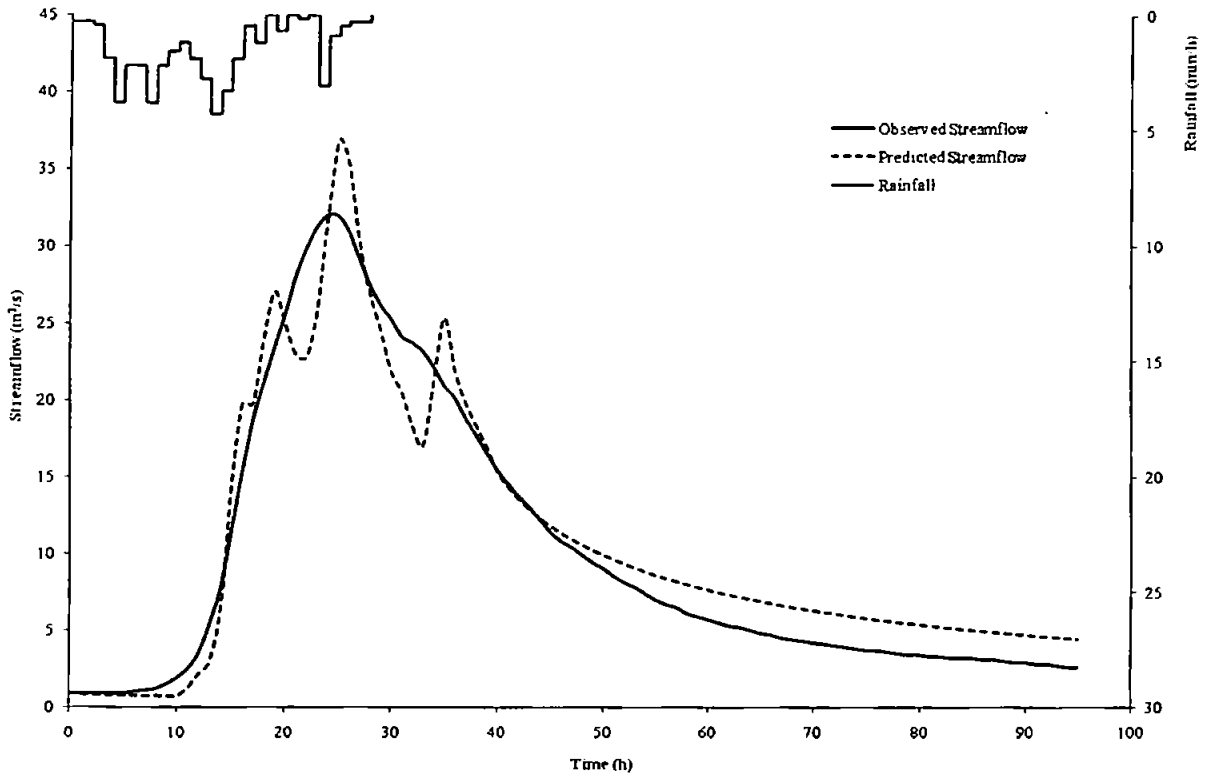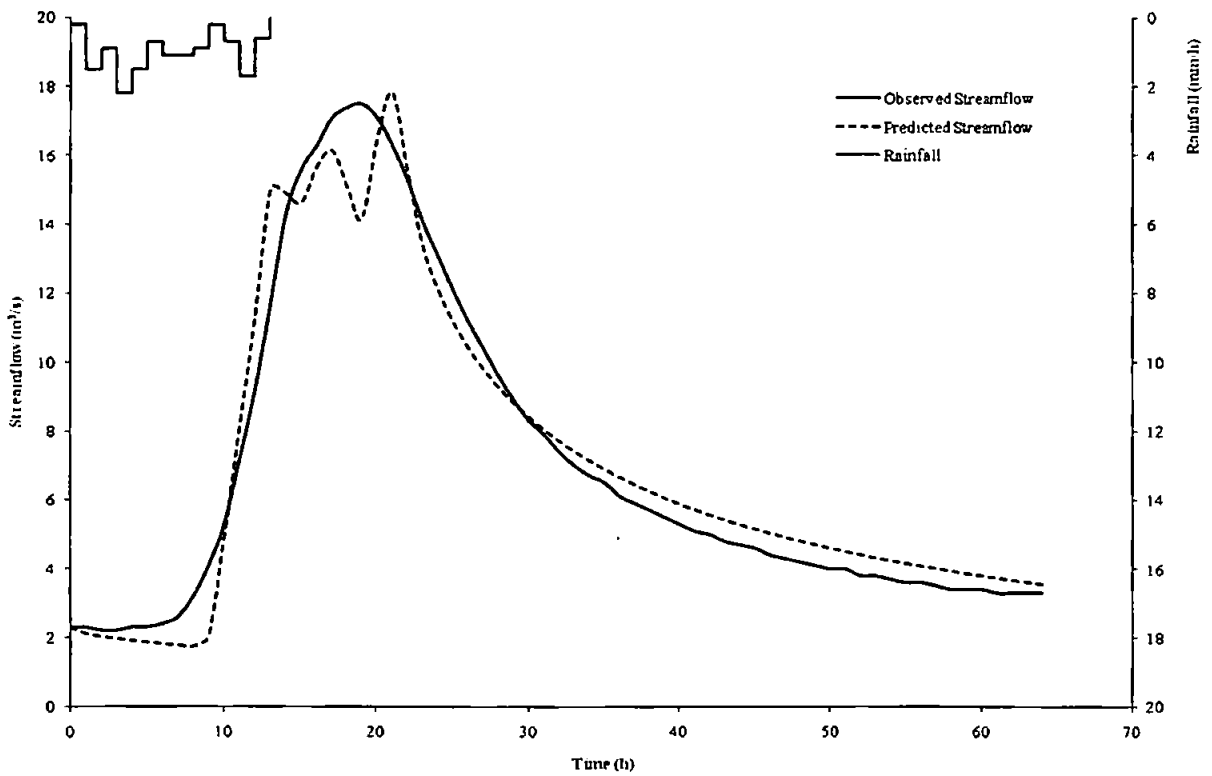**Figure D5.1 Predicted and observed results for event 1559**

Figure D5.2 Predicted and observed results for event 1560

Figure D5.3 Predicted and observed results for event 1561

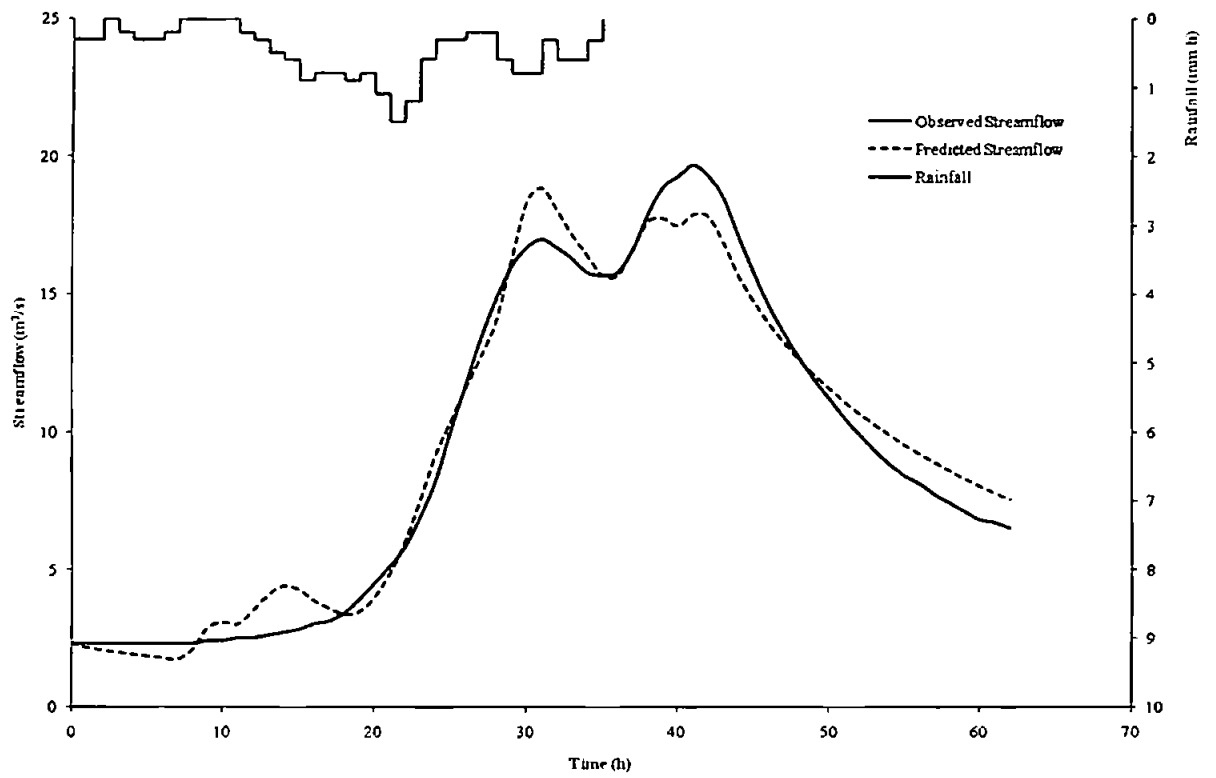**Figure D5.4 Predicted and observed results for event 1562**

305

Figure D5.5 Predicted and observed results for event 1563

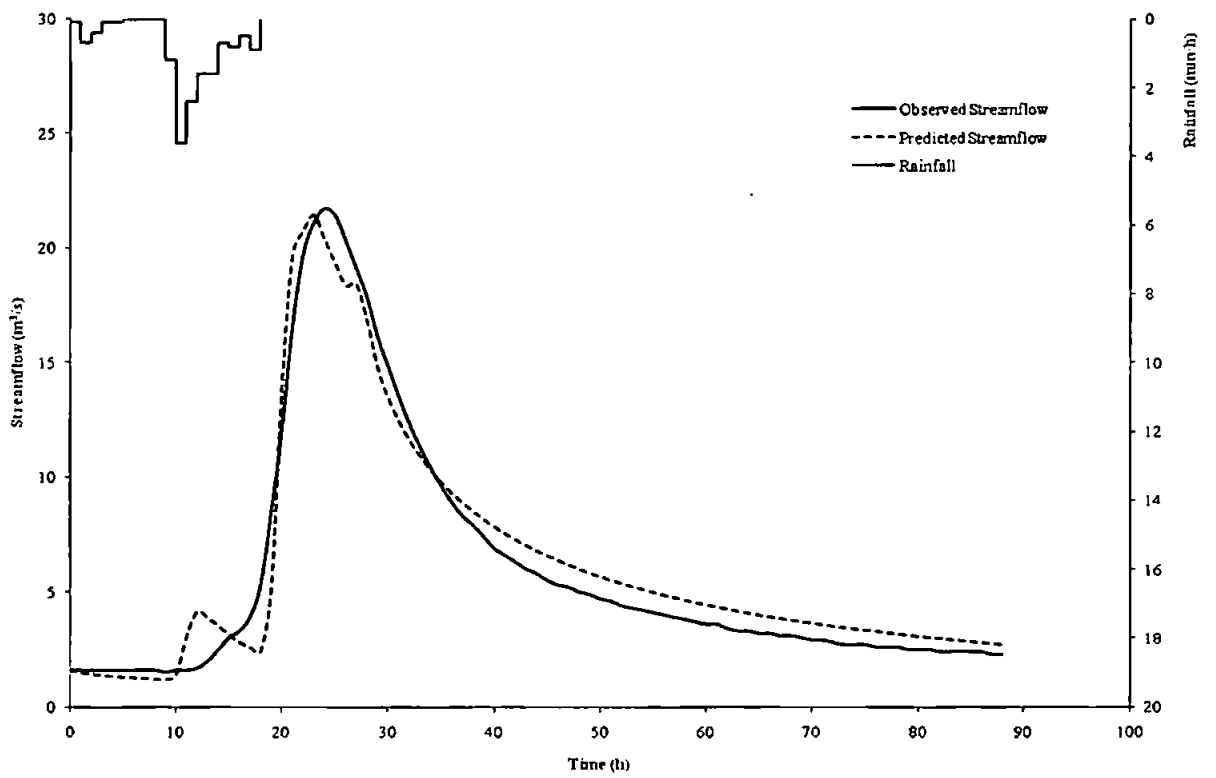**Figure D5.6 Predicted and observed results for event 1564**

306

Figure D5.7 Predicted and observed results for event 1567

Figure D5.8 Predicted and observed results for event 1568

Figure D5.9 Predicted and observed results for event 1570

Figure D5.10 Predicted and observed results for event 1571

308

Figure D5.11 Predicted and observed results for event 1572

D6: Catchment 37001 – River Roding at Redbridge

Figure D6.1 Predicted and observed results for event 650

Figure D6.2 Predicted and observed results for event 651

Figure D6.3 Predicted and observed results for event 653

Figure D6.4 Predicted and observed results for event 656

Figure D6.5 Predicted and observed results for event 657

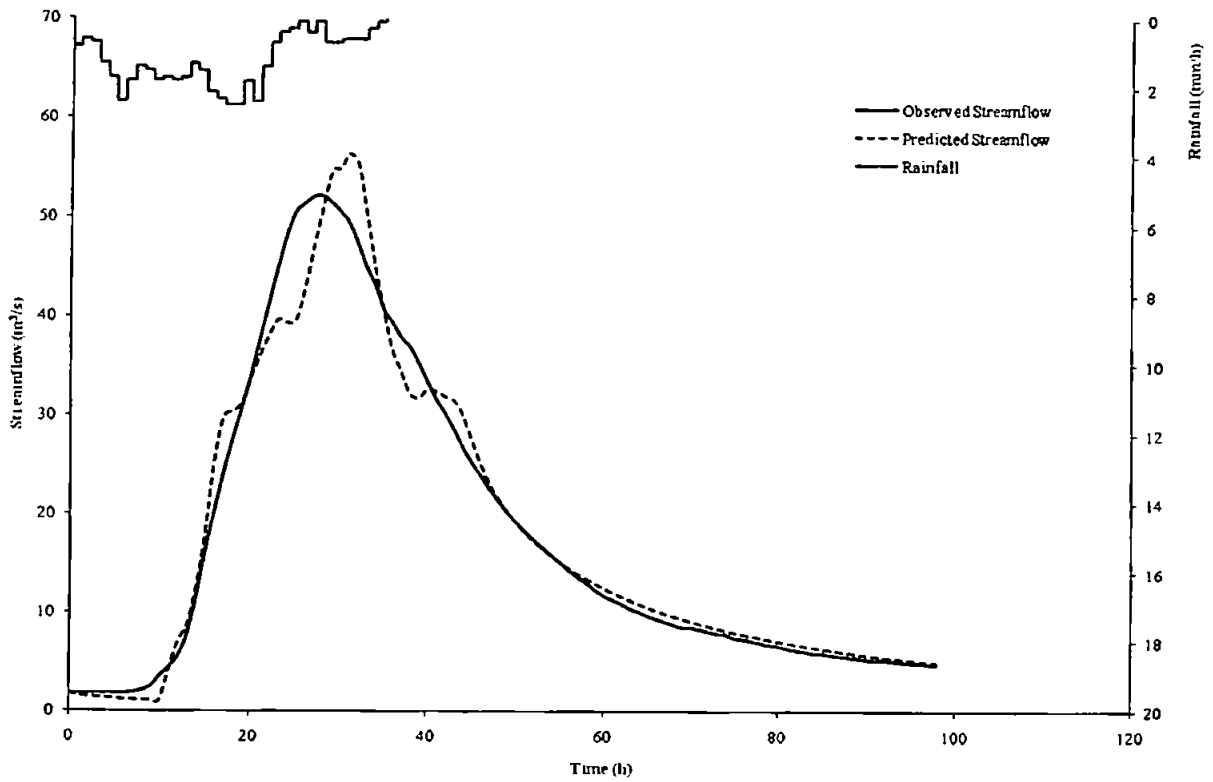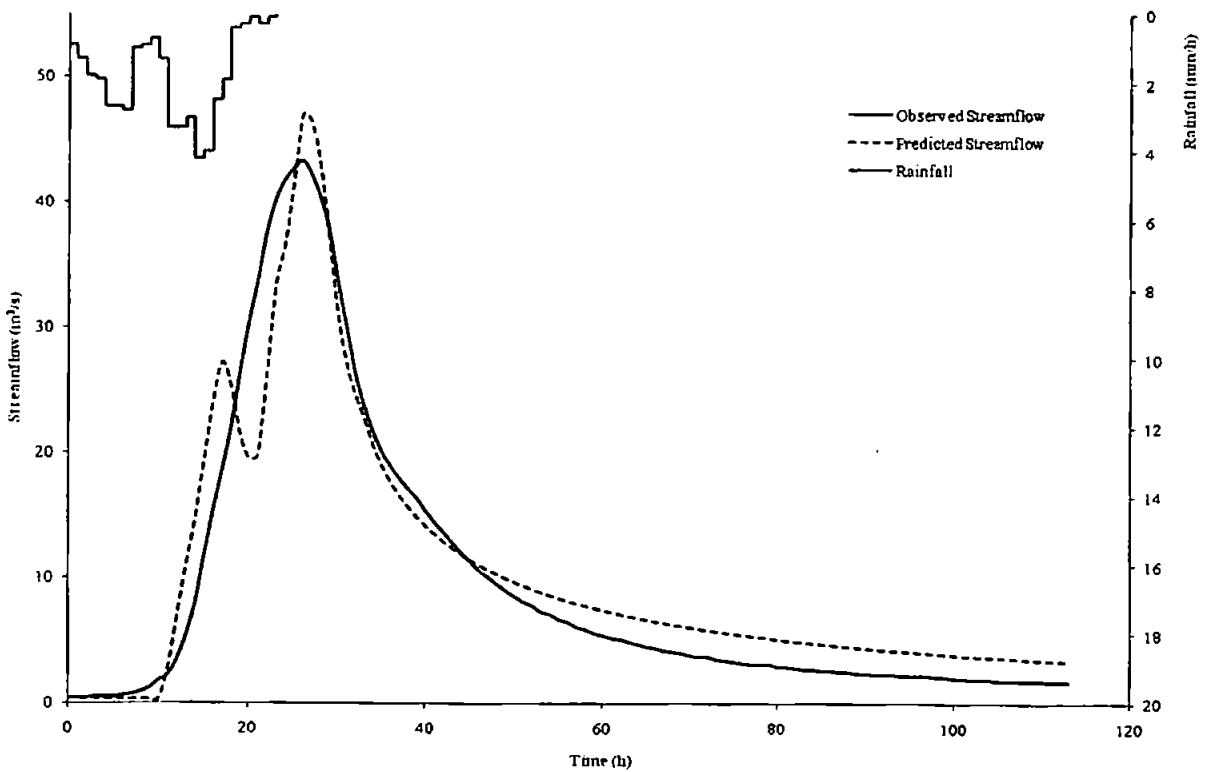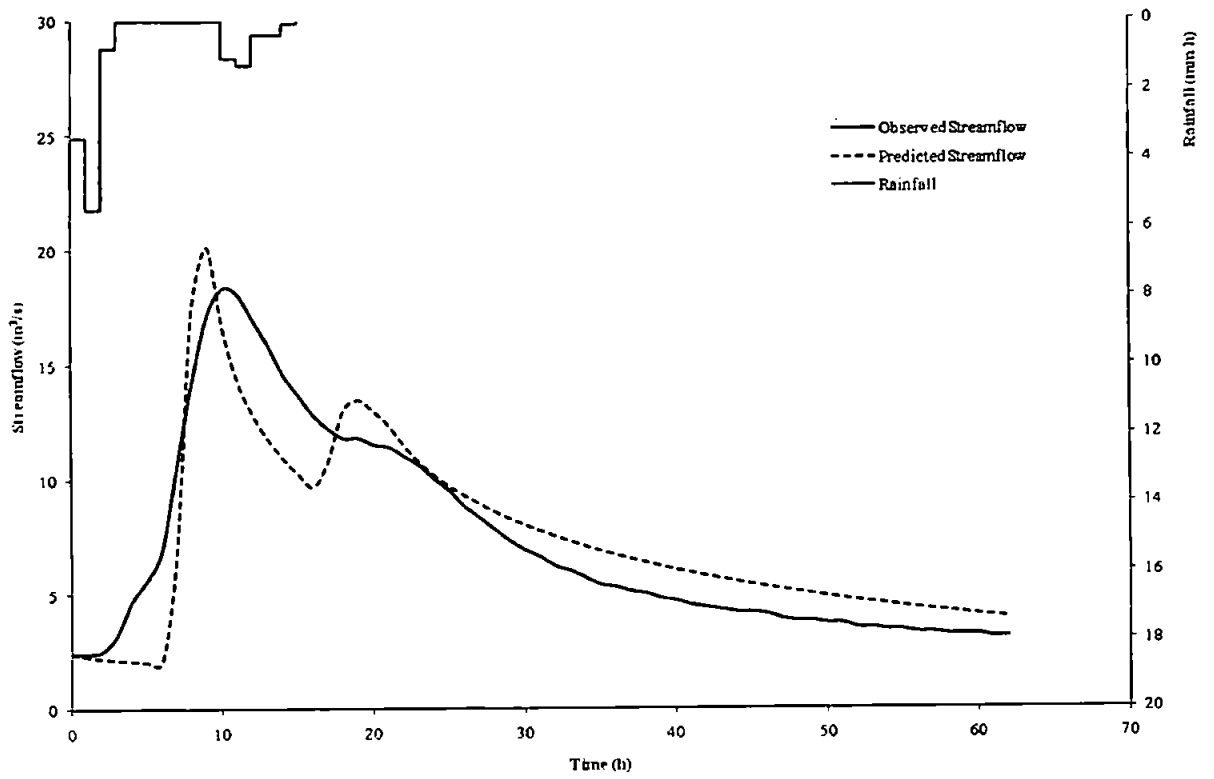**Figure D6.6 Predicted and observed results for event 658**

312

Figure D6.7 Predicted and observed results for event 659

# D7: Catchment 66011 – River Conwy at Cwm Llanerch

Figure D7.1 Predicted and observed results for event 2072

Figure D7.2 Predicted and observed results for event 2073

314

Figure D7.3 Predicted and observed results for event 2074

Figure D7.4 Predicted and observed results for event 2075

315

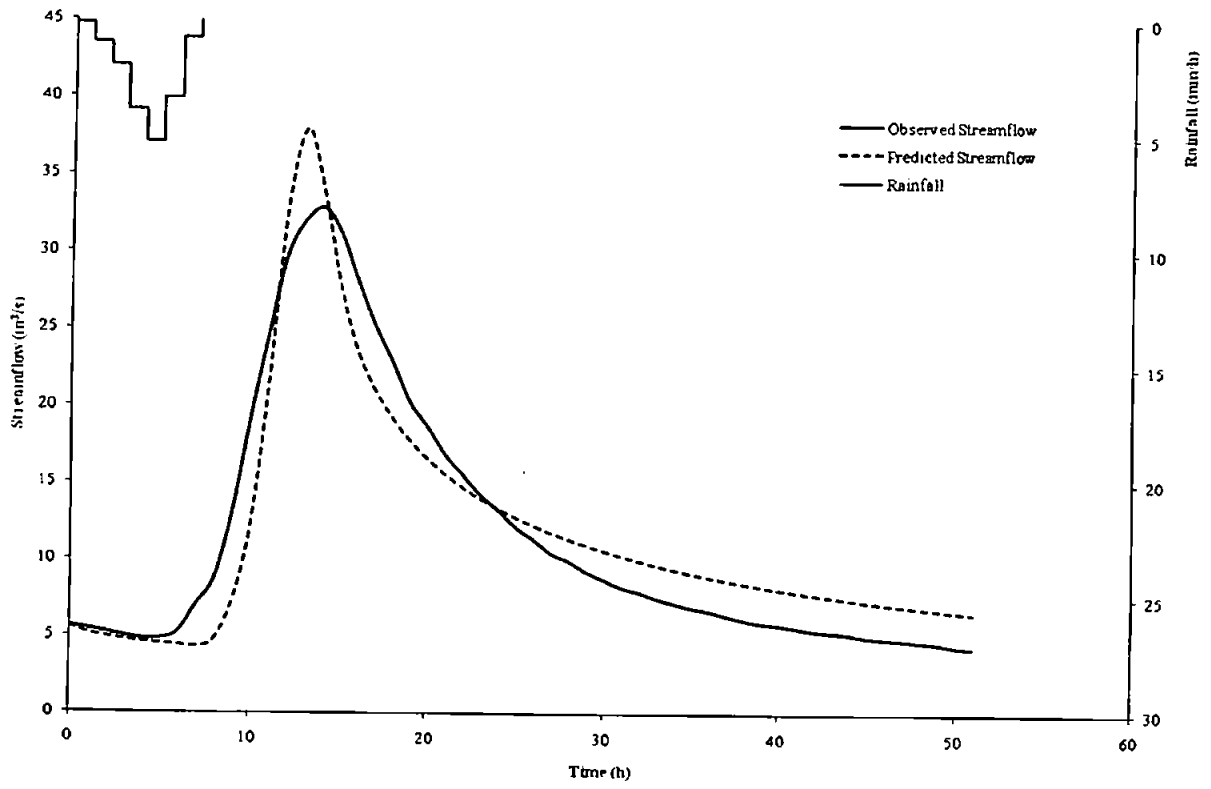**Figure D7.5 Predicted and observed results for event 2076**

Figure D7.6 Predicted and observed results for event 2077

Figure D7.7 Predicted and observed results for event 2078

Figure D7.8 Predicted and observed results for event 2079

317

Figure D7.9 Predicted and observed results for event 2080
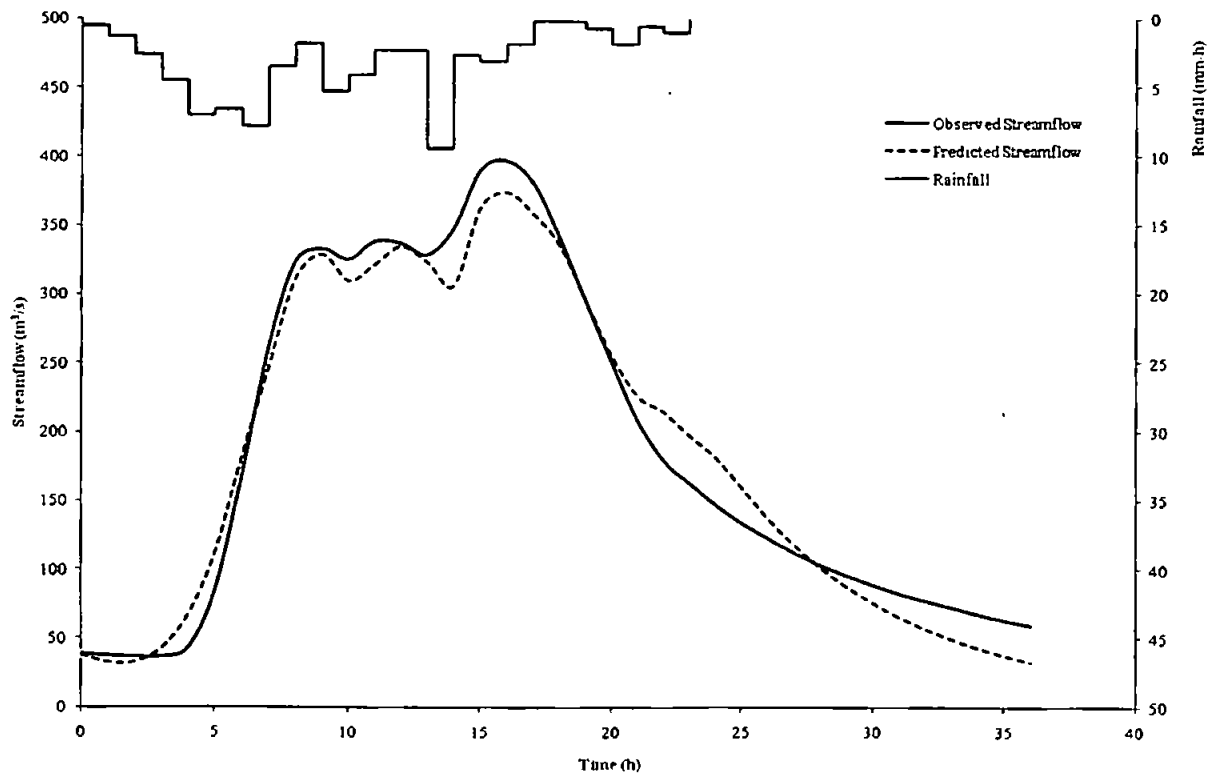
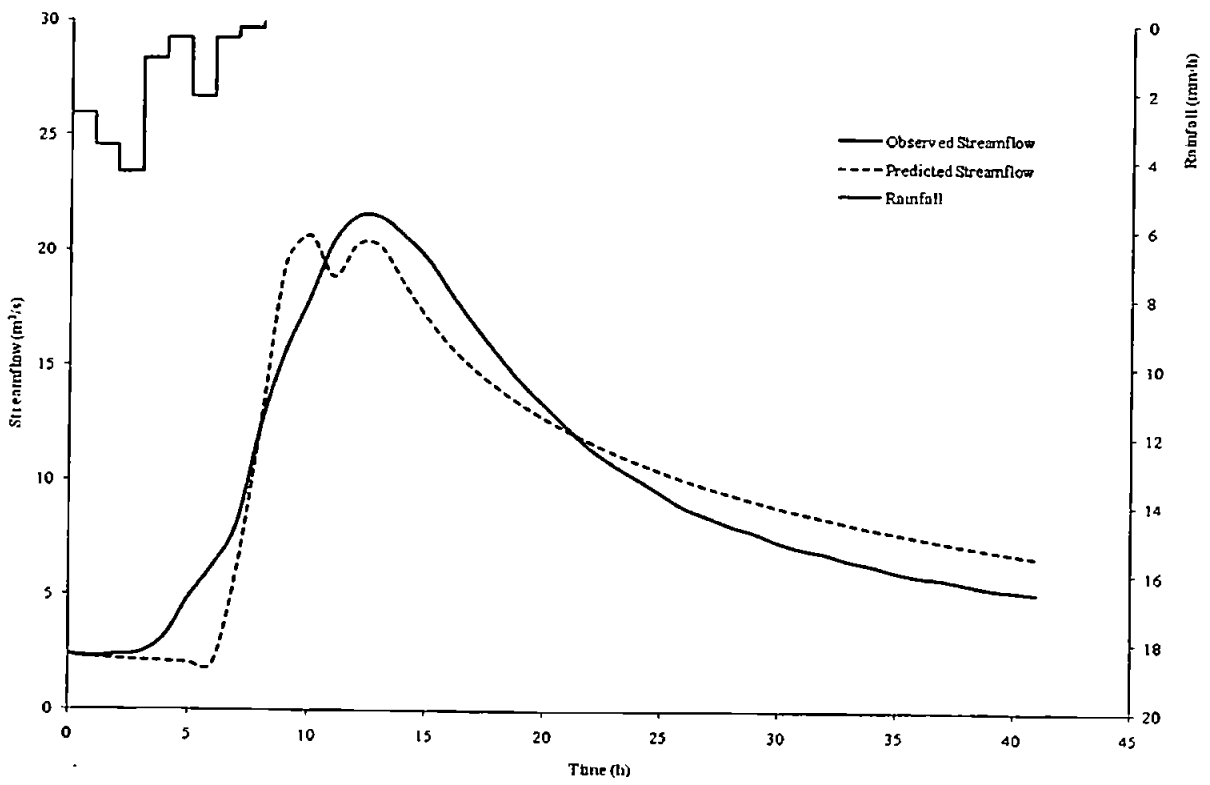**Figure D7.10 Predicted and observed results for event 2081**
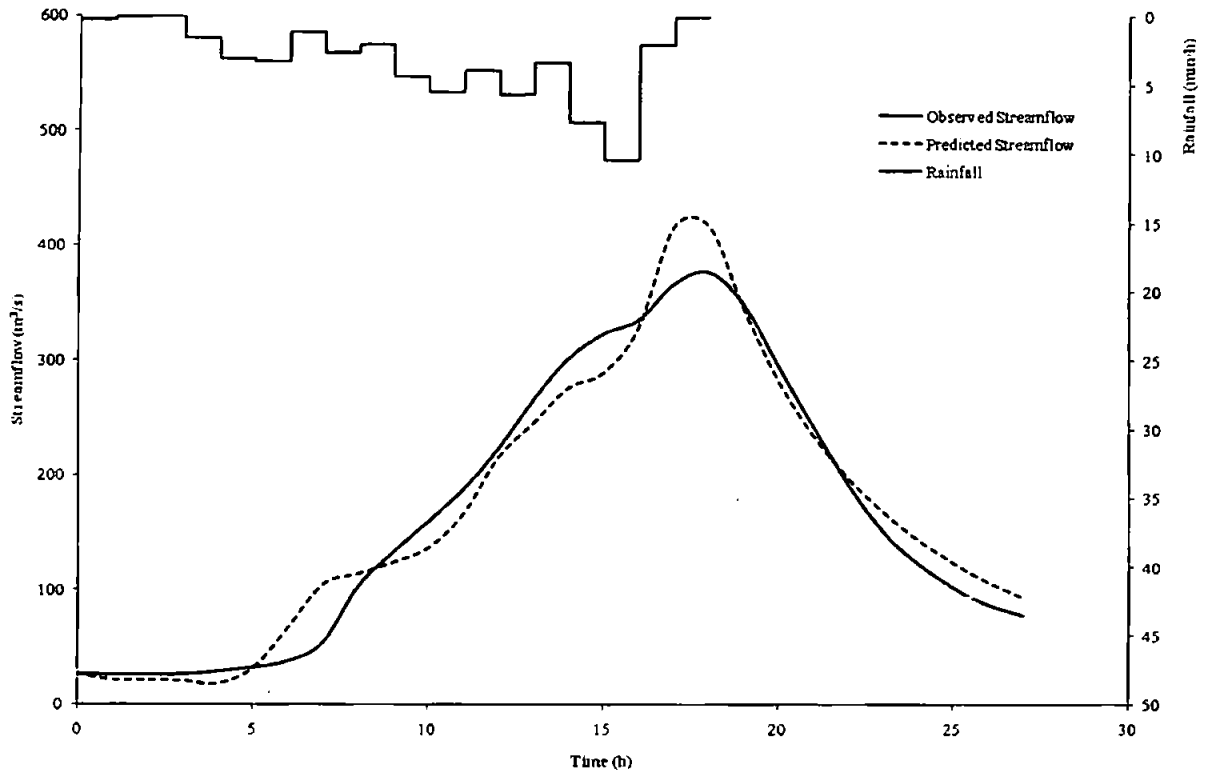
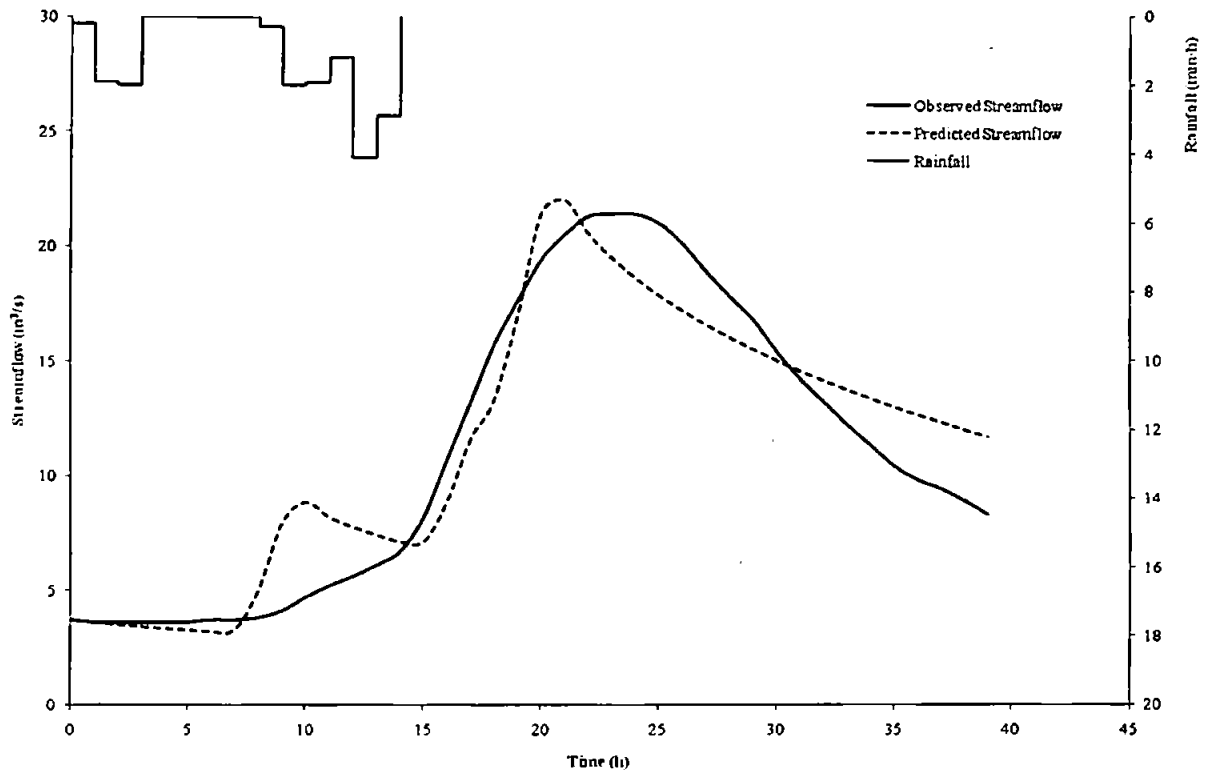**Figure D7.11 Predicted and observed results for event 2082**
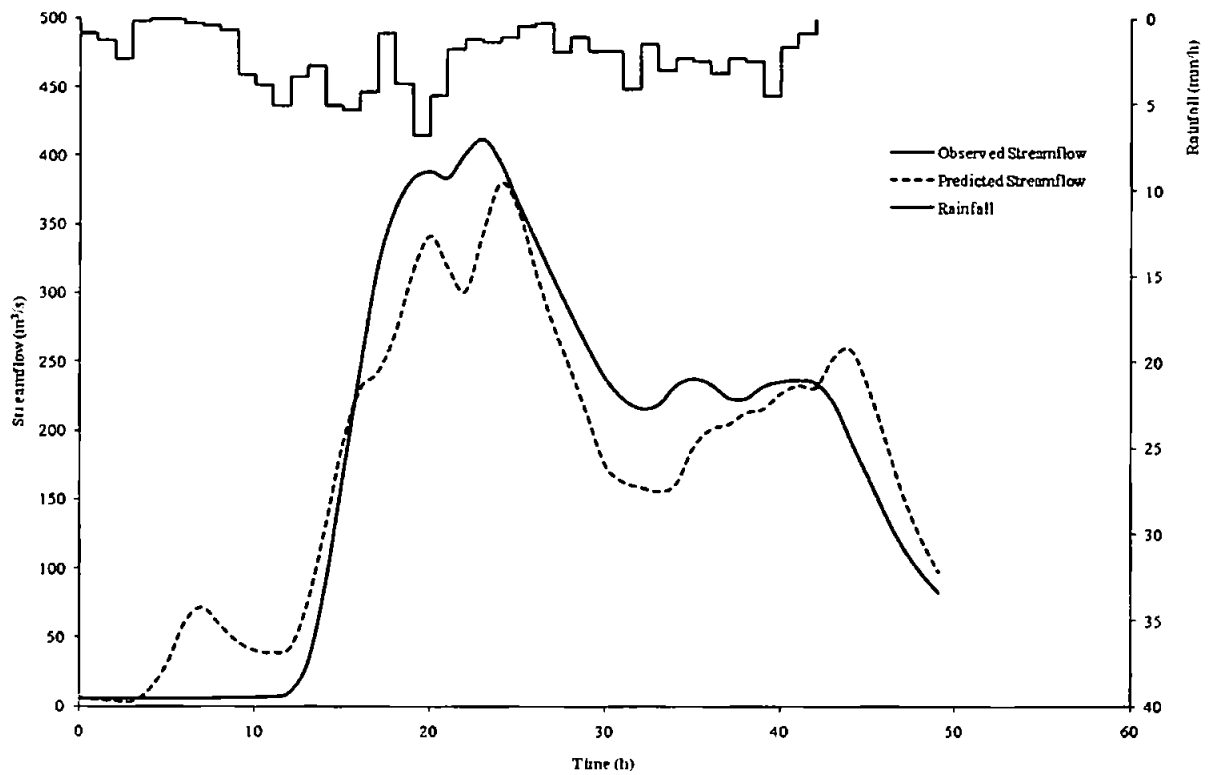
Figure D7.12 Predicted and observed results for event 2083
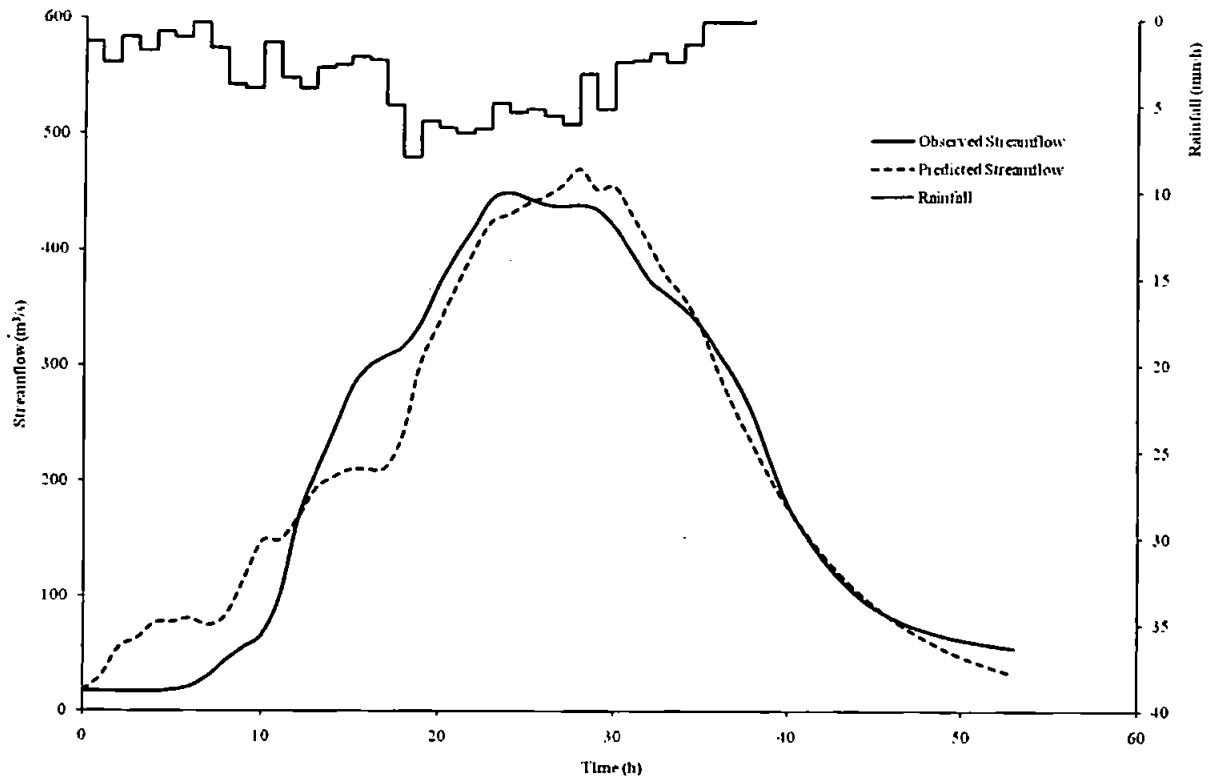
Figure D7.13 Predicted and observed results for event 2084

D8: Catchment 28026 – River Anker at Polesworth
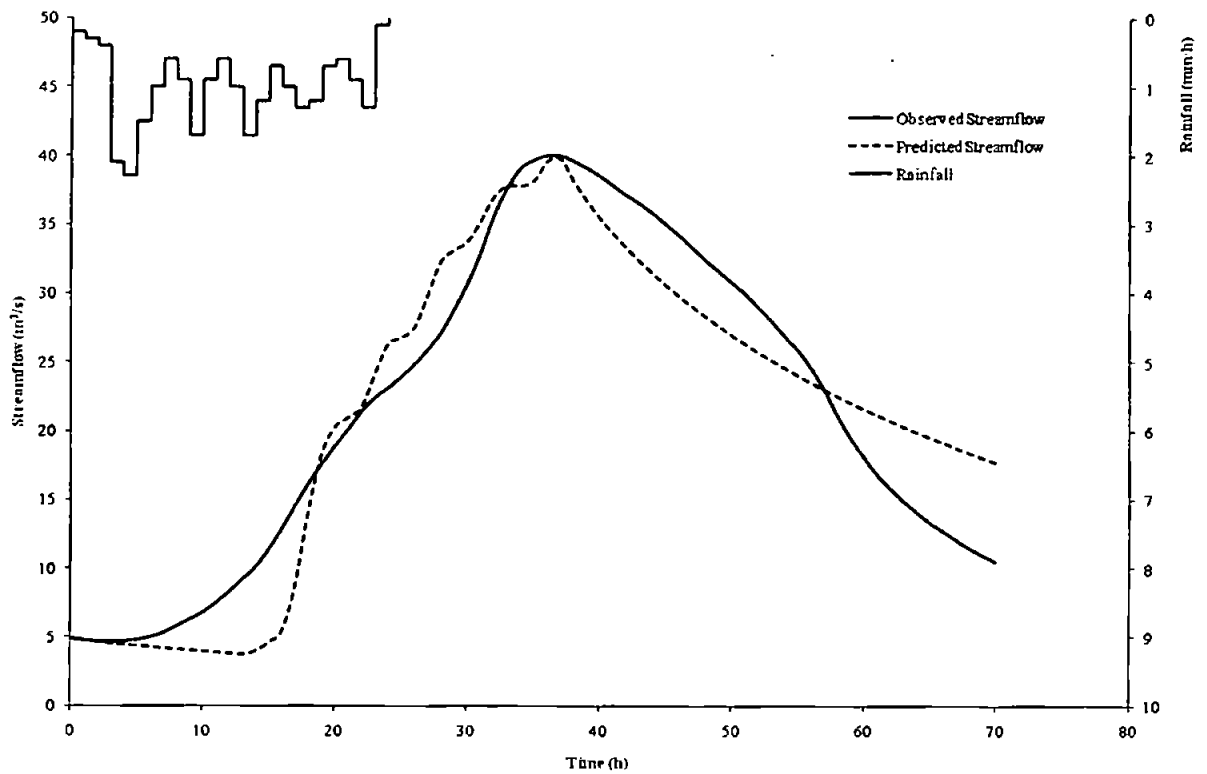
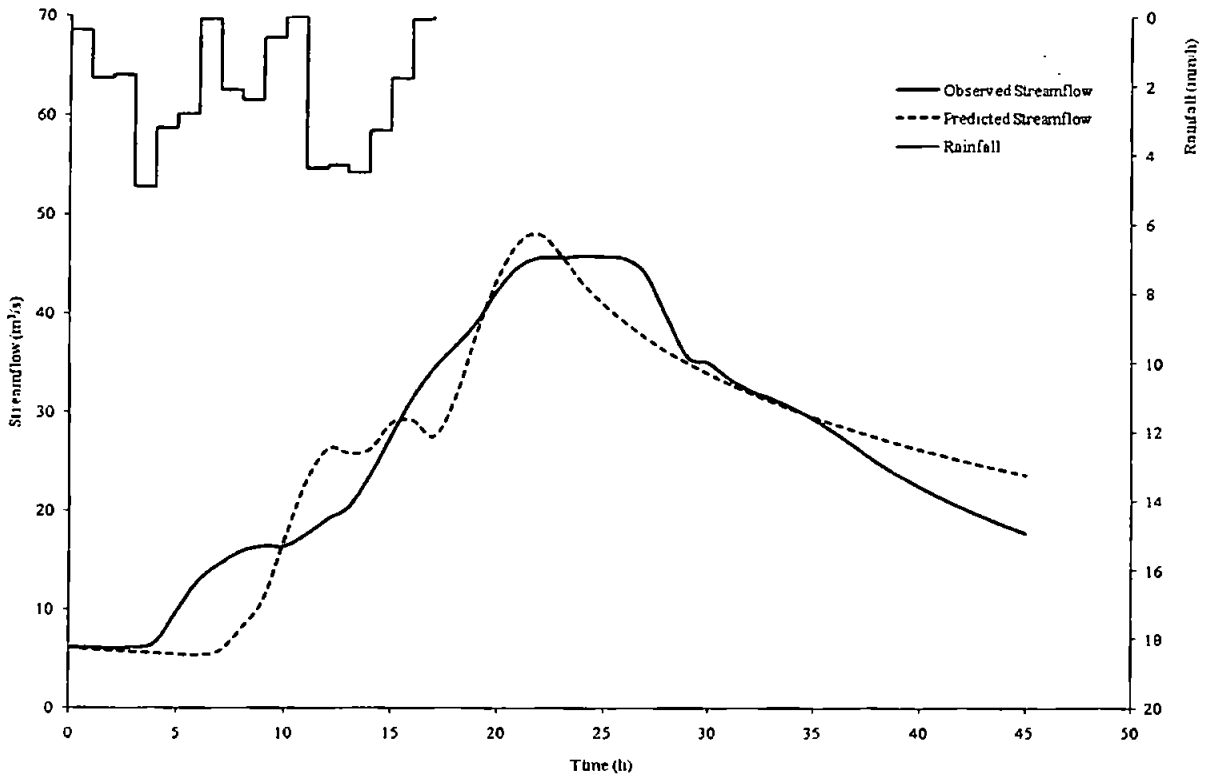**Figure D8.1 Predicted and observed results for event 409**
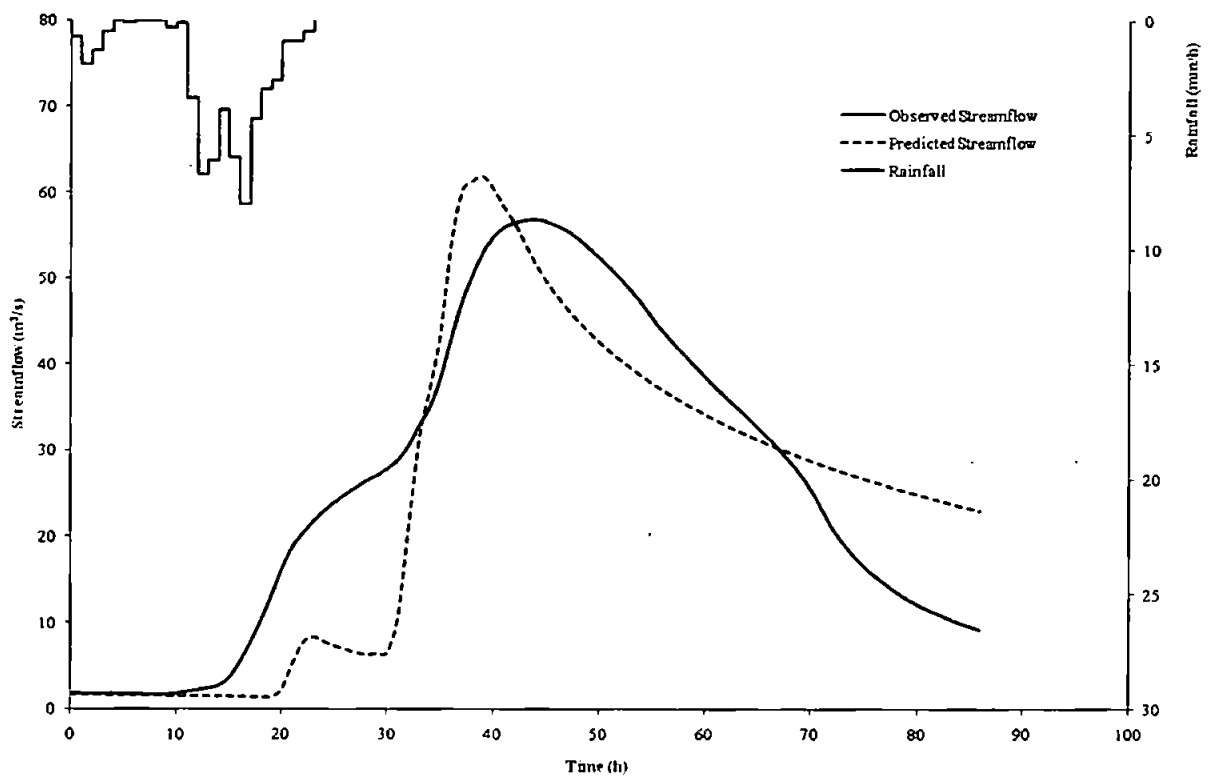
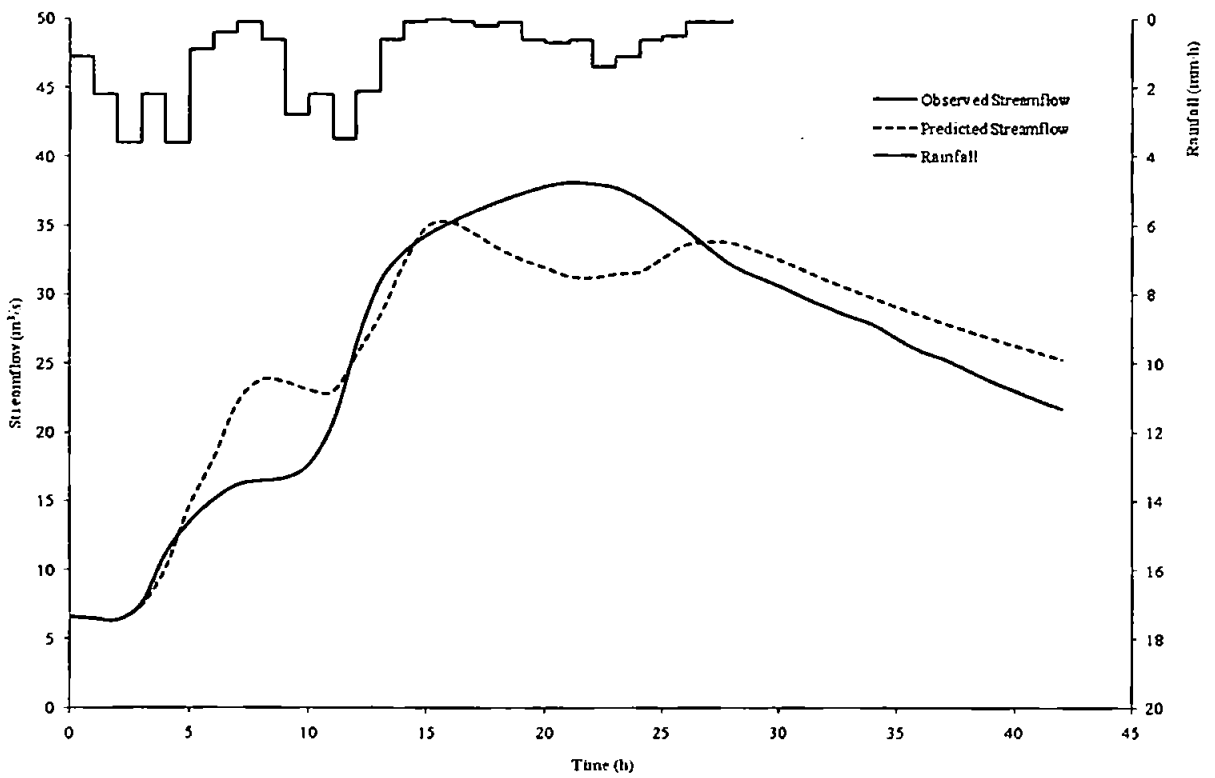**Figure D8.2 Predicted and observed results for event 410**
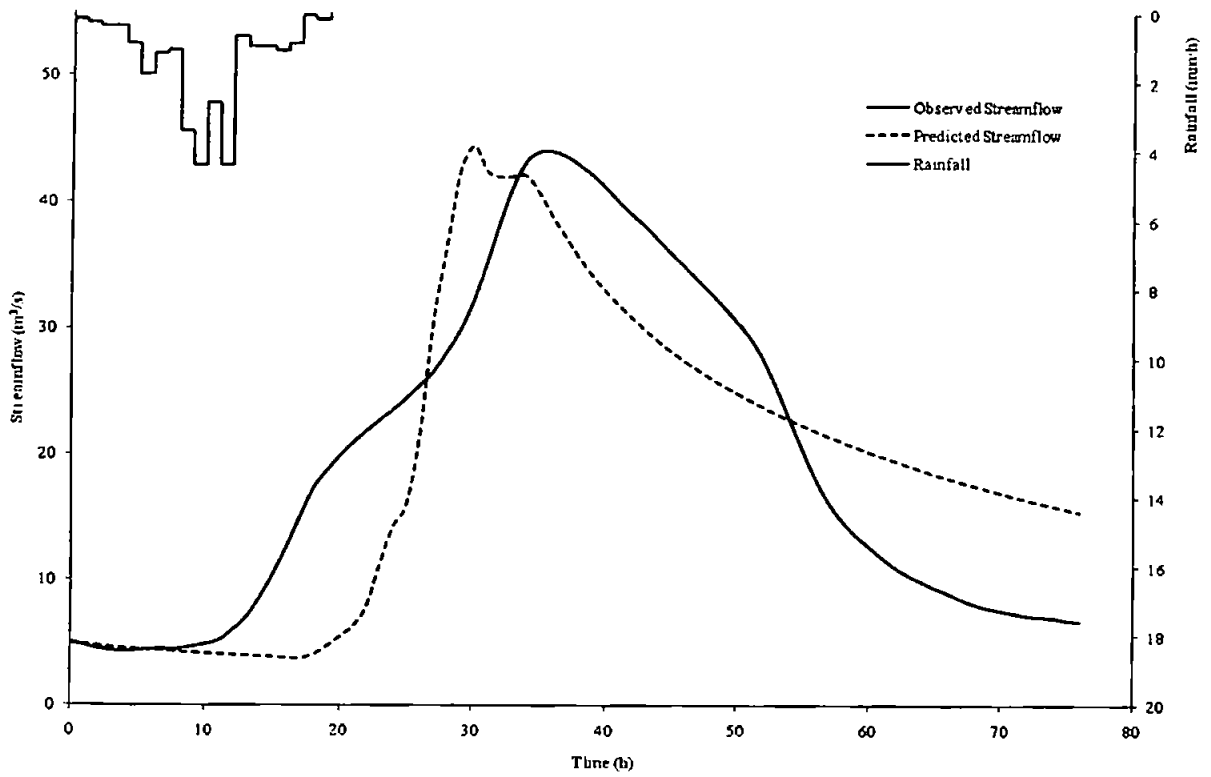
Figure D8.3 Predicted and observed results for event 411
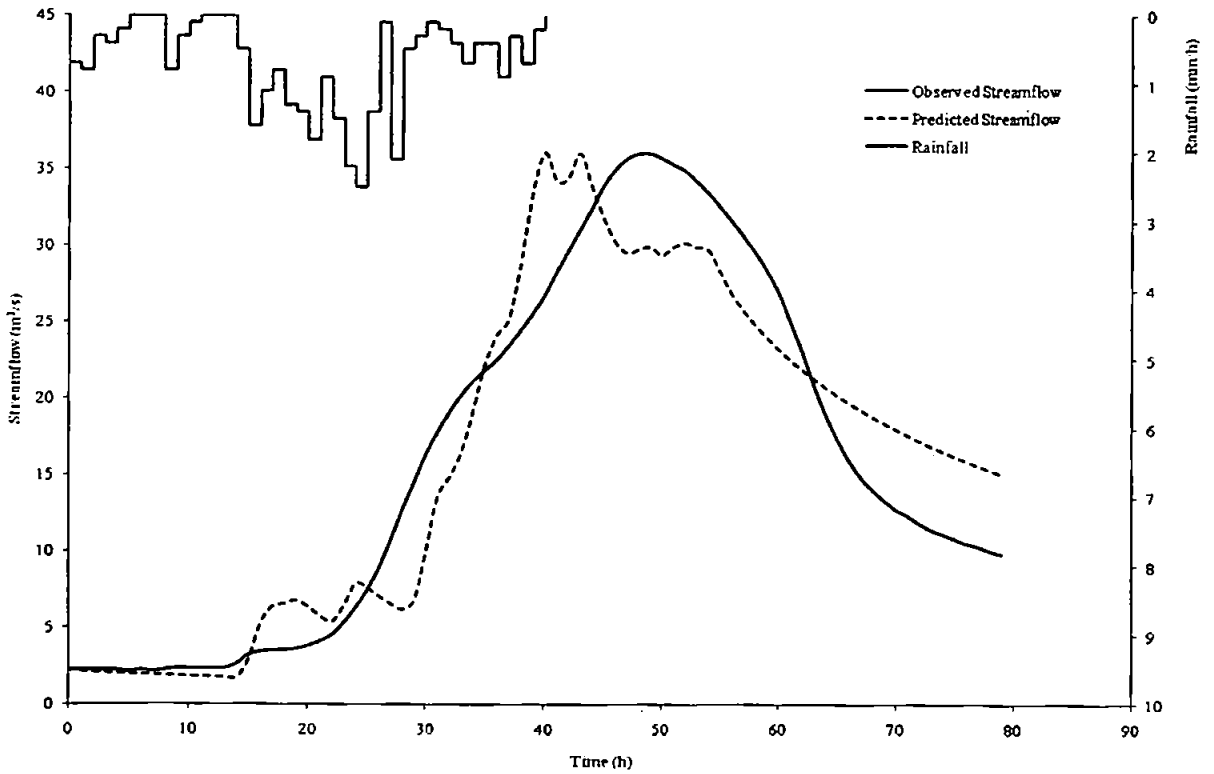
Figure D8.4 Predicted and observed results for event 412

322
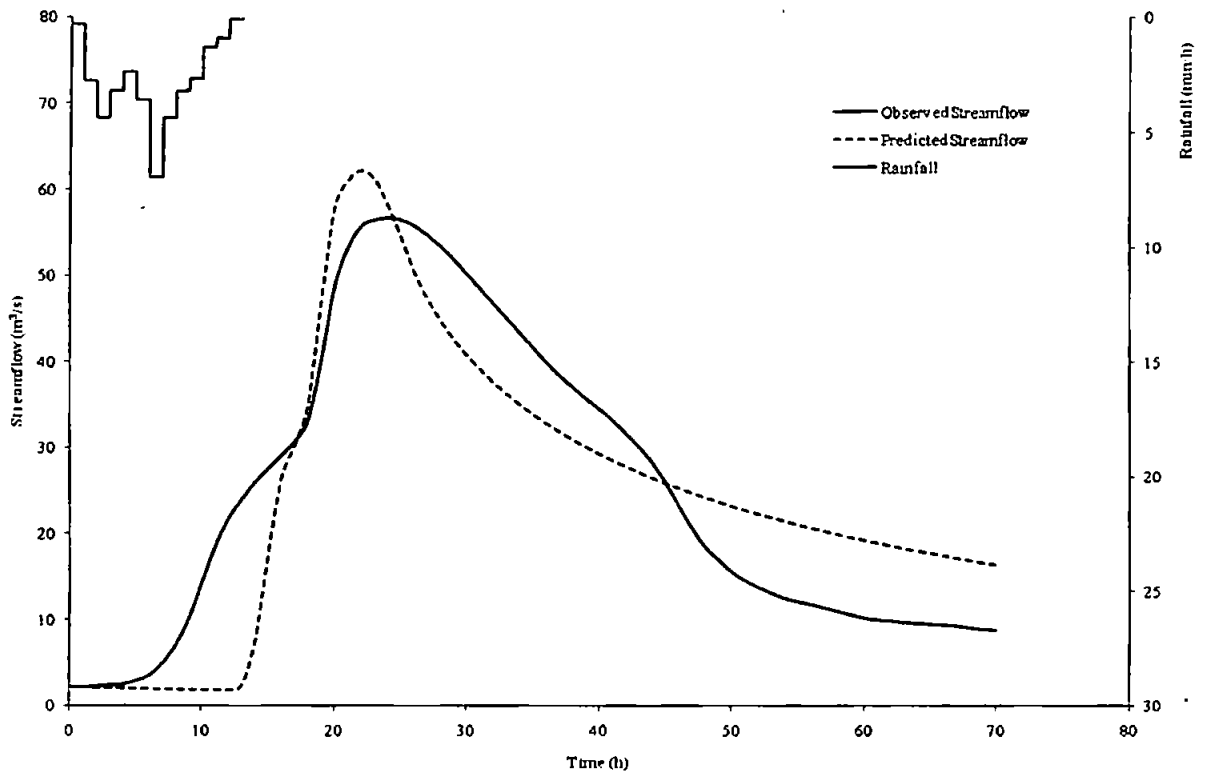
Figure D8.5 Predicted and observed results for event 413

D9: Catchment 7001 – River Findhorn at Shenachie
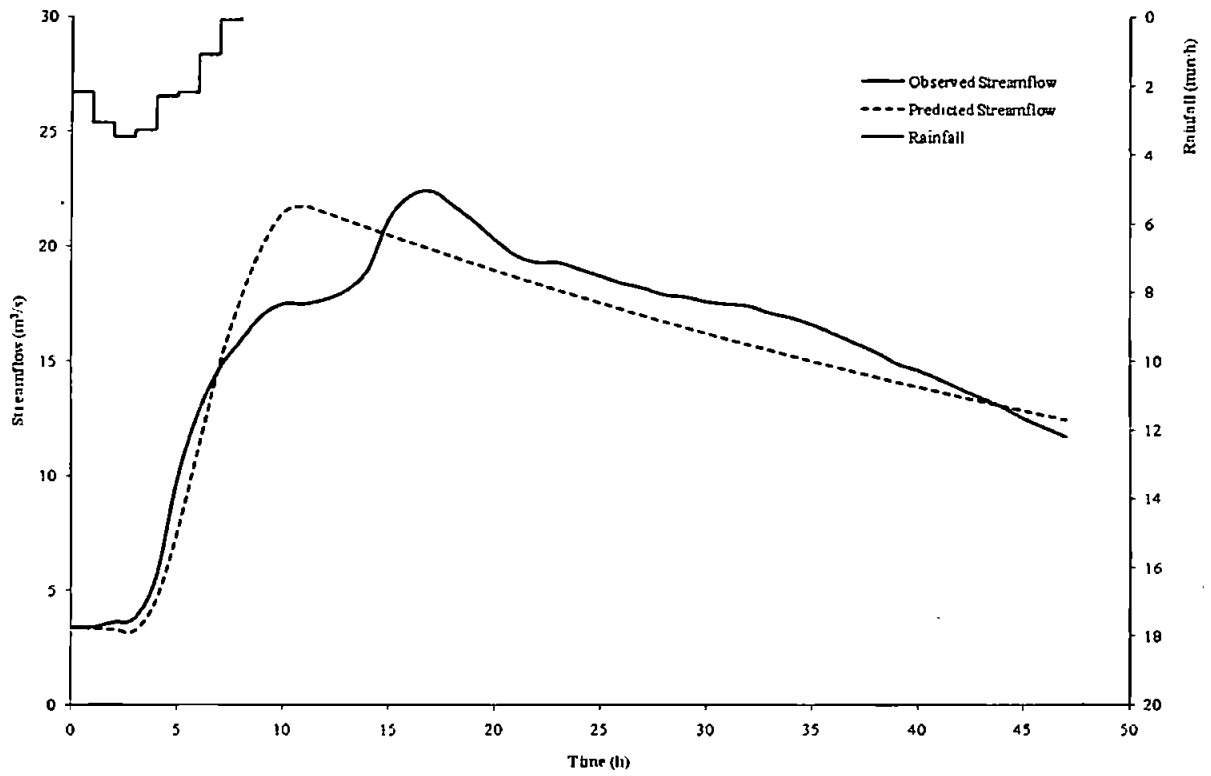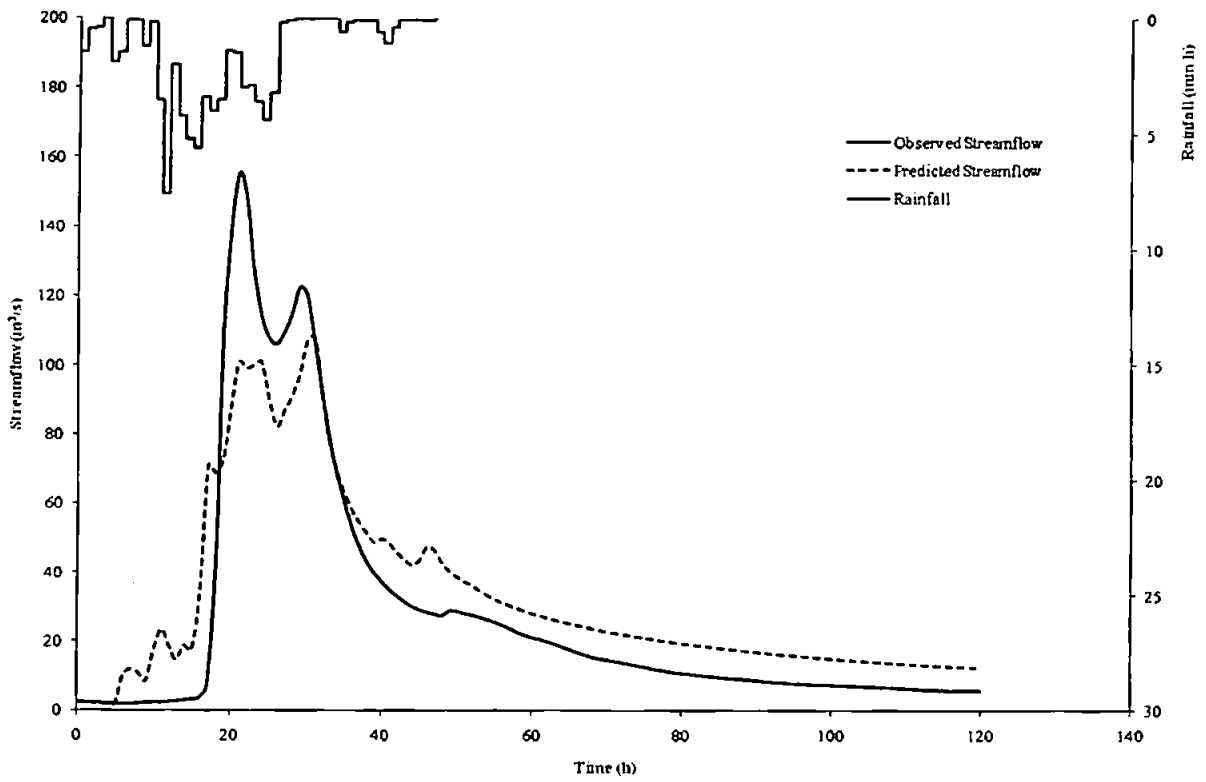

Figure D9.1 Predicted and observed results for event 3671
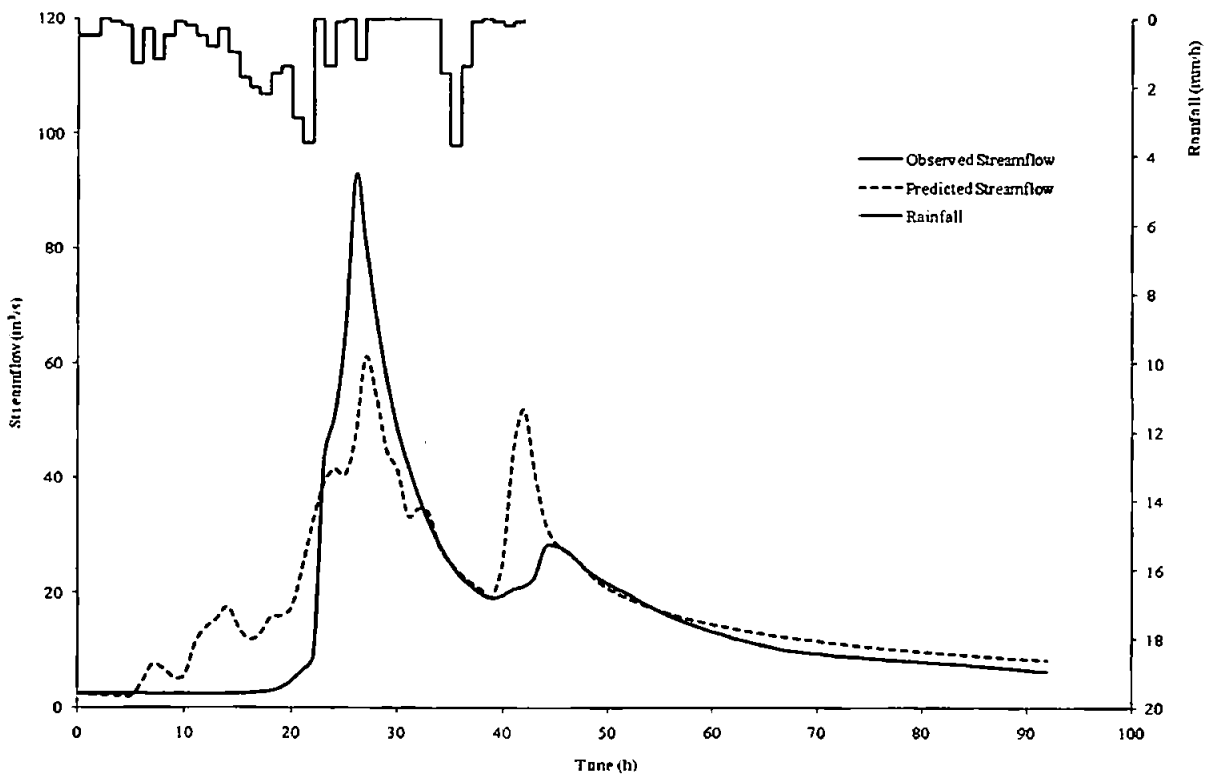
Figure D9.2 Predicted and observed results for event 3673
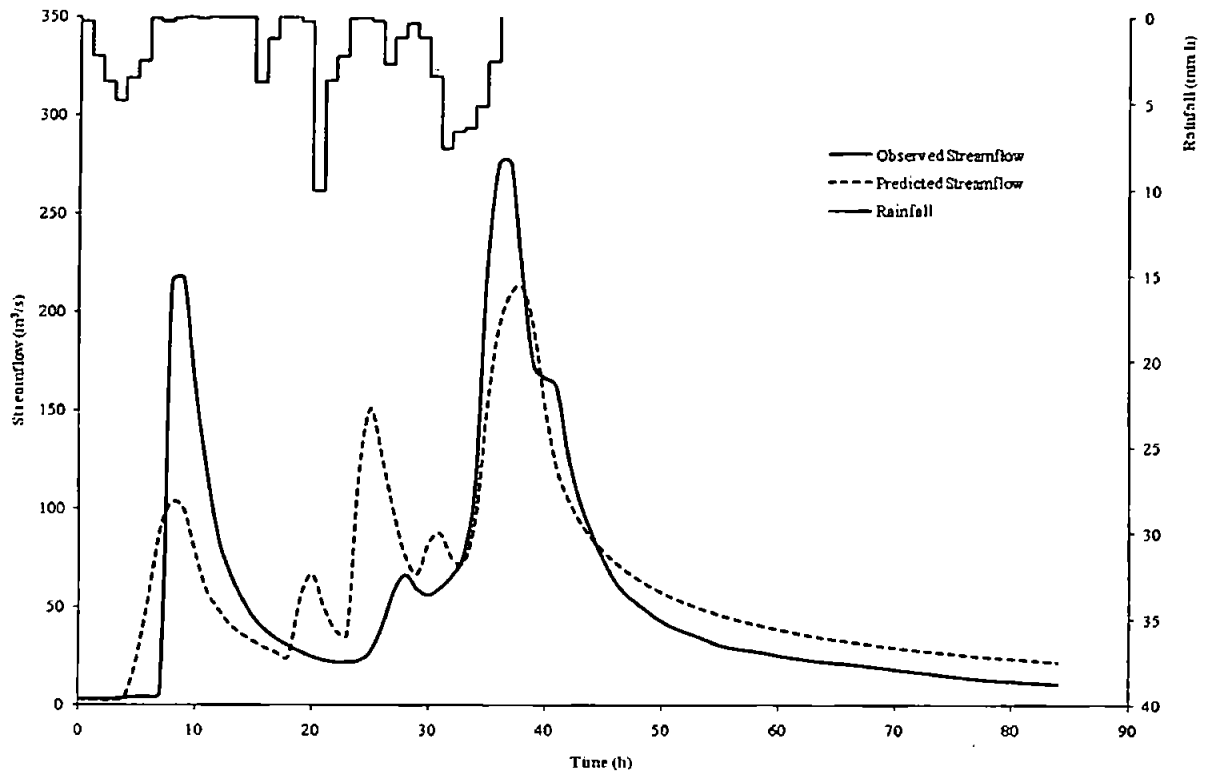
Figure D9.3 Predicted and observed results for event 3675
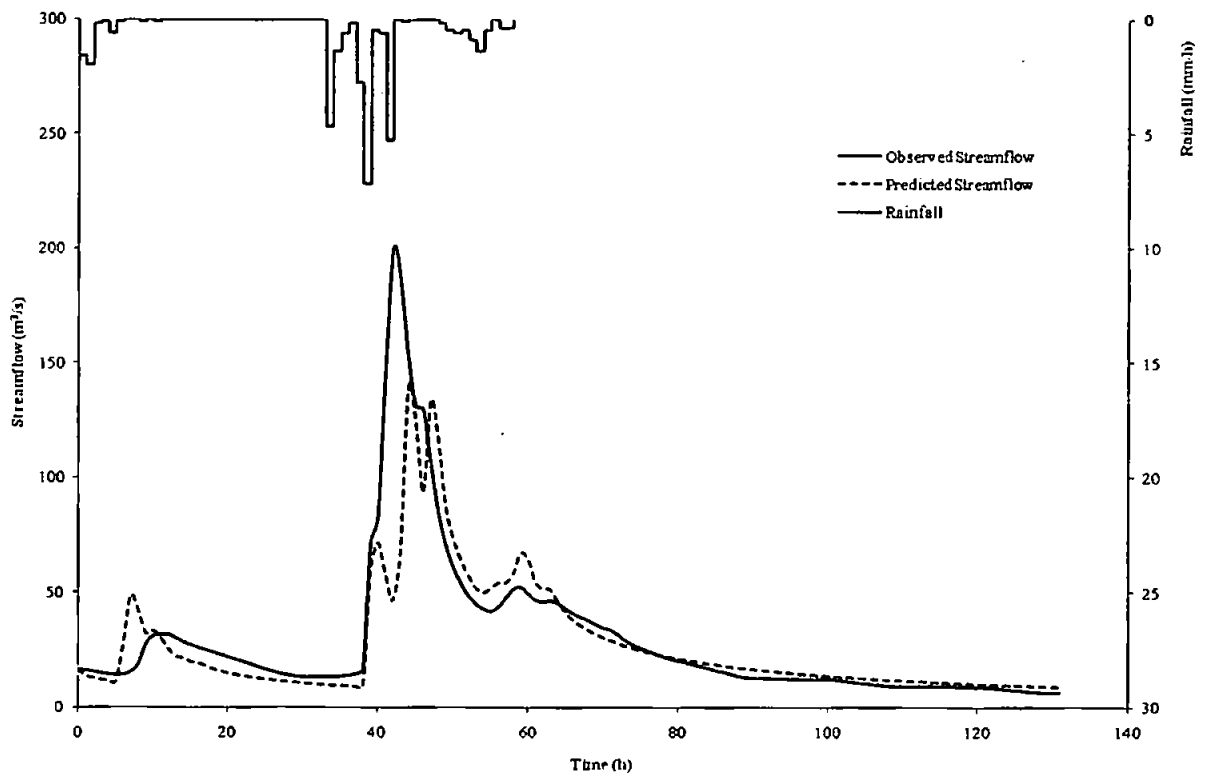
Figure D9.4 Predicted and observed results for event 3677

325
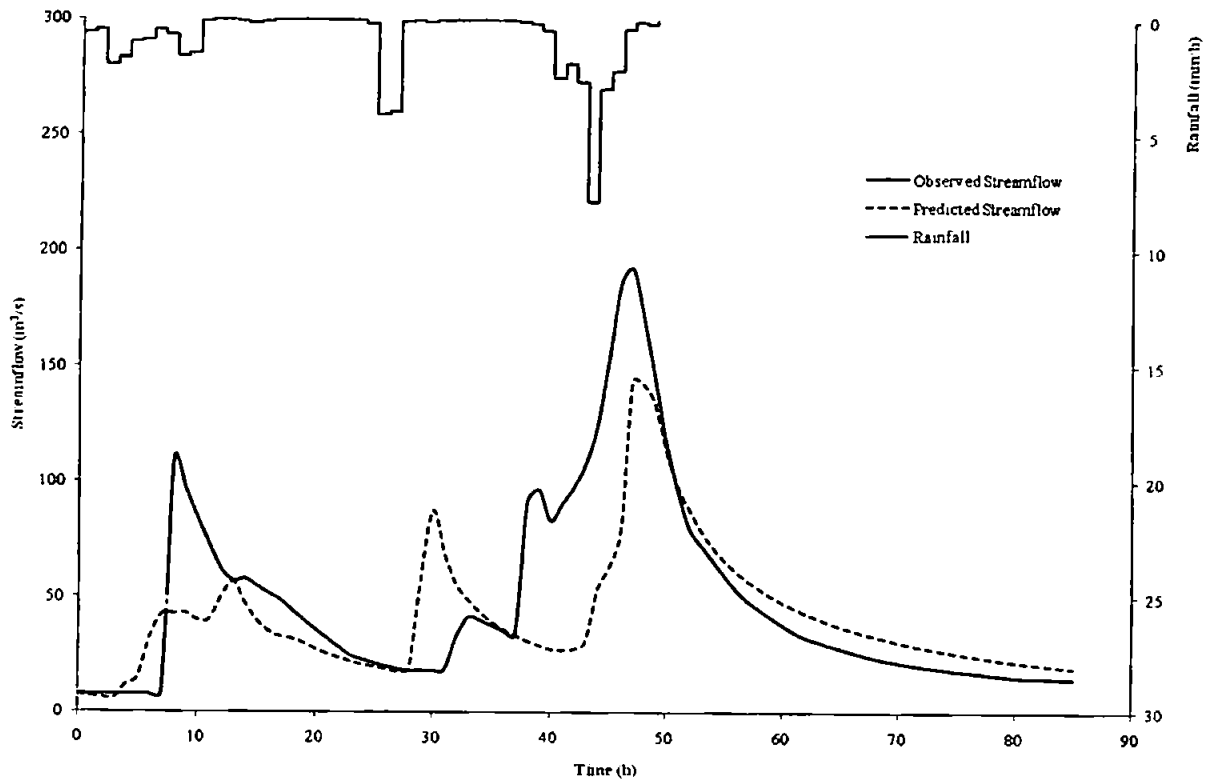
Figure D9.5 Predicted and observed results for event 3678
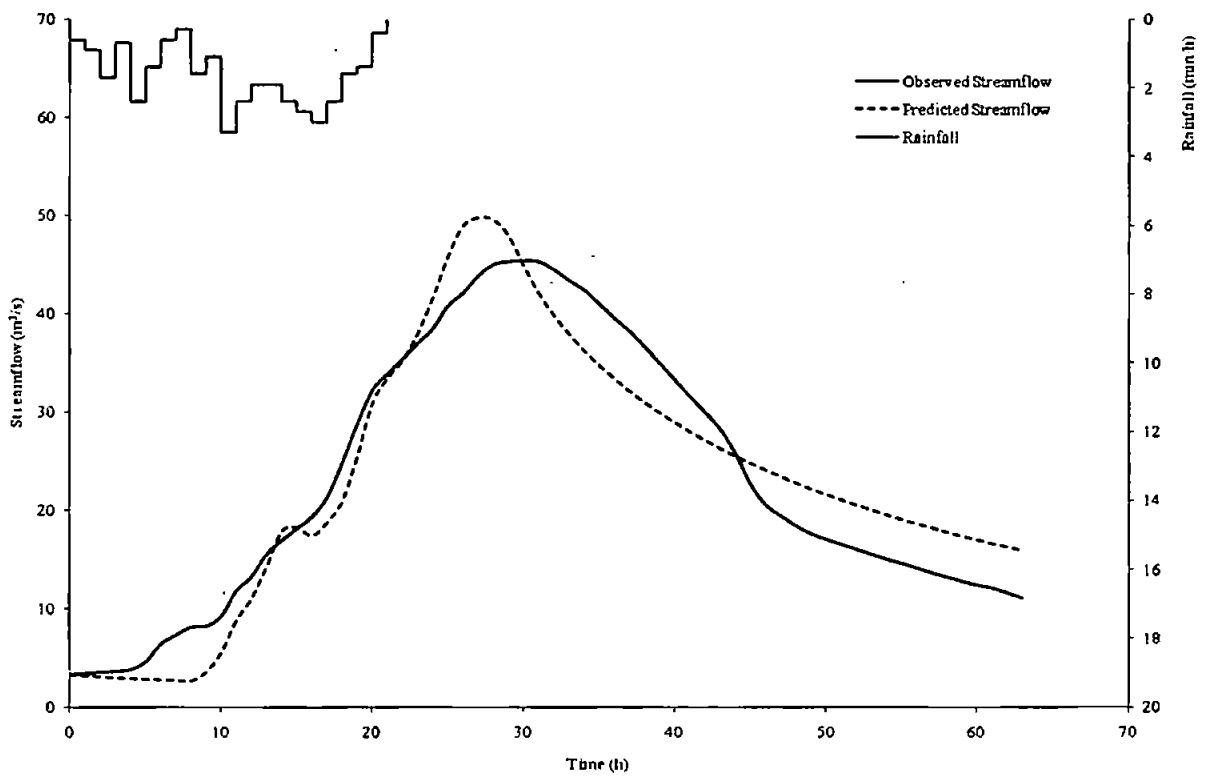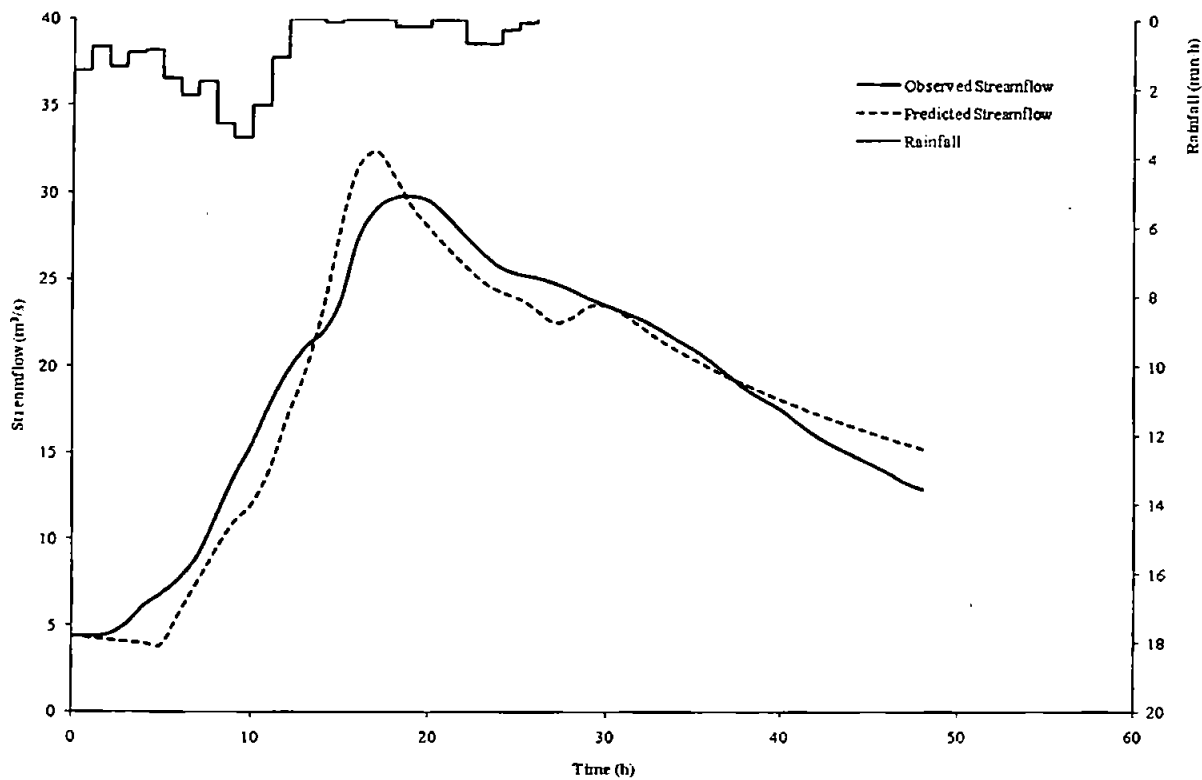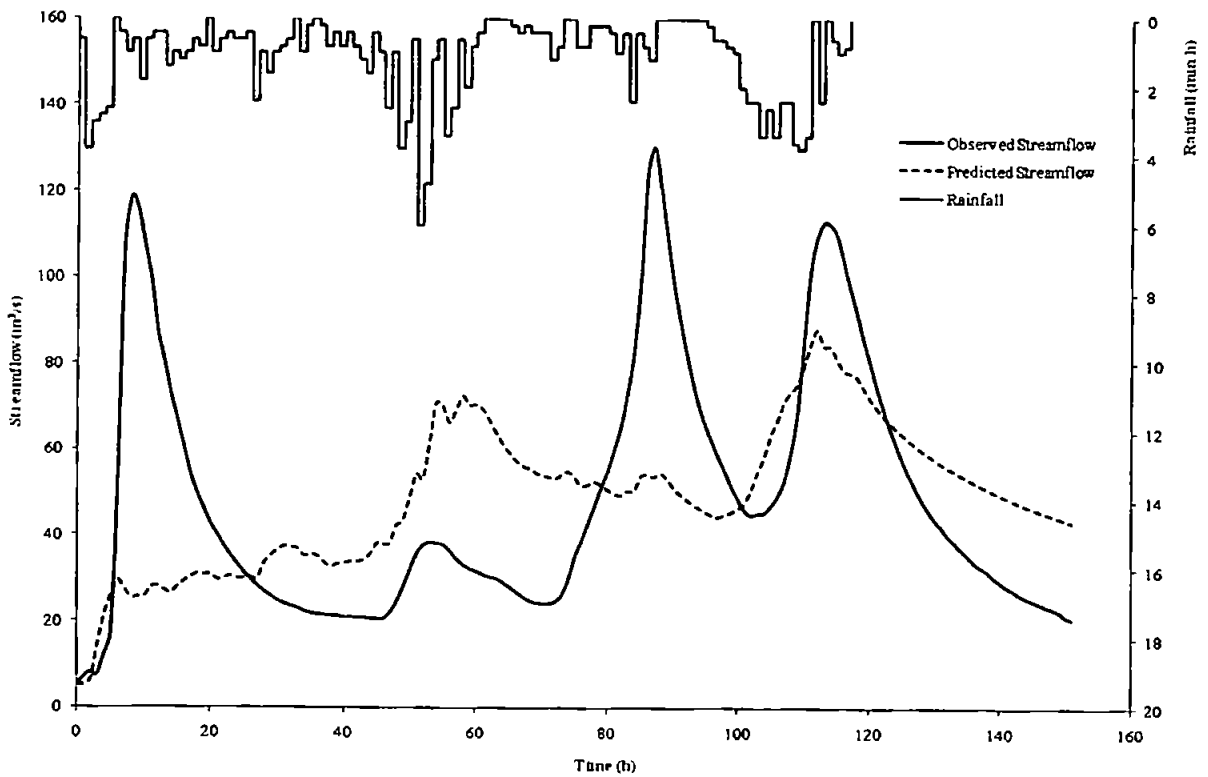

Figure D9.6 Predicted and observed results for event 3680

326
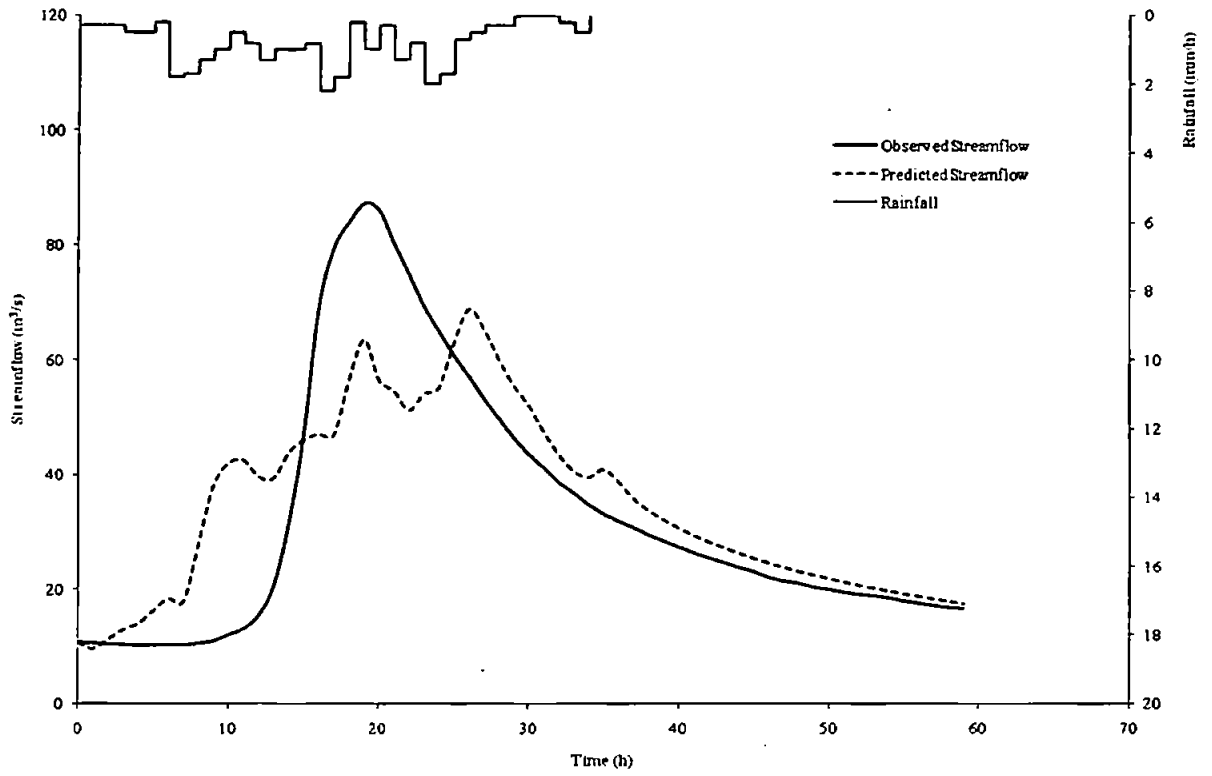
Figure D9.7 Predicted and observed results for event 3682
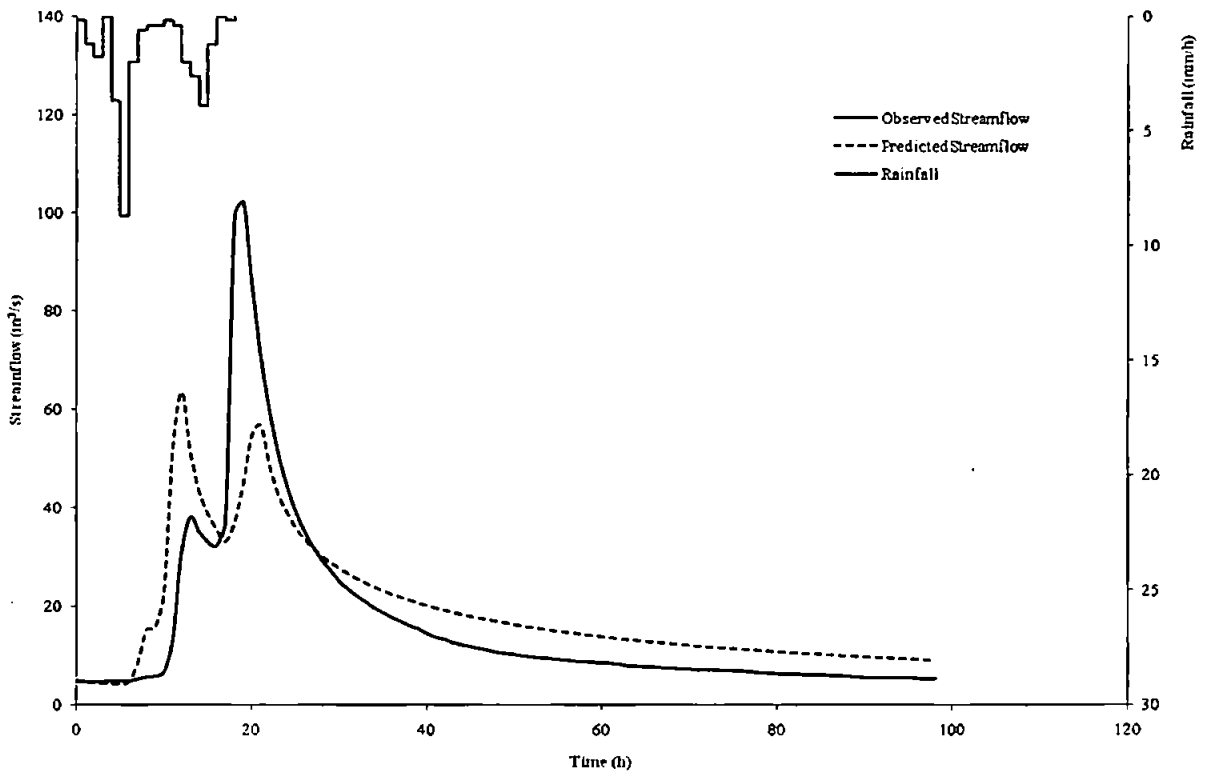
Figure D9.8 Predicted and observed results for event 3686

327
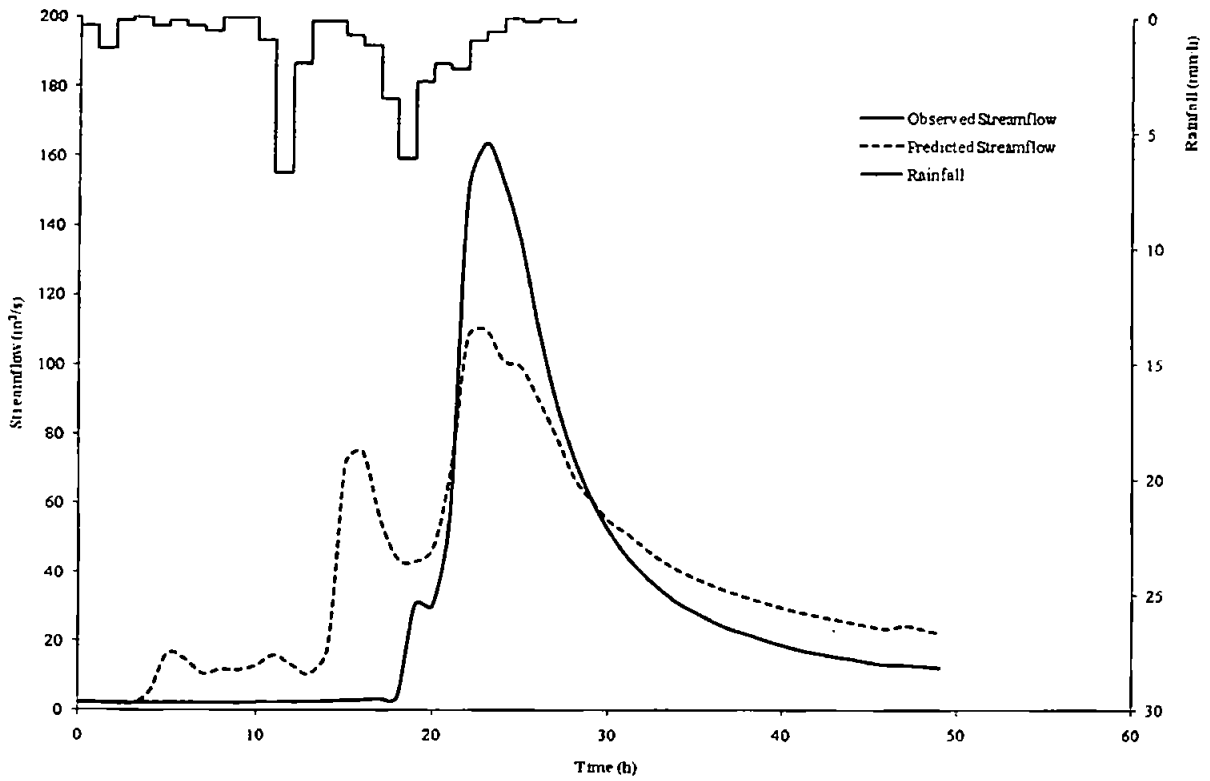
Figure D9.9 Predicted and observed results for event 3687
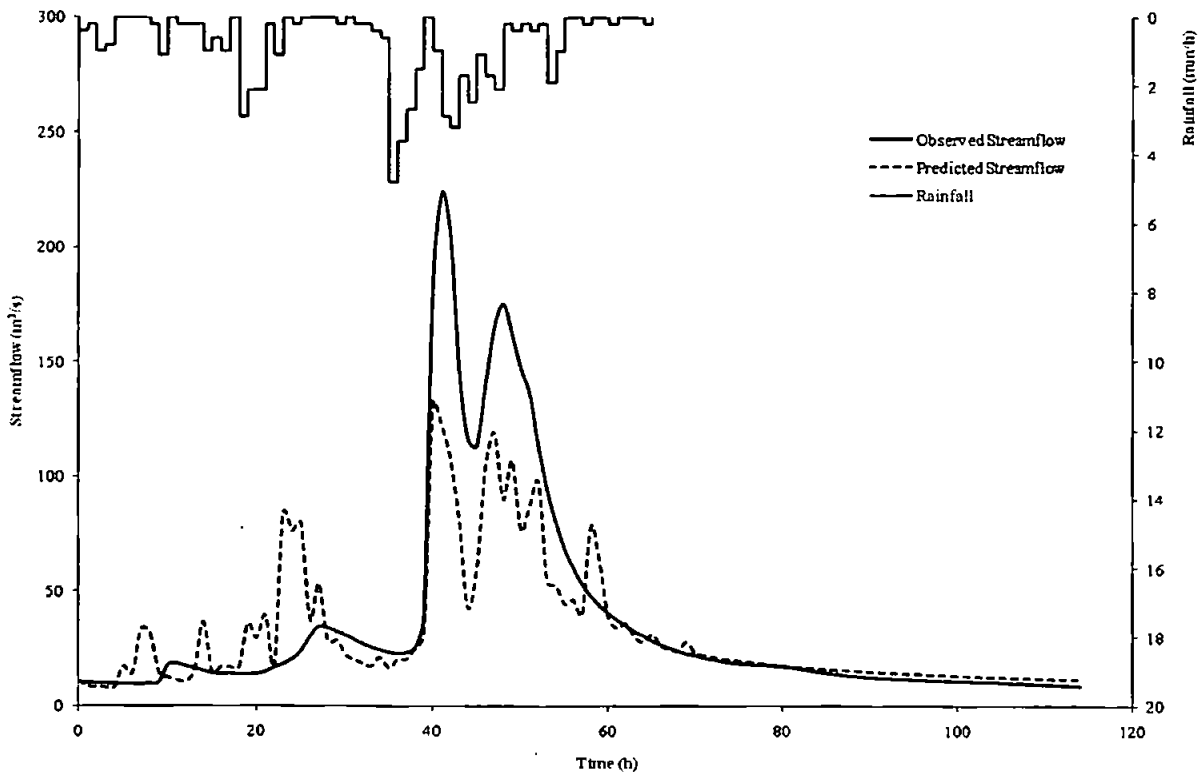
Figure D9.10 Predicted and observed results for event 3688

328
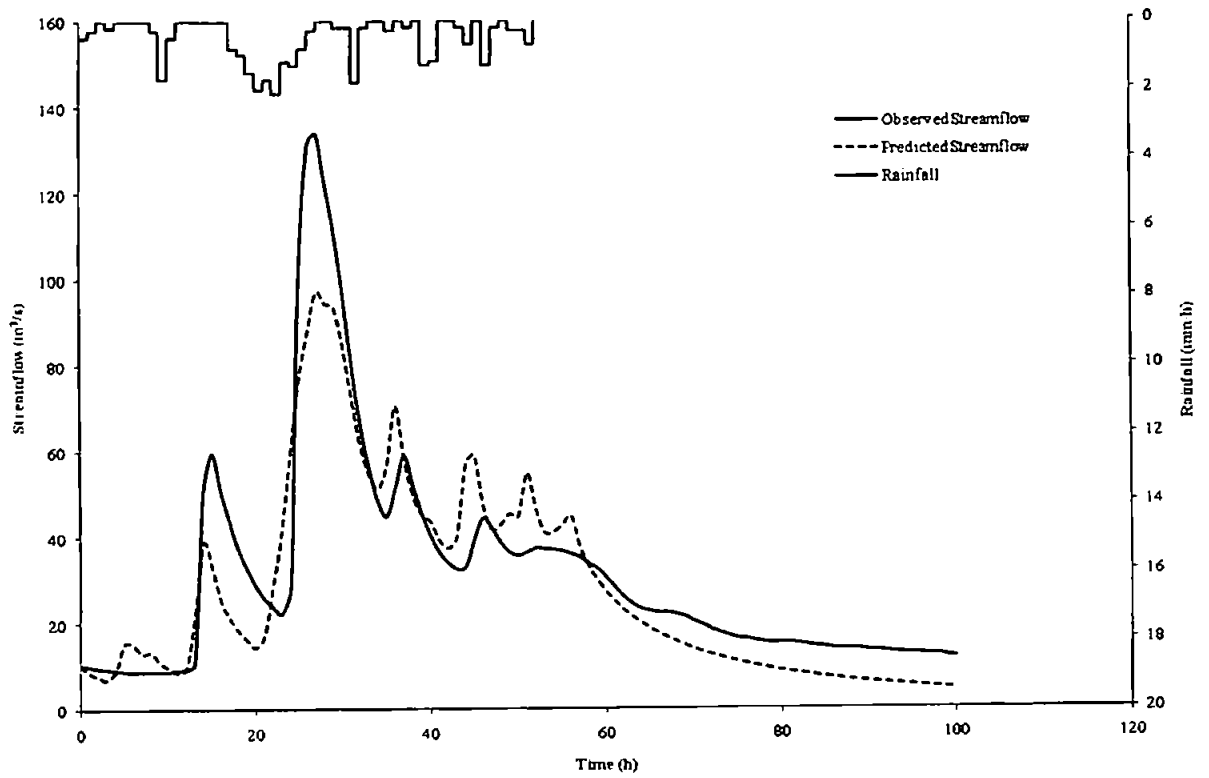
Figure D9.11 Predicted and observed results for event 3691
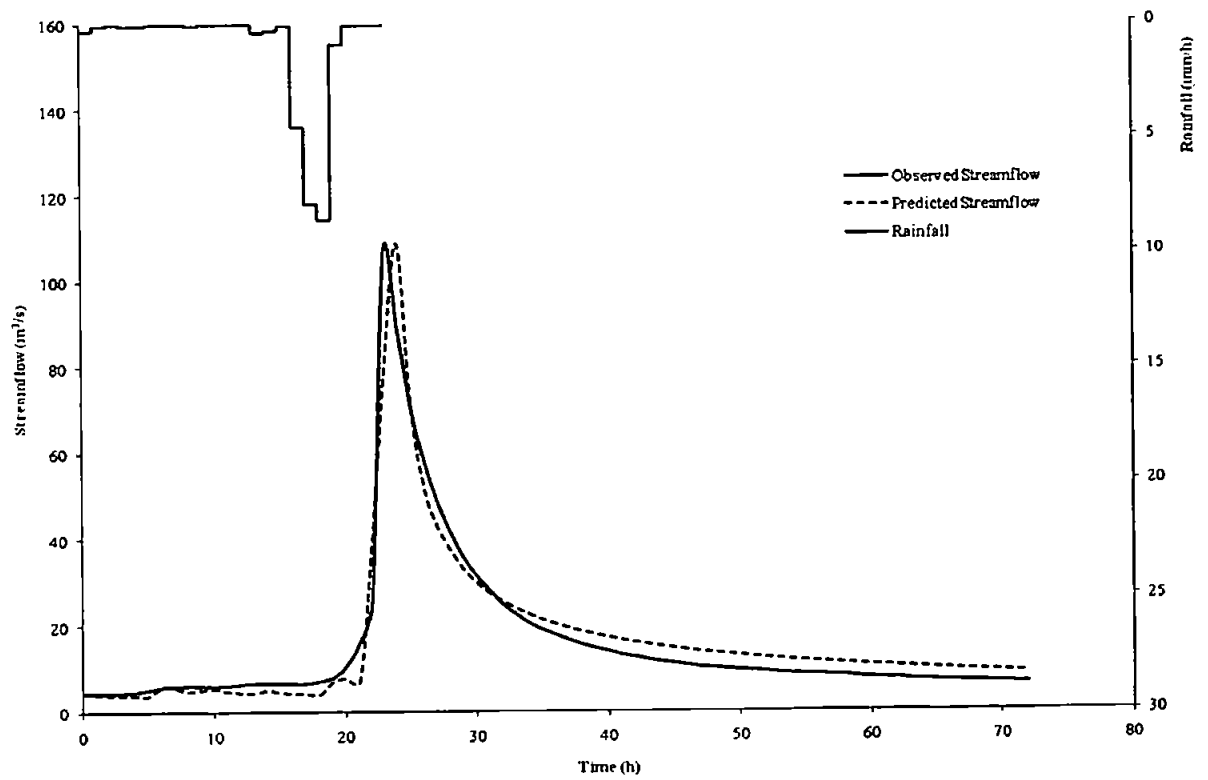
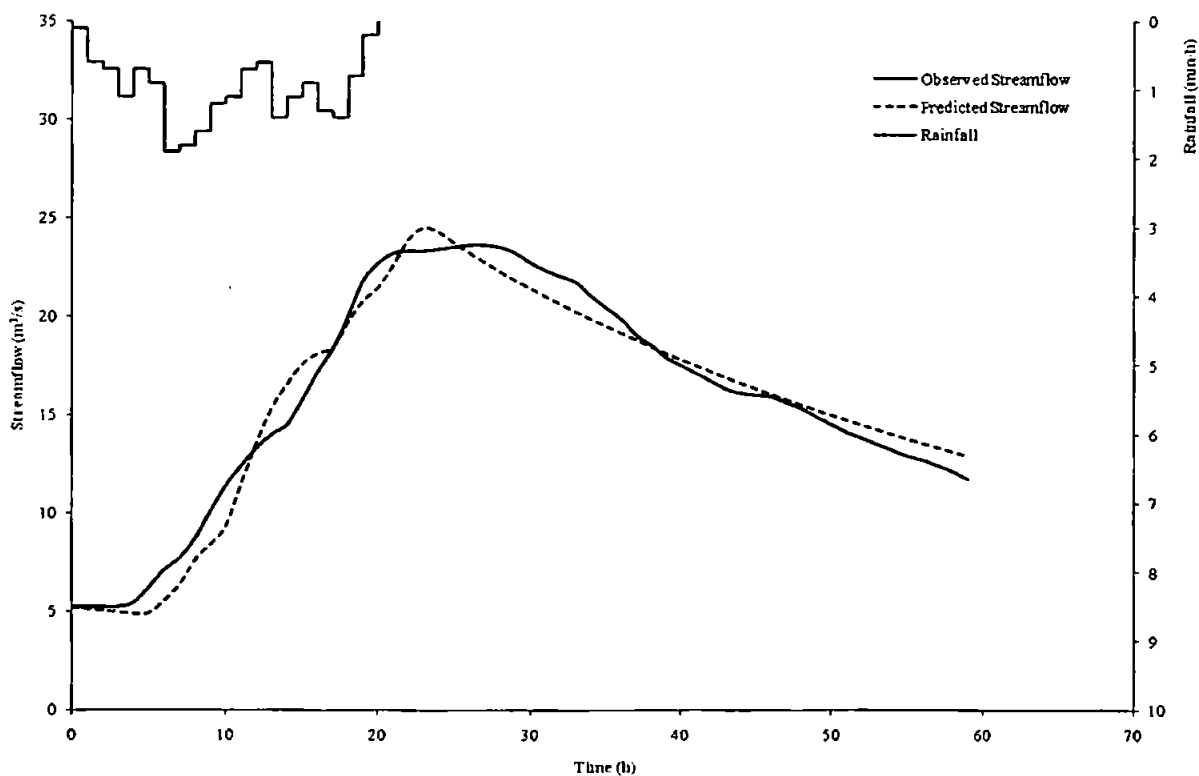**Figure D9.12 Predicted and observed results for event 3697**

329
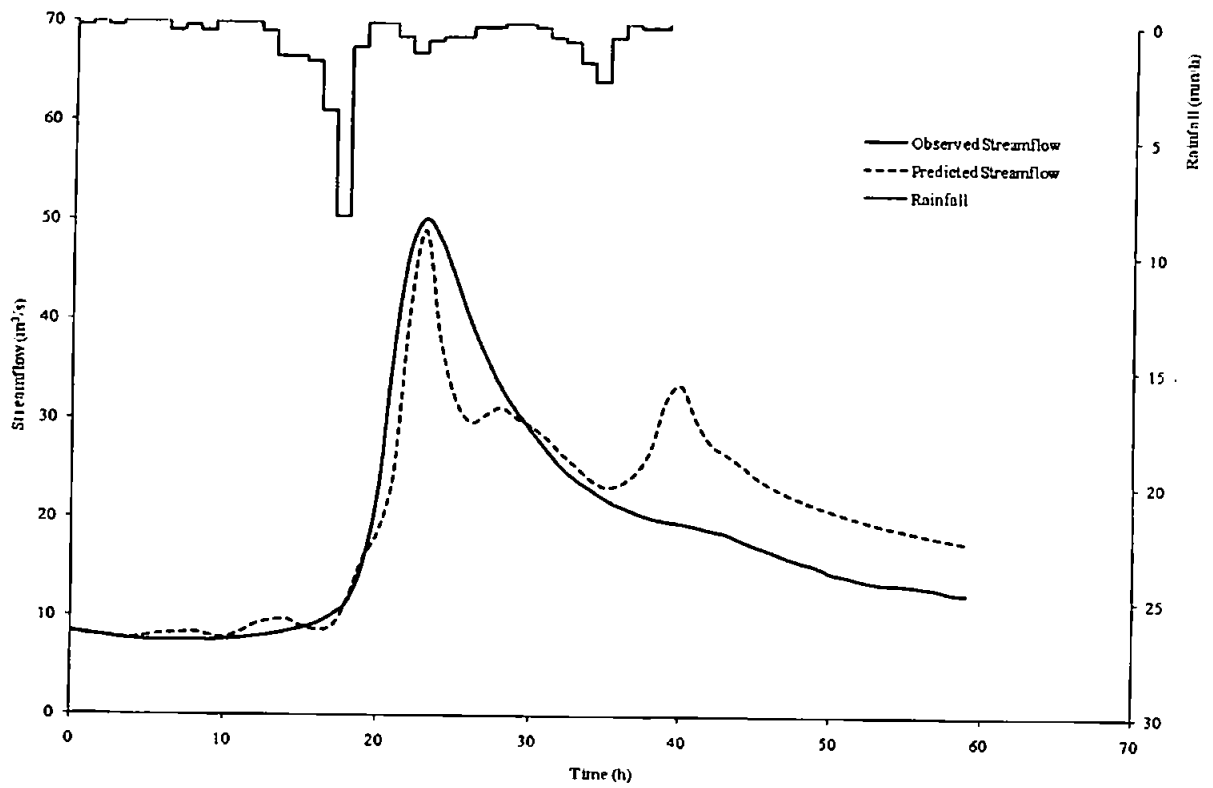
Figure D9.13 Predicted and observed results for event 3698
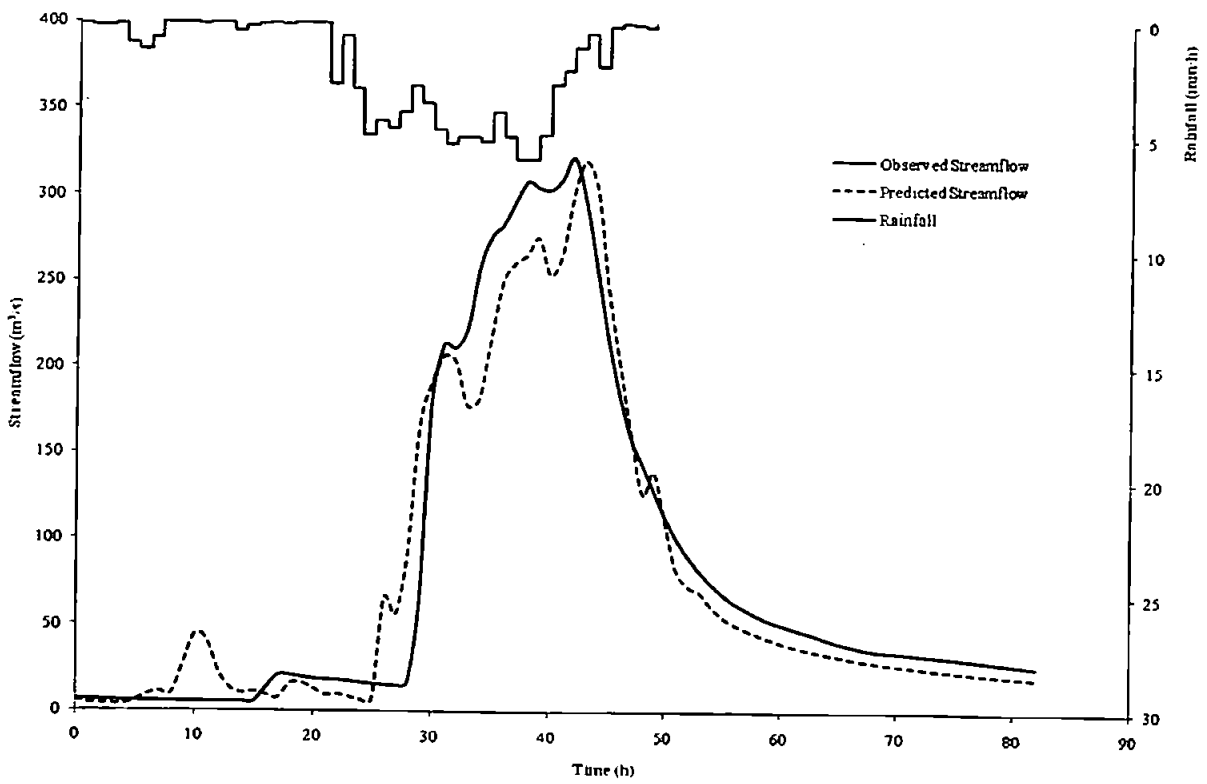
Figure D9.14 Predicted and observed results for event 3704
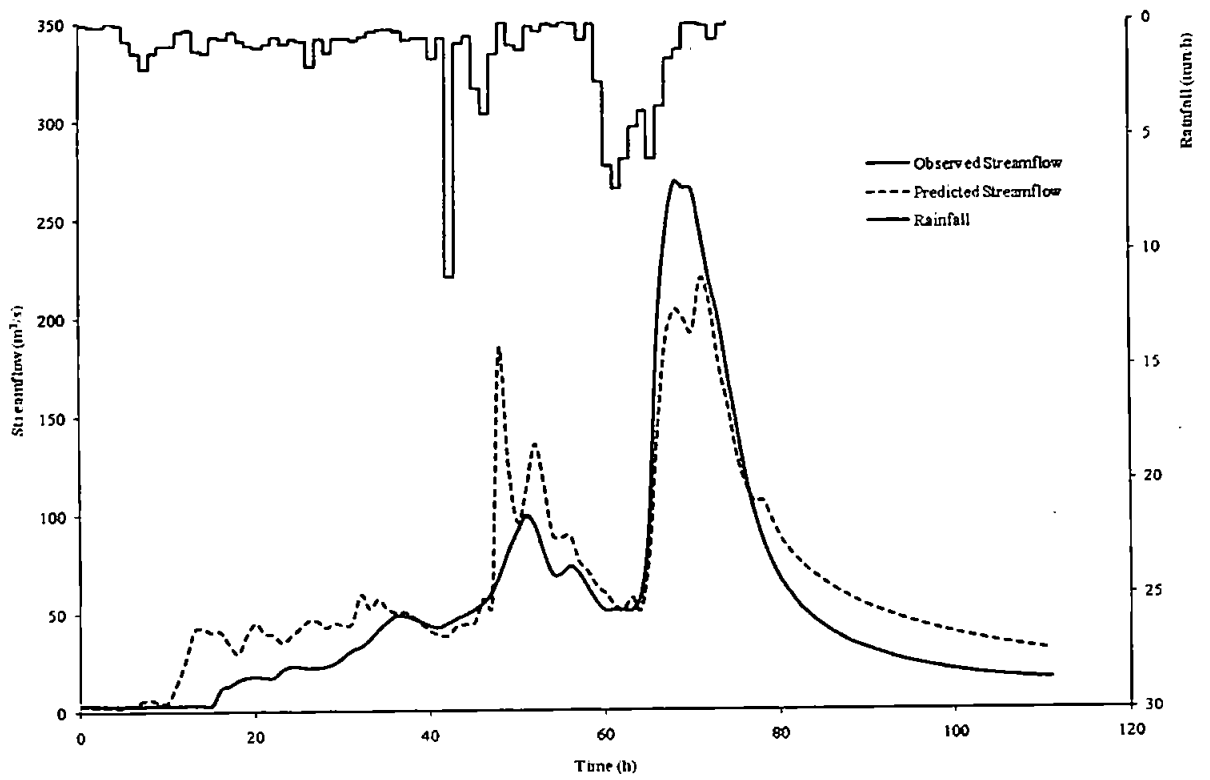
Figure D9.15 Predicted and observed results for event 3705

D10: Catchment 57005 – River Taff at Pontypridd
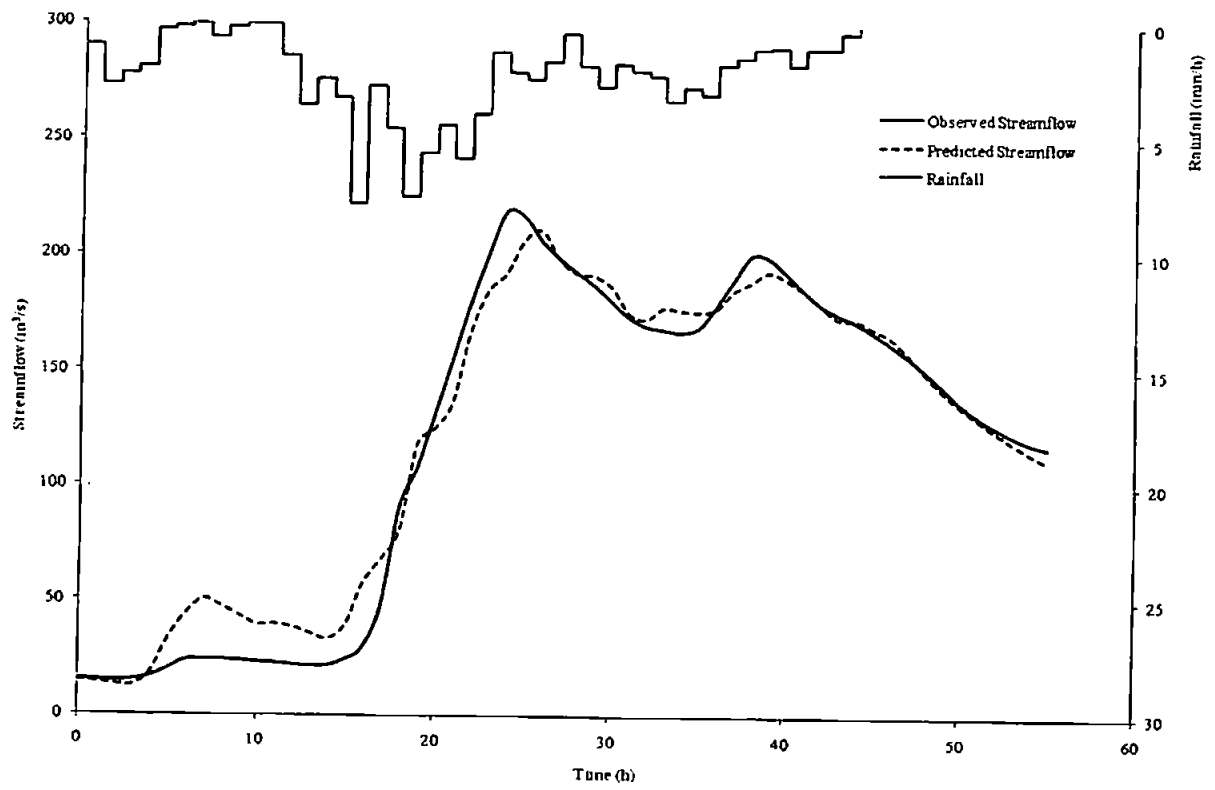
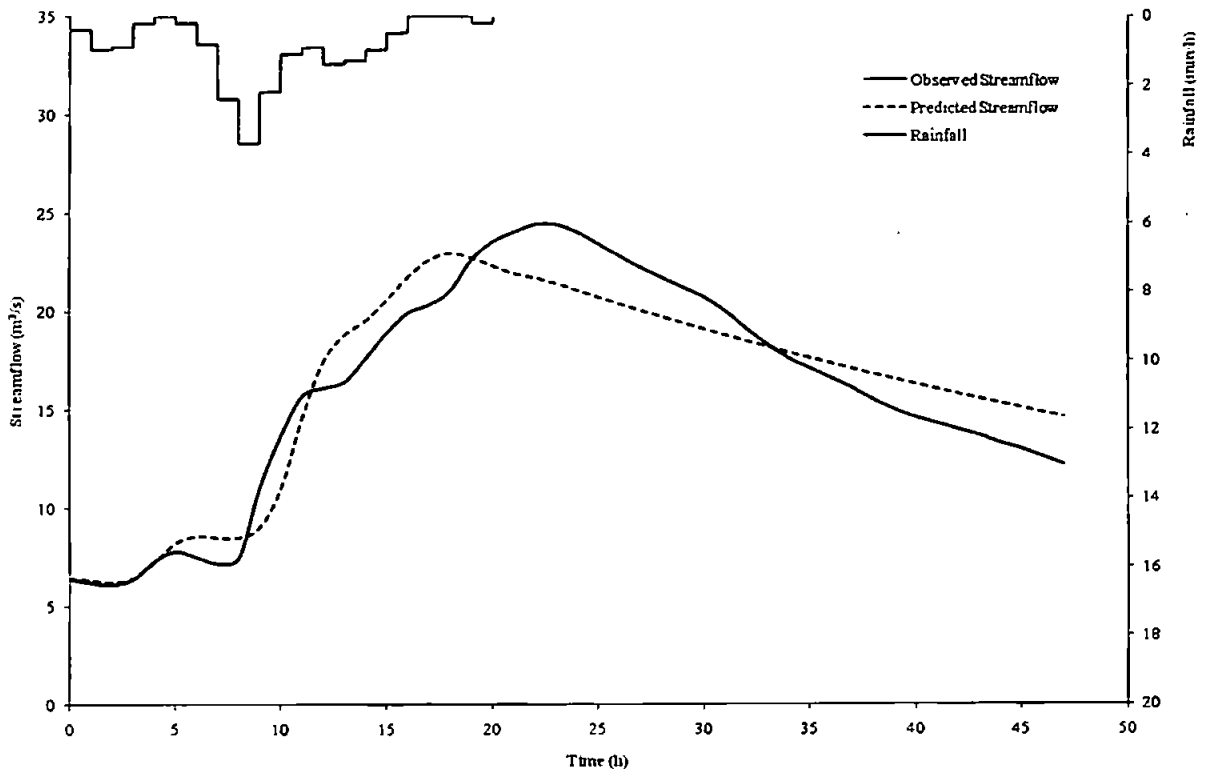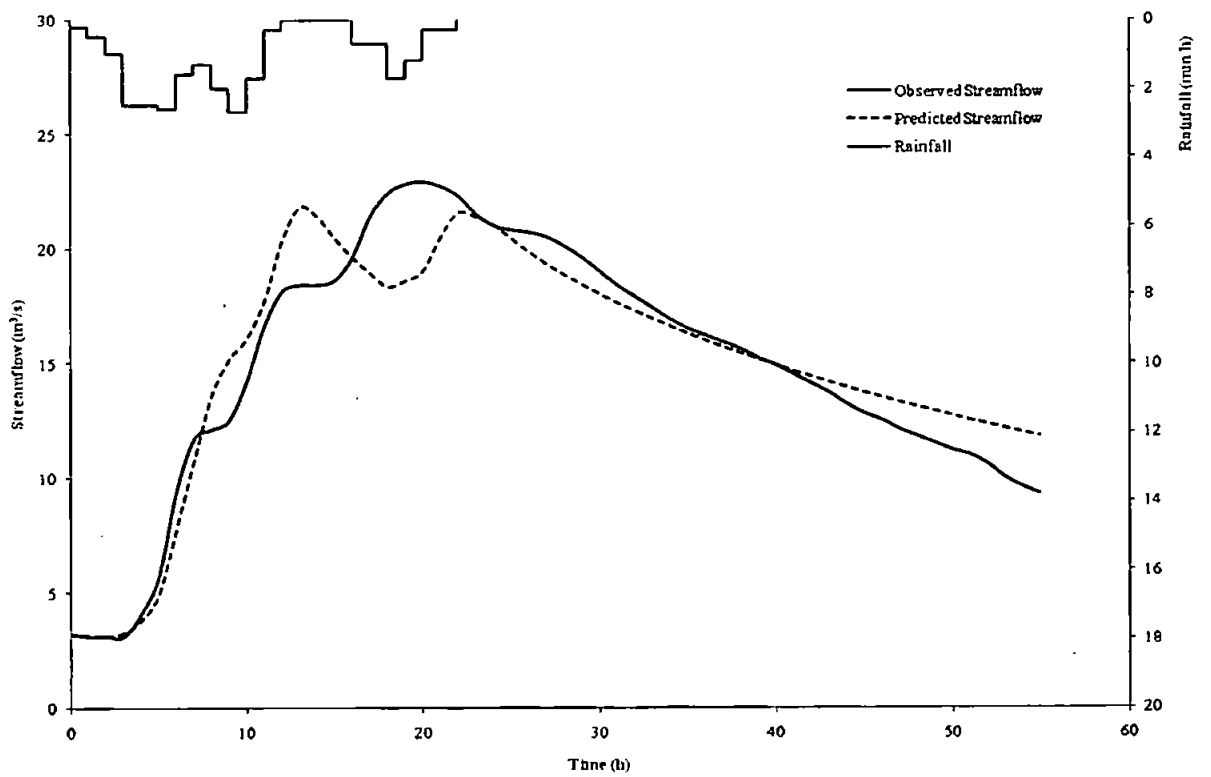
Figure D10.1 Predicted and observed results for event 1836
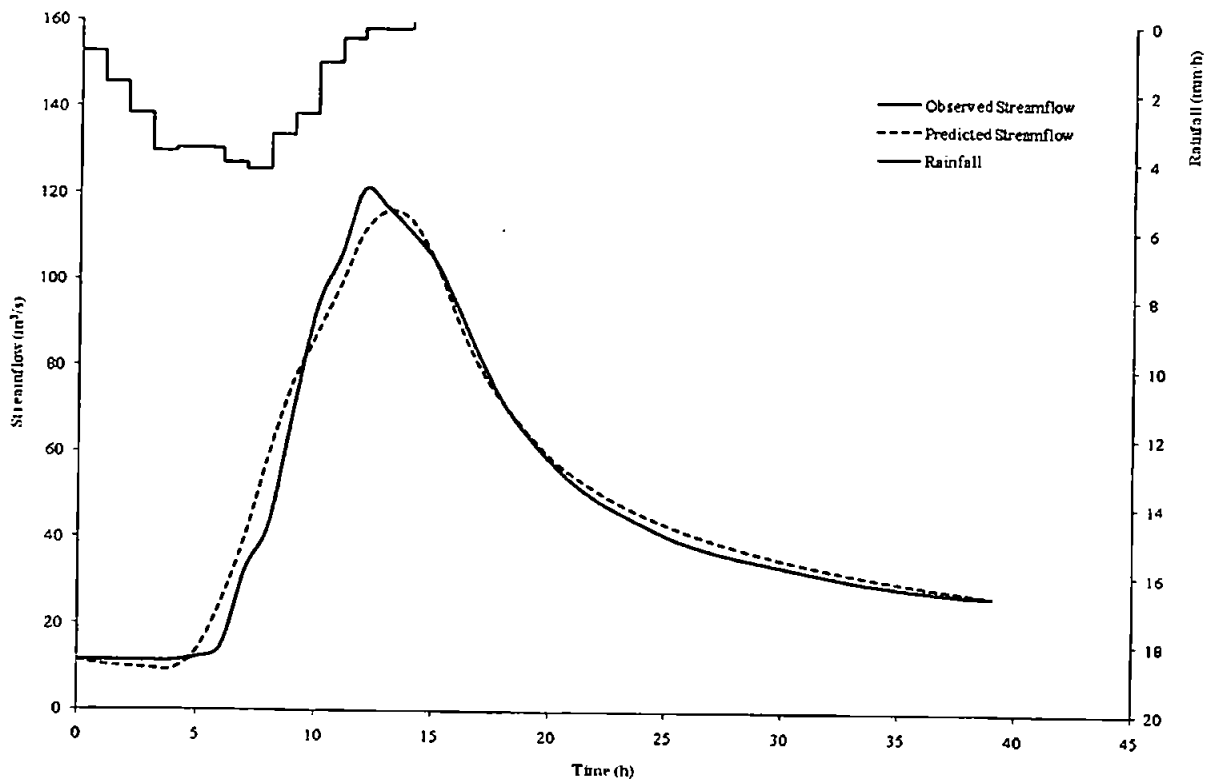
Figure D10.2 Predicted and observed results for event 1837
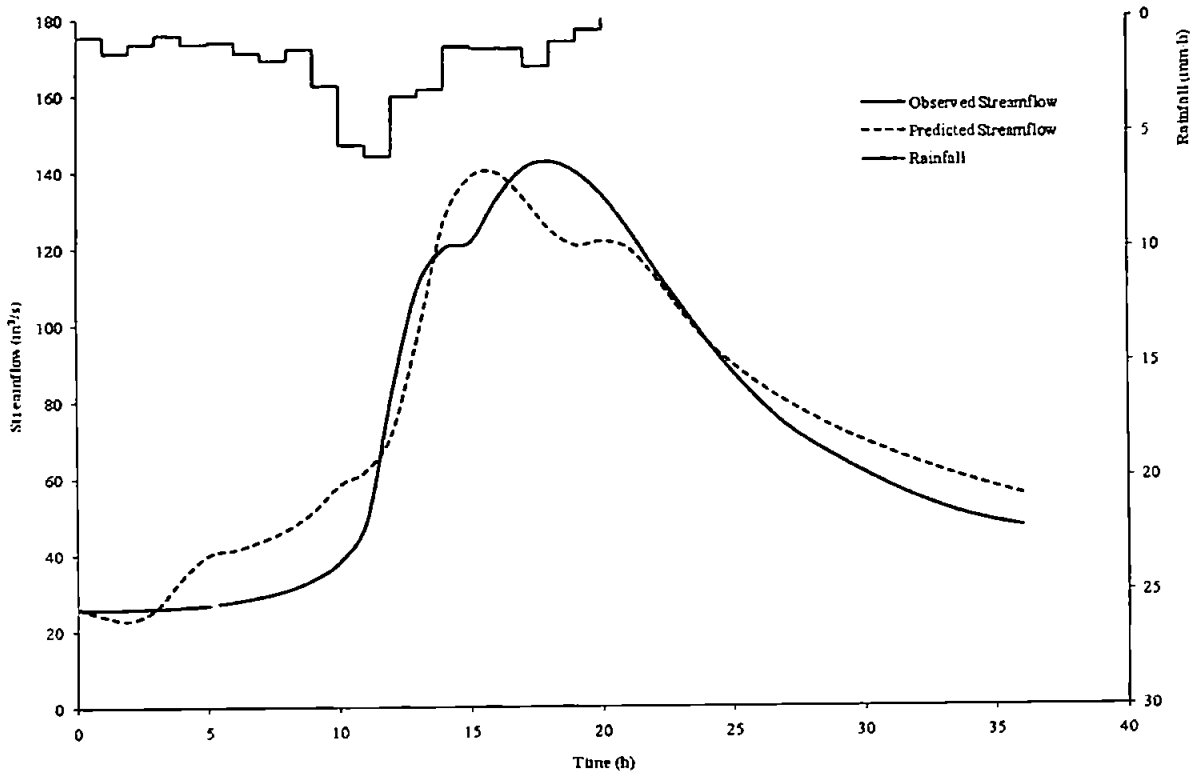
Figure D10.3 Predicted and observed results for event 1838
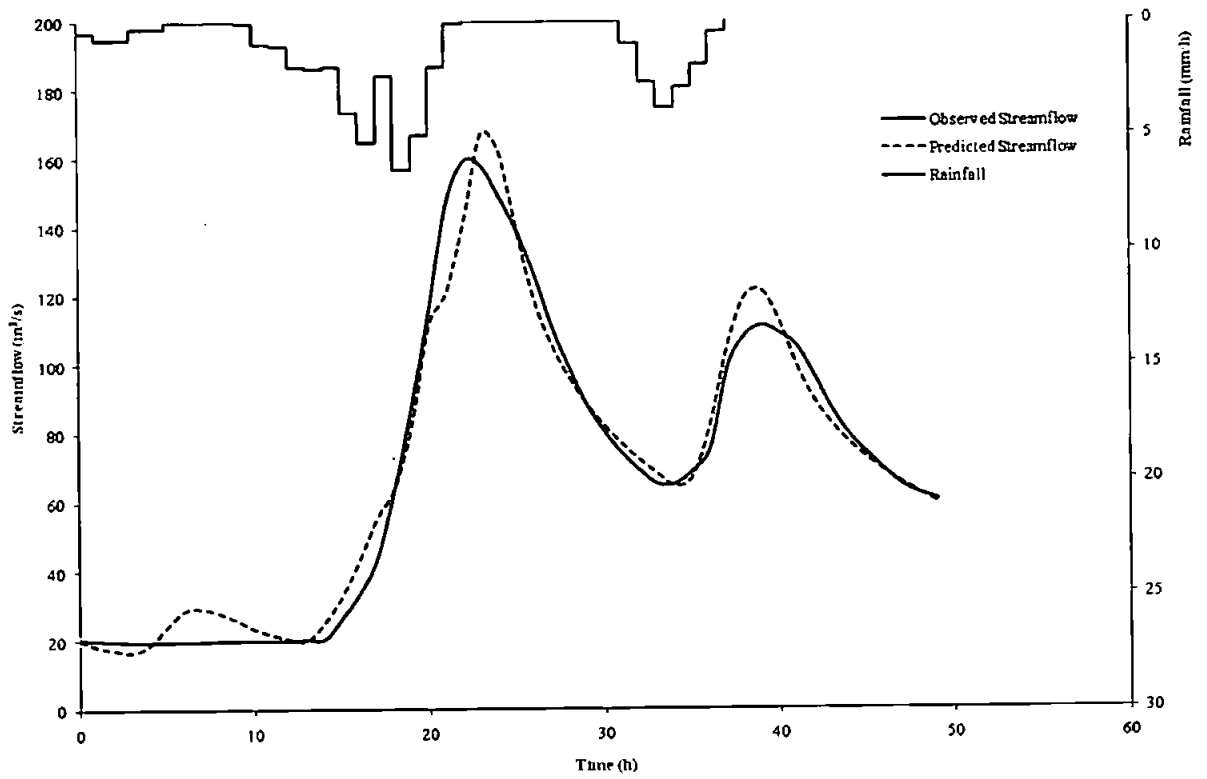
Figure D10.4 Predicted and observed results for event 1840
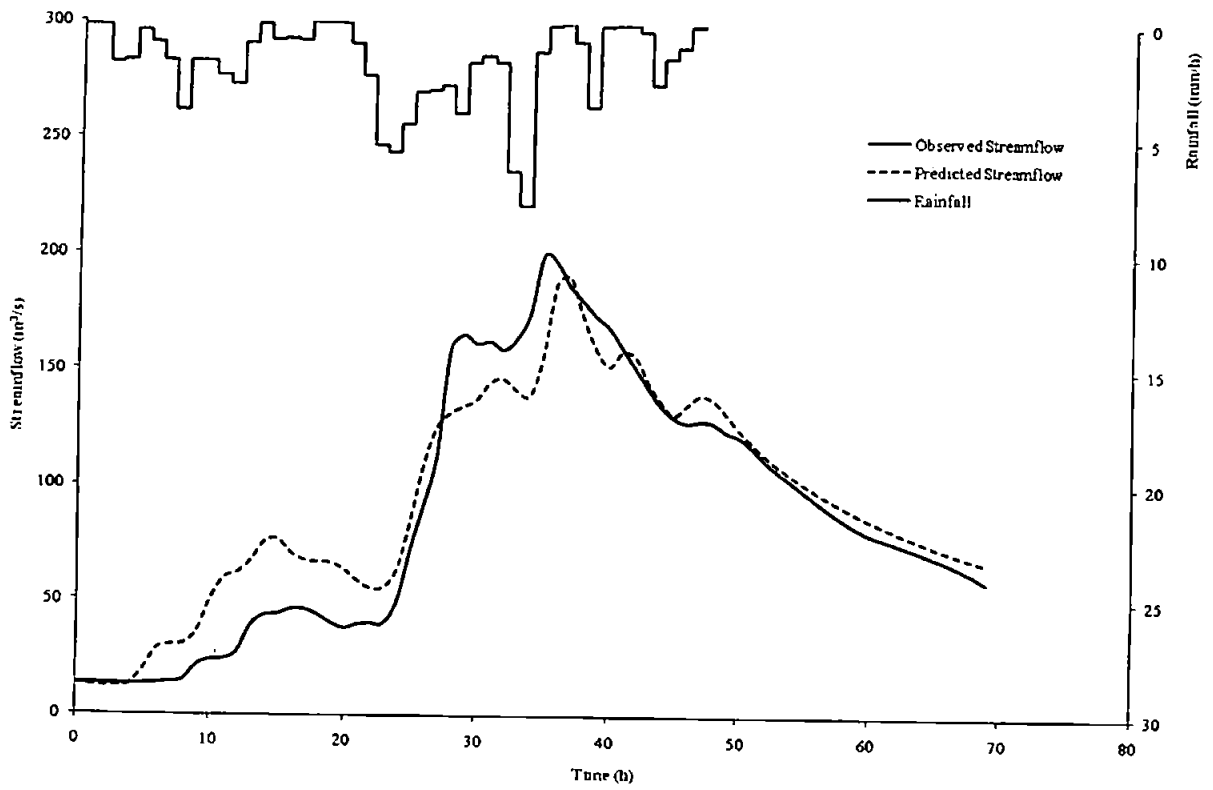
Figure D10.5 Predicted and observed results for event 1841
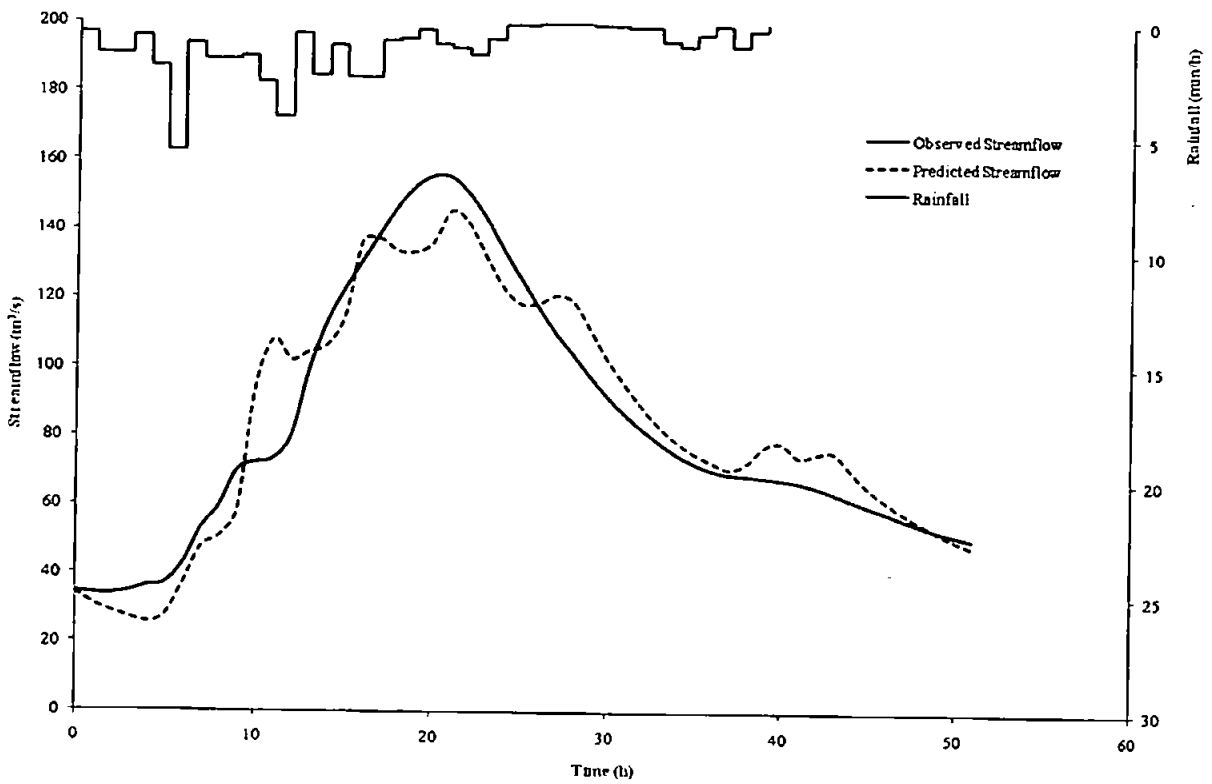
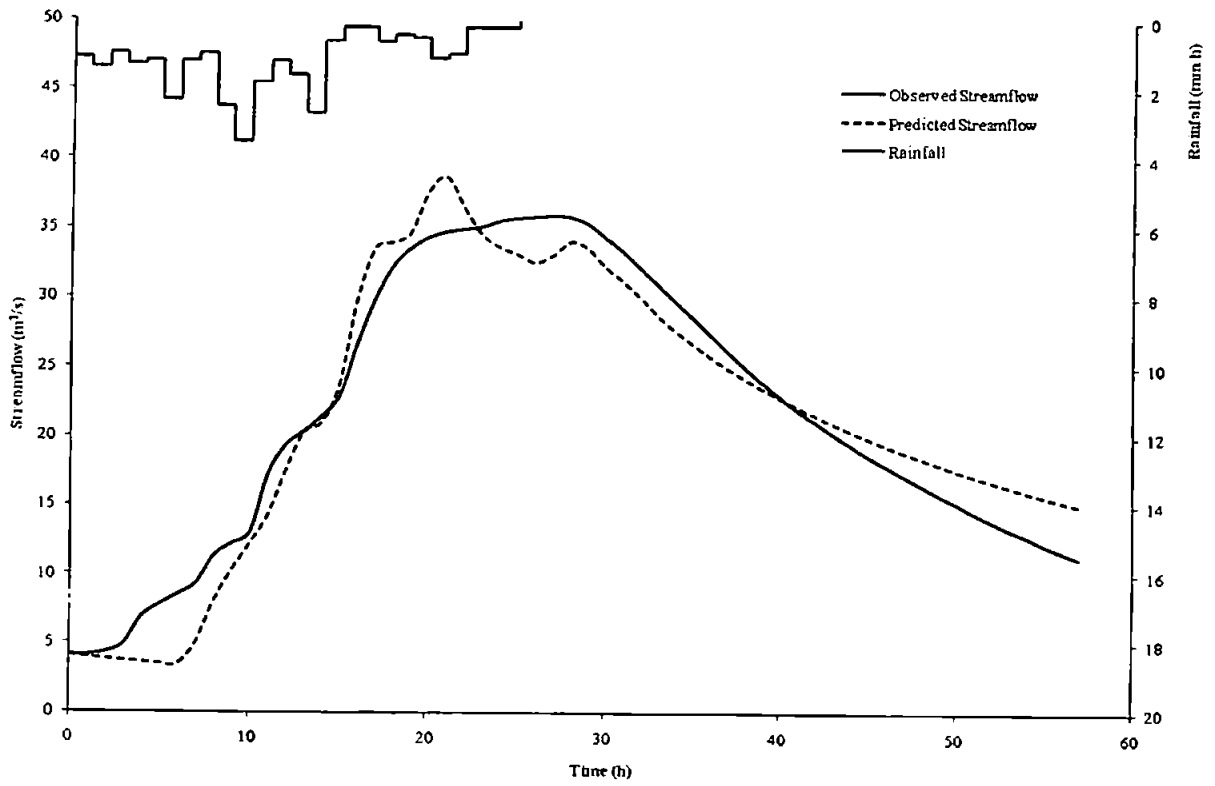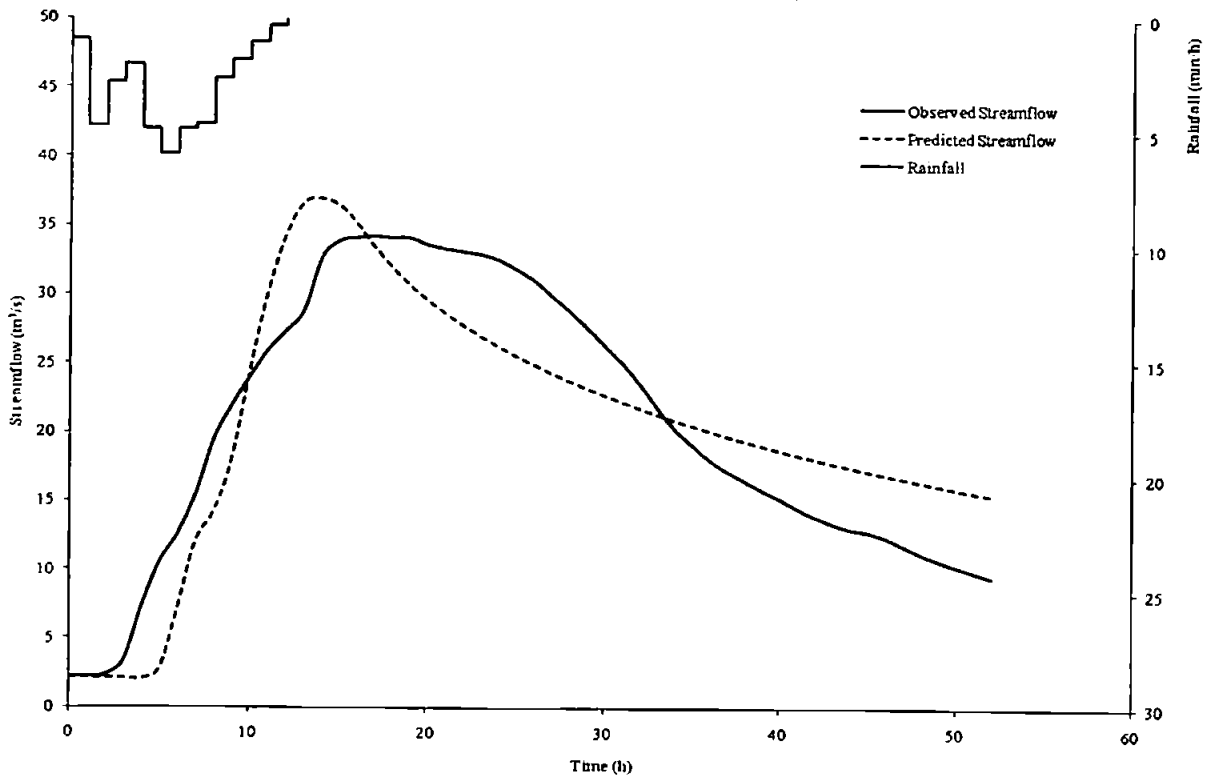**Figure D10.6 Predicted and observed results for event 1842**
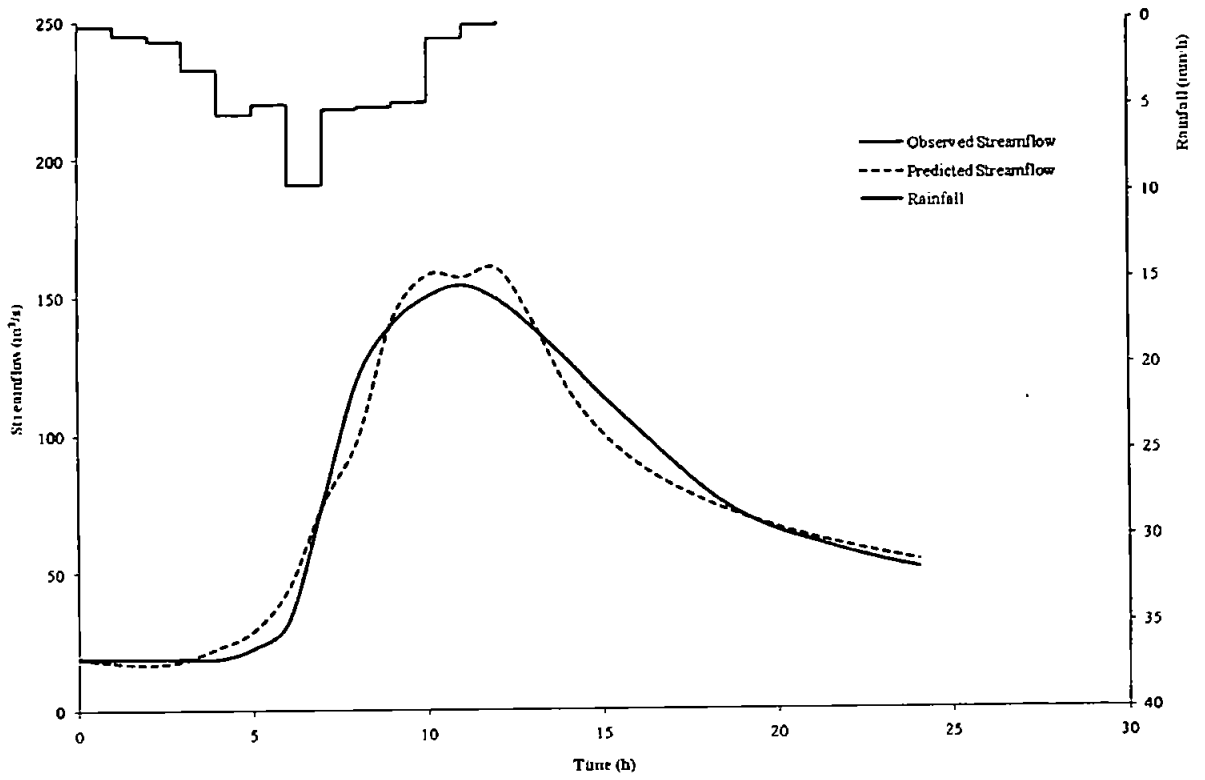
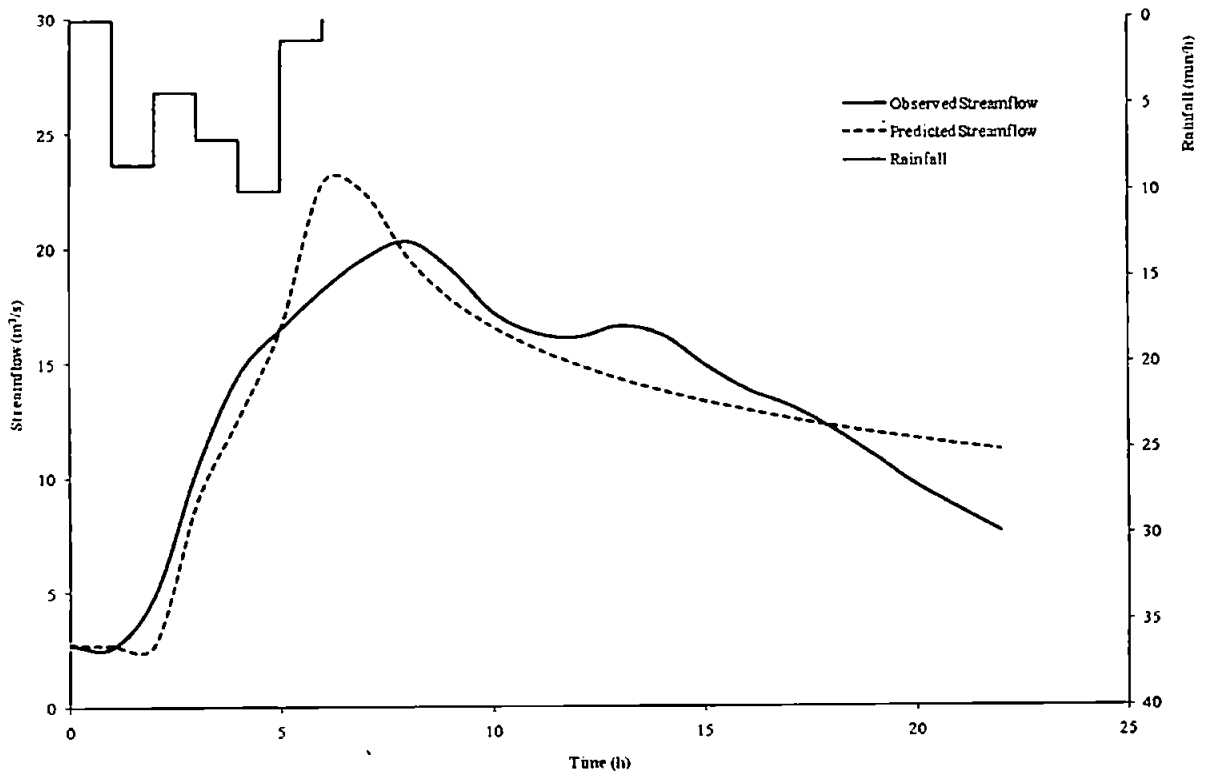**Figure D10.7 Predicted and observed results for event 1843**
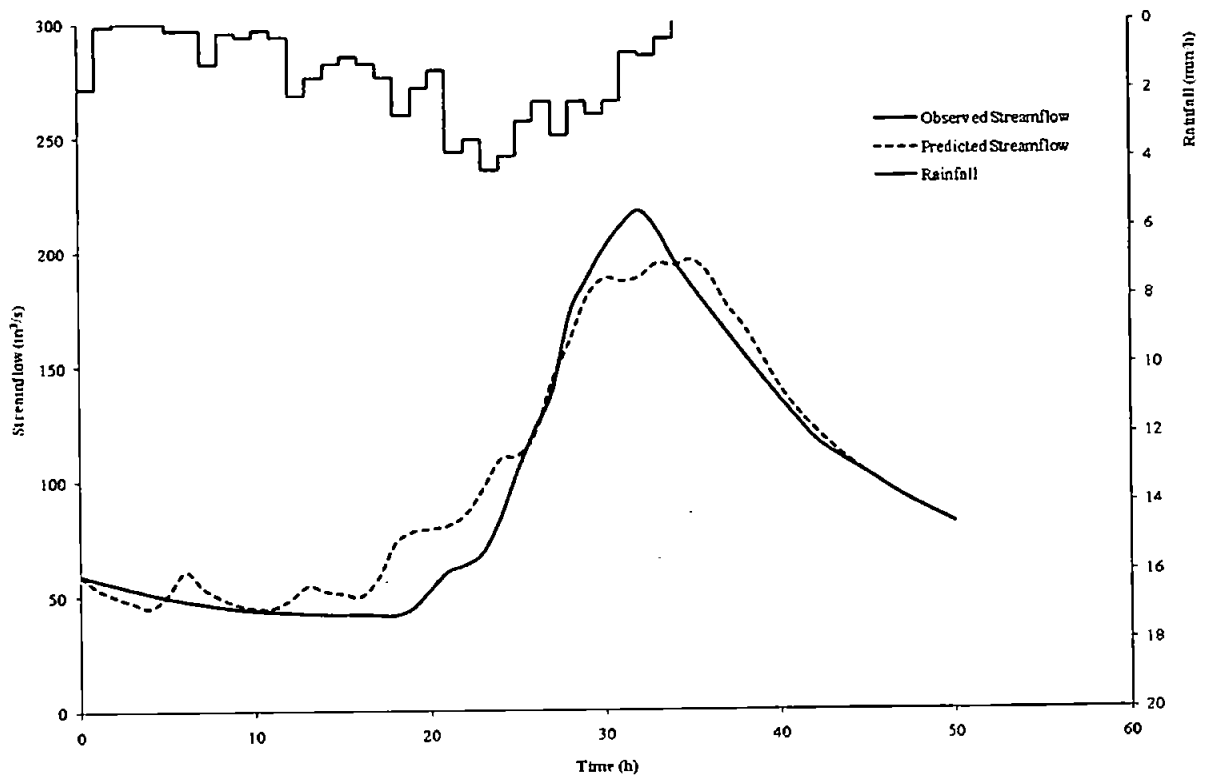
Figure D10.8 Predicted and observed results for event 1844
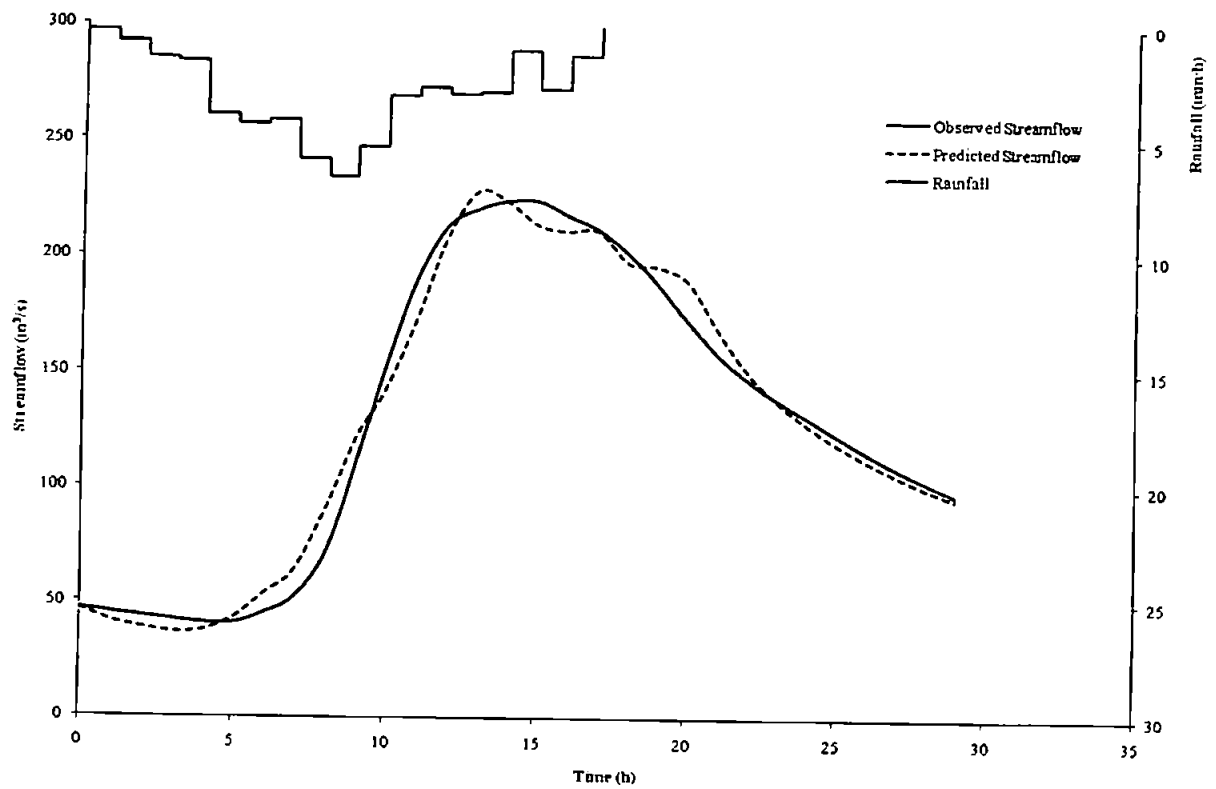
Figure D10.9 Predicted and observed results for event 1845
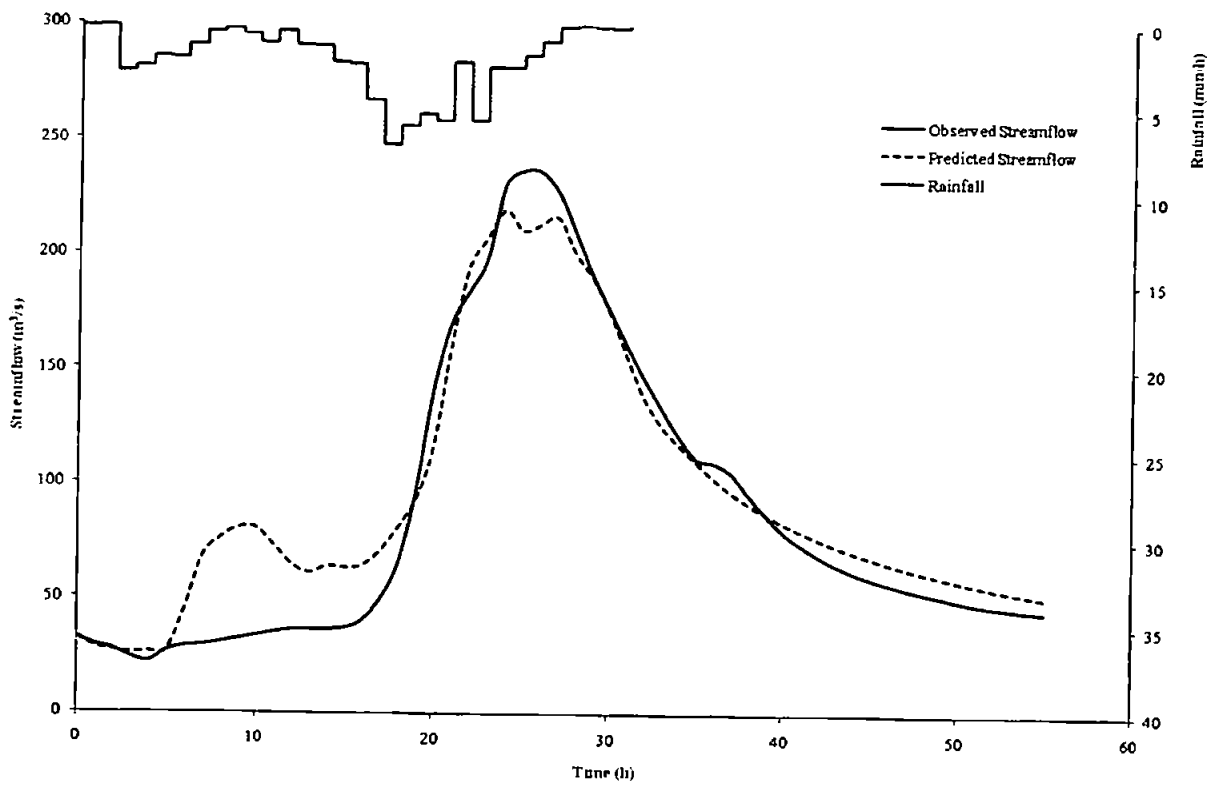
Figure D10.10 Predicted and observed results for event 1846

336
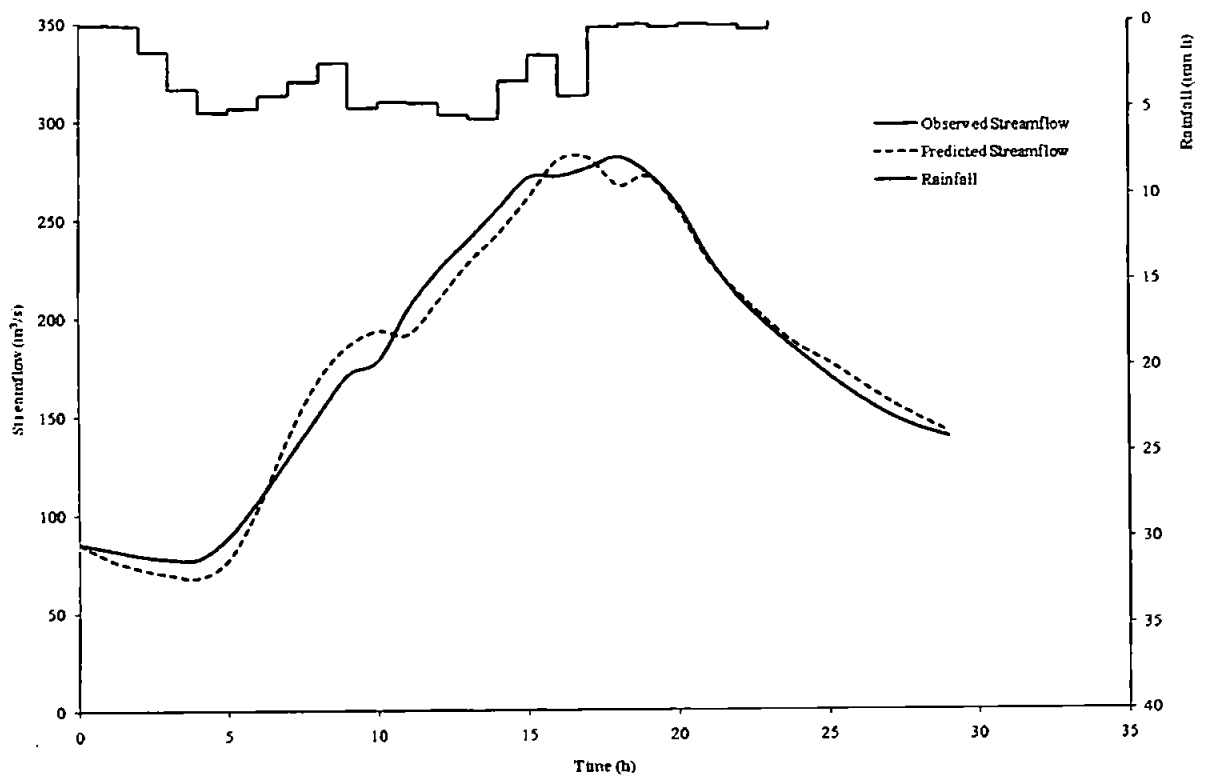
Figure D10.11 Predicted and observed results for event 1847

337

D11: Catchment 72006 – River Lune at Kirkby Lonsdale
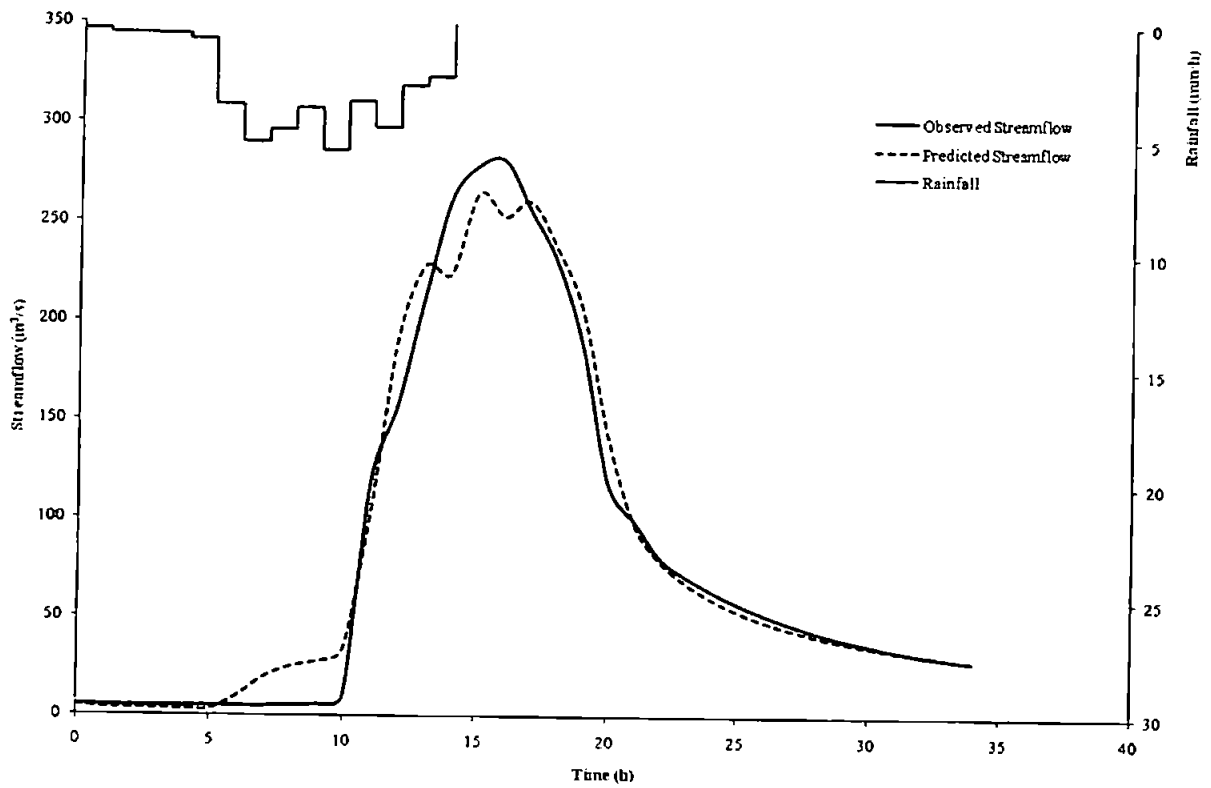
Figure D11.1 Predicted and observed results for event 2282
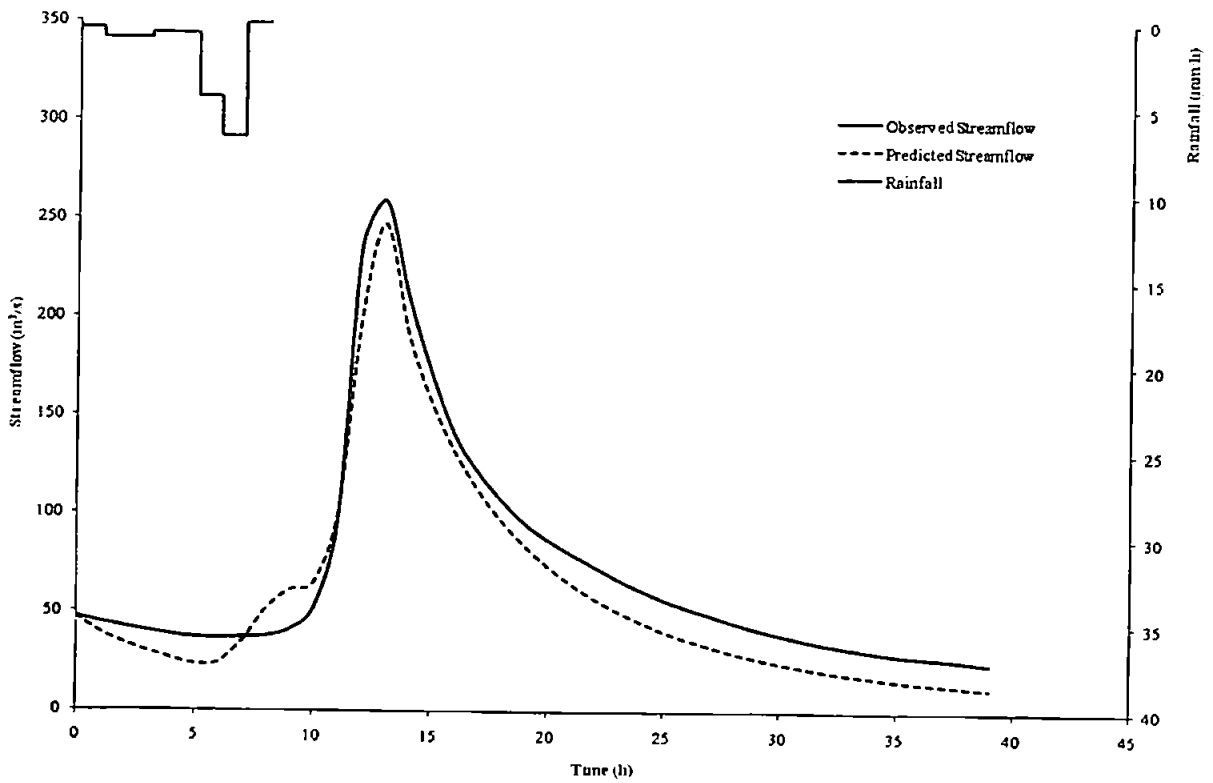
Figure D11.2 Predicted and observed results for event 2283
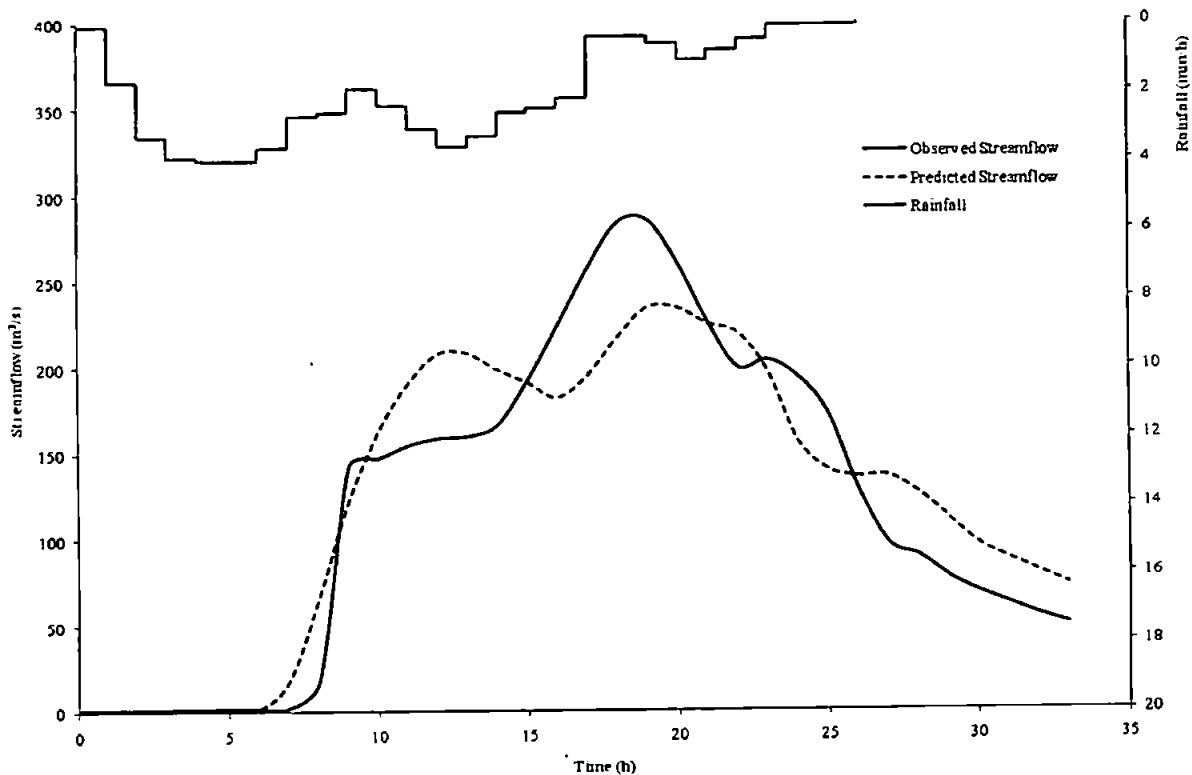
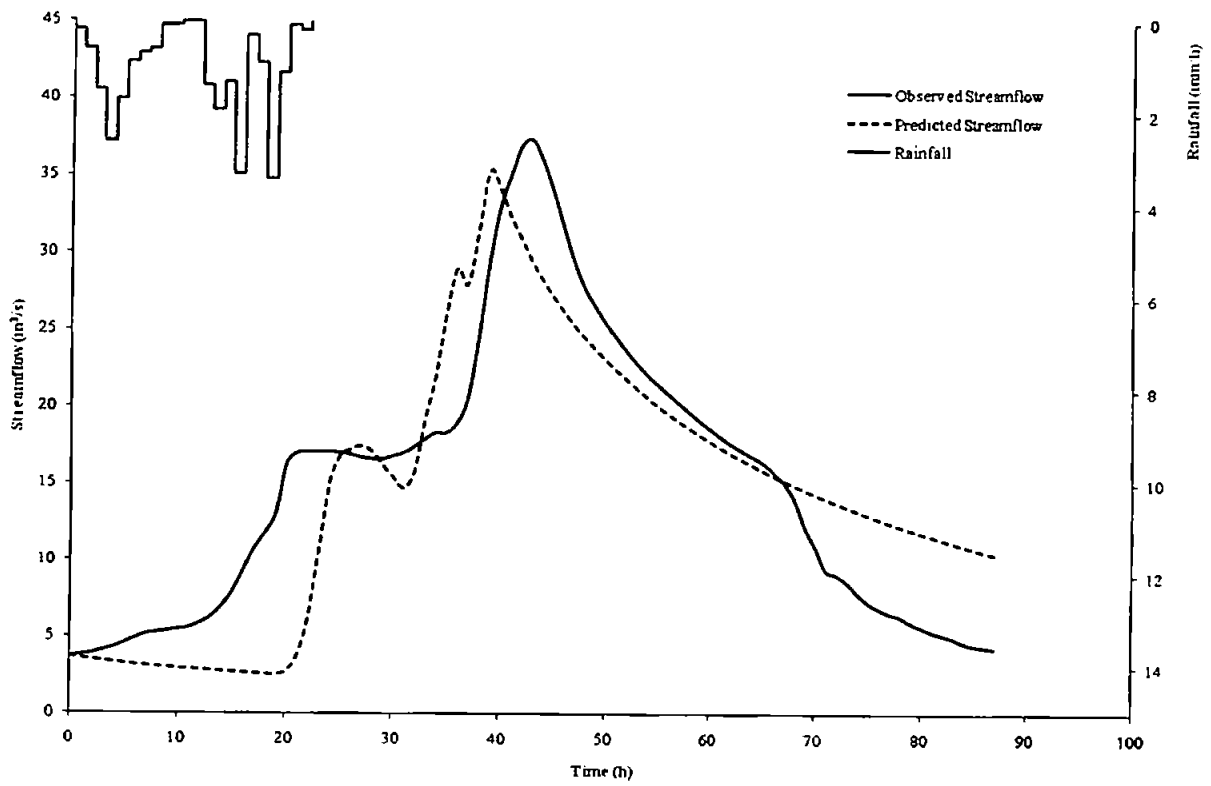**Figure D11.3 Predicted and observed results for event 2284**

Figure D11.4 Predicted and observed results for event 2285

339
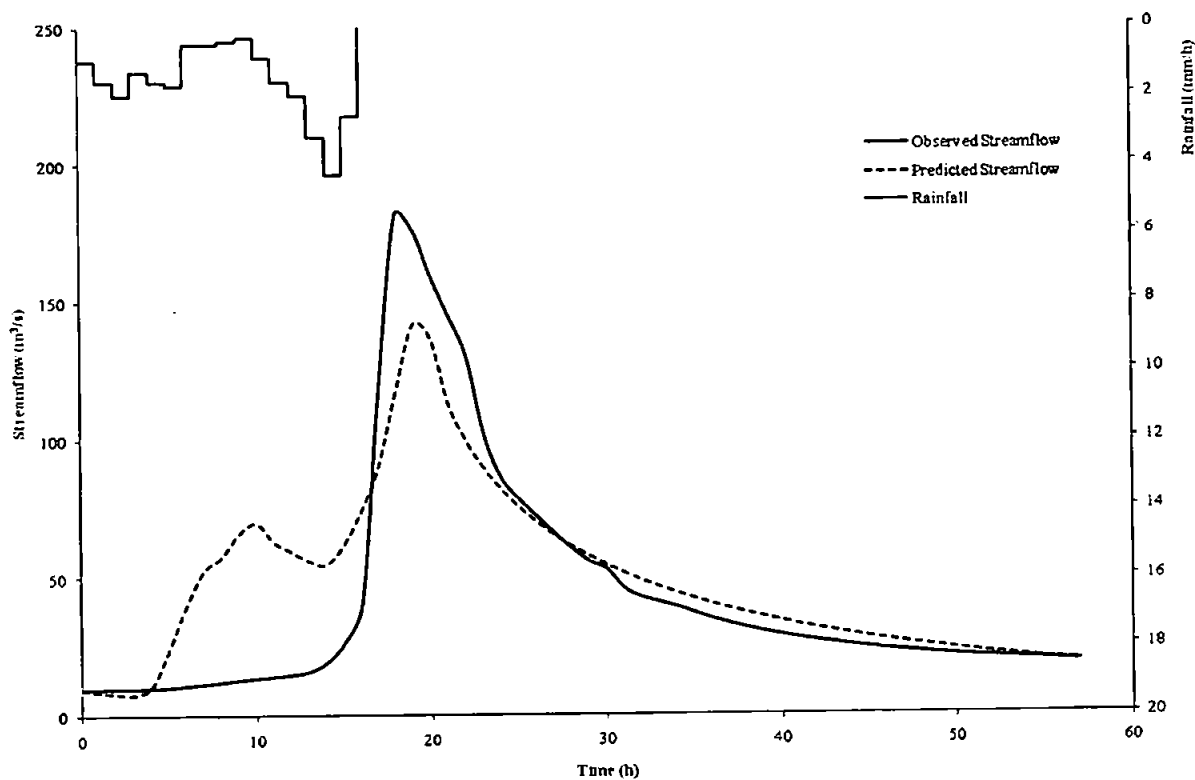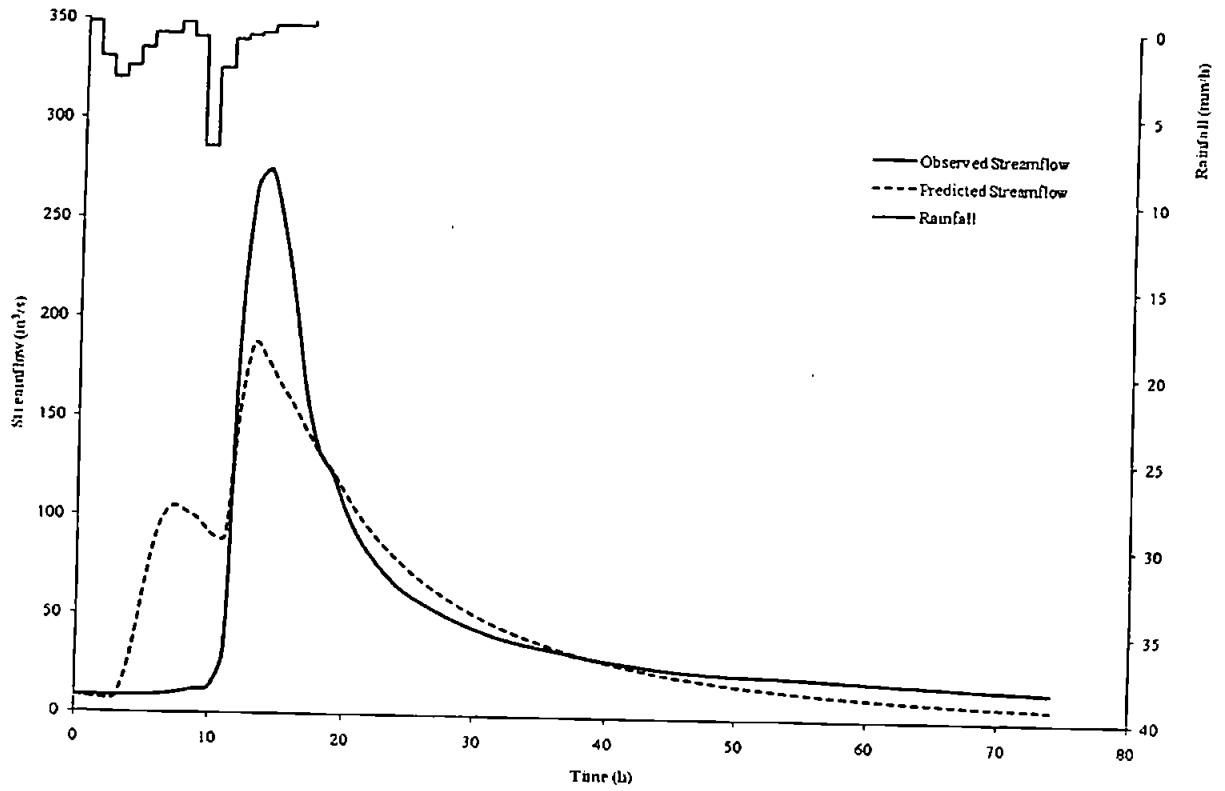
Figure D11.5 Predicted and observed results for event 2286
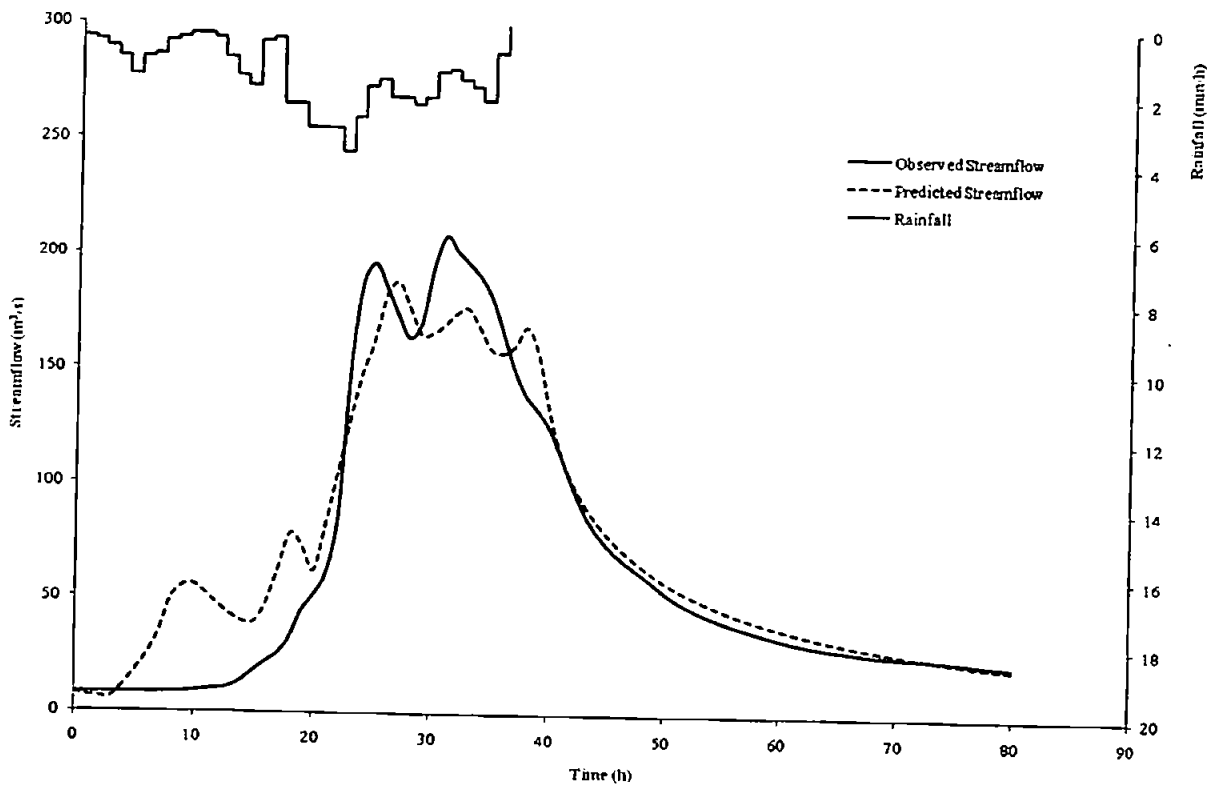
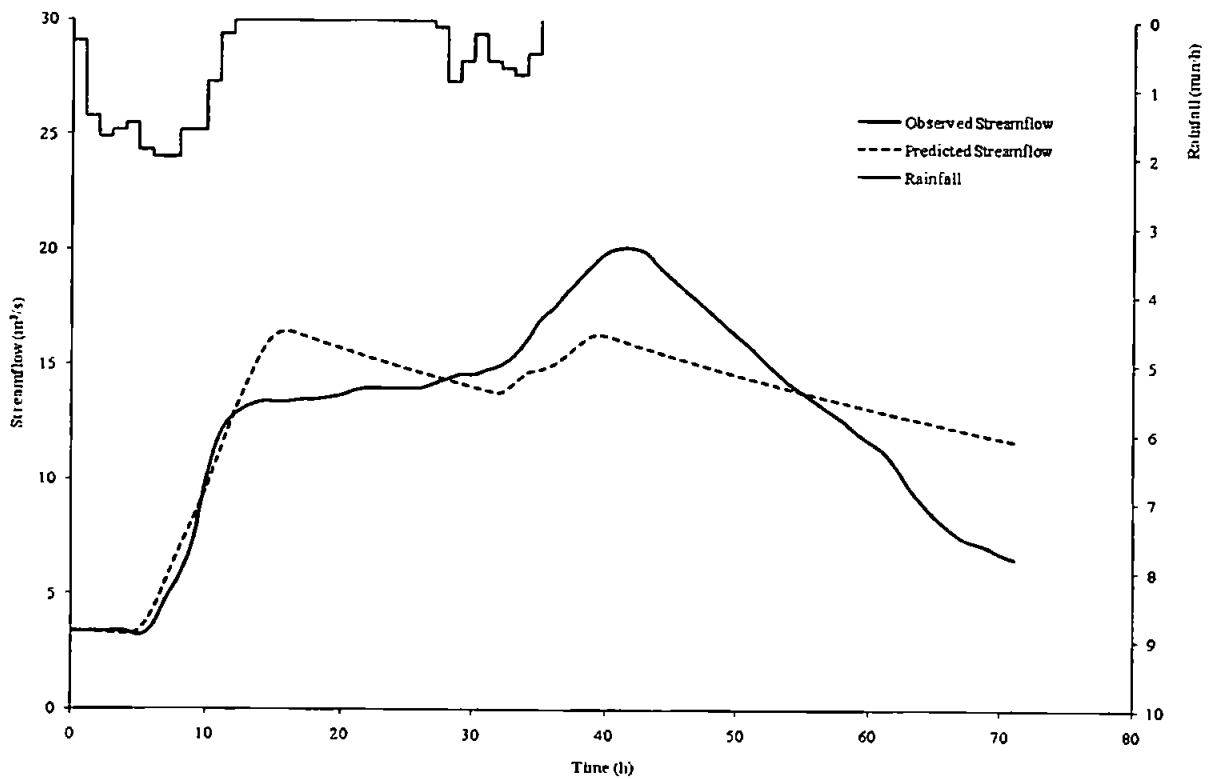**Figure D11.6 Predicted and observed results for event 2287**

340
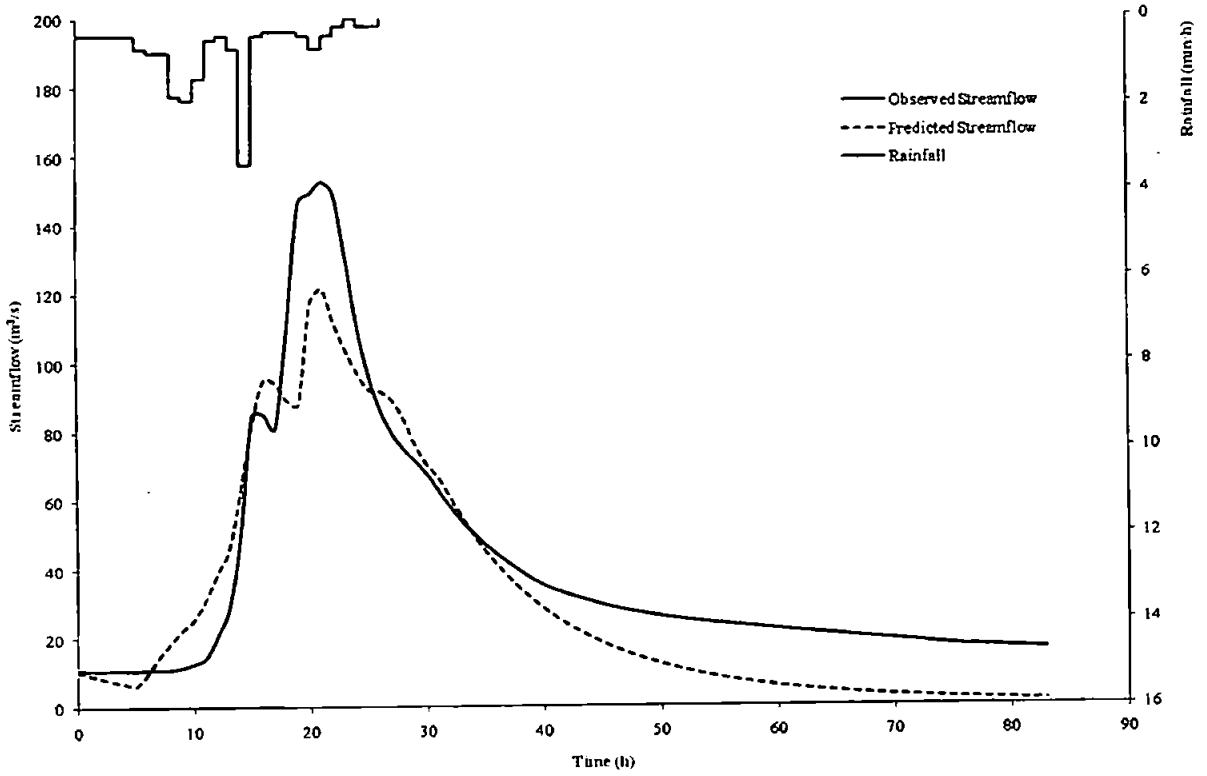
Figure D11.7 Predicted and observed results for event 2288
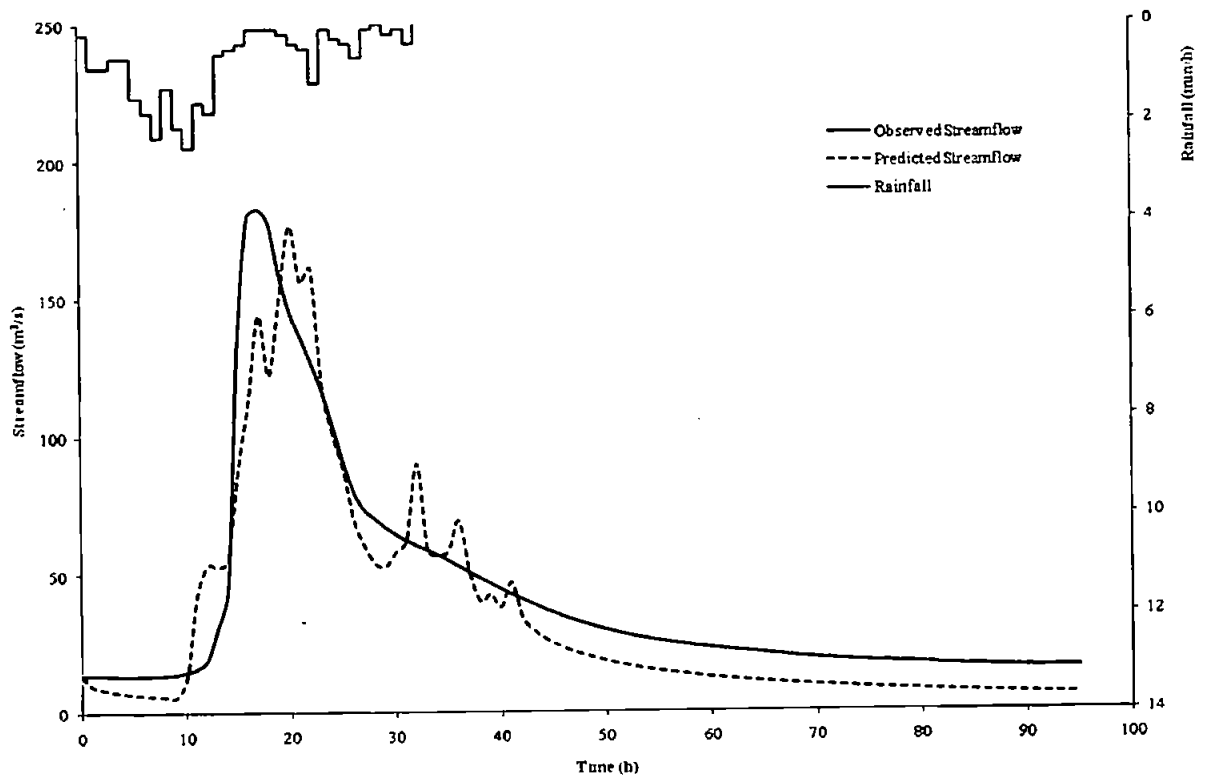
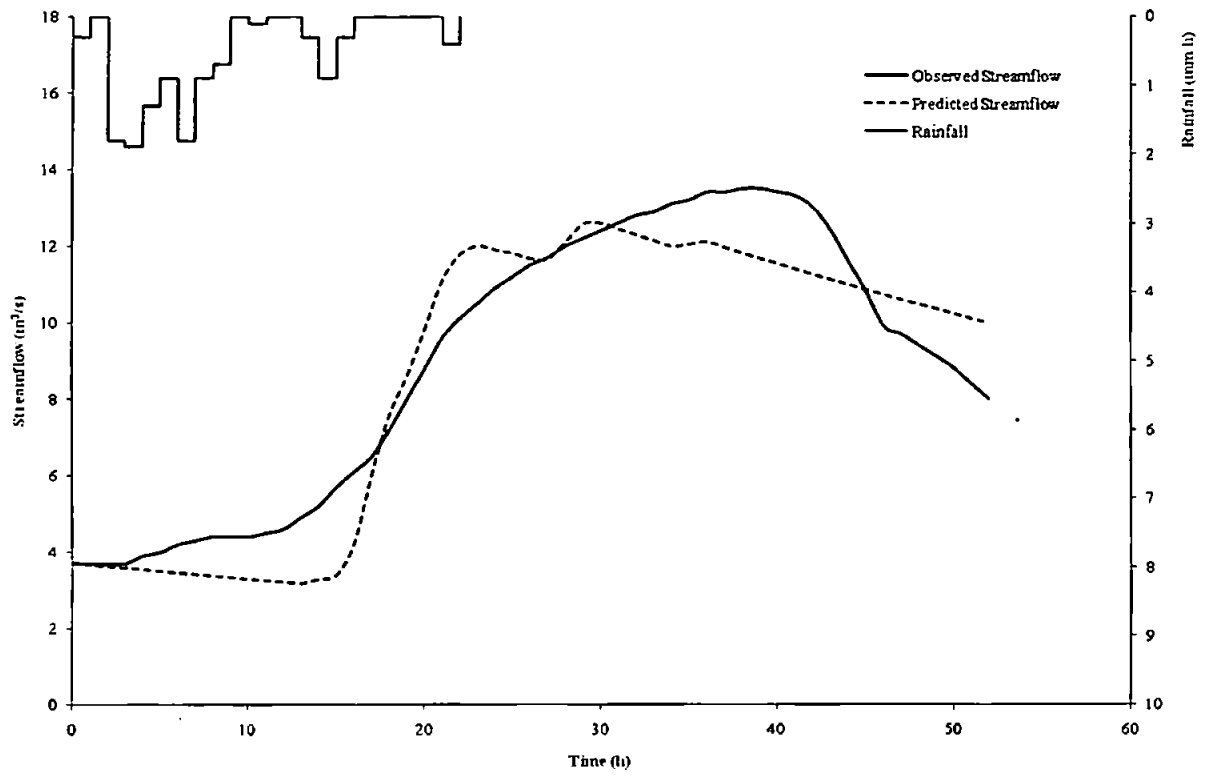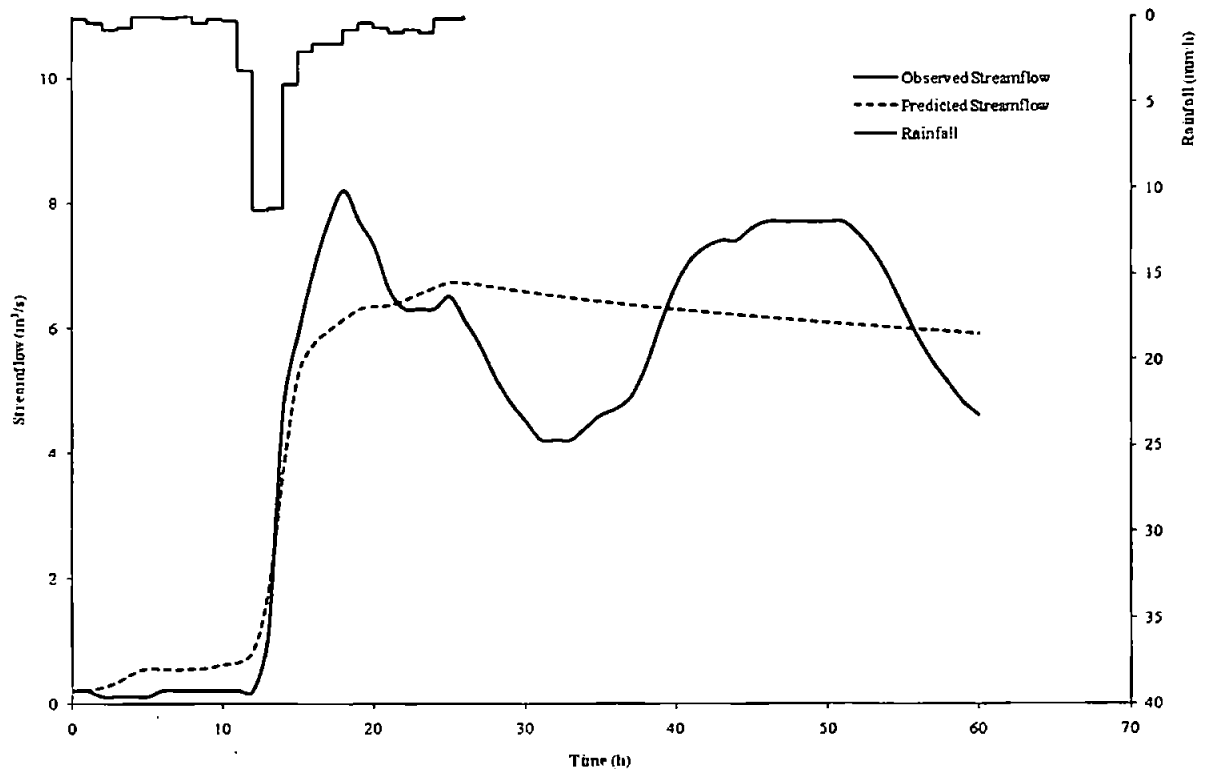**Figure D11.8 Predicted and observed results for event 2289**

341
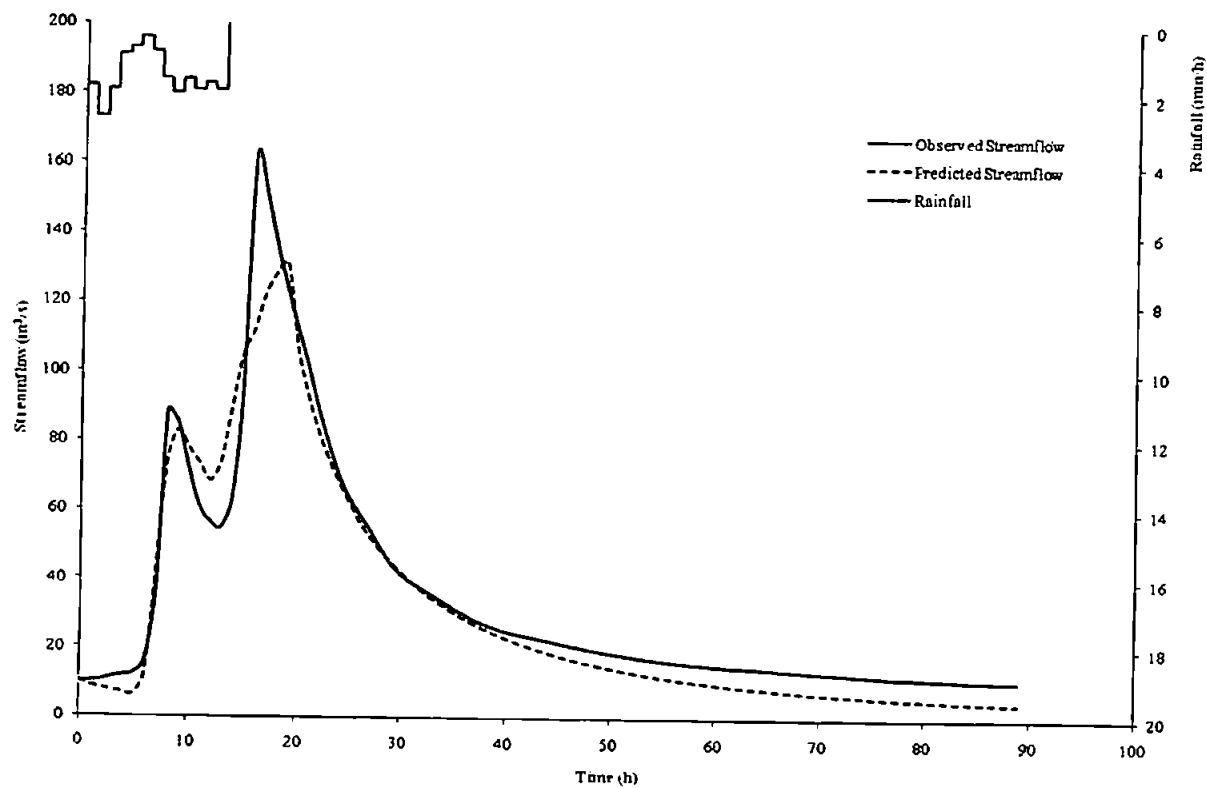
Figure D11.9 Predicted and observed results for event 2290
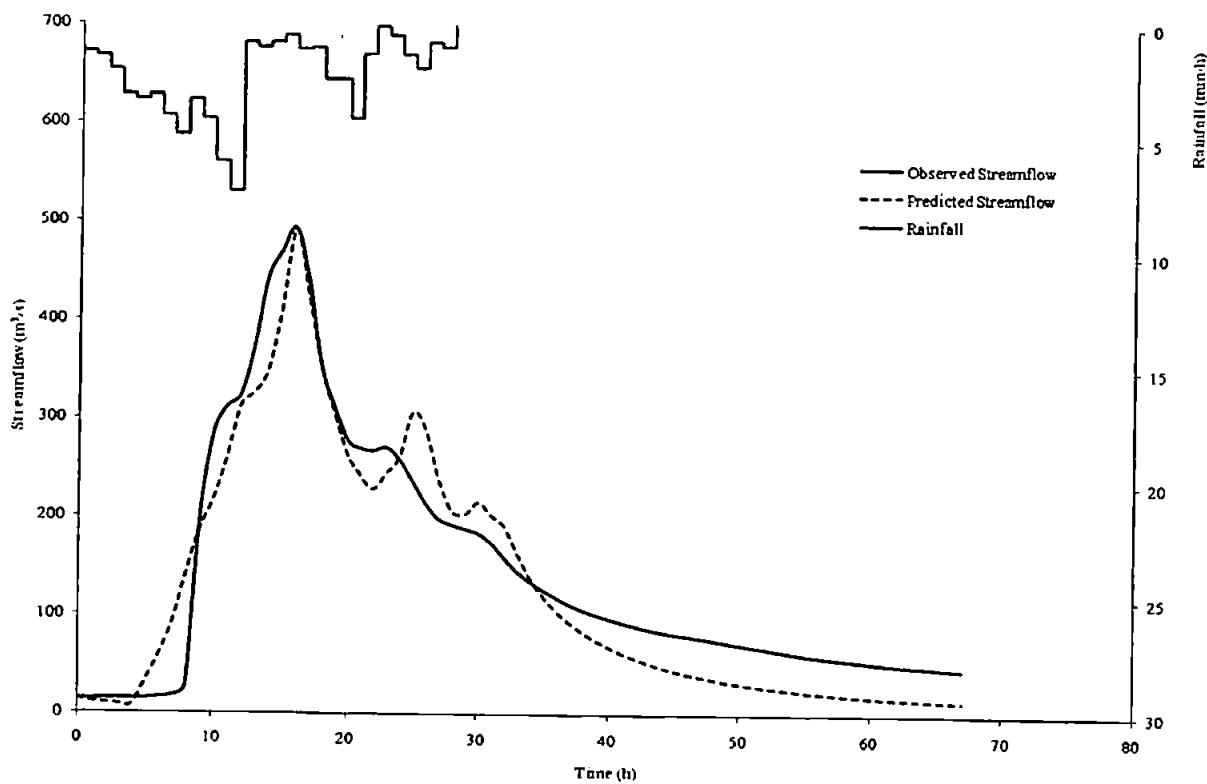
Figure D11.10 Predicted and observed results for event 2291

342

Appendix E: Single Fractional Reservoir Results Using Calibration Set 14

The following Figures show the predicted and observed streamflow hydrographs together with the observed event rainfall hyetograph for the initialised, single, fractional-order, time-lagged, linear reservoir with a non-linear rainfall filter using calibration set 14 (re. section 6.2.4) for the East Dart at Bellever (river gauge no. 46005).
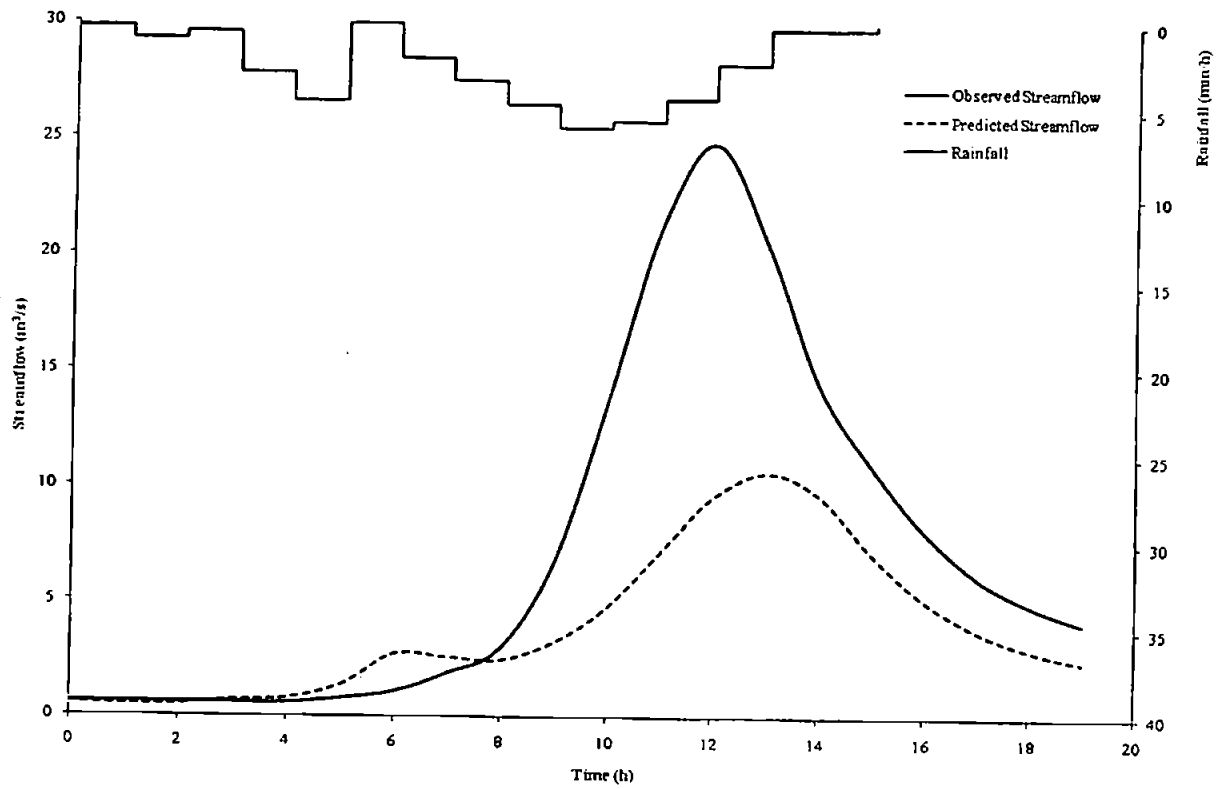
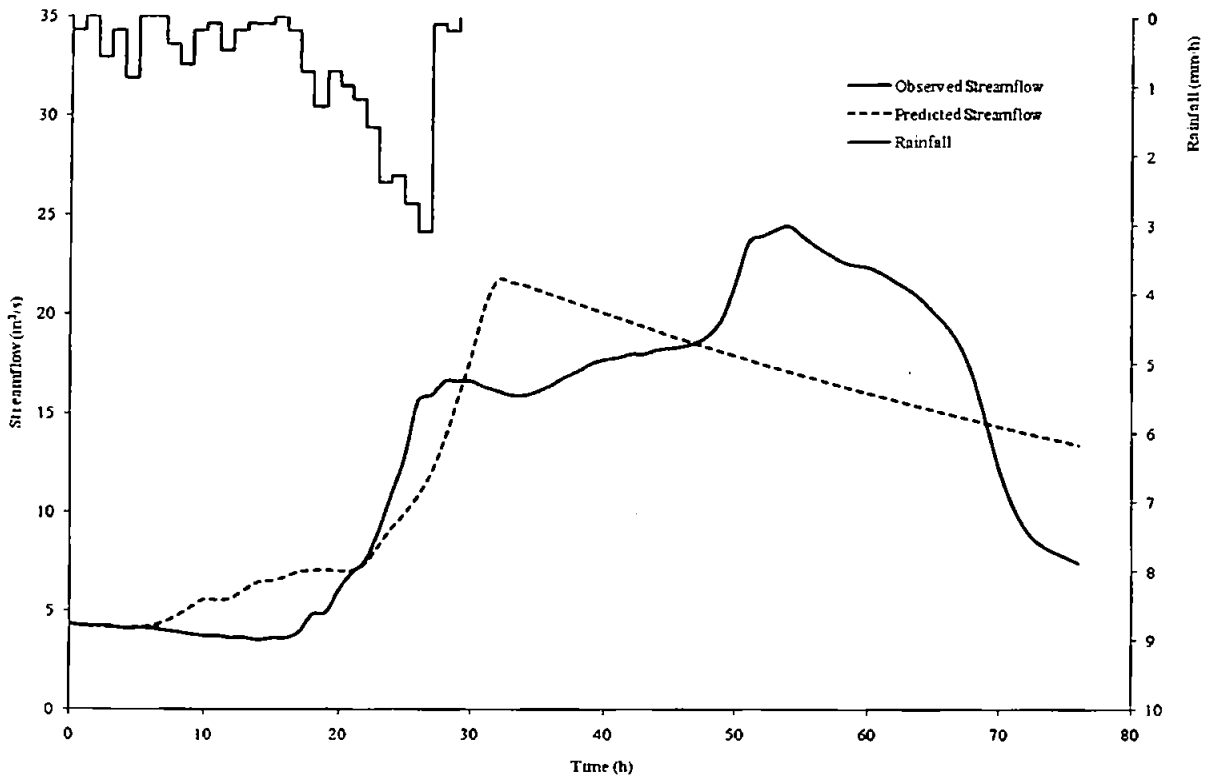**Figure E1 Predicted and observed results for event 1287**
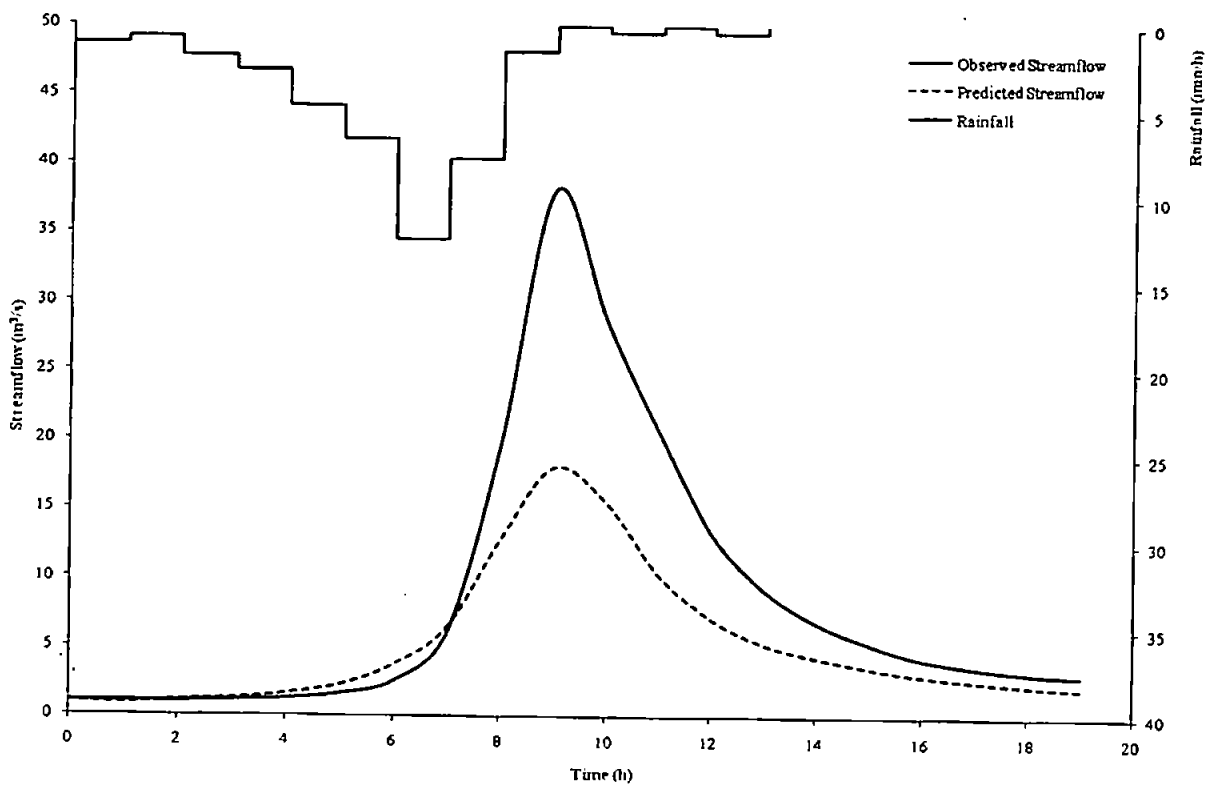
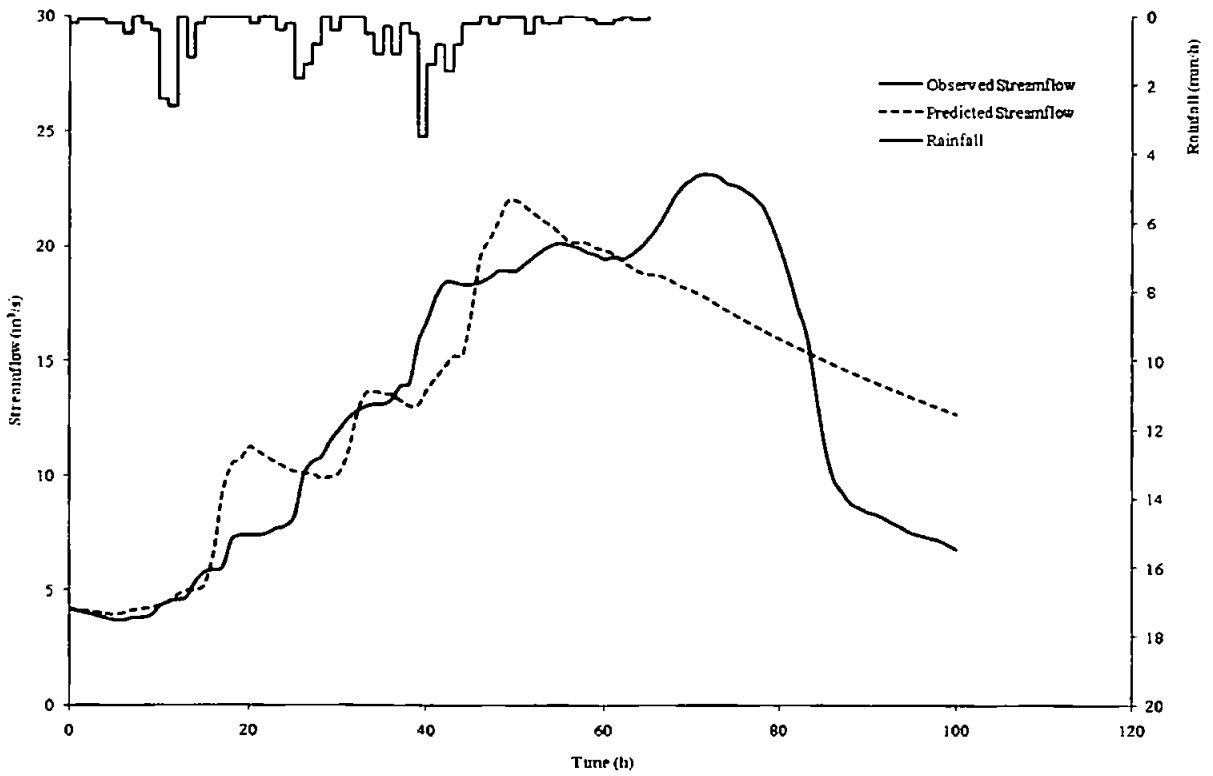**Figure E2 Predicted and observed results for event 1289**
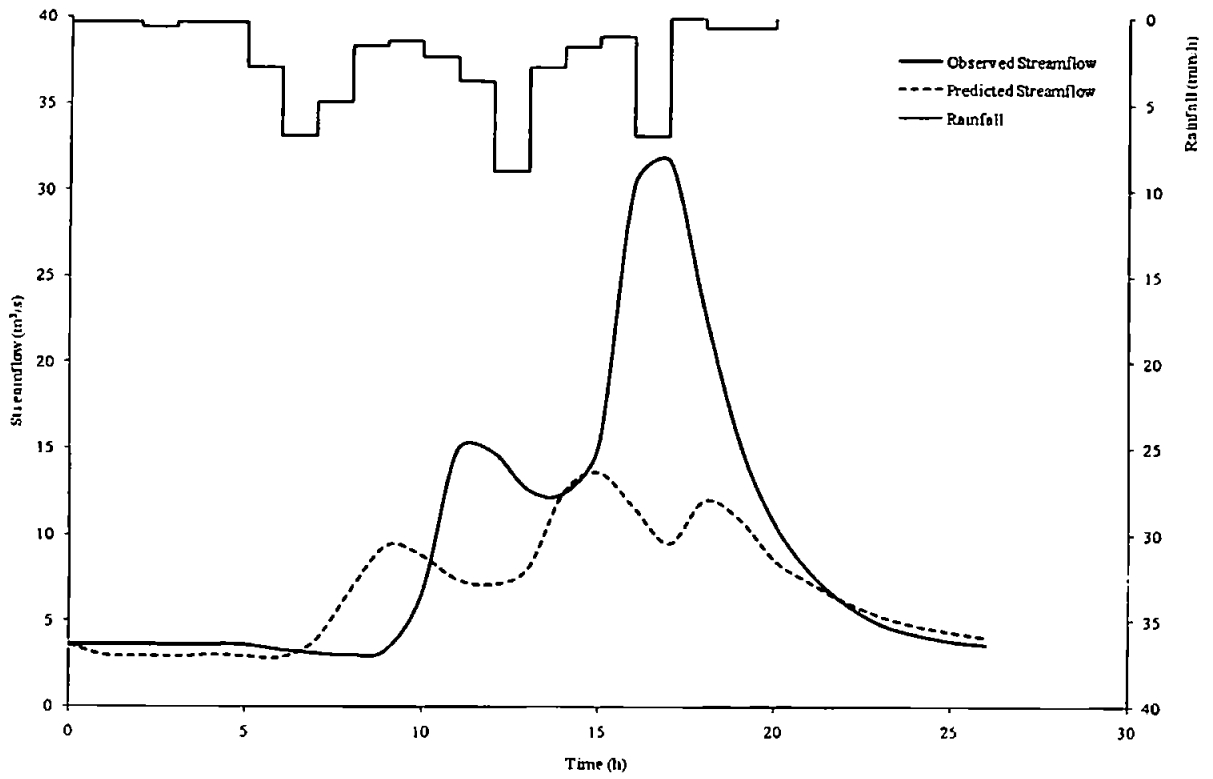
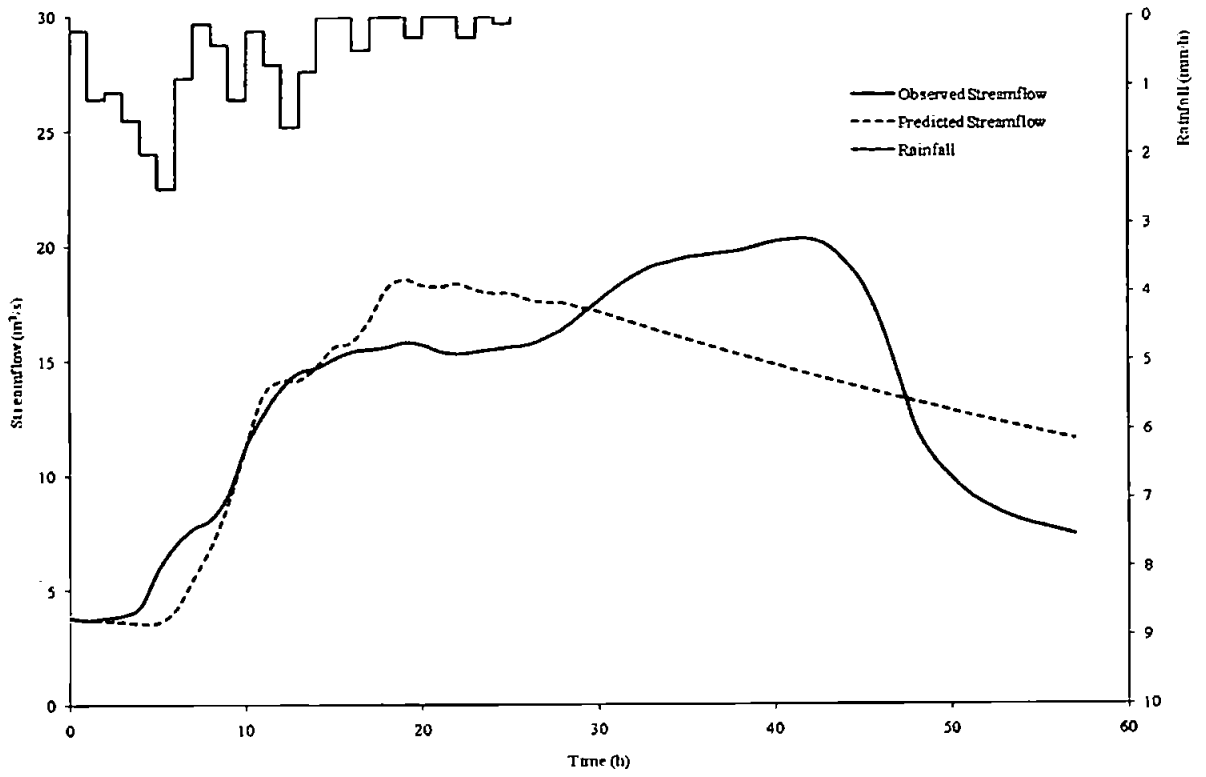**Figure E3 Predicted and observed results for event 1292**
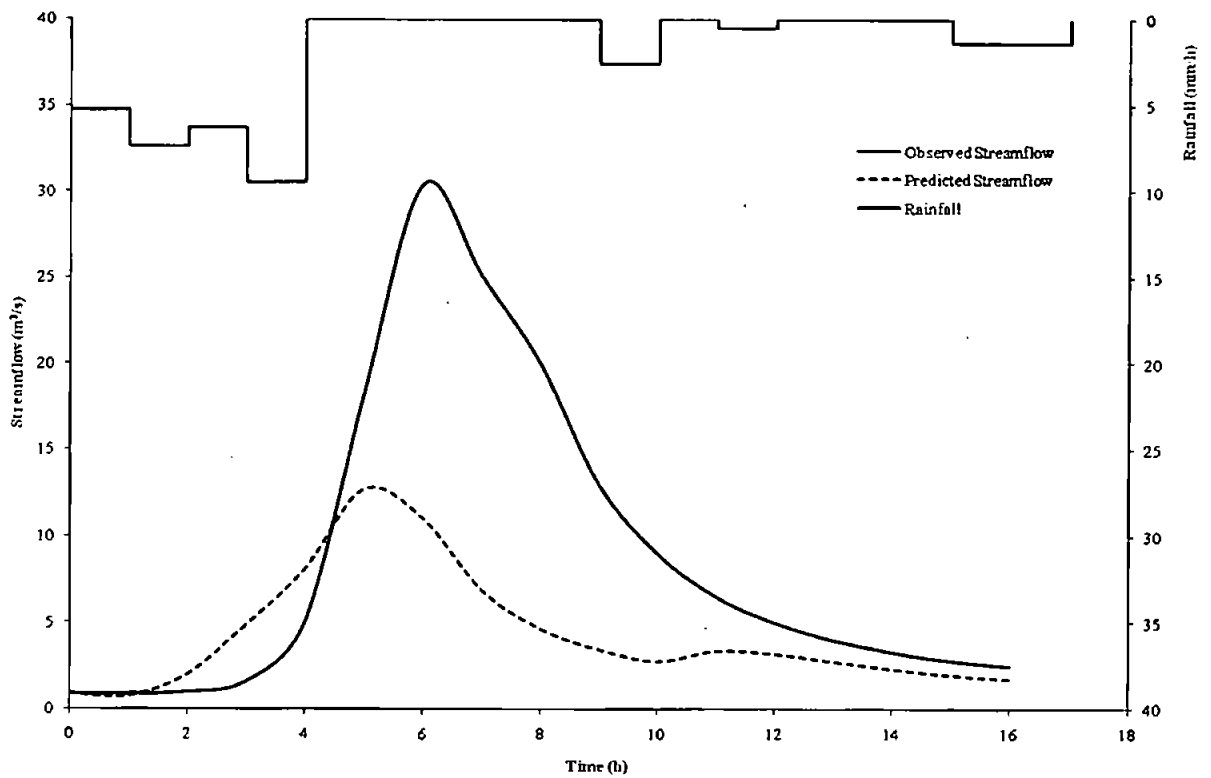
Figure E4 Predicted and observed results for event 1297

345
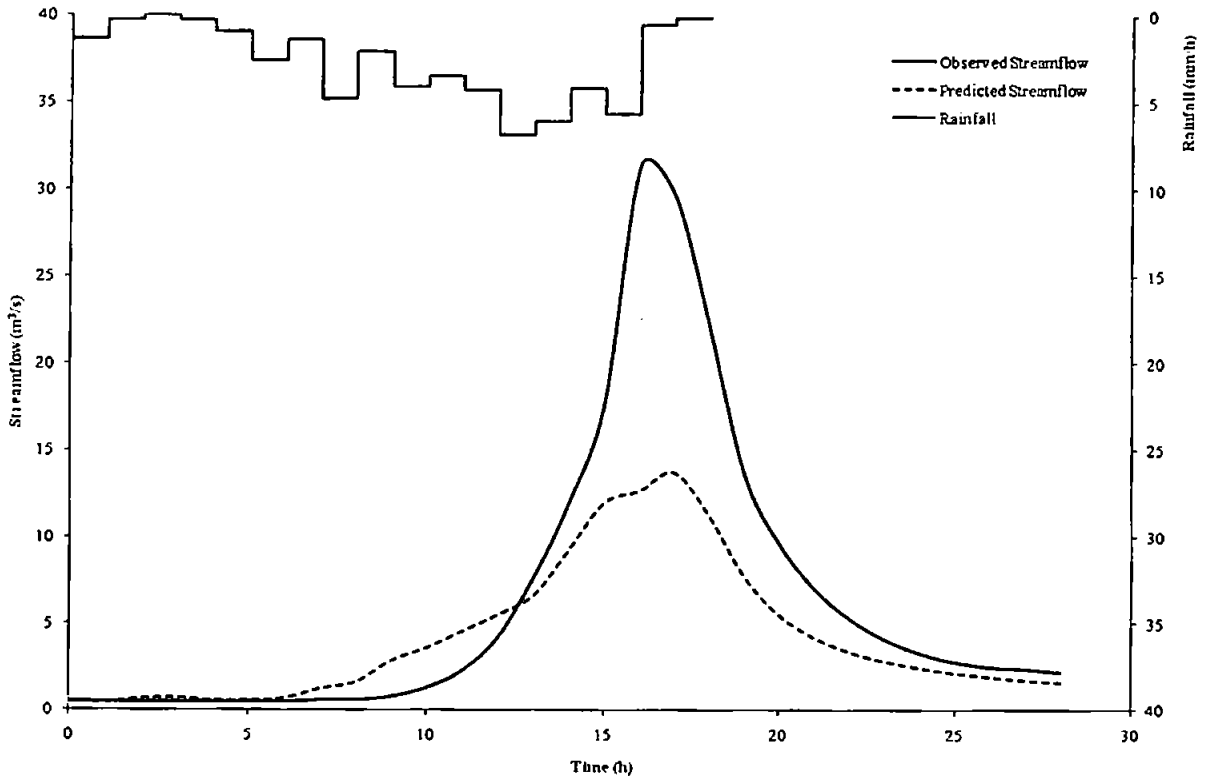
Figure E5 Predicted and observed results for event 1298
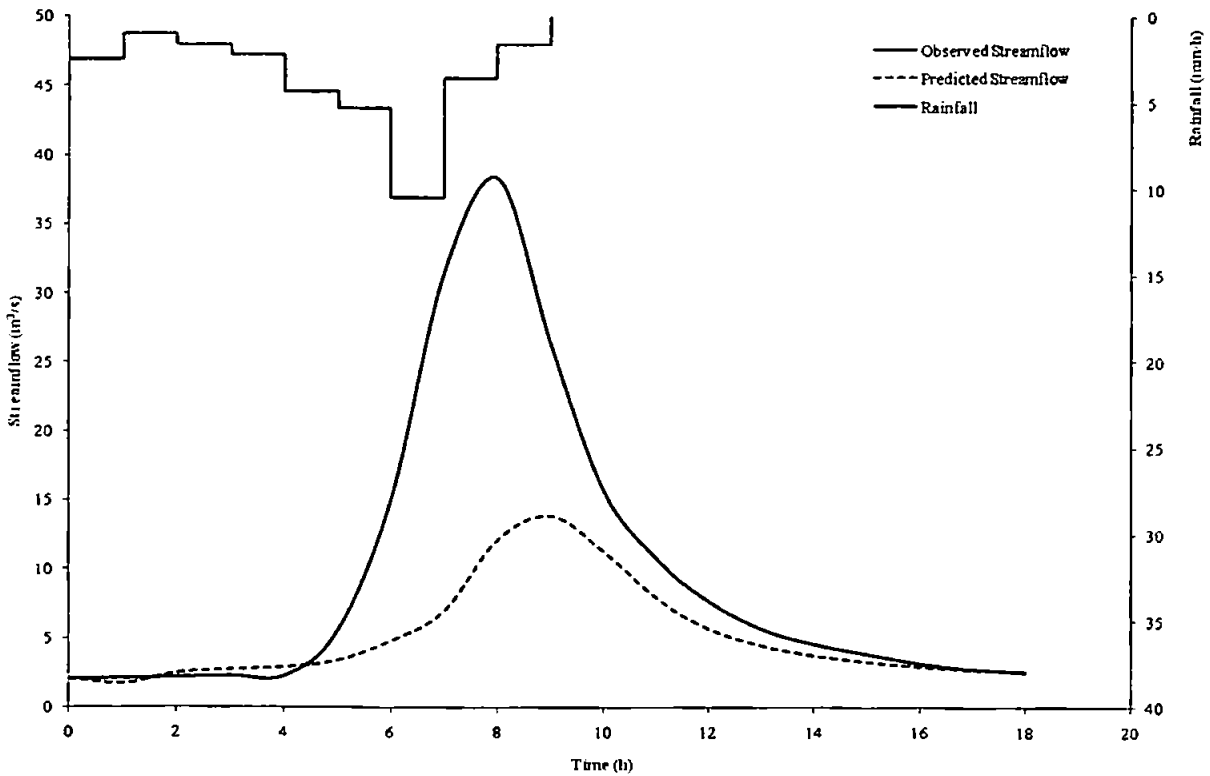
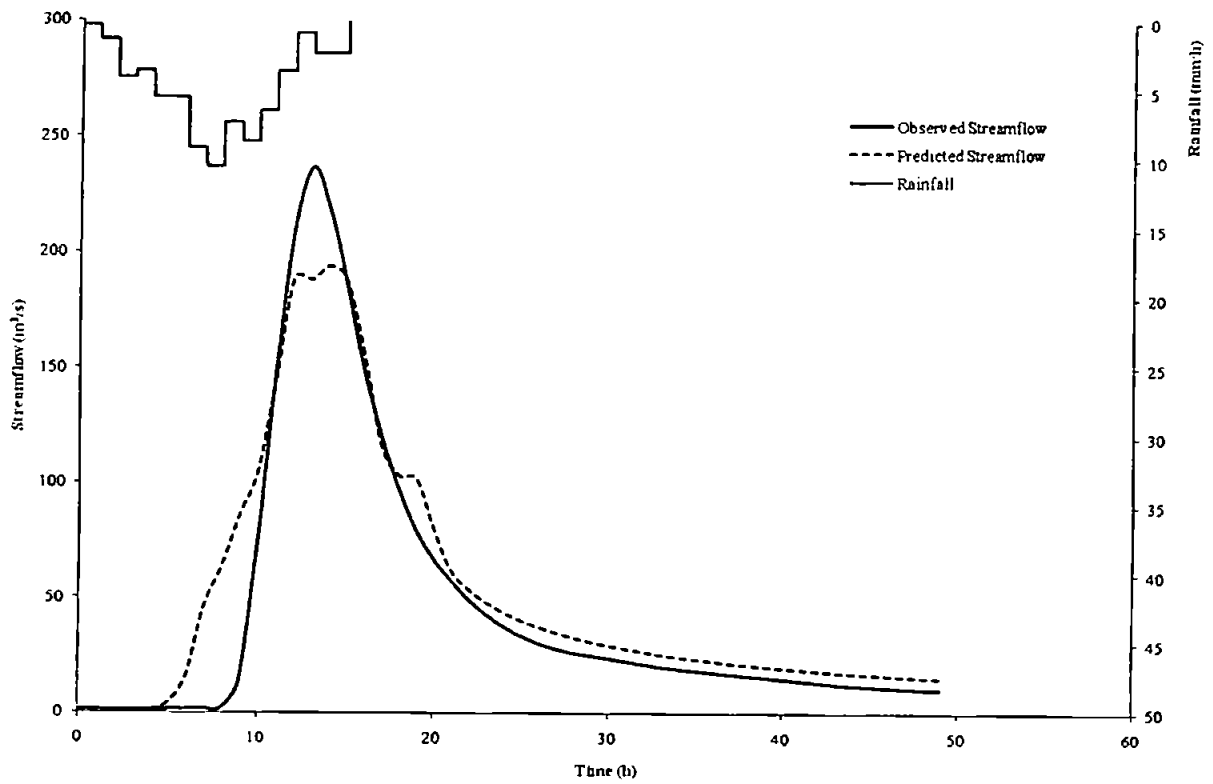**Figure E6 Predicted and observed results for event 1299**

346
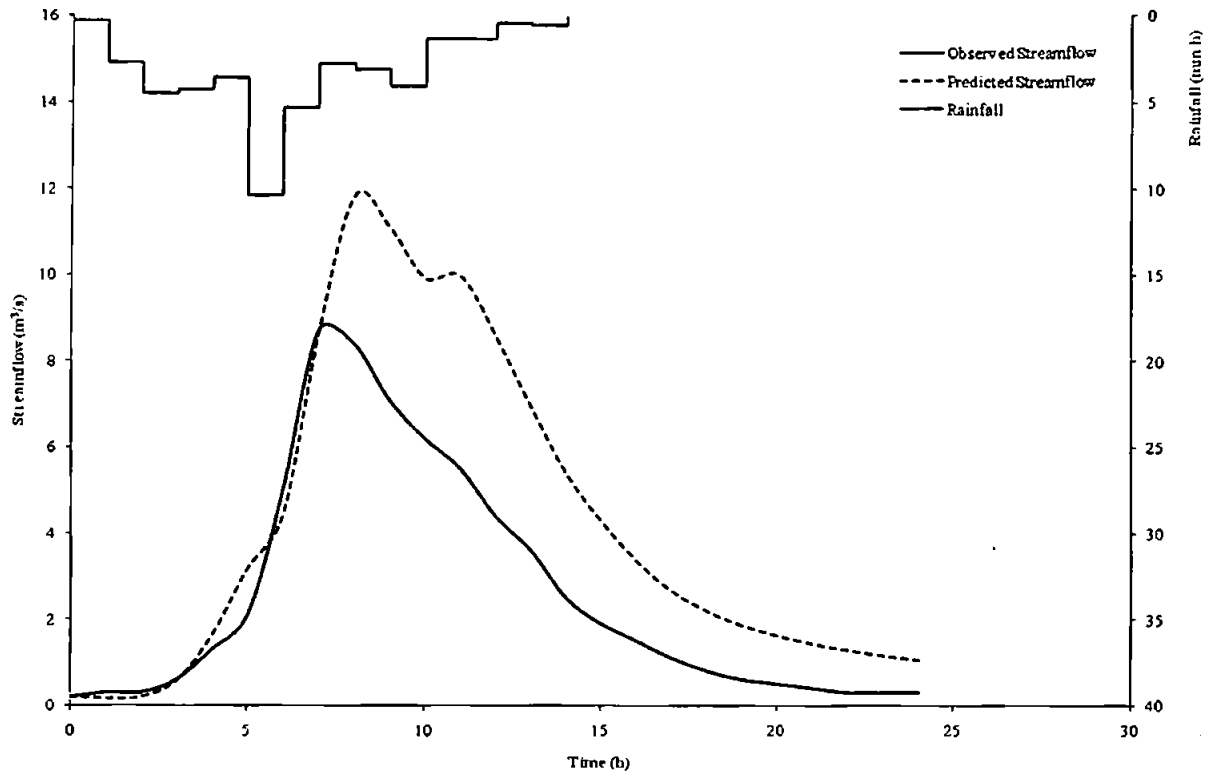
Figure E7 Predicted and observed results for event 1300
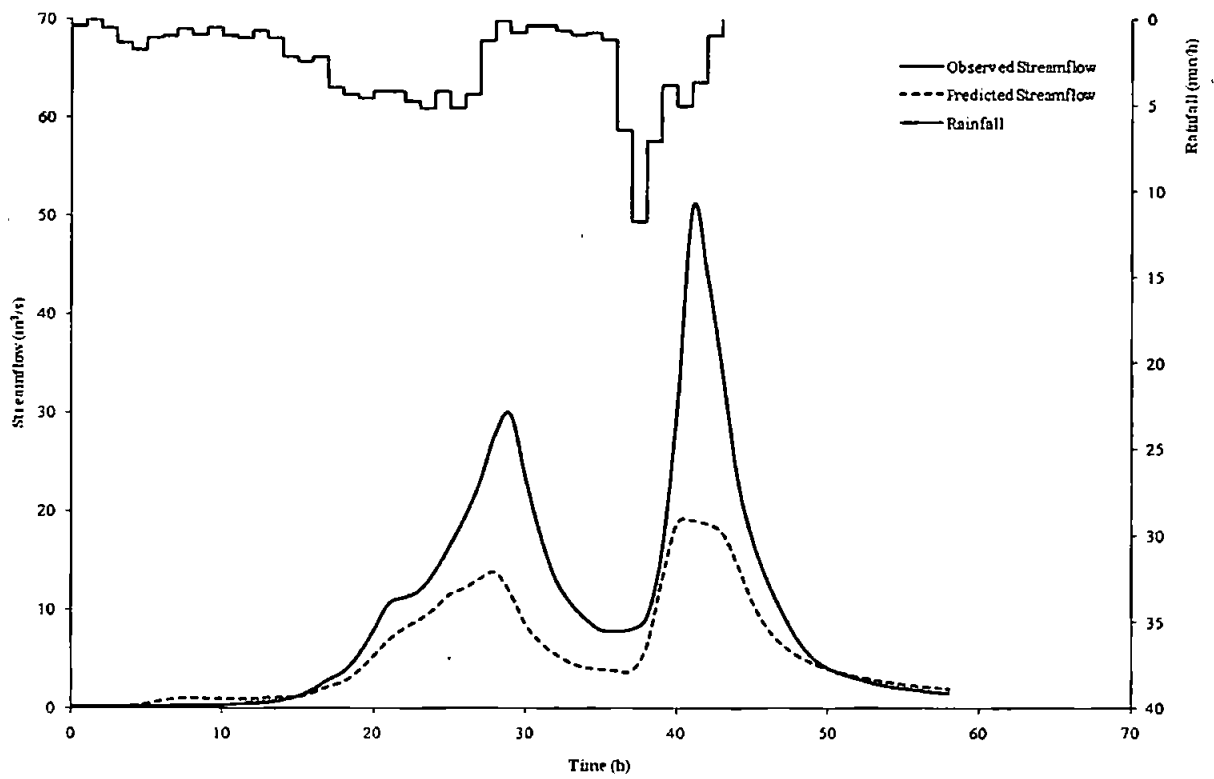
Figure E8 Predicted and observed results for event 1301

347
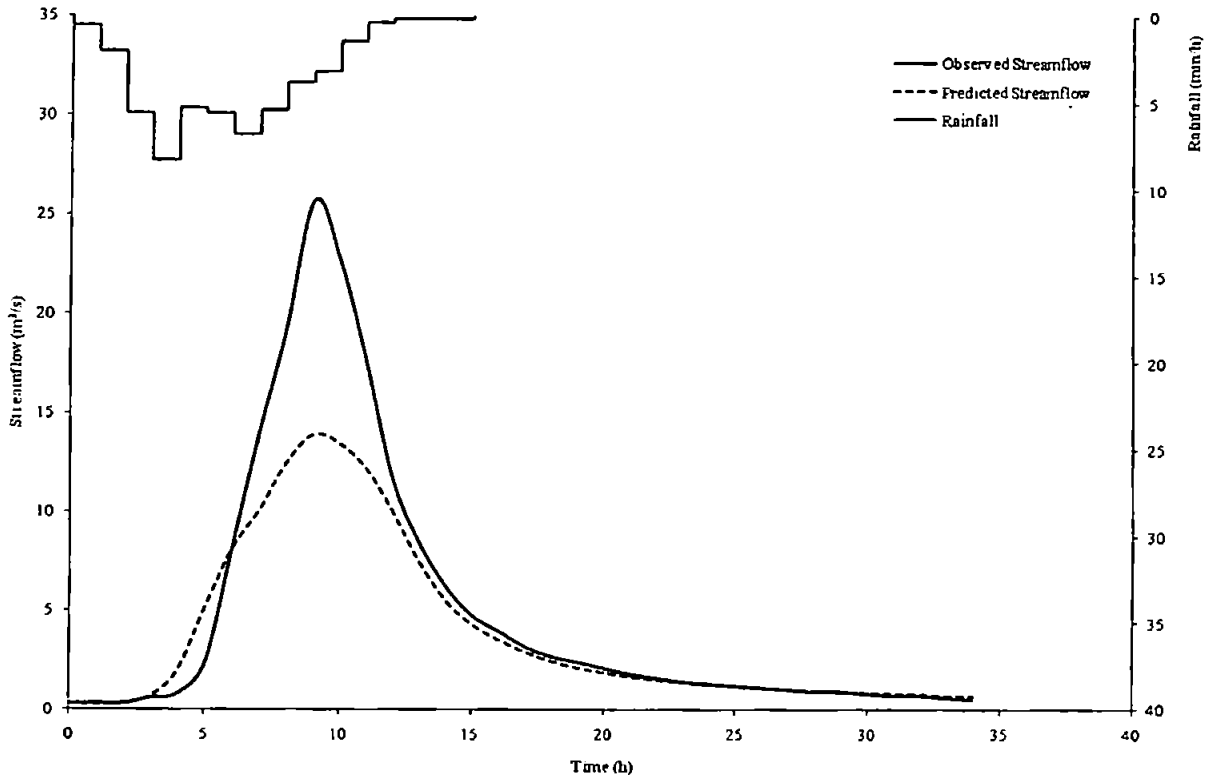
Figure E9 Predicted and observed results for event 1302
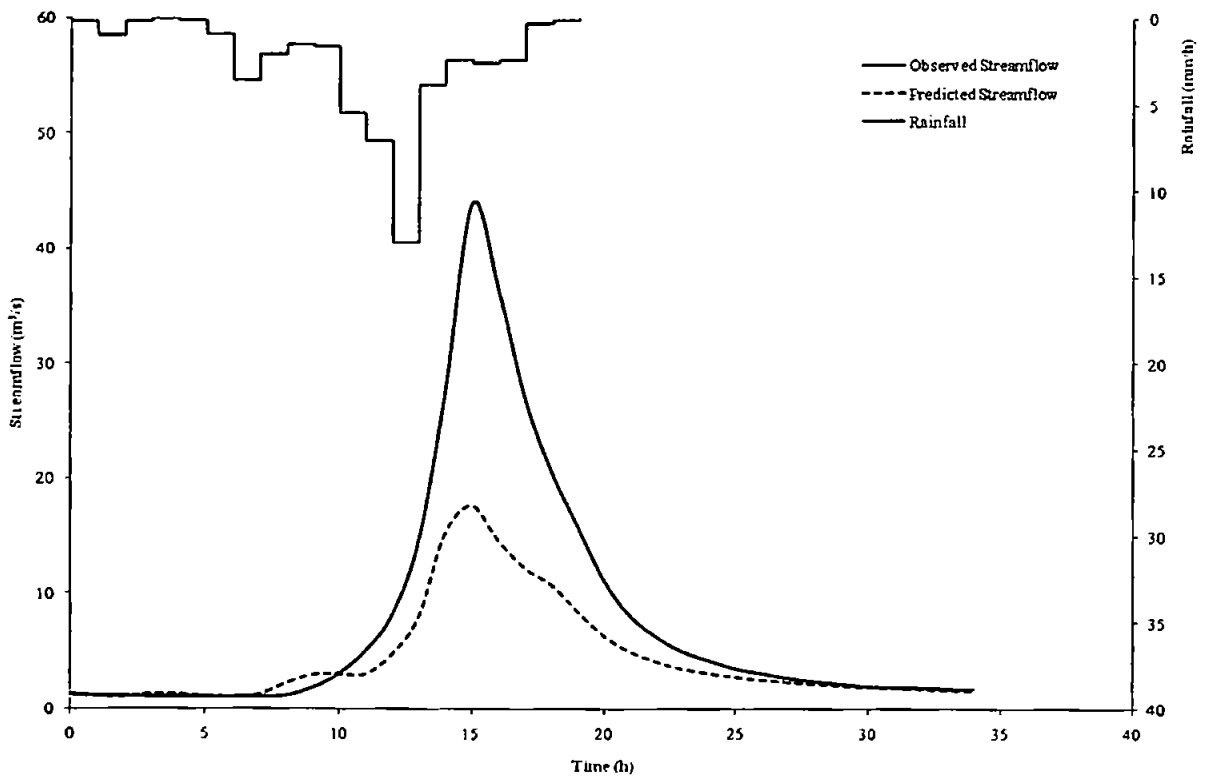
Figure E10 Predicted and observed results for event 1303
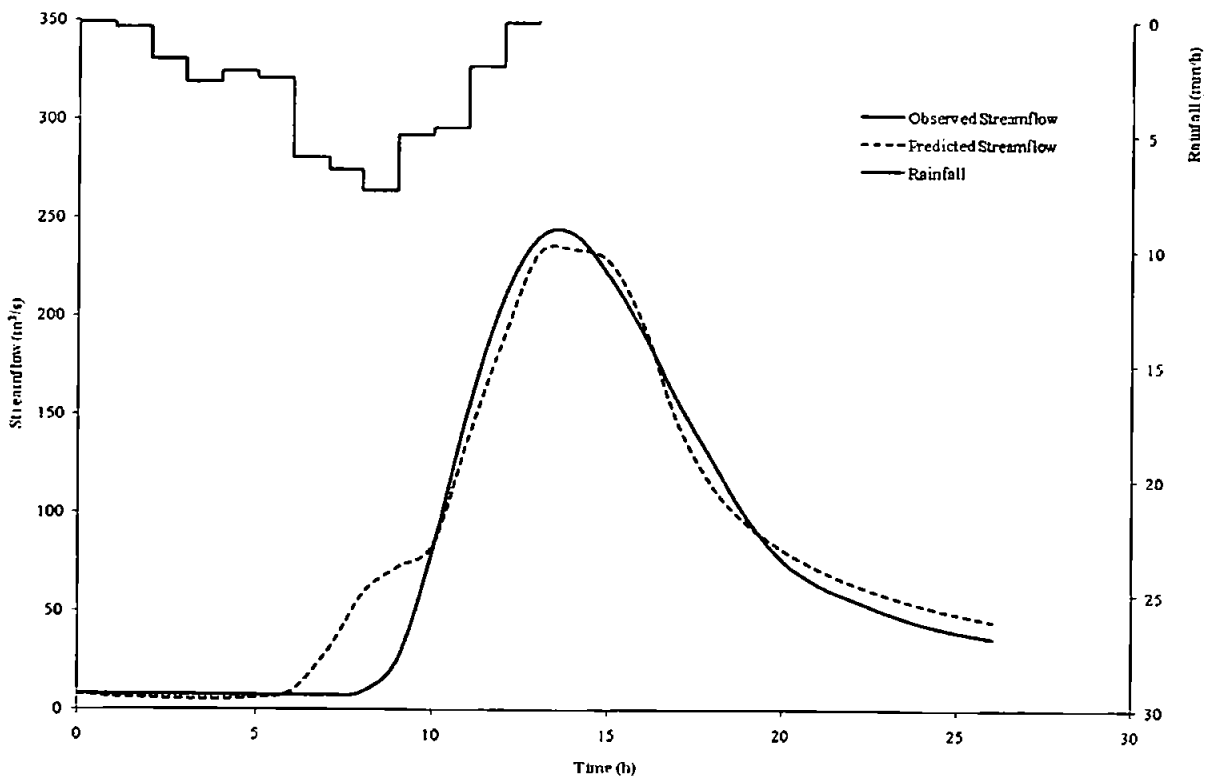
348
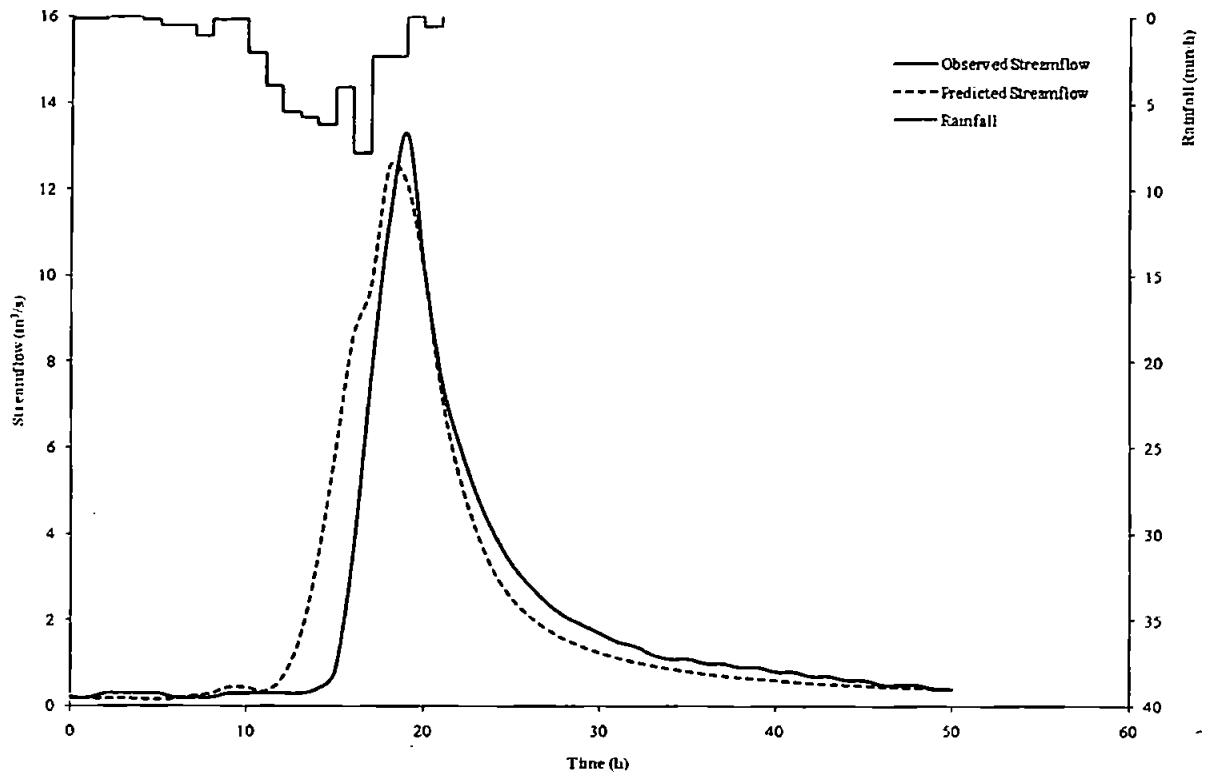
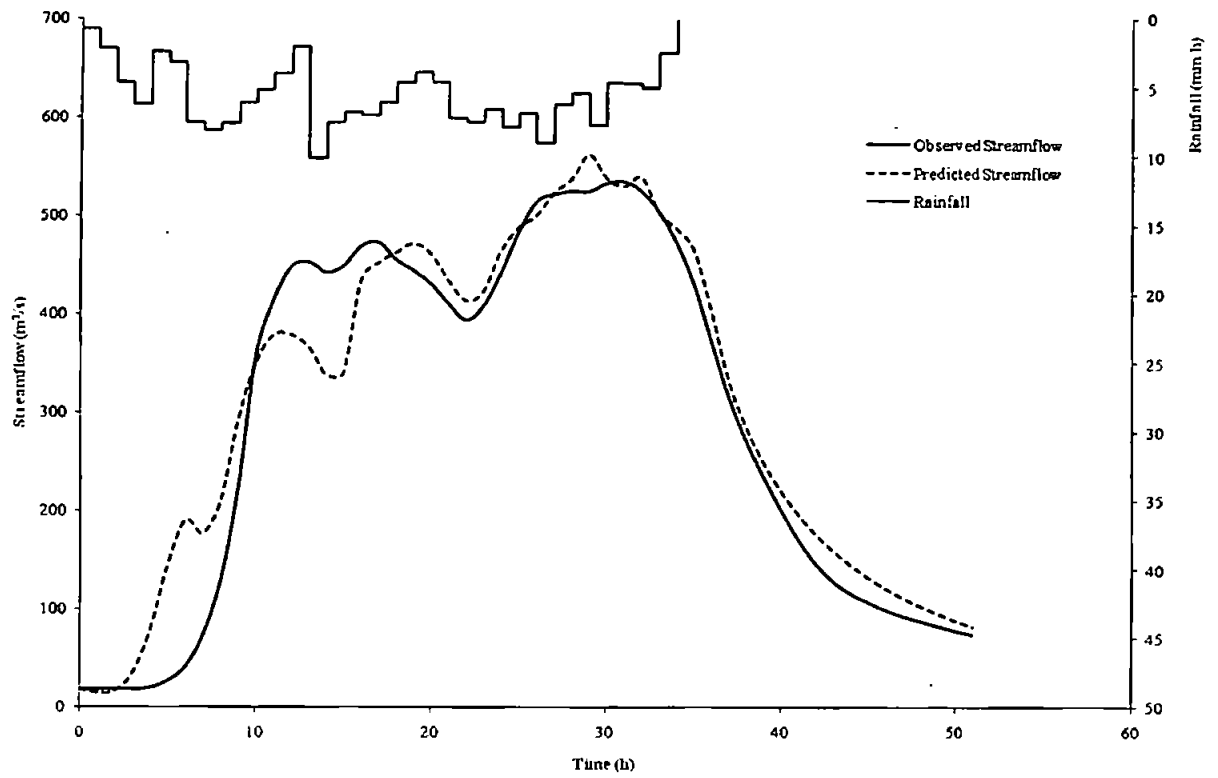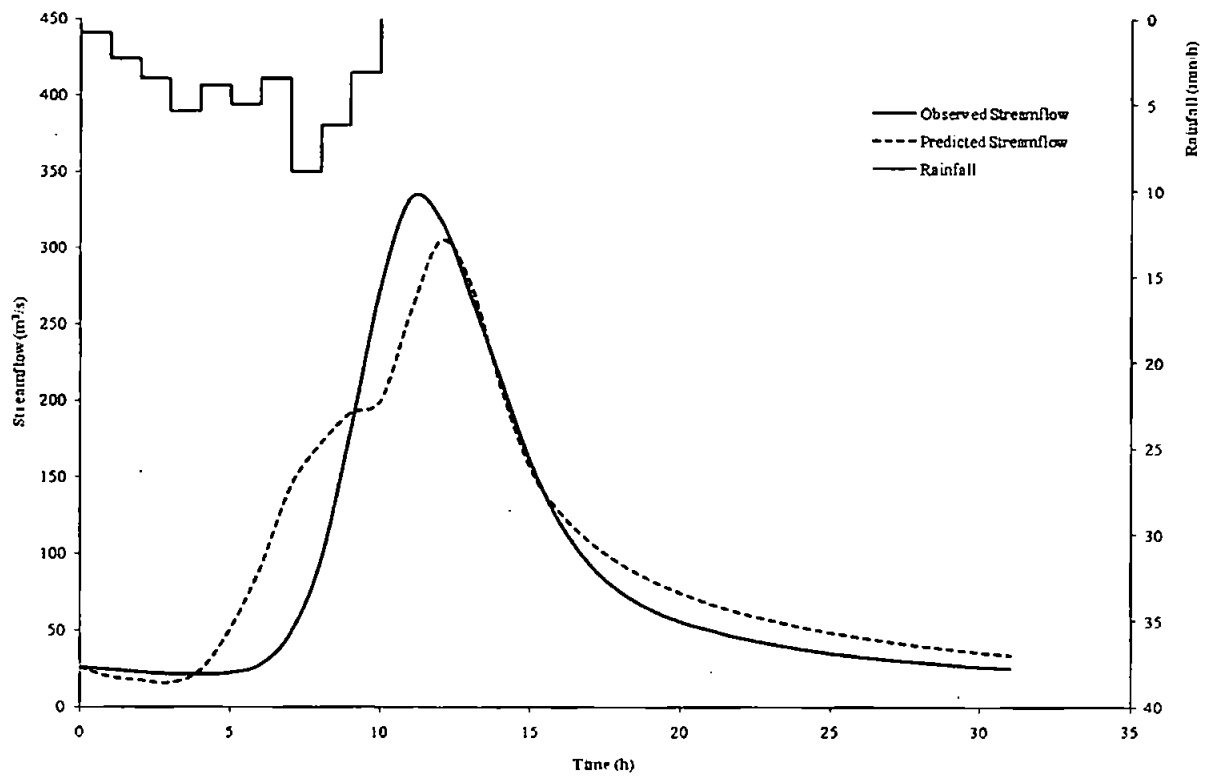**Figure E11 Predicted and observed results for event 1304**
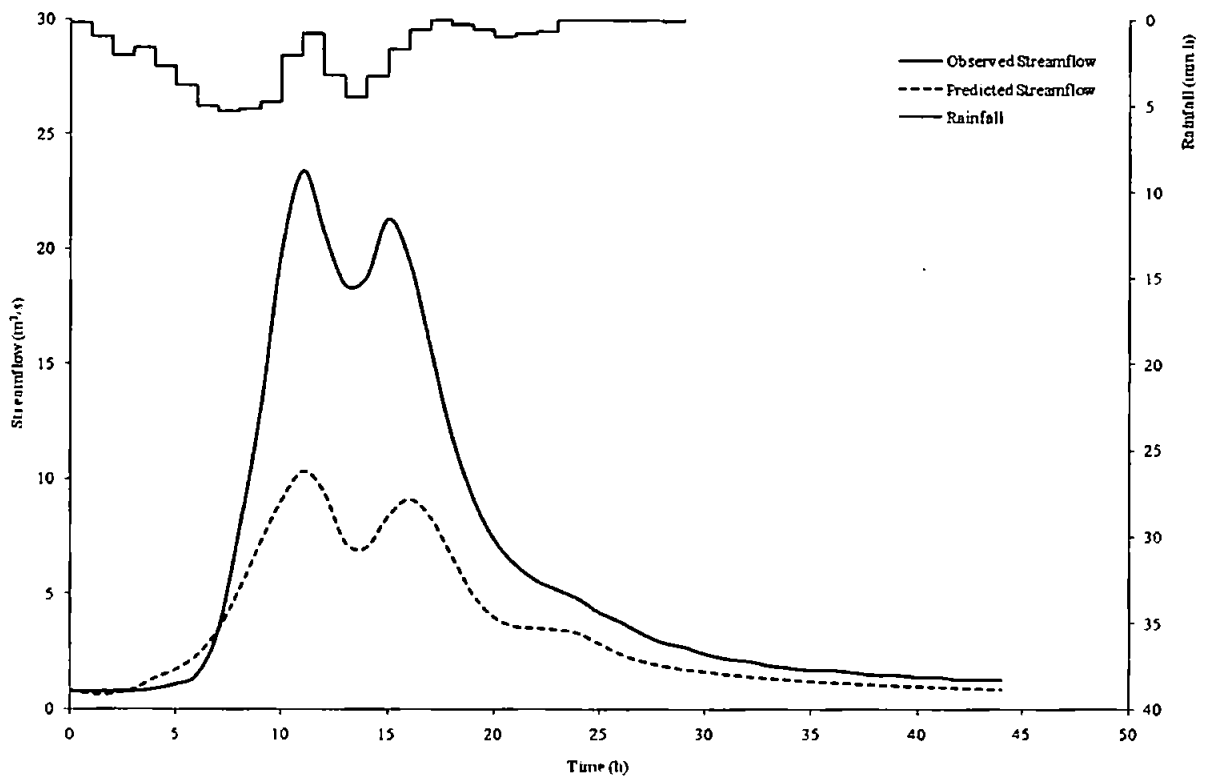
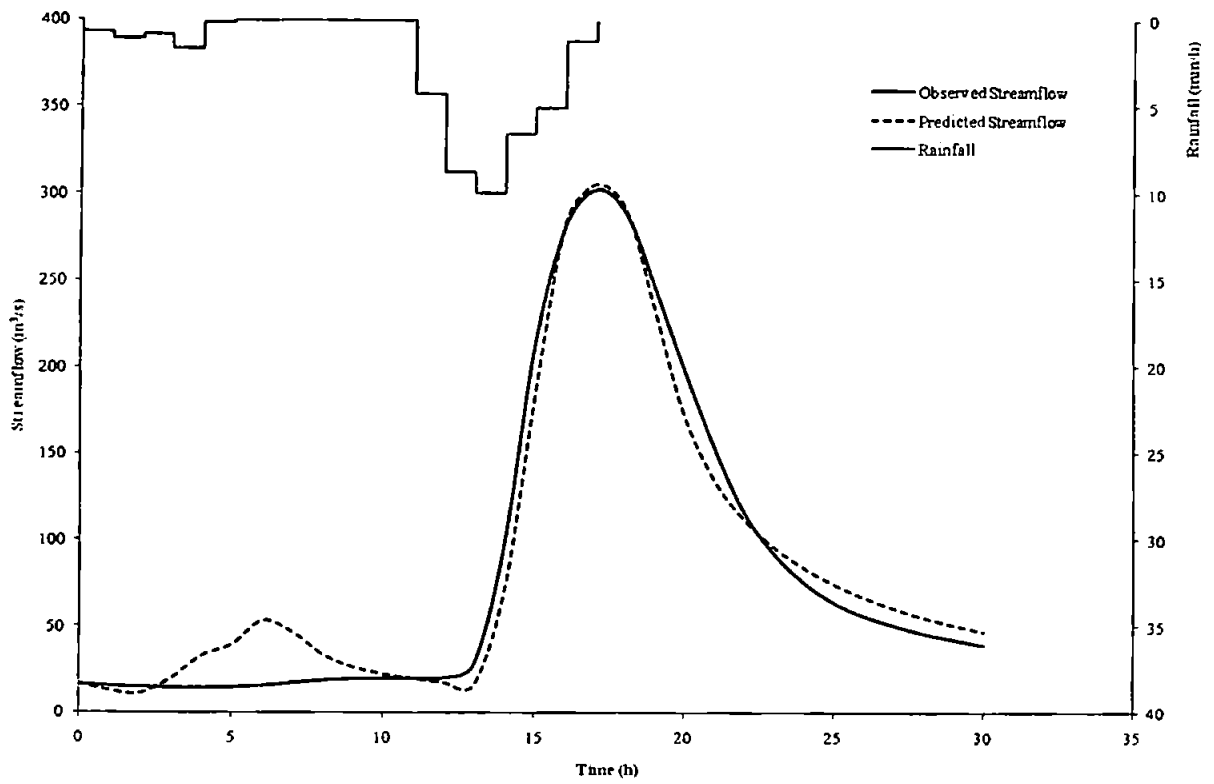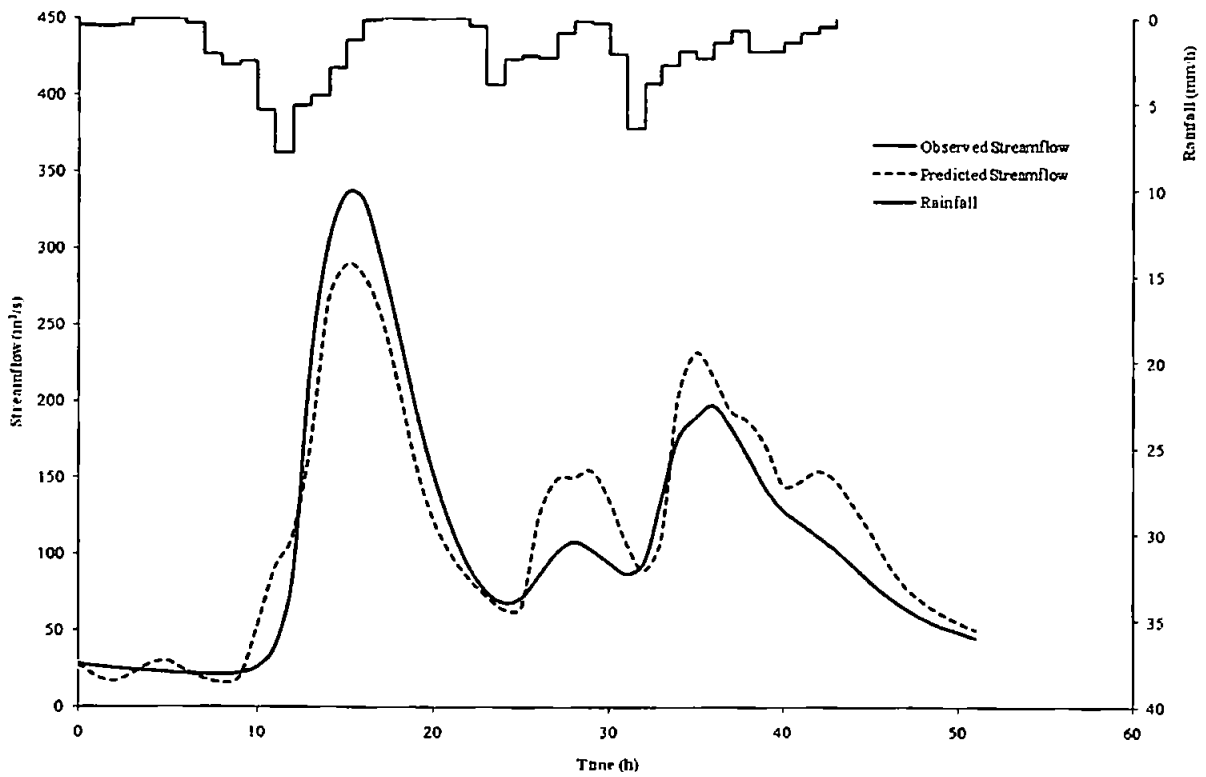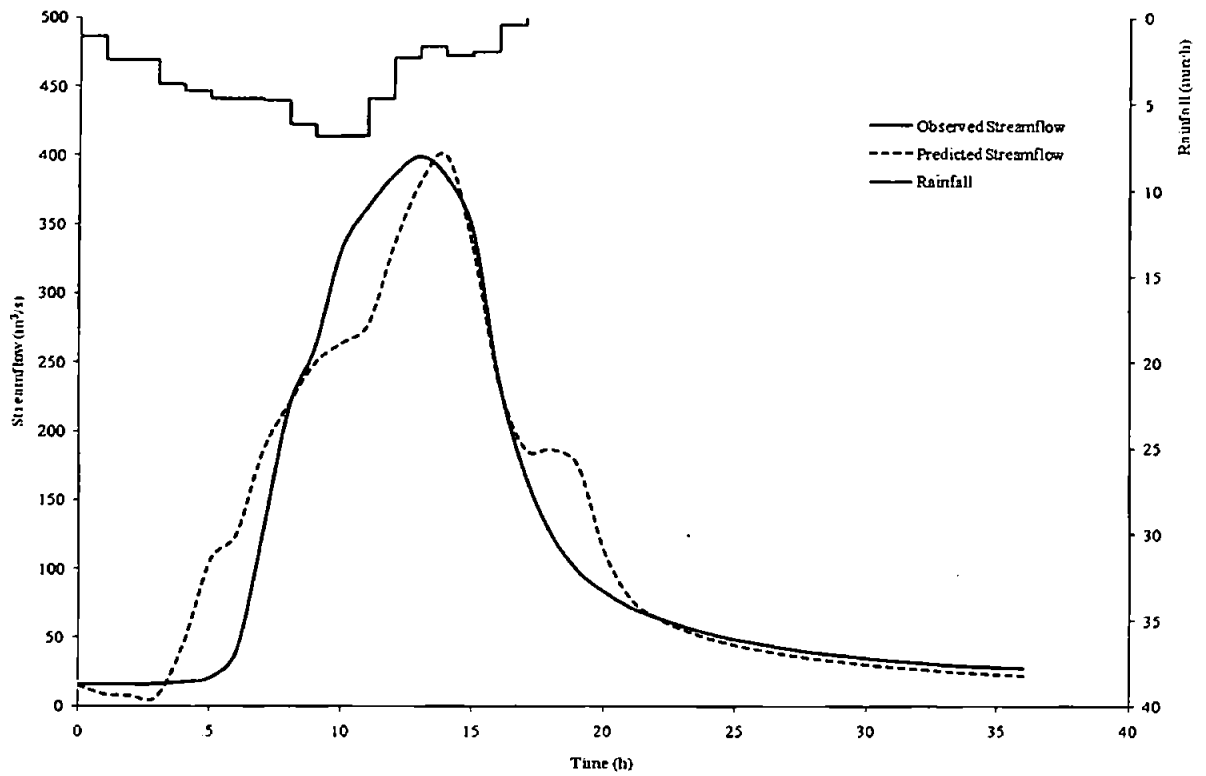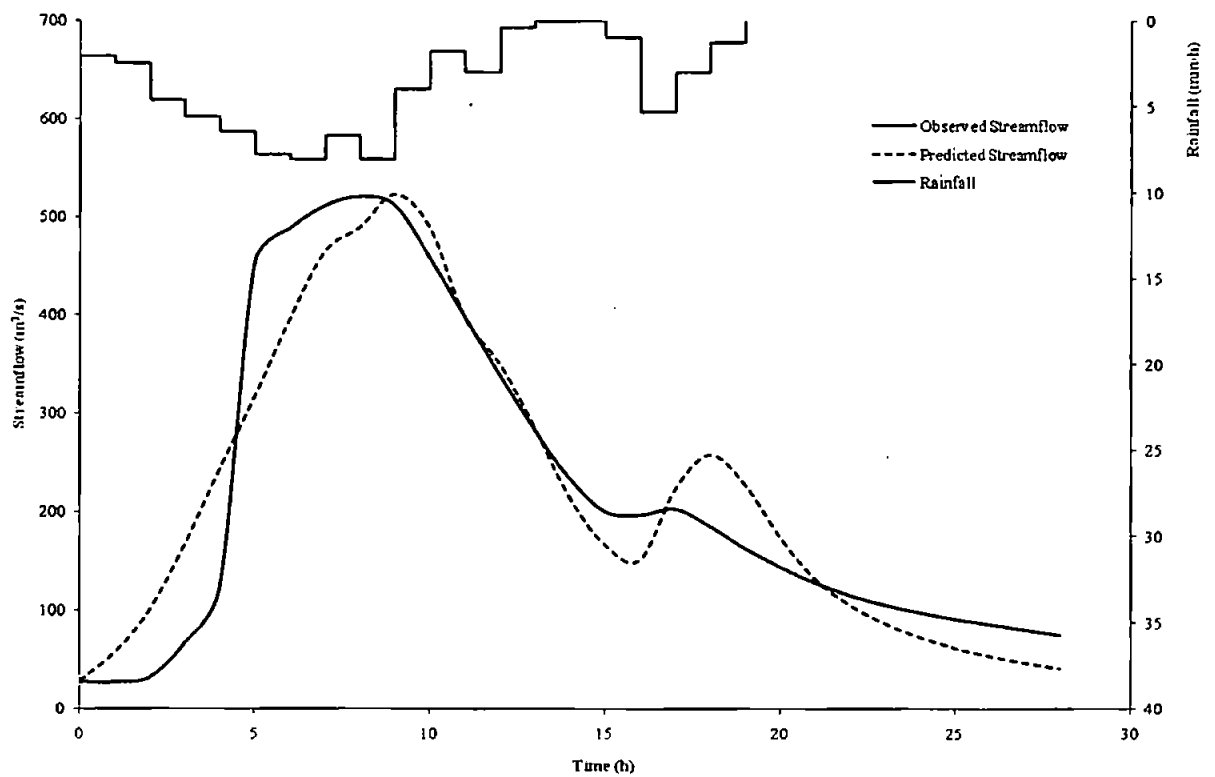**Figure E12 Predicted and observed results for event 4351**
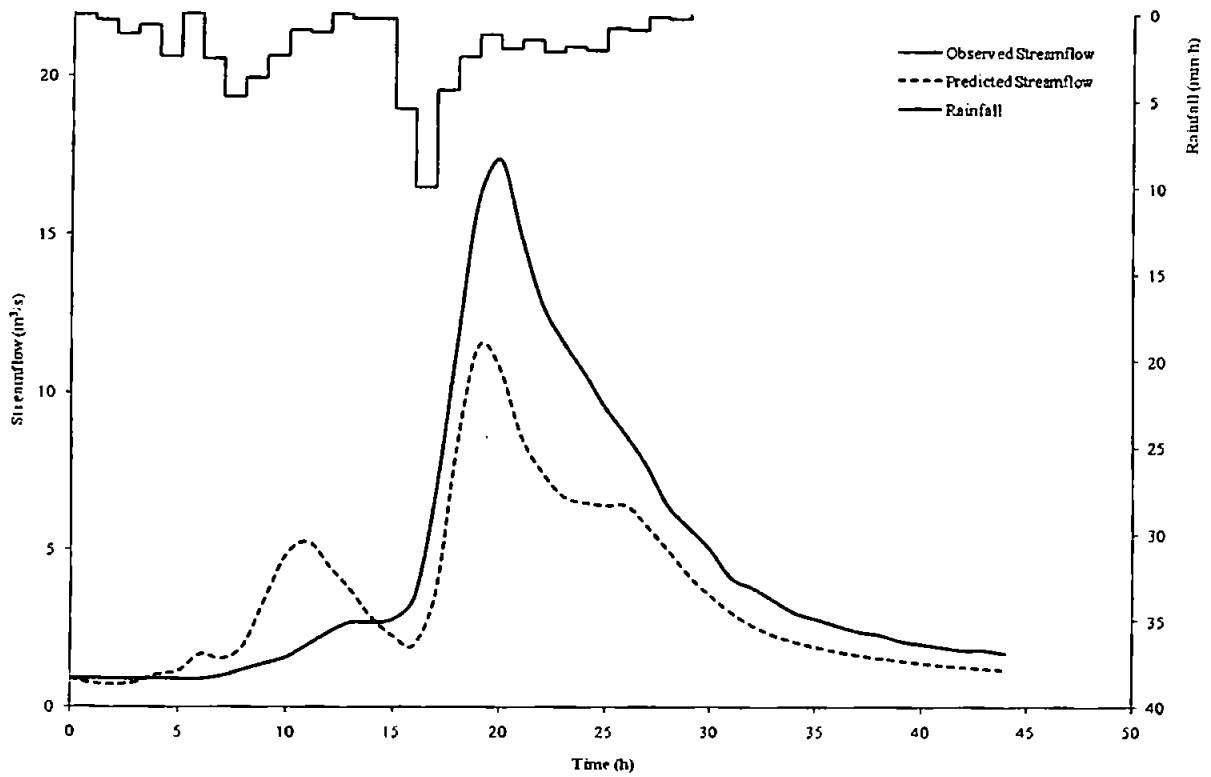
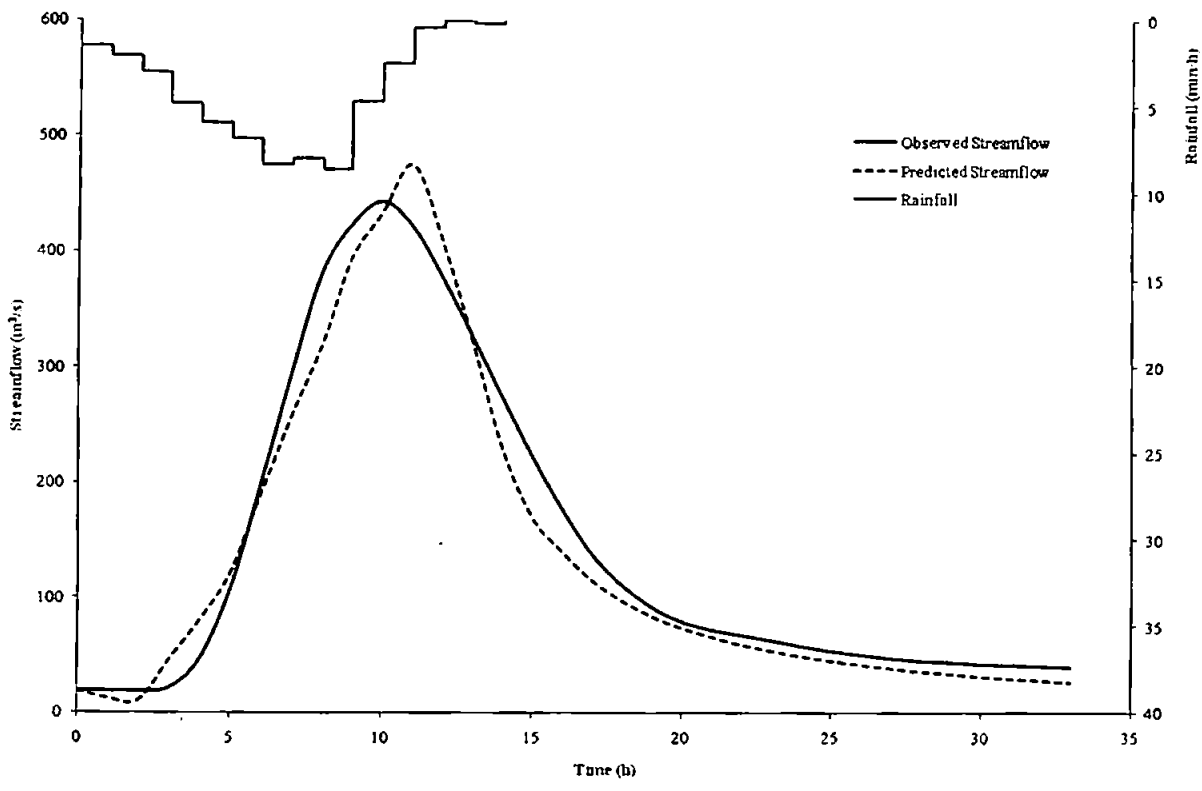**Figure E13 Predicted and observed results for event 4352**
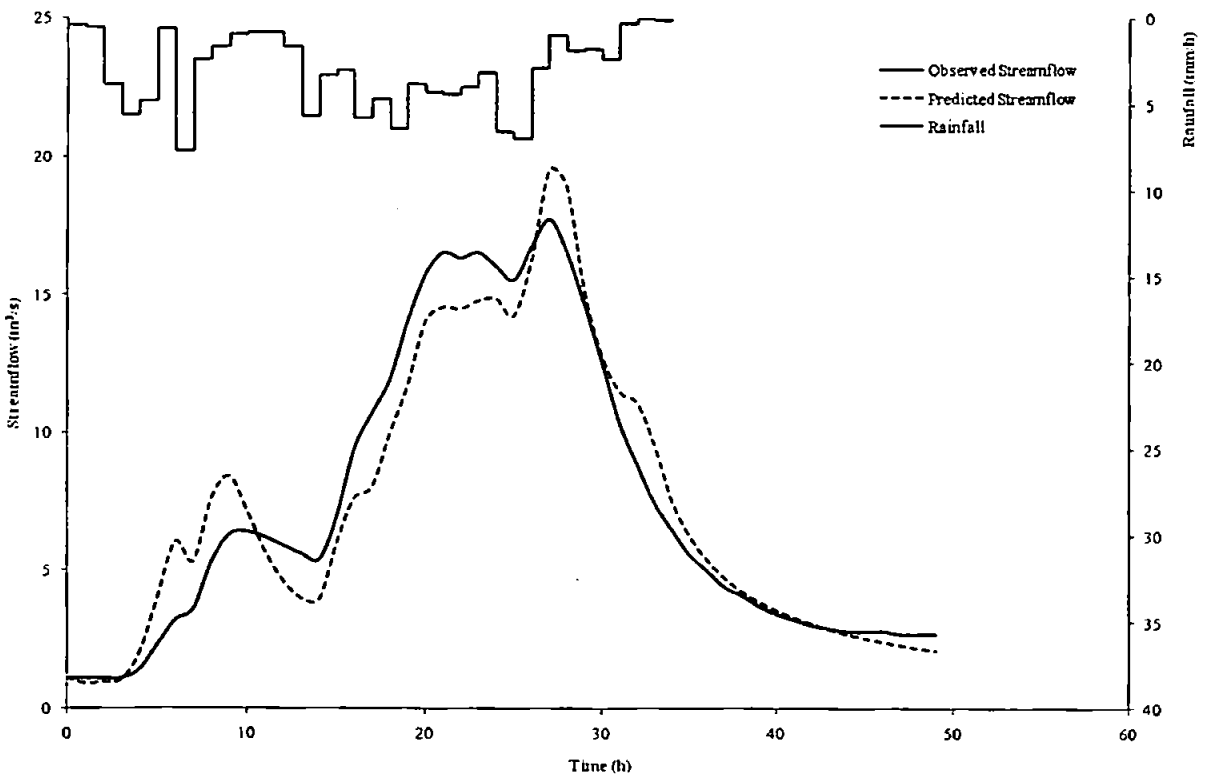
Figure E14 Predicted and observed results for event 4353

350

References

Abbott, M. B., Bathurst, J. C., Cunge, J. A., O'Connell, P. E. and Rasmussen, J. (1986a)
An introduction to the European Hydrological System - Systeme Hydrologique
Europeen, "SHE", 1: History and philosophy of a physically-based, distributed
modelling system. *Journal of Hydrology*, **87**(1-2): 45-59.

Abbott, M. B., Bathurst, J. C., Cunge, J. A., O'Connell, P. E. and Rasmussen, J. (1986b)
An introduction to the European Hydrological System - Systeme Hydrologique
Europeen, "SHE", 2: Structure of a physically-based, distributed modelling
system. *Journal of Hydrology*, **87**(1-2): 61-77.

Achar, B. N. N., Lorenzo, C. and Hartley, T. (2007). The Caputo fractional derivative:
Initialization issues relative to fractional differential equation. In: Sabatier, J.,
Agrawal, O.P. and Machado, J.A.T. (Eds) *Advances in Fractional Calculus:
Theoretical Developments and Applications in Physics and Engineering.*
Dordrecht: Springer. pp 27-42.

Amorocho, J. (1973). Nonlinear hydrologic analysis. In: Chow, V.T. (Ed) *Advances in
Hydroscience.* Academic Press. pp 203-251.

Argawal, R. P. (1953) A propos d'une note de M. Pierre Humbert. *Comptes Rendus de
l'Academie des Sciences*, **236**(21): 2031-2032.

Babovic, V. and Keijzer, M. (2002) Rainfall runoff modelling based on genetic
programming. *Nordic Hydrology*, **33**(5): 331-346.

Baeumer, B., Meerschaert, M. M. and Mortensen, J. (2005) Space-time fractional
derivative operators. *Proceedings of the American Mathematical Society*,
133(8): 2273-2282.

Baumann, G., Sudland, N. and Nonnenmacher, T. F. (2000) Anomalous relaxation and
diffusion processes in complex systems. *Transport Theory and Statistical
Physics*, **29**(1-2): 157-171.

Benson, D. A., Schumer, R., Meerschaert, M. M. and Wheatcraft, S. W. (2001)
Fractional dispersion, Levy motion, and the MADE tracer tests. *Transport in
Porous Media*, **42**(1-2): 211-240.

Beven, K. (1989) Changing ideas in hydrology - The case of physically-based models.
Journal of Hydrology, **105**(1-2): 157-172.

Beven, K. (1993) Prophecy, reality and uncertainty in distributed hydrological
modeling. *Advances in Water Resources*, **16**(1): 41-51.

Beven, K. (2002) Towards a coherent philosophy for modelling the environment.
Proceedings of the Royal Society of London - A, **458**(2026): 2465-2484.

Beven, K. (2006a) A manifesto for the equifinality thesis. *Journal of Hydrology*,
320(1-2): 18-36.

Beven, K. (2006b) Searching for the holy grail of scientific hydrology: $Q_f = (S,R,\Delta t)A$ as closure. *Hydrology and Earth System Sciences*, **10**(5): 609-618.

Beven, K. and Binley, A. (1992) The future of distributed models - model calibration and uncertainty prediction. *Hydrological Processes*, **6**(3): 279-298.

Beven, K. and Freer, J. (2001) Equifinality, data assimilation, and uncertainty estimation in mechanistic modelling of complex environmental systems using the GLUE methodology. *Journal of Hydrology*, **249**(1-4): 11-29.

Beven, K. J. (2000) *Rainfall-Runoff Modelling: The Primer*. London: John Wiley & Sons. 360 pp.

Bloschl, G. and Sivapalan, M. (1995) Scale issues in hydrological modeling - a review. *Hydrological Processes*, **9**(3-4): 251-290.

Boorman, D. B. and Reed, D. W. (1981). *Derivation of a Catchment Average Unit Hydrograph*. Report No. 71. Institute of Hydrology, Wallingford, UK. 50 pp.

Borthwick, M. F., Packham, I. S. and Rafiq, M. Y. (2008) Interactive visualization for evolutionary optimization of conceptual rainfall-streamflow models. *Journal of Computing in Civil Engineering*, **22**(1): 40-49.

Boyle, D. P., Gupta, H. V. and Sorooshian, S. (2000) Toward improved calibration of hydrologic models: Combining the strengths of manual and automatic methods. *Water Resources Research*, **36**(12): 3663-3674.

Bras, R. L. and Rodriguez-Iturbe, I. (1985) *Random Functions and Hydrology*. New York: Dover Publications. 559 pp.

Bree, T. (1978) The stability of parameter estimation in the general linear model. *Journal of Hydrology*, **37**(1-2): 47-66.

Burnash, R. J. E., Ferral, R. L. and McGuire, R. A. (1973). *A generalized streamflow simulation system - Conceptual modeling for digital computers*. Joint Federal and State River Forecast Center, U.S. National Weather Service and California Department of Water Resources, Sacramento, California. 204 pp.

Caputo, M. (1967) Linear model of dissipation whose Q is almost frequency dependent II. *Geophysical Journal of the Royal Astronomical Society*, **13**: 529-539.

Caputo, M. (2000) Models of flux in porous media with memory. *Water Resources Research*, **36**(3): 693-705.

Carpinteri, A. and Mainardi, F. (Eds) 1997. *Fractals and Fractional Calculus in Continuum Mechanics*. CISM International Centre for Mechanical Sciences. Courses and Lectures. New York: Springer-Verlag. 348 pp.

Cavallini, F. (2002). *Causal generalized functions in geophysical and environmental modelling*. Workshop: From Waves to Diffusion and Beyond. Bologna. 20 Dec 2002.

Cavallini, F. (2006). Fractional calculus application. Borthwick, M., Trieste. Personal communication.

Chadwick, A., Morfett, J. and Borthwick, M. (2004) *Hydraulics in Civil and Environmental Engineering.* London: Spon Press. 644 pp.

Chang, F. X., Chen, J. and Huang, W. (2005) Anomalous diffusion and fractional advection-diffusion equation. *Acta Physica Sinica*, 54(3): 1113-1117.

Chow, V. T. and Kulandaiswamy, V. C. (1971) General hydrologic system model. *Journal of the Hydraulics Division, Proceedings of American Society of Civil Engineers*, 97(HY6): 791-804.

Clark, M. P., Rupp, D. E., Woods, R. A., Meerveld, H. J. T.-v., Peters, N. E. and Freer, J. E. (2009) Consistency between hydrological models and field observations: linking processes at the hillslope scale to hydrological responses at the watershed scale. *Hydrological Processes*, 23(2): 311-319.

Cook, H. L. (1946) The infiltration approach to the calculation of surface runoff. *Transactions of the American Geophysical Union*, 27(5): 726–747.

Cooper, V. A., Nguyen, V. T. V. and Nicell, J. A. (1997) Evaluation of global optimization methods for conceptual rainfall-runoff model calibration. *Water Science and Technology*, 36(5): 53-60.

Davidson, J. W., Savic, D. A. and Walters, G. A. (2003) Symbolic and numerical regression: experiments and applications. *Information Sciences*, 150(1-2): 95-117.

de Vos, N. J. and Rientjes, T. H. M. (2007) Multi-objective performance comparison of an artificial neural network and a conceptual rainfall–runoff model. *Hydrological Sciences Journal*, 52(3): 397-413.

Debnath, L. (2003a) Fractional integral and fractional differential equations in fluid mechanics. *Fractional Calculus and Applied Analysis*, 6(2): 119-156.

Debnath, L. (2003b) Recent applications of fractional calculus to science and engineering. *International Journal of Mathematics and Mathematical Sciences*, 2003(54): 3413-3442.

Deng, Z. Q., de Lima, J. and Singh, V. P. (2005) Fractional kinetic model for first flush of stormwater pollutants. *Journal of Environmental Engineering*, 131(2): 232-241.

Ding, J. Y. (2005) A measure of watershed nonlinearity: interpreting a variable instantaneous unit hydrograph model on two vastly different sized - watersheds. *Hydrology and Earth System Sciences Discussions*, 2: 2111-2151.

Diskin, M. H. (1970) On the computer evaluation of Thiessen weights. *Journal of Hydrology*, 11(1): 69-78.

Diskin, M. H., Boneh, A. and Golan, A. (1984) Identification of a Volterra series conceptual model based on a cascade of nonlinear reservoirs. *Journal of Hydrology*, **68**(1-4): 231-245.

Diskin, M. H. and Simon, E. (1977) A procedure for the selection of objective functions for hydrologic simulation models. *Journal of Hydrology*, **34**(1-2): 129-149.

Doetsch, G. (1974) *Introduction to the Theory and Application of the Laplace Transformation*. New York: Springer-Verlag. 326 pp.

Dong, S.-H. (2008) Genetic algorithm based parameter estimation of Nash model. *Water Resources Management*, **22**(4): 525-533.

Dooge, J. C. I. (1959) A general theory of the unit hydrograph. *Journal of Geophysical Research*, **64**(2): 241-256.

Dooge, J. C. I. (1973). *Linear Theory of Hydrologic Systems*. Report No. 1468. Agricultural Research Service, United States Department of Agriculture, Washington, D.C. 327 pp.

Dooge, J. C. I. (2005) Bringing it all together. *Hydrology and Earth System Sciences*, **9**: 3 - 14.

Dooge, J. C. I. and O'Kane, J. P. (2003) *Deterministic Methods in Systems Hydrology*. Lisse: Balkema. 309 pp.

Dorado, J., Rabunal, J. R., Puertas, J., Santos, A. and Rivero, D. (2002). Prediction and modelling of the flow of a typical urban basin through genetic programming. *Applications of Evolutionary Computing, Proceedings*. pp 190-201.

Duan, Q. Y., Gupta, H. V., Sorooshian, S., Rousseau, A. N. and Turcotte, R. (Eds) 2003. *Calibration of Watershed Models*. Water Science and Application. Washington, DC: American Geophysical Union. 346 pp.

Duan, Q. Y., Sorooshian, S. and Gupta, V. (1992) Effective and efficient global optimization for conceptual rainfall-runoff models. *Water Resources Research*, **28**(4): 1015-1031.

Engeland, K. and Gottschalk, L. (2002) Bayesian estimation of parameters in a regional hydrological model. *Hydrology and Earth System Sciences*, **6**(5): 883-898.

Environment Agency. (2009) *HiFlows*. Available at: http://www.environment-agency.gov.uk/hiflowsuk (Accessed: 1/09/2009).

Evans, J. P. and Jakeman, A. J. (1998) Development of a simple, catchment-scale, rainfall-evapotranspiration-runoff model. *Environmental Modelling and Software*, **13**(3-4): 385-393.

Franchini, M. (1996) Use of a genetic algorithm combined with a local search method for the automatic calibration of conceptual rainfall-runoff models. *Hydrological Sciences Journal*, **41**(1): 21-39.

Freeze, R. A. and Harlan, R. L. (1969) Blueprint for a physically-based, digitally-simulated hydrologic response model. *Journal of Hydrology*, 9(3): 237-258.

Gaume, E. and Gosset, R. (2003) Over-parameterisation, a major obstacle to the use of artificial neural networks in hydrology? *Hydrology and Earth System Sciences*, 7(5): 693 - 706.

Goldberg, D. E. (1989) *Genetic Algorithms in Search, Optimization and Machine Learning.* Reading, Massachusetts: Addison-Wesley. 412 pp.

Goldberg, D. E. and Kuo, C. H. (1987) Genetic algorithms in pipeline optimization. *Journal of Computing in Civil Engineering*, 1(2): 128-141.

Goodrich, D. C., Lane, L. J., Shillito, R. M., Miller, S. N., Syed, K. H. and Woolhiser, D. A. (1997) Linearity of basin response as a function of scale in a semiarid watershed. *Water Resources Research*, 33(12): 2951–2966.

Gorenflo, R. and Mainardi, F. (1996). *Fractional oscillations and Mittag-Leffler functions.* Proceedings of the International Workshop on the Recent Advances in Applied Mathematics (RAAM '96). Kuwait. 4-7 May. pp 193-208.

Gorenflo, R. and Mainardi, F. (2000). Fractional calculus: integral and differential equations of fractional order. In: Carpinteri, A. and Mainardi, F. (Eds) *Fractals and Fractional Calculus in Continuum Mechanics.* (Revised ed) New York: Springer Verlag. pp 223-276.

Gupta, H. V., Bastidas, L. A., Vrugt, J. A. and Sorooshian, S. (2003a). Multiple criteria global optimization for watershed model calibration. In: Duan, Q.Y., Gupta, H.V., Sorooshian, S., Rousseau, A.N. and Turcotte, R. (Eds) *Calibration of Watershed Models.* Washington, DC: American Geophysical Union. pp 125-132.

Gupta, H. V., Sorooshian, S., Hogue, T. S. and Boyle, D. P. (2003b). Advances in automatic calibration of watershed models. In: Duan, Q.Y., Gupta, H.V., Sorooshian, S., Rousseau, A.N. and Turcotte, R. (Eds) *Calibration of Watershed Models.* Washington, DC: American Geophysical Union. pp 9-28.

Gupta, H. V., Sorooshian, S. and Yapo, P. O. (1998) Toward improved calibration of hydrologic models: Multiple and noncommensurable measures of information. *Water Resources Research*, 34(4): 751-763.

Gupta, V. K. (1982) *Calibration of conceptual rainfall-runoff models: Problems caused by model structure.* Thesis, MSc Thesis, Case Western Reserve University.

Hall, M. J. and Minns, A. W. (1993). *Rainfall-runoff modelling as a problem in artificial intelligence: Experience with a neural network.* Proceedings 4th National Hydrology Symposium. Cardiff, UK. British Hydrological Society. pp 5.51-5.57.

355

Hartley, T. T. and Lorenzo, C. F. (2008) Application of incomplete gamma functions to the initialization of fractional-order systems. *Journal of Computational and Nonlinear Dynamics*, 3(2): 021103.

Hilfer, R. (2008). Threefold introduction to fractional derivatives. In: Klages, R., Radons, G. and Sokolov, I.M. (Eds) *Anomalous Transport: Foundations and Applications*. Weinheim: Wiley-VCH. pp 17-73.

Holland, J. H. (1975) *Adaptation in Natural and Artificial Systems*. Ann Arbor: University of Michigan Press. 211 pp.

Horton, R. E. (1933) The role of infiltration in the hydrologic cycle. *Transactions of the American Geophysical Union* 14: 446 -460.

Horton, R. E. (1940) An approach toward a physical interpretation of infiltration capacity. *Proceedings of the Soil Science Society of America*, 5: 399-417.

Hosking, J. R. M. (1981) Fractional differencing. *Biometrika*, 68(1): 165-176.

Hurst, H. E. (1951) Long-term storage capacity of reservoirs. *Transactions of the ASCE*, 116: 776-808.

Institute of Hydrology (1999) *Flood Estimation Handbook*. Wallingford, UK: Institute of Hydrology.

Jain, A. and Srinivasulu, S. (2004) Development of effective and efficient rainfall-runoff models using integration of deterministic, real-coded genetic algorithms and artificial neural network techniques. *Water Resources Research*, 40: W04302, doi:10.1029/2003WR002355.

Jain, A. and Srinivasulu, S. (2006) Integrated approach to model decomposed flow hydrograph using artificial neural network and conceptual techniques. *Journal of Hydrology*, 317(3-4): 291.

Jakeman, A. J. and Hornberger, G. M. (1993) How much complexity Is warranted in a rainfall-runoff model. *Water Resources Research*, 29(8): 2637-2649.

Jakeman, A. J., Littlewood, I. G. and Whitehead, P. G. (1990) Computation of the instantaneous unit hydrograph and identifiable component flows with application to two small upland catchments. *Journal of Hydrology*, 117(1-4): 275-300.

Jayawardena, A. W., Muttil, N. and Lee, J. H. W. (2006) Comparative analysis of data-driven and GIS-based conceptual rainfall-runoff model. *Journal of Hydrologic Engineering*, 11(1): 1-11.

Jeng, R. I. and Coon, G. C. (2003) True form of instantaneous unit hydrograph of linear reservoirs. *Journal of Irrigation and Drainage Engineering*, 129(1): 11-17.

Jones, S. B. (1983). *The estimation of catchment average point rainfall profiles*. Report No. 87. Institute of Hydrology, Wallingford, UK. 34 pp.

Kachroo, R. K. and Liang, G. C. (1992) River flow forecasting. Part 2. Algebraic development of linear modelling techniques. *Journal of Hydrology*, 133(1-2): 17-40.

Kavetski, D., Franks, S. W. and Kuczera, G. (2002). Confronting input uncertainty in environmental modelling. In: Duan, Q., Gupta, H.V., Sorooshian, S., Rousseau, A.N. and Turcotte, R. (Eds) *Calibration of Watershed Models*. Washington, DC: American Geophysical Union. pp 49-68.

Kilbas, A. A., Saigo, M. and Saxena, R. K. (2004) Generalized Mittag-Leffler function and generalized fractional calculus operators. *Integral Transforms and Special Functions*, 15(1): 31 - 49.

Kilbas, A. A., Srivastava, H. M. and Trujillo, J. J. (2006) *Theory and Applications of Fractional Differential Equations*. Amsterdam: Elsevier. 540 pp.

Kim, S. and Kavvas, M. L. (2006) Generalized Fick's law and fractional ADE for pollution transport in a river: detailed derivation. *Journal of Hydrologic Engineering*, 11(1): 80-83.

Kirchner, J. W. (2003) A double paradox in catchment hydrology and geochemistry. *Hydrological Processes*, 17(4): 871 - 874.

Kirchner, J. W. (2006) Getting the right answers for the right reasons: Linking measurements, analyses, and models to advance the science of hydrology. *Water Resources Research*, 42: W03S04, doi:10.1029/2005WR004362.

Kirchner, J. W., Feng, X. and Neal, C. (2000) Fractal stream chemistry and its implications for contaminant transport in catchments. *Nature*, 403: 524-527.

Kirchner, J. W., Feng, X. and Neal, C. (2001) Catchment-scale advection and dispersion as a mechanism for fractal scaling in stream tracer concentrations. *Journal of Hydrology*, 254(1-4): 82-101.

Kjeldsen, T. R., Stewart, E. J., Packman, J. C., Folwell, S. S. and Bayliss, A. C. (2005). *Revitalisation of the FSR/FEH Rainfall-Runoff Method*. Report No. FD1913/TR. CEH, Wallingford. 133 pp.

Klemes, V. (1974) The Hurst phenomenon: a puzzle? *Water Resources Research*, 10(4): 675-688.

Kohler, M. A. and Linsley, R. K. (1951). *Predicting runoff from storm rainfall*. Research Paper No 34, U.S.Weather Bureau, Washington, D.C. 9 pp.

Koutsoyiannis, D. (2002) The Hurst phenomenon and fractional Gaussian noise made easy. *Hydrological Sciences Journal*, 47(4): 573-595.

Koutsoyiannis, D. and Xanthopoulos, T. (1989) On the parametric approach to unit hydrograph identification. *Water Resources Management*, 3(2): 107-128.

Koza, J. R. (1992) *Genetic Programming: On the Programming of Computers by Means of Natural Selection*. Cambridge, MA, USA: MIT Press.

Kuczera, G. (1983) Improved parameter inference in catchment models: 1. Evaluating parameter uncertainty. *Water Resources Research*, **19**(5): 1151-1162.

Kuczera, G. and Parent, E. (1998) Monte Carlo assessment of parameter uncertainty in conceptual catchment models: the Metropolis algorithm. *Journal of Hydrology*, **211**(1-4): 69-85.

Lees, M. J. (2000) Data-based mechanistic modelling and forecasting of hydrological systems. *Journal of Hydroinformatics*, **2**(1): 15-34.

Legates, D. R. and McCabe, G. J. (1999) Evaluating the use of "goodness-of-fit" measures in hydrologic and hydroclimatic model validation. *Water Resources Research*, **35**(1): 233-241.

Li, C. and Deng, W. (2007) Remarks on fractional derivatives. *Applied Mathematics and Computation*, **187**(2): 777-784.

Liong, S. Y., Chan, W. T. and Shreeram, J. (1995) Peak-flow forecasting with genetic algorithm and SWMM. *Journal of Hydraulic Engineering*, **121**(8): 613-617.

Loague, K. and VanderKwaak, J. E. (2004) Physics-based hydrologic response simulation: platinum bridge, 1958 Edsel, or useful tool. *Hydrological Processes*, **18**(15): 2949-2956.

Lorenzo, C. F. and Hartley, T. T. (1998). *Initialization, Conceptualization, and Application in the Generalized Fractional Calculus*. Report No. TP-1998-208415. NASA, Washington, DC. 107 pp.

Lorenzo, C. F. and Hartley, T. T. (2008) Initialization of fractional-order operators and fractional differential equations. *Journal of Computational and Nonlinear Dynamics*, **3**(2): 021101.

Lovejoy, S. and Schertzer, D. (2006). *Scale, scaling and multifractals in geophysics: twenty years on*. Tsonis, A.A. and Elsner, J.B. (Eds) Proceedings: 20 Years of Nonlinear Dynamics in Geosciences. Rhodes, Greece. Springer. June 11-16. pp 311-337.

Madsen, H. (2000) Automatic calibration of a conceptual rainfall-runoff model using multiple objectives. *Journal of Hydrology*, **235**(3-4): 276-288.

Maillet, E. (1905) *Essais d'Hydraulique Souterraine et Fluviale*. Paris: Hermann. 218 pp.

Malti, R., Aoun, M., Sabatier, J. and Oustaloup, A. (2006). *Tutorial on system identification using fractional differentiation models*. Ninness, B. and Hjalmarsson, H. (Eds) 14th IFAC Symposium on System Identification. Newcastle, Australia. IFAC. pp 606-611.

Mandelbrot, B. B. (2002) *Gaussian Self-affinity and Fractals: Globality, the Earth, 1/f Noise and R/S*. New York: Springer-Verlag. 654 pp.

358

Mandelbrot, B. B. and Van Ness, J. W. (1968) Fractional Brownian motions, fractional noises and applications. *SIAM Review*, 10(4): 422–437.

Matsoukas, C., Islam, S. and Rodriguez-Iturbe, I. (2000) Detrended fluctuation analysis of rainfall and streamflow time series. *Journal of Geophysical Research*, 105(D23): 29165–29172.

Miller, K. S. and Ross, B. (1993) *An Introduction to the Fractional Calculus and Fractional Differential Equations*. New York: Wiley. 366 pp.

Minns, A. W. (2000) Subsymbolic methods for data mining in hydraulic engineering. *Journal of Hydroinformatics*, 2(1): 3-13.

Minns, A. W. and Hall, M. J. (1996) Artificial neural networks as rainfall-runoff models. *Hydrological Sciences Journal*, 41(3): 399-417.

Minshall, N. E. (1960) Predicting storm runoff from small experimental watersheds. *Journal of the Hydraulics Division, Proceedings of American Society of Civil Engineers*, 86(HY8): 17-38.

Mittag-Leffler, M. G. (1903) Sur la nouvelle fonction $E_\alpha (x)$. *Comptes Rendus de l'Academie des Sciences*, 137: 554-558.

Mohan, S. and Vijayalakshmi, D. P. (2008) Estimation of Nash's IUH parameters using stochastic search algorithms. *Hydrological Processes*, 22(17): 3507-3522.

Montanari, A. (2005) Large sample behaviors of the generalized likelihood uncertainty estimation (GLUE) in assessing the uncertainty of rainfall-runoff simulations. *Water Resources Research*, 41: W08406, doi:10.1029/2004WR003826.

Moore, R. J. (1985) The probability-distributed principle and runoff production at point and basin scales. *Hydrological Sciences Journal*, 30(2): 273-297.

Moore, R. J. and Clarke, R. T. (1981) A distribution function-approach to rainfall runoff modeling. *Water Resources Research*, 17(5): 1367-1382.

Napiorkowski, J. J. and Piotrowski, A. (2005) Artificial neural networks as an alternative to the Volterra series in rainfall-runoff modelling. *Acta Geophysica Polonica*, 53(4): 459 - 472.

Napiorkowski, J. J. and Strupczewski, W. G. (1979) The analytical determination of the kernels of the Volterra series describing the cascade of nonlinear reservoirs. *Journal of Hydrological Sciences*, 6(3-4): 121-142.

Napiorkowski, J. J. and Strupczewski, W. G. (1984) Problems involved in identification of the kernels of Volterra series. *Acta Geophysica Polonica*, 32(4): 375 - 391.

Nash, J. E. (1957). *The form of the instantaneous unit hydrograph*. International Association of Hydrological Sciences, General Assembly. Toronto. IAHS Press. 3-14 Sep. pp 114-121.

Nash, J. E. (1960) A unit hydrograph study, with particular reference to British catchments. *Proceedings of the ICE*, 17(3): 249-282.

Nash, J. E. and Sutcliffe, J. V. (1970) River flow forecasting through conceptual models part 1 - A discussion of principles. *Journal of Hydrology*, 10(3): 282-290.

Natural Environment Research Council (1975a). *Flood Studies Report: Volume I Hydrological Studies*. NERC, London. 550 pp.

Natural Environment Research Council (1975b). *Flood Studies Report: Volume IV Hydrological Data*. NERC, London. 541 pp.

Natural Resources Conservation Service (2007). Hydrographs. *National Engineering Handbook, Part 630, Chapter 16 - Hydrology*. Washington, DC: United States Department of Agriculture.

Ndiritu, J. G. and Daniell, T. M. (1999) An improved genetic algorithm for continuous and mixed discrete-continuous optimization. *Engineering Optimization*, 31(5): 589-614.

Odibat, Z. M. and Shawagfeh, N. T. (2007) Generalized Taylor's formula. *Applied Mathematics and Computation*, 186(1): 286-293.

Oldham, K. B. and Spanier, J. (1974) *The Fractional Calculus: Theory and Applications of Differentiation and Integration to Arbitrary Order*. New York: Academic Press. 234 pp.

Orjuela, R., Malti, R., Moze, M. and Oustaloup, A. (2006). *Prise en compte des conditions initiales lors de la simulation de fonctions de transfert non entières*. Conférence Internationale Francophone d'Automatique, CIFA 2006. Bordeaux, France. e-STA, Sciences et Technologies de l'Automatique. 30 May - 1 Jun.

Ortigueira, M. D. (2003) On the initial conditions in continuous-time fractional linear systems. *Signal Processing*, 83(11): 2301-2309.

Ortigueira, M. D. and Coito, F. J. (2008). *The initial conditions of Riemann-Liouville and Caputo derivatives*. Fradkov, A. (Ed) 6th EUROMECH Nonlinear Dynamics Conference ENOC 2008. Saint Petersburg, Russia. Open Access Electronic Library. 30 Jun - 4 Jul.

Oustaloup, A. and Sabatier, J. (1995) Study of the relaxation of water on a porous dyke: a non-integer approach. *Annales Geophysicae*, 13.

Oustaloup, A., Sabatier, J. and Lanusse, P. (1999) From fractal robustness to the CRONE approach. *Fractional Calculus and Applied Analysis*, 2(1): 1-30.

Pachepsky, Y., Benson, D. and Rawls, W. (2000) Simulating scale-dependent solute transport in soils with the fractional advective–dispersive equation. *Soil Science Society of America Journal*, 64(4): 1234-1243.

Pachepsky, Y., Timlin, D. and Rawls, W. (2003) Generalized Richards' equation to simulate water transport in unsaturated soils. *Journal of Hydrology*, **272**(1-4): 3-13.

Packham, I. S. J., Rafiq, M. Y., Borthwick, M. F. and Denham, S. L. (2005) Interactive visualisation for decision support and evaluation of robustness - in theory and in practice. *Advanced Engineering Informatics*, **19**(4): 263-280.

Pandey, G., Lovejoy, S. and Schertzer, D. (1998) Multifractal analysis of daily river flows including extremes for basins of five to two million square kilometres, one day to 75 years. *Journal of Hydrology*, **208**(1-2): 62-81.

Pilgrim, D. H. (1976) Travel times and nonlinearity of flood runoff from tracer measurements on a small watershed. *Water Resources Research*, **12**(3): 487-496.

Podlubny, I. (1999) *Fractional Differential Equations: An Introduction to Fractional Derivatives, Fractional Differential Equations, to Methods of their Solution and Some of their Applications.* San Diego: Academic Press. 368 pp.

Prabhakar, T. R. (1971) A singular integral equation with a generalized Mittag-Leffler function in the kernel. *Yokohama Mathematical Journal*, **19**: 7-15.

Reggiani, P., Hassanizadeh, S. M., Sivapalan, M. and Gray, W. G. (1999) A unifying framework for watershed thermodynamics: constitutive relationships. *Advances in Water Resources*, **23**(1): 15-39.

Reggiani, P. and Rientjes, T. H. M. (2005) Flux parameterization in the representative elementary watershed approach: Application to a natural basin. *Water Resources Research*, **41**: W04013, doi:10.1029/2004WR003693.

Reggiani, P., Sivapalan, M. and Majid Hassanizadeh, S. (1998) A unifying framework for watershed thermodynamics: balance equations for mass, momentum, energy and entropy, and the second law of thermodynamics. *Advances in Water Resources*, **22**(4): 367-398.

Rigden, T. and Borthwick, M. (2008). *Evolutionary computing approach to instantaneous unit hydrograph identification.* Rafiq, Y., de Wilde, P. and Borthwick, M. (Eds) Intelligent Computing in Engineering (ICE08) - 15th International Workshop of EG-ICE. Plymouth, UK. 2-4 Jul. pp 157-166.

Robinson, J. S., Sivapalan, M. and Snell, J. D. (1995) On the relative roles of hillslope processes, channel routing, and network geomorphology in the hydrologic response of natural catchments. *Water Resources Research*, **31**(12): 3089-3101.

Rodriguez-Iturbe, I. and Rinaldo, A. (1997) *Fractal River Basins : Chance and Self-Organization.* Cambridge: Cambridge University Press. 564 pp.

Samko, S. G., Kilbas, A. A. and Marichev, O. I. (1993) *Fractional Integrals and Derivatives: Theory and Applications.* London: Gordon and Breach. 1006 pp.

Scher, H., Margolin, G., Metzler, R., Klafter, J. and Berkowitz, B. (2002) The dynamical foundation of fractal stream chemistry: The origin of extremely long retention times. *Geophysical Research Letters*, **29**(5): 1061, doi:10.1029/2001GL014123.

Schertzer, D. and Lovejoy, S. (1987) Physically based rain and cloud modeling by anisotropic, multiplicative turbulent cascades. *Journal of Geophysical Research*, **92**(D8): 9693-9714.

Schütze, N., Schmitz, G. H. and Petersohn, U. (2005) Self-organizing maps with multiple input-output option for modeling the Richards equation and its inverse solution. *Water Resources Research*, **41**(3): W03022, doi:10.1029/2004WR003630.

Sherman, L. K. (1932) Streamflow from rainfall by the unit-graph method. *Engineering News Record*, **108**: 501-505.

Shrestha, R. R., Theobald, S. and Nestmann, F. (2005) Simulation of flood flow in a river system using artificial neural networks. *Hydrology and Earth System Sciences*, **9**(4): 313-321.

Silverman, B. W. (1986) *Density Estimation for Statistics and Data Analysis*. London: Chapman and Hall.

Singh, K. P. (1964) Nonlinear instantaneous unit hydrograph theory. *Journal of the Hydraulics Division, Proceedings of American Society of Civil Engineers*, **90**(HY2): 313-347.

Singh, V. P. (1988) *Hydrologic Systems. Vol. 1, Rainfall-Runoff Modelling*. Englewood Cliffs, N.J.: Prentice Hall. 480 pp.

Singh, V. P. and Woolhiser, D. A. (2002) Mathematical modeling of watershed hydrology. *Journal of Hydrologic Engineering*, **7**(4): 270-292.

Sivapalan, M., Zhang, L., Vertessy, R. and Bloschl, G. (2003) Downward approach to hydrological prediction. *Hydrological Processes*, **17**(11): 2101-2111.

Sklash, M. G. and Farvolden, R. N. (1979) The role of groundwater in storm runoff. *Journal of Hydrology*, **43**(1-4): 45-65.

Sorooshian, S. and Dracup, J. A. (1980) Stochastic parameter estimation procedures for hydrologic rainfall-runoff models: correlated and heteroscedastic error cases. *Water Resources Research*, **16**(2): 430-442.

Spanier, J. and Oldham, K. B. (1987) *An Atlas of Functions*. Berlin: Springer-Verlag. 700 pp.

Sudheer, K. P. (2005) Knowledge extraction from trained neural network river flow models. *Journal of Hydrologic Engineering*, **10**(4): 264-269.

Tallaksen, L. M. (1995) A review of baseflow recession analysis. *Journal of Hydrology*, **165**(1-4): 349-370.

Tessier, Y., Lovejoy, S., Hubert, P., Schertzer, D. and Pecknold, S. (1996) Multifractal analysis and modeling of rainfall and river flows and scaling, causal transfer functions. *Journal of Geophysical Research*, **101**(D21): 26427-26440.

Uhlenbrook, S., Seibert, J., Leibundgut, C. and Rodhe, A. (1999) Prediction uncertainty of conceptual rainfall-runoff models caused by problems in identifying model parameters and structure. *Hydrological Sciences Journal*, **44**(5): 779-797.

Valdes, J. B., Fiallo, Y. and Rodrigueziturbe, I. (1979) A rainfall-runoff analysis of the geomorphological IUH. *Water Resources Research*, **15**(6): 1421-1434.

Vrugt, J. A., Gupta, H. V., Bastidas, L. A., Bouten, W. and Sorooshian, S. (2003) Effective and efficient algorithm for multiobjective optimization of hydrologic models. *Water Resources Research*, **39**(8): 1214, doi:10.1029/2002WR001746.

Wagener, T., Boyle, D. P., Lees, M. J., Wheater, H. S., Gupta, H. V. and Sorooshian, S. (2001) A framework for development and application of hydrological models. *Hydrology and Earth System Sciences*, **5**(1): 13-26.

Wang, C. T., Gupta, V. K. and Waymire, E. (1981) A geomorphologic synthesis of nonlinearity in surface runoff. *Water Resources Research*, **17**(3): 545-554.

Wang, G.-T. and Wu, K. (1983) The unit-step function response for several hydrological conceptual models. *Journal of Hydrology*, **62**(1-4): 119-128.

Wang, Q. J. (1991) The genetic algorithm and its application to calibrating conceptual rainfall-runoff models. *Water Resources Research*, **27**(9): 2467-2471.

Wang, Q. J. (1997) Using genetic algorithms to optimise model parameters. *Environmental Modelling & Software*, **12**(1): 27-34.

Webster, P. and Ashfaq, A. (2003) Comparison of UK flood event characteristics with design guidelines. *Proceedings of the ICE - Water and Maritime Engineering*, **156**(1): 33-40.

Wheatcraft, S. W. and Meerschaert, M. M. (2008) Fractional conservation of mass. *Advances in Water Resources*, **31**(10): 1377-1381.

Wheater, H. S. (2002) Progress in and prospects for fluvial flood modelling. *Philosophical Transactions of the Royal Society, London A*, **360**(1796): 1409-1431.

Whigham, P. A. and Crapper, P. F. (1997). *Applying genetic programming to model rainfall-runoff.* McDonald, D. and McAleer, M. (Eds) International Congress on Modelling and Simulation: Proceedings. 8-11 Dec.

Whitehead, P., Young, P. and Hornberger, G. (1979) A systems model of stream flow and water quality in the Bedford-Ouse river - 1. Stream flow modelling. *Water Research*, **13**(12): 1155-1169.

Williams, A. G., Borthwick, M. F., Mtika, E., Ternan, J. L. and Sullivan, A. (2004). *The influence of changes in farming patterns on the runoff characteristics of the River Camel, Cornwall, UK.* Webb, B., Arnell, N.W., Onof, C., MacIntyre, N., Gurney, R. and Kirby, C. (Eds) BHS International Conference on "Hydrology: Science & Practice for the 21st Century". London, UK. British Hydrological Society. 12-16 Jul. pp 526-533.

Wiman, A. (1905) Über den fundamentalsatz in der teorie der funktionen $E_a(x)$. *Acta Mathematica,* 29(1): 191-201.

Yang, R. and Douglas, I. (1998) Simple genetic algorithm with local tuning: Efficient global optimizing technique. *Journal of Optimization Theory and Applications,* 98(2): 449-465.

Yapo, P. O., Gupta, H. V. and Sorooshian, S. (1998) Multi-objective global optimization for hydrologic models. *Journal of Hydrology,* 204(1-4): 83-97.

Yawson, D. K., Kongo, V. M. and Kachroo, R. K. (2005) Application of linear and nonlinear techniques in river flow forecasting in the Kilombero River basin, Tanzania. *Hydrological Sciences Journal,* 50(5): 783-796.

Young, P. (2003) Top-down and data-based mechanistic modelling of rainfall-flow dynamics at the catchment scale. *Hydrological Processes,* 17(11): 2195-2217.

Young, P. and Beven, K. (1991) Computation of the instantaneous unit-hydrograph and identifiable component flows with application to 2 small upland catchments - comment. *Journal of Hydrology,* 129(1-4): 389-396.

Young, P. C. (2002) Advances in real-time flood forecasting. *Philosophical Transactions of the Royal Society, London A,* 360(1796): 1433-1450.

Young, P. C. and Beven, K. J. (1994) Data-based mechanistic modelling and the rainfall-flow non-linearity. *Environmetrics,* 5(3): 335-363.

Zhang, X., Crawford, J. W., Deeks, L. K., Stutter, M. I., Bengough, A. G. and Young, I. M. (2005) A mass balance based numerical method for the fractional advection-dispersion equation: Theory and application. *Water Resources Research,* 41: W07029, doi:10.1029/2004WR003818.

Zoch, R. T. (1934) On the relation between rainfall and streamflow - I. *Monthly Weather Review,* 62(9): 315–322.

Copies of Publications

The preprint of the following journal paper published during the programme of research is included below.

Interactive Visualization for Evolutionary Optimization of Conceptual Rainfall-Streamflow Models

M. F. Borthwick[1]; I. S. Packham[2]; and M. Y. Rafiq, M.ASCE[3]

Abstract:
Calibration is an essential part of the application of conceptual rainfall-streamflow models to watershed management problems for civil engineers. However the identification of a unique set of parameters is difficult, if not impossible, for commonly used models. Most multi-objective methods and uncertainty assessment tools require substantial numbers of function evaluations and limit the intervention of experienced modelers in the calibration process. This paper demonstrates the application of an efficient user-driven calibration-support system to conceptual rainfall-streamflow models. The system is designed to assist the hydrological modeler by means of rapid sampling of solutions, clustering and visualization, together with interactivity to exploit the expertise of the user and/or the knowledge revealed by the clustering technique. The efficiency of the multiobjective calibration is enhanced through the use of a novel objective function based on hydrograph slope. The application of the system to the calibration of the SIXPAR conceptual rainfall-streamflow model using a synthetic time series is shown to be effective.

CE Database subject headings: Calibration, Optimization, Evolutionary computing, Multiple objective analysis, Genetic algorithms, Hydrologic models, Visualization

[1]Martin Borthwick, Lecturer, School of Engineering, University of Plymouth, Drake Circus, Plymouth, PL4 8AA, UK. mborthwick@plymouth.ac.uk
[2]Ian Packham, Researcher, Lightwave Technologies Ltd, Innovation Centre, NovaUCD, University College Dublin, Belfield, Dublin 4, Ireland. ian.packham@ucd.ie
[3]Yaqub Rafiq, Senior Lecturer, School of Engineering, University of Plymouth, Drake Circus, Plymouth, PL4 8AA, UK. mrafiq@plymouth.ac.uk

Introduction

Computational modeling of the transformation of rainfall to streamflow is important for a number of civil engineering applications, for example flood and drought forecasting, flood defense design, and predicting the effects of climate and land use change on the hydrological response of watersheds. An essential aspect of computational rainfall-streamflow modeling is calibration of the parameters for the numerical model to fit a set of field observed data, particularly given the number of conceptual models in use that have parameters that cannot be measured independently. However, the multi-dimensional nature of such models, parameter interaction and sensitivity often results in non-smooth, multimodal response surfaces leading to problems in the attempt to identify the model uniquely (Gupta et al. 2003b). Manual calibration, whereby the user chooses or makes a best-estimate of the set of parameter values, tests the model against an observed calibration data set, evaluates some measure of fitness (e.g. a numerical objective function) and then revises the parameter estimates, is time-consuming and requires experience. Although evolutionary computing-based techniques have been developed for automatic global calibration of models, notably the shuffled complex evolution, SCE-UA (Duan et al. 1992), there is evidence when used with single objective function measures of model fitness to suggest that there are different sets of parameter values with similar fitness, which Beven (1993) describes as "equifinality" (see also Beven 2006). In addition to errors in the observed data, the structure of the model and over-parameterization may render it impossible to identify a unique set of parameters for calibration. For example Duan et al (1992), Gan and Biftu (1996) and Wang (1997) found that calibration of multi-parameter conceptual rainfall-runoff models using a single objective function even with synthetic data (for a hypothetical set of global optimal parameter values) produced multiple local optima of similar fitness; and Uhlenbrook et al (1999) showed that even conceptually unrealistic sets of parameter values could produce good predictions.

A number of computer-based tools for helping the user to quantify the calibration uncertainty have been proposed by Kuczera (1983), Kuczera and Parent (1998), Beven and Binley (1992), Beven and Freer (2001), Kavetski et al (2002), and Wagener et al (2003), among others. The techniques generally rely upon Monte Carlo sampling of the parameter space and require substantial numbers of objective function evaluations which can be computationally expensive for complex models. Montesinos and Beven (1999) used a genetic algorithm, GA (Goldberg 1989; Holland 1975), to reduce the number of function evaluations when assessing the model uncertainty using the Generalised Likelihood Uncertainty Estimation (GLUE) technique (Beven and Binley 1992) and found that over several generations, the GA solutions tended to converge on a region of attraction around an optimum. Werner and Khu (2001) extended this approach by incorporating niching (Goldberg 1989) to avoid convergence on a local optimum before applying the GLUE technique and tested the method on a river routing model. Khu and Werner (2003) have gone on to use artificial neural networks to represent the behavior of a rainfall-streamflow model during the sampling stage of the GLUE technique (where sets of parameter values that produce above a threshold fitness are retained). The actual rainfall-streamflow model is then used with the selected parameter sets to evaluate the corrected fitness.

An alternative approach has been to use multiple objective functions to extract more information from the observed data and thereby constrain the calibration. Yapo et al (1998) developed a multi-objective complex evolution technique (MOCOM-UA) derived from the SCE-UA method (Duan et al. 1992) which uses Pareto ranking (Goldberg 1989) and has been tested using 2 objective functions on the Sacramento soil

moisture accounting model, SAC-SMA (Burnash et al. 1973) with observed data; and extended to 3 objectives (Gupta et al. 1998). Madsen (2000) used 4 objectives to represent the runoff volume, hydrograph shape, peak flows and low flows and then computed an overall fitness measure using the Euclidean distance incorporating user-defined transformation constants for each component objective function. This was then optimized using the SCE-UA. Gupta et al (2003a) followed Boyle et al (2000) and partitioned the streamflow hydrograph into driven and non-driven components and used the root mean square error for each component as the objectives in the MOCOM-UA technique, but found that the endpoints of the Pareto optimal parameter sets identified were not well defined. Consequently, Vrugt et al (2003) developed the multi-objective shuffled complex evolution Metropolis (MOSCEM-UA) algorithm based on the SCE-UA but using the Metropolis Hastings sampling strategy in place of the downhill simplex to avoid convergence on a single optimum. This permits the estimation of the most likely parameter set based on Pareto dominance and the underlying posterior probability distribution to attempt to quantify uncertainty. The use of multi-objective calibration involves large numbers of model runs with the associated computational overhead. There has been research into reducing the calibration time of multi-objective techniques. For example Liu et al (2004) have applied a k-nearest neighbor classifier system to predict the subsets of good solutions from an initial multi-objective genetic algorithm (MOGA) run and used them to update the population of parameter sets before running the next generation of the MOGA with the rainfall-streamflow model. They found a substantial reduction of function evaluations required to produce the Pareto front (albeit smaller than that obtained by just running the MOGA).

Alongside the development of automatic calibration tools has been work on incorporating the expertise of the hydrological modeler through user interaction. A number of comparative studies have demonstrated the value of semi-automatic multi-objective calibration tools when used in combination with the user's qualitative knowledge of the reliability of the data and the model being used to make the calibration suit the application (Bender and Simonovic 1994; Rafiq et al. 2003; Gupta et al. 1999; Harlin 1991; Houghton-Carr 1999; Madsen et al. 2002; Zhang and Lindström 1997; Hogue at al 2000). Visualization helps the modeler to observe the complexity of the parameter and objective function spaces and assists in the process of selecting a set of parameter values for the particular watershed application. The GLOBE system developed by Solomatine (1995, 1999) includes a computer-generated visualization of single objective function clusters in 2D parameter sub spaces, although without a facility for the user to examine other regions or interact with the calibration algorithms unless the system is restarted. The Real-time Interactive Basin Simulator of Garrote and Becchi (1997) incorporates both a distributed real-time flood forecasting model and user-interactive tools for the visualization of flow parameters at user-defined locations within a river basin as the storm simulation progresses. Wagener et al (2001) have developed a toolkit for identifying both the model structure and calibration of the parameters which uses Monte Carlo sampling of the parameter space and provides the user with a selection of visualization techniques for the parameter and objective function spaces.

This paper presents the application of an efficient user-driven calibration-support system that relies upon rapid visualization of the model parameter sub-spaces and objective function spaces obtained from a GA-based search. A key feature of the system is the facility for the user to interactively select regions of interest for refined search or for testing the robustness of potentially good solutions based on either their experience and/or the knowledge revealed by a clustering technique. The system allows

different objective functions to be tested. It is accepted that there may not be a single parameter set but a number of sets from which the user must select for the model. A particularly novel aspect of this application is the introduction of an objective function based on the changing slope of the streamflow hydrograph.

Objective Functions

A number of reviews have been undertaken of the use of common single objective functions in rainfall-streamflow model calibration (Cooper et al. 1997; Diskin and Simon 1977; Legates and McCabe 1999). In many cases the simple least squares (or root mean square error, RMSE) or the Nash-Sutcliffe efficiency, NSE (a normalized version of the RMSE) has been used, but these tend to emphasize the fitting of peak flows. Sorooshian and Dracup (1980) introduced the heteroscedastic maximum likelihood estimator (HMLE) to account for non-constant variance error in the observed streamflow data. With the exception of selecting at least one objective function which takes account of the error in the measurement data, there does not appear to be a consensus on which group of objective functions should be used in multi-criteria calibration (see the review in the introduction of this paper). For the purposes of demonstrating the calibration system presented in this paper 2 objective functions were used. The first objective was the commonly-used RMSE (given that error-free synthetic streamflow data was used):

$$RMSE = \sqrt{\frac{1}{n}\sum_{t=1}^{n}\left(q_{obs,t} - q_t(\theta)\right)^2} \tag{1}$$

where $q_{obs,t}$ is the observed streamflow at time t, $q_t(\theta)$ is the streamflow predicted by the model at time t, and n is the number of daily streamflow values used in the calibration. To account for the limitations of the RMSE, a second objective function was required that would fit the observed hydrograph shape across the range of flows. A novel approach was to compare the slopes (after Rafiq et al (2006b)) of the observed and predicted hydrographs, expressed as the root mean square error of slope, RMSslope, given by in equation 2.

$$RMSslope = \sqrt{\frac{1}{n}\sum_{t=1}^{n}\left(slope_{obs,t} - slope_t(\theta)\right)^2} \tag{2}$$

where
$$slope_t = \frac{q_{t+1} - q_{t-1}}{2\Delta t} \tag{3}$$

for $1 < t < n$ using a central difference approximation; and at the end points of the time series the slopes were estimated using forward and backward differences as follows:

$$slope_1 = \frac{q_2 - q_1}{\Delta t} \tag{4}$$

$$slope_n = \frac{q_n - q_{n-1}}{\Delta t} \tag{5}$$

Δt is the timestep (1 day for the daily time series used) and q_t is the streamflow at a particular time, t.

Optimization Algorithm

Duan et al (1992) identified the existence of a number of regions of attraction in the parameter space for a typical conceptual model where the calibration algorithm can converge to a solution. These regions were found to contain numerous minor local optima. The response surfaces tended to be discontinuous and non-convex with areas of parameter interaction. These types of spaces make the search for an optimum set of parameter values by traditional gradient-based methods difficult or impossible. Consequently, emphasis has been placed on the use of evolutionary search techniques, such as genetic algorithms. GA search operates in a similar manner to Darwinian natural selection (Goldberg 1989; Holland 1975). In the algorithm an initial population of randomly selected sets of parameter values is tested for fitness (by comparing model predictions using each set of parameters with observed streamflow) and a new population of parameter sets is evolved by applying reproduction, crossover and mutation operations on selected members of the parent population. The selection is made using a probabilistic rule weighted according to fitness. The process is repeated with a view to evolving fitter populations. Goldberg and Kuo (1987) were the first to apply the GA to a flow problem in civil engineering, by optimization of a pipeline. The application has been extended to pipe networks and multi-reservoir systems for the optimization of water resource systems (for example Jeong and Abraham 2006; Sharif and Wardlaw 2000; Wu and Simpson 2001). Wang (1991) first used a genetic algorithm-based automatic calibration of multi-parameter conceptual rainfall-runoff models. This application has been further tested by a number of researchers (Franchini 1996; Liong et al. 1995; Ndiritu and Daniell 1999; Wang 1997; Yang and Douglas 1998, among others). One of the outcomes of this work is that the GA may not always converge to the global optimum solution (where one has been identified by the use of data synthesized for a model run with a predefined set of parameter values) and that it may require a gradient-based optimization technique to refine the search once the GA has converged. In order to avoid convergence onto a single optimum region a low generational GA with moderately high mutation rates was adopted in the calibration system described in this paper. This also enabled the system to rapidly generate diverse parameter solutions of varying fitness, for subsequent visualization and analysis by the user. In this way the user can continually refine and test their chosen parameter region for calibration, without the need for large numbers of function evaluations (unlike Monte Carlo sampling systems).

User-Driven Calibration-Support System

The interactive calibration-support system was developed by Packham (2003) for the visualization of multivariate data and for decision support in engineering design tasks through user interaction. The system uses evolutionary computing and clustering techniques to visualize the optimization of multidimensional models and to evaluate robust regions of the parameter spaces. The system, together with a review of the development of interactive visualization techniques for engineering design, using evolutionary computing, is presented in Packham et al (2005).

In outline the system has been designed with the following features:

- o Rapid sampling of the feasible parameter and objective spaces by using short GA runs of 20 generations with, typically, 100 members in the population (i.e. 2100 model simulations, including evaluating the initial population of solutions). The low number of generations avoids convergence onto a single optimum region, and the use of moderately high crossover and mutation rates, particularly if duplicate solutions are generated, maintains diversity. This allows the user to subsequently select regions for further search, whilst limiting the computational overhead.

- Easy to use graphical user interface. This has been designed in accordance with Shneiderman's (1998) principles of presenting the user with an overview, zoom facility, and details on demand.

- High dimensional visualization of the parameter and objective function spaces, including 2-D and 3-D views, scatterplot matrix (Chambers et al. 1983), parallel coordinates (Inselberg and Dimsdale 1994), and plots in transformed coordinate systems if required. In this way the user can investigate parameter interaction and model sensitivity to particular parameters.

- Automatic clustering option. A kernel density estimation algorithm (Silverman 1986) is applied to identify clusters of solutions in either the parameter or objective function space. The technique is described in the following section.

- To aid visualization color is applied: where more intense, pure color (i.e. darker) is used within a particular cluster to emphasize higher fitness solutions; and different color hues are used to distinguish between clusters.

- Interactive features. The user can quickly zoom into subspaces and select regions for additional GA searches to generate further solutions or for the identification of clusters – either automatically or manually. All the solutions (i.e. high and low fitness) generated by the GA search are retained by the system. In this way the user has control over both how and where the investigation of the search space takes place, including regions outside of clusters of good solutions found by the GA. The user can also visualize the model output for any of the parameter sets generated by the system, by simply selecting a solution with the mouse. A plot of the predicted and observed streamflow hydrographs is displayed, enhancing the user's perception of the goodness of fit of the chosen solution.

- Robustness evaluation of selected solutions. The user can select a region containing potentially good solutions and carry out a "negative GA" search. This essentially allows the user to search for the worst solution in the selected region instead of the best (thus, for a maximization problem, the user chooses to minimize the objective instead). This method allows the user to evaluate the robustness of solutions in the selected region as the likely worst solutions can be generated (and again highlighted using the clustering technique). The user needs to keep in mind that the same limitations such as being trapped in local optima apply to the negative GA search as to the positive. However, because of the low number of solutions generated in each run, the user can quickly build up a picture of the robustness and nature of the landscape using all the interactive tools described above.

The system has been applied to the multiobjective optimization of the design of biaxial columns (Rafiq et al. 2006a), and to investigate the single objective function calibration of a simple time-series model of rainfall-runoff (Packham et al. 2004; 2005).

In this paper the GA search was carried out using the single objective functions (equations 1 and 2) in turn as fitness measures and also using a weighted average fitness measure given by:

$$\text{Fitness} = w_1 RMSE + w_2 RMS_{slope} \qquad (6)$$

where w_1 and w_2 are weightings. Weights between 0 and 1 such that $w_1 + w_2 = 1$ were used in this study. It should be emphasized that this weighted fitness measure is only used in the system to facilitate the selection operators in the GA. As an entirely separate operation to the GA fitness calculation, the system can evaluate and visualize the associated spaces for any number of objective functions. Depending upon the number of objectives, these can be included in the weighted fitness measure used for the selection mechanism in the GA in equation 6, such that the total of the weights equals 1.

370

However, for a large number of objectives it may be preferable to use a subset in the weighted fitness for the GA search and calculate the remaining functions for visualization purposes only.

Clustering Technique

There are many clustering techniques that have been developed for various applications and they can be sensitive to certain parameters (Jain et al. 1999). The aim of clustering in this case is to identify high performance regions of a search space as generated by the GA with minimal computation time and parameter setting. Such data tends to contain dense regions where the GA has converged, but may be incomplete due to the characteristics of the search. Future runs could fill in the missing data; therefore it is not necessary to find the 'true' clusters using Euclidean distance. Instead, a simple clustering technique was developed that combines the density information from the either the parameter or objective space with the fitness of the solutions.

A full explanation and description of the clustering technique used is given in Packham and Denham (2003). In summary, a univariate kernel density estimate (Silverman 1986) of each variable is made and the minima from each estimate are computed. The bounds of each cluster are thus identified in each variable. The first cluster chosen (to be displayed to the user) is that containing the highest fitness from the GA, this data is removed and the second cluster identified is that with the fittest individual of the remaining data, and so on.

Clustering can be performed in either parameter or objective space using the univariate kernel density estimation procedure described. The clustering itself is an aid to visualization of the high performance regions of the search space, not part of the search itself (although could be used in this way if it was deemed useful). The user can manually create and modify the clusters generated, hence the interaction of the user is as important (if not more so) than the definition of the clusters in this system.

After some investigation of the parameters used in kernel density estimation (such as the type of kernel used, number of points along each variable and smoothing parameter), those that produced the widest and most generic clusters were chosen for this visualization system (Packham et al. 2005). These were found to sufficiently highlight the important regions for most continuous problems (theoretical and practical).

The Rainfall-Streamflow Model and Calibration Data

The conceptual rainfall-streamflow model used in this study was the SIXPAR model (Gupta 1982) which is a reduced parameter version of the Sacramento soil moisture accounting model, SAC-SMA (Burnash et al. 1973), and is described in full in Gupta and Sorooshian (1983). The simplified model shown in Figure 1 permits testing of the calibration system and comparison with the results of Duan et al's (1992) study of the global optimization of conceptual rainfall-runoff models.

Fig 1 about here

In outline the model consists of an upper soil water storage layer (of maximum capacity UM), which is supplied by the daily rainfall. The outflow from this store occurs as interflow (controlled by a recession constant, UK) or percolation into a lower soil water store (controlled by a partitioning parameter, A, which determines the separation of percolation into actual and potential rates; and a parameter X which controls the degree of nonlinearity of the percolation process). Excess precipitation (once the upper zone is full) becomes runoff. The lower store has a maximum capacity BM and the baseflow rate is controlled by a recession constant, BK. Evapotranspiration and channel flow

routing are not simulated for simplicity. For comparison with Duan et al's (1992) study the same 200 day synthetic daily series of precipitation and streamflow for a known set of parameter values was used. Similarly the same constraints were applied to the permitted ranges for each parameter value, as shown in Table 1.

Table 1

Guidance on the selection of the length and characteristics of calibration and verification data for operational rainfall-streamflow models may be found in Yapo et al (1996).

Demonstration of the Interactive Calibration System

Note that the interactive visualization system was designed for maximization problems so negative values of RMSE, RMSslope and hence Fitness were used in the rainfall-streamflow calibration. As a means of comparing the best solutions obtained using different objective functions the commonly used Nash-Sutcliffe efficiency, NSE (Nash and Sutcliffe 1970), has been evaluated for presentation in this paper by:

$$NSE = 1 - \left(\frac{\sum_{t=1}^{n} \left(q_{obs,t} - q_t(\theta)\right)^2}{\sum_{t=1}^{n} \left(q_{obs,t} - \bar{q}_{obs}\right)^2} \right) \qquad (7)$$

where $\bar{q}_{obs}$ is the average observed streamflow.

Figure 2 shows 2-D scatter plots of the parameter subspaces from a 20 generation run of the visualization system with the RMSE used as the GA fitness function in (a), and the RMSslope used as fitness in (b). The user can choose the order of the axes to view different subspaces in the main plot, as necessary.

Fig 2

The scatter plots show all the solutions obtained by the GA. The automatic clustering algorithm generates 2 clusters of the fittest solutions over the entire parameter range (the number of clusters is set by the user). These clusters are shown as highlighted points (in different colors: the main (first) cluster is shown in green (the light points in Figure 2); the second cluster is shown in blue (the darker points); and the remaining solutions are shown in grey. For the RMSE fitness function (Figure 2(a)), the system identified 70 solutions in the first (fittest) cluster, 14 of which had an equivalent NSE of at least 0.999. The best solution found had UM = 16.815, UK = 0.325, BM = 12.065, BK = 0.227, A = 0.665, and X = 0.537, which is somewhat remote from the global solution (re. Table 1). The second cluster had 24 solutions, 10 of which had an equivalent NSE between 0.996 and 0.998, the best of which was relatively far from that in the first cluster with UM = 30.046, UK = 0.231, BM = 3.486, BK = 0.055, A = 0.627, and X = 1.635.

For the RMSslope fitness function (Figure 2(b)), the system identified different clusters to those for the RMSE fitness, but, again, the best solutions from each cluster were far apart from each other. The equivalent NSE values of the best solutions were in the range 0.998 to 0.999. It is clear that there is considerable spread in the good solutions over the parameter subspaces, consistent with the existence of different regions of attraction (convergence) with multiple local optima found by the computationally-intensive visualizations undertaken by Duan et al (1992). Furthermore the different clusters for the 2 objective functions illustrate the effect that the choice of single objective functions has on automatic calibration.

One of the sets of multi-objective results is shown in Figure 3 for a 20 generation run using equation 6 with $w_1 = 0.4$ and $w_2 = 0.6$ to calculate the fitness for the GA search. Figure 3(a) shows all the solutions obtained in the 2-D parameter subspaces and Figure

3(b) shows 3-D function spaces of 2 clusters of good solutions found by running the automatic clustering algorithm.

Fig 3

With the combined objective functions, the clustered solutions also included the region of attraction around the global parameter set. The model output for the best solution obtained can be rapidly displayed by the user (by right clicking with the mouse on the highlighted point) as displayed in Figure 4. At the display scale of Figure 4 the observed and predicted flows appear almost coincident. The zoom facility of the system allows the user to investigate the quality of the fit more closely. It should be noted that the daily rainfall and streamflow rates are expressed in terms of equivalent water depth over the contributing watershed area, commonly used in streamflow modeling, and are given in inches/day (where 1 inch/day = 25.4mm/day) to be consistent with the units used in Duan et al's (1992) SIXPAR model and original data.

Fig 4

In order to investigate the relationships between the parameters, the clustered solutions from the multi-objective search can be visualized in a parallel coordinates plot, as shown in Figure 5.

Fig 5

This indicates the range of values for each parameter associated with the region of good solutions. The results for the 2 clusters show the significant differences between the parameter sets for similar fitness measures, which can be an indicator of model structural error. However these plots have the limitation of being difficult to interpret when a large number of solutions are displayed.

The best solutions identified for a 20 generation run of the multiobjective system with a range of weighting factors between 0 and 1 used in equation 6 are summarized in Table 2.

Table 2

The results show that where the RMSE objective dominates the Fitness (i.e. for $w_1 > 0.5$ and $w_2 < 0.5$) the 20 generation GA search does not identify the region of attraction around the global optimum parameter set. This illustrates the positive influence of the new RMSslope objective function on the effectiveness of the calibration-support system.

The results shown in Table 2 indicate the need for the user to test the effect of different weightings on the identification of clusters. For the model and data used in this study, the results highlight the existence of multiple parameter sets of similar fitness because many conceptual models are subject to over parameterization, parameter interaction and poor sensitivity. From a practical viewpoint the decision of which of the similar-fitness parameter sets constitutes an acceptable calibration will depend upon validation of the selected model with further observed data. This is important given that the user will not know whether the system has identified the true global optimum parameter set (if such a single set exists for a given model and data). The benefit of the interactive system based on visualization is that the user can rapidly test the influence of the fitness weightings and explore the regions of attraction identified by the clustering. In this way the system allows the user to discover the nature of the search space. This knowledge can assist the user in evaluating whether the selected conceptual model is appropriate for the application or if a different model should be tested.

The user-directed interactive search capability of the system is demonstrated in Figure 6(a) where the user has selected a region around the best solution identified from the

initial clustering (for the case with w_1 = 0.4 and w_2 = 0.6). A further 20 generation GA search was carried out within this region where the parameter ranges were constrained by the boundaries of the selection box drawn by the user by simply using the mouse. The automatic clustering algorithm has been run to generate a cluster of the fittest solutions over this zoomed region, which is shown in Figure 6 (b).

Fig 6

From the fittest solution identified in this zoomed region, the best parameter set is converging towards the global, with UM = 9.546, UK = 0.499, BM = 20.226, BK = 0.208, A = 0.319, and X = 2.702, and an equivalent NSE of 0.9999. Given that a total of 40 generations of a 100 member population was run using the GA (i.e. 4100 model simulations, including evaluating the initial population of solutions) the system has been effective in locating the region of the global solution without the computational expense of a large number of model runs. In order to investigate the robustness of this region around the best parameter set found so far, the user can run a "negative GA" search (i.e. minimization rather than maximization). A filter was applied to the system to identify the top 10% of solutions within the best cluster (i.e. closest to the global parameter set found so far). A 20 generation "negative GA" was then run within this refined cluster. Figure 7 shows clusters of least fit solutions following a negative GA search together with the top 10% of solutions. The plot provides an approximate evaluation of the robustness of the best parameter set found so far by using the visual representation of the distance between the clusters of good and poor solutions. This information is valuable as it aids the user in deciding whether to continue with a refined search in this region for the best parameter set, or to continue to interact with the system and search in a different part of the space. Once the user has decided upon a promising convergence region then a more detailed search can be undertaken (possibly using a gradient based technique) without wasting computational time. Additionally, the negative GA search tool helps identify ranges for each parameter value which tend to produce sub-optimal calibration within the region around the best-so-far solution. By retaining these poor solutions (as different colored clusters) the user can avoid selecting sub-optimal regions when interactively exploring the parameter space within the visualization system.

Fig 7

Conclusions and Further Work

The application of a user-driven calibration-support system to the SIXPAR conceptual rainfall-streamflow model using synthetic data has been shown to be effective. The system was able to locate the region containing the global parameter set with a relatively modest number of model runs. This is important to hydrological modelers when calibrating high dimensional operational models with long data records (e.g 8 years) because of the large number of function evaluations required. Rapid sampling and clustering procedures, coupled with a range of high dimensional visualization techniques, promote the user's understanding of the complex nature of the parameter space, without excessive computational overheads. The system was able to display the existence of major convergence regions, local optima, and parameter interaction. The interactive features of the system allowed the user to select regions of the parameter space that the initial GA run had identified as potentially good calibration sets. However, the user is still free to select other regions on the basis of their experience of the calibration of a given model and knowledge of a particular watershed. The efficiency of the system was also shown by the facility to make an initial assessment of the robustness of the region around a potential parameter using a "negative GA" search. This allowed rapid sampling of the low fitness parameter sets without the need for computationally expensive model evaluation along a fine grid of values of each parameter. Consequently the user can quickly decide whether to continue refining the

search of a particular region of the parameter space or to return to one of the other clusters of good solutions.

The effect of the choice of objective functions on the calibration performance was demonstrated. A novel objective function, the RMSslope that represents the changing slope of the streamflow hydrograph was proposed. When used singly with an initial 20 generation GA search, the RMSE and RMSslope objective functions identified different optima but failed to find the global solution. However, when combined as a weighted sum, the region of the global solution was detected, particularly where the RMSslope dominated the fitness function. The interactive nature of the system allowed the user to exploit the knowledge revealed by the automatic clustering technique and select a promising region for further exploration, leading to convergence towards the global solution. The combination of search efficiency, visualization and interaction is valuable both for the novice and the experienced hydrological modeler. Thus the system could be used as a decision support tool for the calibration of conceptual rainfall-streamflow models by practicing engineering hydrologists or as a teaching aid for hydrology students.

The standard GA has been used in this visualization system and in the results presented. These GA runs could also be performed in alternative coordinate systems (such as the principal components of previously generated data (Packham and Denham (2003)). It would be also be possible to replace the standard GA with one known to perform well on calibration problems, such as SCE-UA (Duan et al. 1992). If such a technique was implemented in the system and complemented by an appropriate clustering mechanism, it could be very effective in revealing the contours of the search space to the user.

The use of the system with an operational rainfall-streamflow model on a physical watershed with alternative objective functions to the RMSE, such as the HMLE (Sorooshian and Dracup 1980) to account for nonstationary variance in observed streamflow data, is the subject of ongoing research.

Notation
The following symbols are used in this paper:

n	=	the number of daily streamflow values used in the calibration;
$q_{obs,t}$	=	the observed streamflow at time t;
$\bar{q}_{obs}$	=	the average observed streamflow;
q_t	=	the streamflow at a particular time, t;

$q_t(\theta)$ = the streamflow predicted by the model at time t;

Δt = the timestep (1 day for the daily time series used);

w_1, w_2 = weightings.

References

Bender, M., and Simonovic, S. P. (1994). "Decision-support system for long-range stream flow forecasting." *Journal of Computing in Civil Engineering*, 8(1), 20-34.

Beven, K. (1993). "Prophecy, reality and uncertainty in distributed hydrological modeling." *Advances in Water Resources*, 16(1), 41-51.

Beven, K. (2006). "A manifesto for the equifinality thesis." *Journal of Hydrology*, 320(1-2), 18-36.

Beven, K., and Binley, A. (1992). "The future of distributed models - model calibration and uncertainty prediction." *Hydrological Processes*, 6(3), 279-298.

Beven, K., and Freer, J. (2001). "Equifinality, data assimilation, and uncertainty estimation in mechanistic modelling of complex environmental systems using the GLUE methodology." *Journal of Hydrology*, 249(1-4), 11-29.

Boyle, D. P., Gupta, H. V., and Sorooshian, S. (2000). "Toward improved calibration of hydrologic models: Combining the strengths of manual and automatic methods." *Water Resources Research*, 36(12), 3663-3674.

Burnash, R. J. E., Ferral, R. L., and McGuire, R. A. (1973). "A generalized streamflow simulation system - Conceptual modeling for digital computers." Joint Federal and State River Forecast Center, U.S. National Weather Service and California Department of Water Resources, Sacramento, California.

Chambers, J. M., Cleveland, W. S., Kleiner, B., and Tukey, P. A. (1983). *Graphical Methods for Data Analysis*, Chapman & Hall, New York.

Cooper, V. A., Nguyen, V. T. V., and Nicell, J. A. (1997). "Evaluation of global optimization methods for conceptual rainfall-runoff model calibration." *Water Science and Technology*, 36(5), 53-60.

Diskin, M. H., and Simon, E. (1977). "A procedure for the selection of objective functions for hydrologic simulation models." *Journal of Hydrology*, 34(1-2), 129-149.

Duan, Q. Y., Sorooshian, S., and Gupta, V. (1992). "Effective and efficient global optimization for conceptual rainfall-runoff models." *Water Resources Research*, 28(4), 1015-1031.

Franchini, M. (1996). "Use of a genetic algorithm combined with a local search method for the automatic calibration of conceptual rainfall-runoff models." *Hydrological Sciences Journal*, 41(1), 21-39.

Gan, T. Y., and Biftu, G. F. (1996). "Automatic calibration of conceptual rainfall-runoff models: Optimization algorithms, catchment conditions, and model structure." *Water Resources Research*, 32(12), 3513-3524.

Garrote, L., and Becchi, I. (1997). "Object-oriented software for distributed rainfall-runoff models." *Journal of Computing in Civil Engineering*, 11(3), 190-194.

Goldberg, D. E. (1989). *Genetic Algorithms in Search, Optimization and Machine Learning*, Addison-Wesley, Reading, Massachusetts.

Goldberg, D. E., and Kuo, C. H. (1987). "Genetic algorithms in pipeline optimization." *Journal of Computing in Civil Engineering*, 1(2), 128-141.

Gupta, H. V., Bastidas, L. A., Vrugt, J. A., and Sorooshian, S. (2003a). "Multiple criteria global optimization for watershed model calibration." Calibration of Watershed Models, Q. Y. Duan, H. V. Gupta, S. Sorooshian, A. N. Rousseau, and R. Turcotte, eds., American Geophysical Union, Washington, DC, 125-132.

Gupta, H. V., Sorooshian, S., Hogue, T. S., and Boyle, D. P. (2003b). "Advances in automatic calibration of watershed models." Calibration of Watershed Models, Q. Y. Duan, H. V. Gupta, S. Sorooshian, A. N. Rousseau, and R. Turcotte, eds., American Geophysical Union, Washington, DC, 9-28.

Gupta, H. V., Sorooshian, S., and Yapo, P. O. (1998). "Toward improved calibration of hydrologic models: Multiple and noncommensurable measures of information." Water Resources Research, 34(4), 751-763.

Gupta, H. V., Sorooshian, S., and Yapo, P. O. (1999). "Status of automatic calibration for hydrologic models: comparison with multilevel expert calibration." Journal of Hydrologic Engineering, 4(2), 135-143.

Gupta, V. K. (1982). "Calibration of conceptual rainfall-runoff models: Problems caused by model structure," MSc Thesis, Case Western Reserve University, Cleveland, Ohio.

Gupta, V. K., and Sorooshian, S. (1983). "Uniqueness and observability of conceptual rainfall-runoff model parameters - the percolation process examined." Water Resources Research, 19(1), 269-276.

Harlin, J. (1991). "Development of a process oriented calibration scheme for the HBV hydrological model." Nordic Hydrology, 22(1), 15-36.

Hogue, T. S., Sorooshian, S., Gupta, H., Holz, A., and Braatz, D. (2000). "A multistep automatic calibration scheme for river forecasting models." Journal of Hydrometeorology, 1(6), 524-542.

Holland, J. H. (1975). Adaptation in Natural and Artificial Systems, University of Michigan Press, Ann Arbor.

Houghton-Carr, H. A. (1999). "Assessment criteria for simple conceptual daily rainfall-runoff models." Hydrological Sciences Journal, 44(2), 237-261.

Inselberg, A., and Dimsdale, B. (1994). "Multidimensional lines I: Representation." SIAM Journal on Applied Mathematics, 54(2), 559-577.

Jain, A. K., Murty, M. N. & Flynn, P. J. (1999). "Data Clustering: A Review". ACM Computing Surveys, 31(3), 264-323.

Jeong, H. S., and Abraham, D. M. (2006). "Operational response model for physically attacked water networks using NSGA-II." Journal of Computing in Civil Engineering, 20(5), 328-338.

Kavetski, D., Franks, S. W., and Kuczera, G. (2002). "Confronting input uncertainty in environmental modelling." Calibration of Watershed Models, Q. Duan, H. V. Gupta, S. Sorooshian, A. N. Rousseau, and R. Turcotte, eds., American Geophysical Union, Washington, DC, 49-68.

Khu, S. T., and Werner, M. G. F. (2003). "Reduction of Monte-Carlo simulation runs for uncertainty estimation in hydrological modelling." Hydrology and Earth System Sciences, 7(5), 680-692.

Kuczera, G. (1983). "Improved parameter inference in catchment models: 1. Evaluating parameter uncertainty." Water Resources Research, 19(5), 1151-1162.

Kuczera, G., and Parent, E. (1998). "Monte Carlo assessment of parameter uncertainty in conceptual catchment models: the Metropolis algorithm." Journal of Hydrology, 211(1-4), 69-85.

Legates, D. R., and McCabe, G. J. (1999). "Evaluating the use of "goodness-of-fit" measures in hydrologic and hydroclimatic model validation." Water Resources Research, 35(1), 233-241.

Liong, S. Y., Chan, W. T., and Shreeram, J. (1995). "Peak-flow forecasting with genetic algorithm and SWMM." Journal of Hydraulic Engineering, 121(8), 613-617.

Liu, Y., Khu, S.-T., and Savic, D. (2004). "A hybrid optimization method of multi-objective genetic algorithm (MOGA) and k-nearest neighbor (KNN) classifier

for hydrological model calibration." Lecture Notes in Computer Science, Z. R. Yang, H. Yin, and R. Everson, eds., Springer 3177, Berlin, 546-551.

Madsen, H. (2000). "Automatic calibration of a conceptual rainfall-runoff model using multiple objectives." *Journal of Hydrology*, 235(3-4), 276-288.

Madsen, H., Wilson, G., and Ammentrop, H. C. (2002). "Comparison of different automated strategies for calibration of rainfall-runoff models." *Journal of Hydrology*, 261(1-4), 48-59.

Montesinos, P., and Beven, K. J. (1999). "Application of a genetic algorithm as sampler selector within the GLUE approach. Poster Presentation." *XXIV European Geophysical Society General Assembly*, The Hague, Netherlands.

Nash, J. E., and Sutcliffe, J. V. (1970). "River flow forecasting through conceptual models part 1 - A discussion of principles." *Journal of Hydrology*, 10(3), 282-290.

Ndiritu, J. G., and Daniell, T. M. (1999). "An improved genetic algorithm for continuous and mixed discrete-continuous optimization." *Engineering Optimization*, 31(5), 589-614.

Packham, I. S. J. (2003). "An Interactive Visualisation System for Engineering Design using Evolutionary Computing." PhD Thesis, University of Plymouth.

Packham, I. S. J., and Denham, S. L. (2003). "Visualisation methods for supporting the exploration of high dimensional problem spaces in engineering design". *International Conference on Coordinated & Multiple Views in Exploratory Visualization*. Roberts, J. C. (ed.), London, UK: IEEE Computer Soc, 2-13.

Packham, I. S. J., Borthwick, M., Rafiq, Y., and Denham, S. (2004). "Improved understanding of rainfall runoff modelling using interactive visualisation and evolutionary computing." *11th International Workshop, European Group for Intelligent Computing in Engineering*, Weimar, Germany.

Packham, I. S. J., Rafiq, M. Y., Borthwick, M. F., and Denham, S. L. (2005). "Interactive visualisation for decision support and evaluation of robustness - in theory and in practice." *Advanced Engineering Informatics*, 19(4), 263-280.

Rafiq, M. Y., Mathews, J. D., and Bullock, G. N. (2003). "Conceptual building design-evolutionary approach." *Journal of Computing in Civil Engineering*, 17(3), 150-158.

Rafiq, M. Y., Packham, I. S. J., Easterbrook, D. J., and Denham, S. L. (2006a). "Visualizing search and solution spaces in the optimum design of biaxial columns." *Journal of Computing in Civil Engineering*, 20(2), 88-98.

Rafiq, Y., Sui, C., Easterbrook, D., and Bugmann, G. (2006b). "Prediction of the behaviour of masonry wall panels using evolutionary computation and cellular automata." *13th EG-ICE Workshop "Intelligent Computing in Engineering & Architecture"*, Ascona, Switzerland. (Accepted for publication).

Sharif, M., and Wardlaw, R. (2000). "Multireservoir systems optimization using genetic algorithms: case study." *Journal of Computing in Civil Engineering*, 14(4), 255-263.

Shneiderman, B. (1998). *Designing the User Interface*, Addison-Wesley, Reading, Massachusetts.

Silverman, B. W. (1986). *Density Estimation for Statistics and Data Analysis*, Chapman and Hall, London.

Solomatine, D. P. (1995). "The use of global random search methods for models calibration." *HYDRA 2000 Proceedings of the XXVIth IAHR Congress*, London, 224-229.

Solomatine, D. P. (1999). "Two strategies of adaptive cluster covering with descent and their comparison to other algorithms." *Journal of Global Optimization*, 14(1), 55-78.

Sorooshian, S., and Dracup, J. A. (1980). "Stochastic parameter estimation procedures for hydrologic rainfall-runoff models: correlated and heteroscedastic error cases." *Water Resources Research*, 16(2), 430-442.

Uhlenbrook, S., Seibert, J., Leibundgut, C., and Rodhe, A. (1999). "Prediction uncertainty of conceptual rainfall-runoff models caused by problems in identifying model parameters and structure." *Hydrological Sciences Journal*, 44(5), 779-797.

Vrugt, J. A., Gupta, H. V., Bastidas, L. A., Bouten, W., and Sorooshian, S. (2003). "Effective and efficient algorithm for multiobjective optimization of hydrologic models." *Water Resources Research*, 39(8), 1214, doi:10.1029/2002WR001746.

Wagener, T., Boyle, D. P., Lees, M. J., Wheater, H. S., Gupta, H. V., and Sorooshian, S. (2001). "A framework for development and application of hydrological models." *Hydrology and Earth System Sciences*, 5(1), 13-26.

Wagener, T., Wheater, H. S., and Gupta, H. V. (2003). "Identification and evaluation of watershed models." Advances in Calibration of Watershed Models, Q. Duan, S. Sorooshian, H. V. Gupta, A. Rousseau, and R. Turcotte, eds., AGU Monograph, 29-47.

Wang, Q. J. (1991). "The genetic algorithm and its application to calibrating conceptual rainfall-runoff models." *Water Resources Research*, 27(9), 2467-2471.

Wang, Q. J. (1997). "Using genetic algorithms to optimise model parameters." *Environmental Modelling & Software*, 12(1), 27-34.

Werner, M., and Khu, S. T. (2001). "Monte-Carlo based uncertainty analysis framework using a multi-modal genetic algorithm." *XXIX IAHR Congress "21st Century: The New Era for Hydraulic Research and Its Applications"*, Beijing, China.

Wu, Z. Y., and Simpson, A. R. (2001). "Competent genetic-evolutionary optimization of water distribution systems." *Journal of Computing in Civil Engineering*, 15(2), 89-101.

Yang, R., and Douglas, I. (1998). "Simple genetic algorithm with local tuning: Efficient global optimizing technique." *Journal of Optimization Theory and Applications*, 98(2), 449-465.

Yapo, P. O., Gupta, H. V., and Sorooshian, S. (1996). "Automatic calibration of conceptual rainfall-runoff models: Sensitivity to calibration data." *Journal of Hydrology*, 181(1-4), 23-48.

Yapo, P. O., Gupta, H. V., and Sorooshian, S. (1998). "Multi-objective global optimization for hydrologic models." *Journal of Hydrology*, 204(1-4), 83-97.

Zhang, X., and Lindström, G. (1997). "Development of an automatic calibration scheme for the HBV hydrological model." *Hydrological Processes*, 11(12), 1671-1682.

Table 1. True parameter values used to synthesize streamflow data and ranges permitted for GA search

Parameter	True Value	Lower Bound	Upper Bound
UM	10	0	50
UK	0.5	0	1
BM	20	0	50
BK	0.2	0	1
A	0.31	0	1
X	3	0	10

Table 2. Best solutions identified from first cluster for different weighting factors used in evaluation of multiobjective Fitness (equation 6)

w_1	w_2	UM	UK	BM	BK	A	X	NSE
0.1	0.9	9.937	0.454	19.951	0.206	0.300	4.850	0.9997
0.2	0.8	9.866	0.542	19.621	0.209	0.287	5.936	0.9997
0.3	0.7	10.535	0.432	16.105	0.237	0.362	1.470	0.9989
0.4	0.6	12.899	0.439	16.916	0.208	0.242	1.260	0.9995
0.5	0.5	10.929	0.487	19.761	0.182	0.312	3.631	0.9995
0.6	0.4	25.305	0.250	.2.524	0.392	0.237	7.192	0.9988
0.7	0.3	28.393	0.249	2.214	0.149	0.358	5.788	0.9991
0.8	0.2	30.136	0.236	4.664	0.013	0.733	7.814	0.9988
0.9	0.1	10.076	0.480	17.257	0.241	0.653	1.503	0.9991
True solution:		10.000	0.500	20.000	0.200	0.310	3.000	1.0000
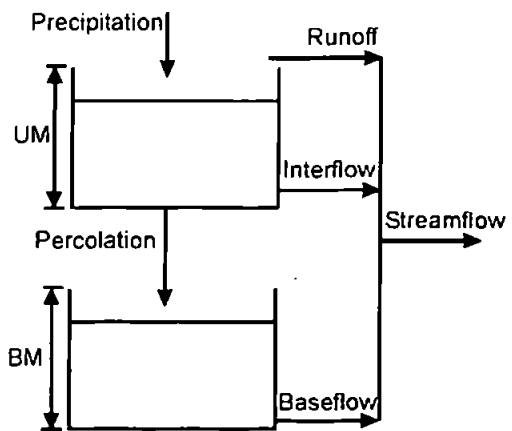
Figure 1: Schematic structure of SIXPAR model
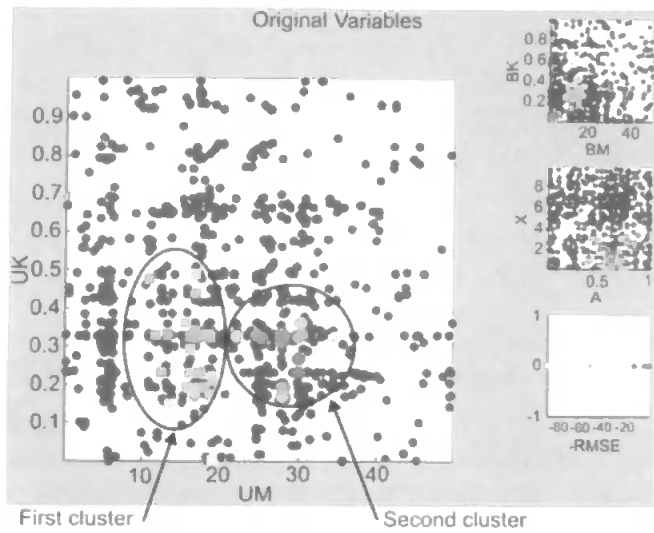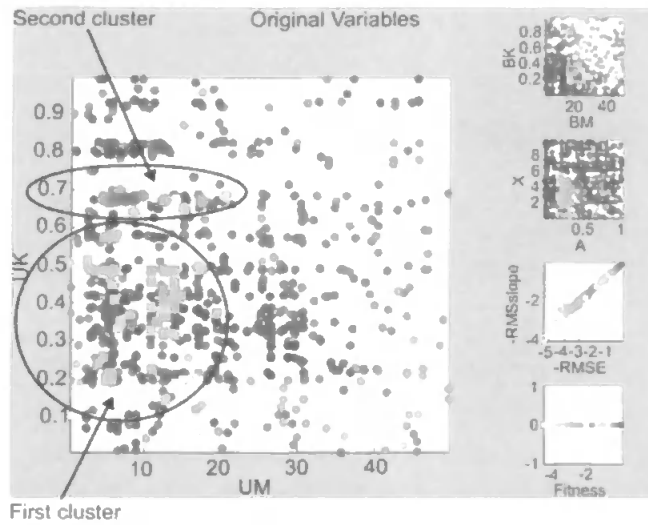
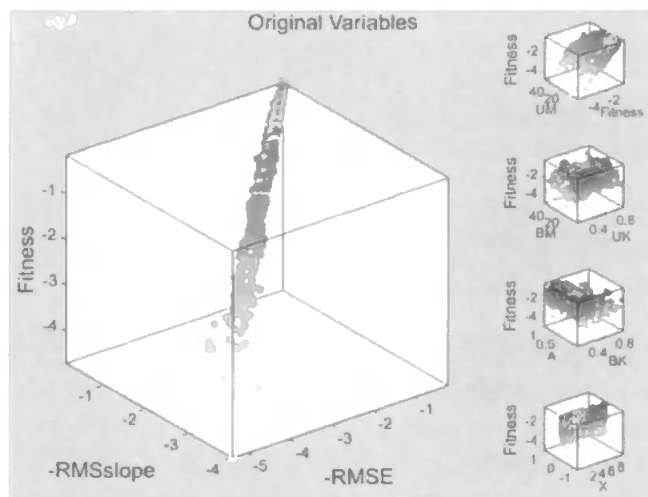**(a) RMSE used as fitness in GA search**
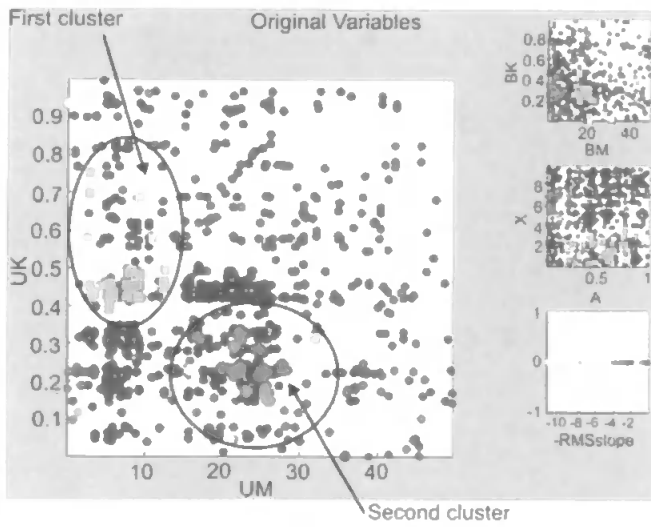
(b) RMSslope used as fitness in GA search

Figure 2: 2-D scatter plots of parameter subspaces

(a) 2-D parameter subspaces

(b) 3-D function subspaces showing clusters only

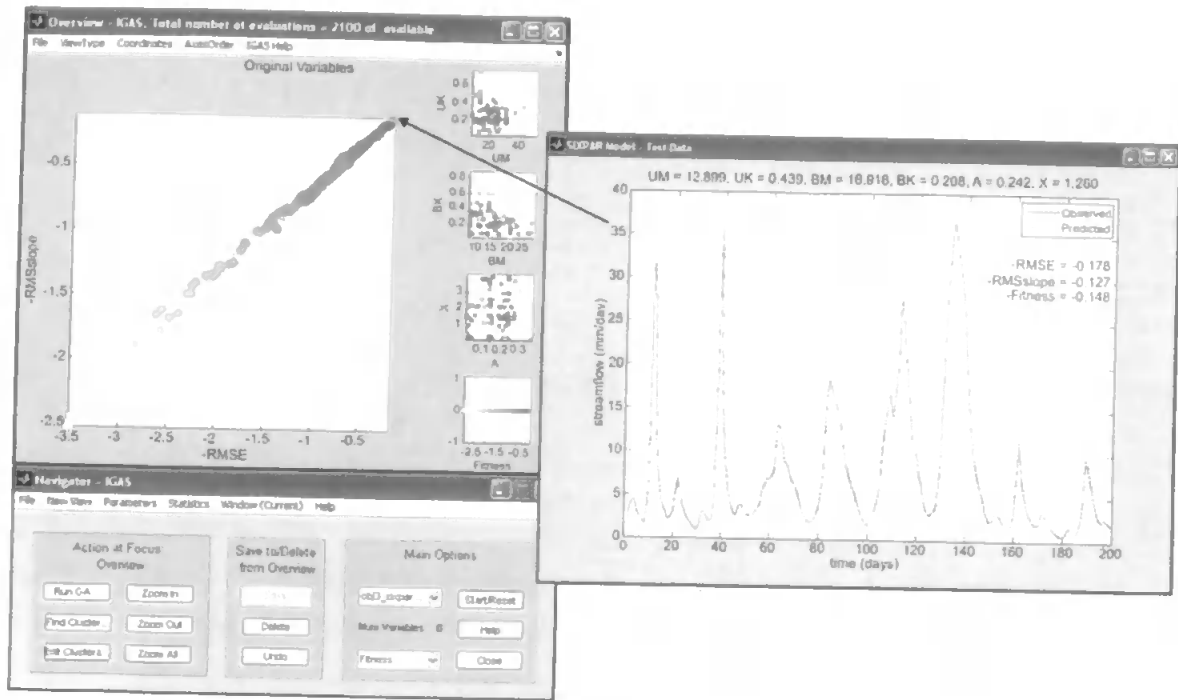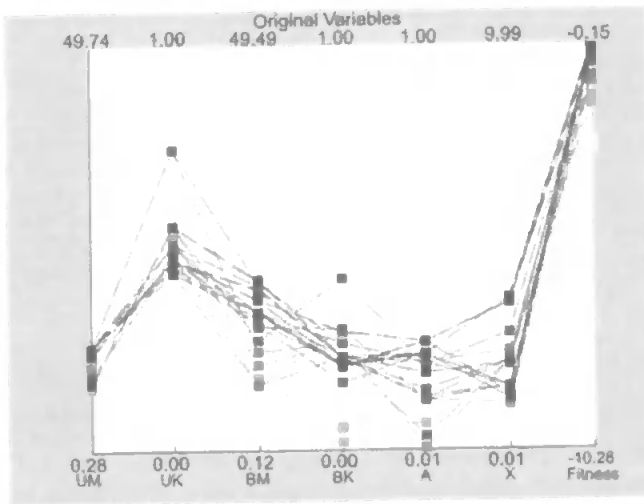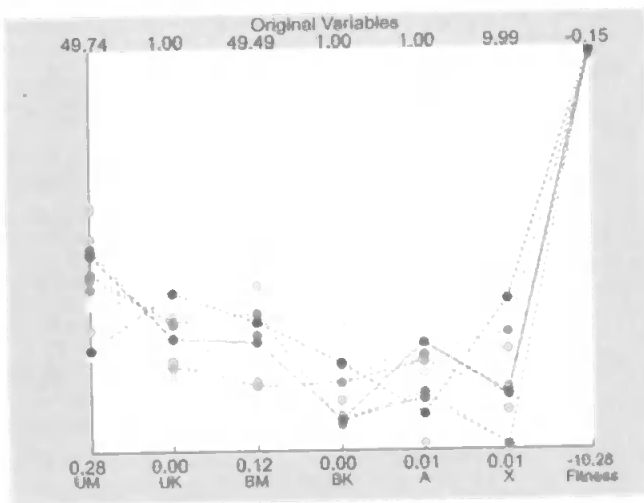Figure 3: Scatter plots of the multi-objective GA search

383

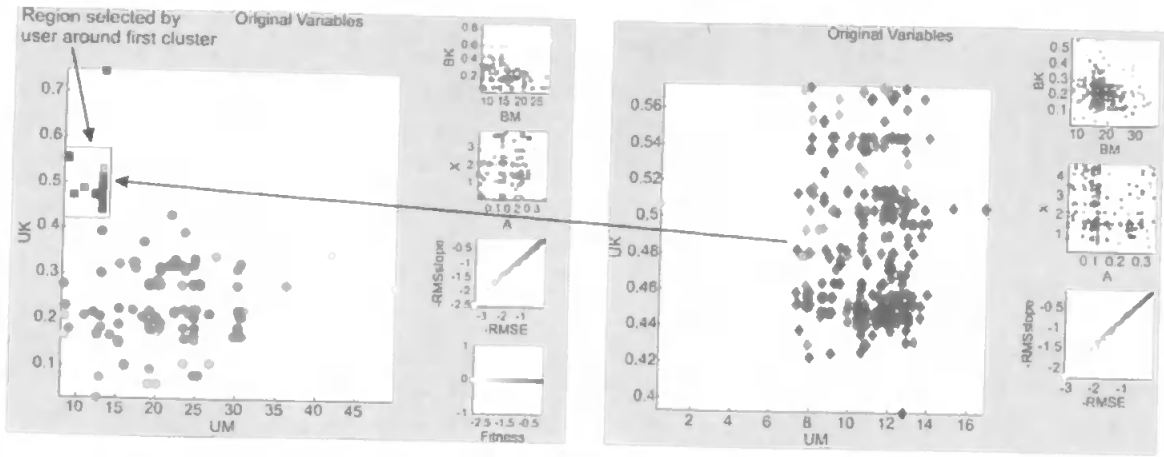Figure 4: Best solution from 20 generational multi-objective GA search

(a) first cluster

(b) second cluster

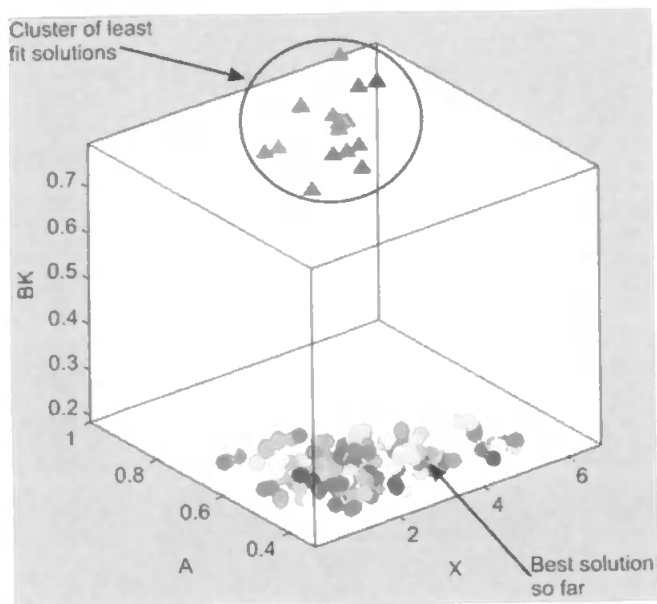Figure 5: Parallel coordinates plot of parameters from multi-objective GA search

(a) User selected region around initial best solution

(b) Cluster of best solutions identified in selected space

Figure 6: Interactive search capability

Figure 7: Clusters of best and worst solutions following "negative GA" search within user-selected region